Nickel and Palladium Complexes of Di-N-Heterocyclic Carbenes

by

Peter J. Silcock

A thesis submitted in part fulfilment of the requirements for
the degree of Doctor of Philosophy
at the University of Oxford.

Balliol College

Oxford

December 1999

The work described in this thesis was carried out in the Inorganic Chemistry Laboratory, South Parks Road, Oxford, from September 1996 to August 1999 under the supervision of Professor Malcolm L.H. Green, FRS. All the work is my own unless stated to the contrary, and has not previously been submitted for any degree at this, or any other, university.

Abstract:

Nickel and Palladium Complexes of Di-N-Heterocyclic Carbenes

Peter J. Silcock
Balliol College

Michaelmas Term 1999
Submitted for D. Phil.

This thesis is concerned with the synthesis of two di-N-heterocyclic carbene ligands, and their reactivity towards nickel and palladium precursors in order to synthesise new organometallic pre-catalysts for a number of important reactions. The catalytic properties of a new rhodium C_{60} compound are also investigated, with relevance to the evaluation of C_{60} as a hydrogen storage medium.

Chapter 1 reviews the preparation and chemistry of N-heterocyclic carbenes, emphasising their organometallic reactivity and role as ancillary ligands in homogeneous transition metal catalysis. An overview of relevant nickel and palladium catalysis is also presented, including olefin polymerisation, olefin / CO copolymerisation and Heck coupling reactions.
Chapter 2 describes the synthesis and characterisation of the dicarbene ligands $^{tBu}CC^{meth}$ and $^{tBu}CC^{eth}$ ‡ and their reactions with various nickel precursors in attempts to prepare chelating dicarbene nickel *cis*-dihalide complexes. The synthesis, characterisation and chemical reactivity of the cations $[Ni(^{tBu}CC^{meth})_2]^{2+}$, $[(^{tBu}CC^{meth})NiCl(PMe_3)]^+$ and $[(^{tBu}CC^{eth})NiCl(PMe_3)]^+$ is detailed, and their X-ray structures are compared. The unsuccessful preparation of $[Ni(^{tBu}CC^{eth})_2]^{2+}$ and the relative stability of the monocations with respect to dicarbene substitution is discussed and attributed to steric factors.
Chapter 3 describes the synthesis, characterisation, reactivity and catalytic studies of simple nickel and palladium *cis*-dimethyl complexes of the chelating dicarbene ligands. Variable temperature ^1H NMR spectroscopy showed contrasting rates of thermal hydrocarbon elimination from $Ni(^{tBu}CC^{meth})Me_2$ and $Ni(^{tBu}CC^{eth})Me_2$, which has previously been observed for chelating *bis*-phosphine analogues with various P,P' linkages $(CH_2)_n$. These observations further corroborate the analogy between dicarbene and *bis*-phosphine ligands. It was demonstrated that the compounds $Pd(^{tBu}CC^{meth})Me_2$ and $Pd(^{tBu}CC^{eth})Me_2$ are effective pre-catalysts for the Heck coupling of 4-bromoanisole and n-butyl acrylate. In addition cations of the type $[(^{tBu}CC^{meth/eth})PdMe(L)]^+$ (L = pyridine, THF) which are relevant to olefin / CO copolymerisation were prepared. The X-ray structures of $M(^{tBu}CC^{eth})Me_2$ (M = Ni, Pd) are discussed as well as the synthesis and structural characterisation of $[(\mu\text{-}^{tBu}CC^{meth})\{Ni(PMe_3)Me_2\}_2]$.
Chapter 4 presents a brief introduction to some relevant C_{60} chemistry and to the concept of hydrogen storage. The synthesis and characterisation of a new rhodium C_{60} compound is described. The compound catalysed the hydrogenation and hydroformylation of simple alkenes as well as the hydrogenation of C_{60} to $C_{60}H_{36}$. The recovery of hydrogen gas from $C_{60}H_{36}$ was investigated in order to evaluate C_{60} as a hydrogen storage medium.
Chapter 5 outlines the experimental details for the synthesis, characterisation, reactions and catalytic studies of the new compounds described in the preceding three chapters.
Chapter 6 presents the characterising data for the new compounds described in chapters 2 and 3.
Appendices contain details of the crystallographic data for the eight structurally characterised compounds described in chapters 2 and 3.

---

‡ $^{tBu}CC^{meth}$ = 1,1'-methylene-3,3'-di-*tert*-butyldiimidazol-2,2'-diylidene
$^{tBu}CC^{eth}$ = 1,1'-(1,2-ethylene)-3,3'-di-*tert*-butyldiimiadazol-2,2'-diylidene

For Mum and Dad

Acknowledgements

I am indebted to Professor Malcolm Green FRS for creating, within a few hectic days of June 1996, my opportunity to commence a D. Phil. in his unique research group, and for his inspirational supervision and kind support thereafter. Thank you.

I am also grateful to EPSRC and Johnson Matthey plc for a CASE award, and to my industrial supervisors Jack Frost and Stan Golunski, for their attention and input during my visits to Sonning with Malcolm.

Special thanks must now go to Richard Douthwaite and Pedro Gomes for their huge contributions to the work in this thesis. Richard solved my eight crystal structures, proof-read all of this thesis after moving to Birmingham and on a day-to-day basis provided help, wisdom, instruction, focus, a loud stereo system and his acid wit for the majority of three years. He liked to run a tight ship in T3, so I'm sure it tickled his famous sense of irony when I moved in for a D. Phil. never having used a Schlenk line. Of course I could not forget Pedro, who during the summer months of 1998 provided ideas which kick-started the nickel carbene chemistry. His enthusiasm and industry, all the way from Lisbon, inspired many of us on the top floor. Other useful contributions to this thesis were made by Daniel Haüßinger (2-D NMR spectroscopy), Ana Martins (help with attempted dicarbene nickel dihalide syntheses), Jeremy Sloan (electron microscopy), Andreas Danopolous (ideas on dicarbene ligand synthesis), Andy York (help with BET surface area measurement), Greg Mullen and Phil Arnold (electrospray MS) and Gerry Clancy (proof-reading). I am also grateful to Steve Brogden and co. of the stores, Anne and Jim of the analytical department, and the glassblowers and workshop for all their help over the years.

Since my arrival to the Green group many have come, gone, and been part of the furniture. Of these, I would most like to thank the following: Gerry Clancy and Ronan Bellabarba for all their help and for rapidly becoming great mates after our kick off in September 1996; Richard and Hanif for putting up with me in T3; Ronan who tolerated our invasion of T17 (where new music volume and oven temperature ensured visitors left with fingers burnt, ears ringing and no glassware); Arran 'Azza' Tulloch who was never entirely averse to a sly pint, and Sofia Pascu, who became a good friend sometime after dropping the arsenic chemistry. Andy, Jeremy, Cliff, Daniel, Linda, Steve and Ino must also be noted for their helpfulness and conviviality, which really goes for everyone in the Green group. If you are affronted by my negligence in leaving you out, or indeed greatly put out to see your name in the list then please forgive me: I thank you all! Skinner, Dribs and Nige of the Mountford group deserve a cheeky mention for shaking-up the Oxford scene on arrival.

1999 will be remembered by many as the glory-year in which Man. U. were crowned World, European and domestic champions, and picked up the FA Cup along the way. However, I wish to shift the emphasis and make mention of another celebrity crowd, which graced the beautiful streets of Lisbon for 10 days in August. Gerry, Sofia, Ronan, Chris, Cliff, Sean, Malcolm and above all Pedro and Ana who were such great hosts, all have my gratitude for making it such an unforgettable conference to be at, and a story in itself.

No list of my acknowledgements would be complete without mention of my friends outside the lab, who often saw me right when the damn chemistry didn't work! So to Mike, Steve, Semps, Ezz of Dubai, Bob and the London / Crete boys. Cheers lads.

Finally, the most important thanks of all go to Mum, John and Hannah for unflagging support and understanding throughout my D. Phil.

'Yes Percy I don't want to be pedantic or anything but the colour of gold is gold.
That's why it's called "gold". What you have discovered, if it has a name,
is some "*green*".'

Edmund Blackadder to the aspiring alchemist.

Abbreviations

Ac	:	Acetyl
BET	:	Brunauer, Emmett and Teller
bpy	:	2,2'-Bipyridyl
COD	:	1,5-Cyclooctadiene
COE	:	Cyclooctene
DME	:	1,2-Dimethoxyethane
DMSO	:	Dimethylsulphoxide
DOE	:	Department of Energy
dppe	:	1,2-*bis*(Diphenylphosphino)ethane
dppp	:	1,3-*bis*(Diphenylphosphino)propane
EDX	:	Energy dispersive X-ray
EI	:	Electron impact
Et	:	Ethyl
FAB	:	Fast Atom Bombardment
GC	:	Gas Chromatography
GCMS	:	Gas chromatography-mass spectrometry
GNFs	:	Graphite nanofibres
HOMO	:	Highest Occupied Molecular Orbital
IR	:	Infrared
LUMO	:	Lowest Unoccupied Molecular Orbital
MAO	:	Methylaluminoxane
Me	:	Methyl
Mes	:	(2,4,6-$(CH_3)_3C_6H_2$)
MO	:	Molecular Orbital
MS	:	Mass spectrometry
^{n}Bu	:	($CH_2CH_2CH_2CH_3$)
NMR	:	Nuclear Magnetic Resonance
NOE	:	Nuclear Overhauser Effect
NOESY	:	2-D Nuclear Overhauser Spectroscopy
py	:	Pyridine
^{R}CC^{meth}	:	1,1'-Methylene-3,3'-dialkyldiimidazol-2,2'-diylidene (R = alkyl)
r.t.	:	Retention time
RCM	:	Ring Closing Metathesis
ROMP	:	Ring Opening Metathesis Polymerisation
SWNTs	:	Single-walled nanotubes
^{t}Bu	:	*tert*-Butyl
^{tBu}CC^{meth}	:	1,1'-Methylene-3,3'-di-*tert*-butyldiimidazol-2,2'-diylidene
^{tBu}CC^{eth}	:	1,1'-(1,2-Ethylene)-3,3'-di-*tert*-butyldiimidazol-2,2'-diylidene
^{tBu}C(D)C^{meth}	:	1,1'-Methylene -3,3'-di-*tert*-butyl(2-deuteroimidazolium)-imidazol-2-ylidene
^{tBu}C(D)C^{meth}	:	1,1'-(1,2-ethylene)-3,3'-di-*tert*-butyl(2-deuteroimidazolium)-imidazol-2-ylidene
TEM	:	Transmission electron microscopy
THF	:	Tetrahydrofuran
tmiy	:	1,3,4,5-Tetramethylimidazol-2-ylidene
TON	:	Turnover Number (mol product / mol catalyst)
TPD	:	Temperature-programmed desorption
XRD	:	X-Ray diffraction
40-60 petroleum ether	:	Petroleum ether with boiling point in the range 40-60 °C

Contents

Appendices: X-Ray Crystal Structure Data

CHAPTER 1

Introduction

1.1 Introduction

The majority of this thesis is concerned with the synthesis of two new bidentate N-heterocyclic carbene ligands, and their reactivity towards various nickel and palladium precursors in order to synthesise new organometallic pre-catalysts for a number of important reactions.

This chapter provides an introduction to the chemistry of N-heterocyclic carbenes with an emphasis on their organometallic reactivity and ability to act as ancillary ligands in homogeneous transition metal catalysis. An overview of nickel and palladium catalysis relevant to the aims of the work in this thesis is also presented.

1.2 N-Heterocyclic Carbenes

1.2.1 Discovery and Synthesis

Complexes of N-heterocyclic carbenes were first prepared in 1968 by Öfele (**1**) and Wanzlick et al. (**2**) by reaction between imidazolium salts and metal-containing precursors of sufficient basicity to deprotonate the salts (Eqs. 1, 2):[1,2]

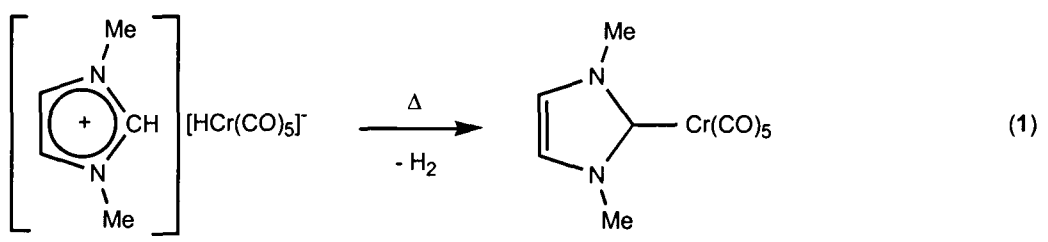

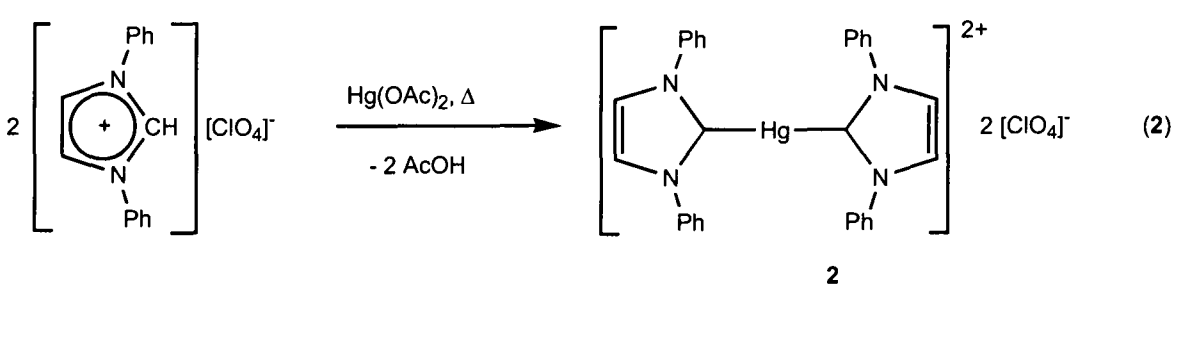

Wanzlick and co-workers went on to demonstrate that imidazolium salts such as **3** and **6** are deprotonated by potassium *tert*-butoxide to give carbenes **4** and **7** respectively, which were then trapped, but not isolated. The carbene **4** was trapped using phenyl isothiocyanate to give the zwitterion **5**, and **7** using $HgCl_2$ which gave the mercury complex **8** (Eqs. 3, 4):[3,4]

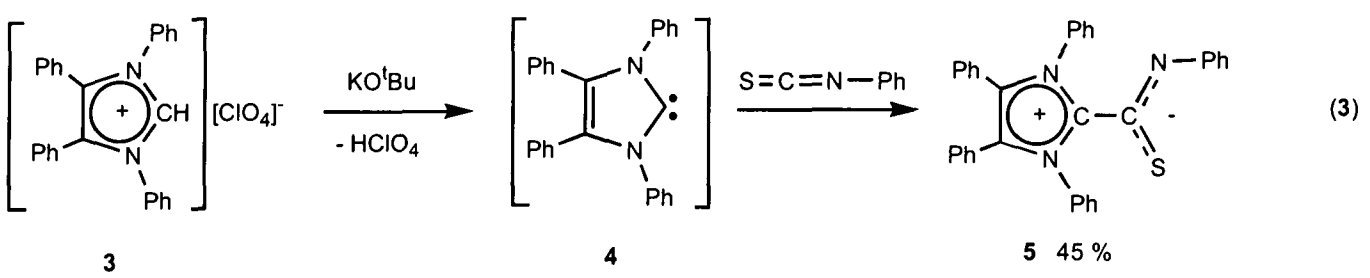

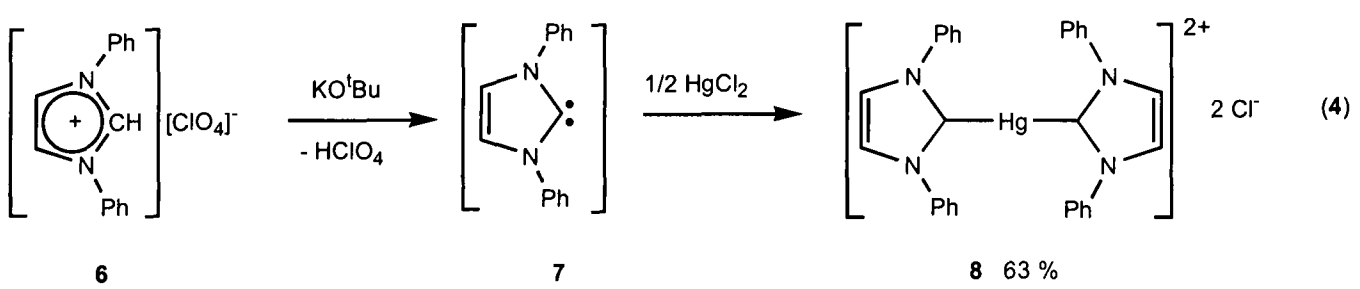

The same principle was used almost two decades later when Arduengo deprotonated 1,3-diadamantylimidazolium chloride with sodium hydride in THF in the presence of a catalytic amount of DMSO anion to precipitate the colourless, crystalline and thermally stable (melting point 240-241 °C without decomposition) free N-heterocyclic carbene **9** (figure 1.1).[5]

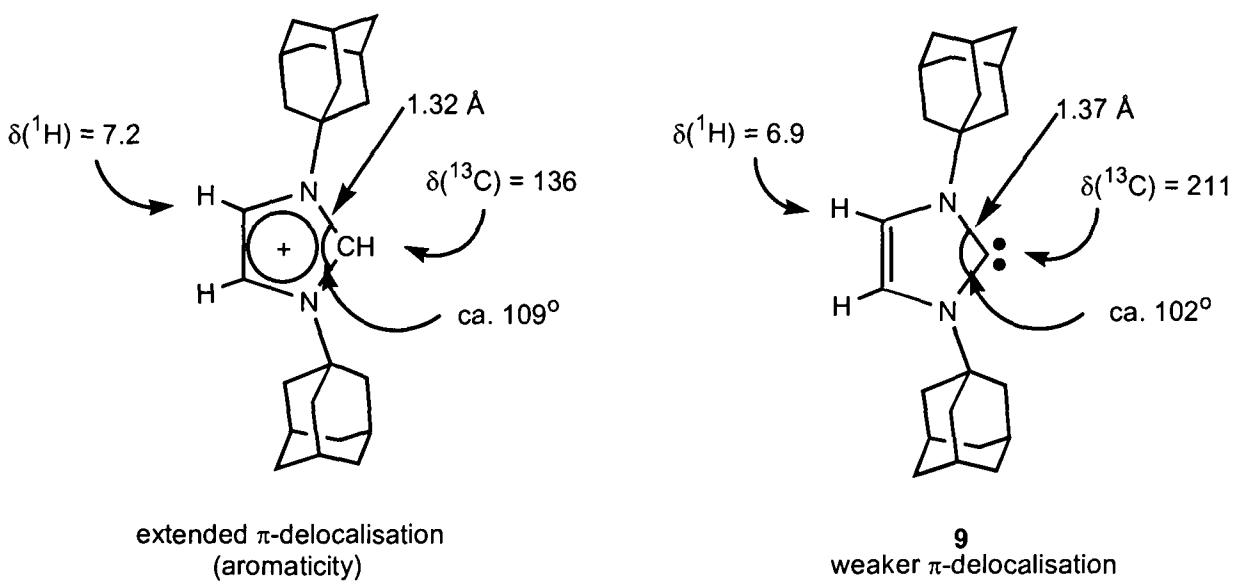

Figure 1.1 Geometric and spectroscopic parameters of the first isolated free carbene **9** and the corresponding imidazolium cation.

Since this development the common method to synthesise free N-heterocyclic carbenes established by Arduengo is deprotonation of the corresponding imidazolium salt using NaH with a catalytic amount of KO^{t}Bu in THF at ambient temperatures (Eq. 5).[6] Catalytic amounts of KO^{t}Bu or DMSO anion are necessary to obtain a reasonable rate of deprotonation because sodium hydride, and typically the imidazolium salt, are insoluble in THF. Alternatively a stoichiometric amount of KO^{t}Bu can be used (Eq. 6).[6] However, rather than hydrogen *tert*-butyl alcohol is generated, which can rapidly reprotonate the less stable free carbenes thus restricting the scope of this method.

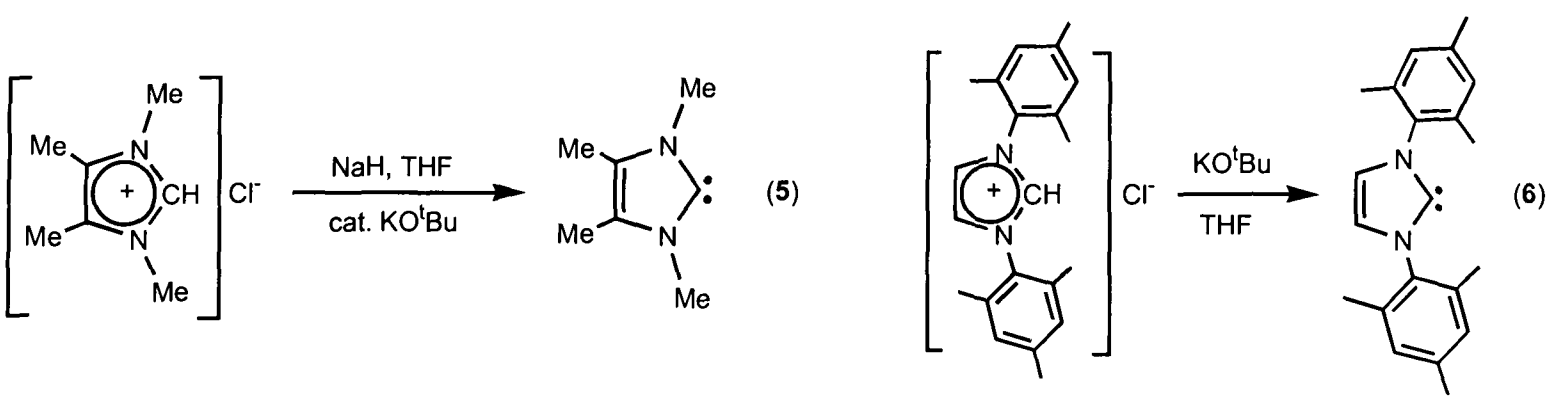

In 1993 Kuhn et al. discovered an alternative synthesis for 1,3-dialkylimidazol-2-ylidenes by condensing **10** with thioureas to give imidazole thiones which could be subsquently reduced with metallic potassium in THF (scheme 1.1).[7] The N-heterocyclic carbene products were obtained in good yields, although 24 hours refluxing in THF is required which excludes the preparation of thermally sensitive carbenes using this method.

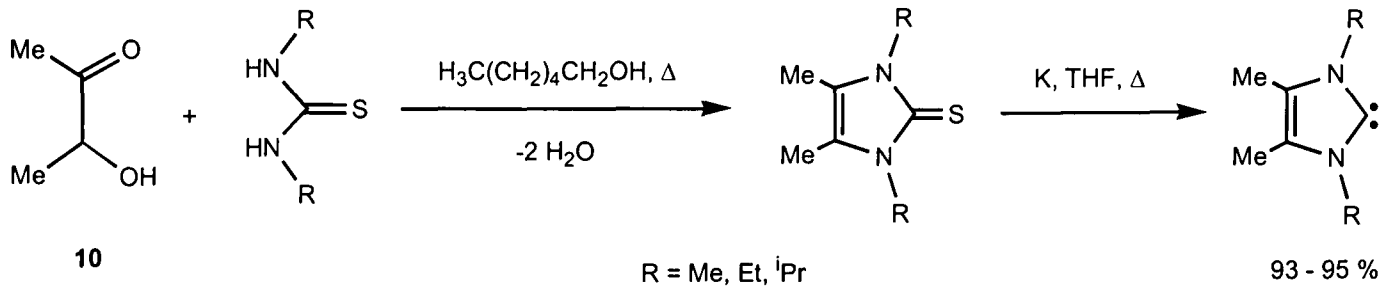

Scheme 1.1

In 1996 Herrmann and co-workers synthesised N-heterocyclic carbenes that were not previously accessible using liquid ammonia as the solvent.[8] The imidazolium salt is dissolved or suspended in a mixture (ca. 5 : 1) of liquid ammonia and THF and is then treated with sodium hydride. The deprotonation reaction occurs between -80 and -30 °C with the deprotonation reagent being either sodium hydride or sodium amide (formed by solvolysis). Liquid ammonia provides increased solubility for the deprotonation reagent and imidazolium salt at lower temperatures, allowing thermally sensitive carbenes to be synthesised. Temperatures can be kept below -30 °C throughout, with the reaction going to completion within minutes. Using this method the first free dicarbene **11** was synthesised, as well as carbenes with linear, branched, cyclic, heteroatom substituted (O, N, P) and chiral hydrocarbon residues (**12-17**) (figure 1.2):[8]

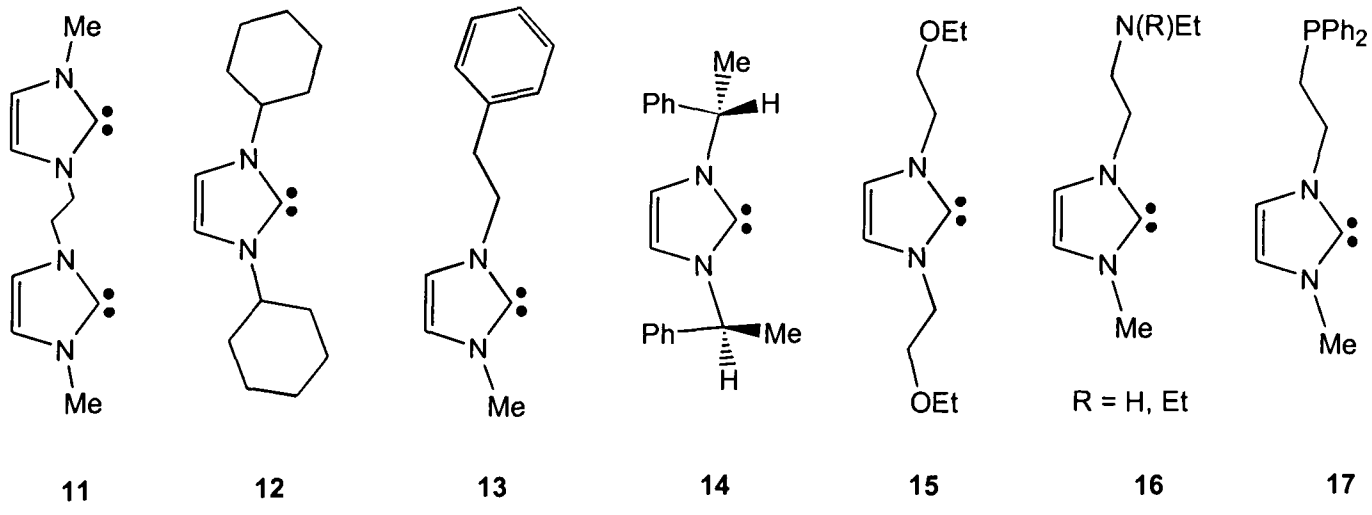

Figure 1.2 N-heterocyclic carbenes synthesised using liquid ammonia as the solvent.

1.2.2 Electronic Properties

The stability of 1,3-diadamantylimidazol-2-ylidene (**9**) was initially attributed to both steric and electronic factors[5,9], but the discovery of stable carbenes bearing less bulky substituents in the 1 and 3 positions such as 1,3-dimethylimidazol-2-ylidene[8] has since proved that thermodynamic stabilisation due to electronic effects is the essential feature.

Firstly, stability for the carbene electron pair may be gained from the σ-electron withdrawl effects on the carbene centre by the more electronegative nitrogens. Secondly, π-electron transfer occurs from the electron-rich π system of the heterocyclic ring into the *p* orbital of the carbene carbon atom that is perpendicular to the ring plane (figure 1.3).

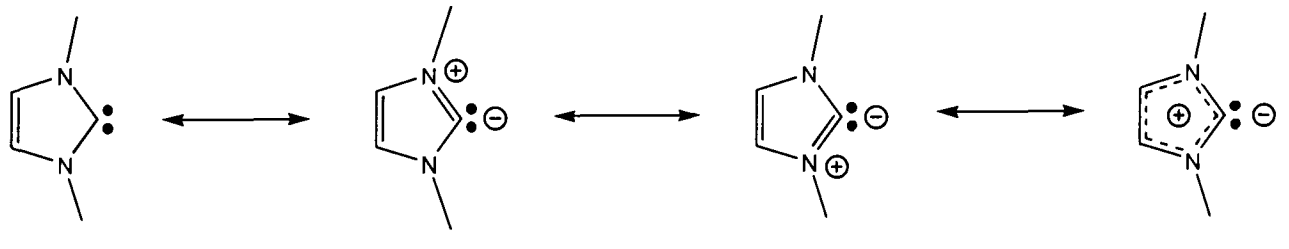

Figure 1.3 Resonance structures for π-electron transfer throughout the heterocyclic ring.

The imidazolium salt precursors to free N-heterocyclic carbenes are themselves electron-rich heteroaromatic compounds, with a ^{13}C NMR resonance within the range δ 135-138 for the N-C-N sp^2 carbon, and a ^{1}H NMR signal at δ 8.1-7.3 for the $H^4(H^5)$ ring protons (the heterocyclic ring atoms are numbered as shown in figure 1.4). In contrast, the corresponding N-heterocyclic carbene spectra show much lower field resonances for the N-C-N sp^2 carbon (δ = 210-220) and significantly higher field chemical shifts for the $H^4(H^5)$ protons (δ = 6.4-7.0). The data indicates a magnetic anisotropy difference for free carbenes consistent with a decrease in aromaticity, or 6 π-electron delocalisation.[10-12] Also, X-ray and neutron diffraction techniques showed that the carbenic (N^1-C^2-N^1) angles (102.2(2)° for **9**) are significantly smaller than the typical range known for imidazolium salts (108.6(2)-109.7(3)°), and that the $N^1(N^3)$-C^2 bonds (1.367(2) and 1.373(2) Å for **9**) are longer than in the corresponding imidazolium cations (1.328(4) and 1.331(3) Å for that of **9**).[5,13] Considering this together with the knowledge that the $N^1(N^3)$-$C^5(C^4)$ bonds are also slightly longer for free carbenes, it was concluded that π-delocalisation is less pronounced in N-heterocyclic carbenes than in imidazolium cations (figure 1.1).

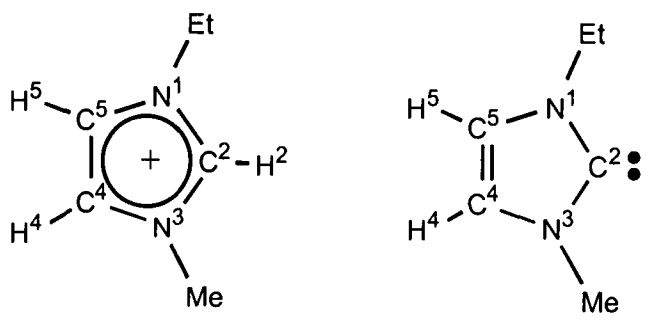

Figure 1.4 Ring atom numbering system commonly used for imidazolium salts and N-heterocyclic carbenes, exemplified by the 1-ethyl-3-methylimidazolium cation and 1-ethyl-3-methylimidazol-2-ylidene.

Despite this decrease in aromatic character upon deprotonation, the π-electron transfer into the carbene carbon *p* orbital leads to a significant moderation of the electrophilic reactivity normally associated with carbenes. Likewise, the inductive σ-electron withdrawl effect on the carbene centre serves to decrease the nucleophilic reactivity: The combination of these σ- and π- effects increases the energy gap between the singlet and triplet states, thus stabilising the singlet carbene over the more reactive triplet state. *Ab initio* MO calculations determined a singlet ground state for imidazolylidene.[14]

NB. The singlet-triplet energy gap is smaller for the less stable N-heterocyclic carbenes in which the C-C bond is saturated (the first of which was isolated by Arduengo et al. in 1995[15]), because the five-centre six-electron π-delocalisation (represented by the resonance structure on the far right of figure 1.3) cannot contribute to their stabilisation.

1.2.3 Reactivity

As opposed to triplet carbenes which show radical-like reactivity, singlet carbenes are expected to have nucleophilic and electrophilic reactivity due to the σ-donating lone pair and the vacant *p* orbital respectively. However, N-heterocyclic carbenes do not perform electrophilic reactions like insertions into C-H bonds or cycloadditions with nucleophilic olefins (e.g. hexene), and can be handled in typical donor solvents including THF, liquid ammonia and acetonitrile. N-heterocyclic carbenes are also stable with respect to dimerisation (nucleophilic perpendicular attack of one singlet carbene at the vacant out-of-plane *p* orbital of another singlet carbene).[16] This lack of electrophilic reactivity shows that

the LUMO lies rather high in energy as a result of the interaction of the vacant *p* orbital with the delocalised π system, and suggests that the term 'carbene' is misleading.

N-heterocyclic carbenes show nucleophilic reactivity and can act as Lewis bases. Reaction between **18** and **9** and the soft and weak Lewis acids iodine and iodopentafluorobenzene respectively form the adducts **19** and **20**, which have characteristic linear arrangements and positively charged imidazolium moieties of increased π-delocalisation (Eqs. 7, 8).[17,18]

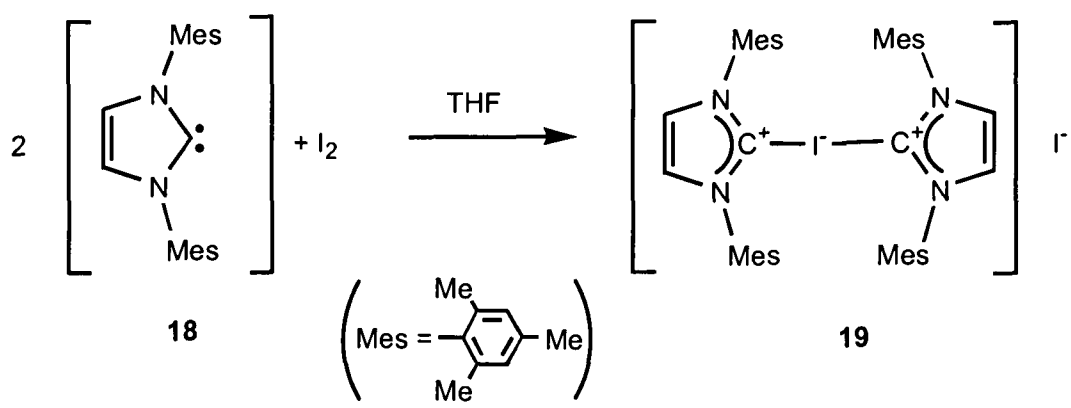

18 **19** (7)

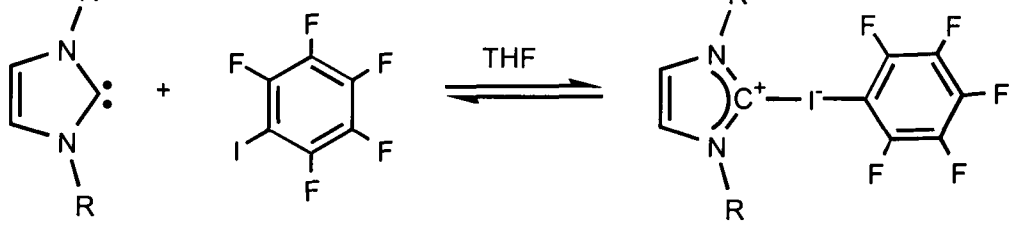

9 (R = adamantyl) **20** (8)

Complexation to a Lewis acid decreases the electron density at the carbene carbon and the mesomeric structures shown in figure 1.3 become more important. In this sense an imidazolium salt is an adduct of the corresponding free carbene and the Lewis acidic proton.

Adduct formation of N-heterocyclic carbenes with Lewis acids containing main group elements as the central atom is widespread, as exemplified by complexation of carbenes **21a-f** to diethylmagnesium, borane, boron trifluoride, aluminium hydride, silicon tetrachloride and germanium diiodide. Adducts **22a-f** are formed in high yields (figure 1.5).[19-23]

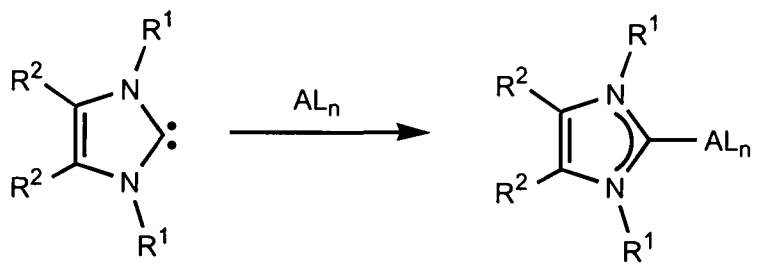

21a - f **22a - f**

22	R^1	R^2	AL_n
a	adamantyl	H	$MgEt_2$
b	Me	Me	BH_3
c	Me	Me	BF_3
d	Mes	H	AlH_3
e	^{i}Pr	Me	$SiCl_4$
f	Mes	H	GeI_2

Figure 1.5 Lewis acid-base adducts of N-heterocyclic carbenes with main group elements.

Traditionally the literature has dealt with the reactivity of transition metal carbene complexes by discriminating between electrophilic (Fischer) and nucleophilic (Schrock) carbenes (figure 1.6).[24] In these complexes the $:CR^1R^2$ carbene ligands exhibit both σ-donor and π-acceptor properties resulting in a metal-carbon 'double bond' (in all cases the metal-carbon bonds are shorter than single bonds in metal-alkyl complexes). The σ-donation is rather weak, and bonding to metals depends on pronounced π-backbonding.

Fischer Schrock

Figure 1.6 Examples of Fischer- (electrophilic) and Schrock-type (nucleophilic) carbene complexes.

Such conventional carbene complexes are very reactive and often react with cleavage of the metal-carbon bond: Cyclopropanation and olefin metathesis are important examples where the carbene ligand is transferred to other substances.[25]

N-heterocyclic carbene complexes cannot be classified into either the Fischer- or Schrock-type system, because the negligible π-acceptor and strong σ-donor properties of the ligand (in total contrast to conventional carbenes) lead to a moderated reactivity of the M-C bond. Comparison of the CO stretching frequencies of $[Fe(CO)_4L]$ shows that the ratio of σ-donors to π-acceptors (electron density induced at the metal centre) increases with ligand L in the order $:C(OR)R < :C(NR_2)R < :C(NR_2)_2$ < N-heterocyclic carbenes.[26] A similar study of $[MoL_3(CO)_3]$ CO stretching frequencies shows that the π-acceptor character decreases in the order NO > CO > RNC > PF_3 > $P(OR)_3$ > $P(aryl)_3$ > $P(alkyl)_3$ > RCN > N-heterocyclic carbenes > pyridine:[26,27] N-heterocyclic carbene transition metal adducts very much resemble adducts of electron-rich alkylphosphines and of N donors such as nitriles and pyridine, and structurally characterised complexes show long metal-carbon bonds in contrast with Fischer- and Schrock-type carbenes, suggesting a bond order of one. N-heterocyclic carbenes are simply strongly σ-donating Lewis bases. Therefore in contrast with Fischer and Schrock carbene complexes, N-heterocyclic carbene-transition metal bonds do not react with nucleophiles such as amines or alkyl lithium salts, and will not add to unsaturated nucleophiles such as allenes, acetylenes, arenes or olefins.

1.2.4 Transition Metal Complexes

Complexes of N-heterocyclic carbenes are known for almost all of the transition metals, and in many cases for more than one oxidation state of the particular metal. In contrast to Fischer- and Schrock-type complexes, thermodynamic stability does not rely on pπ-dπ back-donation of electron density from the metal. This allows the preparation of N-heterocyclic carbene complexes of electron-deficient metals with high formal oxidation states (figure 1.7),[28,29] as well as complexes with more electron-rich metal centres (figure 1.8).[30-33] The existence of the low-coordinate 14-electron Ni(0) and Pt(0) complexes (figure 1.9) is attributed to kinetic stabilisation with bulky R-groups, and an increase in the usually negligible pπ-dπ back-donation.[34]

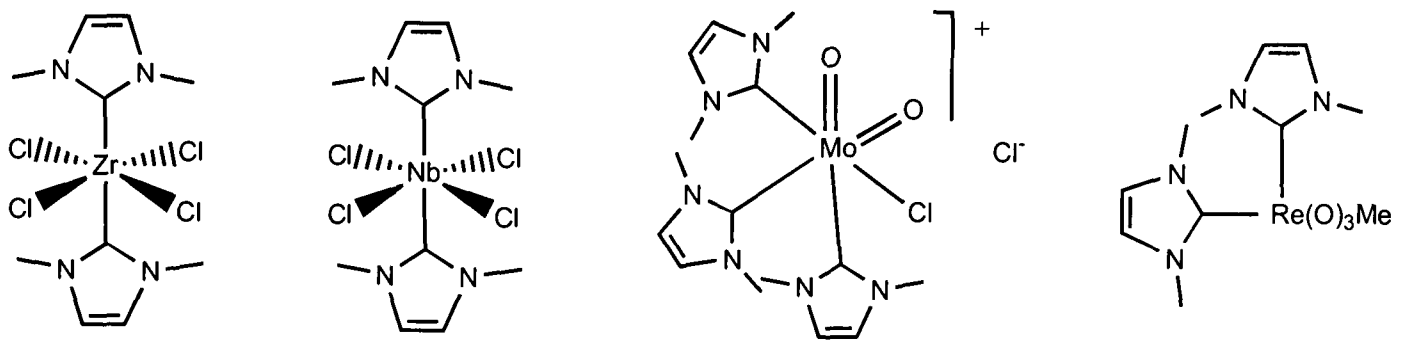

Figure 1.7 Examples of high oxidation state transition metal (Zr^{IV}, Nb^{IV}, Mo^{VI} and Re^{VII}) carbene complexes.

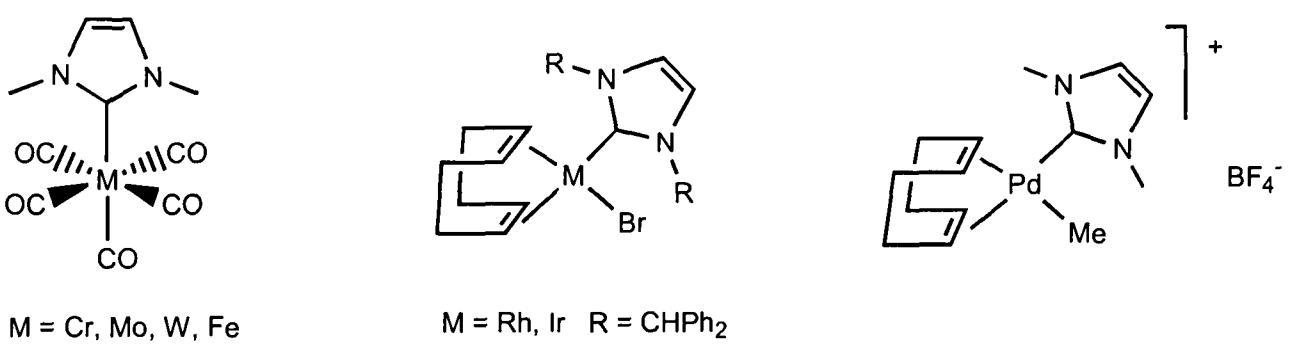

Figure 1.8 Examples of lower oxidation state transition metal (Cr^0, Mo^0, W^0, Fe^0, Rh^I, Ir^I and Pd^{II}) carbene complexes.

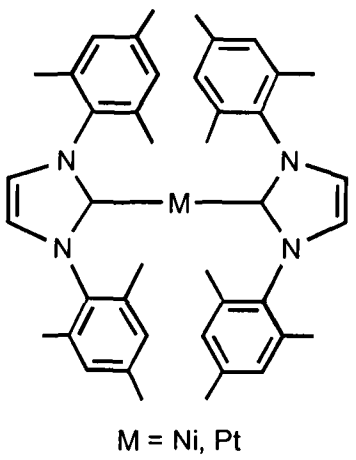

Figure 1.9 Electron-rich Ni^0 and Pt^0 carbene complexes.

The vast majority of transition metal N-heterocyclic carbene complexes have been synthesised using one of two routes. This is exemplified by the formation of nickel(II) carbene dihalides from nickel(II) precursors (a) by reaction with free carbenes or (b) by *in situ* deprotonation of the corresponding imidazolium salts (scheme 1.2).[35]

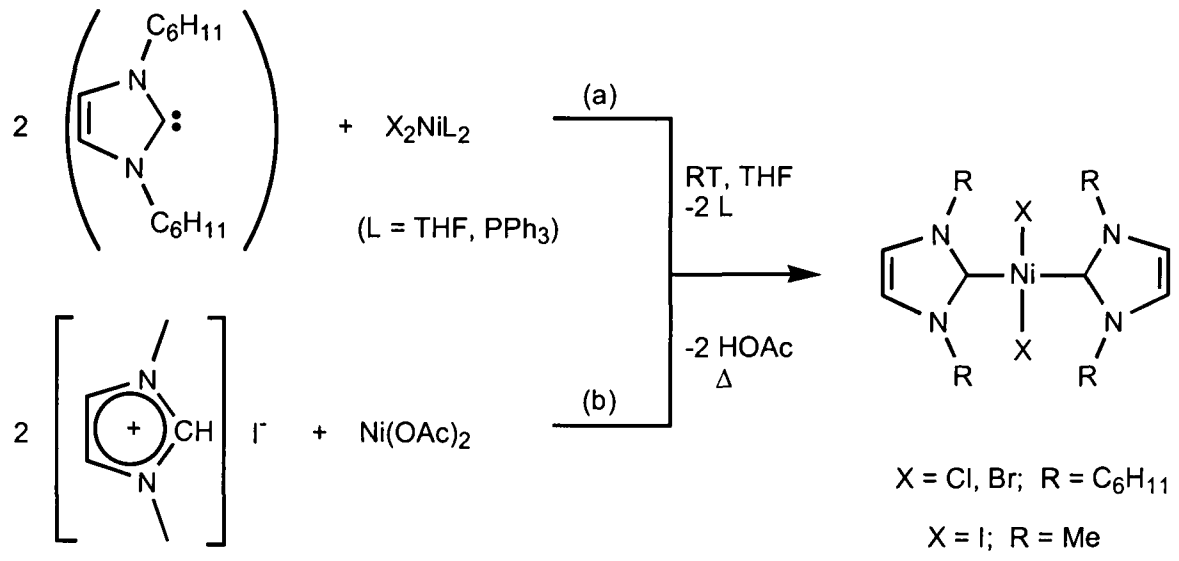

Scheme 1.2 Formation of Ni^{II} carbene dihalide complexes by *in situ* deprotonation of the imidazolium salt or by the free carbene route.

The imidazolium salt route has the advantage that, in comparison to free carbenes, a much wider variety of imidazolium salt precursors are available due to their thermal- and air-stability and ease of synthesis. However, it is necessary to have a basic ligand such as acetate, alkoxide or hydride in the precursor to effect deprotonation of the imidazolium salt, which restricts the range of precursors available. The types of complexes formed by this route are also limited, because of the need to accommodate the anion of the imidazolium salt either inside or out of the coordination sphere of the resulting carbene complex.

In contrast, free N-heterocyclic carbenes react as two-electron donors with a broad variety of precursors. Free carbenes may replace other ligands in the precursor complex such as CO, THF, PR_3, MeCN and halides: A molecule of carbon monoxide is displaced from carbonyl complexes $[M(CO)_6]$ (M = Cr, Mo, W) to form the compounds shown in figure 1.8,[33] and other two-electron donors are displaced by free carbenes from the adducts $[(Me_2S)MCl]$ (M = Cu, Ag, Au), $[MCl_4(THF)_2]$ (M = Ti, Zr, Hf), $[MCl_4(Py)_2]$ (M = Nb, Ta), and $[VCl_2(tmeda)_2]$.[29,36] As well as performing substitution reactions, free carbenes also form straight adducts with coordinatively unsaturated complexes,[29] and split bridging moieties of dinuclear precursor complexes to form mononuclear carbene complexes in excellent yields (scheme 1.3).[37]

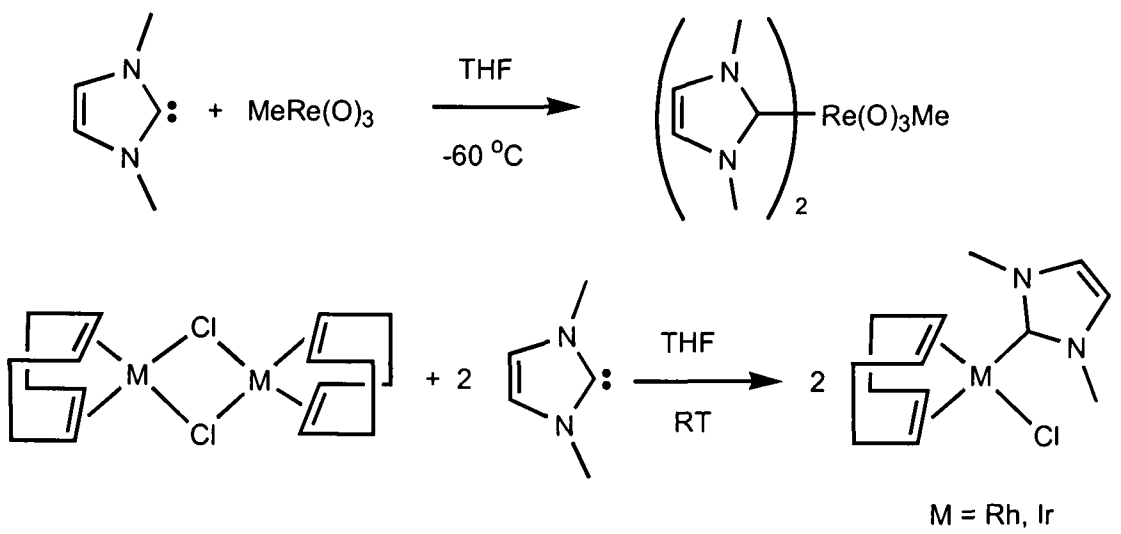

Scheme 1.3 Additions of free carbenes to transition metal precursors.

The observation of this simple reactivity of free carbenes as σ-donating Lewis bases, with the ability to coordinate to a wide variety of transition metals in a wide variety of oxidation states, has led to the analogy with the ubiquitous phosphines which are important as ligands in organometallic catalytic reactions.

1.2.5 Transition Metal Complexes of Chelating Carbene Ligands

The first chelating N-heterocyclic carbene complex **23** was synthesised in 1980 with the *in situ* formation of a macrocyclic di-N-heterocyclic carbene ligand (abbreviated as L_2^{cyclam}) by insertion of a Rh atom into the corresponding electron-rich olefin (Eq. 9). On bubbling CO through a dichloromethane solution of **23** for 15 minutes at room temperature the COD ligand of the anion is replaced by two molecules of CO to form the orange-yellow compound $[Rh(L_2^{cyclam})(COD)][Rh(CO)_2Cl_2]$-*cis* which was structurally characterised.[38]

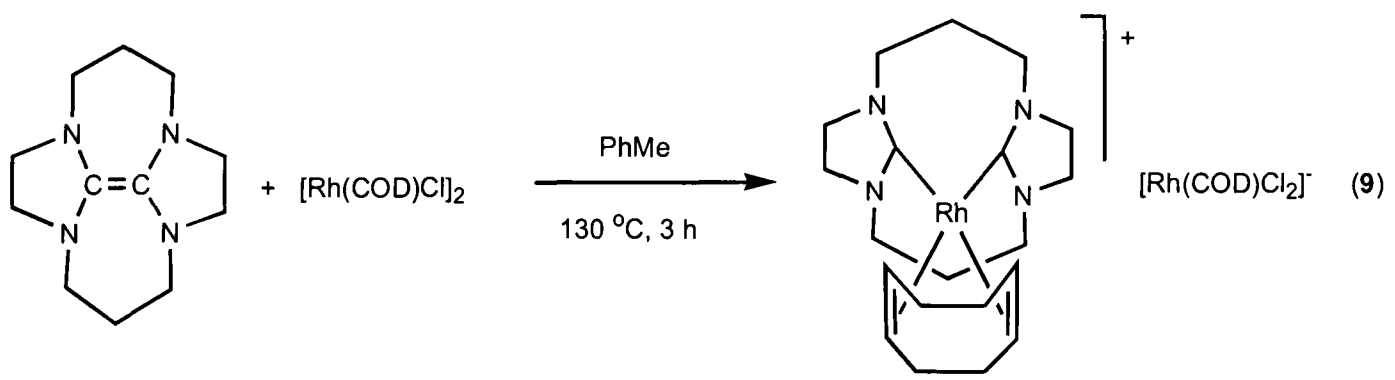

In 1993 Öfele et al. synthesised the first examples of chelating carbene transition metal complexes derived from imidazolium salt precursors, which were deprotonated *in situ* using NaH / KO^{t}Bu in the presence of $M(CO)_6$ (M = Cr, Mo, W). Two CO ligands are

displaced by the resulting bidentate carbene ligand to form the carbene complexes **24** in 10 % yield (Eq. 10).[33]

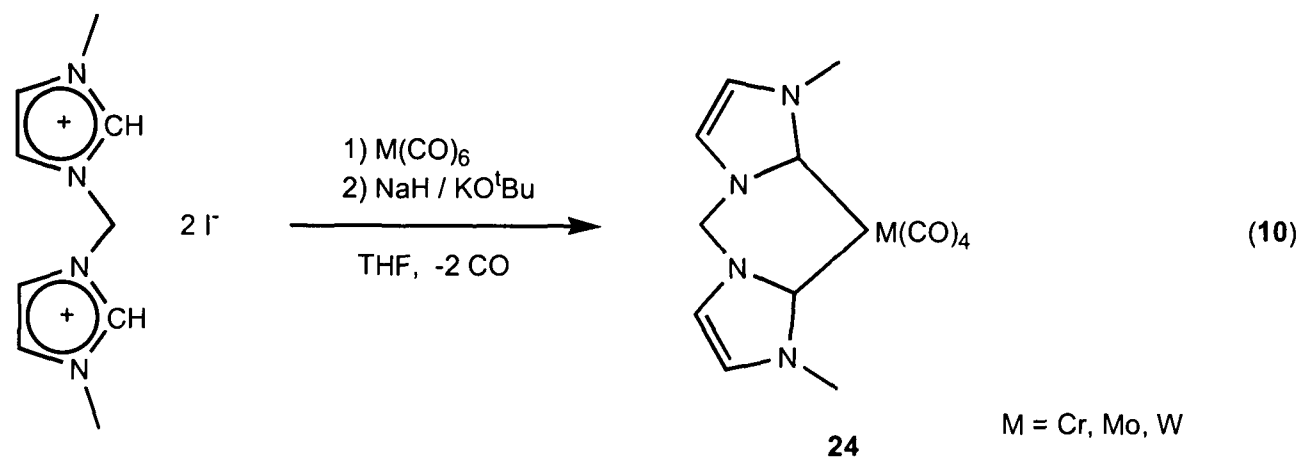

(10)

In 1995 variable temperature NMR spectroscopy showed a dynamic behaviour for the chelating carbene ligand in complexes **24**. The ^{1}H NMR signal for the methylene bridge protons is a singlet (δ 6.11) at room temperature, which broadens and collapses on cooling to -40 °C, and reappears as two doublets (δ 6.45 and 5.89) at -60 °C. The interconversion of H_{exo} and H_{endo} on the NMR timescale implies a 'butterfly type' conformational movement of the ligand through a planar intermediate (figure 1.10).[39]

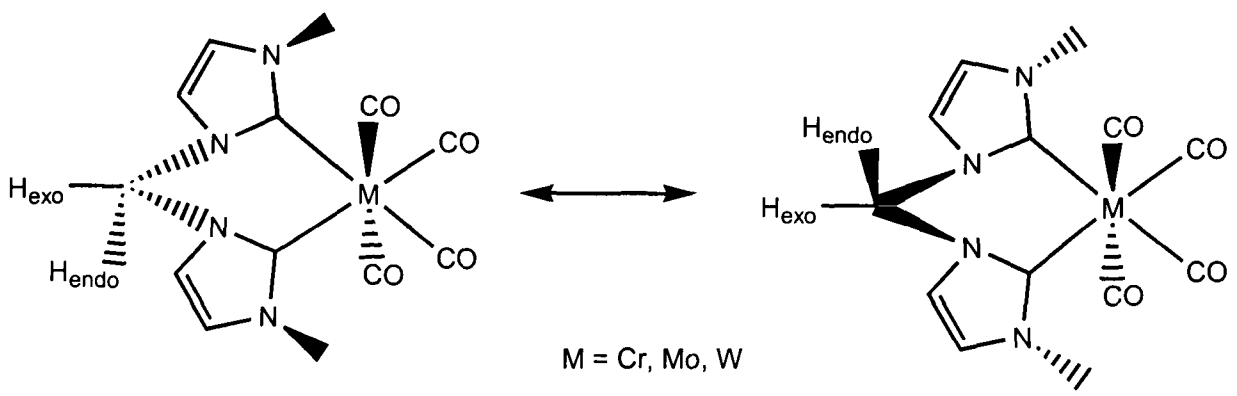

Figure 1.10 Interconversion of the magnetically inequivalent H_{exo} and H_{endo} is caused by a 'butterfly type' conformational movement of the ligand.

Homoleptic *bis*(dicarbene) palladium(II) dicationic complexes **25** were synthesised in 1995 by Fehlhammer et al. (Eq. 11), and the BF_4^- salt structurally characterised. The X-ray structure showed the two six-membered metallocycles adopting boat-like conformations, strongly bending out of the PdC_4 coordination plane in opposite directions. Furthermore, the heterocyclic rings are seen to deviate from this coordination plane by +42 and -43°. The C-Pd-C bite angle of 81.8(2)° shows the degree of distortion from true square planar (90°) geometry. The room temperature ^{1}H NMR spectra showed two doublets at δ 6.75 and 6.48

for the methylene bridge protons H_{exo} and H_{endo}, and ^1H NMR spectra at temperatures up to 410 K showed this magnetic inequivalence on the NMR timescale to be preserved: In contrast with complexes **24** the structure is rigid with respect to equilibration of the methylene bridge protons, probably due to steric congestion that would be present in the putative planar intermediate.[40]

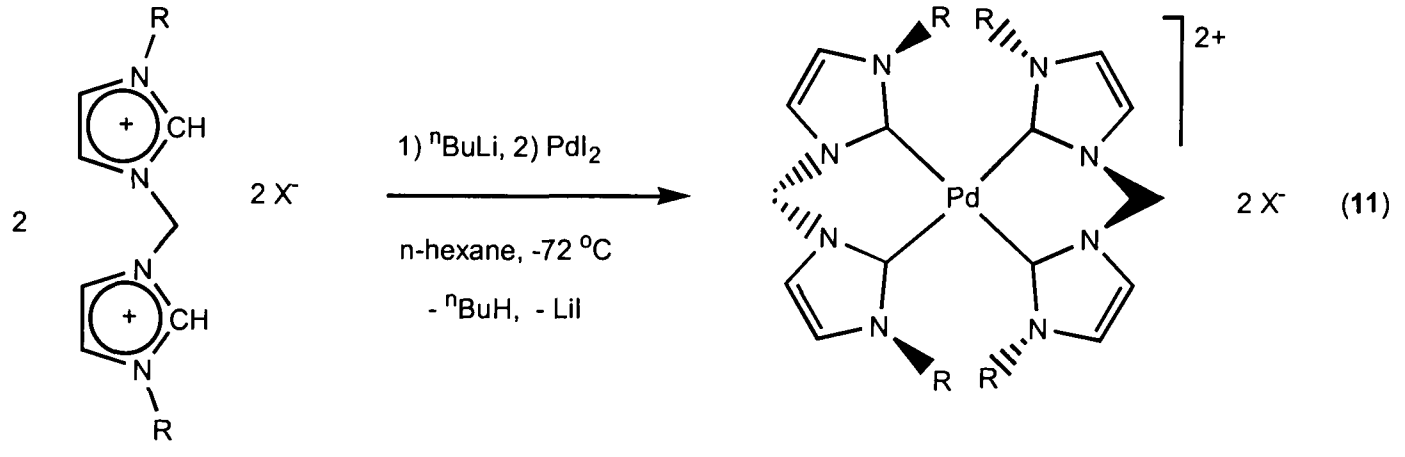

A novel tridentate tris(methylimidazolyl)borate ligand and its hexacarbene iron(III) complex **26** were synthesised, and the latter structurally characterised, by Fehlhammer et al. in 1996.[41] The ligand was deprotonated *in situ* using 3 equivalents of ^{n}BuLi in hexane (-78 °C) before anhydrous $FeCl_2$ was added. The solid was isolated after 24 h at room temperature, dissolved in methanol, and the product **26** precipitated on addition of a saturated solution of $NaBPh_4$ in methanol (Eq. 12). It is unclear how the oxidation to Fe(III) occurred, to form this extremely stable 17-electron species.

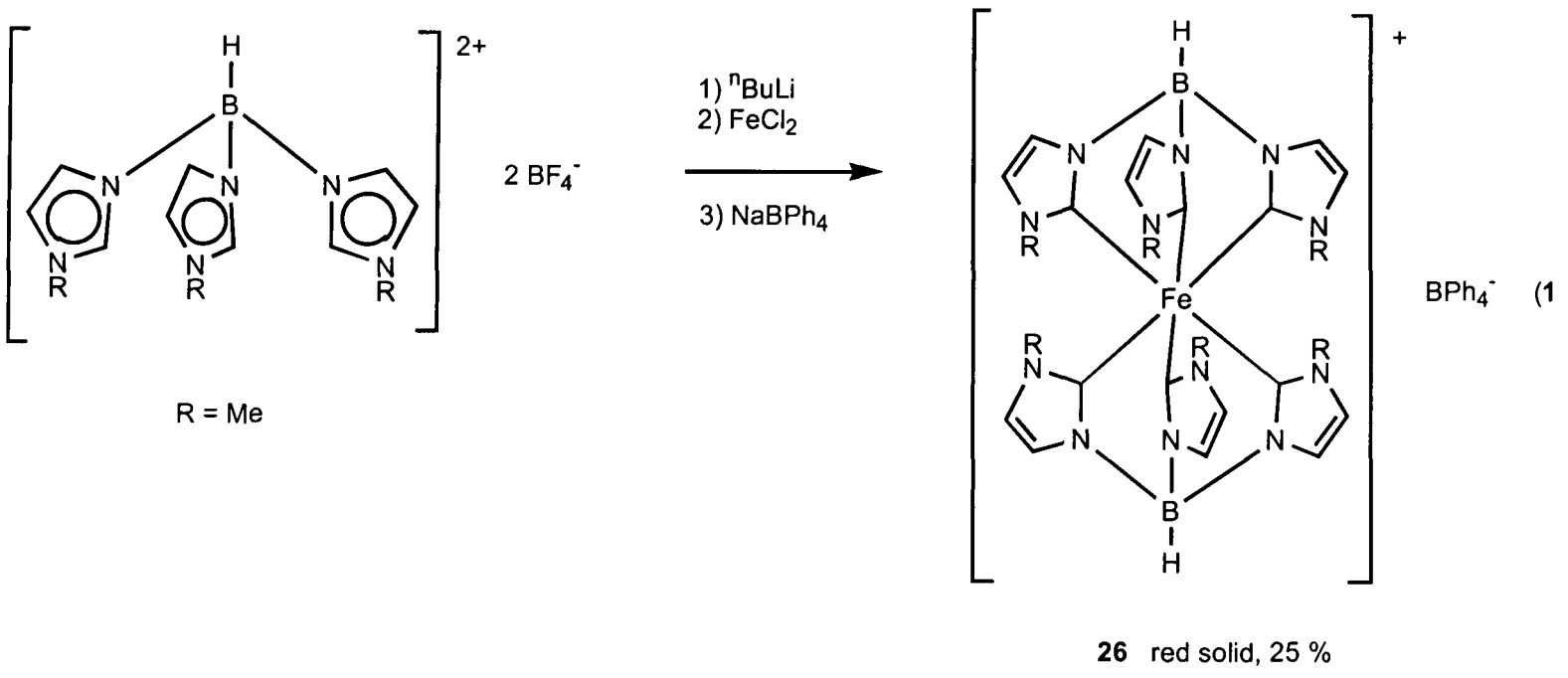

From 1998 to 1999 Herrmann et al. developed the high yield synthesis and investigated the reactivity of chelating dicarbene palladium(II) dihalide complexes **27a-c** (scheme 1.4).[42,43] Complex **27a** was structurally characterised and, as observed for the homoleptic complex **25**, the six-membered palladacycle is fixed in a boat conformation with the two heterocyclic rings deviating from the coordination plane (in this case by +51.3(3) and - 52.5(3)°). The C-Pd-C bite angle of 83.2(3)° shows that the degree of distortion from true square planar (90°) geometry is only slightly less than for the more sterically crowded *bis*(dicarbene) complex **25** (81.8(2)°). Compared to **25**, which has Pd-C distances of 2.137(5) and 2.049(4) Å, the Pd-C bonds are shortened to 1.989 and 1.988 Å due to the weaker *trans* influence of the iodide ligands. The ^{1}H NMR spectrum shows a singlet (δ 6.28) for the methylene bridge protons, implying that the same 'butterfly type' conformational movement of the dicarbene ligand (planar intermediate) is causing the interconversion of H_{exo} and H_{endo} on the NMR timescale, as observed for complexes **24**.

Herrmann used the imidazolium salt route to synthesise complexes **27a-c**, with $Pd(OAc)_2$ as the metal precursor. DMSO was chosen as the solvent because of the high solubility of the reactants, and because of the higher boiling point than the acetic acid by-product. This ensured that after removing the solvent under reduced pressure there was no residual acetic acid to cause product decomposition. The complexes were purified by Soxhlet extraction with acetonitrile, and were found to be soluble in DMSO and hot acetonitrile, sparingly soluble in dichloromethane and THF, and insoluble in diethyl ether and hydrocarbon solvents.

The dihalide complexes were then treated with an equivalent of KPF_6 or two equivalents of $NaPF_6$ or $AgBF_4$, in the presence of acetonitrile, to generate the cationic complex **28** and the dicationic complexes **29a** and **29b** respectively, in which one or two halide ligands are replaced by acetonitrile (scheme 1.4). These cationic complexes were found to be soluble and stable in methanol (as well DMSO, acetonitrile and nitromethane).

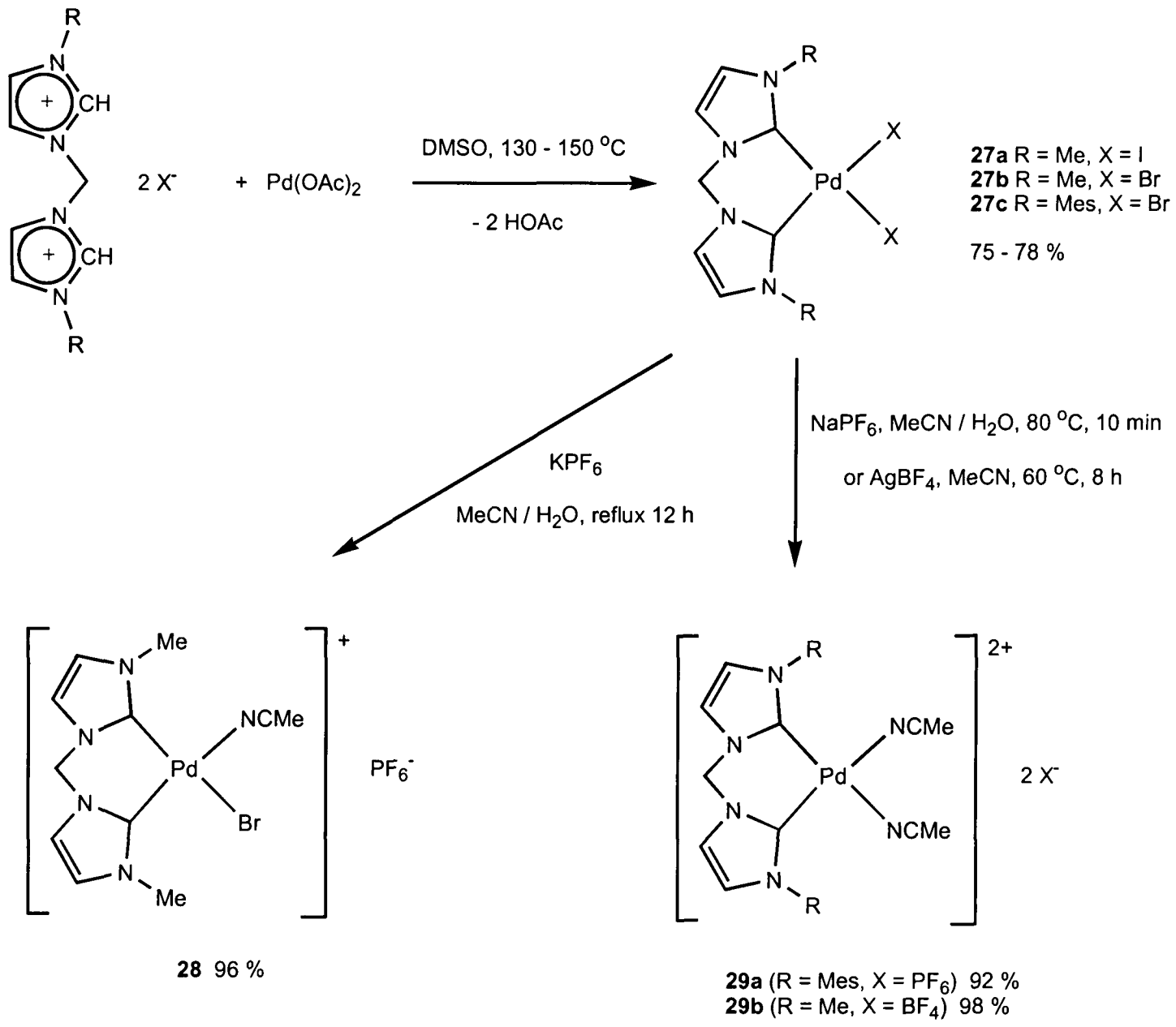

Scheme 1.4 Synthesis and reactivity of chelating dicarbene palladium (II) dihalide complexes.

Herrmann also synthesised homoleptic *bis*(dicarbene) palladium(II) dicationic complexes **31a** and **31b** using the dihalide complexes **27a** and **27b** via two routes, one of which involves the synthesis of the dicarbene palladium(II) diacetate complex **30** (scheme 1.5).[44] The yields using these imidazolium salt routes are considerably greater than for Fehlhammer's synthesis of **25** by generation of the free carbene *in situ*. Herrmann's routes also allow for the synthesis of complexes like **31b** which contain two different chelating dicarbene ligands.

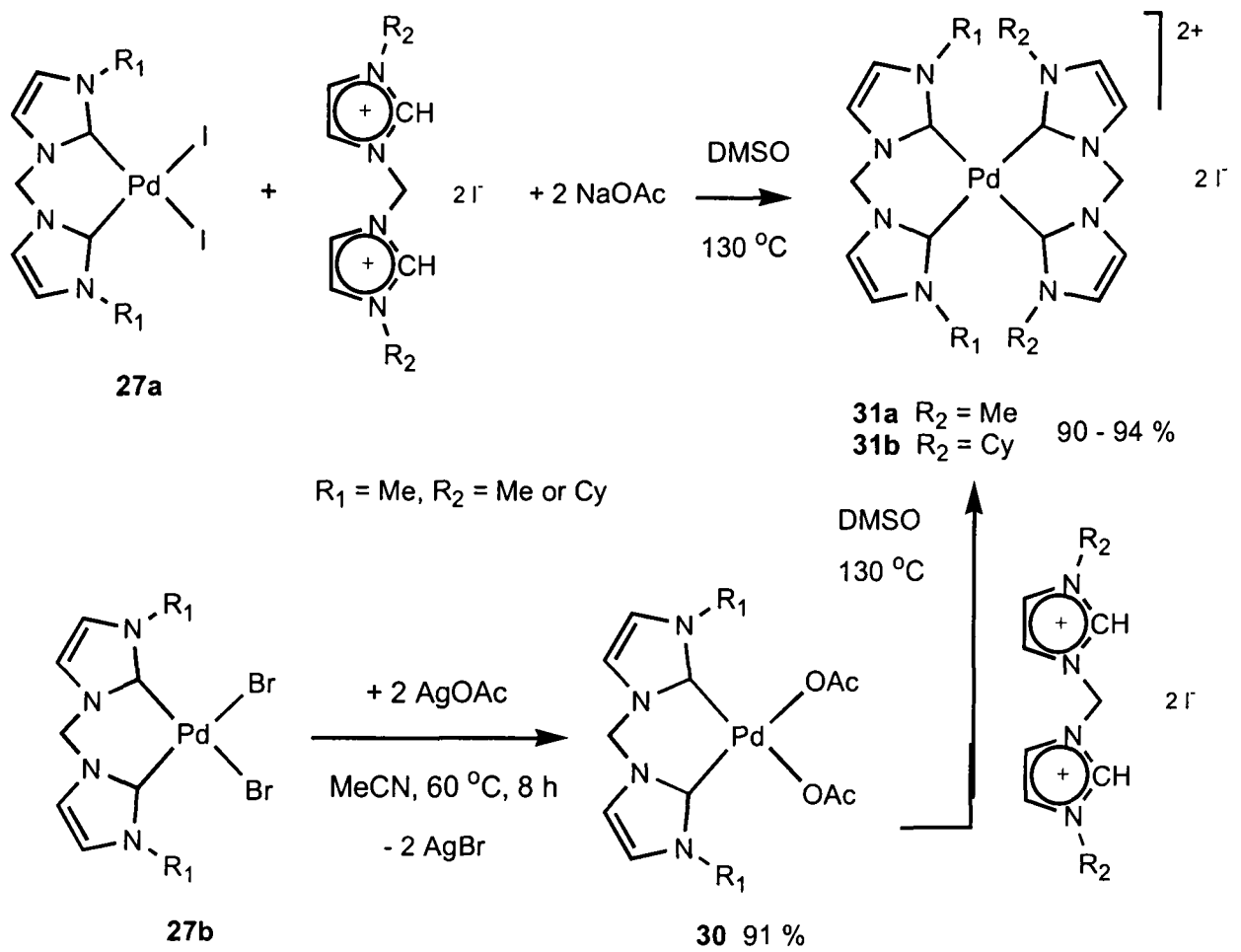

Scheme 1.5 Synthesis of homoleptic *bis*(dicarbene) palladium(II) dications.

Homoleptic *bis*(dicarbene) nickel(II) dicationic complexes **32** were synthesised by Herrmann and co-workers in good yields by treating the corresponding diimidazolium diiodide salts with an equivalent of anhydrous $Ni(OAc)_2$ (Eq. 13).[44] DMSO was the solvent of choice, and on work-up is removed under reduced pressure with the acetic acid by-product. The yellow residue is washed with methanol to give a crude product. Recrystallisation from DMSO / methanol affords yellow crystals of the particular complex. The X-ray structure of complex **32** with dicarbene N-substituent R = Me showed the two six-membered metallocycles to adopt a *trans* double-boat conformation similar to the palladium analogue **25**. The Ni-C bond distances are 1.909(2) Å, and the C-Ni-C bite angle of 86.64(9)° shows a smaller distortion from square planar geometry than observed for the palladium analogue **25** (C-Pd-C = 81.8(2)°). Furthermore, the heterocyclic rings deviate from the NiC_4 coordination plane (+39.64(9) and -40.85(8)°) to a lesser extent than for the palladium analogue **25** (+42 and -43 °).

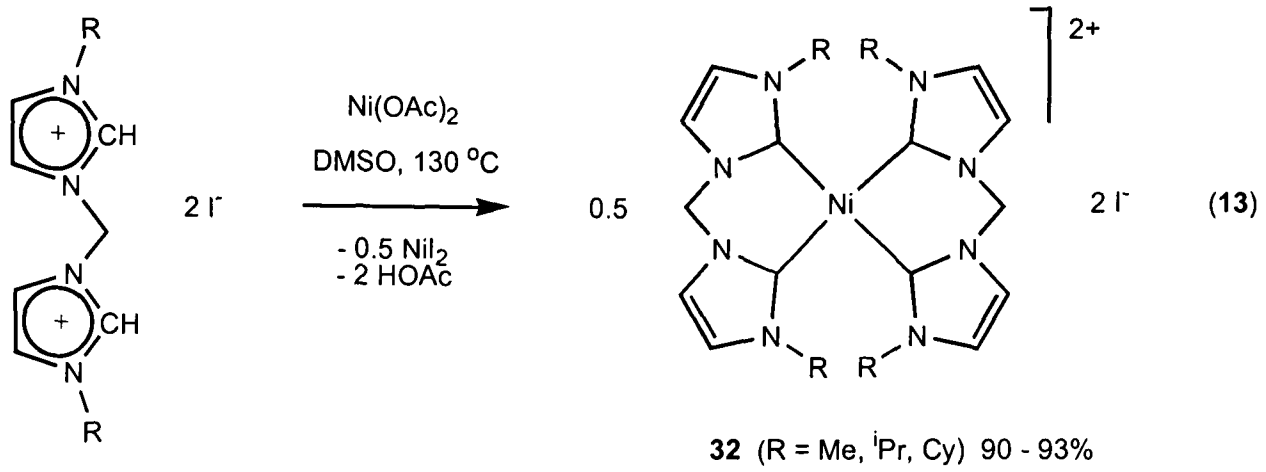

32 (R = Me, ^{i}Pr, Cy) 90 - 93% **(13)**

Both the palladium and the nickel homoleptic *bis*(dicarbene) dicationic complexes were found to be air and water stable and thermally robust in the solid state at temperatures up to 225 °C. The dications are soluble in DMSO and methanol but insoluble in other common organic solvents. As with **25**, ^{1}H NMR spectra of all the palladium and nickel dications showed two doublets (δ 6-7) for the methylene bridge protons, and spectra at 150 °C showed their magnetic inequivalence on the NMR timescale to be preserved: In contrast with complexes **24** and the *cis*-dihalide palladium(II) complexes **27a-c** the structures are rigid with respect to equilibration of the methylene bridge protons.

Two of Herrmann's observations were of particular significance as far as this thesis is concerned: Firstly, it was found that using diimidazolium salts with bulkier N-substituents such as isopropyl and cyclohexyl did not prevent exclusive formation of the homoleptic *bis*(dicarbene) nickel(II) dications, i.e. *formation of the neutral* cis-*dihalide nickel(II) complexes analogous to the palladium compounds* ***27*** *was never observed*. Secondly, no reaction at all occurred between $Ni(OAc)_2$ and the *N*-^{t}Bu-substituted diimidazolium salt analogue (i.e. the precursor to the $^{tBu}CC^{meth}$ free carbene ligand used in this thesis): In the *tert*-butyl case neither the neutral *cis*-dihalide nor the homoleptic *bis*(dicarbene) dicationic nickel(II) complexes could be synthesised using this route.

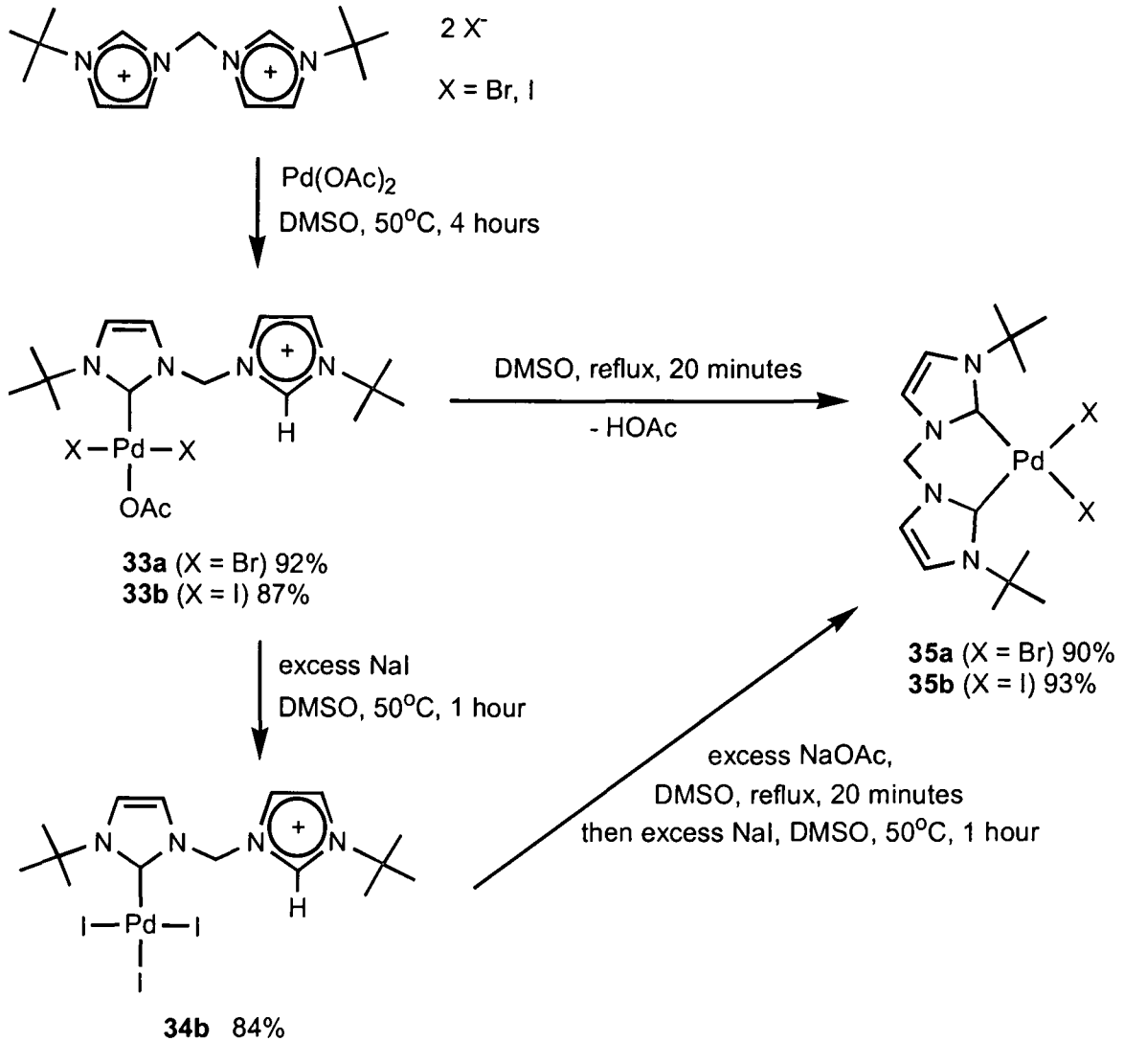

Scheme 1.6 Synthesis of Pd^{II} dihalide complexes of the *N-tert*-butyl substituted dicarbene ligand $^{tBu}CC^{meth}$, and isolation of the monocarbene intermediates.

Most recently Herrmann et al. synthesised the palladium(II) *cis*-dihalide complexes **35a** and **35b** (scheme 1.6), which incorporate the methylene bridged dicarbene ligand $^{tBu}CC^{meth}$ used in this thesis ($^{R}CC^{meth}$ and $^{R}CC^{eth}$ henceforth denote di-N-heterocyclic carbene ligands with N-substituents R, and methylene and ethylene N,N' linkages respectively).[45] The diiodide complex **35b** was structurally characterised, and the structure compared to that of **27a** which contains the less bulky methyl substituted dicarbene ligand: No significant increased angular distortions in the geometry about the palladium centre due to the sterically more demanding *N-tert*-butyl substituents were noted (C-Pd-C bite angle = 83.3(2)°). However, the heterocyclic rings deviate from the NiC_4 coordination plane (±62.6(2)°) to a greater extent than for the *N*-methyl substituted analogue **27a** (+51.3(3) and -52.5(3)°), and the Pd-C bonds are slightly longer (2.004(3) Å for **35b** versus 1.989(8) and 1.988(7) Å for **27a**). Furthermore, the ^{1}H NMR spectra of **35a** and **35b** showed two doublets (δ 6.60, 6.20 (**35a**) and δ 6.60, 6.30 (**35b**)) for the magnetically inequivalent methylene bridge protons: In contrast with complex **27a** the structure is rigid with respect

to equilibration of the methylene bridge protons, due to the increased steric congestion (caused by the *tert*-butyl ligand substituents) that would be present in the putative planar intermediate.

By heating a DMSO solution of the diimidazolium salt and one equivalent of palladium acetate for 4 hours at 50 °C, Herrmann and co-workers were able to synthesise the intermediate acetato-monocarbene dihalide complexes **33a** and **33b**. The X-ray crystal structure of complex **33b** showed a hydrogen bond between the acidic NC(H)N proton of the pendant imidazolium ring and the noncoordinated oxygen centre of the acetate anion. The monocarbene triiodide complex **34b**, prepared by reaction of **33b** with an excess of NaI was also structurally characterised. Refluxing **33a** or **33b** in DMSO for 20 minutes caused deprotonation and complexation of the pendant imidazolium ring to give acetic acid and the dicarbene dihalide complex **35a** or **35b** (scheme 1.6).

Using the same method Herrmann et al. prepared a large range of complexes analogous to **35**, featuring dicarbene ligands with primary, secondary and tertiary *N*-alkyl substituents as well as *N*-aryl substituents.[45] Although the intermediate monocarbene complexes analogous to **33** were not isolated or observed by ^{1}H NMR it was postulated that the reactions proceeded in the same manner. Herrmann et al. could not, however, prepare analogues to **35** using N,N' linkages between the heterocyclic rings other than methylene: Ethylene- and propylene-bridged diimidazolium salts led to decomposition products on reaction with $Pd(OAc)_2$. Herrmann proposed that monocarbene intermediates are formed, but that the lengthened N,N' linkage disfavours hydrogen bonding between the acidic NC(H)N proton of the pendant imidazolium ring and the noncoordinated oxygen centre of the acetate anion (as observed for **33b**). This could then favour deprotonation at an alternative position of the pendant arm at the elevated reaction temperature (50 °C) leading to unidentified decomposition products.

Furthermore, Herrmann et al. postulated that intermediate species such as **36** have prevented the preparation of chelating dicarbene nickel(II) *cis*-dihalide complexes via the imidazolium salt route: Reaction of the diimidazolium diiodide salts with an equivalent of anhydrous $Ni(OAc)_2$ leads to the homoleptic *bis*(dicarbene) nickel(II) dicationic complexes **32** (see above). This could be explained by initial formation of the intermediate **36** (figure

1.11), followed by deprotonation of the pendant imidazolium rings in the presence of acetate anions to yield the observed dicationic complexes **32**.

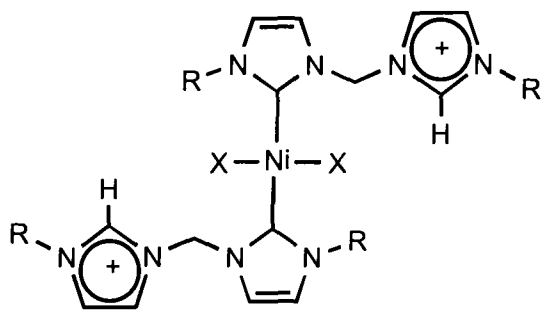

36 (X = OAc or I)

Figure 1.11 Proposed intermediate in the synthesis of the homoleptic *bis*(dicarbene) nickel(II) dicationic complexes **32**.

1.2.6 Homogeneous Catalysis

(a) Hydrosilylation of Alkenes, Alkynes and Ketones

The first investigation of the catalytic properties of N-heterocyclic carbene complexes was reported in 1977, when rhodium(I) complexes containing a C-C saturated N-heterocyclic carbene ligand were found to be active catalysts for the hydrosilylation of terminal alkenes, alkynes and ketones.[46-48] Complexes including **37** and **38** (figure 1.12) led to selective anti-Markovnikov addition of silanes to terminal alkenes as had previously been observed using many rhodium phosphine compounds such as Wilkinson's compound, $RhCl(PPh_3)_3$, and $[RhCl(CO)(PPh_3)_2]$. Yields of up to 98% were obtained, depending on the silane and the rhodium-carbene catalyst (Eq. 14).

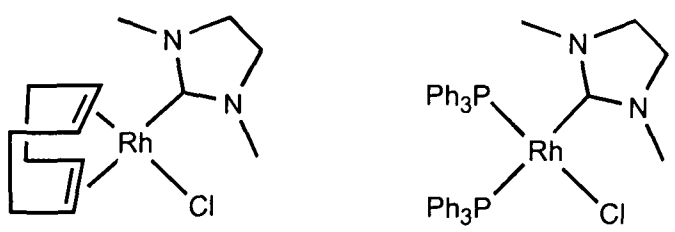

37 **38**

Figure 1.12 Examples of rhodium(I) hydrosilylation catalysts incorporating N-heterocyclic carbene ligands.

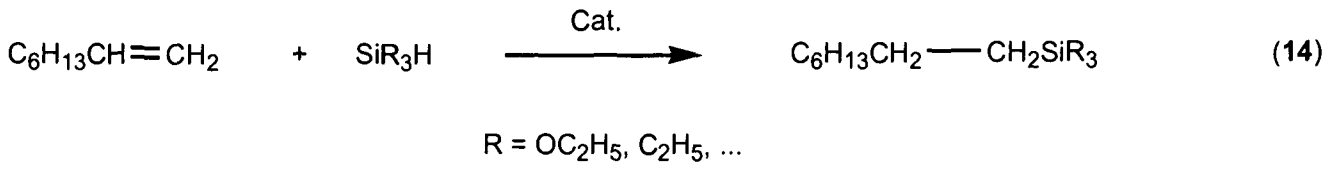

(14)

Complexes **37** and **38** also catalysed the hydrosilylation of alkynes, giving mixtures of *cis* and *trans* alkenes, and further heating in the presence of both the silane reactant and the catalyst caused complete *cis* to *trans* isomerisation (Eq. 15).

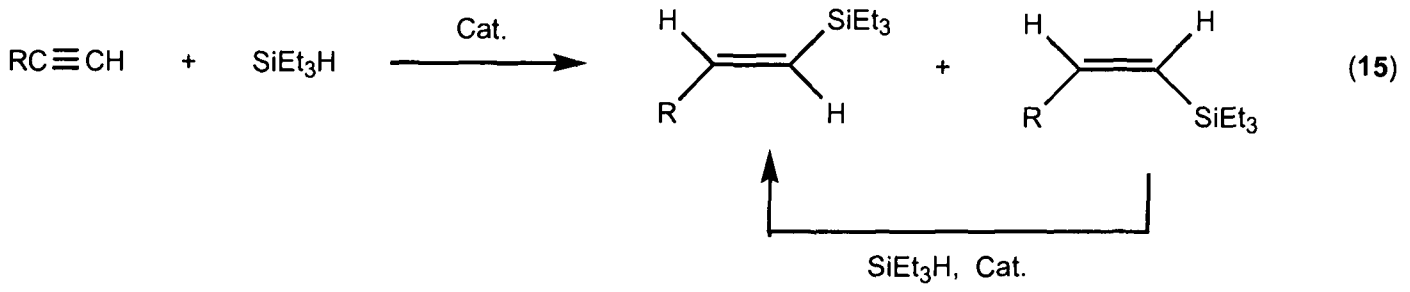

(15)

The hydrosilylation of ketones to silylethers (Eq. 16) was also catalysed by **37** and **38**, with **38** achieving 98% conversion after 4 h at 100 °C. The silylether can be hydrolysed to give the corresponding alcohol, resulting in a mild synthetic route for reducing ketones to secondary alcohols. The catalytic activity was affected on changing the N-substituents of the carbene ligand, indicating that the carbene ligand is involved in the catalysis.

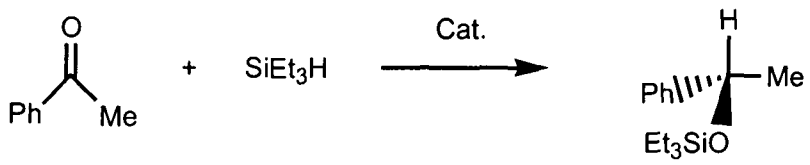

(16)

In 1996 chiral rhodium(I) carbene complexes **39** (figure 1.13) were used to catalyse the asymmetric hydrosilylation of acetophenone (a prochiral ketone) (Eq. 17) giving products which may be hydrolysed to produce optically active secondary alcohols.[49] Although the enantiomeric excess was only 30 %, this represented the first successful asymmetric catalysis using chiral carbene complexes.

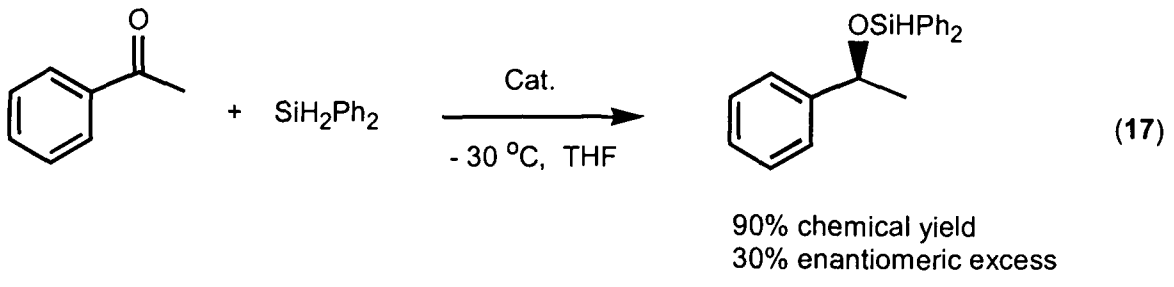

(17)

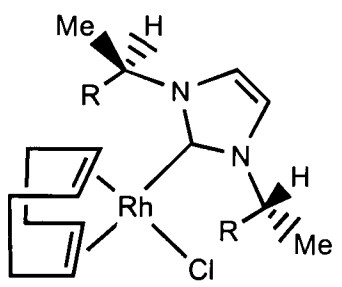

(R, R)-**39** R = Ph, $C_{10}H_7$

Figure 1.13 Chiral rhodium(I) asymmetric hydrosilylation catalysts incorporating N-heterocyclic carbene ligands.

(b) Hydrogenation of Alkenes

The hydrogenation of alkenes at atmospheric pressure is possible with late transition metal carbene complexes. The most active carbene catalysts have been found to be the mixed phosphine-carbene rhodium(I) complex **38** or a ruthenium(II) analogue. No significant enantiomeric excesses were observed using a chiral analogue of complex **37** (Eq. 18).[47]

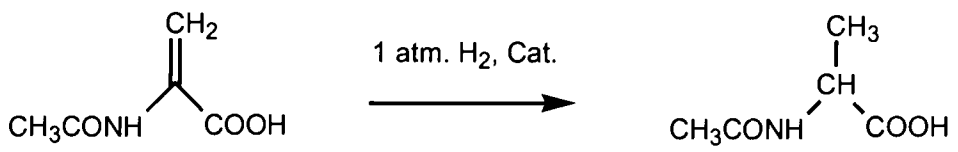

(18)

(c) Hydroformylation of Alkenes

Rhodium(I) carbene complexes such as **37** and **38** can be used for the hydroformylation of alkenes.[10] The conventional catalysts for this process are rhodium(I) phosphine complexes, which have to be used in the presence of a large excess (up to 1000-fold) of free phosphine to (a) avoid decomposition of the complex and (b) obtain a good ratio of linear to branched products. N-heterocyclic carbene complexes, however, have a greater long-term stability, and can be used without ligand excess. This obvious advantage is coupled with the disadvantage of reduced activities, caused by the higher electron density at the metal centre of the carbene catalysts. This can be overcome to a certain extent by using mixed rhodium(I) carbene phosphine complexes, which catalyse alkene hydroformylation with higher activities and have greater long-term stability.[50]

(d) Catalytic 2,3-Dimethylfuran Synthesis

The synthesis of 2,3-dimethylfuran from (Z)-3-methylpent-2-en-4-yn-1-ol (Eq. 19) was catalysed by ruthenium(II) carbene complexes such as **40** (figure 1.14). The activity of the catalyst was found to be strongly dependent on the nature of the N-substituent (R) on the carbene ligand. The most efficient catalyst was a dimer, with R a propylene bridge linking two monomers via the carbene ligands (R' = Et).

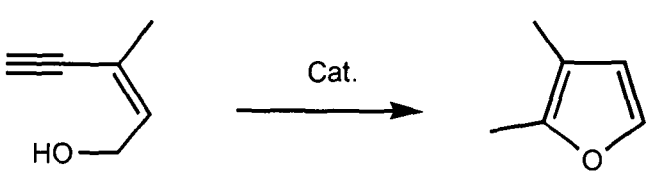

(19)

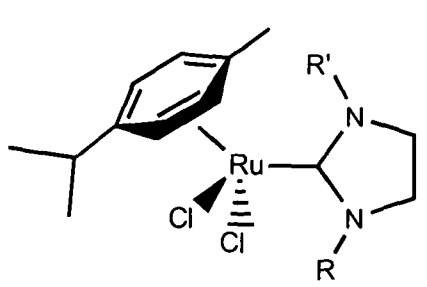

40

Figure 1.14 Ruthenium(II) carbene catalyst for the synthesis of 2,3-dimethylfuran.

(e) Heck Coupling of Aryl Halides with n-Butyl Acrylate

In 1995 Herrmann et al. used the iodo palladium(II) carbene complex **41** (figure 1.15) as a pre-catalyst for the Heck coupling of aryl halides (Eq. 20).[51] Using 0.5 mol % catalyst, conversions proceeded quantitatively (turnover number (TON) = 200 mol product / mol Pd) within 24 h at 130 °C for activated electron-poor aryl halides (R = CHO, $COCH_3$, NO_2), although only 60 % conversion (0.67 mol %, TON = 90) after 50 h was achieved for R = OCH_3 (deactivated, electron-rich). The high turnovers result from the long-term stability of **41**, which is stable towards oxygen and moisture, and melts at 299 °C with only partial decomposition. No deposition of palladium metal was observed during catalysis, even when high temperatures and long reaction times were employed. It was postulated that the active species is $Pd^0(Carbene)_2$ in line with the generally accepted phosphine equivalent: The induction time required to form the active species was reduced significantly on addition of either sodium formate, hydrazine or tetrabutylammonium bromide (thought by

Herrmann to act as reducing agents which generate the Pd^0 active species), or when the aryl halide contained the reducing formyl (CHO) residue. Formation of $Pd^0(Carbene)_2$ *in situ* by reaction of $[Pd(dba)_2]$ (dba = dibenzylidene acetone) with two equivalents of 1,3-dimethylimidazol-2-ylidene resulted in the absence of an induction period and high TON's of over 250000 (quantitative conversions in under 3 h).

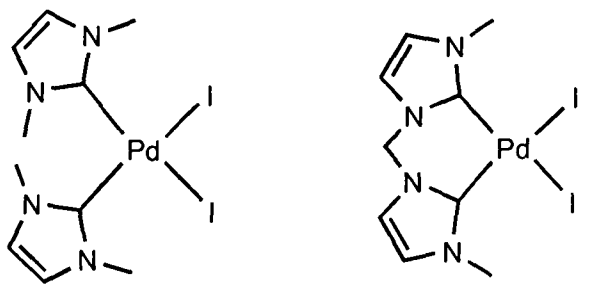

Figure 1.15 Palladium(II) N-heterocyclic carbene pre-catalysts for the Heck coupling of aryl halides.

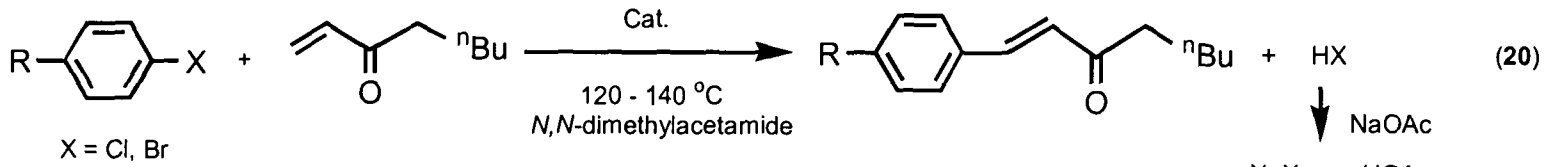

The chelating dicarbene palladium(II) diiodide **27a** (figure 1.15) is a more active pre-catalyst for the Heck reaction of aryl halides with n-butyl acrylate.[42,52] The complex is thermally robust (stable in solution at 150 °C) and 0.1 mol % quantitatively converts 4-bromoacetophenone (TON = 1000) within 5 h at 140 °C. The TON is only 120 for 4-chloroacetophenone after 24 h under the same conditions, reflecting the higher activation energy required for aryl chloride oxidative addition to the palladium centre. Compound **27a** (0.5 mol %) also achieves a 95 % conversion (TON = 190) of the deactivated aryl bromide 4-bromoanisole (R = OCH_3). Tetrabutylammonium acetate was used to minimise the induction period.

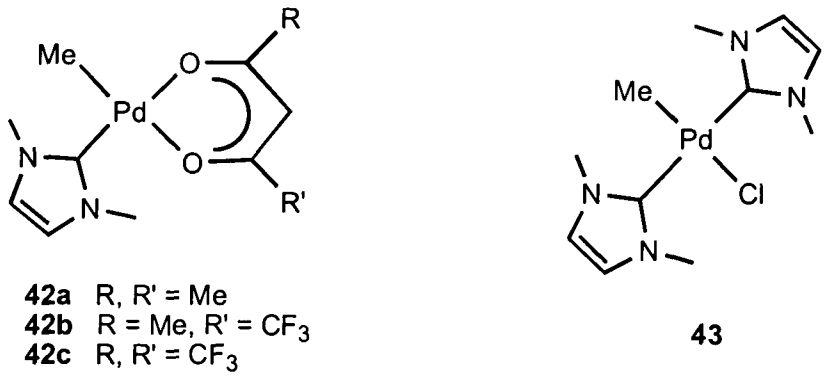

Figure 1.16 Highly active palladium(II) methyl N-heterocyclic carbene pre-catalysts for the Heck coupling of aryl halides.

In 1998 Cavell and co-workers found methyl palladium(II) carbene complexes **42a-c** and **43** (figure 1.16) to be excellent Heck catalysts, showing significantly greater activity than Herrmann's diiodide complexes in the coupling of the activated aryl halide 4-bromoacetophenone (R = $COCH_3$) with n-butyl acrylate.[31] Quantitative conversions were observed in under 25 minutes, using up to 0.6 mol % **42a** or **42b**, at 120 °C. Turnover numbers were then accurately measured for complexes **42a**, **42c** and **43** as 74500, 109000 and 100500 respectively, and are higher than values observed for traditional phosphine based catalysts. High initial activities were achieved, with little or no induction period, in the absence of a reducing agent. This is in contrast to Herrmann's work, where the absence of a reducing agent resulted in a long induction period. Cavell et al. concluded that the presence of a methyl group on the palladium centre provides a facile pathway for formation of the palladium(0) active species, probably via olefin insertion into the Pd-CH_3 bond followed by β-hydride elimination and then reductive elimination of HX in the presence of the base NaOAc (scheme 1.7). The higher turnover number of the *bis*-carbene complex **43** compared with the monocarbene complex **42a** was attributed to the stabilising effect of a second carbene ligand increasing the lifetime of the catalyst.

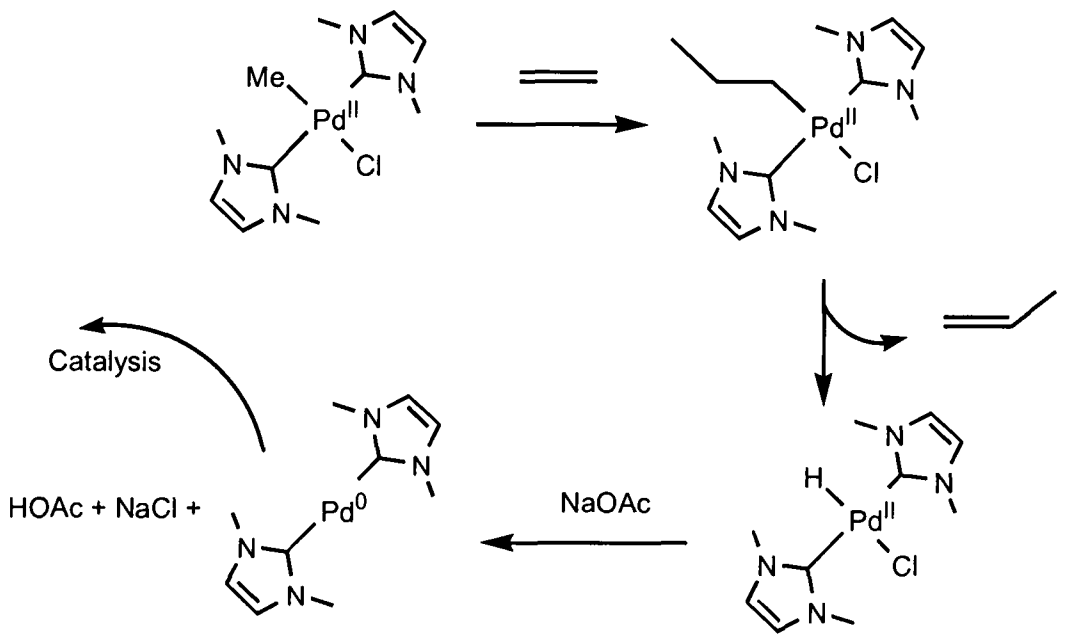

Scheme 1.7 Role of the methyl group in generation of the Pd^0 active species.

(f) Aryl Coupling Reactions

Palladium(II) N-heterocyclic carbene complexes **27a** (figure 1.15) and **44** (figure 1.17) are catalysts for the Suzuki coupling of aryl halides with arylboronic acids (Eq. 21). Complexes **44** also catalyse the Stille coupling of aryl halides with aryl tin compounds (Eq. 22).[42,53] The products of these reactions, unsymmetrically substituted biaryl derivatives, are used as drug intermediates and nonlinear optical materials.[54,55]

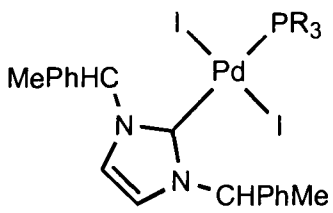

44 $PR_3 = PPh_3, PCy_3$

Figure 1.17 Mixed carbene-phosphine palladium(II) aryl coupling pre-catalysts.

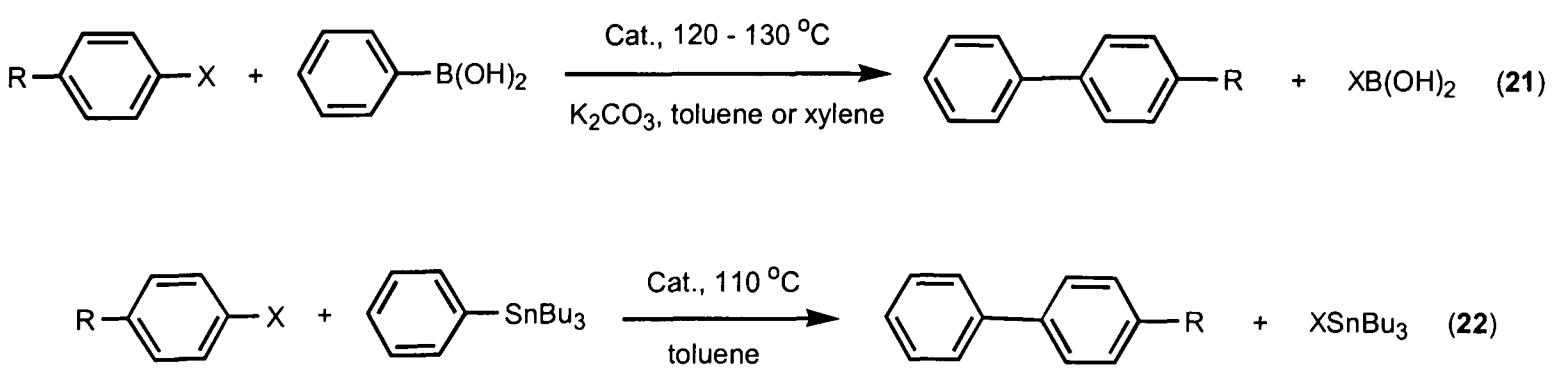

The chelating dicarbene palladium(II) diiodide complex **27a** (1 mol %) catalysed the Suzuki coupling reaction of aryl bromides (R = OCH_3, $COCH_3$, NH_2, NO_2, H) and aryl chlorides (R = $COCH_3$) with yields varying between 99 % after 12 h (X = Br, R = NO_2) and 60 % after 48 h (X = Cl, R = $COCH_3$). However Herrmann and co-workers were able to use the mixed N-heterocyclic carbene-phosphine complexes **44** to obtain turnover numbers of up to 1000 (mol product / mol Pd), with quantitative conversion of all aryl bromides (R = $COCH_3$, OCH_3, H) within 12-14 h, and up to 87 % conversion of aryl chlorides within 32 h. These yields and turnovers are generally superior to results obtained using the *bis*(N-heterocyclic carbene) palladium(II) diiodide catalysts **41** and **27a**: The mixed phosphine carbene complex combines the good activity of conventional *bis*-phosphine complexes with the advantageous stability of *bis*-carbene complexes (the thermal stabilities of complexes **44** are comparable to the *bis*-carbene complexes, wheras corresponding *bis*-phosphine complexes $(R_3P)_2PdX_2$ readily decompose to palladium black at elevated reaction temperatures). Using catalyst **44** (PR_3 = PPh_3) 91-99 % yields (17-25 h) were obtained for the Stille coupling of aryl bromides (R = $COCH_3$, OCH_3, H) (Eq. 22), although aryl chloride coupling proceeded in poor yield (4 %, 17 h).

In 1999 Cavell and co-workers improved on the results of Herrmann et al. by achieving turnovers of up to 55700 for the Suzuki coupling of 4-bromoacetophenone with phenylboronic acid.[56] Using 2 x 10^{-3} mol % of the palladium(II) aryl complex **45** (figure 1.18) a TON of 28000 is obtained after 24 hours. The high activity of **45** was attributed to the presence of the aryl group, which provides a facile route to the palladium(0) *bis*-monocarbene active species. The diiodide complexes **27a** and **44** used by Herrmann are not so readily reduced, requiring a significant induction period before they become active, leading to a loss of catalyst activity. The palladium(0) complex **46** (figure 1.18) is even more active, giving a TON of 55700 with 1 x 10^{-3} mol % catalyst. In this case the high activity results from its ability to readily undergo oxidative addition of aryl halide, and hence undergo the first (possibly rate-determining) step in the catalytic cycle.

The Suzuki coupling reaction is also catalysed by nickel(II) N-heterocyclic carbene complexes **47** and **48** (figure 1.18), although not as efficiently as observed for Pd.[56] The diiodide complex **47** achieved 19 % conversion of aryl halide after 24 hours, with a TON of 630. Under the same conditions the aryl complex **48** achieved a 58 % conversion (TON =

1930). Thus, introduction of an aryl group into the pre-catalyst leads to an increase in activity, although not as pronounced as for the palladium case.

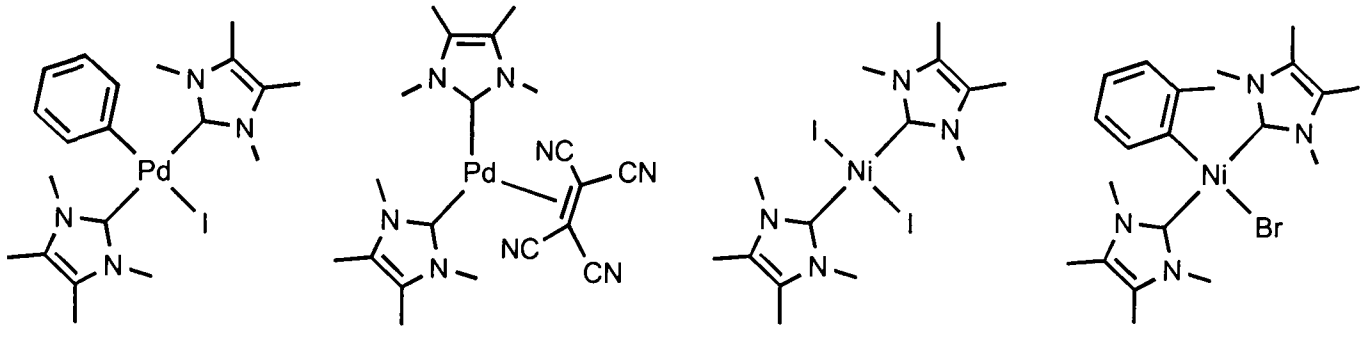

45 46 47 48

Figure 1.18 Nickel(II) and palladium(II) N-heterocyclic carbene pre-catalysts for the Suzuki coupling of aryl halides.

(g) Copolymerisation of C_2H_4 and CO

Dicationic complexes **29a** and **29b** (figure 1.19) were found by Herrmann and co-workers in 1999 to catalyse the copolymerisation of ethylene and carbon monoxide (Eq. 23).[43] Optimum turnover numbers were obtained at 50 °C using 50 bar ethylene and 20 bar CO, and either complex **29a** (20 mg, 23 μmol) or complex **29b** (10 mg, 19 μmol) as the pre-catalyst, in the presence of *p*-benzoquinone (3 mg, 28 μmol). The yield of copolymer under these conditions was 810 g / g Pd. The absence of *p*-benzoquinone resulted in decreased turnovers and the solvent of choice was methanol, with other coordinating solvents such as CH_3CN rendering the catalyst inactive. The catalysts were also active at room temperature. The copolymer product, insoluble in methanol, was separated from the palladium black arising from catalyst decomposition by extraction into 1,1,1,3,3,3-hexafluoro-*iso*-propanol, and characterised by infrared (C=O stretch at 1692 cm^{-1}), ^1H NMR (δ 2.40-2.55 ppm) and ^{13}C NMR spectroscopy. The latter spectrum showed the perfect alternation of monomers in the copolymer, with no signals other than for the methylene and carbonyl carbons of poly(C_2H_4-*alt*-CO) at δ 35.0 and δ 212.1 ppm respectively. An estimation of the average molecular weight of the copolymer was not determined.

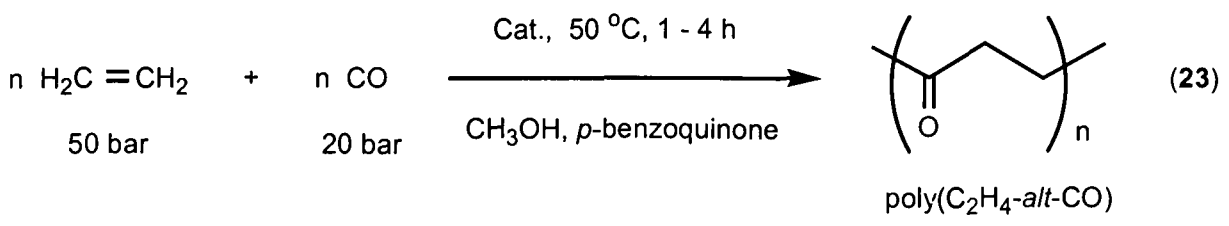

(**23**)

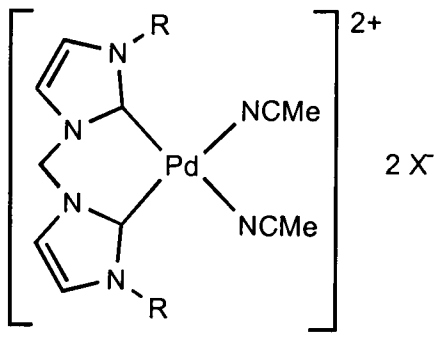

29a (R = Mes, X = PF_6)
29b (R = Me, X = BF_4)

Figure 1.19 Dicationic palladium(II) dicarbene pre-catalysts for the copolymerisation of ethylene and CO.

(h) Ring Opening Metathesis Polymerisation (ROMP) and Ring Closing Metathesis (RCM)

In 1998 Herrmann and co-workers synthesised the first ruthenium complexes **49a-d** (figure 1.20) containing alkylidene groups as well as N-heterocyclic carbenes. These were shown to be active catalysts for the ring opening metathesis polymerisation (ROMP) of 2-norbornene (Eq. 24) and cyclooctene (Eq. 25), as well as for the ring closing metathesis (RCM) of 1,7-octadiene (Eq. 26).[57]

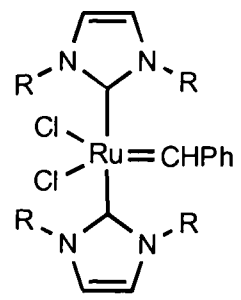

49a R = ^{i}Pr
49b R = Cy
49c R = CHMePh
49d R = CHMeNaph

Figure 1.20 Ruthenium(II) alkylidene ROMP and RCM catalysts incorporating N-heterocyclic carbene ligands.

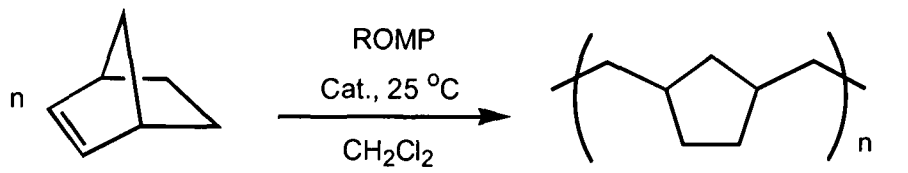

(24)

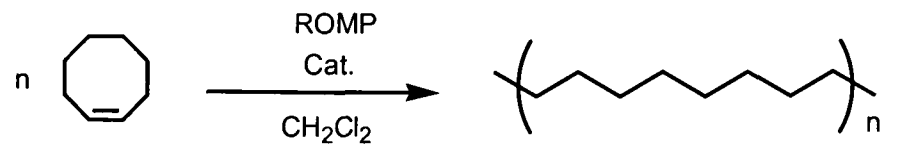

(25)

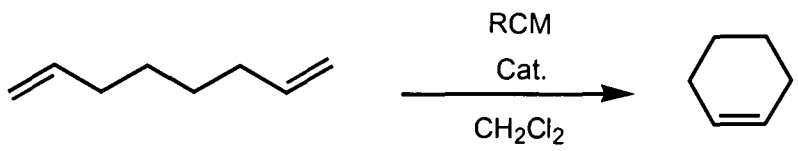

(26)

The compounds **49a-d** are synthesised by treating the phosphine complexes $[RuCl_2(PR_3)_2(=CHPh)]$ (R = Ph, Cy) developed by Grubbs et al.[58] (themselves highly efficient metathesis pre-catalysts) with 2.2 equivalents of the appropriate N-heterocyclic carbene. ROMP of 2-norbornene is catalysed by **49a** and **49b** (1 mol %) with near quantitative yields in 1 minute reaction time at room temperature. ROMP of cyclooctene is catalysed by **49a** and **49b** (0.2 mol %) with near quantitative yields in 1 h at room temperature, or by **49c** and **49d** (0.2 mol %) with near quantitative yields in 1 h at 60 °C and significantly lower activity at room temperature. This suggests that steric effects (changing the carbene N-substituents) can be exploited to tune the catalytic performance to a greater extent than with phosphine ligands. RCM of 1,7-octadiene proceeds in quantitative yields in 10 minutes for catalysts **49a-d** (2 mol %) at 60 °C, with **49a** (2 mol %) attaining a 51 % yield within 10 minutes at room temperature.

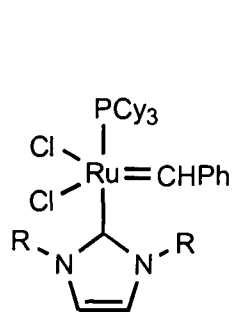

50

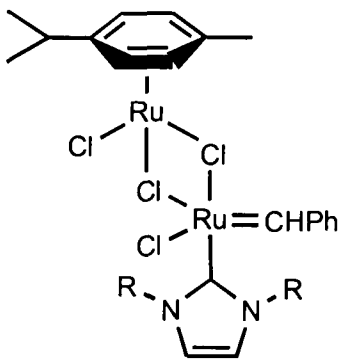

51

Figure 1.21 Mixed phosphine-carbene and bimetallic carbene ruthenium(II) catalysts for ring closing metathesis.

More recent work includes the development of mixed phosphine-carbene ruthenium(II) catalysts **50** (figure 1.21) which show increased RCM activity at elevated temperatures relative to the parent phosphine compounds, due to greater thermal stability. The

compounds **50** and bimetallic complexes such as **51** (figure 1.21) even allow the formation of tetrasubstituted cycloalkenes by RCM (e.g. Eq. 27), which were previously unobtainable using ruthenium-based metathesis catalysts.[59-61]

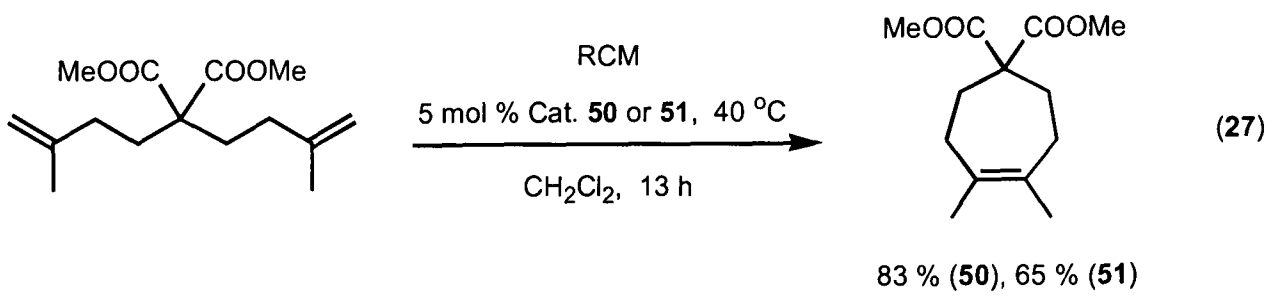

(**27**)

83 % (**50**), 65 % (**51**)

1.3 Overview of Relevant Homogeneous Catalysis of Nickel and Palladium Complexes

1.3.1 Polymerisation of Ethylene and α-Olefins using Nickel(II) or Palladium(II) Diimine Catalysts

In 1995 Brookhart and co-workers reported polymerisation of ethylene and α-olefins using Ni(II)- or Pd(II)-based catalysts.[62] Such late transition metal systems had previously only been observed to dimerise or oligomerise olefins due to competing β-hydride elimination (followed by associative displacement). The resulting high molecular weight polymers have unique microstructures because they are far more highly branched than those produced by the early transition metal metallocene catalysts. The nickel catalysts exhibit high activities which are comparable to those of the metallocenes, and the degree of branching in the polymer can be controlled by simple variation of pressure, temperature and ligand substituents. When polymerisations are carried out at lower temperatures (e.g. -10 °C) and low monomer concentrations (< 1 M) the polyolefins produced have very narrow molecular weight distributions suggestive of a living polymerisation.[63]

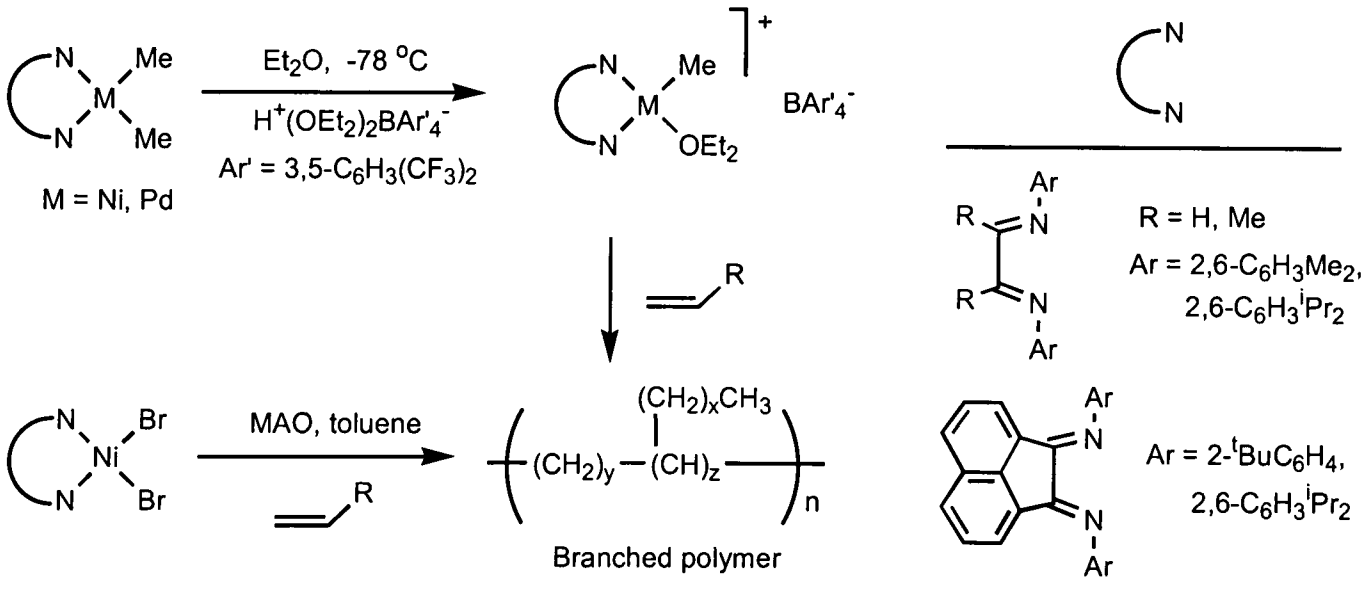

Scheme 1.8 Formation of Ni^{II} and Pd^{II} diimine olefin polymerisation initiators.

The polymerisation initiators are produced by protonation of the nickel and palladium dimethyl precursors (which incorporate bulky diimine ligands) with $[H(OEt_2)_2]^+[B\{C_6H_3(CF_3)_2\}_4]^-$ to produce the cationic diethyl ether adducts (scheme 1.8).

The nickel initiators, however, are more conveniently generated *in situ* by methylaluminoxane (MAO) activation (1000 equiv., toluene) of the diimine nickel dibromide complexes (scheme 1.8).

Polymerisation and the high degree of branching observed can be explained by the mechanism shown in scheme 1.9, given that NMR studies have established alkyl olefin complexes as the catalyst resting states.[62] Polyethylene chain propagation occurs via the migratory insertion of ethylene into the metal-alkyl bond, with the subsequent species being rapidly trapped by ethylene to reform an alkyl ethylene species. Repetition of these steps results in a linear hydrocarbon chain. However, instead of being trapped by ethylene, the coordinatively unsaturated species can β-hydride eliminate to give an olefin hydride. Reinsertion of the olefin into the metal-hydride bond may then occur with opposite regiochemistry to introduce a branched alkyl group. In this case, subsequent trapping by ethylene and insertion results in chain propagation and a new methyl branch in the polymer, although further chain migration (via repeated β-hydride elimination and opposite reinsertion) may occur beforehand to produce longer branches before chain propagation recommences.

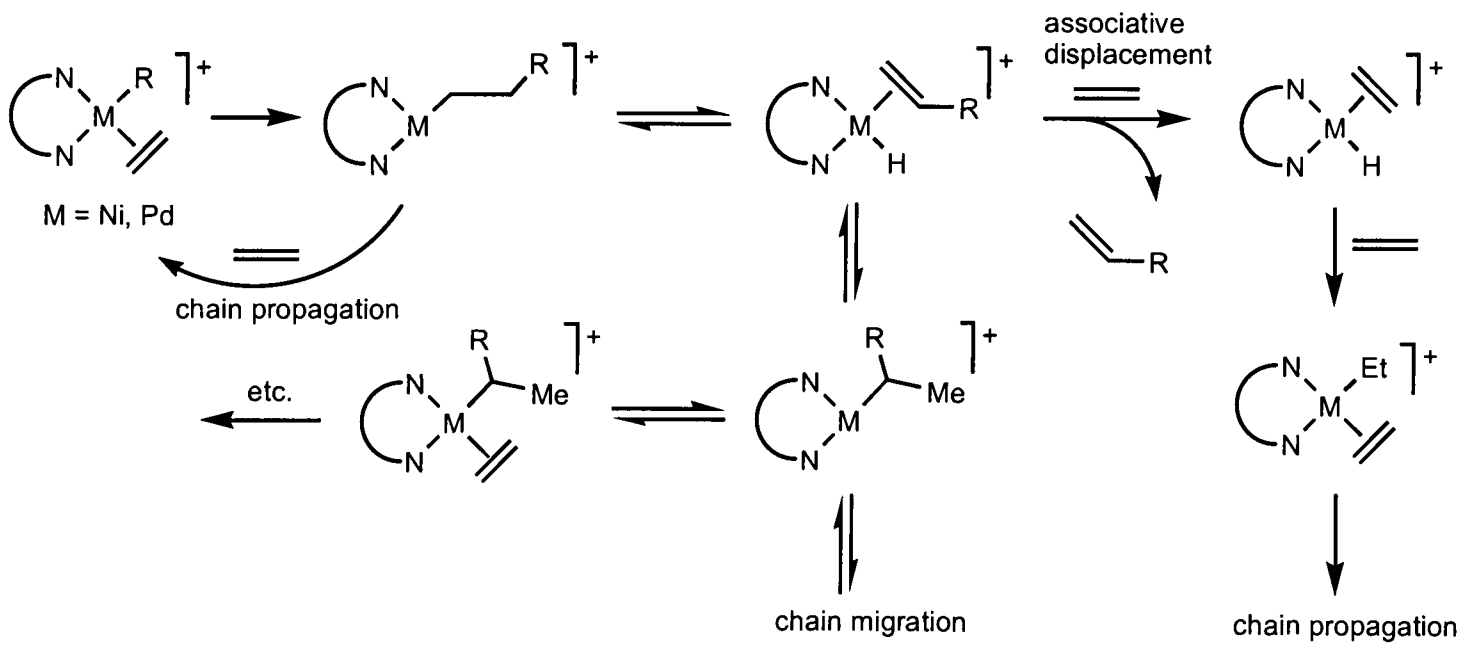

Scheme 1.9 Mechanism for the formation of highly branched polyethylene.

After β-hydride elimination has occurred at any point during the polymerisation, it is possible for the polymer chain to be displaced by a molecule of ethylene. This displacement is an associative process, and results in the termination of growth of that

particular polymer chain, and initiation of a new polymer chain. Thus associative displacement results in a 'chain transfer' process.

Fortunately the extreme steric bulk of the diimine ligands greatly reduces the rates of associative displacement and chain transfer, because the aryl rings lie roughly perpendicular to the square plane, and the *ortho* substituents block axial approach of olefins, retarding association. This feature had previously been absent in late transition metal systems, which explains why dimerisation and oligomerisation rather than the formation of high molecular weight polymers had only previously been observed.

The unique polymer microstructures which are highly dependent on the bulky diimine ligand substituents, in addition to living polymerisation which allows the synthesis of polymers (and block copolymers) with specific molecular weights, make late transition metal olefin polymerisation catalysis an exciting area to develop. Furthermore, the moderate electrophilicity of late transition metal catalysts makes them tolerant to a variety of heteroatom functionalities in the olefin substrate, allowing the preparation of functionalised polymers and reducing their sensitivity to oxygen and water. In this respect the late transition metal catalysts can have a wider applicability than the early transition metal metallocene systems. Therefore an aim of the work in this thesis was to synthesise potential olefin polymerisation pre-catalysts using bulky bidentate N-heterocyclic carbenes (CC), themselves highly sterically tuneable, in place of Brookhart's diimine ligands. Nickel and palladium dihalide and dimethyl complexes of the type $[(CC)MX_2]$ were targeted.

1.3.2 Alternating Copolymerisation of Alkenes and Carbon Monoxide

Copolymers of olefins with carbon monoxide (polyketones) are of great interest to industry for a number of reasons. Firstly, the presence of carbonyl groups ensures that the polymers can be chemically modified, so the polyketones are excellent starting materials in the synthesis of many other types of functionalised polymers. Secondly, alternating ethylene-carbon monoxide copolymer has high mechanical strength resulting from its high crystallinity. Other advantages are that the carbon monoxide monomer is cheap and plentiful, and, from an environmental standpoint, the presence of the carbonyl chromophore in the polymer backbone makes these copolymers photodegradable.

Copolymerisation may be initiated either by free radicals or using γ-rays, which generates random olefin-carbon monoxide copolymer (C_nH_{2n}:CO > 1). However, metal-catalysed copolymerisation has the advantages that it occurs at ambient temperatures and significantly lower pressures, and the resultant polymers have higher molecular weights and a strictly alternating structure (olefin:CO =1).

Cationic palladium(II) complexes involving chelating 1,3-*bis*(phosphino)propane ligands and weakly coordinating anions such as tetrafluoroborate (e.g. $[(dppp)Pd(MeCN)_2][BF_4]_2$, dppp = $Ph_2P(CH_2)_3PPh_2$) have been established by Drent and co-workers at Shell as the most efficient catalysts for the copolymerisation of ethylene or simple α-olefins with carbon monoxide.[64,65] For ethylene and CO copolymerisation these catalysts achieve yields above 10^6 g / g Pd, at high rates (~6000 g (g Pd)$^{-1}$ h^{-1}) under mild conditions (90 °C, 45 bar).

The catalysts are easy to prepare either separately, or *in situ* from palladium acetate, a stoichiometric amount of the bidentate phosphine ligand dppp and a Brønsted acid of a weakly or non-coordinating anion (e.g. OTs^-). Methanol is the solvent of choice. With ethylene as the olefin, a perfectly alternating ethylene / CO copolymer (100 % selectivity) is the result: It has a high melting point (~260 °C), and because it is insoluble in most organic solvents it precipitates during copolymerisation as a snow-white solid.

Variation of the chain length n of the diphosphine ligand $Ph_2P(CH_2)_nPPh_2$ affects the rate of ethylene / CO copolymerisation and the molecular weight of the product. The highest rates (~6000 g (g Pd)$^{-1}$ h^{-1}) and molecular weights (~5000) are achieved for n = 3.

A sensible mechanism for formation of the strictly alternating ethylene / CO copolymer involves the alternate insertions of carbon monoxide and ethylene into a preformed Pd-alkyl or Pd-hydride bond (scheme 1.10). The first step involves carbon monoxide insertion into the Pd-alkyl bond to form a Pd-acyl. Clearly ethylene is also able to insert into Pd-alkyl bonds, since the same catalyst system is effective for the dimerisation of olefins under identical conditions.[66,67] There is therefore no thermodynamic barrier to ethylene insertion into the Pd-alkyl bond, so the reason that CO insertion is preferential must be due to kinetics: Ethylene insertion is too slow to compete with CO insertion. Also, since CO is a

better π-acid compared to olefins, it should bind more readily to the electron-rich palladium centre. The second step (ethylene insertion into the resulting Pd-acyl bond) is determined by thermodynamics: Sen et al. showed, using α-keto acyl complexes of palladium(II), that CO insertion into Pd-acyl bonds is thermodynamically 'uphill'. They also found that olefins readily inserted into the Pd-acyl bond of $[(PPh_3)_2Pd(MeCN)(COR)]^+$. Therefore only ethylene insertion into the Pd-acyl is observed during copolymerisation.

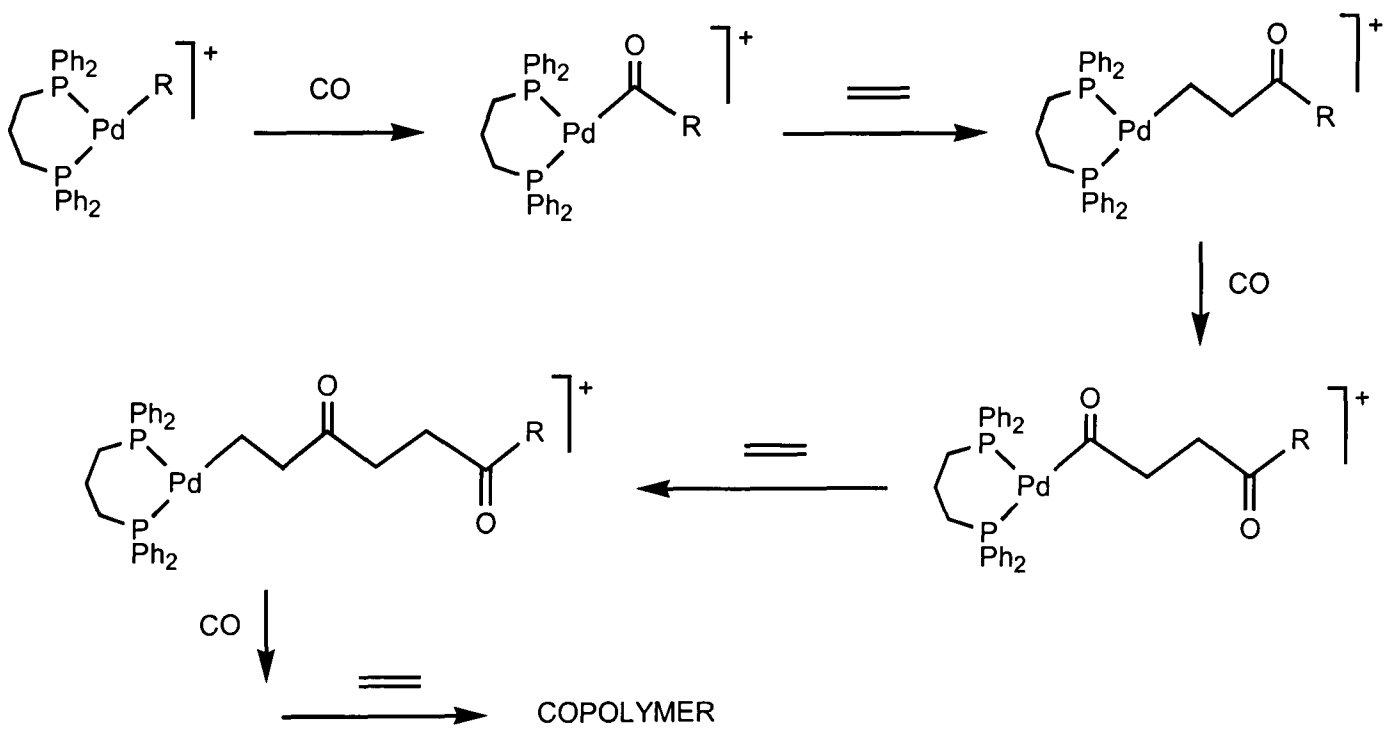

Scheme 1.10 Mechanism for formation of strictly alternating ethylene / CO copolymer.

An analysis of the end groups of alkene / CO copolymers, formed in methanol / nitromethane using $[(dppp)Pd(MeCN)_2][BF_4]_2$ as the catalyst, was carried out.[68,69] The presence of methoxycarbonyl, alkyl and alkenyl end-groups proved that both Pd-hydride and Pd-methoxide must act as initiators (with Pd-hydride generation occuring via β-hydrogen abstraction from Pd-alkoxide generated *in situ*). Chain termination can occur through β-hydrogen abstraction from a Pd-alkyl species, although this is a rare event because alkene insertion into the Pd-acyl bond is the rate-limiting step in the chain propagation mechanism (scheme 1.10).

A ligand displacement step is necessary for the alkene to insert into the initial Pd-acyl bond. This accounts for the observation by Sen et al. that cationic weakly solvated palladium(II) complexes (e.g. $[(PPh_3)_2Pd(R)(solvent)]^+$) catalyse copolymerisation, whereas their neutral analogues (e.g. $[(PPh_3)_2Pd(R)(X)]$, X = halide) are inactive

(displacement of halide by the alkene cannot occur in the latter complex).[66,67] Despite the activity of such complexes containing two monodentate phosphine ligands, a marked increase in activity was observed by Drent and co-workers when bidentate phosphines such as dppp were used. The chelating ligands enforce *cis* coordination of the monomer and growing polymer chain, allowing insertion to occur more readily.[64]

Great potential exists, therefore, for the synthesis of new alkene / CO copolymerisation catalysts using chelating N-heterocyclic carbenes as ancillary ligands in place of *bis*(phosphines). Hence a particular aim of the work in this thesis was to design cationic palladium (II) complexes of the type $[(CC)Pd(R)(solvent)]^+$ or dicationic complexes such as $[(CC)Pd(solvent)_2]^{2+}$, with (CC) a bidentate N-heterocyclic carbene ligand.

1.3.3 Heck Coupling Reactions

Carbon-carbon bond forming reactions are key steps in the syntheses of many organic chemicals both in nature and in industry, making such reactions important tools for synthetic chemists.[70] Many frequently used cross coupling reactions involve palladium catalysts (figure 1.22).[71]

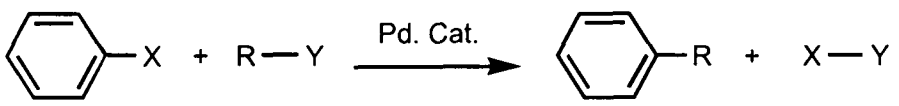

Figure 1.22 Palladium catalysed cross coupling reactions. X = I, Br, Cl, OTf, COCl, CO-O-COR, $OPO(OR)_2$, $N_2^+BF_4^-$, IR^+X^-; R = aryl, vinyl, alkynyl; Y = H, MgX, ZnX, SnR_3, $B(OR)_2$, Li, HgX, AlR_2, CuX, Cp_2ZrCl, SiF_3.

The Heck reaction (arylation of olefins with aryl halides) has received increasing attention in the last decade because of its synthetic potential for generating carbon-carbon bonds and its tolerance towards a wide range of functional groups.[25,72] Herrmann et al. investigated the Heck reaction of aryl bromides with n-butyl acrylate, because the products (cinnamic ester derivatives) are used industrially as UV absorbers, as anti-oxidants in plastics and as intermediates for pharmaceuticals. Palladium phosphine catalysts generated *in situ* from $Pd(OAc)_2$ + 4 P(*o*-Tol)$_3$ have traditionally been used to catalyse such reactions, with best literature results for activated, electron-poor aryl bromides (e.g. 4-bromoacetophenone, 4-

bromobenzaldehyde) being turnover numbers (TON's) of around 134000 mol product / mol Pd.[73] However, Herrmann and co-workers found that the dimeric palladacycle $Pd_2(\mu\text{-}OAc)_2\{o\text{-}CH_2C_6H_4P(o\text{-}Tol)_2\}_2$ achieves a TON about 10 times greater.[52] Herrmann also investigated N-heterocyclic carbene palladium(II) diiodide complexes and found that both the di(monocarbene) and chelating dicarbene Pd complexes efficiently catalysed the Heck reactions of aryl bromides and activated aryl chlorides with n-butyl acrylate (see section 1.2.6(e)). The highest TON of 1000 was observed for the coupling of 4-bromoacetophenone using the chelating dicarbene complex. Cavell et al. then found that methyl palladium(II) carbene complexes showed significantly greater activity than Herrmann's diiodide complexes, with turnover numbers as high as 109000 for 4-bromoacetophenone (see section 1.2.6(e)). High initial activities were also achieved, with little or no induction period, in the absence of a reducing agent. This is in contrast to Herrmann's work, where the absence of a reducing agent resulted in long induction periods. Based on their results, Cavell et al. concluded that the presence of a methyl group on the palladium centre provides a facile pathway for formation of the palladium(0) active species (scheme 1.7), and proposed a mechanism for Heck coupling with dicarbene palladium complexes (scheme 1.11).

In summary, Herrmann has demonstrated that palladium Heck catalysts with a chelating dicarbene ligand can show greater activities than their di(monocarbene) equivalents, and Cavell has shown that the presence of a methyl group on the palladium centre markedly improves catalyst activity. It therefore seemed obvious to combine the two advantages, and incorporate into this work the aim of investigating the ability of chelating dicarbene palladium dimethyl complexes to catalyse Heck reactions.

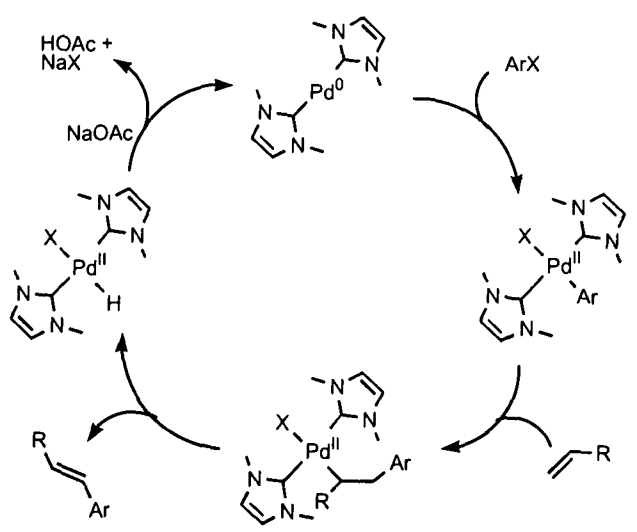

Scheme 1.11 Proposed mechanism for Heck coupling with dicarbene-Pd complexes.

1.4 References

1) Öfele, K. *J. Organomet. Chem.* **1968**, *12*, P42.
2) Wanzlick, H.-W.; Schönherr, H.-J. *Angew. Chem. Int. Ed. Engl* **1968**, *7*, 141.
3) Schönherr, H.-J.; Wanzlick, H.-W. *Chem. Ber.* **1970**, *103*, 1037.
4) Wanzlick, H.-W.; Schönherr, H.-J. *Liebigs Ann. Chem.* **1970**, *731*, 176.
5) Arduengo III, A. J.; Harlow, R. L.; Kline, M. *J. Am. Chem. Soc.* **1991**, *113*, 361.
6) Arduengo III, A. J.; Rasika Dias, H. V.; Harlow, R. L.; Kline, M. *J. Am. Chem. Soc.* **1992**, *114*, 5530.
7) Kuhn, N.; Kratz, T. *Synthesis* **1993**, 561.
8) Herrmann, W. A.; Elison, M.; Fischer, J.; Köcher, C.; Artus, G. R. J. *Chem. Eur. J.* **1996**, *2*, 1627.
9) Dixon, D. A.; Arduengo III, A. J. *J. Phys. Chem.* **1991**, *95*, 4180.
10) Herrmann, W. A.; Köcher, C. *Angew. Chem. Int. Ed. Engl.* **1997**, *36*, 2162.
11) Arduengo III, A. J.; Dixon, D. A.; Kumashiro, K. K.; Lee, C.; Power, W. P.; Zilm, K. W. *J. Am. Chem. Soc.* **1994**, *116*, 6361.
12) Rasika Dias, H. V.; Jin, W. *Tetrahedron Lett.* **1994**, *35*, 1365.
13) Langer, V.; Huml, K.; Reck, G. *Acta Crystallogra. Sect. B* **1982**, *38*, 298.
14) Kuhn, N.; Bohnen, H.; Henkel, G. *Z. Naturforsch. B* **1994**, *49*, 1473.
15) Arduengo III, A. J.; Goerlich, J. R.; Marshall, W. J. *J. Am. Chem. Soc.* **1995**, *117*, 11027.
16) Regitz, M. *Angew. Chem. Int. Ed. Engl.* **1991**, *30*, 674.
17) Arduengo III, A. J.; Kline, M.; Calabrese, J. C.; Davidson, F. *J. Am. Chem. Soc.* **1991**, *113*, 9704.
18) Arduengo III, A. J.; Tamm, M.; Calabrese, J. C. *J. Am. Chem. Soc.* **1994**, *116*, 3625.
19) Arduengo III, A. J.; Dias, H. V. R.; Calabrese, J. C.; Davidson, F. *J. Am. Chem. Soc.* **1992**, *114*, 9724.
20) Arduengo III, A. J.; Dias, H. V. R.; Davidson, F.; Harlow, R. L. *J. Organomet. Chem.* **1993**, *462*, 13.
21) Arduengo III, A. J.; Dias, H. V. R.; Calabrese, J. C.; Davidson, F. *Inorg. Chem.* **1993**, *32*, 1541.
22) Kuhn, N.; Henkel, G.; Kratz, T.; Kreutzberg, J.; Boese, R.; Maulitz, A. H. *Chem. Ber.* **1993**, *126*, 2041.
23) Kuhn, N.; Kratz, T.; Bläser, D.; Boese, R. *Chem. Ber.* **1995**, *128*, 245.
24) Fischer, E. O.; Maasböl, A. *Angew. Chem. Int. Ed. Engl.* **1964**, 580.
25) Cornils, B.; Herrmann, W. A. *Applied Homogeneous Catalysis with Organometallic Complexes*; VCH: Weinheim, 1996
26) Elison, M. : Dissertation,Technische Universität München, 1995.
27) Elschenbroich, C.; Salzer, A. *Organometallchemie*; Teubner: Stuttgart, 1990
28) Herrmann, W. A.; Lobmaier, G. M.; Elison, M. *J. Organomet. Chem.* **1996**, *520*, 231.
29) Herrmann, W. A.; Öfele, K.; Elison, M.; Kühn, F. E.; Roesky, P. W. *J. Organomet. Chem.* **1994**, *480*, C7.
30) Köcher, C.; Herrmann, W. A. *J. Organomet. Chem.* **1997**, *532*, 261.
31) McGuinness, D. S.; Green, M. J.; Cavell, K. J.; Skelton, B. W.; White, A. H. *J. Organomet. Chem.* **1998**, *565*, 165.
32) Öfele, K.; Kreiter, C. G. *Chem. Ber.* **1972**, *105*, 529.
33) Öfele, K.; Herrmann, W. A.; Mihalios, D.; Elison, M.; Herdtweck, E.; Scherer, W.; Mink, J. *J. Organomet. Chem.* **1993**, *459*, 177.

34) Arduengo III, A. J.; Gamper, S. F.; Calabrese, J. C.; Davidson, F. *J. Am. Chem. Soc.* **1994**, *116*, 4931.
35) Herrmann, W. A.; Gerstberger, G.; Spiegler, M. *Organometallics* **1997**, *16*, 2209.
36) Kuhn, N.; Kratz, T.; Bläser, D.; Boese, R. *Inorg. Chim. Acta.* **1995**, *238*, 179.
37) Herrmann, W. A.; Elison, M.; Fischer, J.; Köcher, C. A., G.R.J. *Chem. Eur. J.* **1996**, *2*, 772.
38) Hitchcock, P. B.; Lappert, M. F.; Terreros, P.; Wainwright, K. P. *J. Chem. Soc., Chem. Commun.* **1980**, 1180.
39) Öfele, K.; Herrmann, W. A.; Mihalios, D.; Elison, M.; Herdtweck, H.; Priermeier, T.; Kiprof, P. *J. Organomet. Chem.* **1995**, *498*, 1.
40) Fehlhammer, W. P.; Bliss, T.; Kernbach, U.; Brüdgam, I. *J. Organomet. Chem.* **1995**, *490*, 149.
41) Kernbach, U.; Ramm, M.; Luger, P.; Fehlhammer, W. P. *Angew. Chem. Int. Ed. Engl.* **1996**, *35*, 310.
42) Herrmann, W. A.; Reisinger, C.-P.; Spiegler, M. *J. Organomet. Chem.* **1998**, *557*, 93.
43) Gardiner, M. G.; Herrmann, W. A.; Reisinger, C.-P.; Schwarz, J.; Spiegler, M. *J. Organomet. Chem.* **1999**, *572*, 239.
44) Herrmann, W. A.; Schwarz, J.; Gardiner, M. G.; Spiegler, M. *J. Organomet. Chem.* **1999**, *575*, 80.
45) Herrmann, W. A.; Schwarz, J.; Gardiner, M. G. *Organometallics* **1999**, *18*, 4082.
46) Lappert, M. F.; Maskell, R. K. *J. Organomet. Chem.* **1984**, *264*, 217.
47) Lappert, M. F. *Transition Metal Chemistry*; (Eds.: A. Müller, E. Diemann) Verlag Chemie: Weinheim, 1981
48) Hill, J. E.; Nile, T. A. *J. Organomet. Chem.* **1977**, *137*, 293.
49) Herrmann, W. A.; Goossen, L. J.; Köcher, C.; Artus, G. R. J. *Angew. Chem. Int. Ed. Engl.* **1996**, *35*, 2805.
50) Köcher, C. ; Dissertation, Technische Universität München, 1997.
51) Herrmann, W. A.; Elison, M.; Fischer, J.; Köcher, C.; Artus, G. R. J. *Angew. Chem. Int. Ed. Engl.* **1995**, *34*, 2371.
52) Herrmann, W. A.; Böhm, V. P. W.; Reisinger, C.-P. *J. Organomet. Chem.* **1999**, *576*, 23.
53) Weskamp, T.; Böhm, V. P. W.; Herrmann, W. A. *J. Organomet. Chem.* **1999**, *585*, 348.
54) Hsieh, K.-H.; LaHann, T.; Speth, R. *J. Med. Chem.* **1989**, *32*, 898.
55) Williams, D. J. *Angew. Chem. Int. Ed. Engl.* **1984**, *23*, 640.
56) McGuinness, D. S.; Cavell, K. J.; Skelton, B. W.; White, A., H. *Organometallics* **1999**, *18*, 1596.
57) Weskamp, T.; Schattenmann, W. C.; Spiegler, M.; Herrmann, W. A. *Angew. Chem. Int. Ed. Engl.* **1998**, *37*, 2490.
58) Schwab, P.; France, M. B.; Ziller, J. W.; Grubbs, R. H. *Angew. Chem. Int. Ed. Engl.* **1995**, *34*, 2039.
59) Ackermann, L.; Fürstner, A.; Weskamp, T.; Kohl, F. J.; Herrmann, W. A. *Tetrahedron Lett.* **1999**, *40*, 4787.
60) Huang, J. K.; Stevens, E. D.; Nolan, S. P.; Petersen, J. L. *J. Am. Chem. Soc.* **1999**, *121*, 2674.
61) Scholl, M.; Trnka, T. M.; Morgan, J. P.; Grubbs, R. H. *Tetrahedron Lett.* **1999**, *40*, 2247.
62) Johnson, L. K.; Killian, C. M.; Brookhart, M. *J. Am. Chem. Soc.* **1995**, *117*, 6414.

63) Killian, C. M.; Tempel, D. J.; Johnson, L. K.; Brookhart, M. *J. Am. Chem. Soc.* **1996**, *118*, 11664.
64) Drent, E.; Budzelaar, P. H. M. *Chem. Rev.* **1996**, *96*, 663.
65) Sen, A. *Acc. Chem. Res.* **1993**, *26*, 303.
66) Lai, T.-W.; Sen, A. *Organometallics* **1984**, *3*, 866.
67) Sen, A.; Lai, T.-W. *J. Am. Chem. Soc.* **1982**, *104*, 3520.
68) Jiang, Z.; Dahlen, G. M.; Houseknecht, K.; Sen, A. *Macromolecules* **1992**, *25*, 2999.
69) Jiang, Z.; Dahlen, G. M.; Houseknecht, K.; Sen, A. *Polym. Prepr. - Am. Chem. Soc., Div. Polym. Chem.* **1992**, *33(1)*, 1233.
70) Weissermel, K.; Arpe, H.-J. *Industrial Organic Chemistry*; 3rd ed., VCH: Weinheim, 1988
71) Heck, R. F. *Palladium Reagents In Organic Synthesis*; Academic Press: New York, 1985
72) Heck, R. F. *Comprehensive Organic Synthesis*; Pergamon: Oxford, 1991; Vol. 4, pp. 833
73) Blaser, H.-U.; Spencer, A. *J. Organomet. Chem.* **1982**, *233*, 267.

CHAPTER 2

Cationic Nickel(II) Complexes of Chelating Di-N-Heterocyclic Carbenes

2.1 Introduction

The aim of the work described in chapters 2 and 3 was to prepare new nickel(II) and palladium(II) complexes of chelating bidentate N-heterocyclic carbenes, and explore their activity as pre-catalysts for olefin polymerisation, olefin / CO copolymerisation and the Heck coupling reaction. Chapter 2 is concerned with ligand synthesis and reactivity with nickel(II) precursors.

Currently, N-heterocyclic carbene ligands are regarded as strongly σ-donating Lewis bases with poor π-acceptor properties, and are therefore very similar as ligands to electron-rich alkylphosphines and N donors such as pyridine or acetonitrile (section 1.2.3).[1] Phosphines are widely used in transition metal chemistry, and are important as ancillary ligands in homogeneous catalysis (e.g. hydroformylation (Co^I / PR_3, Rh^I / PR_3), hydrogenation (Rh^I / PPh_3), hydrocyanation (Ni^0 / P(*o*-$C_6H_4Me)_3$) and C-C coupling (Pd^{II} / P(*o*-$C_6H_4Me)_3$). Furthermore, chelating *bis*-phosphines are often used to improve the activity or selectivity of certain catalytic systems compared to the mono-phosphine equivalents: Palladium(II) complexes such as $[(dppp)Pd(MeCN)_2][BF_4]_2$ (dppp = $Ph_2P(CH_2)_3PPh_2$) have been established as the most efficient catalysts for the copolymerisation of α-olefins with carbon monoxide[2] (section 1.3.2) and chiral *bis*-phosphine ligands are used in numerous enantioselective reactions (e.g. rhodium(I) catalysts convert prochiral alkenes of the type R'CH=C(NHR_2)CO_2R" to chiral amino acids with optical yields greater than 95 %).[3-6] Great potential exists to develop N-heterocyclic carbene ligands as alternatives to phosphines in homogeneous catalysis: Of the reactions studied to date carbene complexes are more thermally robust than their phosphine equivalents, because degradation of phosphine ligands via P-C bond cleavage readily occurs at elevated temperatures limiting the temperature range of catalysis. In addition, metal carbene bonds are kinetically robust negating the need for excess ligand as is the case for phosphine-based cataysts.[7] Furthermore, chelating dicarbene ligands (figure 2.1) can be easily modified by variation of the N-substituents R and the backbone (CR'R")$_n$ of the diimidazolium salt precursor. This would allow for relatively easy ligand design with respect to improving the properties, e.g. stereoselectivity, of a particular catalyst.

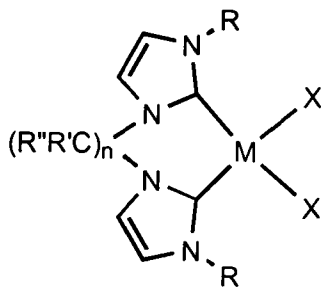

M = Ni, Pd

X = halide, alkyl

Figure 2.1 Palladium(II) and nickel(II) target compounds, incorporating chelating bidentate N-heterocyclic carbene ligands.

Given the similar electronic properties of N-heterocyclic carbenes and N-donor ligands, it was also conceivable that chelating dicarbene complexes of nickel(II) and palladium(II) could act as pre-catalysts for the polymerisation of α-olefins, in an analogous manner to the diimine catalysts prepared by Brookhart et al. in 1995.[8] Section 1.3.1 contains a more detailed account of olefin polymerisation using diimine pre-catalysts, and explains that an essential feature of the diimine ligands is their extreme steric bulk: It was therefore relevant to the aim of the work in this thesis to synthesise bidentate N-heterocyclic carbene ligands with bulky N-substituents R (figure 2.1).

Brookhart et al. showed that the degree of branching in the polymer (and hence the physical properties of the polymer) is sensitive to the nature of the diimine ligand, and in particular to the nature of the bulky aryl groups.[9] This ability to directly affect the nature of the polymer products by variation of ligand properties was also observed by Drent et al. for the palladium(II) / phosphine catalysed copolymerisation of ethylene and CO (as mentioned above): It was shown that the molecular weight of the copolymer product was sensitive to the chain length n of the palladium(II) catalyst diphosphine ligand $Ph_2P(CH_2)_nPPh_2$.[2] It was therefore conceivable that variation of the N-substituents R, as well as the backbone $(CR'R'')_n$ bridging the two N-heterocyclic carbene functionalities, could lead to variation in the physical properties of any polymer or copolymer produced using chelating dicarbene catalysts.

The nickel(II) and palladium(II) *cis*-dihalide or -dialkyl dicarbene complexes shown in figure 2.1 were considered suitable target compounds because of their potential to act as

olefin polymerisation pre-catalysts similar to the Brookhart diimine systems, and because of their potential to act as olefin / CO copolymerisation pre-catalysts similar to the palladium(II) diphosphine systems described by Drent.

At the commencement of the research described in this thesis there were no known nickel complexes incorporating chelating dicarbene ligands, although Herrmann et al. had synthesised the *trans*-di(monocarbene) nickel(II) dihalide complexes shown in scheme 2.1. The compounds were synthesised by treating $Ni(THF)_2X_2$ or $Ni(PPh_3)_2X_2$ (X = Cl, Br, I) with two equivalents of the free carbene, and also via reaction of two equivalents of the corresponding imidazolium salt with nickel acetate.[10]

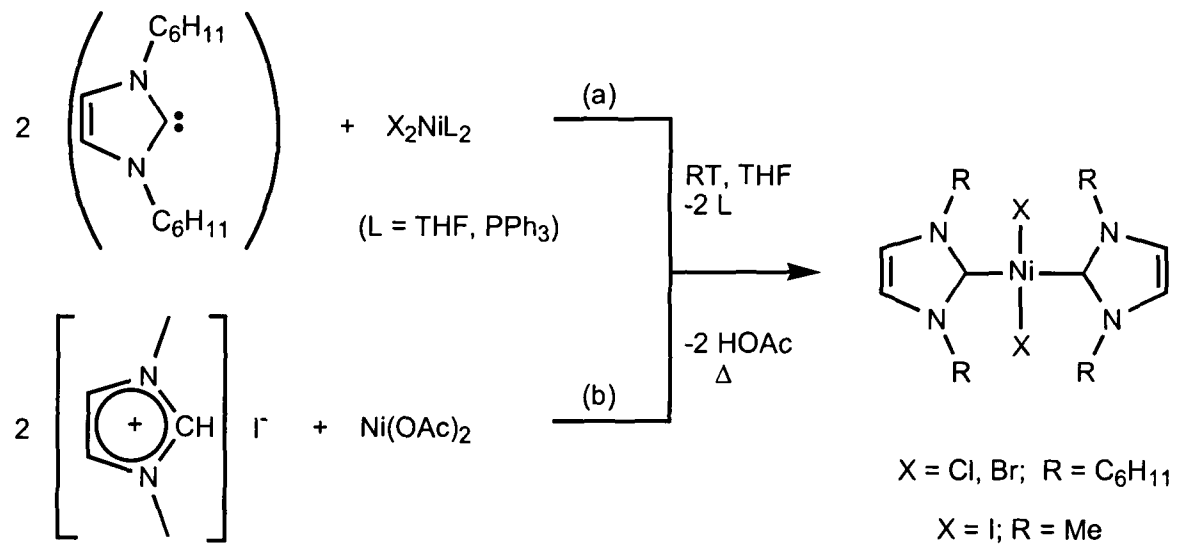

Scheme 2.1 Formation of *trans*-di(monocarbene) Ni^{II} dihalide complexes by *in situ* deprotonation of the imidazolium salt or by the free carbene route.

Furthermore, in 1995 Herrmann et al. claimed to have synthesised a chelating dicarbene palladium(II) diiodide complex by reaction of the diimidazolium salt with palladium acetate (Eq. 28),[7] but the compound was not structurally characterised: It was later shown to be a dinuclear palladium(II) complex with two bridging dicarbene ligands resulting in a similar elemental analysis and NMR spectrum, but with slightly different chemical shifts to the chelating compound (which was eventually synthesised and structurally characterised by Herrmann et al. in 1998 (section 1.2.5)).[11] These, and similar monocarbene complexes were subsequently studied as pre-catalysts for several C-C coupling reactions (sections 1.2.6(e) and 1.2.6(f)).

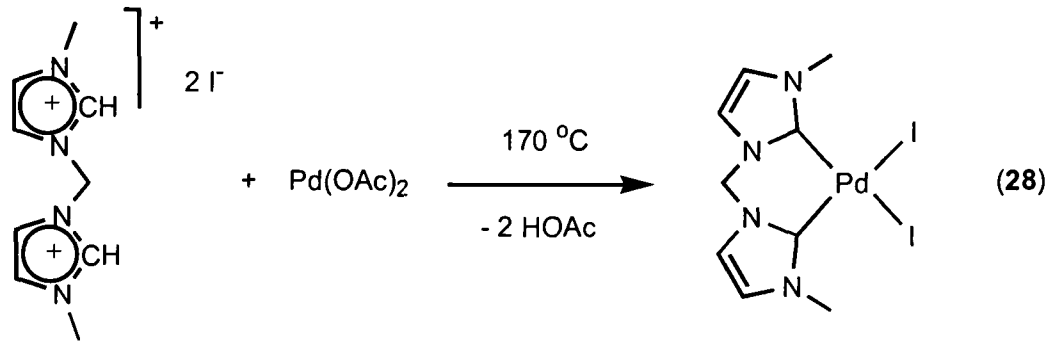

(28)

No olefin polymerisation or olefin / CO copolymerisation studies using N-heterocyclic carbene compounds had been reported at the commencement of the research in this thesis. However, in 1999 Herrmann et al. synthesised a dicationic palladium(II) dicarbene complex which catalysed the copolymerisation of ethylene and CO (section 1.2.6(g)).[12]

2.2 Synthesis and Characterisation of Diimidazolium Salts

2.2.1 Synthesis of 1-*tert*-Butylimidazole

1-*tert*-Butylimidazole was chosen as the precursor to the diimidazolium salts in order to fulfil the aim of having bulky N-substituent (*tert*-butyl) groups on the carbene ligand. 1-*tert*-butylimidazole was prepared by a modification of the imidazole synthesis discovered by Radziszewski, involving the condensation of a dicarbonyl compound with an aldehyde and ammonia.[13,14] This method can be applied to the synthesis of substituted imidazoles,[15] and 1-*tert*-butylimidazole can be synthesised via condensation of glyoxal with formaldehyde, *tert*-butylamine and ammonia (Eq. 29). An equimolar mixture of the reactants in propan-2-ol and water is refluxed at 70-80 °C for 2 hours. After evaporation of the propan-2-ol and water the product is isolated by vacuum distillation as a colourless to pale yellow liquid. The following signals are observed in the ^{1}H NMR spectrum (C_6D_6) of pure 1-*tert*-butylimidazole: δ 0.93 (9H, s, C(C*H*$_3$)$_3$), 6.63 (1H, s, NC*H*), 7.31 (1H, s, NC*H*), 7.48 (1H, s, NC*H*). Typically yields of over 70 g (44 %) were obtained.

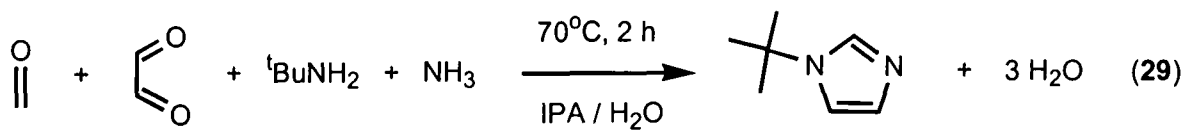

(29)

2.2.2 Synthesis of 1,1'-Methylene*bis*(3-*tert*-butylimidazolium) Diiodide (1)

In 1989 Williams et al. reported the synthesis of 1,1-methylene*bis*(3-methylimidazolium) diiodide (Eq. 30). A mixture of diiodomethane, 2 equivalents 1-methylimidazole and ethyl acetate (solvent) are refluxed for 12 hours to give a white precipitate (crude yield = 70 %). Recrystallisation from hot ethanol produces white needles which analyse as pure product:[16]

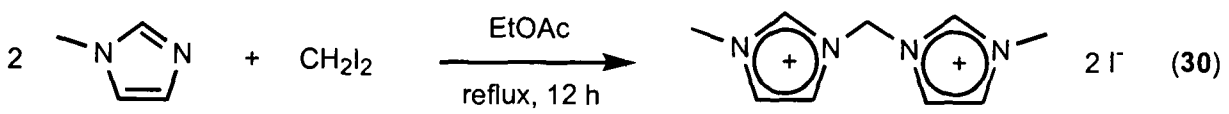

(**30**)

This synthesis was repeated using a mixture of diiodomethane, 2 equivalents 1-*tert*-butylimidazole and ethyl acetate. Refluxing for 12 hours gave a white precipitate. The precipitate was isolated by filtration, washed with diethyl ether and recrystallised from hot ethanol which gave white needles. However, ^{1}H NMR spectroscopy and elemental analysis were consistent with monomeric imidazolium salt (scheme 2.2), rather than the desired product. Repeating the synthesis at a higher temperature (130 °C) and longer reaction time (24 h) also gave the monomeric salt. It was therefore decided to change the solvent from ethyl acetate to 1,4-dioxane, based on the synthesis of a trimeric imidazolium salt using 1-*tert*-butylimidazole.[17] Refluxing a mixture of diiodomethane, 2 equivalents 1-*tert*-butylimidazole and 1,4-dioxane (24 h, 120 °C) gave a cream precipitate. Elemental analysis and ^{1}H and ^{13}C{^{1}H} NMR spectroscopy were consistent with the desired product 1,1'-methylene*bis*(3-*tert*-butylimidazolium) diiodide (**1**) (scheme 2.2).

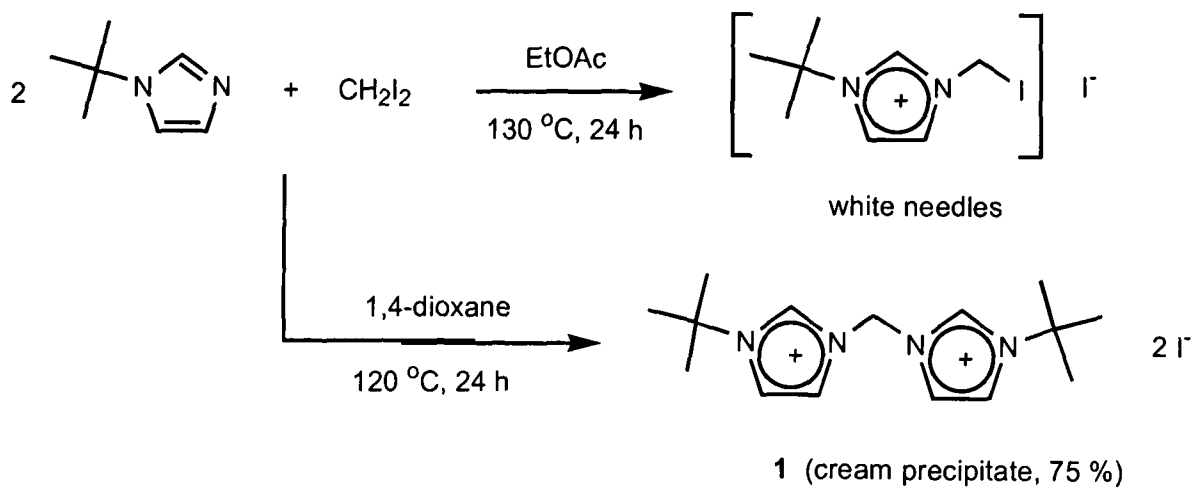

Scheme 2.2 Contrasting reactions between 1-*tert*-butylimidazole and diiodomethane using two different solvents.

2.2.3 Syntheses of 1,1'-Methylene*bis*(3-*tert*-butylimidazolium) Dibromide (2) and 1,1'-(1,2-Ethylene)*bis*(3-*tert*-butylimidazolium) Dibromide (3)

Refluxing mixtures of dibromomethane or 1,2-dibromoethane, 2 equivalents 1-*tert*-butylimidazole and 1,4-dioxane (24 h, 150 °C) gave cream precipitates. Elemental analyses and ^{1}H and $^{13}C\{^{1}H\}$ NMR spectroscopy were consistent with the desired products 1,1'-methylene*bis*(3-*tert*-butylimidazolium) dibromide (**2**) and 1,1'-(1,2-ethylene)*bis*(3-*tert*-butylimidazolium) dibromide (**3**) (scheme 2.3). Typically, near quantitative yields of over 30 g were obtained. Although air-stable, the diimidazolium dibromide salts are hygroscopic and were stored under nitrogen or argon.

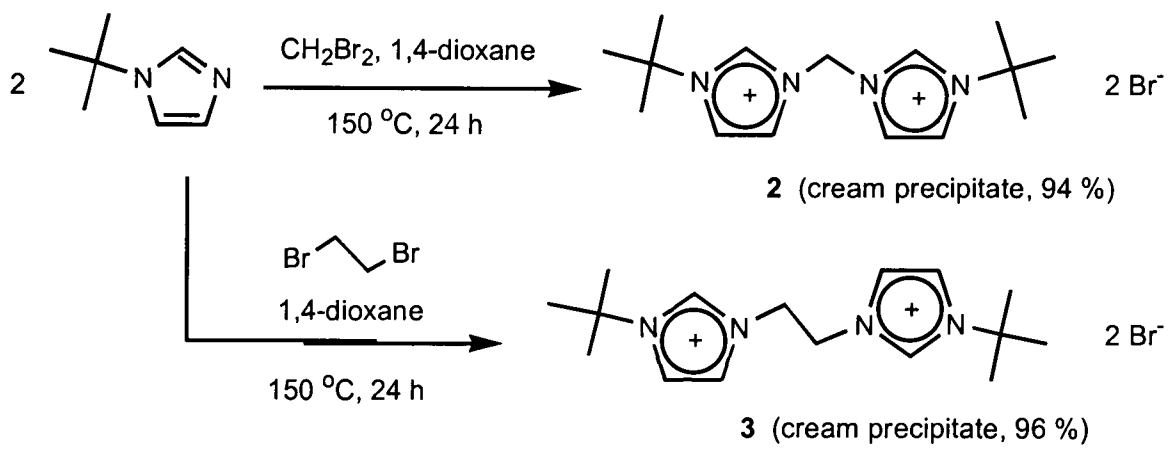

Scheme 2.3 Synthesis of diimidazolium dibromide salts.

The diimidazolium salts **1-3** were found to be soluble in water, alcohols, DMSO and dichloromethane, and insoluble in 1,4-dioxane, THF, diethyl ether and hydrocarbon solvents.

2.2.4 NMR Spectroscopy of Diimidazolium Salts 1-3

^{1}H and $^{13}C\{^{1}H\}$ NMR spectroscopy (CD_3OD) of compounds **1-3** is as expected for imidazolium salts.[1,17] Characteristic low field chemical shifts (δ 9.5-9.8) are observed for the H^2 protons (the heterocyclic ring atoms are numbered as shown in figure 1.4). Furthermore, the H^2 protons are observed to undergo deuterium exchange; the low field signal disappears after 24 hours, accompanied by an increase in intensity of the CD_3OH residual protio solvent peak (δ 4.8). The H^4 and H^5 ring protons (δ 7.7-8.2) were not observed to exchange with deuterium. However, in a previous study by Avent et al.,

deuterium exchange with all three imidazolium ring protons was observed for 1-ethyl-3-methylimidazolium chloride in D_2O: Exchange was observed to be more rapid for H^2 than for H^4 and H^5.[18] Hence it may be concluded that all three protons of the imidazolium ring are acidic, and that H^2 is more acidic than H^4 and H^5.

2.2.5 X-Ray Crystal Structure of 1,1'-Methylene*bis*(3-*tert*-butylimidazolium) Dibromide (2)

Crystals suitable for X-ray structure determination (performed by Dr Richard Douthwaite) were grown by cooling a saturated aqueous solution of 1,1'-methylene*bis*(3-*tert*-butylimidazolium) dibromide (**2**) to 5 °C, and leaving it to stand for 1 week. Two views of the structure are shown in figure 2.2 with selected bond distances and angles shown in table 2.1. The asymmetric unit contains one molecule of **2** and two molecules of water of crystallisation. The distances and angles between the imidazolium ring atoms are very similar to those of other structurally characterised imidazolium salts.[19,20]

Bond	Length (Å)	Bond	Angle (°)
N(3)-C(4)	1.315(5)	N(3)-C(4)-N(5)	109.0(3)
C(4)-N(5)	1.336(5)	C(4)-N(5)-C(6)	108.6(3)
N(5)-C(6)	1.386(5)	N(5)-C(6)-C(7)	106.2(3)
C(6)-C(7)	1.342(6)	C(6)-C(7)-N(3)	108.1(3)
C(7)-N(3)	1.383(5)	C(7)-N(3)-C(4)	108.2(3)
N(5)-C(8)	1.449(5)	N(5)-C(8)-N(9)	111.0(3)
N(3)-C(18)	1.493(5)		

Table 2.1 Selected bond lengths and angles for 1,1'-methylene*bis*(3-*tert*-butylimidazolium) dibromide (**2**).

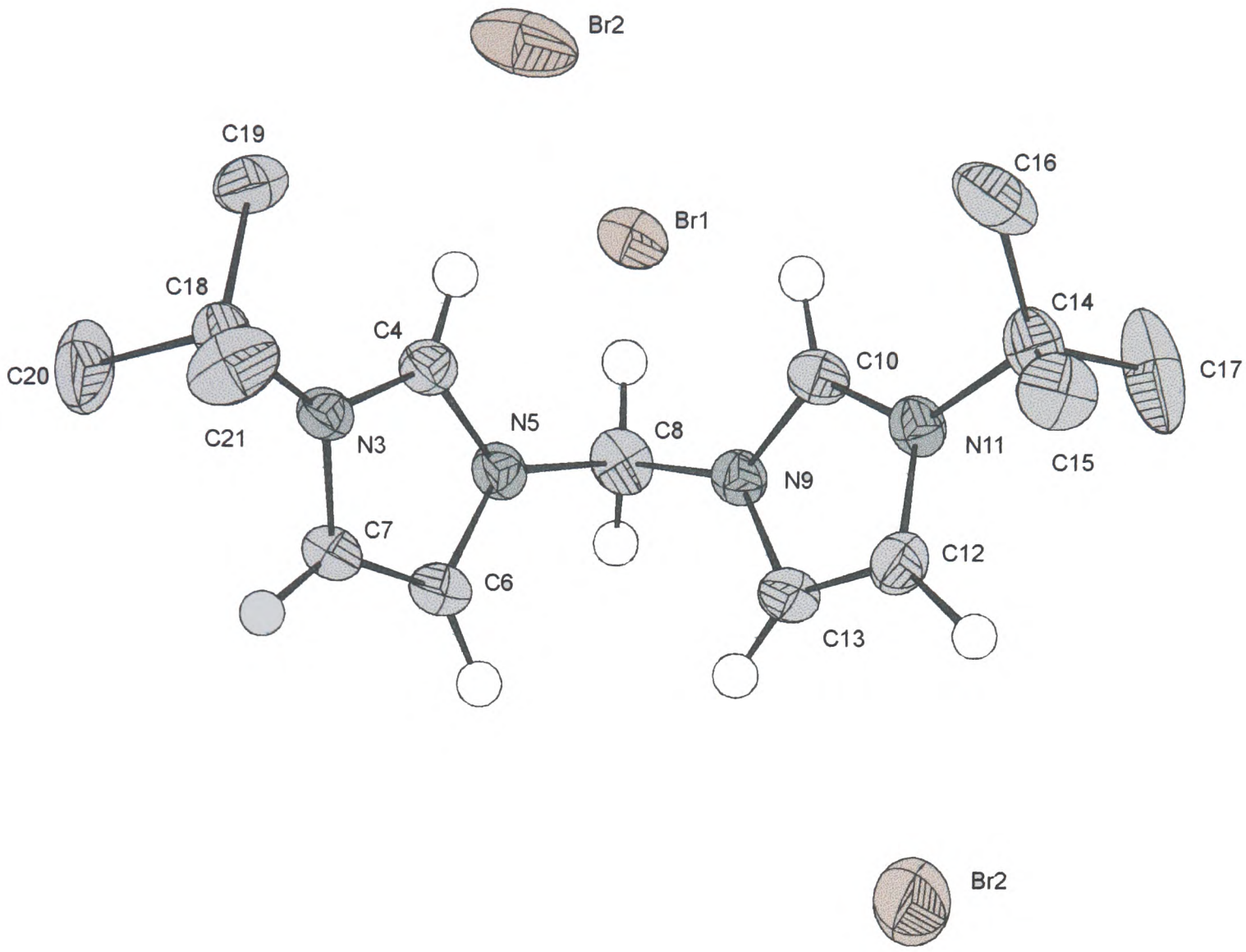

Figure 2.2 Two views of the X-ray structure of 1,1'-methylene*bis*(3-*tert*-butylimidazolium) dibromide (**2**). The *tert*-butyl hydrogen atoms are omitted for clarity.

2.3 Synthesis and Characterisation of Di-N-Heterocyclic Carbenes $^{tBu}CC^{meth}$ (4) and $^{tBu}CC^{eth}$ (5)

2.3.1 Synthesis of $^{tBu}CC^{meth}$ (4)

Two initial attempts were made, using published methods, to deprotonate 1,1'-methylene*bis*(3-*tert*-butylimidazolium) diiodide (**1**). The first attempt was made by treating diimidazolium salt **1** with 2 equivalents of sodium hydride and 10 mol % potassium *tert*-butoxide in THF, as established by Arduengo et al.[21] The reaction mixture, a brown suspension, was filtered to give a deep red solution, and the volatiles were removed under reduced pressure. ^{1}H NMR spectroscopy (C_6D_6) of the resulting red oil was consistent with that of 1-*tert*-butylimidazole, and the $^{13}C\{^{1}H\}$ NMR spectrum (C_6D_6) contained no signal within the range δ 210-220 characteristic of free N-heterocyclic carbenes. During reaction of **1** with NaH / KO^{t}Bu the deprotonation is supposedly effected in solution by the $^{t}BuO^{-}$ anion to give ^{t}BuOH, which in turn reacts with NaH forming hydrogen gas and regenerating the $^{t}BuO^{-}$ anion. However, it is conceivable that the rate of reprotonation of the dicarbene product $^{tBu}CC^{meth}$ (**4**) by ^{t}BuOH is comparable to the rate of reaction of ^{t}BuOH with NaH to give hydrogen gas. It was suspected that the free dicarbene product $^{tBu}CC^{meth}$ (**4**) is sensitive to protic species such as ^{t}BuOH, and the extreme moisture sensitivity of **4** has since confirmed this to be the case. With hindsight it is not surprising that the free dicarbene **4** could not be synthesised using NaH / KO^{t}Bu.

A second attempt at deprotonation of **1** using the liquid ammonia route established by Herrmann et al.[22] was also unsuccessful. After drying with potassium metal, liquid ammonia was condensed onto the diimidazolium salt **1** at -78 °C. Sodium hydride (2.2 equivalents) was added and the suspension immediately turned from white to pale yellow. The mixture was refluxed at -30 °C for 1 hour, after which the ammonia was allowed to evaporate. ^{1}H NMR spectroscopy of the THF extract in C_6D_6 was consistent with 1-*tert*-butylimidazole, and the $^{13}C\{^{1}H\}$ NMR spectrum contained no characteristic carbene signal in the range δ 210-220.

It was not understood why the liquid ammonia / NaH attempt failed, but it was nevertheless desirable to find a reliable method for deprotonation. It was therefore decided to use

potassium *bis*(trimethylsilyl)amide as the deprotonation reagent, rather than NaH. An obvious advantage is that the solubility of potassium *bis*(trimethylsilyl)amide in THF negates the need for a catalytic amount of a soluble base such as KO^{t}Bu. Furthermore, after deprotonation the *bis*-trimethylsilylamine by-product is volatile enough to be removed under reduced pressure, leaving only the free dicarbene product and the potassium halide salt, which can be separated by extraction of the former into a hydrocarbon solvent.

The free dicarbene $^{tBu}CC^{meth}$ (**4**) is prepared by stirring a THF suspension of 1,1'-methylene*bis*(3-*tert*-butylimidazolium) diiodide (**1**) or 1,1'-methylene*bis*(3-*tert*-butylimidazolium) dibromide (**2**) and 2.2 equivalents potassium *bis*(trimethylsilyl)amide for 12 hours at 25 °C (Eq. 31). The volatiles are removed and the residue extracted with 40-60 petroleum ether to give an orange solution. Cooling the solution to -80 °C gives a white powder, **4**. Yields of up to 5.0 g (63 %) are obtained and **4** can be stored in the solid state at -20 °C, under argon or nitrogen, without decomposition (discoloration was observed at room temperature).

The white powder **4** was found to decompose to a soluble brown oil within seconds of exposure to air. Furthermore, hydrocarbon, ether or THF solutions of **4** turned from pale yellow to green and then to dark red-brown within minutes of exposure to air, with no precipitation. ^{1}H NMR spectra (C_6D_6) of the decomposed carbene showed an imidazole-type *tert*-butyl resonance at δ 0.93, in contrast with the free carbene resonance normally observed at δ 1.41. Similarly, three imidazole ring proton resonances consistent with 1-*tert*-butylimidazole were also observed (δ 6.63, 7.31, 7.48), with no other resonance for the protons of the methylene bridge. The solubility and ^{1}H NMR spectroscopy of this decomposition product are not consistent with those of imidazolium cations, so exposure to air clearly causes a more complex decomposition (possibly to 1-*tert*-butylimidazole) than a simple protonation at each carbene carbon centre.

2.3.2 Synthesis of $^{tBu}CC^{eth}$ (5)

$^{tBu}CC^{eth}$ (**5**) is also synthesised by treating the corresponding diimidazolium salt, in this case 1,1'-(1,2-ethylene)*bis*(3-*tert*-butylimidazolium) dibromide (**3**), with 2.2 equivalents potassium *bis*(trimethylsilyl)amide in THF (Eq. 31). However, on completion of the

reaction the product is extracted into THF instead of 40-60 petroleum ether. This is because, in contrast with **4**, the ethylene-bridged equivalent is only sparingly soluble in 40-60 petroleum ether, and THF was found to be a more efficient extraction solvent than other alternatives such as toluene and diethyl ether. Cooling the THF extract to -80 °C gives a white powder, **5**. Yields of up to 5.7 g (60 %) are obtained. **5** was stored in the solid state at -20 °C, under argon or nitrogen, without decomposition (discoloration was observed at room temperature).

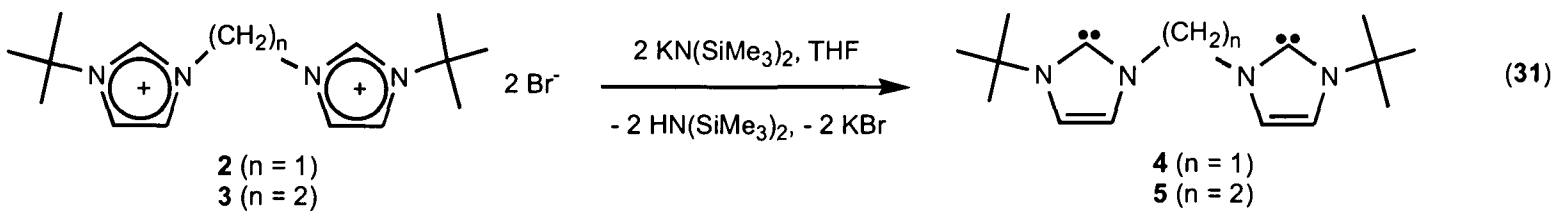

2 (n = 1)
3 (n = 2)

4 (n = 1)
5 (n = 2)

(31)

5 is apparently slightly less air-sensitive in the solid state than **4**, with exposure to air causing solid **5** to turn red-brown only within minutes. However, solutions behaved in a similar manner to those of **4**.

^{1}H NMR spectroscopy showed that dry, degassed C_6D_6 solutions of $^{tBu}CC^{meth}$ (**4**) and $^{tBu}CC^{eth}$ (**5**) are stable over hours at temperatures up to 100 °C, and that decomposition occurs at an appreciable rate above this temperature. Temperatures greater than 100 °C are therefore unsuitable for reactions of **4** and **5** which require long (> 12 hour) reaction times. ^{1}H NMR spectroscopy also showed that dry, degassed CD_2Cl_2 solutions of **4** and **5** decompose within minutes at 25 °C. Therefore dichloromethane is an unsuitable solvent for reactions of **4** and **5**.

2.3.3 Characterisation of $^{tBu}CC^{meth}$ (4) and $^{tBu}CC^{eth}$ (5)

The free dicarbenes were characterised by ^{1}H and $^{13}C\{^{1}H\}$ NMR spectroscopy (C_6D_6) with the latter showing resonances for the carbene carbon atoms of $^{tBu}CC^{meth}$ (**4**) and $^{tBu}CC^{eth}$ (**5**) at δ 214.5 and δ 214.0 respectively. This is much lower field than for the corresponding diimidazolium salts **2** and **3**, whose N(*C*H)N carbons resonate at δ 137.6 and δ 136.6 respectively. The heterocyclic ring protons of the free carbenes **4** and **5** resonate within the range δ 6.50-7.11, which is, as expected, significantly higher field than for the corresponding diimidazolium salts (δ 7.72-8.19). This NMR data indicates an increase in magnetic anisotropy of the heterocyclic rings, which is consistent with a decrease in the

aromaticity of the rings, upon deprotonation of the diimidazolium salts to form the free dicarbenes.[23]

Electron impact mass spectrometry showed a molecular ion peak at m/z = 274 for **5**, although only fragment ions such as [M^+ - ^{t}Bu] were observed for **4** which is more air-sensitive in the solid state. Both compounds were too air-sensitive for accurate C, H, N microanalyses.

2.4 Attempts to Prepare Nickel(II) *cis*-Dihalide Complexes of $^{tBu}CC^{meth}$ (4) and $^{tBu}CC^{eth}$ (5): Synthesis, Characterisation and Reactivity of Cationic Nickel(II) Complexes of 4 and 5

Nickel(II) *cis*-dihalide complexes of $^{tBu}CC^{meth}$ (**4**) and $^{tBu}CC^{eth}$ (**5**) were desirable not only because of their potential to act as pre-catalysts for a number of reactions including olefin polymerisation (sections 2.1 and 1.3.1), but also because of their synthetic potential. Standard metathesis reactions could be used to replace one or both of the halides with functionalities such as alkyls, alkoxides, amides and sulphides (scheme 2.4).

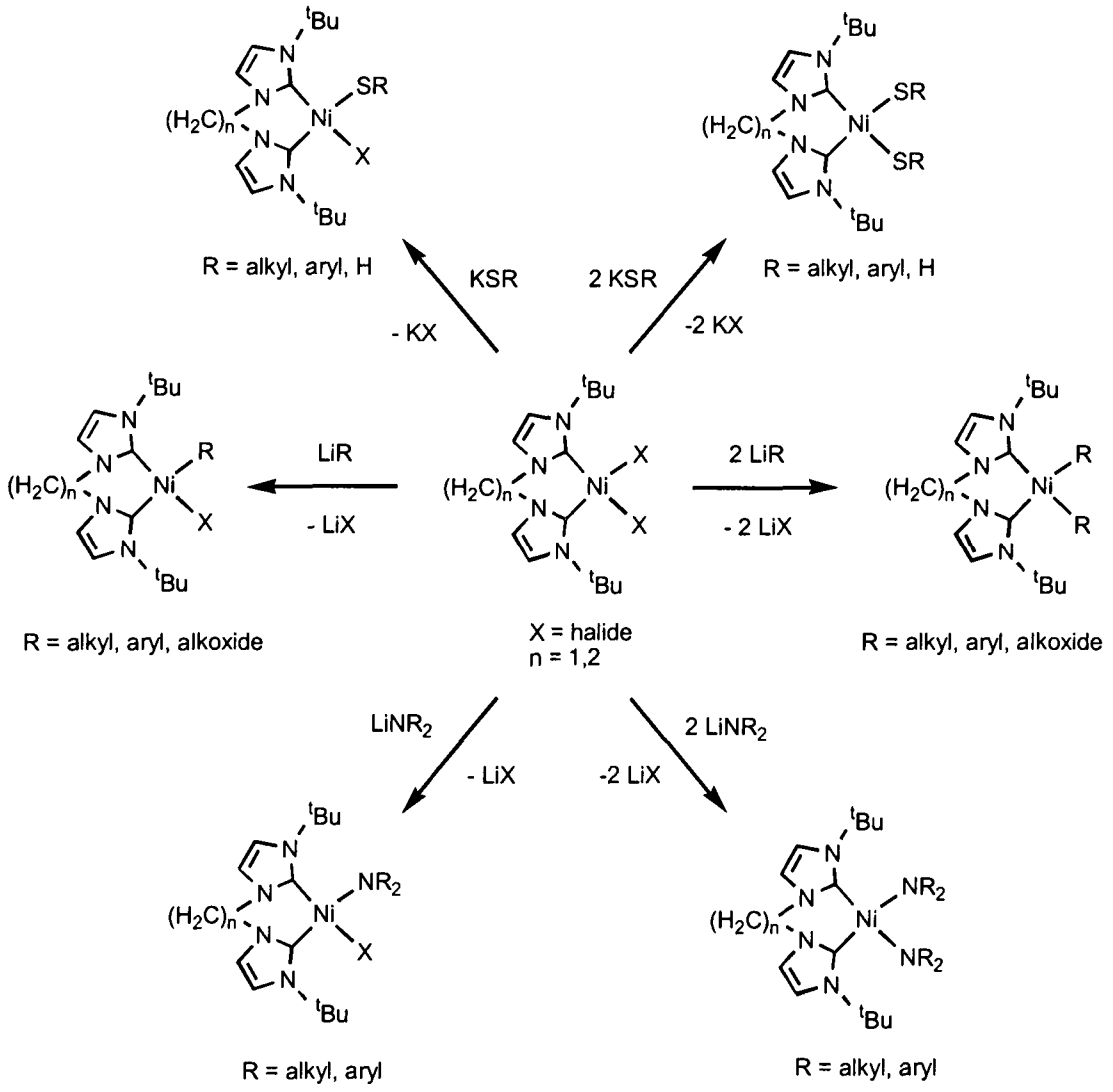

Scheme 2.4 Possible metathesis reactions of dicarbene *cis*-dihalide complexes of Ni^{II}.

2.4.1 Reaction Between $^{tBu}CC^{meth}$ (4) and $NiBr_2$(DME): Synthesis of $[Ni(^{tBu}CC^{meth})_2][Br]_2$ (6)

In an attempt to prepare $(^{tBu}CC^{meth})NiBr_2$ via dicarbene substitution of the labile DME ligand, $NiBr_2$(DME) was treated with 1 equivalent of $^{tBu}CC^{meth}$ (**4**) in DME (0 °C). After

reaction a pale yellow precipitate was isolated. ^{1}H NMR spectroscopy (CD_3OD) showed a mixture of products, with many peaks observed in the *tert*-butyl region (δ 1.0-2.5) and the methylene bridge / imidazole ring proton region (δ 6.0-8.5). However, a small quantity of single crystals suitable for X-ray structure determination were grown by cooling the impure NMR sample to -20 °C for 1 month.

The X-ray crystal structure was successfully determined by Dr Richard Douthwaite, showing the compound to be the dicationic *bis*(dicarbene) nickel(II) complex $[Ni(^{tBu}CC^{meth})_2][Br]_2$ (**6**) (Eq. 32). The compound **6** was also characterised by ^{1}H and $^{13}C\{^{1}H\}$ NMR spectroscopy (CD_3OD) of the remaining crystals.

Several attempts were made to prepare **6** in high yield by addition of 2 equivalents of **4** to 1 equivalent of $NiBr_2$(DME) (Eq. 32). After the addition, the pale yellow precipitate was isolated and recrystallised from methanol at -20 °C. However, ^{1}H NMR spectroscopy (CD_3OD) showed that the products invariably contained approximately 20 % of an unknown impurity, from which **6** could not be readily separated. Crude yields of up to 27 % were obtained. Complex **6**, a pale yellow powder, is air-stable and soluble in alcohols, water and DMSO but insoluble in other common organic solvents such as dichloromethane and THF.

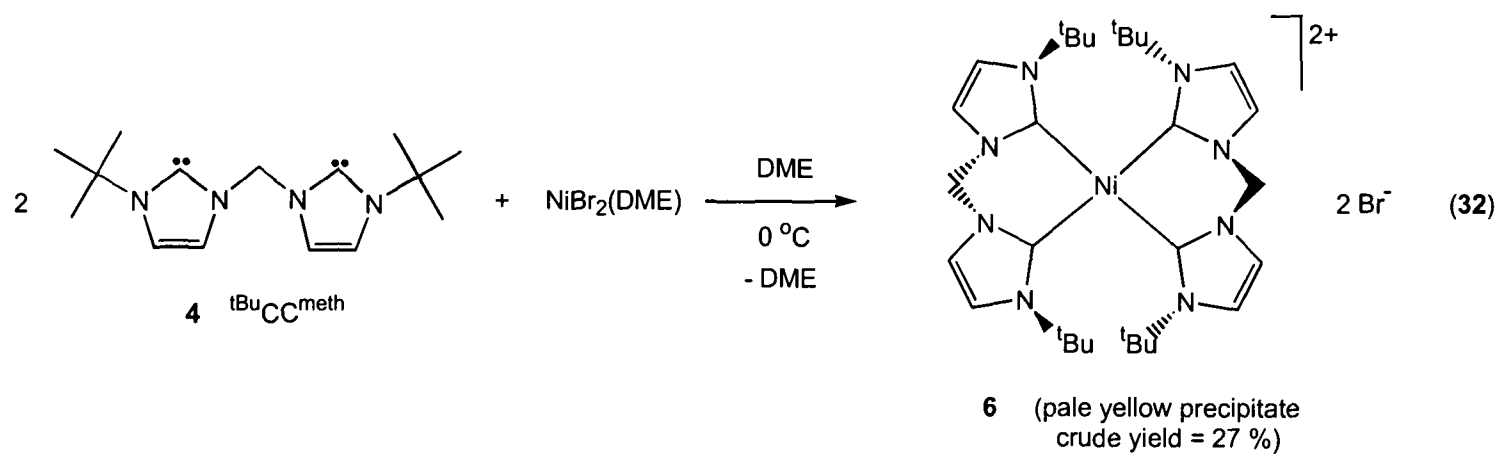

The reaction showed in equation 32 is in contrast to that described by Herrmann et al. between the diimidazolium diiodide salt **1** and $Ni(OAc)_2$ in DMSO, where reaction does not occur to give $[Ni(^{tBu}CC^{meth})_2][I]_2$ (Eq. 33).[24] This discrepency between the free carbene and diimidazolium salt routes is most likely due to the latter metathesis reaction requiring a more congested transition state compared to substitution by free dicarbene, even if via predominantly an associative mechanism. An intermediate in the synthesis of homoleptic

bis(dicarbene) nickel(II) complexes by the diimidazolium salt route, proposed by Herrmann and co-workers,[25] is shown in figure 1.11.

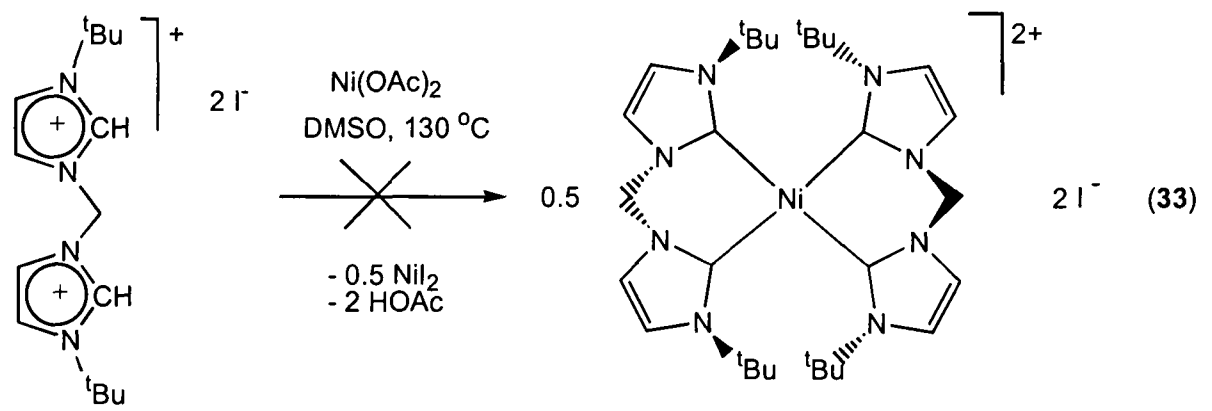

(33)

2.4.2 Characterisation of $[Ni(^{tBu}CC^{meth})_2][Br]_2$ (6)

^1H and $^{13}C\{^1H\}$ NMR spectroscopy of the single crystals of **6** in CD_3OD were consistent with a *bis*(dicarbene) nickel(II) complex 'locked' in a *trans*-double boat conformation. The ^1H NMR spectrum is shown in figure 2.3. A single resonance for the four *tert*-butyl groups is observed at δ 1.45, and two doublets ($^2J_{HH}$ = 14 Hz) at δ 6.65 and 7.11 are assigned to the magnetically inequivalent protons of each methylene bridge, showing the structure to be rigid at this temperature with respect to equilibration of these protons. This is probably due to steric congestion that would be present in the planar intermediate of a 'butterfly-type' conformational movement (figure 1.10) of the ligands. The lack of equilibration of the methylene bridge protons is therefore unsurprising, given that *bis*(dicarbene) nickel(II) dicationic analogues with less bulky *N*-alkyl substituents also show no equilibration.[24] $^{13}C\{^1H\}$ NMR spectroscopy shows a singlet at δ 170.3 attributable to the four equivalent carbene carbon atoms. This value is shifted ca. 30 ppm upfield with respect to those observed for the neutral nickel N-heterocyclic carbene complexes **12** and **13** studied in chapter 3, and is characteristic of a cationic metal complex.[12,24,26] $^{13}C\{^1H\}$ NMR spectroscopy of the palladium complex $[Pd(^{Me}CC^{meth})_2][I]_2$, prepared in low yield from free dicarbene and PdI_2 (Eq. 11), shows a similar singlet for the carbene carbons at δ 168.8,[26] and several nickel complexes $[Ni(^{R}CC^{meth})_2][I]_2$ formed in high yield from diimidazolium salts and $Ni(OAc)_2$ (Eq. 13) show singlets in the range δ 171.07-173.08 attributable to the carbene carbon atoms.[24]

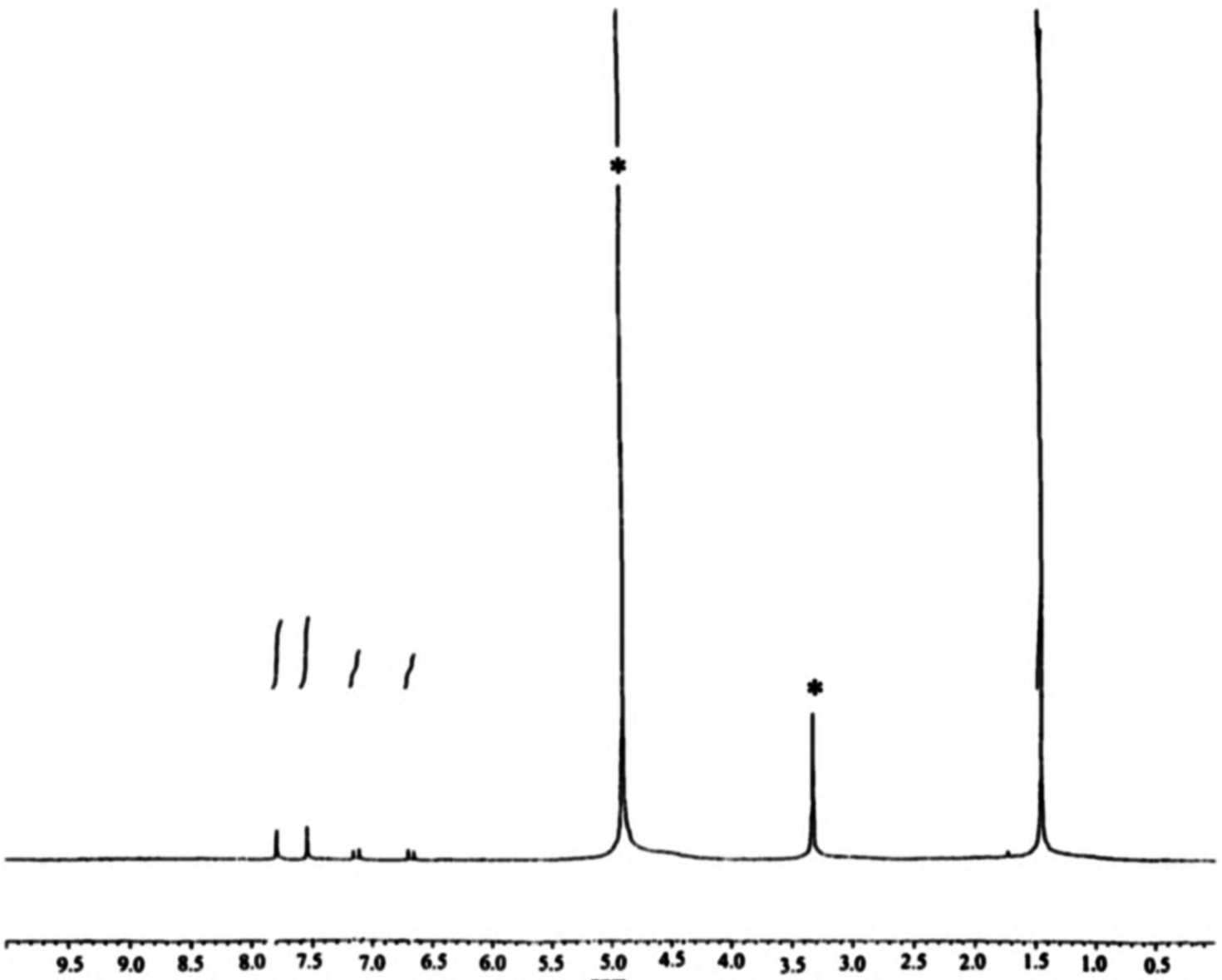

Figure 2.3 300 MHz ^{1}H NMR spectrum of [Ni(^{tBu}CC^{meth})$_2$][Br]$_2$ (**6**) in CD_3OD (* = solvent).

The X-ray crystal structure of **6** is shown in figure 2.4 and selected bond lengths and angles are shown in table 2.2. The asymmetric unit contains one half of the dication, one bromide, and two molecules of methanol. The nickel atom is located at the centre of inversion; therefore half of the dication shown in figure 2.4 is symmetry-generated. The homoleptic carbene cation of **6** is analogous to that of the palladium complex [Pd(^{Me}CC^{meth})$_2$][I]$_2$ (Eq. 11),[26] and the nickel complexes shown in equation 13, of which the *N*-methyl substituted derivative [Ni(^{Me}CC^{meth})$_2$][I]$_2$ was structurally characterised.[24] A *trans* double boat conformation is adopted by the cation of **6** in a manner similar to that for [Pd(^{Me}CC^{meth})$_2$][I]$_2$ and [Ni(^{Me}CC^{meth})$_2$][I]$_2$. Coordination at the nickel atom is close to square planar with Ni-C bond lengths Ni(2)-C(3) = 1.936(4) Å and Ni(2)-C(7) = 1.928(4) Å which are longer than those observed for [Ni(^{Me}CC^{meth})$_2$][I]$_2$ (1.909(2) Å). Comparison of the bite angles of **6** C(3)-Ni(2)-N(7) (83.57(17)°) and [Ni(^{Me}CC^{meth})$_2$][I]$_2$

(86.64(9)°) and the twist angles of the heterocyclic rings relative to the coordination plane of **6** (54.6(6) and 56.5(7)°) and $[Ni(^{Me}CC^{meth})_2][I]_2$ (39.64(9) and 40.85(8)°) indicate that the conformation adopted primarily results from minimisation of ^{t}Bu-^{t}Bu nonbonding interactions.

Electrospray mass spectrometry showed a molecular ion (m/z = 289 $[M^{2+}]$) corresponding to the dication $[Ni(^{tBu}CC^{meth})_2]^{2+}$.

Bond	Length (Å)	Bond	Angle (°)
Ni-C(3)	1.936(4)	C(3)-Ni-C(7)	83.57(17)
Ni-C(7)	1.928(4)	C(3)-Ni-C(7')	96.43(17)
C(3)-N(4)	1.366(5)	N(4)-C(3)-N(17)	104.1(4)
C(3)-N(17)	1.354(6)	N(6)-C(7)-N(8)	104.0(3)
N(6)-C(7)	1.346(5)	Ni-C(3)-N(4)	114.3(3)
C(7)-N(8)	1.354(5)	C(3)-N(4)-C(5)	123.1(4)
C(9)-C(10)	1.336(7)	N(4)-C(5)-N(6)	107.8(3)
C(15)-C(16)	1.326(7)	C(5)-N(6)-C(7)	122.4(3)
		Ni-C(7)-N(6)	115.7(3)
		C(5)-N(4)-C(15)	124.0(4)
		C(3)-N(4)-C(5)	123.1(4)
		C(5)-N(6)-C(10)	125.0(3)
		C(7)-N(6)-C(10)	112.4(4)
		ring $twist_{C(3)}$*	54.6(6)
		ring $twist_{C(7)}$	56.5(7)

* The angle between the coordination plane defined by nickel and carbene carbon atoms and the heterocyclic ring containing C(n).

Table 2.2 Selected bond lengths and angles for $[Ni(^{tBu}CC^{meth})_2][Br]_2$ (**6**).

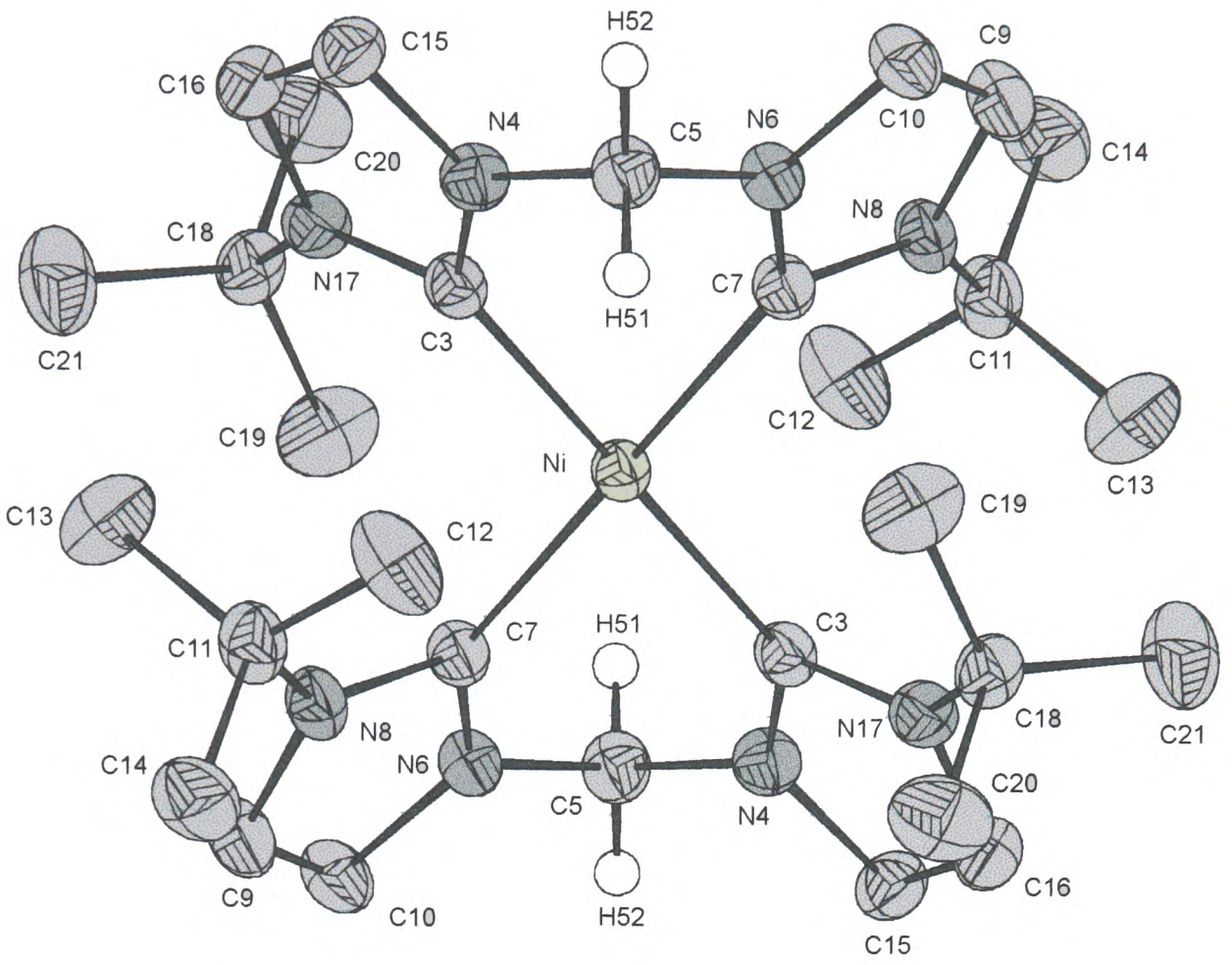

Figure 2.4 Two views of the dication $[Ni(^{tBu}CC^{meth})_2]^{2+}$ from the X-ray structure of **6**. Hydrogen atoms except for H51 and H52 are omitted for clarity.

2.4.3 Reaction of $^{tBu}CC^{meth}$ (4) with $NiBr_2(DME)$ in the Presence of Na/Hg Amalgam

In an attempt to prepare the neutral nickel(0) complex $Ni(^{tBu}CC^{meth})_2$, $NiBr_2(DME)$ was treated with 2 equivalents $^{tBu}CC^{meth}$ (**4**) in the presence of excess Na/Hg amalgam (Eq. 34). After reaction the mixture was extracted with 40-60 petroleum ether and toluene. ^1H NMR spectroscopy of the extracts showed a mixture of free **4** and 1-*tert*-butylimidazole, the latter possibly a decomposition product of the former. The toluene extract also contained unidentified decomposition products.

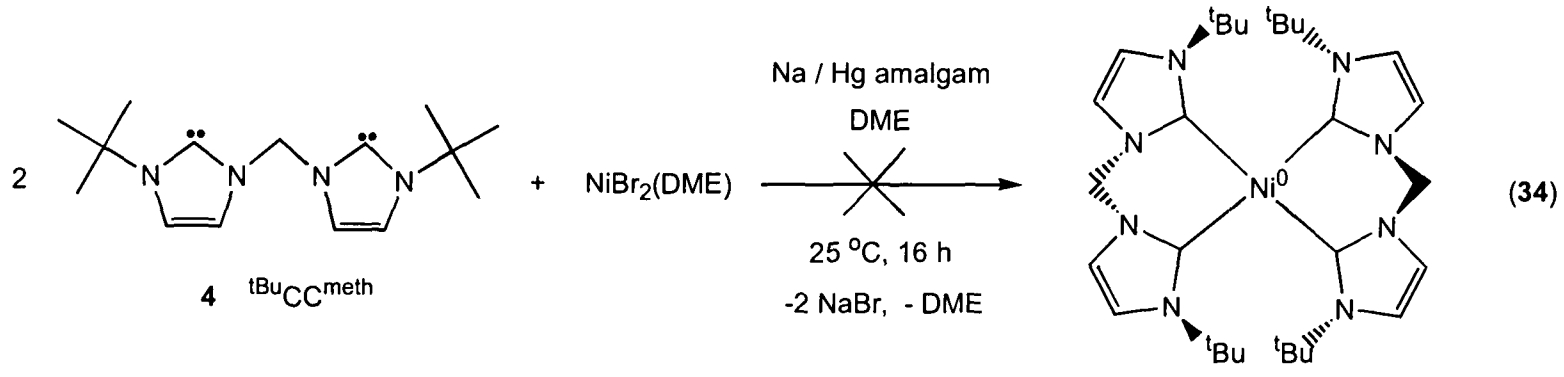

(34)

A *bis*(monocarbene) nickel(0) 14-electron complex is known (figure 1.9),[27] but no examples of 18-electron *tetrakis*(monocarbene) or *bis*(dicarbene) nickel(0) complexes have been reported, which is probably due to charge buildup at the nickel atom as a consequence of strong σ-donation and the absence of appreciable π-acidity of N-heterocyclic carbene ligands.

2.4.4 Reaction Between $^{tBu}CC^{eth}$ (5) and $NiBr_2(DME)$

Attempts to prepare either the *cis*-dibromide complex $(^{tBu}CC^{eth})NiBr_2$ or the ethylene-bridged analogue to **6**, $[Ni(^{tBu}CC^{eth})_2][Br]_2$, by reacting 1 or 2 equivalents respectively of $^{tBu}CC^{eth}$ (**5**) with $NiBr_2(DME)$ were unsuccessful (scheme 2.5). ^1H NMR spectroscopy (CD_3OD) of the pale yellow precipitates obtained showed mixtures of products, with many peaks observed in the *tert*-butyl region (δ 1.0-2.5) and the imidazole ring proton region (δ 6.5-8.5). At least two complex multiplets for the ethylene bridge protons would be expected in the range δ 2.5-7.0 for either of the desired products, although none were observed.

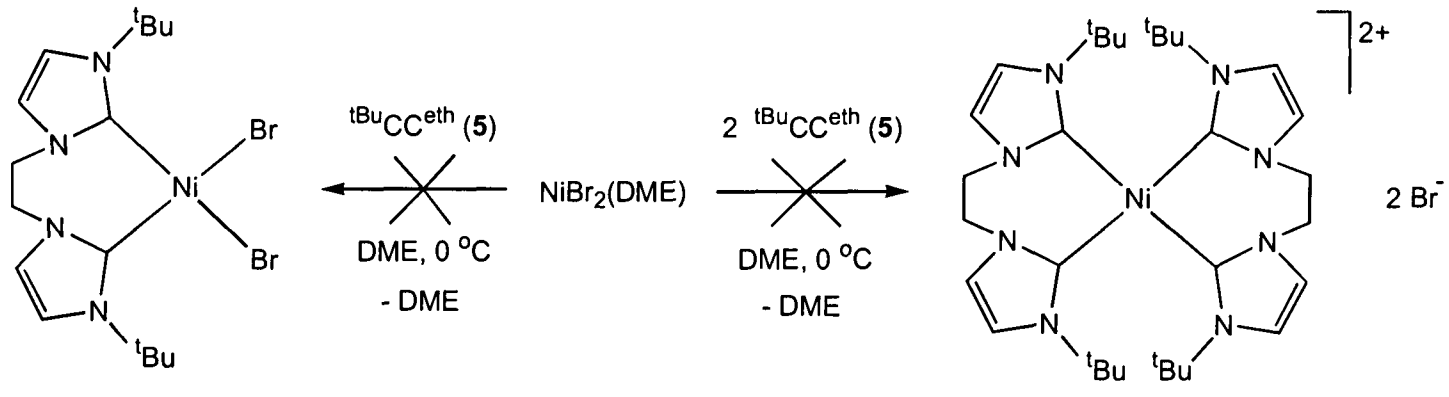

Scheme 2.5

Molecular modelling and examination of the X-ray structure of $[(^{tBu}CC^{eth})NiCl(PMe_3)][BPh_4]$ (**10**) (figure 2.18) indicate that substantial steric congestion would be present in the cation $[Ni(^{tBu}CC^{eth})_2]^{2+}$ due to nonbonding interactions between ^{t}Bu groups and the ethylene bridge of an opposing dicarbene ligand.

2.4.5 Reaction Between $^{tBu}CC^{meth}$ (4) and $NiBr_2(THF)_{1.5}$

In the light of the failure to synthesise $Ni(^{tBu}CC^{meth})Br_2$ by reaction of **4** with $NiBr_2(DME)$, it was decided to use a different nickel(II) precursor to achieve this aim. $NiBr_2(THF)_{1.5}$ was chosen in the light of previous work by Herrmann et al. in which labile THF ligands were substituted by N-heterocyclic carbene ligands to form *trans*-di(monocarbene) nickel(II) dihalide complexes (scheme 2.1).[10]

To a purple THF solution of $NiBr_2(THF)_{1.5}$ was added 1 equivalent of a THF solution of **4** which gave an orange supernatant and a beige precipitate. The precipitate was soluble in DMSO, acetonitrile and pyridine but insoluble in non polar organic solvents, THF and dichloromethane. Carbon, hydrogen and nitrogen microanalysis results were within 0.4 % of the calculated values for $Ni(^{tBu}CC^{meth})Br_2$, or $C_{15}H_{24}N_4NiBr_2$. Based on this empirical formula the yield was calculated to be 29 %.

Despite the analytical purity of the precipitate, ^{1}H NMR spectroscopy (d^6-DMSO and CD_3CN) showed a mixture of products, with many peaks observed in the *tert*-butyl region (δ 1.0-2.5) and the methylene bridge / imidazole ring proton region (δ 6.5-8.5). ^{1}H NMR spectroscopy (d^6-DMSO) showed the supernatant to contain a similar mixture of products. The dication $[Ni(^{tBu}CC^{meth})_2]^{2+}$ was not observed in the ^{1}H NMR spectra of either the beige precipitate or orange supernatant.

FAB mass spectrometry of the precipitate showed no molecular ion peak for Ni(^{tBu}CC^{meth})Br_2 at m/z = 479, although peaks at m/z = 318 and 399 were observed which are consistent with the fragments [Ni(^{tBu}CC^{meth}) – H] and [Ni(^{tBu}CC^{meth})Br] respectively. Peaks were also observed at m/z = 535, 578, 659 and 753 possibly due to fragment ions [Ni_2Br_2(^{tBu}CC^{meth}) – H] (m/z = 536), [Ni(^{tBu}CC^{meth})$_2$ – H] (m/z = 578), [NiBr(^{tBu}CC^{meth})$_2$] (m/z = 659) and [Ni_3Br_4(^{tBu}CC^{meth})] (m/z = 756).

Given the lack of a Ni(^{tBu}CC^{meth})Br_2 molecular ion peak at m/z = 479, and the observation of fragment ions in the range m/z = 535-753, it is reasonable to assume that if present, Ni(^{tBu}CC^{meth})Br_2 is not a major product, and that the products observed by ^{1}H NMR spectroscopy could generally have molecular weights greater than 479, and could therefore be dimers, trimers or oligomers as shown in figure 2.5. All the products shown have an empirical formula of $C_{15}H_{24}N_4NiBr_2$ (except for the neutral oligomer due to the THF end-groups) which is identical to that of Ni(^{tBu}CC^{meth})Br_2 and would account for the observed microanalytical data. Furthermore, the cationic nature of some of the oligomers shown could account for the low solubility of the beige precipitate in THF and dichloromethane.

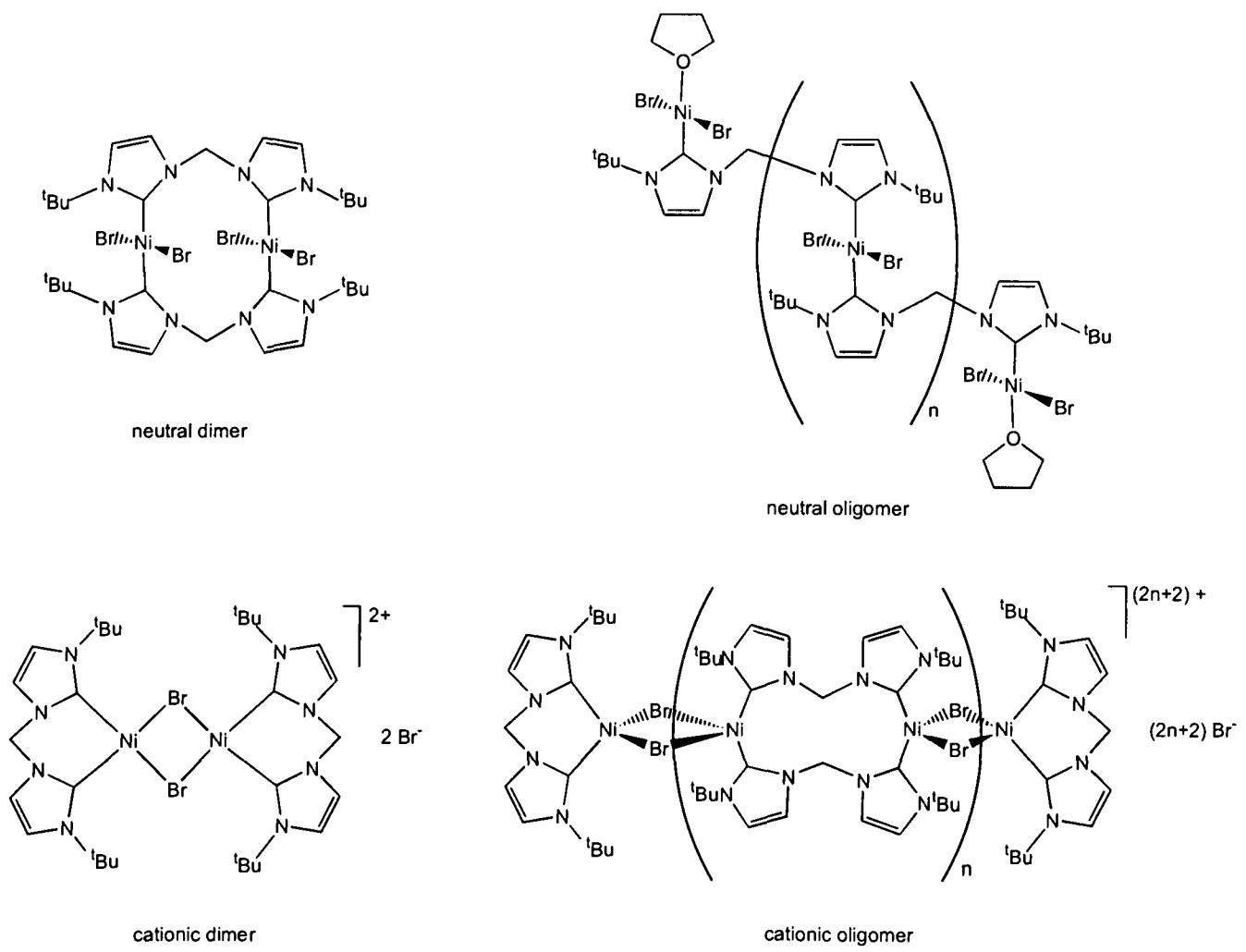

Figure 2.5 Possible dimeric and oligomeric products of the reaction between ^{tBu}CC^{meth} (**4**) and $NiBr_2(THF)_{1.5}$.

2.4.6 Reactions of the Beige Precipitate '[Ni(^{tBu}CC^{meth})Br$_2$]$_n$' with Lewis Bases PMe$_3$ and d^5-Pyridine

Following the characterisation of the stable cationic nickel(II) complex [(^{tBu}CC^{meth})NiCl(PMe$_3$)]Cl (**7**) (section 2.4.9), it was postulated that reaction of PMe$_3$ with the beige precipitate (from the reaction between ^{tBu}CC^{meth} (**4**) and NiBr$_2$(THF)$_{1.5}$) could yield the analogous compound [(^{tBu}CC^{meth})NiBr(PMe$_3$)]Br. A mixture of products with a formula '[Ni(^{tBu}CC^{meth})Br$_2$]$_n$' could conceivably react with n equivalents PMe$_3$ to give n equivalents of [(^{tBu}CC^{meth})NiBr(PMe$_3$)]Br (Eq. 35). This could involve the scission of oligomers (figure 2.5) to form the monomeric product, and/or a simpler reaction between Ni(^{tBu}CC^{meth})Br$_2$ and one equivalent of PMe$_3$.

As predicted, the compound [(^{tBu}CC^{meth})NiBr(PMe$_3$)]Br was formed upon treatment of the beige precipitate '[Ni(^{tBu}CC^{meth})Br$_2$]$_n$' with 1 equivalent PMe$_3$ (Eq. 35). An excess of pentane was added to the filtered *ortho*-dichlorobenzene reaction mixture, affording a yellow precipitate. Carbon, hydrogen and nitrogen microanalysis results were within 0.4 % of the calculated values for [(^{tBu}CC^{meth})NiBr(PMe$_3$)]Br. ^{1}H NMR spectroscopy (d^6-DMSO) showed the presence of [(^{tBu}CC^{meth})NiBr(PMe$_3$)]Br by comparison with the similar spectrum of the chloride analogue **7**, although impurity peaks were also present (estimated purity = 60 %).

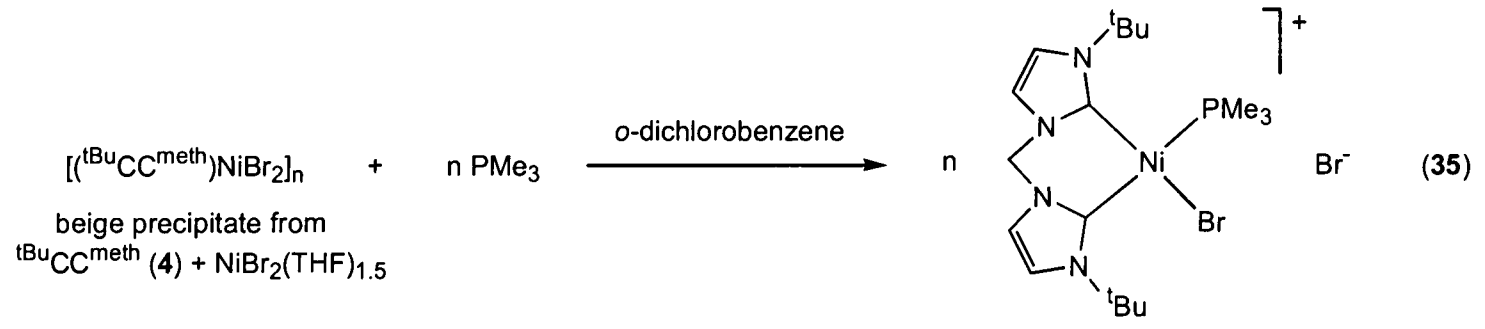

Similarly, ^{1}H NMR spectroscopy of the beige precipitate '[Ni(^{tBu}CC^{meth})Br$_2$]$_n$' in d^5-pyridine was consistent with the formation of the cationic d^5-pyridine adduct [(^{tBu}CC^{meth})NiBr(C$_5$D$_5$N)]Br (Eq. 36). Two singlets are observed for the ^{t}Bu groups, at δ 1.34 and 2.06, and two doublets at δ 8.20 and 8.46 are assigned to the protons of the dicarbene methylene bridge. The four imidazole ring protons resonate at δ 7.32, 7.42, 8.46 and 8.89. The spectrum shows a small amount of impurity (estimated purity = 90 %).

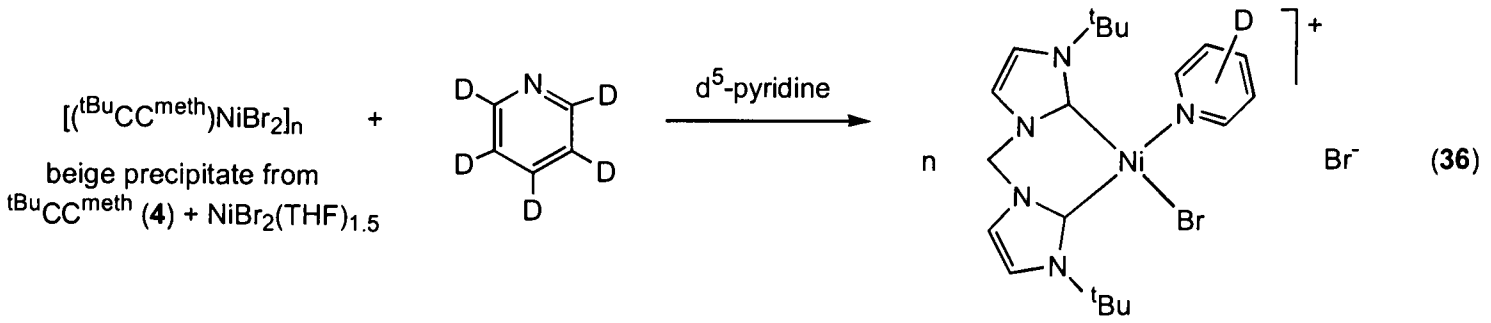

(36)

The formation of the cationic Lewis base adducts $[(^{tBu}CC^{meth})NiBr(PMe_3)]Br$ and $[(^{tBu}CC^{meth})NiBr(C_5D_5N)]Br$ is evidence to support the presence of nickel(II) $^{tBu}CC^{meth}$ bromide compounds, such as the desired *cis*-dihalide product $Ni(^{tBu}CC^{meth})Br_2$ and oligomers with the same empirical formula (figure 2.5), in the mixture of products obtained from reaction of $^{tBu}CC^{meth}$ (**4**) with $NiBr_2(THF)_{1.5}$. The nickel(II) centres of the *cis*-dihalide product $Ni(^{tBu}CC^{meth})Br_2$ and the postulated oligomers (figure 2.5) all possess two bromide ligands, one of which could act as a leaving group to facilitate the formation of a strong nickel-phosphorus or nickel nitrogen bond (depending on the Lewis base employed).

2.4.7 'High Dilution' Reaction Between $^{tBu}CC^{meth}$ (4) and $NiBr_2(THF)_{1.5}$

It was decided to attempt a final reaction between $^{tBu}CC^{meth}$ (**4**) and $NiBr_2(THF)_{1.5}$ using large amounts of solvent to minimise the concentration of the two reactant solutions. It was hoped that dropwise addition of a dilute solution of **4** to a solution of $NiBr_2(THF)_{1.5}$ of the same low concentration would maximise the 1:1 stoichiometry of the reaction throughout addition, and favour the formation of the desired product $Ni(^{tBu}CC^{meth})Br_2$ whilst disfavouring the formation of oligomeric products. The reaction of 2.81 mmol **4** with 2.67 mmol $NiBr_2(THF)_{1.5}$, in 1 litre of THF, resulted in a yellow precipitate. The precipitate was soluble in DMSO but insoluble in dichloromethane, THF and non-polar organic solvents.

^1H NMR spectroscopy (d^6-DMSO) showed that a much cleaner reaction than previously observed between these two reactants had occurred. A singlet (δ 1.31) was observed for the ^{t}Bu groups of the dicarbene ligand as well as two doublets (δ 7.59 and 7.88) for the imidazole ring protons. More surprisingly, the spectrum showed a singlet (δ 6.84) for the methylene bridge protons of the $^{tBu}CC^{meth}$ ligand, rather than the two doublets seen for every other characterised nickel(II) chelating $^{tBu}CC^{meth}$ complex. The magnetic equivalence of the methylene bridge protons indicates that the dicarbene ligand $^{tBu}CC^{meth}$ is most likely acting in a bridging mode between two nickel atoms. Indeed, ^1H NMR spectroscopy (C_6D_6)

of the structurally characterised complex $[(\mu\text{-}^{tBu}CC^{meth})\{Ni(PMe_3)Me_2\}_2]$ (**12**), in which $^{tBu}CC^{meth}$ bridges two nickel centres, also shows a singlet (δ 7.90) for the methylene bridge protons. It was postulated that the product of this second, 'high dilution' reaction of $NiBr_2(THF)_{1.5}$ with $^{tBu}CC^{meth}$ (**4**) could be the bridging dimer $[Br_2Ni(\mu\text{-}^{tBu}CC^{meth})_2NiBr_2]$, shown in equation 37. ^1H NMR spectroscopy of the yellow precipitate also showed the presence of 0.5 equivalents THF and ca. 0.1 equivalents diimidazolium salt impurity. $^{13}C\{^1H\}$ NMR spectroscopy (d^6-DMSO) was consistent with the postulated bridging dimer $[Br_2Ni(\mu\text{-}^{tBu}CC^{meth})_2NiBr_2]$, showing a single resonance at δ 168.0 for the 4 equivalent carbene carbon atoms. C, H, N, Ni, Br microanalysis results were only within 2.3 % of the calculated values for $[Br_2Ni(\mu\text{-}^{tBu}CC^{meth})_2NiBr_2](THF)$ due to the diimidazolium salt impurity observed by NMR spectroscopy.

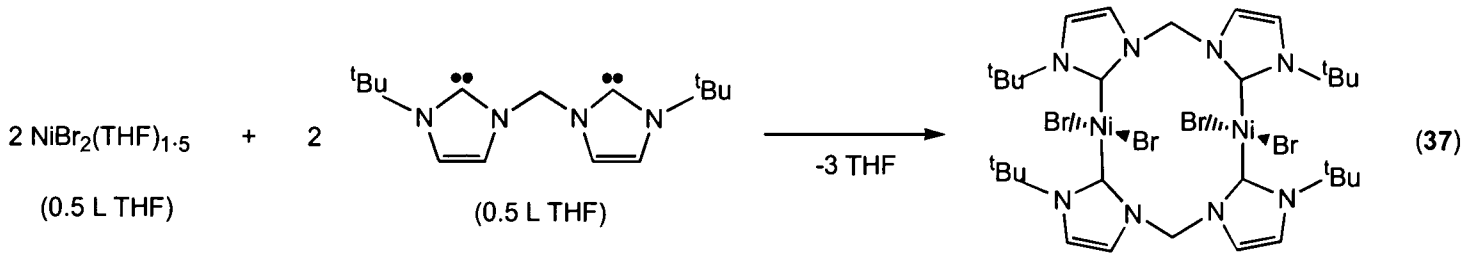

(37)

Unfortunately FAB mass spectrometry showed no molecular ion peaks for either the desired product $Ni(^{tBu}CC^{meth})Br_2$ (m/z = 479) or the postulated dimeric product $[Br_2Ni(\mu\text{-}^{tBu}CC^{meth})_2NiBr_2]$ (m/z = 958). Furthermore, slow evaporation of a SO_2 solution of the yellow precipitate did not afford single crystals suitable for X-ray diffraction, so the compound was not structurally characterised.

The yellow precipitate, possibly $[Br_2Ni(\mu\text{-}^{tBu}CC^{meth})_2NiBr_2]$, dissolved in ethanol to give a yellow solution. After removal of the volatiles, ^1H NMR spectroscopy (d^6-DMSO) of the resulting yellow solid was consistent with the formation of the dicationic *bis*(dicarbene) complex $[Ni(^{tBu}CC^{meth})_2][Br]_2$ (**6**). Herrmann et al. observed that after conversion of organometallic halide precursors into the corresponding ethoxides, the latter had sufficient basicity to deprotonate imidazolium salts, with the carbene ligand thus generated replacing the ethoxide ligand (scheme 2.6).[28] It is possible that a rearrangement process to form the dication **6** may have occurred via reaction of a cationic imidazolium moiety (e.g. a heterocyclic carbene ring which has been protonated by ethanol) with an intermediate nickel(II) ethoxide complex (e.g. scheme 2.7).

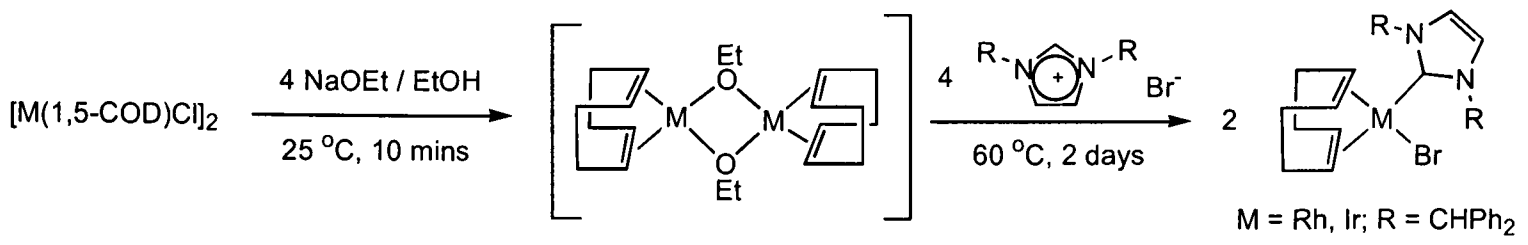

Scheme 2.6 Metal ethoxide complexes formed *in situ* deprotonate imidazolium salts to give N-heterocyclic carbene complexes.

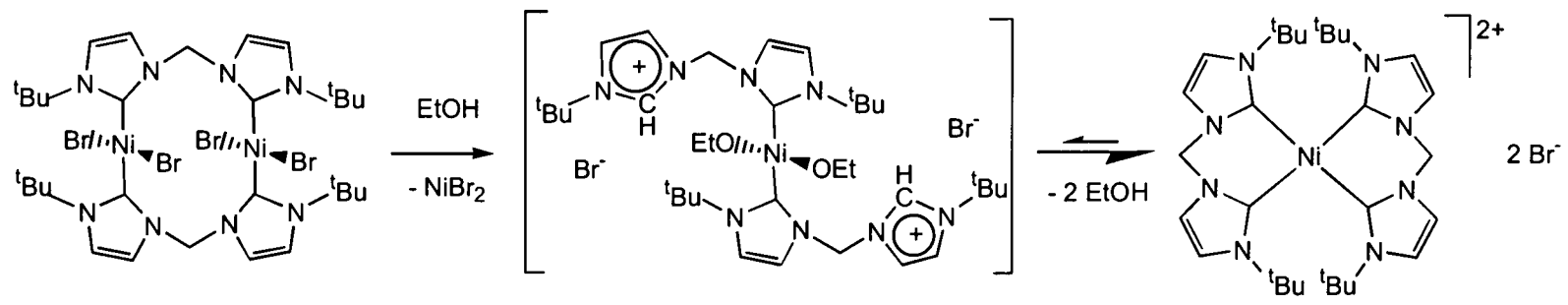

Scheme 2.7 Possible route for conversion of a compound $[Br_2Ni(\mu\text{-}^{tBu}CC^{meth})_2NiBr_2]$ to the dicationic compound $[Ni(^{tBu}CC^{meth})_2][Br]_2$ (**6**), on treatment with ethanol.

2.4.8 Synthesis of $[(^{tBu}CC^{meth})NiCl(PMe_3)]Cl$ (7)

$Ni(PMe_3)_2Cl_2$ was chosen for reaction with $^{tBu}CC^{meth}$ (**4**) and $^{tBu}CC^{eth}$ (**5**) in an attempt to prepare the corresponding chelating dicarbene nickel(II) *cis*-dichloride complexes. A possible advantage was its increased solubility in comparison to $NiBr_2(DME)$ and $NiBr_2(THF)_{1.5}$, of which the former is only sparingly soluble in DME and THF, and neither of which are soluble in less polar solvents such as diethyl ether and toluene. $Ni(PMe_3)_2Cl_2$ is soluble in non-polar solvents such as toluene, and this increased solubility could allow for cleaner, more stoichiometric reactions with the dicarbene ligands.

A toluene solution of **4** was added to a deep red solution of 1 equivalent $Ni(PMe_3)_2Cl_2$ to give a yellow precipitate (Eq. 38), characterised as the monocationic compound $[(^{tBu}CC^{meth})NiCl(PMe_3)]Cl$ (**7**) in 95 % yield.

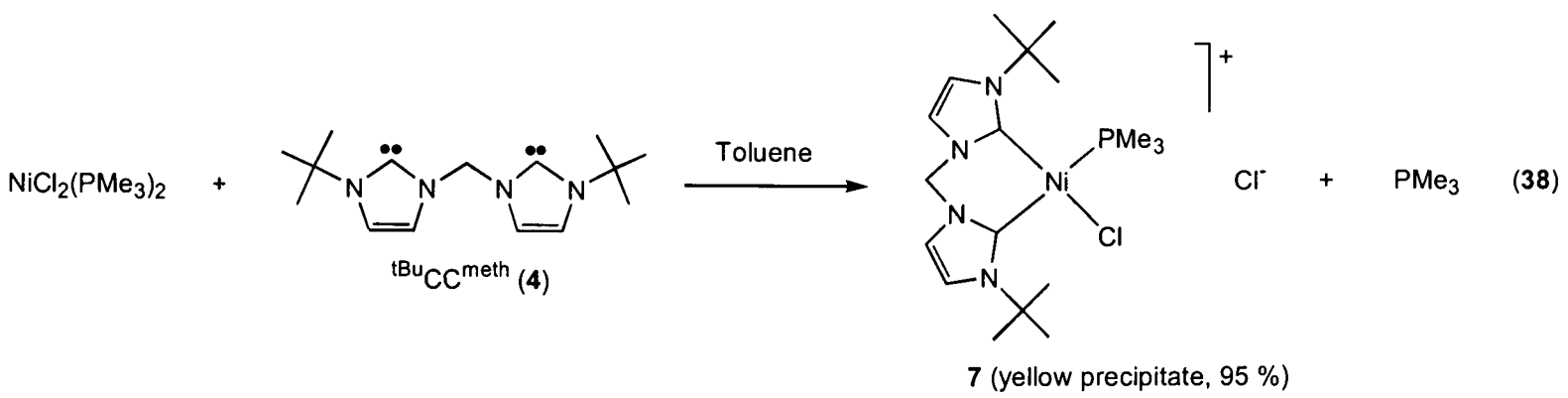

Compound **7** is air stable for days in the solid state and as solutions in polar aprotic solvents such as DMSO and acetonitrile. **7** is also soluble in dichloromethane, although ^{1}H NMR spectroscopy showed that dry degassed CD_2Cl_2 solutions decompose after several days at room temperature. **7** is insoluble in THF and non-polar organic solvents, and solutions of **7** in protic solvents such as alcohols and water degrade within minutes.

2.4.9 Characterisation of [(^{tBu}CC^{meth})NiCl(PMe$_3$)]Cl (7)

The yellow powder [(^{tBu}CC^{meth})NiCl(PMe$_3$)]Cl (**7**) was characterised by electrospray mass spectrometry, ^{1}H, $^{13}C\{^{1}H\}$ and $^{31}P\{^{1}H\}$ NMR studies, and finally by X-ray crystal structure determination. The electrospray mass spectrum contained a single peak (m/z = 429 [M^+]) corresponding to the cation [(^{tBu}CC^{meth})NiCl(PMe$_3$)]$^+$.

The molecular structure of **7** was initially determined using NMR methods. ^{1}H NOESY and ^{1}H-^{13}C-$^{n}J_{CH}$ shift correlation NMR spectra, recorded by Dr Daniel Haüßinger, enabled individual assignment of each ^{1}H and ^{13}C signal.

The ^{1}H and $^{13}C\{^{1}H\}$ NMR spectra of **7**, as well as the 2-D NMR experiments listed above were all recorded successfully in CD_2Cl_2. However, ^{1}H NMR spectroscopy subsequently showed the decomposition of **7** over a period of days in this solvent. For this reason d^6-DMSO became the NMR solvent of choice for the cationic compounds **7-10**, and subsequently for ^{1}H, $^{13}C\{^{1}H\}$, and $^{31}P\{^{1}H\}$ spectra of **7**.

^{1}H NMR spectroscopy of **7** in CD_2Cl_2 (figure 2.6) and d^6-DMSO is consistent with the molecular structure shown in equation 38, in which ^{tBu}CC^{meth} (**4**) is chelating to a nickel atom with square planar coordination geometry, with one N-heterocyclic carbene moiety *trans* to a PMe$_3$ ligand and the other *trans* to a chloride. Two magnetically inequivalent ^{t}Bu

groups are observed (δ 1.79 and 1.87 in CD_2Cl_2, or δ 1.75 and 1.84 in d^6-DMSO), and four inequivalent NC*H* heterocyclic ring protons (in the range δ 6.95-8.43 (CD_2Cl_2) or δ 7.51-7.88 (d^6-DMSO)). The methylene bridge protons are observed as two doublets (δ 6.91 and 8.26 in CD_2Cl_2, or δ 6.76 and 7.10 in d^6-DMSO, $^2J_{HH}$ = 13 Hz). The PMe_3 protons are observed at δ 1.23 (CD_2Cl_2) or δ 1.21 (d^6-DMSO) with $^2J_{PH}$ = 10 Hz. $^5J_{PH}$ coupling (2 Hz) is observed for only one of the NC*H* heterocyclic ring protons which shows a virtual triplet (δ 6.95 in CD_2Cl_2 or δ 7.51 in d^6-DMSO) instead of the doublet which is usually observed due to $^3J_{HH}$ coupling. In the $^1H\{^{31}P\}$ NMR spectrum of **7** in d^6-DMSO, the resonance at δ 7.51 is observed as a doublet due to phosphorus decoupling, and similarly the PMe_3 resonance at δ 1.21 is observed as a singlet.

$^{13}C\{^1H\}$ NMR spectroscopy of (**7**) in CD_2Cl_2 (figure 2.6) and d^6-DMSO is also consistent with the molecular structure shown in equation 38. The inequivalent carbene carbon resonances are observed at δ 162.6 and 165.7 in CD_2Cl_2, or δ 161.6 and 165.8 in d^6-DMSO. These values are shifted ca. 35 ppm upfield with respect to those observed for the neutral nickel N-heterocyclic carbene complexes **12** and **13** studied in chapter 3, and are characteristic of cationic metal complexes.[12,24,26] Both carbene carbon resonances are doublets due to $^2J_{PC}$ coupling which is significantly greater for the carbon *trans* to the PMe_3 ligand (117 Hz) than for the carbon *cis* to PMe_3 (40 Hz). $^2J_{PC}$ *cis* and *trans* coupling constants of similar magnitude have recently been observed in chelating *bis*(phosphine) Pd and Pt dialkyl complexes.[29,30] Four inequivalent heterocyclic ring NC*H* carbons are observed, of which one is a doublet due to $^{4\text{ or }5}J_{PC}$ coupling (5 Hz). Two magnetically inequivalent ^{t}Bu groups are also observed (two quaternary signals, and two methyl signals of which one is a doublet due to $^5J_{PC}$ (= 2 Hz) coupling), as well as a singlet for the methylene bridge and a doublet ($^1J_{PC}$ = 29 Hz) for the PMe_3 carbons.

$^{31}P\{^1H\}$ NMR spectroscopy (d^6-DMSO) of **7** showed a singlet at δ -12.3.

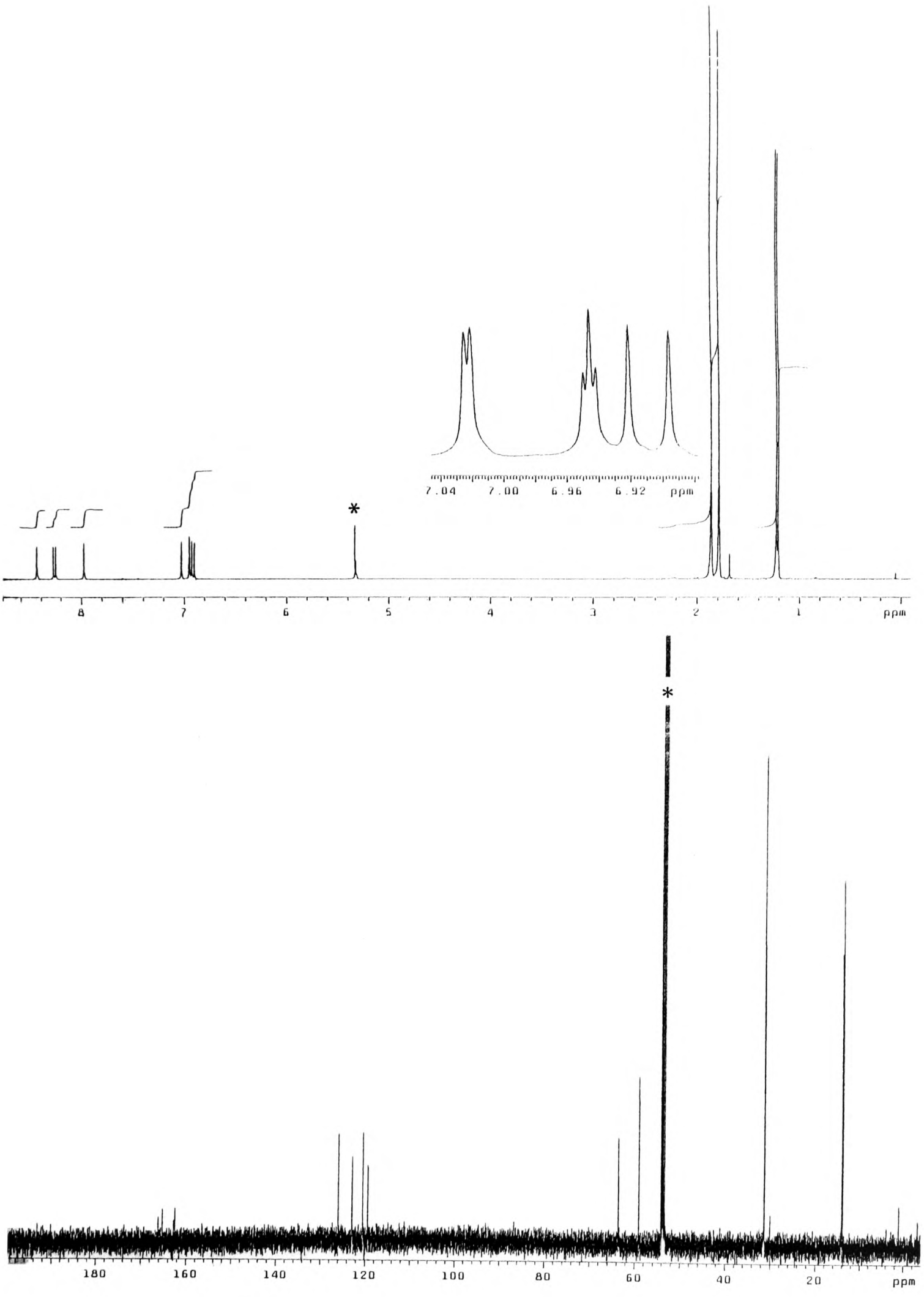

Figure 2.6 500 MHz ^{1}H and 125.7 MHz $^{13}C\{^{1}H\}$ NMR spectra of $[(^{tBu}CC^{meth})NiCl(PMe_3)]Cl$ (**7**) in CD_2Cl_2 (* = solvent).

After recording the ^{1}H, $^{13}C\{^{1}H\}$, and $^{31}P\{^{1}H\}$ spectra a ^{1}H NOESY experiment was performed by Dr Daniel Haüßinger in order to individually assign each proton signal. The NOESY experiment is a 2-dimensional NMR experiment in which the off-diagonal peaks correlate spins which share a dipolar coupling due to the nuclear Overhauser effect.[31,32] The nuclear Overhauser effect (NOE) is an aspect of nuclear relaxation and depends upon dipolar (through-space) magnetic coupling between nuclei. It is revealed when one of the nuclei is irradiated at its resonance frequency and the signal of another nucleus is detected more or less intense than usual. The interaction is dependent upon the relaxation of the observed nucleus by the irradiated nucleus and is only noticeable over short distances.[31,32] The 2-dimensional NOESY experiment is based on transient NOE detection, which shows a strong dependence on internuclear distance, falling off very rapidly as the distance between nuclei increases, and may thus be used in the elucidation of molecular structure.[32]

A ^{1}H NOESY spectrum of **7** in CD_2Cl_2 was recorded which showed off-diagonal peaks corresponding to the magnetically inequivalent protons of **7** which are close in space.

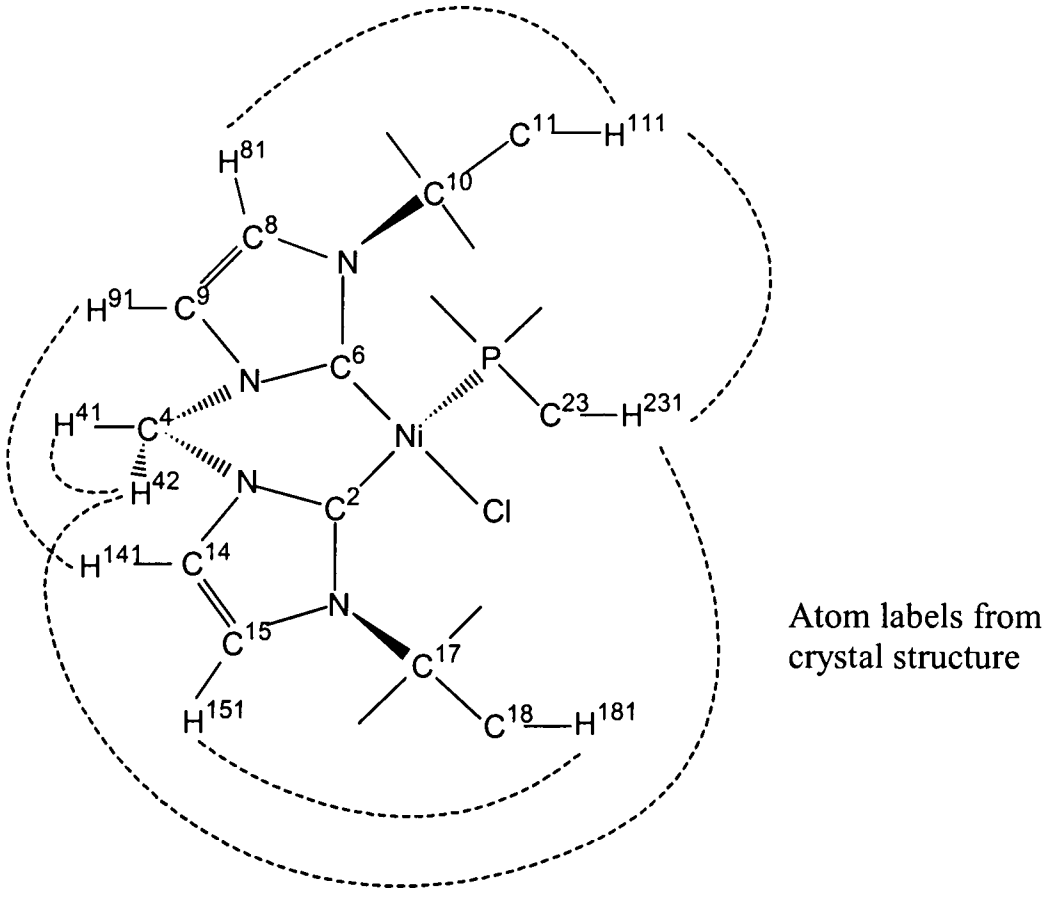

Figure 2.7 Molecular structure of the cation $[(^{tBu}CC^{meth})NiCl(PMe_3)]^{+}$. Dashed lines represent through-space (dipolar) correlations between protons.

The structure of the cation $[(^{tBu}CC^{meth})NiCl(PMe_3)]^+$ is shown in figure 2.7, together with the through-space (dipolar) correlations between protons. The ^1H NOESY spectrum (figure 2.8) shows that only one of the two ^{t}Bu signals, δ 1.87 (H^{111}), is correlated with the PMe_3 signal δ 1.23 (H^{231}). Therefore the ^{t}Bu group with the signal at δ 1.87 must be closer in space to PMe_3, on the heterocyclic ring *cis* to PMe_3, and the ^{t}Bu group with the signal at δ 1.79 (H^{181}) must be further away on the ring *trans* to PMe_3. Both of the ^{t}Bu signals are also correlated with one (different) heterocyclic ring proton. The signal for H^{111} is correlated with δ 7.02 (H^{81}) and that for H^{181} is correlated with δ 6.95 (H^{151}). These ring protons must be the nearest to the ^{t}Bu groups, in the adjacent ring positions, and on the rings *cis* and *trans* to PMe_3 respectively. The only two ring proton signals which showed through-space correlation were those for H^{91} (δ 8.43) and H^{141} (δ 7.97). This is consistent with a deviation of the heterocyclic rings from the nickel coordination plane ('ring twist' - see figure 2.11) which would bring H^{91} and H^{141}, both adjacent to the methylene bridge, closer together in space. The PMe_3 signal is also correlated with only one of the methylene bridge proton signals, δ 6.91 (H^{42}). The H^{42} proton is closer in space to PMe_3 than the other methylene bridge proton H^{41} (δ 8.26). This is also consistent with a deviation of the heterocyclic rings from the nickel coordination plane, causing the ^{t}Bu groups and methylene bridge to point in opposite directions above and below the plane, and the methylene bridge protons to point towards and away from the nickel centre (figure 2.11). H^{42} can be viewed as being in an *endo* position, because the C-H^{42} bond points more in the direction of the Ni centre / PMe_3 ligand than the other methylene bridge C-H bond, which points in an opposite direction to the Ni centre (H^{41} is therefore in an *exo* position). Furthermore, the NOESY correlation of the H^{42} and PMe_3 signals is consistent with a nonbonding interaction between the dicarbene ^{t}Bu groups and the PMe_3 methyls, which perpendicularly displaces the phosphorus atom from the NiC_2 coordination plane, away from the bulky ^{t}Bu groups and towards the nearest proton of the methylene bridge, H^{42}. This distortion can be viewed in the X-ray crystal structure of **7** (figure 2.11). The final NOESY correlation is between the signals for the methylene bridge protons H^{41} and H^{42}, which also show through-bond (scalar) coupling.

The ^1H NOESY experiment was used, as described above, to assign nearly all the proton signals individually. The assignment of the signals at δ 7.97 and 8.43 to the ring protons adjacent to the methylene bridge (H^{91} and H^{141}) is correct, but the NOESY spectrum

provides no evidence as to which of the two signals corresponds to the proton on the ring *cis* to PMe_3 (H^{91}) and which to the proton on the ring *trans* to PMe_3 (H^{141}).

Following the assignment of the proton signals, a ^{1}H-^{13}C-$^{1}J_{CH}$ shift correlation NMR spectrum (figure 2.9) was recorded by Dr Daniel Haüßinger, which enabled individual assignment of the primary, secondary and tertiary carbon signals of **7** (section 6.7). The quaternary carbon signals for the carbene carbons C^2 and C^6 were assigned as δ 165.7 and 162.6 respectively based on the difference in $^{2}J_{PC}$ coupling, which is significantly greater for the carbon *trans* to the PMe_3 ligand (117 Hz) than for the carbon *cis* to PMe_3 (40 Hz). The quaternary ^{t}Bu signals however, observed at δ 59.07 and 59.11, could not be specifically assigned to the particular carbon C^{10} or C^{17}.

The ring proton signals at δ 7.97 and 8.43 were eventually successfully assigned to the protons H^{141} and H^{91} respectively, by recording a ^{1}H-^{13}C-$^{n}J_{CH}$ shift correlation NMR spectrum, where n > 1 (figure 2.10). This spectrum showed correlations due to $^{2}J_{CH}$ coupling between the signal at δ 7.97 and the signal for C^{15} at δ 119.4, and between δ 8.43 and C^8 (δ 120.5), which confirmed which of the heterocyclic rings these protons are bonded to. Furthermore, two correlations due to $^{2}J_{CH}$ coupling were observed between the quaternary ^{t}Bu signals and the ^{t}Bu proton signals, but because of the similar chemical shifts of the carbon resonances (δ 59.07 and 59.11), it was impossible to resolve which of the off-diagonal peaks corresponded to which carbon signal.

The complete individual assignments of the ^{1}H and ^{13}C signals (apart from quaternary ^{t}Bu signals) are summarised in section 6.7. It is interesting to note that the carbon and proton signals corresponding to $NC^{15}H^{151}$ on the ring *trans* to PMe_3, show $^{4\text{ or }5}J_{PC}$ and $^{5}J_{PH}$ coupling respectively, whereas the N*CH* signals on the ring *cis* to PMe_3 show no coupling to phosphorus. Similarly, the C^{11} ^{t}Bu signal (on the ring *cis* to PMe_3) shows $^{5}J_{PC}$ coupling but the C^{18} signal (on the ring *trans* to PMe_3) does not. This could be the result of the contrasting bond angles involved in the *cis* and *trans* cases, with combinations of more favourable bond angles resulting in the observed couplings to phosphorus.

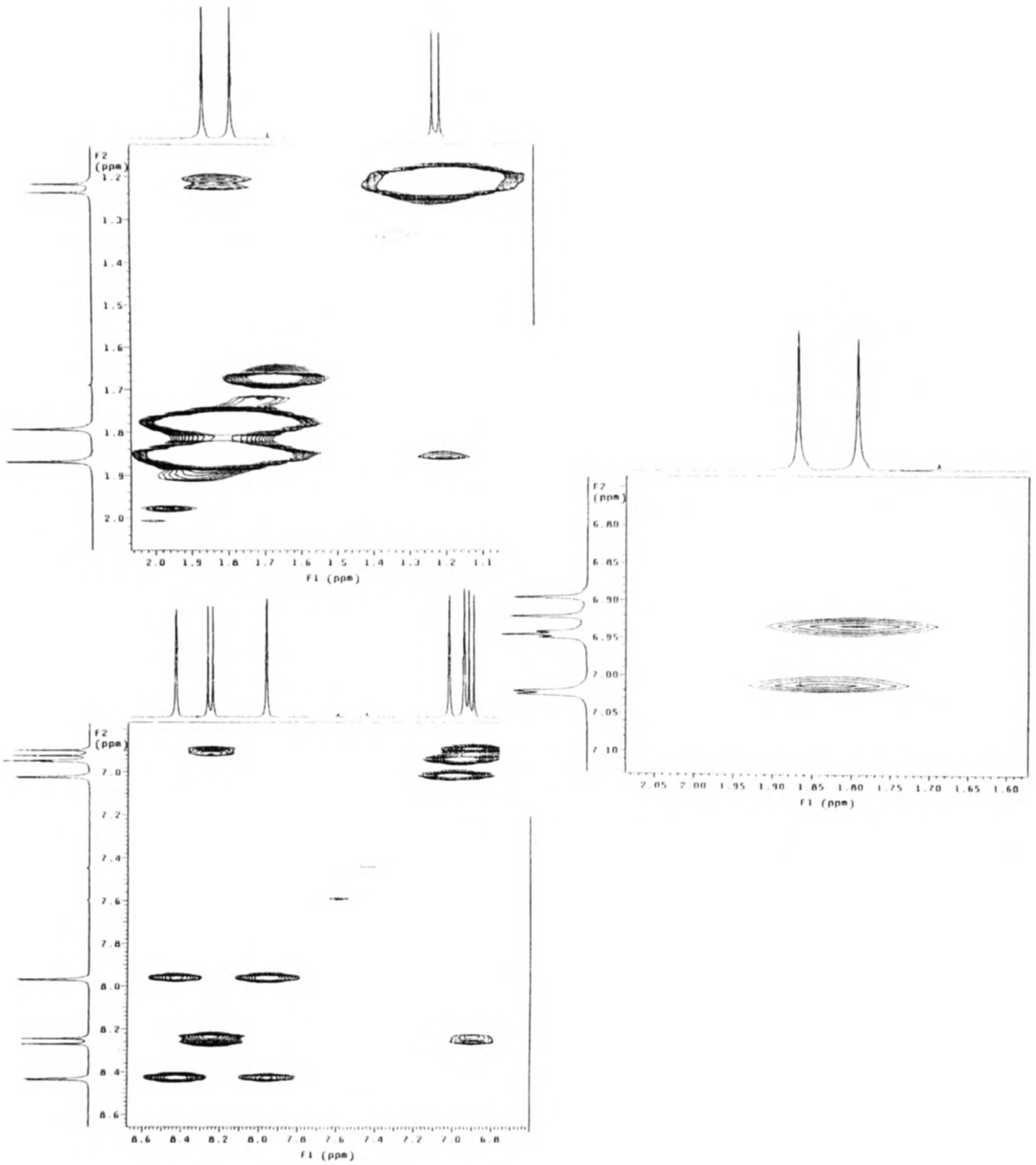

Figure 2.8 500 MHz ^{1}H NOESY spectrum of [(^{tBu}CC^{meth})NiCl(PMe$_3$)]Cl (**7**) in CD_2Cl_2.

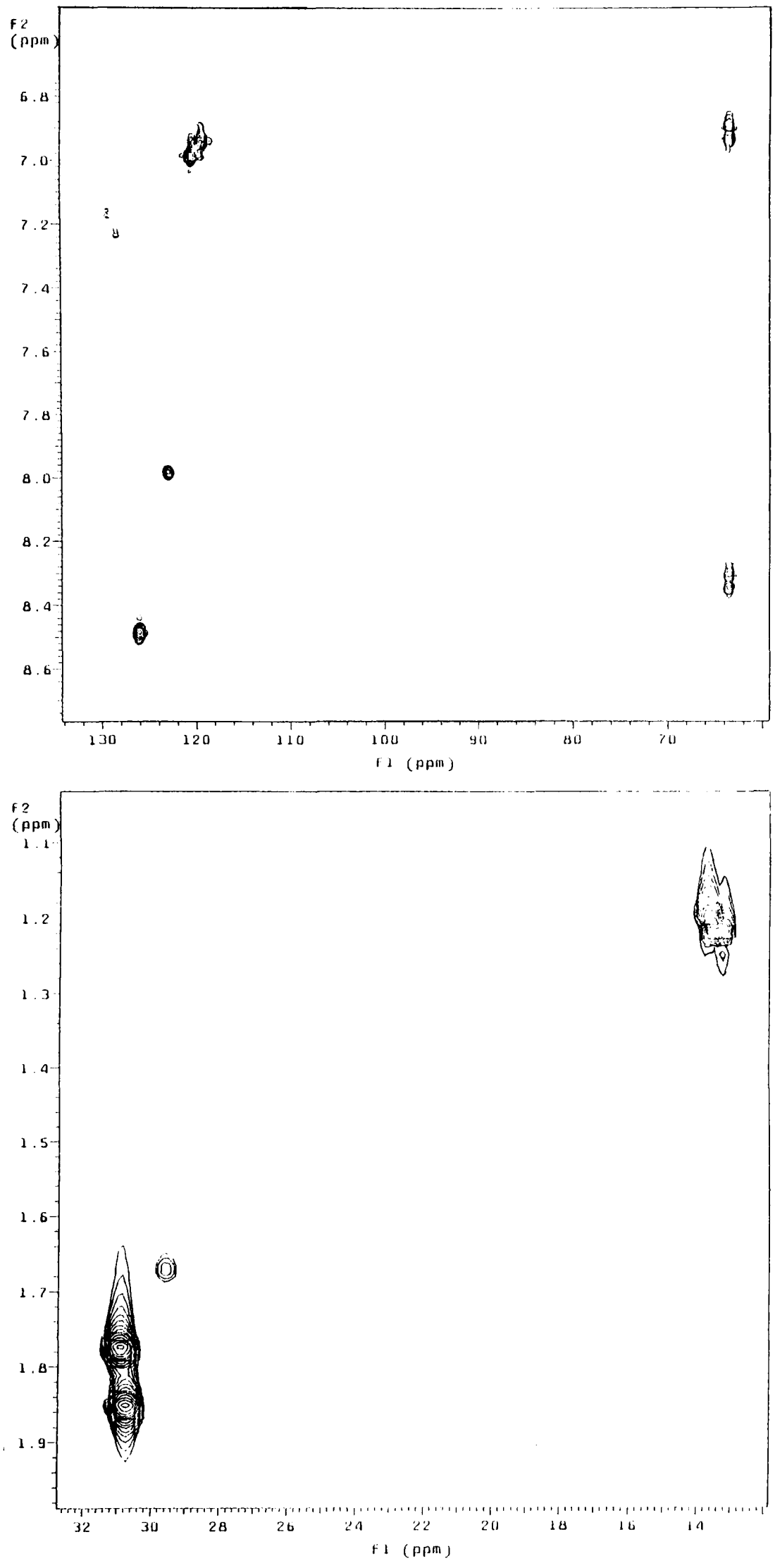

Figure 2.9 500 MHz ^{1}H-^{13}C-$^{1}J_{CH}$ shift correlation NMR spectrum of [($^{tBu}CC^{meth}$)NiCl(PMe_3)]Cl (**7**) in CD_2Cl_2.

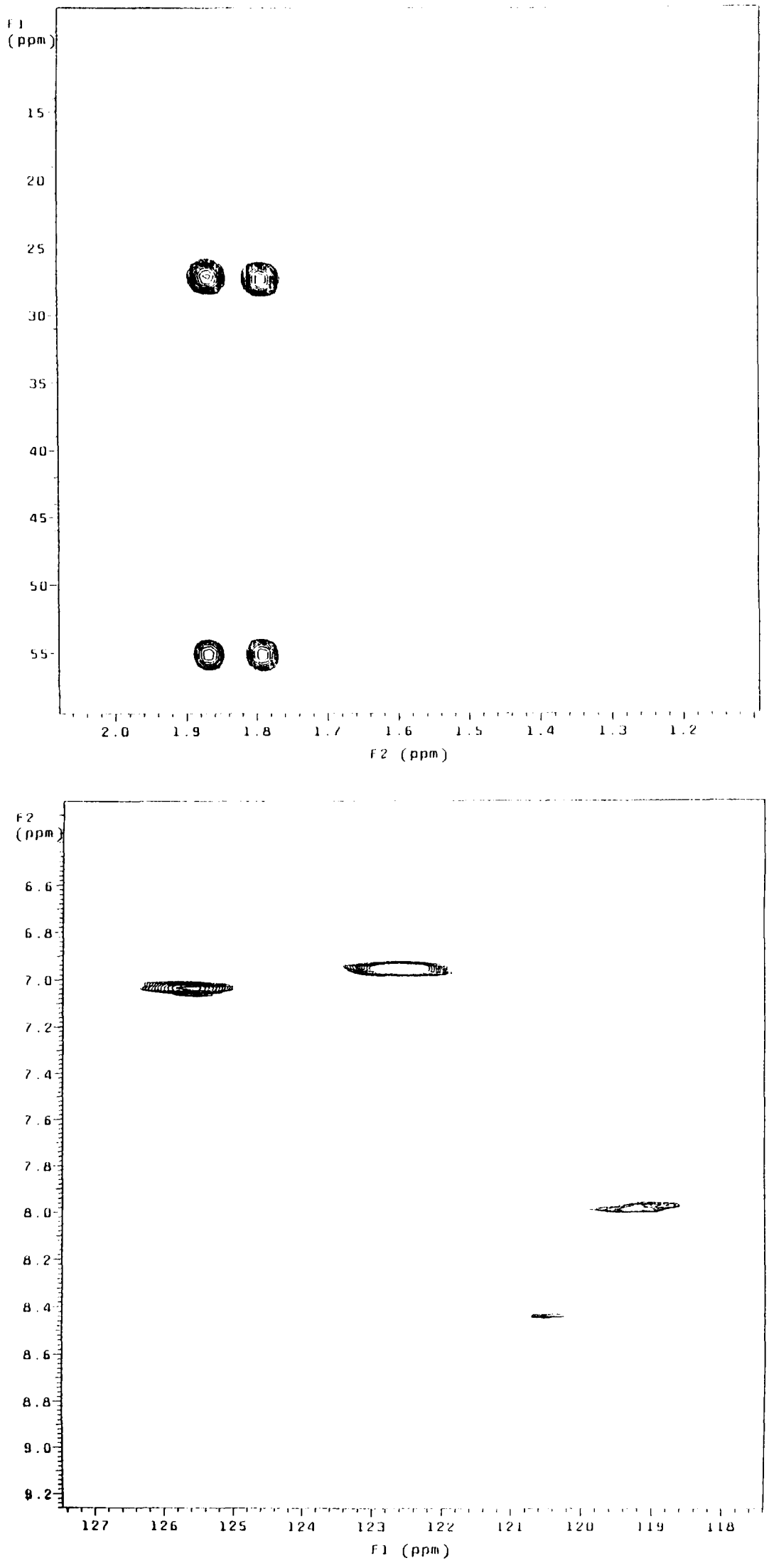

Figure 2.10 500 MHz ^{1}H-^{13}C-$^{n}J_{CH}$ (n > 1) shift correlation spectrum of [($^{tBu}CC^{meth}$)NiCl(PMe_3)]Cl (**7**) in CD_2Cl_2.

Single crystals of **7**, of sufficient quality for X-ray structure determination (performed by Dr Richard Douthwaite), were grown from layering pentane onto a CH_2Cl_2 solution. Selected bond lengths and angles are given in table 2.3. The cation of **7**, shown in figure 2.11, is chiral and crystallises as a racemic mixture. The asymmetric unit contains one molecule of **7** as well as 1.2 molecules of CH_2Cl_2 as solvent of crystallisation. The cation of **7** displays a boat conformation similar to those reported in other transition metal complexes incorporating methylene-bridged chelating di-N-heterocyclic carbenes (section 1.2.5). The geometry at the nickel centre is essentially square planar, although the phosphorus atom is displaced perpendicularly from a plane defined by the nickel and the carbene carbons by 0.903(2) Å. This is due to a nonbonding interaction between the dicarbene ^{t}Bu groups and the phosphine methyl groups. The Ni-C bond lengths *trans* and *cis* to PMe_3 show a marked difference of 0.071(8) Å, reflecting the greater *trans* influence of PMe_3 compared to Cl^-. The *trans* bond length Ni-C(2) = 1.942(4) Å is slightly longer than those observed in the two previously structurally characterised nickel(II) carbene complexes, *trans*-dichlorobis(1,3-dicyclohexylimidazol-2-ylidene)nickel(II) (1.911(2) Å) (scheme 2.1)[10] and $[Ni(^{Me}CC^{meth})_2][I]_2$ (1.909(2) Å) (Eq. 13),[24] and in the dication $[Ni(^{tBu}CC^{meth})_2][Br]_2$ (**6**) (1.928(4) Å), whereas the *cis* bond length Ni-C(6) = 1.871(4) Å is somewhat shorter. The bite angle C(2)-Ni-C(6) = 84.92(18)° is in between those of $[Ni(^{tBu}CC^{meth})_2][Br]_2$ (**6**) (83.57(17)°) and $[Ni(^{Me}CC^{meth})_2][I]_2$ (86.64(9)°), and the twist angles of the heterocyclic rings relative to the coordination plane of **7** (56.7(7) and 56.2(7)°) are similar to those of $[Ni(^{tBu}CC^{meth})_2][Br]_2$ (**6**) (54.6(6) and 56.5(7)°) but significantly greater than those of $[Ni(^{Me}CC^{meth})_2][I]_2$ (39.64(9) and 40.85(8)°), which again indicates that the conformation adopted by the dicarbene ligand $^{tBu}CC^{meth}$ primarily results from minimisation of nonbonding interactions of the *tert*-butyl groups.

Bond	Length (Å)	Bond	Angle (°)
Ni-C(2)	1.942(4)	C(2)-Ni-C(6)	84.92(18)
Ni-C(6)	1.871(4)	C(2)-Ni-Cl(26)	94.05(13)
Ni-P(22)	2.2074(15)	C(6)-Ni-Cl(26)	177.55(16)
Ni-Cl(26)	2.1951(12)	C(2)-Ni-P(22)	155.81(15)
C(2)-N(3)	1.356(6)	C(6)-Ni-P(22)	92.02(14)
C(2)-N(16)	1.340(6)	N(3)-C(2)-N(16)	104.5(4)
N(5)-C(6)	1.345(6)	N(5)-C(6)-N(7)	106.3(4)
C(6)-N(7)	1.343(6)	Ni-C(2)-N(3)	111.8(3)
C(8)-C(9)	1.329(7)	C(2)-N(3)-C(4)	123.2(4)
C(14)-C(15)	1.336(8)	N(3)-C(4)-N(5)	108.3(4)
		C(4)-N(5)-C(6)	120.3(4)
		Ni-C(6)-N(5)	116.7(3)
		C(4)-N(3)-C(14)	125.7(4)
		C(2)-N(3)-C(14)	111.0(4)
		C(4)-N(5)-C(9)	127.4(4)
		C(6)-N(5)-C(9)	110.4(4)
		ring $twist_{C(2)}$*	56.7(7)
		ring $twist_{C(6)}$	56.2(7)

* The angle between the coordination plane defined by nickel and carbene carbon atoms and the heterocyclic ring containing C(n).

Table 2.3 Selected bond lengths and angles for [($^{tBu}CC^{meth}$)NiCl(PMe_3)]Cl (**7**).

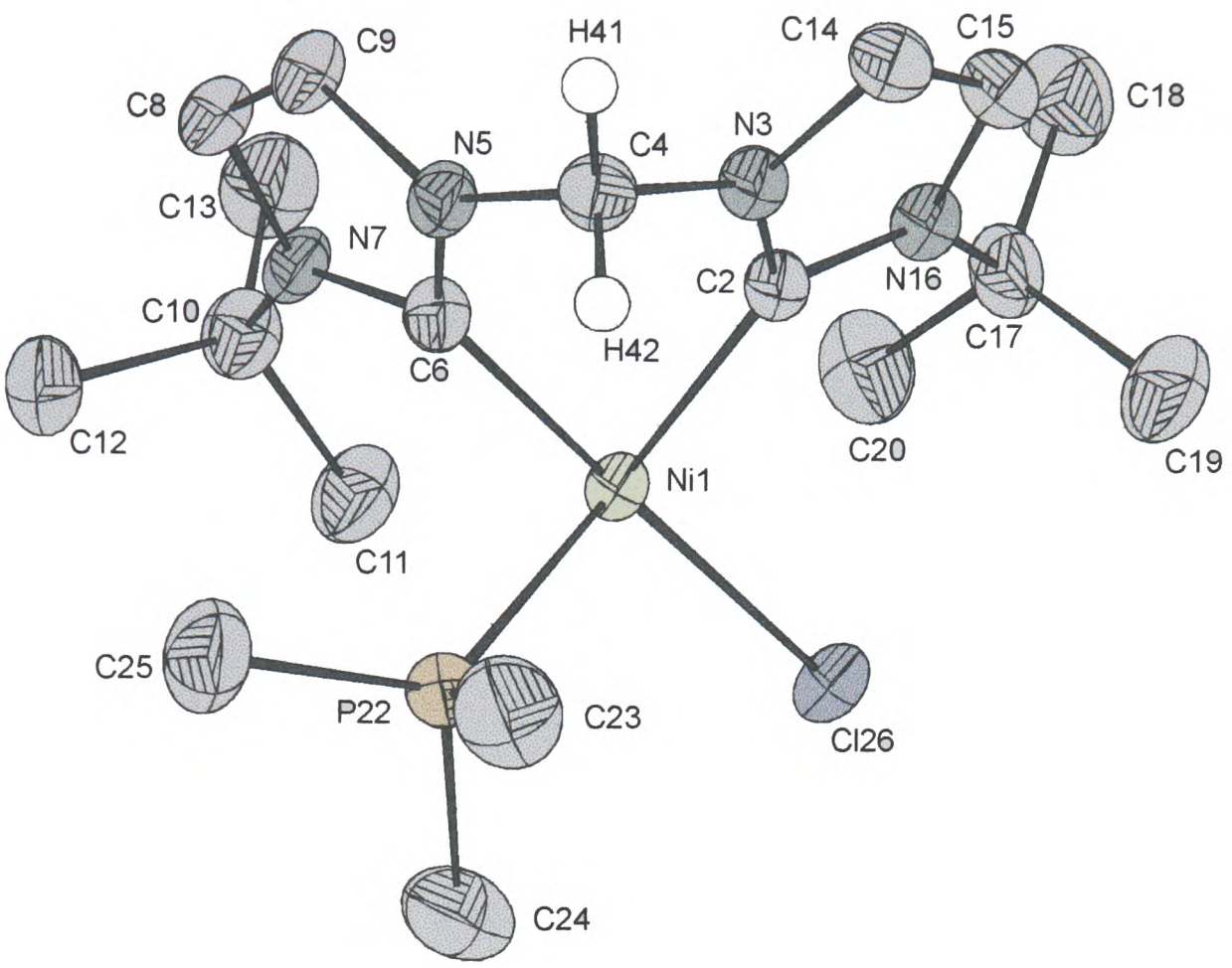

Figure 2.11 Two views of the cation $[(^{tBu}CC^{meth})NiCl(PMe_3)]^+$ from the X-ray structure of **7**. Hydrogen atoms except for H41 and H42 are omitted for clarity.

2.4.10 Synthesis of [(^{tBu}CC^{meth})NiCl(PMe$_3$)][BPh$_4$] (8)

The anion exchange reaction between [(^{tBu}CC^{meth})NiCl(PMe$_3$)]Cl (**7**) and TlBPh$_4$ in dichloromethane gave the tetraphenylborate salt [(^{tBu}CC^{meth})NiCl(PMe$_3$)][BPh$_4$] (**8**) in 51 % yield (Eq. 39).

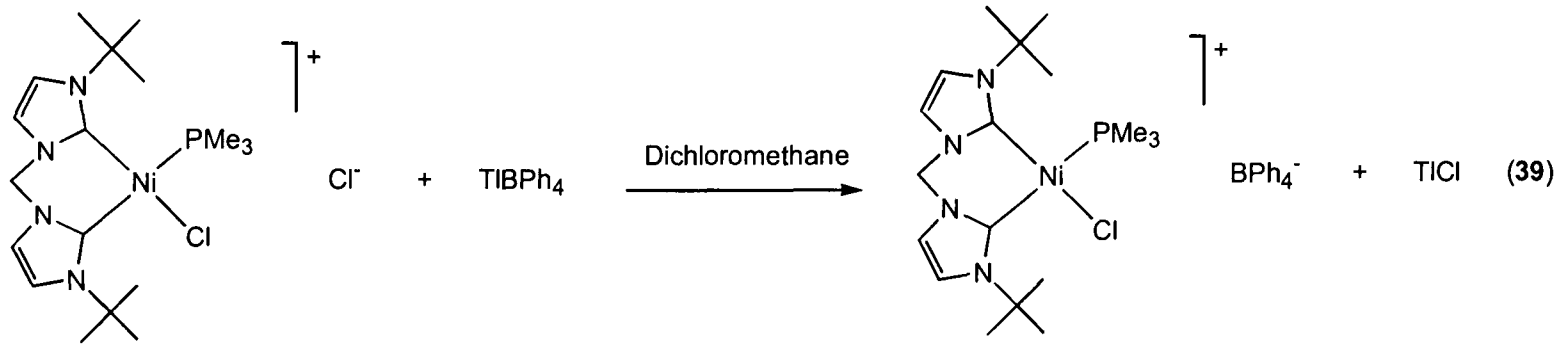

8 (yellow powder, 51 %)

[(^{tBu}CC^{meth})NiCl(PMe$_3$)][BPh$_4$] (**8**) has similar solubility properties as the chloride analogue **7**, is air-stable in the solid state and in solution for days, and solutions of **8** in protic solvents degrade within minutes.

2.4.11 Characterisation of [(^{tBu}CC^{meth})NiCl(PMe$_3$)][BPh$_4$] (8)

The yellow powder [(^{tBu}CC^{meth})NiCl(PMe$_3$)][BPh$_4$] (**8**) was characterised by electrospray mass spectrometry and ^{1}H, ^{13}C{^{1}H} and ^{31}P{^{1}H} NMR spectroscopy. The electrospray mass spectrum contained a single peak (m/z = 429 [M$^+$]) corresponding to the cation [(^{tBu}CC^{meth})NiCl(PMe$_3$)]$^+$. ^{1}H and ^{13}C{^{1}H} NMR spectra of **8** do not significantly differ from those of the precursor chloride salt **7**, other than the presence of additional signals due to the tetraphenylborate anion.

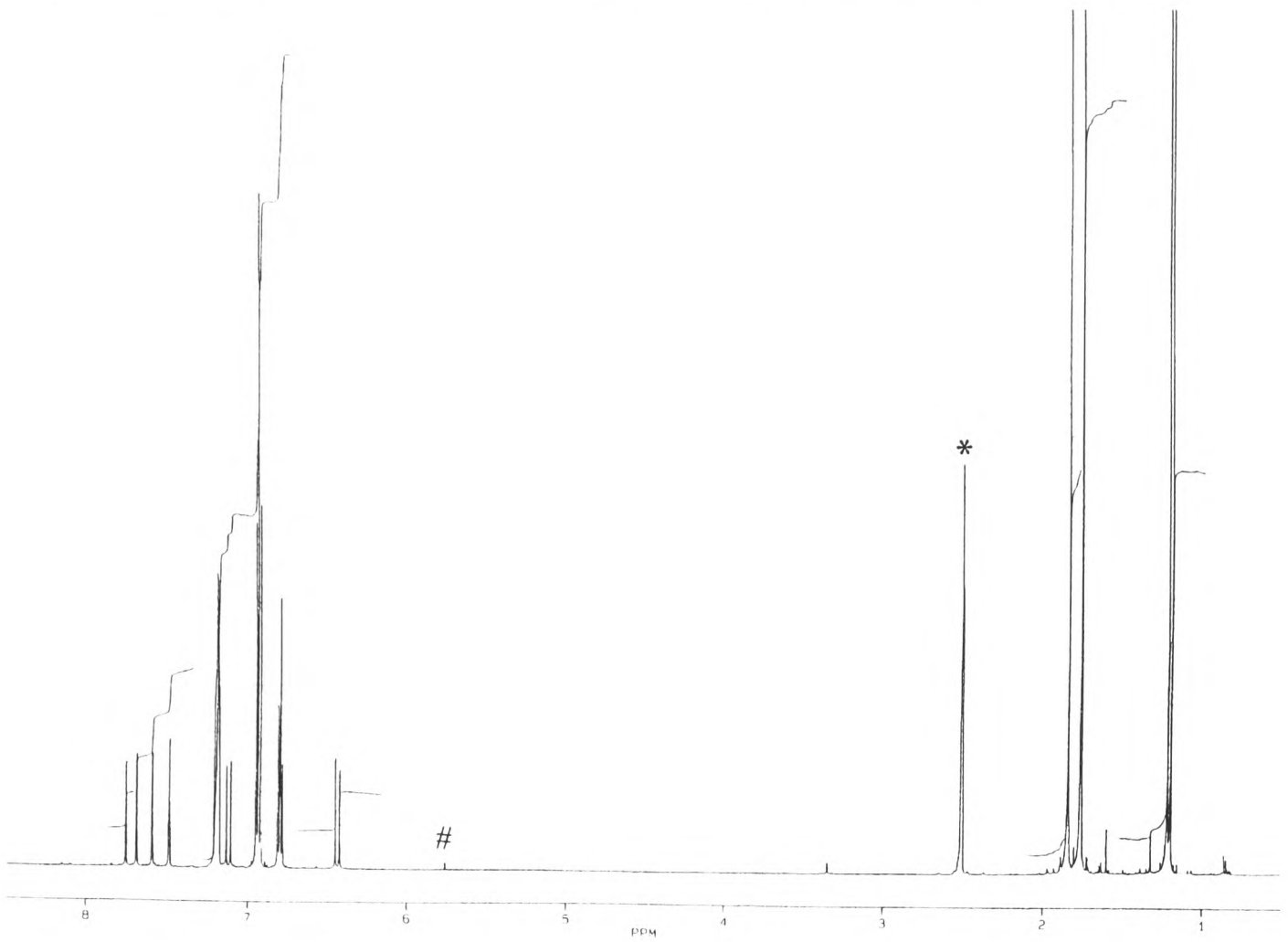

Figure 2.12 500 MHz ^{1}H NMR spectrum of [($^{tBu}CC^{meth}$)NiCl(PMe_3)][BPh_4] (**8**) in d^6-DMSO (* = solvent, # = CH_2Cl_2).

2.4.12 Syntheses of [($^{tBu}CC^{eth}$)NiCl(PMe_3)]Cl (9) and [($^{tBu}CC^{eth}$)NiCl(PMe_3)][BPh_4] (10)

A toluene solution of $^{tBu}CC^{eth}$ (**5**) was added to a deep red solution of 1 equivalent $Ni(PMe_3)_2Cl_2$ to give a yellow precipitate (Eq. 40), characterised as the monocationic compound [($^{tBu}CC^{eth}$)NiCl(PMe_3)]Cl (**9**), in 85 % yield.

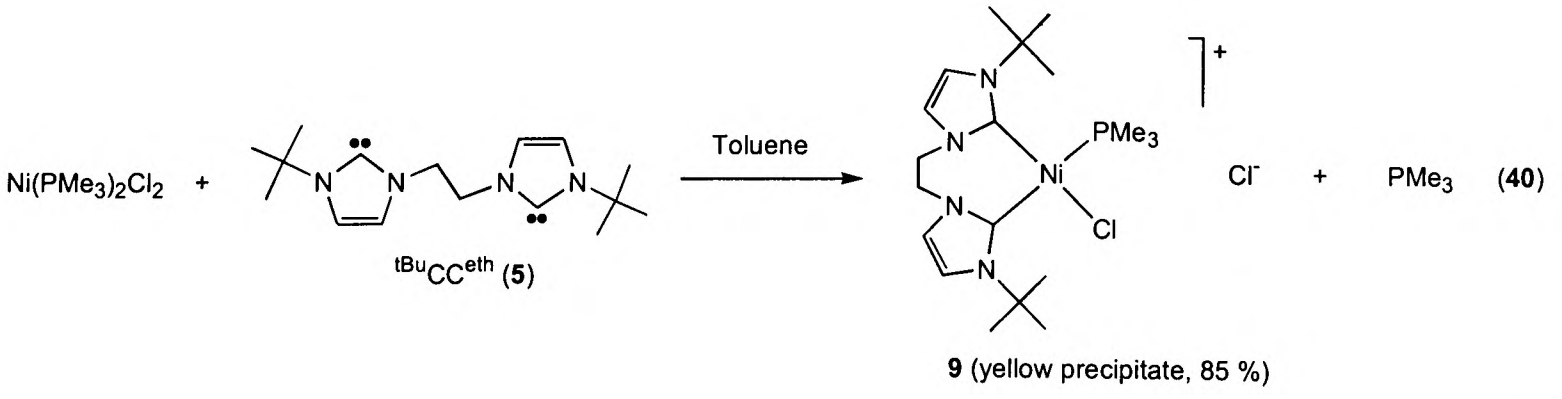

The anion exchange reaction between [($^{tBu}CC^{eth}$)NiCl(PMe_3)]Cl (**9**) and $TlBPh_4$ in dichloromethane gave the tetraphenylborate salt [($^{tBu}CC^{eth}$)NiCl(PMe_3)][BPh_4] (**10**) in 78 % yield (Eq. 41).

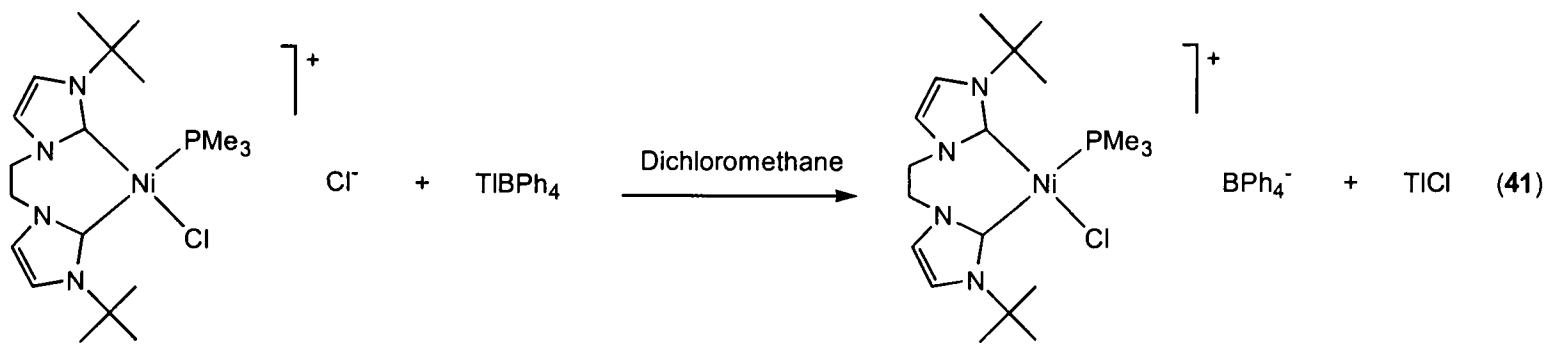

10 (yellow powder, 78 %)

[(^{tBu}CC^{eth})NiCl(PMe$_3$)]Cl (**9**) and [(^{tBu}CC^{eth})NiCl(PMe$_3$)][BPh$_4$] (**10**) are the first examples of chelating ethylene-bridged dicarbene transition metal complexes. Herrmann et. al. could not prepare analogues to the complexes Pd(^{tBu}CC^{meth})X$_2$ (X = Br, I) by reaction between Pd(OAc)$_2$ and diimidazolium dihalides with N,N' linkages other than methylene (section 1.2.5).[25] Compounds **9** and **10** have similar solubility properties to the methylene-bridged analogues **7** and **8** (soluble in polar aprotic solvents such as DMSO, acetonitrile and dichloromethane, but insoluble in THF and non-polar organic solvents). **9** and **10** are air-stable in the solid state and in solution for days, although solutions in protic solvents degrade within minutes, and dichloromethane solutions decompose after several days.

2.4.13 Characterisation of [(^{tBu}CC^{eth})NiCl(PMe$_3$)]Cl (9) and [(^{tBu}CC^{eth})NiCl(PMe$_3$)][BPh$_4$] (10)

The yellow powders [(^{tBu}CC^{eth})NiCl(PMe$_3$)]Cl (**9**) and [(^{tBu}CC^{eth})NiCl(PMe$_3$)][BPh$_4$] (**10**) were characterised by electrospray mass spectrometry, ^{1}H, ^{13}C{^{1}H} and ^{31}P{^{1}H} NMR spectroscopy, and finally [(^{tBu}CC^{eth})NiCl(PMe$_3$)][BPh$_4$] (**10**) was characterised by X-ray diffraction. The electrospray mass spectra of **9** and **10** both contained a single peak (m/z = 443 [M$^+$]) corresponding to the cation [(^{tBu}CC^{eth})NiCl(PMe$_3$)]$^+$.

The molecular structure of **10** was initially determined using NMR methods. ^{1}H NOESY and ^{1}H-^{13}C-$^nJ_{CH}$ shift correlation NMR spectra, recorded by Dr Daniel Haüßinger, enabled individual assignment of each ^{1}H and ^{13}C signal. Since ^{1}H and ^{13}C{^{1}H} NMR spectra of [(^{tBu}CC^{eth})NiCl(PMe$_3$)][BPh$_4$] (**10**) do not differ significantly from those of the precursor chloride salt **9**, other than the presence of additional signals due to the tetraphenylborate anion, discussion of NMR data in this section will henceforth be restricted to compound **10**.

^{1}H NMR spectroscopy of **10** in d^{6}-DMSO (figure 2.13) is consistent with the molecular structure shown in equation 41. Two magnetically inequivalent ^{t}Bu groups are observed (δ 1.80 and 1.91), and four inequivalent NC*H* heterocyclic ring protons (in the range δ 7.47-7.60). Four multiplets (δ 4.67, 4.77, 5.74 and 6.42) are seen for the magnetically inequivalent protons of the ethylene bridge. The PMe_3 protons are observed at δ 1.11 with $^{2}J_{PH}$ = 10 Hz. $^{5}J_{PH}$ coupling (1.5 Hz) is observed for only one of the NC*H* heterocyclic ring protons which shows a virtual triplet (δ 7.51) instead of the doublet which is usually observed due to $^{3}J_{HH}$ coupling. In the $^{1}H\{^{31}P\}$ NMR spectrum of **10** (d^{6}-DMSO), the resonance at δ 7.51 is observed as a doublet due to phosphorus decoupling, and similarly the PMe_3 resonance at δ 1.11 is observed as a singlet.

$^{13}C\{^{1}H\}$ NMR spectroscopy of **10** in d^{6}-DMSO (figure 2.13) is also consistent with the molecular structure shown in equation 41. The inequivalent carbene carbon resonances are observed at δ 156.0 and 163.4. These values are fairly similar to those of the methylene-bridged carbene compounds **7** and **8** in d^{6}-DMSO (δ 162 and 166), and are characteristic of cationic metal carbene complexes (whereas the neutral nickel carbene complexes **12** and **13** show carbene carbon resonances at δ 200.2 and 197.6 respectively).[12,24,26] Both carbene carbon resonances are doublets due to $^{2}J_{PC}$ coupling which is significantly greater for the carbon *trans* to the PMe_3 ligand (111 Hz) than for the carbon *cis* to PMe_3 (41 Hz), as was observed for compound **7**. Four inequivalent heterocyclic ring N*C*H carbons are observed. The two N*C*H carbons of the ring *trans* to the PMe_3 ligand are doublets due to $^{4\text{ or }5}J_{PC}$ coupling (4 Hz), whereas the *cis* ring N*C*H carbons show no coupling to phosphorus. This is in contrast to $^{13}C\{^{1}H\}$ NMR spectroscopy of the methylene-bridged cation $[(^{tBu}CC^{meth})NiCl(PMe_3)]^{+}$, which shows that only one of the N*C*H carbons of the ring *trans* to PMe_3 is coupled to phosphorus. Two magnetically inequivalent ^{t}Bu groups are also observed (two quaternary signals, and two methyl signals none of which are doublets due to $^{5}J_{PC}$ coupling in contrast to **7**), as well as two singlets for the ethylene bridge carbons and a doublet ($^{1}J_{PC}$ = 29 Hz) for the PMe_3 carbons.

$^{31}P\{^{1}H\}$ NMR spectroscopy (d^{6}-DMSO) of **10** shows a singlet at δ -13.5.

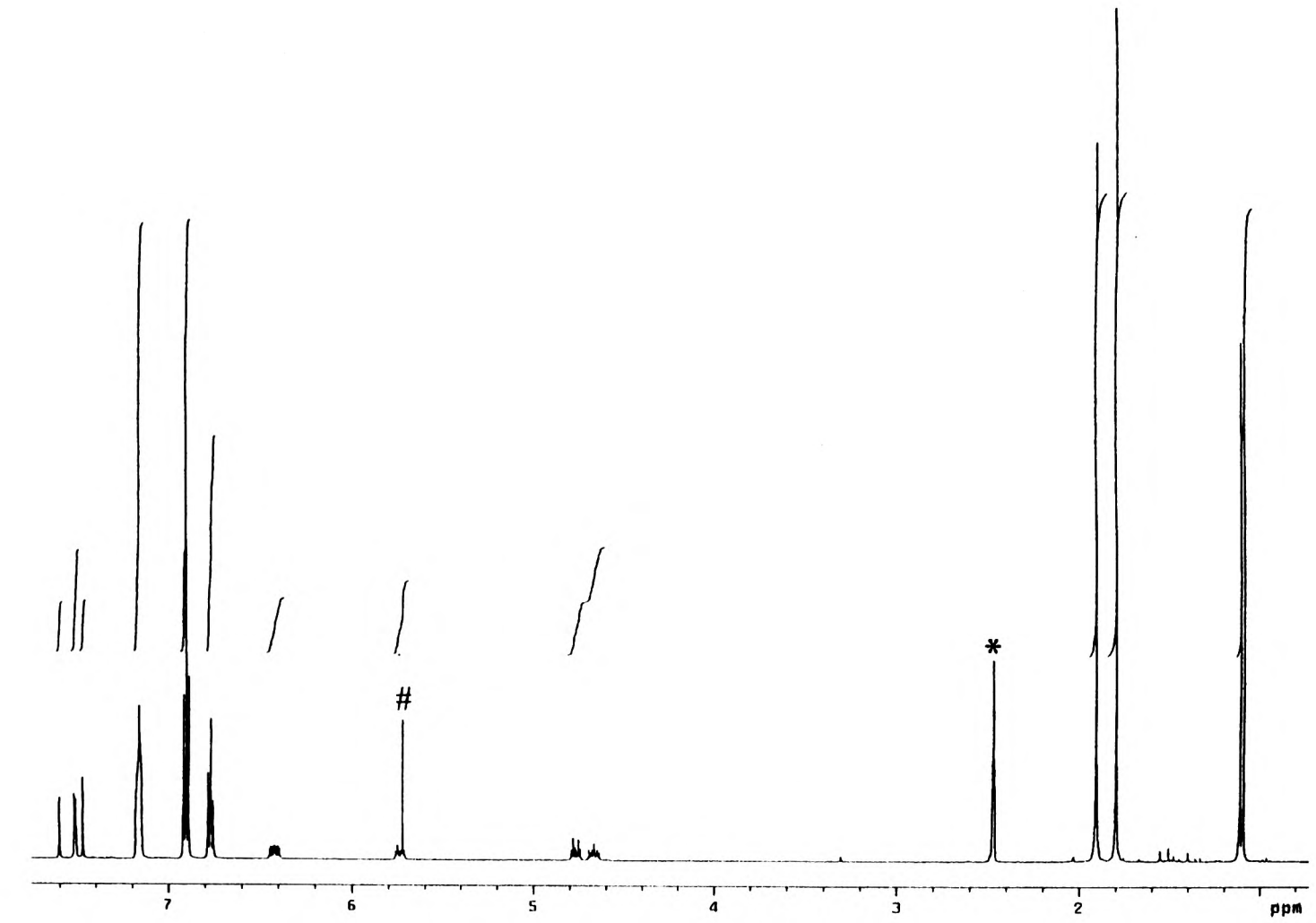

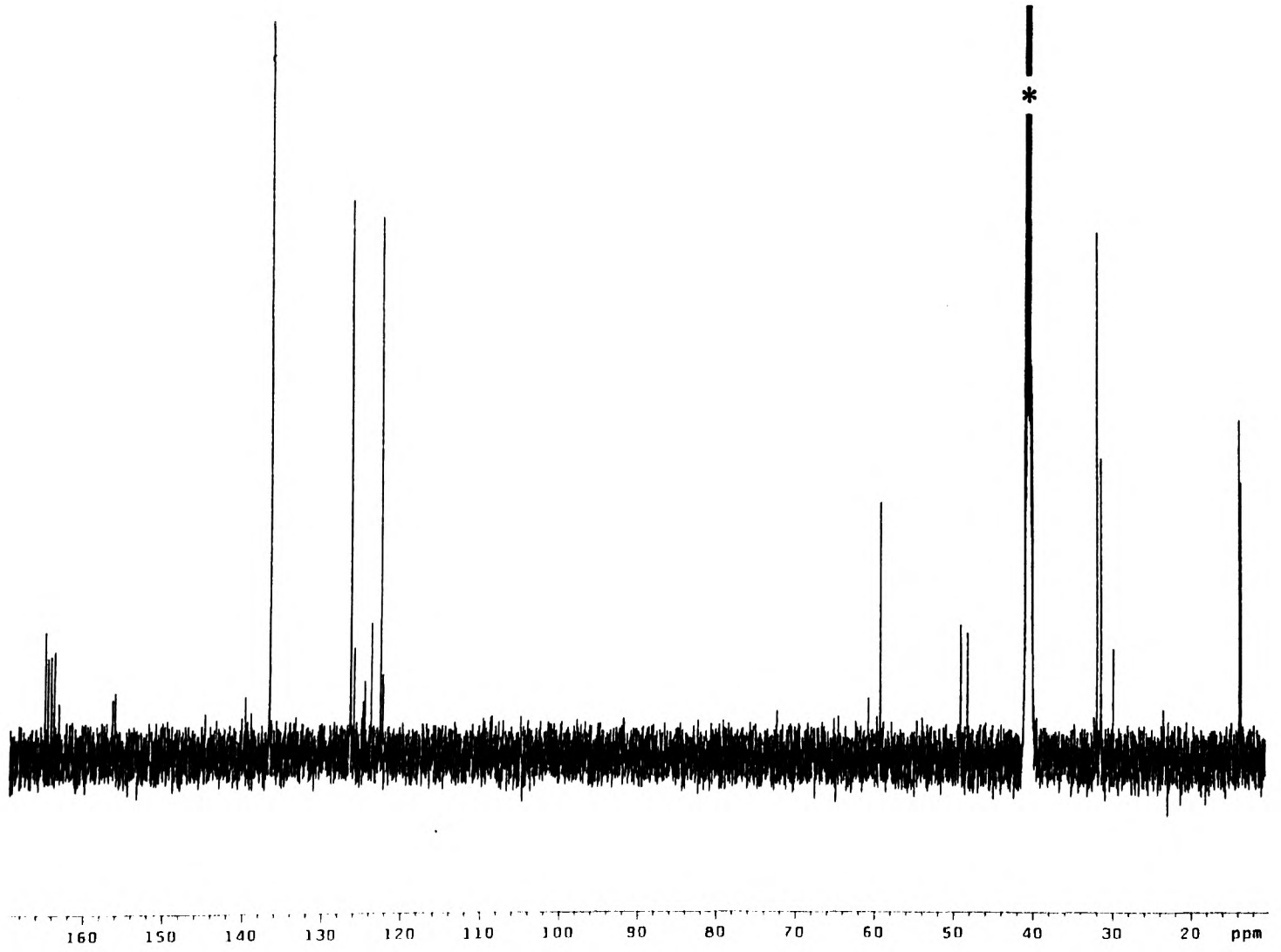

Figure 2.13 500 MHz ^{1}H and 125.7 MHz $^{13}C\{^{1}H\}$ NMR spectra of $[(^{tBu}CC^{eth})NiCl(PMe_3)][BPh_4]$ (**10**) in d^6-DMSO (* = solvent, # = CH_2Cl_2).

A ^{1}H NOESY spectrum of **10** (in d^{6}-DMSO) was recorded by Dr Daniel Haüßinger in order to aid the individual assignment of each proton signal. The structure of the cation $[(^{tBu}CC^{eth})NiCl(PMe_3)]^+$ is shown in figure 2.14, together with the through-space (dipolar) correlations between protons.

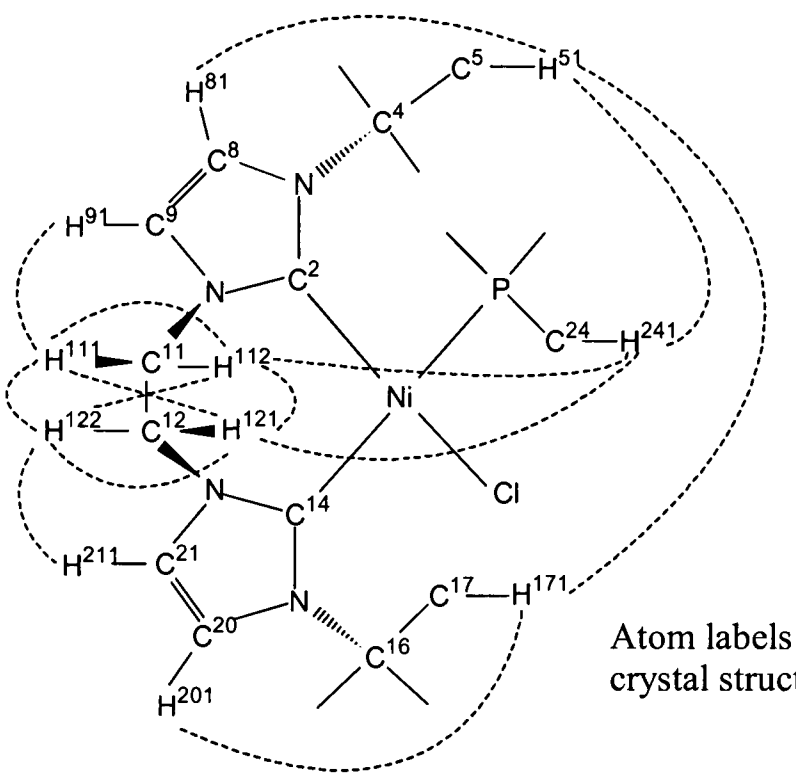

Atom labels from crystal structure

Figure 2.14 Molecular structure of the cation $[(^{tBu}CC^{eth})NiCl(PMe_3)]^+$. Dashed lines represent through-space (dipolar) correlations between protons.

The ^{1}H NOESY spectrum (figure 2.15) shows that only one of the two ^{t}Bu signals, δ 1.91 (H^{51}), is correlated with the PMe_3 signal δ 1.11 (H^{241}). Therefore the ^{t}Bu group with the signal at δ 1.91 must be closer in space to PMe_3, on the heterocyclic ring *cis* to PMe_3, and the ^{t}Bu group with the signal at δ 1.80 (H^{171}) must be further away on the ring *trans* to PMe_3. Both of the ^{t}Bu signals are also correlated with one (different) heterocyclic ring proton signal. The H^{51} signal is correlated with δ 7.60 (H^{81}) and the H^{171} signal is correlated with δ 7.51 (H^{201}). These ring protons must be the nearest to the ^{t}Bu groups, in the adjacent ring positions, and on the rings *cis* and *trans* to PMe_3 respectively. In contrast to the ^{1}H NOESY spectrum of $[(^{tBu}CC^{meth})NiCl(PMe_3)]Cl$ (**7**), the signals for the ^{t}Bu protons H^{51} and H^{171} are correlated with each other. Therefore, the presence of an additional carbon in the bridge causes the ^{t}Bu groups to become closer together in space. By comparing the X-ray structures of **7** and **10** (figures 2.11 and 2.18) it is estimated that the distances between the ^{t}Bu groups are 2.3 Å and 1.9 Å respectively, assuming free rotation about each N-C_{tBu} bond. As observed in the ^{1}H NOESY spectrum of **7**, signals corresponding to adjacent ring

protons on the same ring (H^{81} and H^{91}, or H^{201} and H^{211}) are not correlated. In contrast to the ^1H NOESY spectrum of **7**, signals corresponding to the ring protons adjacent to the bridge, H^{91} and H^{211}, are also not correlated (the extra carbon in the bridge causes H^{91} and H^{211} to be too far apart in space). All of the ethylene bridge proton signals are correlated to each other, but by far the most intense correlations were those observed between the pairs of signals δ 4.67 / 5.74 and δ 4.77 / 6.42, indicating that each pair represents two protons on the same methylene carbon. The ethylene bridge proton signals δ 4.67 and 4.77 are correlated to the signals δ 7.52 and 7.47 respectively, which represent the heterocyclic ring protons H^{91} and H^{211}, that are adjacent to the ethylene bridge. This also indicates that δ 4.67 and 4.77 (and therefore also δ 5.74 and 6.42) represent protons on separate carbons of the ethylene bridge. The PMe_3 signal is correlated with the ethylene bridge proton signals at δ 5.74 and 6.42, which are not on the same carbon. Since the protons at δ 5.74 and 6.42 are not on the same carbon, the signals at δ 5.74 and 6.42 must correspond to H^{112} and H^{121} because they are closer in space to PMe_3 than the two other ethylene bridge protons. This is consistent with the deviation of the heterocyclic rings from the nickel coordination plane ('ring twist') observed in the X-ray crystal structure of **10** (figure 2.18), causing the ^{t}Bu groups and ethylene bridge to point in opposite directions above and below the plane, and the ethylene bridge protons to point towards and away from the nickel centre. H^{112} and H^{121} can be viewed as being in *endo* positions, because the C-H bonds point more in the direction of the Ni centre / PMe_3 ligand than the other ethylene bridge C-H bonds, which point in an opposite direction to the Ni centre: H^{111} and H^{122} are therefore in *exo* positions (figure 2.18).

The ^1H NOESY experiment was used, as described above, to individually assign most of the proton signals. The assignment of the signals at δ 7.47 and 7.52 to the ring protons adjacent to the methylene bridge (H^{91} and H^{211}) is correct, but the NOESY spectrum provides no evidence as to which of the two signals corresponds to which of the two protons. Furthermore, the NOESY cannot indicate which pair of ethylene bridge signals δ 4.67 / 5.74 and δ 4.77 / 6.42 represents the protons of the methylene adjacent to the ring *cis* to PMe_3, and which represents those of the methylene adjacent to the ring *trans* to PMe_3.

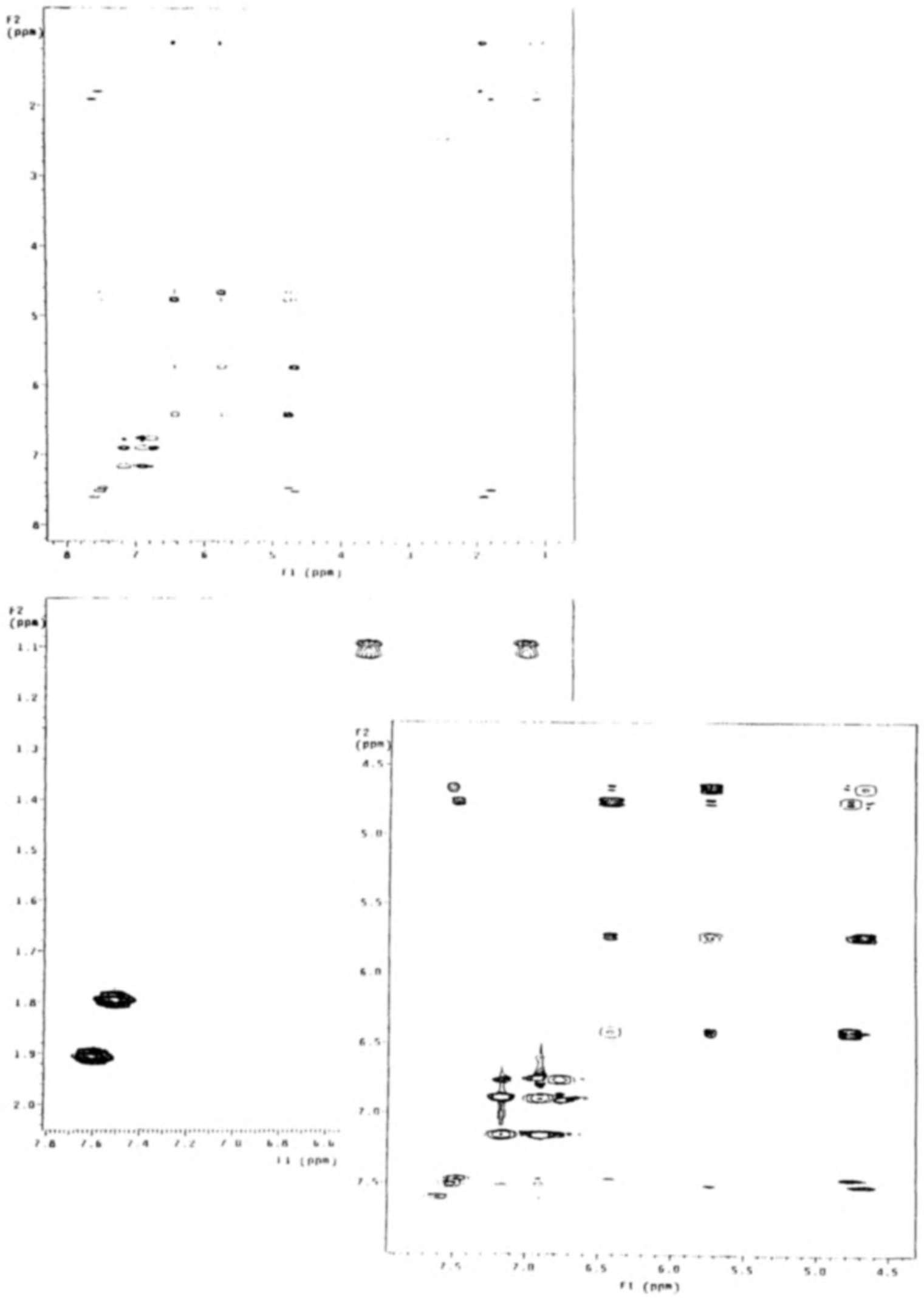

Figure 2.15 500 MHz ^{1}H NOESY spectrum of [(^{tBu}CC^{eth})NiCl(PMe$_3$)][BPh$_4$] (**10**) in d^6-DMSO.

A ^{1}H-^{13}C-$^{1}J_{CH}$ shift correlation NMR spectrum (figure 2.16) was recorded by Dr Daniel Haüßinger. This enabled individual assignment of the primary, secondary and tertiary carbon signals of **10** to the same extent to which the proton signals had already been assigned using the ^{1}H NOESY spectrum. Correlation of the pairs of ethylene bridge proton signals δ 4.67 / 5.74 and δ 4.77 / 6.42 with separate carbon signals (δ 48.9 and 48.1 respectively) confirmed that each pair represents two protons of one methylene carbon.

To complete the individual assignments of all the protons and carbons of the cation $[(^{tBu}CC^{meth})NiCl(PMe_3)]^{+}$, a ^{1}H-^{13}C-$^{n}J_{CH}$ shift correlation NMR spectrum was recorded, where n > 1 (figure 2.17). The signals for the heterocyclic ring protons adjacent to the ethylene bridge at δ 7.47 and 7.52 were successfully assigned to the protons H^{211} and H^{91} respectively. The ^{1}H-^{13}C-$^{n}J_{CH}$ shift correlation NMR spectrum showed correlations due to $^{2}J_{CH}$ coupling between δ 7.47 and the signal for C^{20} at δ 122.0, and between δ 7.52 and C^{8} (δ 123.5), confirming which of the heterocyclic rings these protons are bonded to. It was then possible to use the ^{1}H NOESY correlations between the signals for these ring protons and those for the ethylene bridge protons to complete the individual ^{1}H assignments. The ethylene bridge signals δ 4.77, 6.42, 4.67 and 5.74 correspond to the protons H^{122}, H^{121}, H^{111} and H^{112} respectively. The ^{1}H-^{13}C-$^{1}J_{CH}$ shift correlation NMR spectrum was used thereafter to complete the individual assignments of the primary, secondary and tertiary carbon signals of **10**.

The quaternary carbon signals for the carbene carbons C^{2} and C^{14} were previously assigned as δ 156.0 and 163.4 respectively based on the difference in $^{2}J_{PC}$ coupling, which is significantly greater for the carbon *trans* to the PMe_3 ligand (111 Hz) than for the carbon *cis* to PMe_3 (41 Hz). This assignment was confirmed by the ^{1}H-^{13}C-$^{n}J_{CH}$ shift correlation NMR spectrum (n > 1) which showed $^{3}J_{CH}$ coupling between δ 156.0 (C^{2}) and the signals for H^{81} and H^{91} (δ 7.60 and 7.52), and between δ 163.4 (C^{14}) and the signals for H^{201} and H^{211} (δ 7.51 and 7.47). Furthermore, the quaternary ^{t}Bu signals observed at δ 59.08 and 59.10 were specifically assigned to the carbons C^{16} and C^{4} respectively, since $^{2}J_{CH}$ coupling was observed with the corresponding ^{t}Bu methyl protons H^{171} and H^{51}. Sufficient resolution was achieved in order to ascertain which off-diagonal peak corresponded to which quaternary carbon signal, which was not possible in the case of compound **7**.

The complete individual assignments of the ^{1}H and ^{13}C signals of the cation $[(^{tBu}CC^{eth})NiCl(PMe_3)]^+$ are summarised in section 6.10.

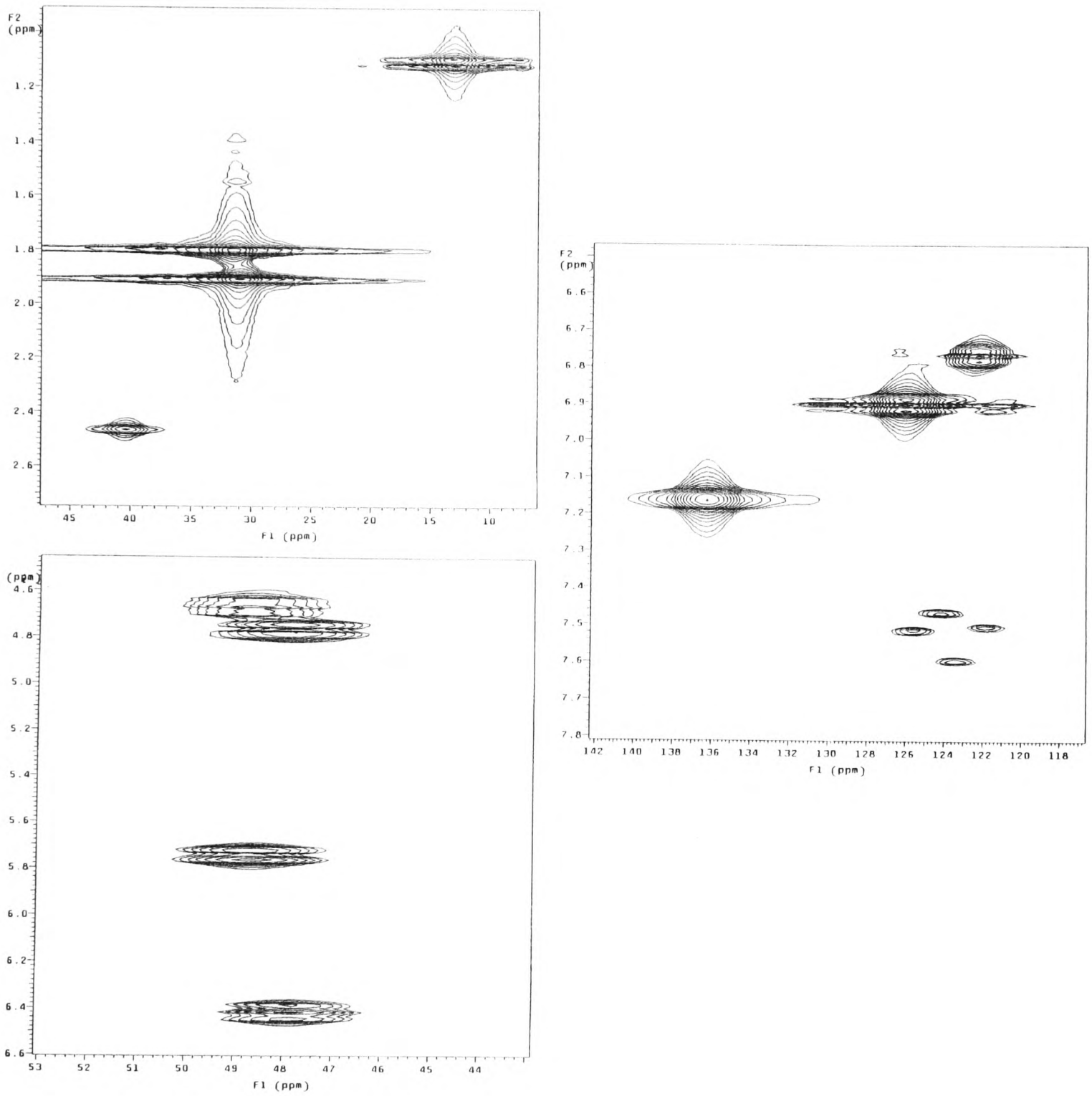

Figure 2.16 500 MHz ^{1}H-^{13}C-$^{1}J_{CH}$ shift correlation NMR spectrum of $[(^{tBu}CC^{eth})NiCl(PMe_3)][BPh_4]$ (**10**) in d^6-DMSO.

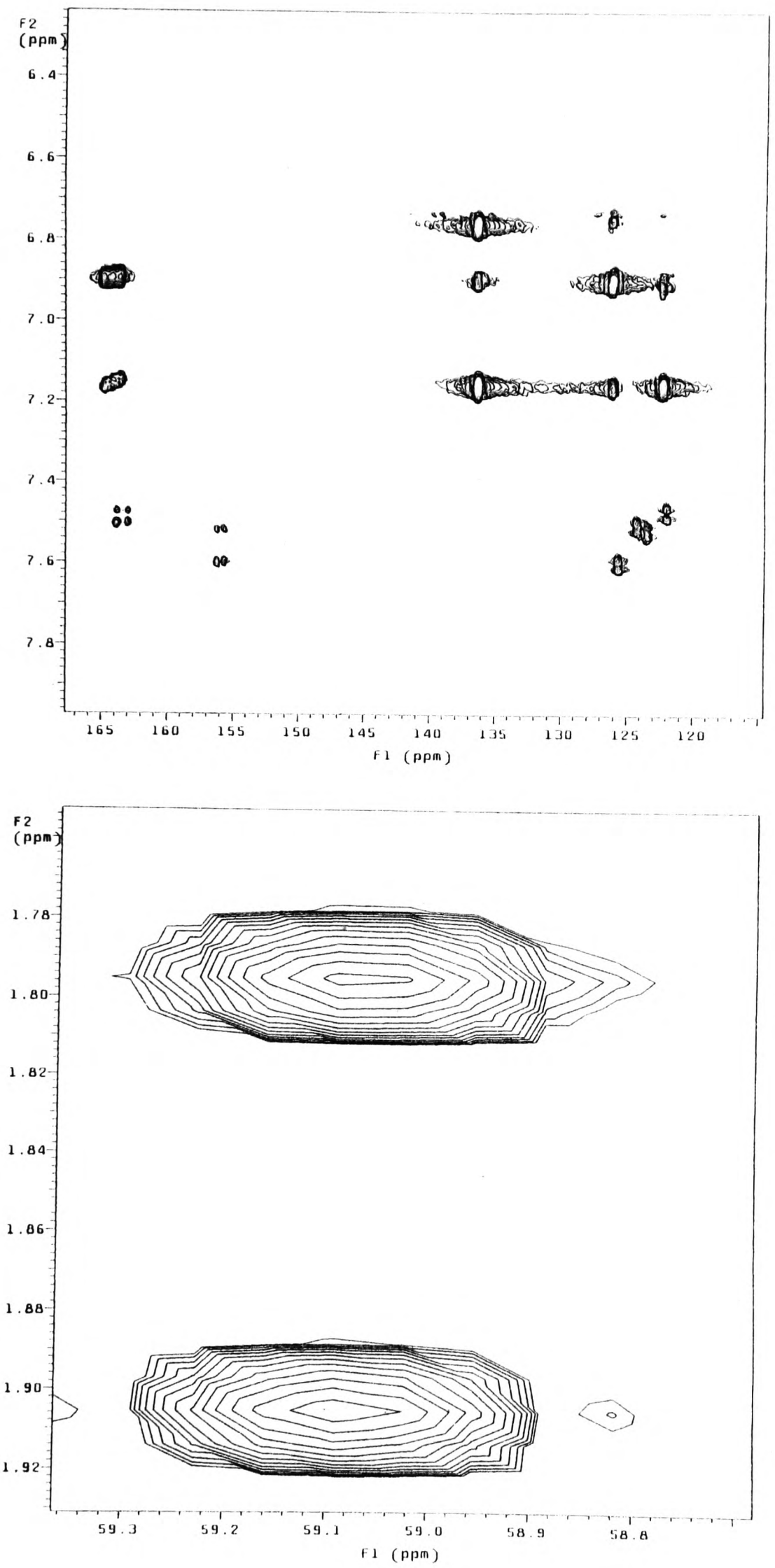

Figure 2.17 500 MHz ^{1}H-^{13}C-$^{n}J_{CH}$ (n > 1) shift correlation NMR spectrum of [($^{tBu}CC^{eth}$)NiCl(PMe_3)][BPh_4] (**10**) in d^6-DMSO.

Single crystals of [(^{tBu}CC^{eth})NiCl(PMe$_3$)][BPh$_4$] (**10**), of sufficient quality for X-ray structure determination (performed by Dr Richard Douthwaite), were grown from layering pentane onto a CH_2Cl_2 solution. Selected bond lengths and angles are given in table 2.4. The cation of **10**, shown in figure 2.18, is chiral and crystallises as a racemic mixture. The asymmetric unit contains one molecule of **10** as well as 1.5 molecules of CH_2Cl_2 as solvent of crystallisation. Prior to this research all structurally characterised transition metal complexes of chelating di-N-heterocyclic carbenes have incorporated a methylene bridge. Although the possibility was not excluded it has been proposed that ethylene-bridged di-N-heterocyclic carbenes prefer to adopt a bridging mode between two metal centres rather than chelate to a single metal atom.[1,33] This is apparently due to an energetically unfavourable eclipsed conformation of the two heterocyclic rings and the four hydrogen atoms of the ethylene bridge. However, the cation of **10** displays a boat-like conformation similar to that of [(^{tBu}CC^{meth})NiCl(PMe$_3$)]Cl (**7**), and projection along the C(11)-C(12) vector clearly shows a staggered conformation with a N(10)-C(11)-C(12)-N(13) torsion angle of 58.7(9)°. The geometry at the nickel centre is essentially square planar. However, the phosphorus atom is displaced perpendicularly from a plane defined by the nickel and the carbene carbons by 0.477(1) Å. The X-ray crystal structure of **7** shows a similar deviation, in which the phosphorus is displaced by 0.903(2) Å. In both cases this is due to nonbonding interactions between ^{t}Bu and phosphine methyl groups, but in **10** there appears to be an opposing interaction between the ethylene bridge and the phosphine methyls, which serves to reduce the deviation. As observed for **7**, the Ni-C bond lengths of **10** *trans* and *cis* to PMe$_3$ show a marked difference (in this case a difference of 0.058(15) Å), reflecting the greater *trans* influence of PMe$_3$ compared to Cl^-. The *trans* bond length Ni-C(14) = 1.915(8) Å is similar to those observed in the two previously structurally characterised nickel(II) carbene complexes, *trans*-dichlorobis(1,3-dicyclohexylimidazol-2-ylidene)nickel(II) (1.911(2) Å) (scheme 2.1)[10] and [Ni(^{Me}CC^{meth})$_2$][I]$_2$ (1.909(2) Å) (Eq. 13),[24] whereas the *cis* bond length Ni-C(2) = 1.857(7) Å is somewhat shorter. The *cis* and *trans* Ni-C bond lengths of the ethylene-bridged cation **10** (1.857(7) and 1.915(8) Å) are shorter than those of the methylene-bridged analogue **7** (1.871(4) and 1.942(4) Å), and are shorter than the Ni-C bond lengths of the compound [Ni(^{tBu}CC^{meth})$_2$][Br]$_2$ (**6**) (1.936(4) and 1.928(4) Å) which incorporates methylene-bridged dicarbene ligands.

The bite angle C(2)-Ni-C(14) = 88.4(4)° in compound **10** and the corresponding ^{tBu}CC^{meth} bite angle C(2)-Ni-C(6) = 84.92(18)° in compound **7** are similar to those of numerous

nickel(II) complexes of chelating *bis*-phosphines which incorporate a two-carbon-atom bridge such as 1,2-*bis*(diphenylphosphino)ethane (dppe), where angles are found within the range 85-90°.[34] By comparison, the limited number of structurally characterised nickel(II) complexes of *bis*-phosphines with one- and three-carbon-atom bridges display angles of 73-79 and 97-103°, overall an increase of typically 8-10° per each additional CH_2 unit. The relatively small difference in bite angle of ca. 3° between **7** and **10** is a consequence of the angle at which the heterocyclic rings are twisted relative to the coordination plane (tables 2.3 and 2.4). Significantly larger twist angles are present in **10** relative to **7**, accomodating the increased length of the bridge and reducing the requirement of a larger bite angle which would result in an energetically unfavourable eclipsed conformation of the ethylene bridged hydrogen atoms. The sum of the angles of **10** at N(13) (360.0(6)°) and N(10) (360.0(7)°) are as expected for sp^2 hybridisation; however, the internal angles of the seven-membered ring C(12)-N(13)-C(14) (130.6(7)°) and C(2)-N(10)-C(11) (121.9(6)°) indicate that a degree of ring strain at N(13) may be present. By comparison there appears to be little strain for the corresponding internal angles C(2)-N(3)-C(4) (123.2(4)°) and C(4)-N(5)-C(6) (120.3(4)°) of the 6-membered ring of **7**. Possibly of more significance is the proximity of adjacent ^{t}Bu substituents in these complexes. Assuming free rotation about each N-C_{tBu} bond, distances between ^{t}Bu groups of 2.3 Å (**7**) and 1.9 Å (**10**) are estimated. The steric pressure induced by these very close contacts cannot be relieved due to the rigid conformation of the dicarbene ligand.

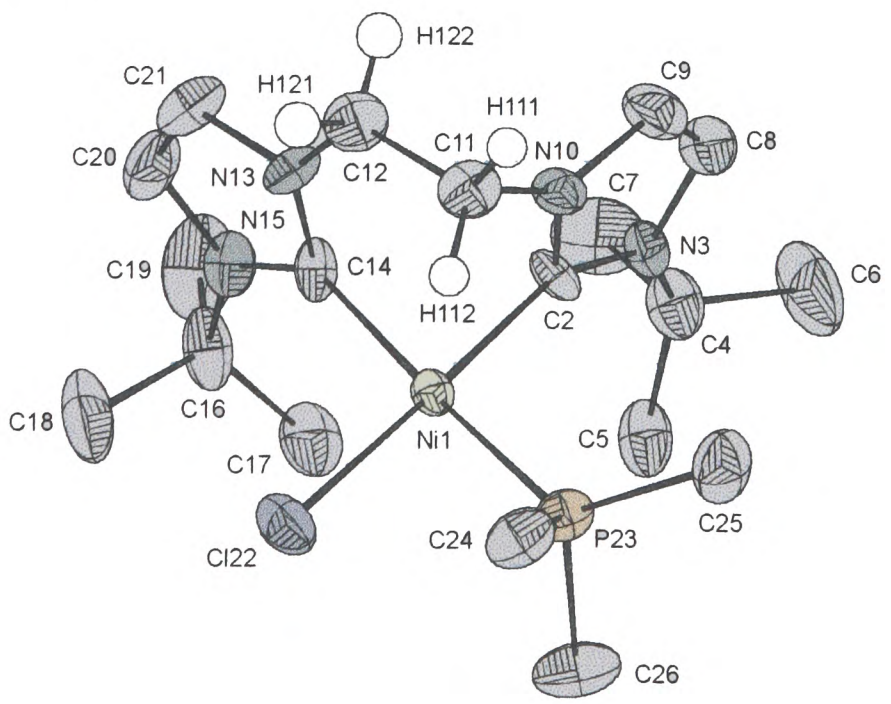

Figure 2.18 (a) View of the cation $[(^{tBu}CC^{eth})NiCl(PMe_3)]^+$ from the X-ray structure of **10**. Hydrogen atoms except for H^{111}, H^{112}, H^{121} and H^{122} are omitted for clarity.

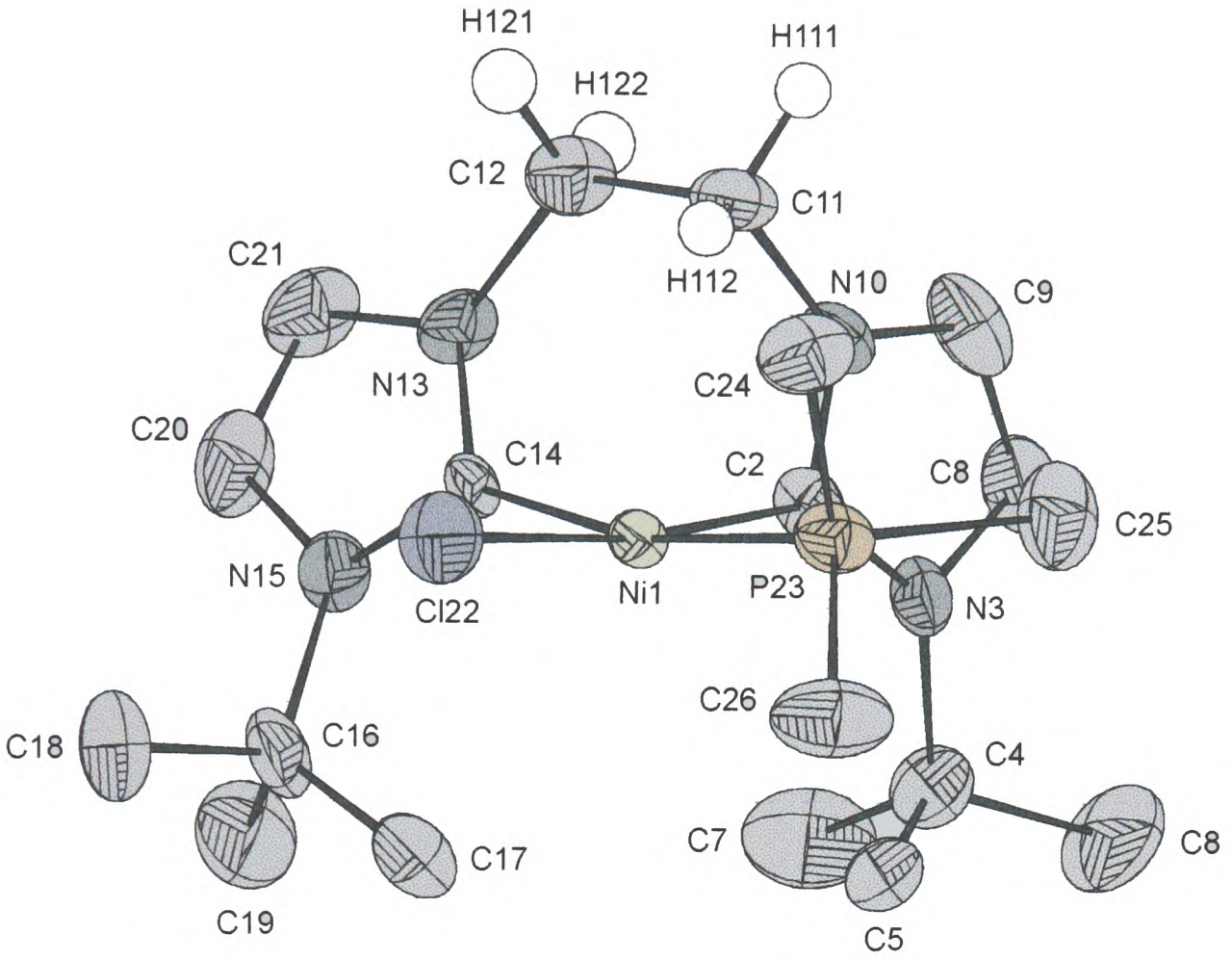

Figure 2.18 (b) Two views of the cation $[(^{tBu}CC^{eth})NiCl(PMe_3)]^+$ from the X-ray structure of **10**. Hydrogen atoms except for H^{111}, H^{112}, H^{121} and H^{122} are omitted for clarity.

Bond	Length (Å)	Bond	Angle (°)
Ni-C(2)	1.857(7)	C(2)-Ni-C(14)	88.4(4)
Ni-C(14)	1.915(8)	C(14)-Ni-Cl(22)	92.0(2)
Ni-P(23)	2.203(3)	C(2)-Ni-Cl(22)	171.3(2)
Ni-Cl(22)	2.200(2)	C(14)-Ni-P(23)	167.4(2)
C(2)-N(3)	1.327(9)	C(2)-Ni-P(23)	89.5(3)
C(2)-N(10)	1.349(9)	N(3)-C(2)-N(10)	106.3(6)
C(14)-N(13)	1.36(1)	N(13)-C(14)-N(15)	103.8(7)
C(14)-N(15)	1.356(9)	Ni-C(2)-N(10)	114.6(5)
C(8)-C(9)	1.322(14)	C(2)-N(10)-C(11)	121.9(6)
C(20)-C(21)	1.321(14)	N(10)-C(11)-C(12)	111.3(7)
		C(11)-C(12)-N(13)	116.0(7)
		C(12)-N(13)-C(14)	130.6(7)
		Ni-C(14)-N(13)	122.8(5)
		C(2)-N(10)-C(9)	110.4(7)
		C(9)-N(10)-C(11)	127.7(7)
		C(12)-N(13)-C(21)	117.7(7)
		C(14)-N(13)-C(21)	111.7(7)
		ring $twist_{C(2)}$*	62.3(8)
		ring $twist_{C(14)}$	73.5(9)

* The angle between the coordination plane defined by nickel and carbene carbon atoms and the heterocyclic ring containing C(n).

Table 2.4 Selected bond lengths and angles for $[(^{tBu}CC^{eth})NiCl(PMe_3)][BPh_4]$ (**10**).

2.4.14 Syntheses of $[Ni(^{tBu}CC^{meth})_2][Cl]_2$ (11)

By changing the reaction solvent from toluene to *ortho*-dichlorobenzene it was possible to obtain the dicationic *bis*(dicarbene) nickel(II) complex $[Ni(^{tBu}CC^{meth})_2][Cl]_2$ (**11**), in high yield, from reaction between $^{tBu}CC^{meth}$ (**4**) and either of $NiCl_2(PMe_3)_2$, $[(^{tBu}CC^{meth})NiCl(PMe_3)]Cl$ (**7**) and $[(^{tBu}CC^{eth})NiCl(PMe_3)]Cl$ (**9**) (scheme 2.8).

Ortho-dichlorobenzene was used as a less reactive alternative to dichloromethane (which causes immediate decomposition of the dicarbenes **4** and **5**) with the aim of solublising the cationic compounds **7** and **9** for further reactions with the free dicarbenes **4** and **5**.

The addition at room temperature of 1 equivalent of an *ortho*-dichlorobenzene solution of **4** to an *ortho*-dichlorobenzene solution of [(^{tBu}CC^{meth})NiCl(PMe$_3$)]Cl (**7**) gave a pale yellow precipitate, characterised as the dicationic *bis*(dicarbene) nickel(II) complex [Ni(^{tBu}CC^{meth})$_2$][Cl]$_2$ (**11**), in 87 % yield. Reaction between NiCl$_2$(PMe$_3$)$_2$ and 2 equivalents **4** in *ortho*-dichlorobenzene resulted in the same pale yellow precipitate, **11**, in 92 % yield. Finally, reaction in *ortho*-dichlorobenzene between the ethylene-bridged cationic nickel(II) complex [(^{tBu}CC^{eth})NiCl(PMe$_3$)]Cl (**9**) and 2 equivalents **4** also afforded the pale yellow precipitate **11** (yield = 90 %).

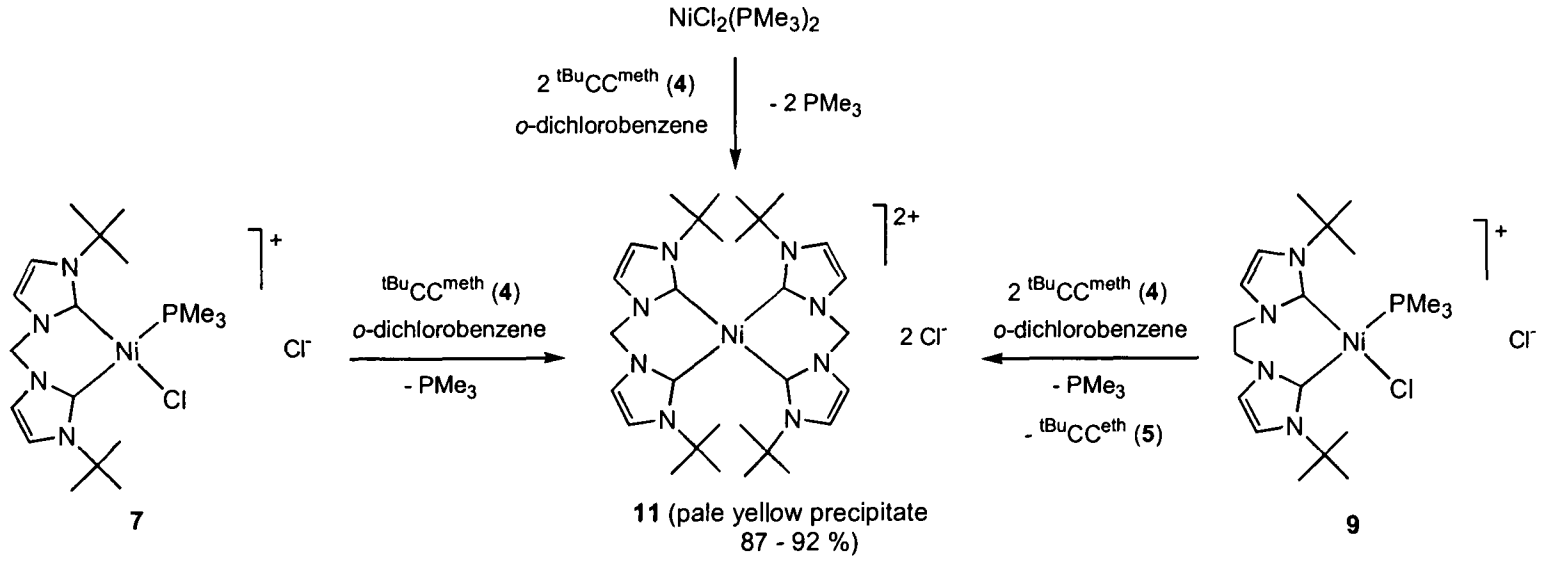

Scheme 2.8 Syntheses of [Ni(^{tBu}CC^{meth})$_2$][Cl]$_2$ (**11**).

Complex **11**, a pale yellow powder, is air-stable and soluble in alcohols, water and DMSO but insoluble in other common organic solvents such as dichloromethane and THF.

In addition to the synthesis of [Ni(^{tBu}CC^{meth})$_2$][Br]$_2$ (**6**) (section 2.4.1), the reactions shown in scheme 2.8 are in contrast to the observation by Herrmann et al. that [Ni(^{tBu}CC^{meth})$_2$][I]$_2$ cannot be synthesised by reaction between the diimidazolium diiodide salt **1** and Ni(OAc)$_2$ in DMSO (Eq. 33).[24] Again, the discrepency between these free dicarbene routes and the diimidazolium salt route is most likely due to the latter metathesis reaction requiring a more congested transition state compared to substitution by free dicarbene, even if via

predominantly an associative mechanism. An intermediate in the synthesis of homoleptic *bis*(dicarbene) nickel(II) complexes by the diimidazolium salt route, proposed by Herrmann and co-workers,[25] is shown in figure 1.11, and based on reactions shown in scheme 2.8, together with the knowledge that **7** is synthesised from $NiCl_2(PMe_3)_2$ and $^{tBu}CC^{meth}$ (**4**), an intermediate in the synthesis of **11** from $NiCl_2(PMe_3)_2$ and the free carbene should be $[(^{tBu}CC^{meth})NiCl(PMe_3)]Cl$ (**7**).

Reaction between $[(^{tBu}CC^{eth})NiCl(PMe_3)]Cl$ (**9**) and 2 equivalents **4** to give $[Ni(^{tBu}CC^{meth})_2][Cl]_2$ (**11**) is the first reported example where a transition metal N-heterocyclic carbene complex undergoes substitution of a carbene ligand. This is in contrast to the generally-held view that the M-C bond in transition metal N-heterocyclic carbene complexes is extremely robust, and kinetically inert to substitution, particularly for metals of groups 8-10.[1] No reaction occurred at room temperature between $[(^{tBu}CC^{meth})NiCl(PMe_3)]Cl$ (**7**) and $^{tBu}CC^{eth}$ (**5**) in *ortho*-dichlorobenzene, i.e. **5** is substituted by **4** but not vice versa.

2.4.15 Characterisation of $[Ni(^{tBu}CC^{meth})_2][Cl]_2$ (11)

The pale yellow powder $[Ni(^{tBu}CC^{meth})_2][Cl]_2$ (**11**) was characterised by electrospray mass spectrometry and ^1H, and $^{13}C\{^1H\}$ NMR spectroscopy. The electrospray mass spectrum contained a single peak (m/z = 289 $[M^{2+}]$) corresponding to the dication $[Ni(^{tBu}CC^{meth})_2]^{2+}$. ^1H and $^{13}C\{^1H\}$ NMR spectra of **11** are identical to those of the bromide analogue **6**.

2.4.16 Reaction Between $^{tBu}CC^{eth}$ (5) and $NiCl_2(PMe_3)_2$

In an attempt to prepare the *bis*(dicarbene) nickel(II) complex $[Ni(^{tBu}CC^{eth})_2][Cl]_2$, addition of 2 equivalents of an *ortho*-dichlorobenzene solution of $^{tBu}CC^{eth}$ (**5**) to an *ortho*-dichlorobenzene solution of $NiCl_2(PMe_3)_2$ resulted in an orange solution after half the addition was complete (i.e. after addition of 1 equivalent of dicarbene). The solution remained orange after the addition was complete, and no precipitate was formed after 16 hours. The product of the reaction (Eq. 42) was isolated and shown by ^1H NMR spectroscopy to be the compound $[(^{tBu}CC^{eth})NiCl(PMe_3)]Cl$ (**9**) (yield = 91 %).

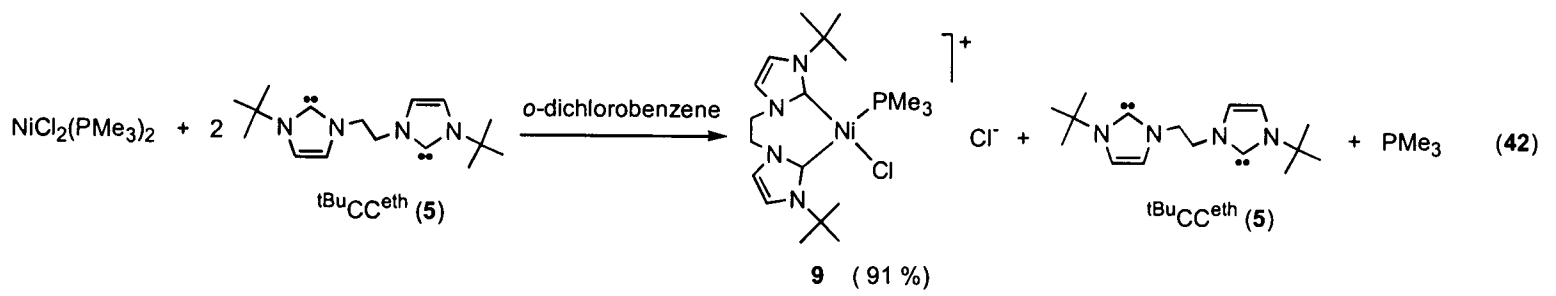

The fact that this attempt to prepare $[Ni(^{tBu}CC^{eth})_2]^{2+}$ was unsuccessful, as well as the previous attempt by reaction of **5** with $NiBr_2(DME)$, supports the view that substantial steric congestion would be present in the dication due to nonbonding interactions between ^{t}Bu groups and the ethylene bridge of an opposing dicarbene ligand. Such interactions can be identified by molecular modelling and by examination of the crystal structure of $[(^{tBu}CC^{eth})NiCl(PMe_3)][BPh_4]$ (**10**).

2.4.17 Attempts to Synthesise $[Ni(^{tBu}CC^{meth})(^{tBu}CC^{eth})][Cl]_2$

Two attempts were made to synthesise the mixed-ligand dicationic complex $[Ni(^{tBu}CC^{meth})(^{tBu}CC^{eth})][Cl]_2$ via reactions analogous to the one between $[(^{tBu}CC^{meth})NiCl(PMe_3)]Cl$ (**7**) and 1 equivalent $^{tBu}CC^{meth}$ (**4**) which gave $[Ni(^{tBu}CC^{meth})_2][Cl]_2$ (**11**) (scheme 2.9).

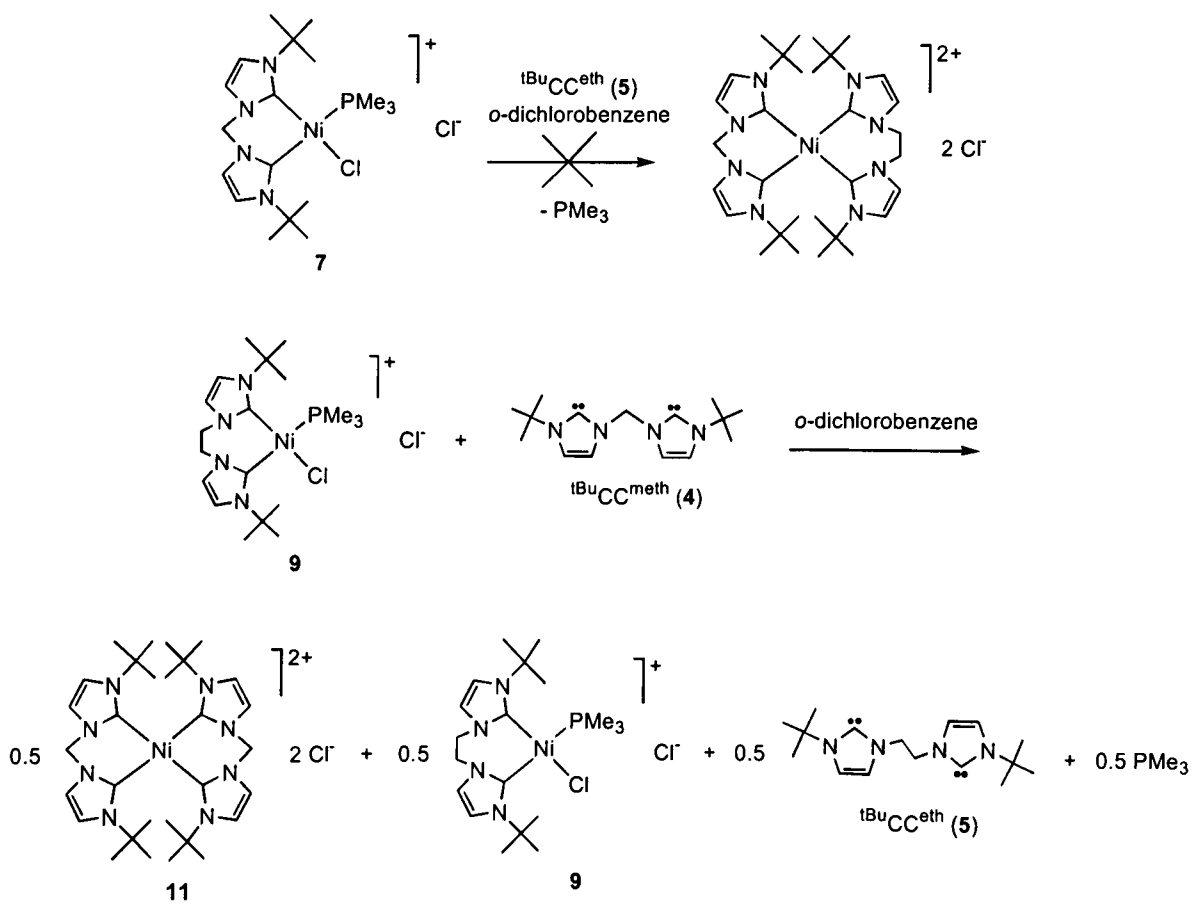

Scheme 2.9 Attempts to synthesise $[Ni(^{tBu}CC^{meth})(^{tBu}CC^{eth})][Cl]_2$.

In the first attempt, no reaction occurred between [(^{tBu}CC^{meth})NiCl(PMe$_3$)]Cl (**7**) and 1 equivalent ^{tBu}CC^{eth} (**5**) in *ortho*-dichlorobenzene. Secondly, a similar reaction between [(^{tBu}CC^{eth})NiCl(PMe$_3$)]Cl (**9**) and 1 equivalent **4** gave a 1:1:1 mixture of [Ni(^{tBu}CC^{meth})$_2$][Cl]$_2$ (**11**), unreacted **9** and **5**.

The inability to synthesise [Ni(^{tBu}CC^{meth})(^{tBu}CC^{eth})]$^{2+}$ is probably also because of the substantial steric congestion that would be present in the dication, in this case caused by nonbonding interactions between ^{t}Bu groups and the ethylene or methylene bridge of the opposing dicarbene ligand.

The formation of [Ni(^{tBu}CC^{meth})$_2$][Cl]$_2$ (**11**) in high yields (scheme 2.8), and the inability to synthesise the dications [Ni(^{tBu}CC^{eth})$_2$]$^{2+}$ (Eq. 42) and [Ni(^{tBu}CC^{meth})(^{tBu}CC^{eth})]$^{2+}$ (scheme 2.9), shows a thermodynamic preference in these complexes for a methylene- rather than an ethylene-bridged dicarbene ligand. This preference is clearly demonstrated by substitution of the ^{tBu}CC^{eth} ligand of [(^{tBu}CC^{eth})NiCl(PMe$_3$)]Cl (**9**) by ^{tBu}CC^{meth} (**4**) to give **11**, when the substitution of a ^{tBu}CC^{meth} ligand by ^{tBu}CC^{eth} (**5**) is never observed. Currently the mechanism by which substitution occurs is undetermined. Two likely intermediates are [(^{tBu}CC^{meth})NiCl(PMe$_3$)]$^+$ and the mixed dicarbene dication [Ni(^{tBu}CC^{meth})(^{tBu}CC^{eth})]$^{2+}$. The thermodynamic preference for the methylene-bridged ligand is probably due to steric rather than electronic factors, because the similarity in structures of **4** and **5** presumably render them comparable σ-donors, and π-bonding is generally considered insignificant in N-heterocyclic carbene complexes of the transition metals. Therefore steric factors likely determine the thermodynamic stability of [(^{tBu}CC^{meth})NiCl(PMe$_3$)]$^+$, a likely intermediate in the substitution reaction, relative to the reactant [(^{tBu}CC^{eth})NiCl(PMe$_3$)]$^+$. Comparison of the crystal structures of these two cations (section 2.4.13) suggests that lower ring strain energy and partial alleviation of a repulsive ^{t}Bu-^{t}Bu interaction drive dicarbene substitution of **9** by **4**.

2.4.18 Attempts to Reduce [Ni(^{tBu}CC^{meth})$_2$][Cl]$_2$ (11) and [(^{tBu}CC^{meth})NiCl(PMe$_3$)]Cl (7)

Attempts to prepare the neutral nickel(0) complex Ni(^{tBu}CC^{meth})$_2$, by reduction of [Ni(^{tBu}CC^{meth})$_2$][Cl]$_2$ (**11**) using zinc and potassium were unsuccessful. Reduction does not occur in the case of zinc (Eq. 43). However, reaction does occur when a pale yellow THF suspension of **11** is stirred over a potassium mirror to give a red suspension. ^{1}H NMR spectroscopy of the 40-60 petroleum ether extract, and subsequent toluene and THF extracts showed mixtures of free ^{tBu}CC^{meth} (**4**), 1-*tert*-butylimidazole (possibly a decomposition product of **4**), and in the latter cases other unidentified decomposition products as well.

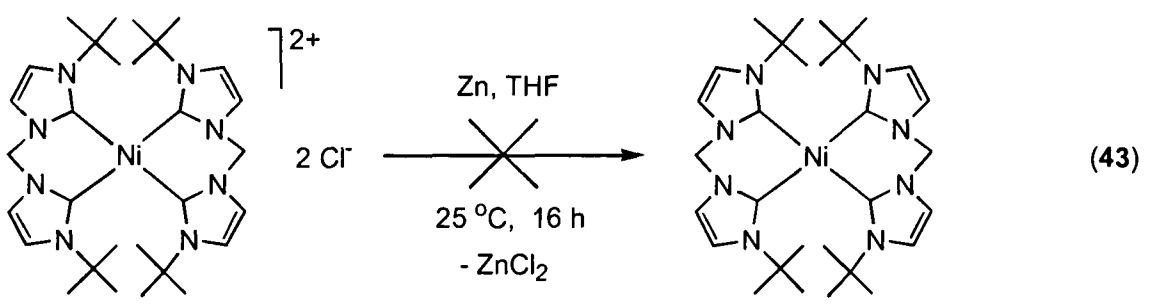

11 (43)

Although a *bis*(monocarbene) nickel(0) 14-electron complex is known (figure 1.9),[27] no examples of 18-electron *tetrakis*(monocarbene) or *bis*(dicarbene) complexes have been reported. This is probably due to charge buildup at the nickel atom as a consequence of strong σ-donation and the absence of appreciable π-acidity of N-heterocyclic carbene ligands. It is therefore reasonable to suggest that **4** is observed as a decomposition product of the nickel(0) species Ni(^{tBu}CC^{meth})$_2$, formed after reduction of **11** with potassium (scheme 2.10).

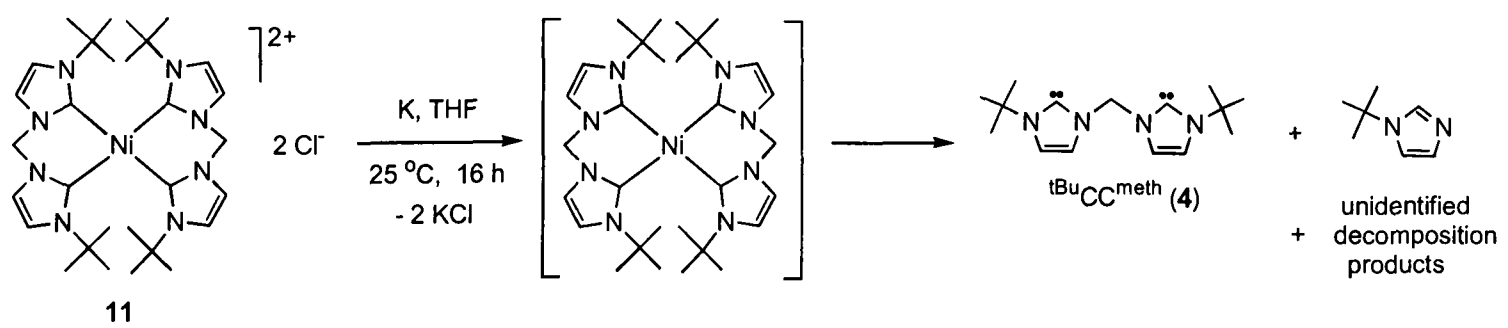

11

Scheme 2.10

An attempt to prepare the neutral complex [(^{tBu}CC^{meth})Ni(PMe$_3$)] was also unsuccessful with no reaction occurring between [(^{tBu}CC^{meth})NiCl(PMe$_3$)]Cl (**7**) and Zn (Eq. 44).

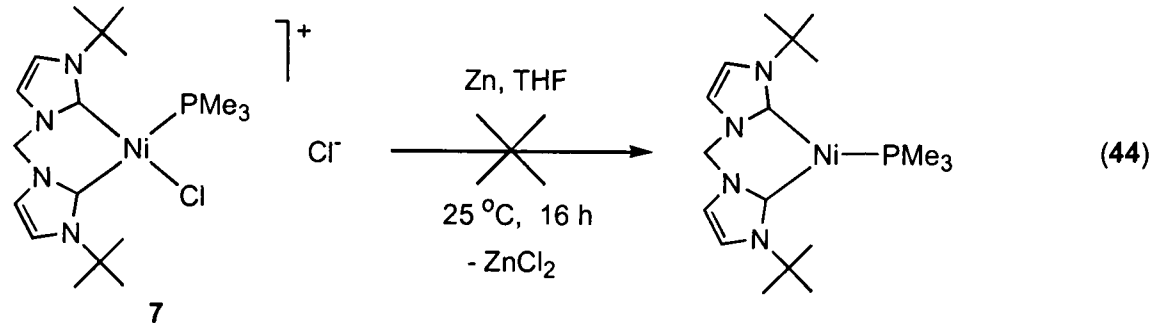

7 (44)

2.4.19 Reactions Between ^{tBu}CC^{meth} (4) and ^{tBu}CC^{eth} (5) and NiCl$_2$(PPh$_3$)$_2$

Reaction of dicarbenes **4** and **5** with NiCl$_2$(PMe$_3$)$_2$ in toluene yielded the cationic complexes **7** and **9** respectively, in which substitution by the dicarbene of only one of the two PMe$_3$ ligands took place. In a final attempt to prepare dicarbene nickel(II) *cis*-dihalide complexes NiCl$_2$(PPh$_3$)$_2$ was treated with the free dicarbenes in the hope that both triphenylphosphine ligands, which are less basic than trialkylphosphines, would be substituted by a dicarbene molecule.

To a dark red THF solution of NiCl$_2$(PPh$_3$)$_2$ was added 1 equivalent of a THF solution of ^{tBu}CC^{meth} (**4**) which gave a green supernatant and a light green precipitate. The precipitate was soluble in DMSO and partially soluble in acetonitrile, but insoluble in non-polar organic solvents, THF and dichloromethane. An analogous reaction between NiCl$_2$(PPh$_3$)$_2$ and 1 equivalent ^{tBu}CC^{eth} (**5**) gave a brown supernatant and grey precipitate. Again the precipitate was soluble in DMSO and partially soluble in acetonitrile, but insoluble in other common aprotic organic solvents.

In both cases ^{1}H NMR spectroscopy (d^6-DMSO and CD$_3$CN) of the precipitate and supernatant showed a similar mixture of products in each, with many peaks observed in the *tert*-butyl region (δ 1.0-2.5) and the ethylene or methylene bridge / imidazole ring proton region (δ 6.0-8.5). Elemental analyses (C, H, N, Ni, Cl) of the green and grey precipitates were within 0-7 % of the calculated values for Ni(^{tBu}CC^{meth})Cl$_2$ and Ni(^{tBu}CC^{eth})Cl$_2$ respectively.

Small quantities of turquoise crystals were grown upon standing acetonitrile solutions of the green and grey precipitates at room temperature for 1 week. However, only the crystals grown from the grey product of the reaction between **5** and $NiCl_2(PPh_3)_2$ were of sufficient quality for X-ray crystal structure determination (performed by Dr Richard Douthwaite). The turquoise compound was structurally characterised as 1,1'-(1,2-ethylene)*bis*(3-*tert*-butylimidazolium) tetrachloronickelate(II). Protonation of the dicarbene to form the diimidazolium salt presumably occurred due to the presence of a small amount of protic impurity. Two views of the structure are shown in figure 2.19, and selected bond lengths and angles are given in table 2.5. The asymmetric unit contains one molecule of 1,1'-(1,2-ethylene)*bis*(3-*tert*-butylimidazolium) tetrachloronickelate(II) and no solvent of crystallisation. The distances and angles between the imidazolium ring atoms are very similar to those of other structurally characterised imidazolium salts,[19,20] and to those of 1,1'-methylene*bis*(3-*tert*-butylimidazolium) dibromide (**2**) (section 2.2.5).

Bond	Length (Å)	Bond	Angle (°)
Ni-Cl(2)	2.2708(13)	Cl(2)-Ni-Cl(3)	121.61(6)
Ni-Cl(3)	2.2443(13)	Cl(2)-Ni-Cl(4)	102.45(6)
Ni-Cl(4)	2.2515(14)	Cl(3)-Ni-Cl(4)	108.35(5)
Ni-Cl(5)	2.2483(14)	Cl(2)-Ni-Cl(5)	112.30(6)
N(6)-C(15)	1.373(6)	Cl(3)-Ni-Cl(5)	100.75(5)
N(6)-C(16)	1.331(6)	Cl(4)-Ni-Cl(5)	111.51(6)
N(6)-C(20)	1.459(6)	C(15)-N(6)-C(16)	108.2(4)
N(8)-C(10)	1.382(6)	C(10)-N(8)-C(16)	108.4(4)
N(8)-C(16)	1.315(6)	N(6)-C(16)-N(8)	108.9(4)
N(8)-C(17)	1.491(6)	N(6)-C(15)-C(10)	107.4(4)
C(10)-C(15)	1.335(7)	N(8)-C(10)-C(15)	107.1(4)
C(20)-C(22)	1.514(7)	N(6)-C(20)-C(22)	109.6(4)
		N(7)-C(22)-C(20)	109.7(4)

Table 2.5 Selected bond lengths and angles for 1,1'-(1,2-ethylene)*bis*(3-*tert*-butylimidazolium) tetrachloronickelate(II).

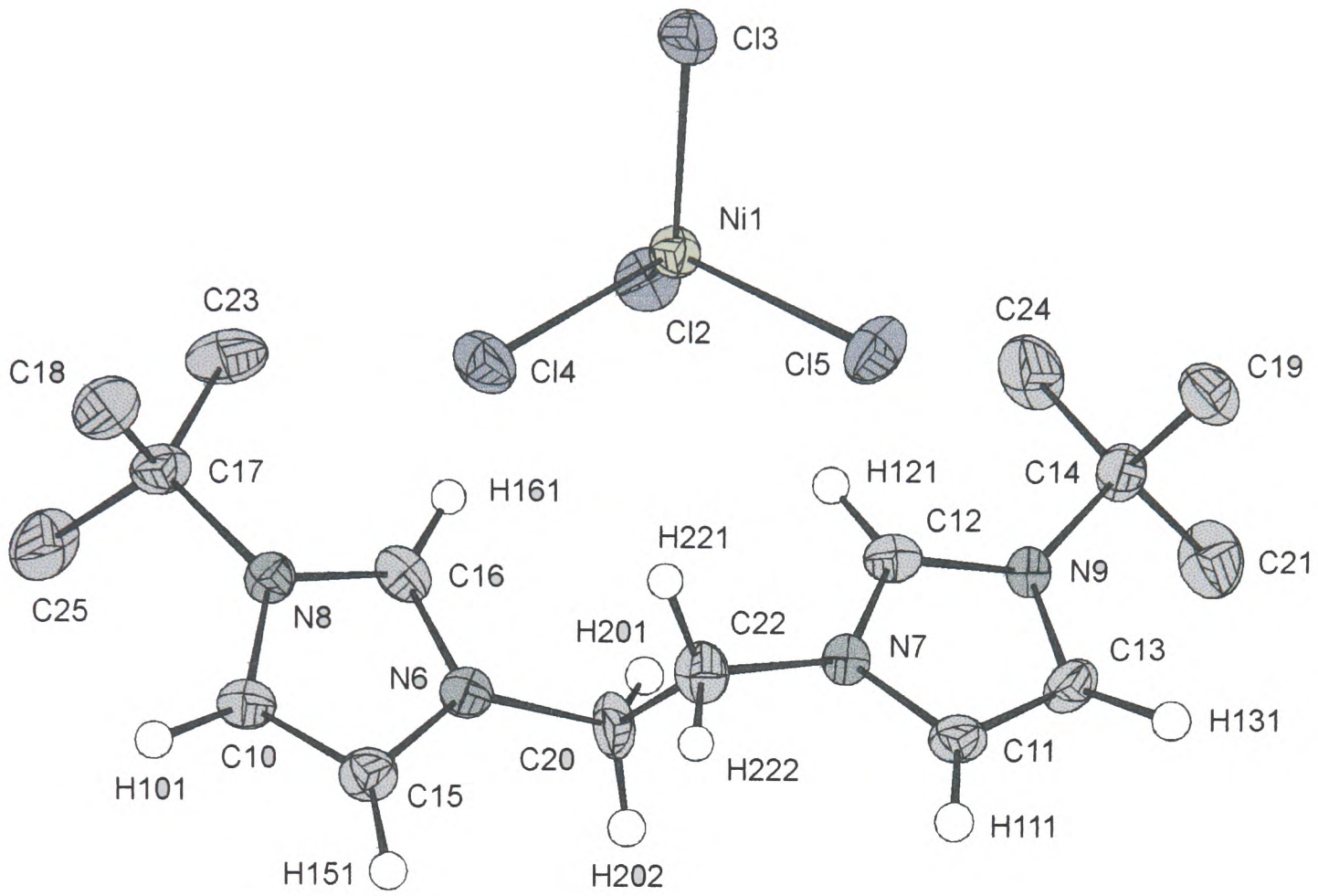

Figure 2.19 Two views of the X-ray structure of 1,1'-(1,2-ethylene)*bis*(3-*tert*-butylimidazolium) tetrachloronickelate(II). ^{t}Bu hydrogen atoms, and in the lower picture all hydrogen atoms, are omitted for clarity.

A similar tetrachloropalladate(II) compound incorporating two monoimidazolium cations (figure 2.20) was structurally characterised by Dullius et. al. in 1998.[35] The X-ray crystal structure showed shorter distances between two of the four chlorine atoms and the NCN carbon atoms of the two imidazolium rings, and Pd-Cl bond distances ca. 0.1 Å longer for the two chlorine atoms in question. This was attributed to strong hydrogen bonding between the two chlorine atoms and N(C*H*)N hydrogens of the cationic imidazolium rings (figure 2.20).

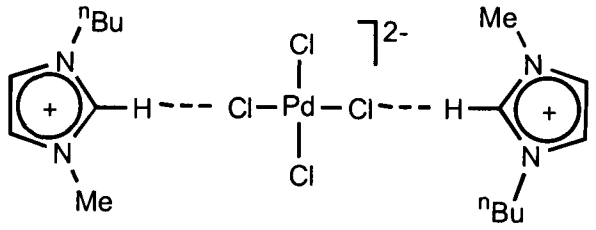

Figure 2.20 *Bis*(1-*n*-butyl-3-methylimidazolium) tetrachloropalladate(II).

The interatomic distances between each of the four chlorine atoms of the $NiCl_4^{2-}$ anion and the N(C*H*)N hydrogen atoms of the dication of 1,1'-(1,2-ethylene)*bis*(3-*tert*-butylimidazolium) tetrachloronickelate(II) are shown in table 2.6. The chlorine - N(*C*H)N carbon distances are also included because of the limited accuracy of Cl-H distances (all C-H bond lengths are fixed because the quality of the crystal structure was such that the hydrogens could not be unambiguously determined from a difference map).

-	C(16)	H(161)	C(12)	H(121)
Cl(2)	3.66	2.80	3.55	2.61
Cl(3)	6.40	5.90	5.95	5.45
Cl(4)	3.41	3.41	5.01	4.62
Cl(5)	5.60	5.28	3.19	3.25

Table 2.6 Interatomic distances (Å) between chlorine atoms of the anion, and N(*C*H)N carbon atoms / N(C*H*)N hydrogen atoms of the cation in the compound 1,1'-(1,2-ethylene)*bis*(3-*tert*-butylimidazolium) tetrachloronickelate(II).

It is apparent that Cl(2) and Cl(4) are significantly closer to C(16) / H(161) than the other chlorines, and that Cl(2) and Cl(5) are significantly closer to C(12) / H(121) than Cl(3) and Cl(4) (table 2.6). Cl(3) is close to neither H(161) nor H(121) and has the shortest Ni-Cl

bond distance (2.2443(13) Å), whereas Cl(2) is close to both hydrogens and has the longest Ni-Cl distance (2.2708(13) Å). This data suggests that a degree of hydrogen bonding exists between Cl(2) and both H(121) and H(161), between Cl(4) and H(161) and between Cl(5) and H(121), with H-Cl bond lengths in the range 2.6-3.4 Å.

2.4.20 Reaction of the Green Precipitate Product of the Reaction Between $NiCl_2(PPh_3)_2$ and $^{tBu}CC^{meth}$ (4) with PMe_3

A dichloromethane suspension of the green precipitate was treated with 1 equivalent (assuming the empirical formula of $Ni(^{tBu}CC^{meth})Cl_2$) of PMe_3. Removal of the volatiles and washing the residue with diethyl ether afforded a yellow powder, shown by ^1H NMR spectroscopy (d^6-DMSO) and elemental analysis to contain the compound $[(^{tBu}CC^{meth})NiCl(PMe_3)]Cl$ (**7**). ^1H NMR spectroscopy also showed the diimidazolium cation of $^{tBu}CC^{meth}$ (**4**) and unidentified impurities (estimated purity = 50 %).

The formation of the cationic PMe_3 adduct **7** is evidence to support the presence of nickel(II) $^{tBu}CC^{meth}$ chloride compounds (e.g. the desired *cis*-dihalide compound $Ni(^{tBu}CC^{meth})Cl_2$, or oligomers similar to those shown in figure 2.5), in the mixture of products of the reaction between $^{tBu}CC^{meth}$ (**4**) and $NiCl_2(PPh_3)_2$. Similarly, the formation of 1,1'-(1,2-ethylene)*bis*(3-*tert*-butylimidazolium)tetrachloronickelate(II) (section 2.4.19) indicates the presence of nickel(II) $^{tBu}CC^{eth}$ compounds in the products of the reaction between $^{tBu}CC^{eth}$ (**5**) and $NiCl_2(PPh_3)_2$.

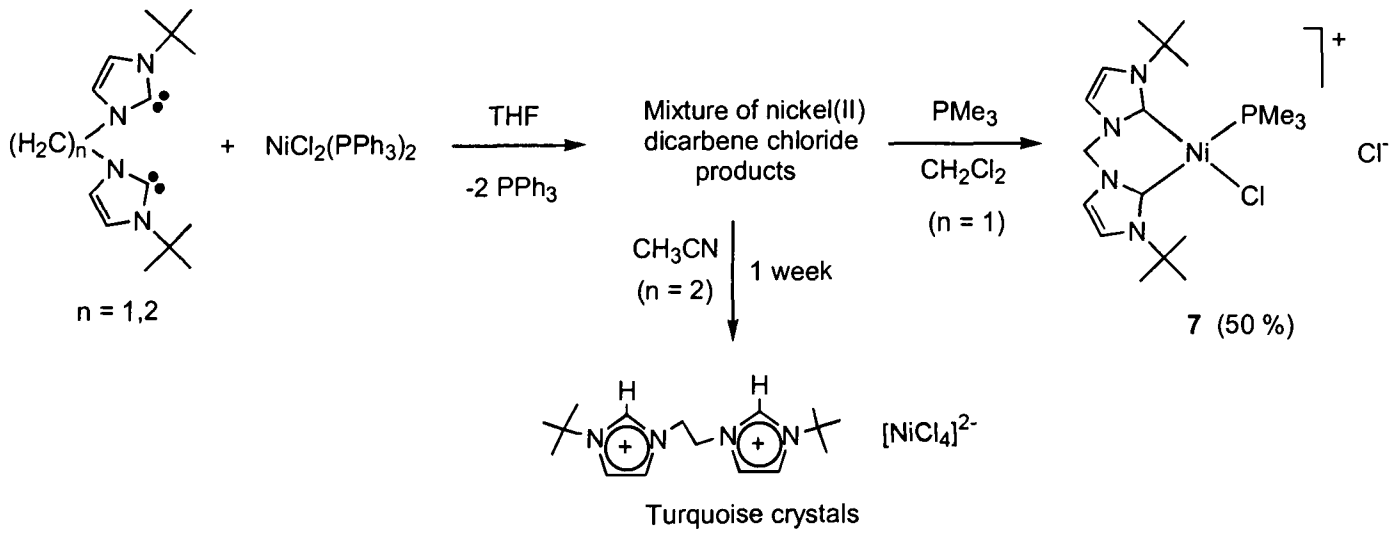

Scheme 2.11 Reactions of the dicarbenes **4** and **5** with $NiCl_2(PPh_3)_2$.

2.5 Ethylene Polymerisation Studies

The beige-coloured product of the reaction between $^{tBu}CC^{meth}$ (**4**) and $NiBr_2(THF)_{1.5}$, shown to be a mixture of nickel(II) dicarbene bromide compounds possibly containing the *cis*-dihalide compound $Ni(^{tBu}CC^{meth})Br_2$ (section 2.4.5), was tested for ability to catalyse ethylene polymerisation in a similar manner to the Brookhart diimine nickel(II) *cis*-dihalide complexes (see section 1.3.1). No polymer formation was observed (Eq. 45). Similarly, no polyethylene formation was observed using $[(^{tBu}CC^{meth})NiCl(PMe_3)]Cl$ (**7**) / MAO as the catalyst system. Experimental details are given in section 5.2.28.

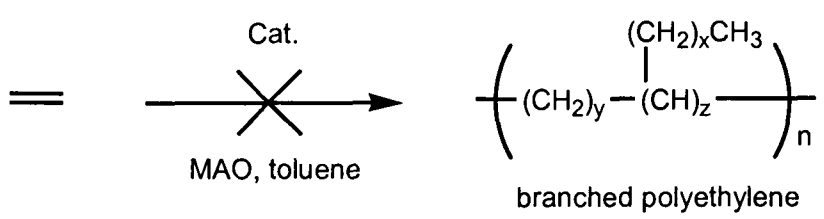

(45)

Cat. = '$[Ni(^{tBu}CC^{meth})Br_2]_n$' or $[(^{tBu}CC^{meth})NiCl(PMe_3)_2]Cl$ (**7**)

2.6 Summary and Conclusions

Typically, the dicarbene ligands $^{tBu}CC^{meth}$ (**4**) and $^{tBu}CC^{eth}$ (**5**) are prepared in ca. 60 % yields of over 5 g by deprotonation of the corresponding diimidazolium dibromide salts **2** and **3**, using potassium *bis*(trimethylsilyl)amide. In an attempt to prepare the chelating dicarbene nickel(II) *cis*-dichloride complexes $Ni(^{tBu}CC^{meth})Cl_2$ and $Ni(^{tBu}CC^{eth})Cl_2$, reaction between $NiCl_2(PMe_3)_2$ and 1 equivalent of **4** or **5** gave the monocationic salts $[(^{tBu}CC^{meth})NiCl(PMe_3)]Cl$ (**7**) and $[(^{tBu}CC^{eth})NiCl(PMe_3)]Cl$ (**9**), which undergo salt metathesis with $TlBPh_4$ to give $[(^{tBu}CC^{meth})NiCl(PMe_3)][BPh_4]$ (**8**) and $[(^{tBu}CC^{eth})NiCl(PMe_3)][BPh_4]$ (**10**). This shows that cationic nickel(II) complexes incorporating chelating di-N-heterocyclic carbenes can be prepared, including the first example of an ethylene-bridged chelating dicarbene transition metal complex. A comparison of the X-ray structures of **7** and **10** shows that the bite angles at the nickel atoms, 84.92(18) and 88.4(4) ° respectively, are comparable to nickel(II) complexes of two-carbon-atom bridging chelating *bis*(phosphines). Comparison of various structural parameters of the cations $[(^{tBu}CC^{meth})NiCl(PMe_3)]^+$ and $[(^{tBu}CC^{eth})NiCl(PMe_3)]^+$ also indicate that ethylene-bridged relative to methylene-bridged dicarbene ligands are sterically more demanding and are under a greater degree of steric strain. This is exemplified by the preparation of $[Ni(^{tBu}CC^{meth})_2]^{2+}$ and failure to prepare $[Ni(^{tBu}CC^{eth})_2]^{2+}$ or $[Ni(^{tBu}CC^{meth})(^{tBu}CC^{eth})]^{2+}$. Furthermore, no reaction is observed between $[(^{tBu}CC^{meth})NiCl(PMe_3)]Cl$ (**7**) and **5**, whereas **4** reacts with $[(^{tBu}CC^{eth})NiCl(PMe_3)]Cl$ (**9**) to give $[Ni(^{tBu}CC^{meth})_2][Cl]$ (**11**), which is the first example of transition metal N-heterocyclic carbene substitution chemistry. $[Ni(^{tBu}CC^{meth})_2][Br]_2$ was synthesised in low yield by reaction between 2 equivalents of **4** and $NiBr_2(DME)$ and was structurally characterised, whereas $[Ni(^{tBu}CC^{meth})_2][Cl]_2$ was prepared in near-quantitative yields by reaction between 2 equivalents of **4** and $NiCl_2(PMe_3)_2$, between 1 equivalent of **4** and **7**, or between 2 equivalents of **4** and **9**. Preparation of the dication $[Ni(^{tBu}CC^{meth})_2]^{2+}$ shows that free carbenes possibly offer a route to late transition metal complexes of bulky dicarbenes that the imidazolium salt method does not. Attempts to prepare the chelating dicarbene nickel(II) *cis*-dihalide complexes $Ni(^{tBu}CC^{meth})X_2$ and $Ni(^{tBu}CC^{eth})X_2$ (X = Cl, Br) were unsuccessful, which is consistent with the recently reported failed attempts using the imidazolium salt method (section 1.2.5).[24,25] Reactions of **4** and **5** with $NiCl_2(PMe_3)_2$ or $NiBr_2(DME)$ lead to the mono- or di-cations described above. Reaction of **4** with

$NiBr_2(THF)_{1.5}$ leads to a mixture of $^{tBu}CC^{meth}$ nickel(II) bromide compounds, which react with Lewis bases PMe_3 and d^5-pyridine to give the cationic compounds $[(^{tBu}CC^{meth})NiBr(PMe_3)]Br$ and $[(^{tBu}CC^{meth})NiBr(d^5\text{-py})]Br$ respectively. Finally, reactions of **4** and **5** with $NiCl_2(PPh_3)_2$ lead to mixtures of dicarbene nickel(II) chloride compounds which react to form the compound $[(^{tBu}CC^{meth})NiCl(PMe_3)]Cl$ (**7**) and the salt 1,1'-(1,2-ethylene)*bis*(3-*tert*-butylimidazolium) tetrachloronickelate(II), which was structurally characterised. There is a clear preference for cationic dicarbene nickel(II) dihalide complexes rather than neutral *cis*-dihalide complexes. This is possibly a consequence of the strong σ-donation and lack of appreciable π-acidity of the dicarbene ligands, which causes a charge buildup at the nickel centre, favouring the observed cationic nickel centres and non-coordinating halide anions. The failure to synthesise the 18-electron nickel(0) derivative $[Ni(^{tBu}CC^{meth})_2]$ by reduction of **11** was also attributed to an unfavourable charge buildup at the nickel centre. Attempts to polymerise ethylene using MAO / **7** and MAO / '$[^{tBu}CC^{meth})NiBr_2]_n$' were unsuccessful. A summary of the new chemistry described in chapter 2 is given in scheme 2.12.

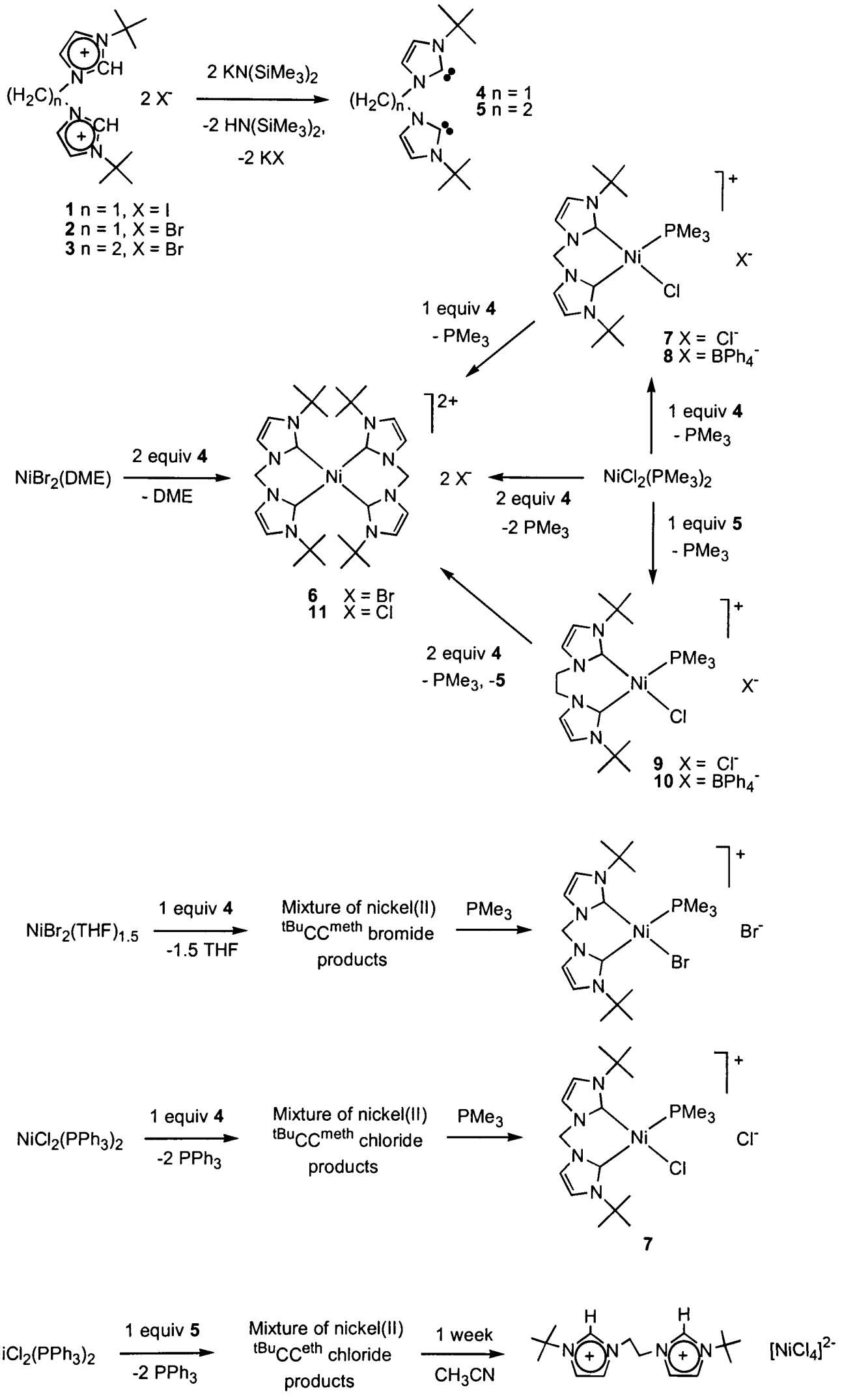

Scheme 2.12 Summary of the new chemistry described in chapter 2.

2.7 References

1) Herrmann, W. A.; Köcher, C. *Angew. Chem. Int. Ed. Engl.* **1997**, *36*, 2162.
2) Drent, E.; Budzelaar, P. H. M. *Chem. Rev.* **1996**, *96*, 663.
3) Gawley, R. E.; Aube, J. *Principles of Asymmetric Synthesis*; Pergamon: Oxford, 1996; Vol. 14
4) Noyori, R. *Asymmetric Catalysis in Organic Chemistry*; Wiley: New York, Chichester, 1994
5) Ojima, I. *Catalytic Asymmetric Synthesis*; VCH: New York, Cambridge, 1993
6) Seyden-Penne, J.; Curran, D. P. *Chiral Auxiliaries and Ligands in Asymmetric Synthesis*; Wiley: New York, Chichester, 1995
7) Herrmann, W. A.; Elison, M.; Fischer, J.; Köcher, C.; Artus, G. R. J. *Angew. Chem. Int. Ed. Engl.* **1995**, *34*, 2371.
8) Johnson, L. K.; Killian, C. M.; Brookhart, M. *J. Am. Chem. Soc.* **1995**, *117*, 6414.
9) Killian, C. M.; Tempel, D. J.; Johnson, L. K.; Brookhart, M. *J. Am. Chem. Soc.* **1996**, *118*, 11664.
10) Herrmann, W. A.; Gerstberger, G.; Spiegler, M. *Organometallics* **1997**, *16*, 2209.
11) Herrmann, W. A.; Reisinger, C.-P.; Spiegler, M. *J. Organomet. Chem.* **1998**, *557*, 93.
12) Gardiner, M. G.; Herrmann, W. A.; Reisinger, C.-P.; Schwarz, J.; Spiegler, M. *J. Organomet. Chem.* **1999**, *572*, 239.
13) Hofmann, K. *The Chemistry Of Heterocyclic Compounds*; Interscience: New York, 1953; Vol. 6, part 1
14) Radziszewski, B. *Chem. Ber.* **1882**, *15*, 1493.
15) Graf, F.; Hupfer, L. ; U.S. Pat. No. 4 450 277, **1984**.
16) Williams, D. J.; Vanderveer, D.; Jones, R. L.; Menaldino, D. S. *Inorg. Chim. Acta* **1989**, *165*, 173.
17) Rasika Dias, H. V.; Jin, W. *Tetrahedron Lett.* **1994**, *35*, 1365.
18) Avent, A. G.; Chaloner, P. A.; Day, M. P.; Seddon, K. R.; Welton, T. *J. Chem. Soc. Dalton Trans.* **1994**, 3405.
19) Arduengo III, A. J.; Harlow, R. L.; Kline, M. *J. Am. Chem. Soc.* **1991**, *113*, 361.
20) Langer, V.; Huml, K.; Reck, G. *Acta Crystallogra. Sect. B* **1982**, *38*, 298.
21) Arduengo III, A. J.; Rasika Dias, H. V.; Harlow, R. L.; Kline, M. *J. Am. Chem. Soc.* **1992**, *114*, 5530.
22) Herrmann, W. A.; Elison, M.; Fischer, J.; Köcher, C.; Artus, G. R. J. *Chem. Eur. J.* **1996**, *2*, 1627.
23) Arduengo III, A. J.; Dixon, D. A.; Kumashiro, K. K.; Lee, C.; Power, W. P.; Zilm, K. W. *J. Am. Chem. Soc.* **1994**, *116*, 6361.
24) Herrmann, W. A.; Schwarz, J.; Gardiner, M. G.; Spiegler, M. *J. Organomet. Chem.* **1999**, *575*, 80.
25) Herrmann, W. A.; Schwarz, J.; Gardiner, M. G. *Organometallics* **1999**, *18*, 4082.
26) Fehlhammer, W. P.; Bliss, T.; Kernbach, U.; Brüdgam, I. *J. Organomet. Chem.* **1995**, *490*, 149.
27) Arduengo III, A. J.; Gamper, S. F.; Calabrese, J. C.; Davidson, F. *J. Am. Chem. Soc.* **1994**, *116*, 4931.
28) Köcher, C.; Herrmann, W. A. *J. Organomet. Chem.* **1997**, *532*, 261.
29) Griffiths, D. C.; MacTavish, D. I.; Male, N. A. H.; Tocher, D. A.; Young, G. B. *J. Chem. Soc., Dalton Trans.* **1997**, 3373.
30) Pan, Y.; Young, G. B. *J. Organomet. Chem.* **1999**, *577*, 257.

31) Williams, D. H.; Fleming, I. *Spectroscopic Methods In Organic Chemistry*; McGraw-Hill: London, 1989
32) Derome, A. E. *Modern NMR Techniques For Chemistry Research*; Pergamon Press: Oxford, 1987
33) Herrmann, W. A.; Elison, M.; Fischer, J.; Köcher, C. A., G.R.J. *Chem. Eur. J.* **1996**, *2*, 772.
34) Allen, F. H.; Davies, J. E.; Galloy, J. J.; Johnson, O.; Kennard, O.; Macrae, C. F.; Mitchell, E. M.; Mitchell, G. F.; Smith, J. M.; Watson, D. G. *J. Chem. Inf. Comput. Sci.* **1991**, *31*, 187.
35) Dullius, J. E. L.; Suarez, P. A. Z.; Einloft, S.; de Souza, R. F.; Dupont, J. *Organometallics* **1998**, *17*, 815.

CHAPTER 3

Nickel(II) and Palladium(II) Methyl Complexes of Di-N-Heterocyclic Carbenes

3.1 Introduction

Nickel(II) and palladium(II) *cis*-dihalide or -dialkyl complexes of chelating di-N-heterocyclic carbenes were considered suitable target compounds for the investigation of dicarbenes as alternatives to chelating diphosphine and diimine ligands used in homogeneous catalysis (section 2.1). The research described in chapter 2 shows a clear preference for cationic nickel(II) complexes of ligands $^{tBu}CC^{meth}$ (**4**) and $^{tBu}CC^{eth}$ (**5**), rather than the desired neutral *cis*-dihalide compounds which could not be synthesised. Therefore it was the aim of subsequent research, described in chapter 3, to synthesise nickel(II) and palladium(II) *cis*-dimethyl complexes of **4** and **5**, and investigate the catalysis thereof.

At the commencement of the research described in this thesis there were no reported N-heterocyclic carbene transition metal alkyl complexes, although in 1998 Cavell and co-workers synthesised the methylpalladium monocarbene complexes shown in figure 3.1.[1] These complexes were shown to have significantly higher Heck coupling activities than N-heterocyclic palladium(II) diiodide complexes synthesised by Herrmann et al.[2-4] (section 1.2.6 (e)). Furthermore, in 1999 Cavell et al. isolated an *o*-tolylnickel *bis*-monocarbene bromide complex (figure 3.1), a catalyst for the Suzuki coupling of aryl halides (section 1.2.6(f)), and observed the methylnickel *bis*-monocarbene iodide complex by ^{1}H NMR spectroscopy (figure 3.1). The latter could not be isolated due to rapid decomposition via elimination of the 1,2,3,4,5-pentamethylimidazolium cation.[5]

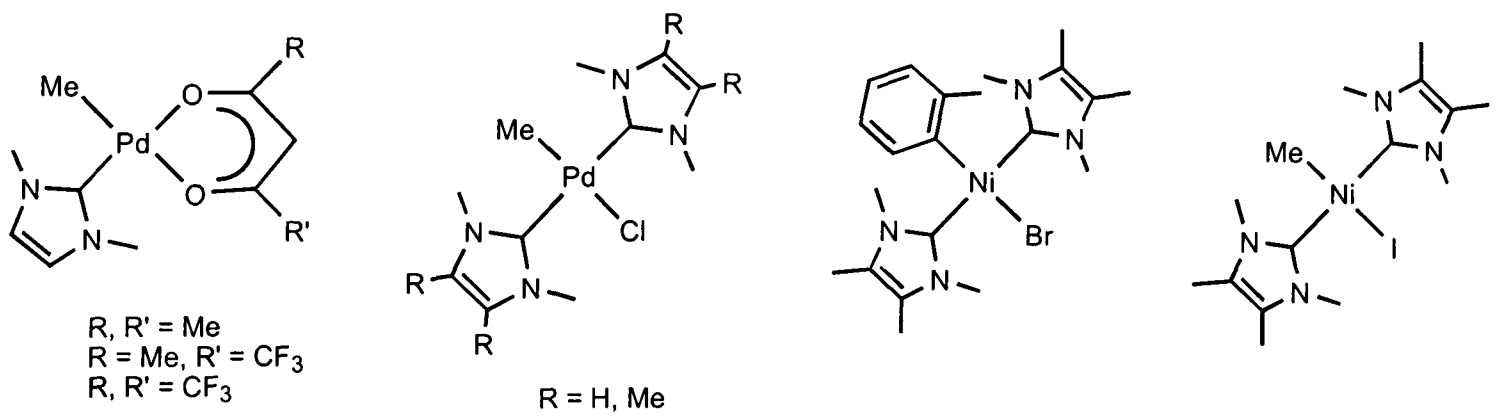

Figure 3.1 Hydrocarbyl nickel and palladium monocarbene complexes.

3.2 Nickel(II) Dimethyl Complexes of $^{tBu}CC^{meth}$ (4) and $^{tBu}CC^{eth}$ (5)

3.2.1 Synthesis of $[(\mu\text{-}^{tBu}CC^{meth})\{Ni(PMe_3)Me_2\}_2]$ (12)

In an attempt to prepare the *cis*-dimethyl compound $Ni(^{tBu}CC^{meth})Me_2$, reaction at -78 °C between $NiMe_2(PMe_3)_2$ and 1 equivalent $^{tBu}CC^{meth}$ (**4**) was performed. Two crops of pale orange crystals of $[(\mu\text{-}^{tBu}CC^{meth})\{Ni(PMe_3)Me_2\}_2].C_5H_{12}$ were isolated at -20 °C from the pentane extract (combined yield = 30 %).

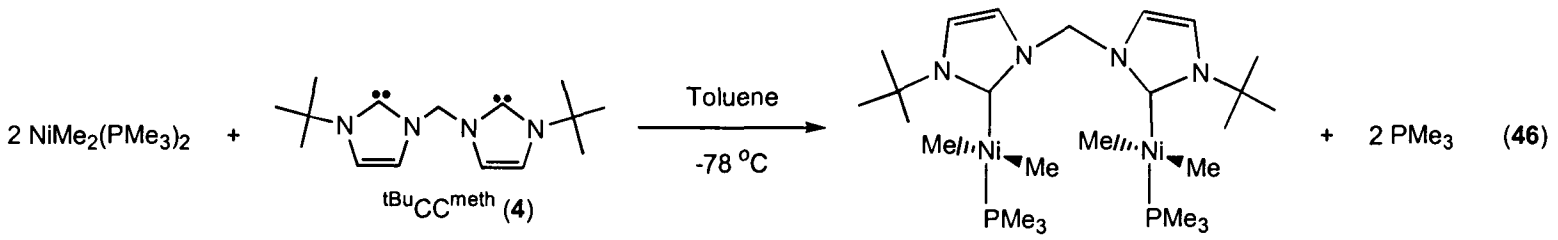

12 (pale orange crystals, 30 %)

$[(\mu\text{-}^{tBu}CC^{meth})\{Ni(PMe_3)Me_2\}_2]$ (**12**), the synthesis of which is shown in equation 46, is air- and thermally sensitive. The orange crystals decompose to form a dark powder after 1 month under nitrogen at -20 °C. **12** is soluble in all common aprotic organic solvents.

3.2.2 Characterisation of $[(\mu\text{-}^{tBu}CC^{meth})\{Ni(PMe_3)Me_2\}_2]$ (12)

The orange crystalline solid **12** was characterised by elemental analysis, ^1H, $^{13}C\{^1H\}$ and $^{31}P\{^1H\}$ NMR studies, and single crystal X-ray diffraction. ^1H NOESY and ^1H-^{13}C-$^nJ_{CH}$ shift correlation NMR experiments, performed by Dr Daniel Haüßinger, enabled individual assignment of each ^1H and ^{13}C signal.

The ^1H NMR spectrum of **12** in d^8-toluene (figure 3.2) is consistent with the molecular structure shown in equation 46. Doublets are observed for the four magnetically equivalent *trans* methyl groups (δ -0.64, $^3J_{PH}$ = 11 Hz) and for the six equivalent PMe_3 methyls (δ 1.05, $^2J_{PH}$ = 8 Hz), and a singlet is observed for the equivalent ^{t}Bu groups (δ 1.70). The ring protons resonate at δ 6.42 and 7.42, and the lowest-field signal, a singlet, corresponds to the two equivalent methylene bridge protons (δ 7.90). The single N(CH_2)N methylene

resonance is consistent with $^{tBu}CC^{meth}$ bridging two nickel centres, and is in contrast to the two resonances observed when $^{tBu}CC^{meth}$ chelates to a single metal centre (the boat conformation adopted by a chelating $^{tBu}CC^{meth}$ ligand renders the methylene protons magnetically inequivalent). In the $^{1}H\{^{31}P\}$ NMR spectrum (d^8-toluene) of **12** the resonances at δ -0.64 and 1.05 are observed as singlets due to phosphorus decoupling.

$^{13}C\{^{1}H\}$ NMR spectroscopy (figure 3.2) shows a doublet at δ 200.2 for the magnetically equivalent carbene carbon atoms of **12**. The magnitude of the coupling constant ($^{2}J_{PC}$ = 106 Hz) indicates that the carbene carbons are *trans* to PMe_3, by comparison with the *cis* and *trans* $^{2}J_{PC}$ values for complexes **6-11**. This resonance is shifted 30-45 ppm downfield with respect to the cationic nickel(II) carbene complexes **6-11**, and is 10-30 ppm further downfield than the carbene carbon resonances of neutral monocarbene late transition metal (including nickel) halide complexes, which are in the range δ 170-190.[6,7] The ring carbons C^5 and C^6 are observed as doublets ($^{4}J_{PC}$ = 4 Hz) and the four Ni-Me carbons are observed as a broad resonance at δ -9.2 (coupling to phosphorus could not be accurately measured).

The $^{31}P\{^{1}H\}$ NMR spectrum (d^8-toluene) of **12** shows a singlet at δ -3.83.

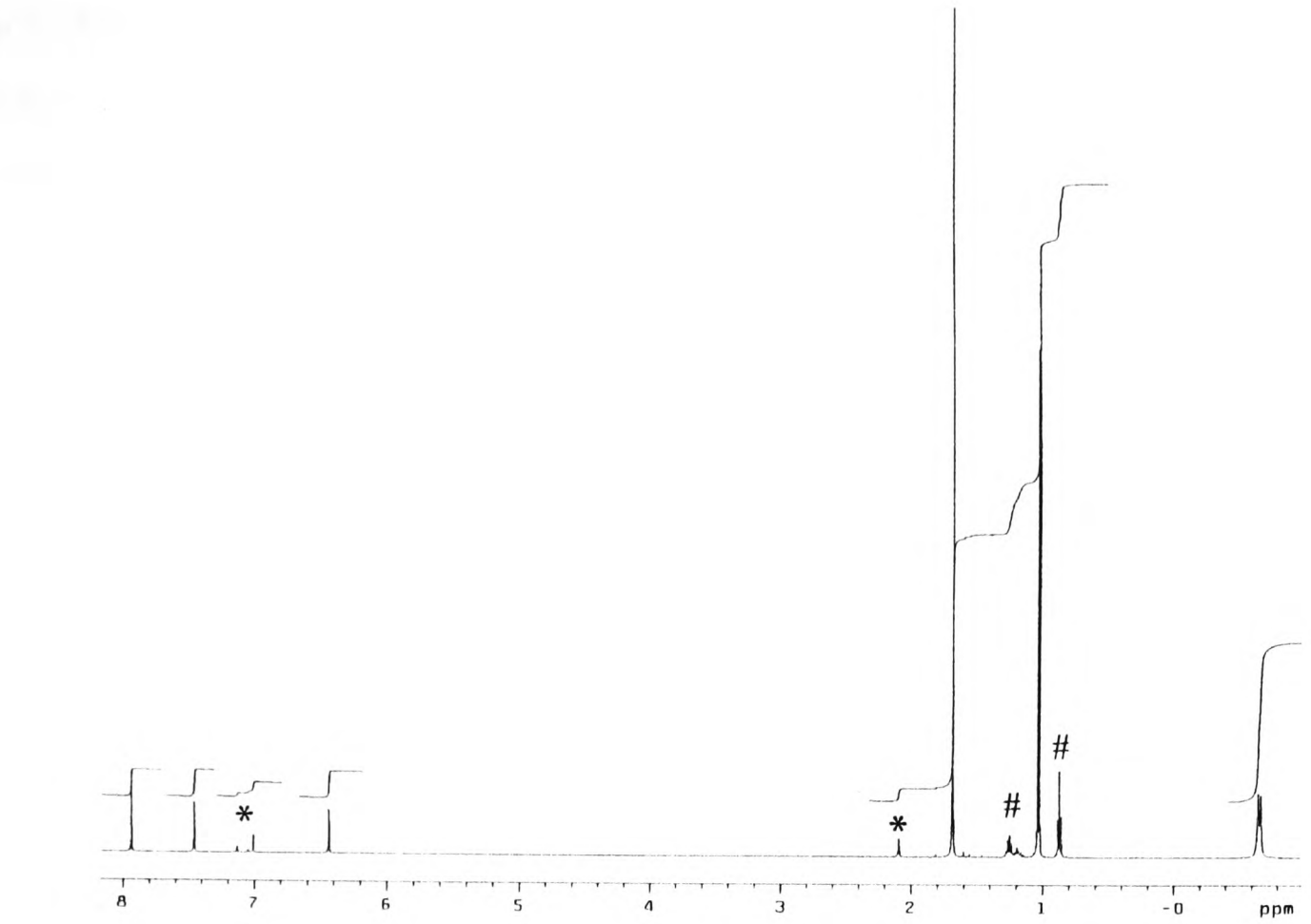

Figure 3.2 500 MHz ^{1}H and 125.7 MHz $^{13}C\{^{1}H\}$ NMR spectra of $[(\mu\text{-}^{tBu}CC^{meth})\{Ni(PMe_3)Me_2\}_2]$ (**12**) in d^8-toluene (* = solvent, # = pentane).

A ^{1}H NOESY spectrum of **12** was recorded by Dr Daniel Haüßinger in order to aid the individual assignment of each proton signal. The structure of **12** is shown in figure 3.3, together with the through-space (dipolar) correlations between protons.

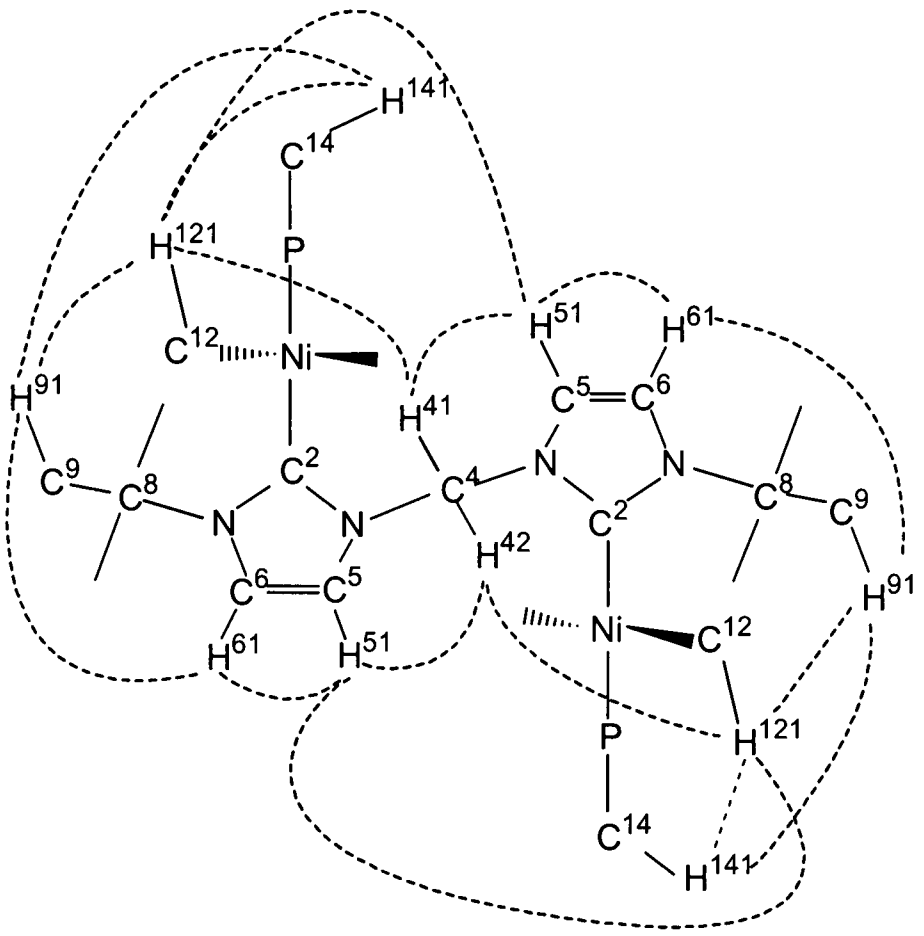

Atom labels from crystal structure

Figure 3.3 Molecular structure of $[(\mu\text{-}^{tBu}CC^{meth})\{Ni(PMe_3)Me_2\}_2]$ (**12**).
Dashed lines represent through-space (dipolar) correlations between protons.

The ^{1}H NOESY spectrum (figure 3.4) shows correlations between the ^{t}Bu signal and the ring proton signal at δ 6.42, and between the methylene bridge signal and the other ring proton signal at δ 7.42. This allows the assignment of the former signal to H^{61} (ring protons adjacent to ^{t}Bu) and the latter to H^{51} (ring protons adjacent to methylene bridge). Unsurprisingly the methyl signal at δ -0.64 (H^{121}) is correlated with the ^{t}Bu and the PMe_3 signals, but the methyl signal is also correlated with the methylene bridge proton signal, and with the heterocyclic ring proton signal for H^{51}. The latter through-space interaction is consistent with a $^{tBu}CC^{meth}$ ligand conformation in which the heterocyclic rings are staggered, i.e. not coplanar, to minimise $NiMe_2(PMe_3)$-$NiMe_2(PMe_3)$ nonbonding interactions such that the $NiMe_2$ protons (H^{121}) of one nickel and the H^{51} proton of the heterocyclic ring bonded to the other nickel are brought into proximity. Finally, correlations are observed between the signals for the ring protons H^{51} and H^{61}, and between the ^{t}Bu and PMe_3 signals.

Following the individual assignment of the proton signals a ^{1}H-^{13}C-$^{1}J_{CH}$ shift correlation NMR spectrum (figure 3.5) was recorded by Dr Daniel Haüßinger which enabled individual assignment of the primary, secondary and tertiary carbon signals of **12**.

A ^{1}H-^{13}C-$^{n}J_{CH}$ (n > 1) shift correlation NMR spectrum (figure 3.6) was also recorded by Dr Daniel Haüßinger. The spectrum showed a correlation between δ 1.70 (H^{91}) and δ 57.0 due to $^{2}J_{CH}$ coupling, which confirmed the assignment of the signal at δ 57.0 to the quaternary ^{t}Bu carbons (C^{8}). Furthermore, the signal at δ 200.2 for the quaternary carbene carbons C^{2} showed two correlations, both due to $^{3}J_{CH}$ coupling, in the first case with the methylene bridge protons and secondly with the $NiMe_2$ protons H^{121}.

The complete individual assignments of the ^{1}H and ^{13}C signals of **12** are summarised in section 6.12.

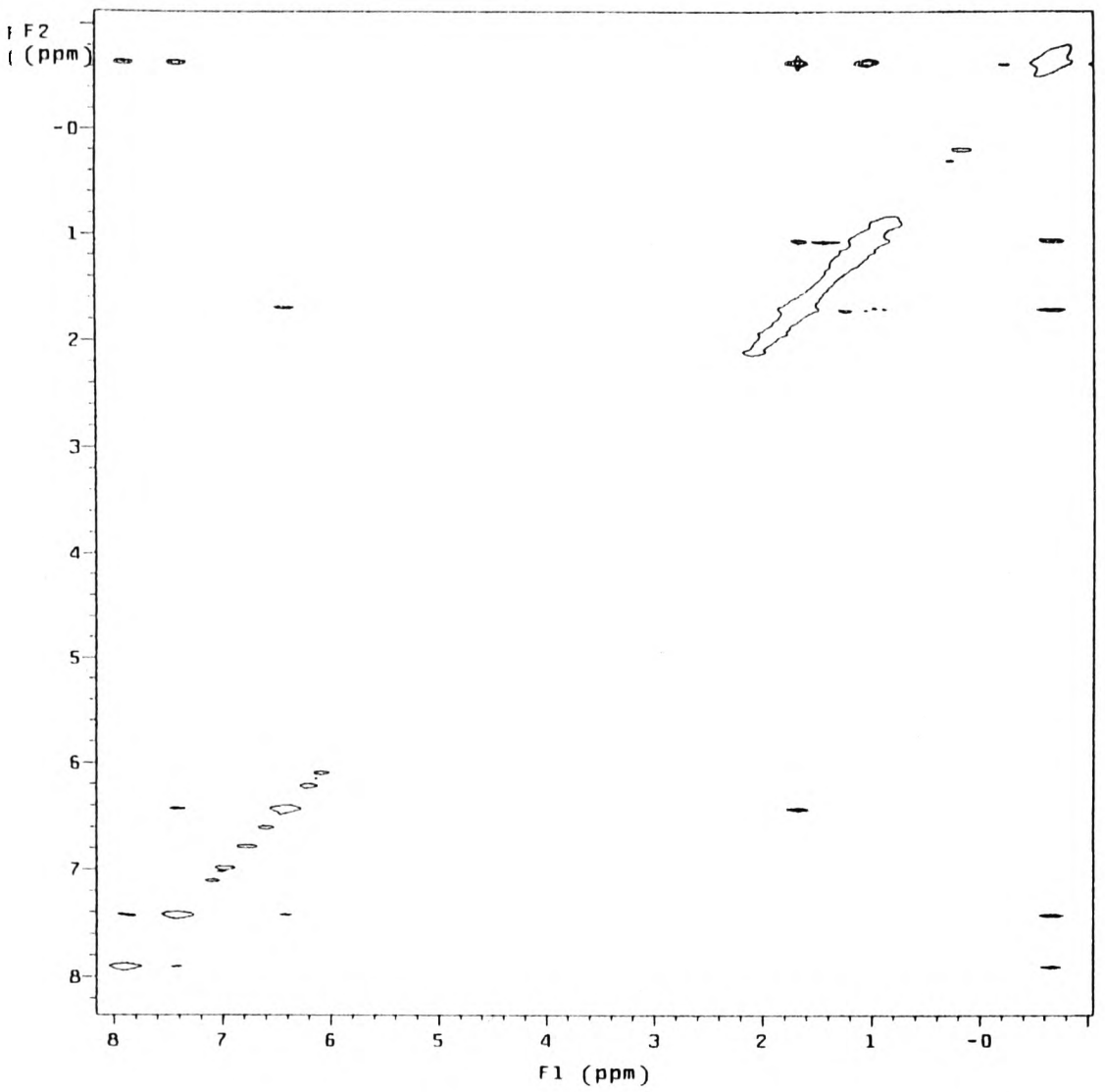

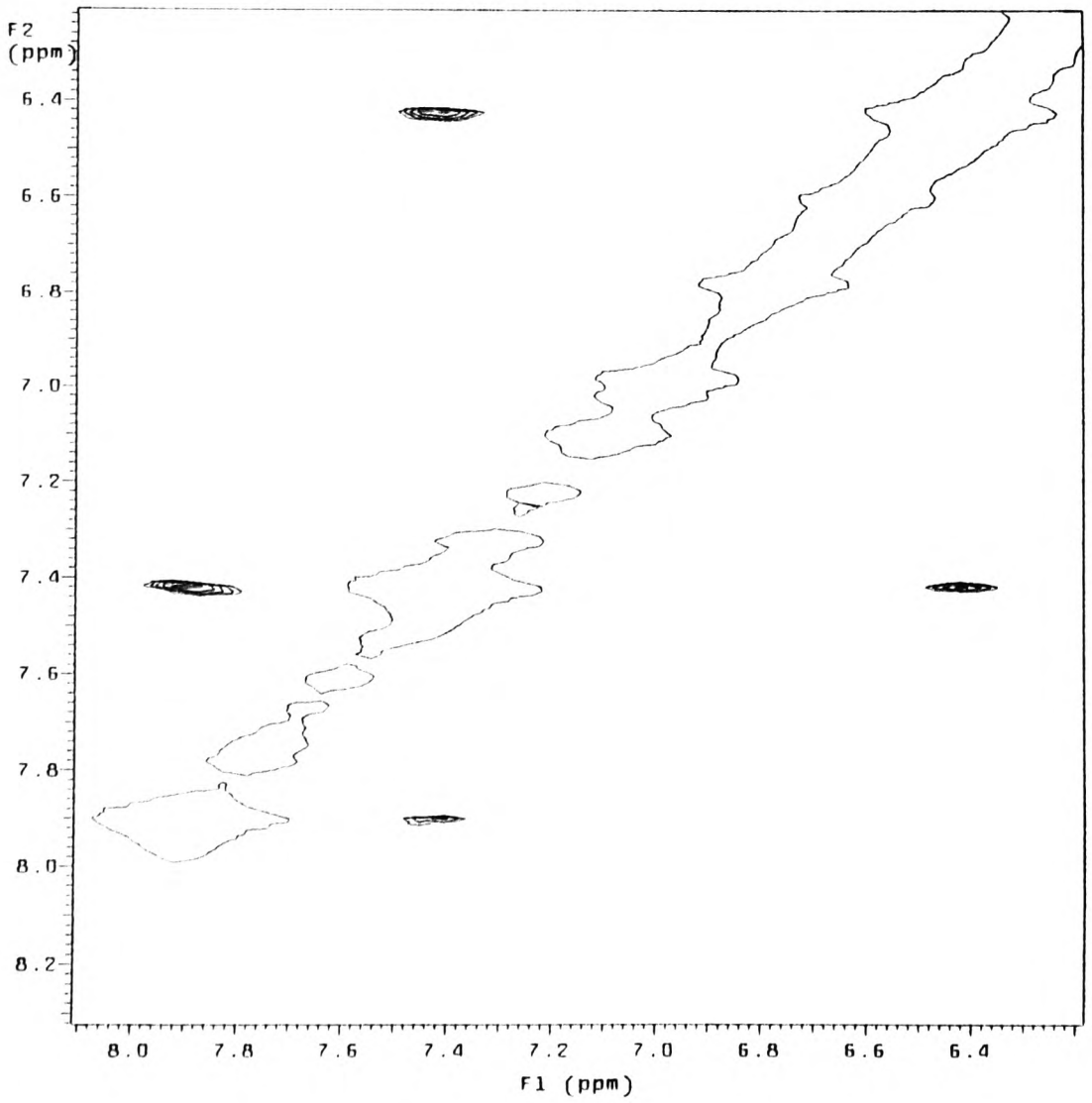

Figure 3.4 500 MHz ^{1}H NOESY spectrum of [(μ-^{tBu}CC^{meth}){Ni(PMe$_3$)Me$_2$}$_2$] (**12**) in d^8-toluene.

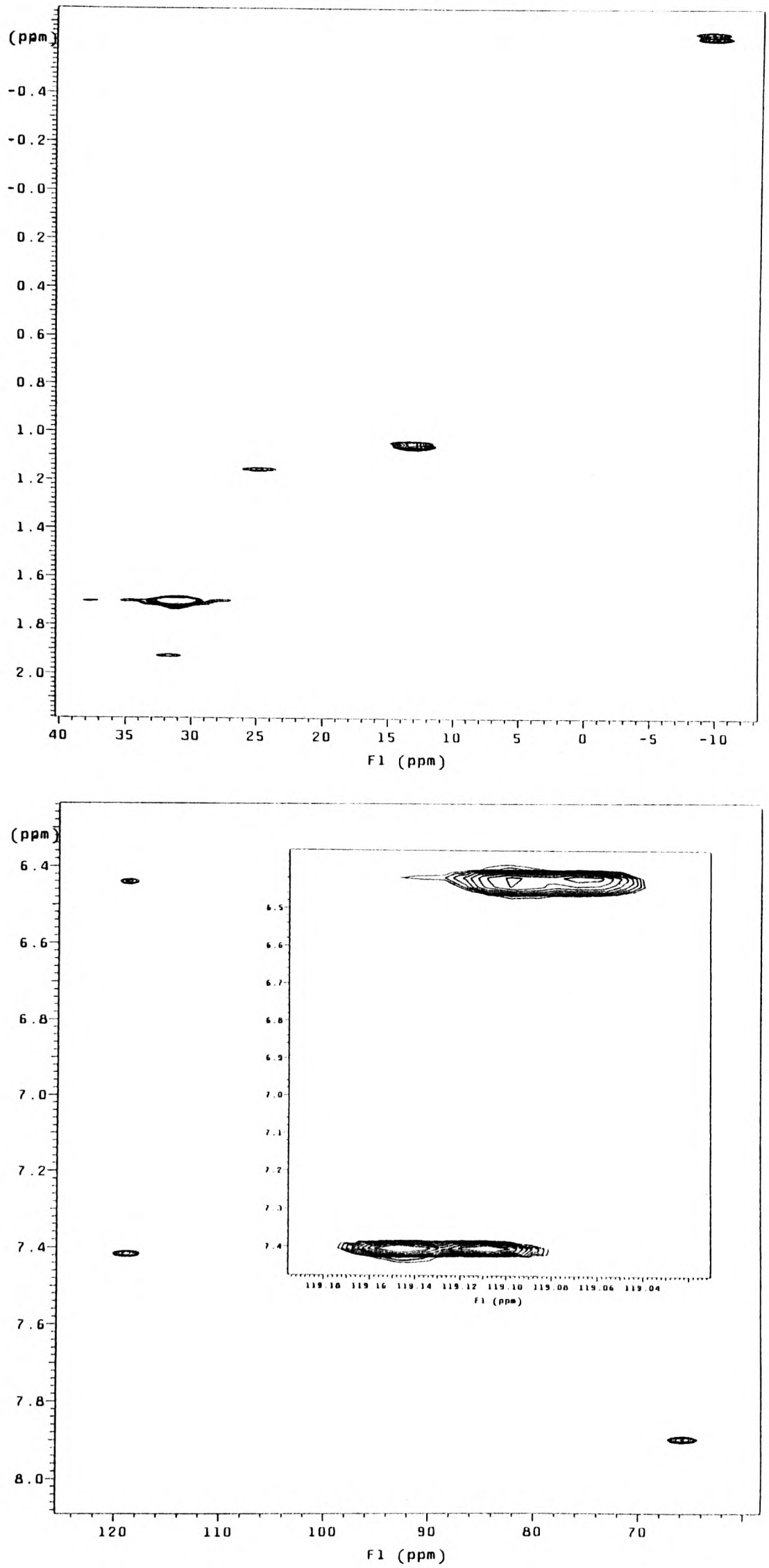

Figure 3.5 500 MHz ^{1}H-^{13}C-$^{1}J_{CH}$ shift correlation NMR spectrum of $[(\mu\text{-}^{tBu}CC^{meth})\{Ni(PMe_3)Me_2\}_2]$ (**12**) in d^8-toluene

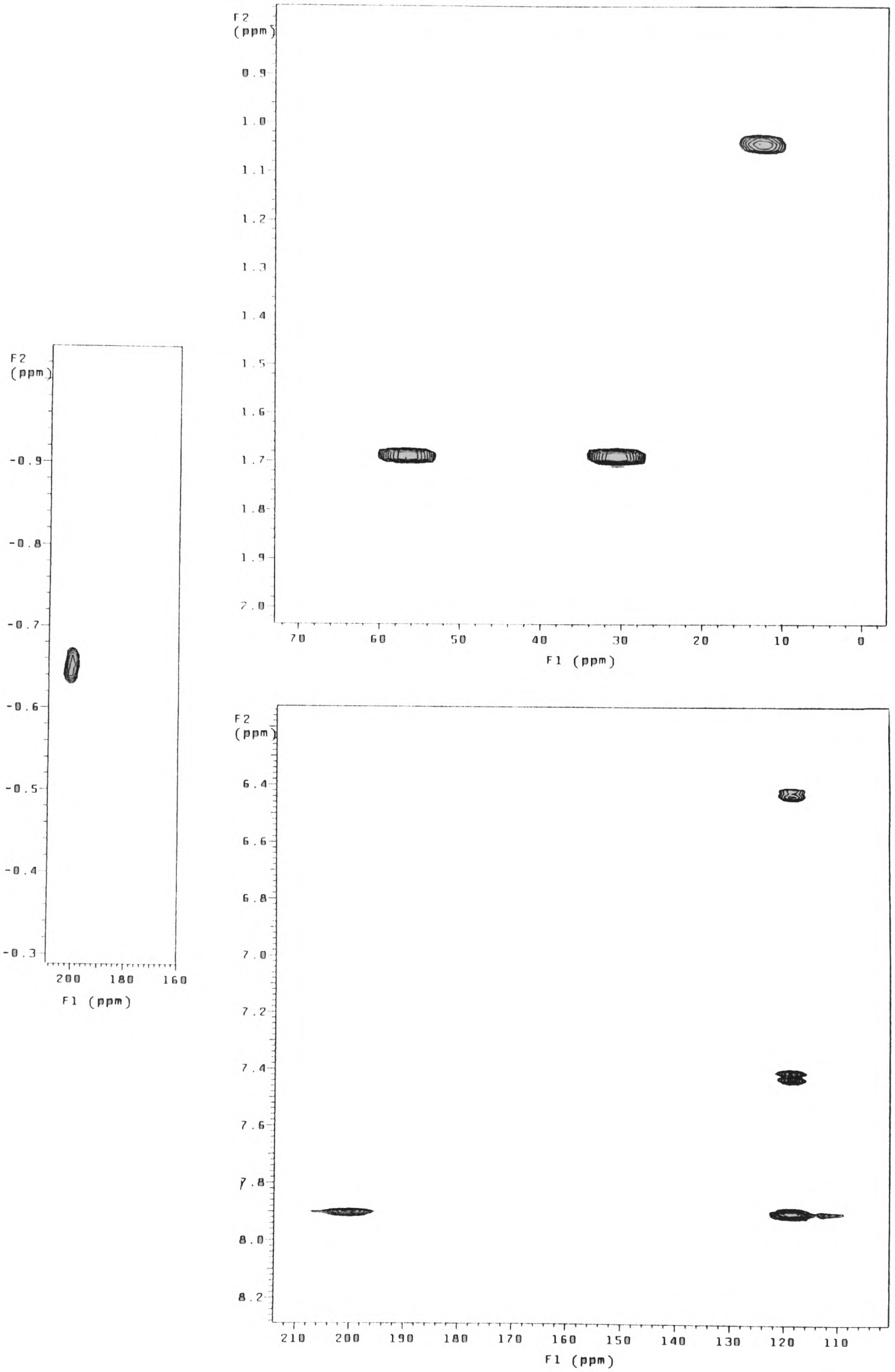

Figure 3.6 500 MHz ^{1}H-^{13}C-$^{n}J_{CH}$ (n > 1) shift correlation NMR spectrum of $[(\mu\text{-}^{tBu}CC^{meth})\{Ni(PMe_3)Me_2\}_2]$ (**12**) in d^8-toluene.

Single crystals of **12** of sufficient quality for X-ray structure determination (performed by Dr Richard Douthwaite) were grown from the pentane extract of the reaction mixture. Selected bond lengths and angles are given in table 3.1. The asymmetric unit contains one half of the molecule **12** and 0.5 molecules of pentane as solvent of crystallisation. The methylene bridge carbon atom C^4 is located at the C_2-axis; therefore half of the molecule shown in figure 3.7 is symmetry-generated. The X-ray structure confirms that compound **12** is a dimer with $^{tBu}CC^{meth}$ bridging two nickel atoms. The geometry at both nickel centres is square planar with the two methyl groups *cis* to the carbene carbon of $^{tBu}CC^{meth}$, and the PMe_3 in the *trans* position. Although the complexes $[(\mu\text{-}^{Me}CC^{meth})\{RhBr(COD)\}_2]$ and $[(\mu\text{-}^{Me}CC^{eth})\{RhCl(COD)\}_2]$ (COD = 1,5-cyclooctadiene) were previously synthesised and the latter structurally-characterised,[7,8] compound **12** is the first example of a group 10 metal complex incorporating a bridging dicarbene ligand. Compound **12** is also the first example of a structurally-characterised nickel *trans*-dimethyl complex. The $Ni\text{-}C_{carbene}$ bond length (1.879(3) Å) is 0.032(5) Å shorter than that observed in the structurally characterised nickel(II) monocarbene complex, *trans*-dichlororo*bis*(1,3-dicyclohexylinidazol-2-ylidene)nickel(II) (scheme 2.1),[6] and is 0.063(7) Å shorter than the Ni-C bond *trans* to PMe_3 in the cation of **7**, $[(^{tBu}CC^{meth})NiCl(PMe_3)]^+$. A probable contributing factor in the latter comparison is the increased steric bulk imposed at the nickel centre by chelating dicarbenes relative to bridging dicarbenes. The $Ni\text{-}C_{Me}$ bond lengths (1.983(4) and 2.001(4) Å) are slightly longer than those of $Ni(^{tBu}CC^{eth})Me_2$ (**13**) (1.972(6) and 1.962(6) Å) and longer than those of $Ni(bpy)Me_2$ (1.923(4) Å).[9] The angle between planes containing the two heterocyclic rings, 80.4(3)°, and the Ni-C(2)-C(2')-Ni' torsion angle, 111.74(13)°, reflect a conformation adopted by the $^{tBu}CC^{meth}$ ligand primarily to minimise $NiMe_2(PMe_3)$-$NiMe_2(PMe_3)$ nonbonding interactions. This is consistent with the observation in the ^1H NOESY spectrum that the $NiMe_2$ protons (H^{121}) of one nickel and the H^{51} proton of the hetrocyclic ring bonded to the other nickel are close in space.

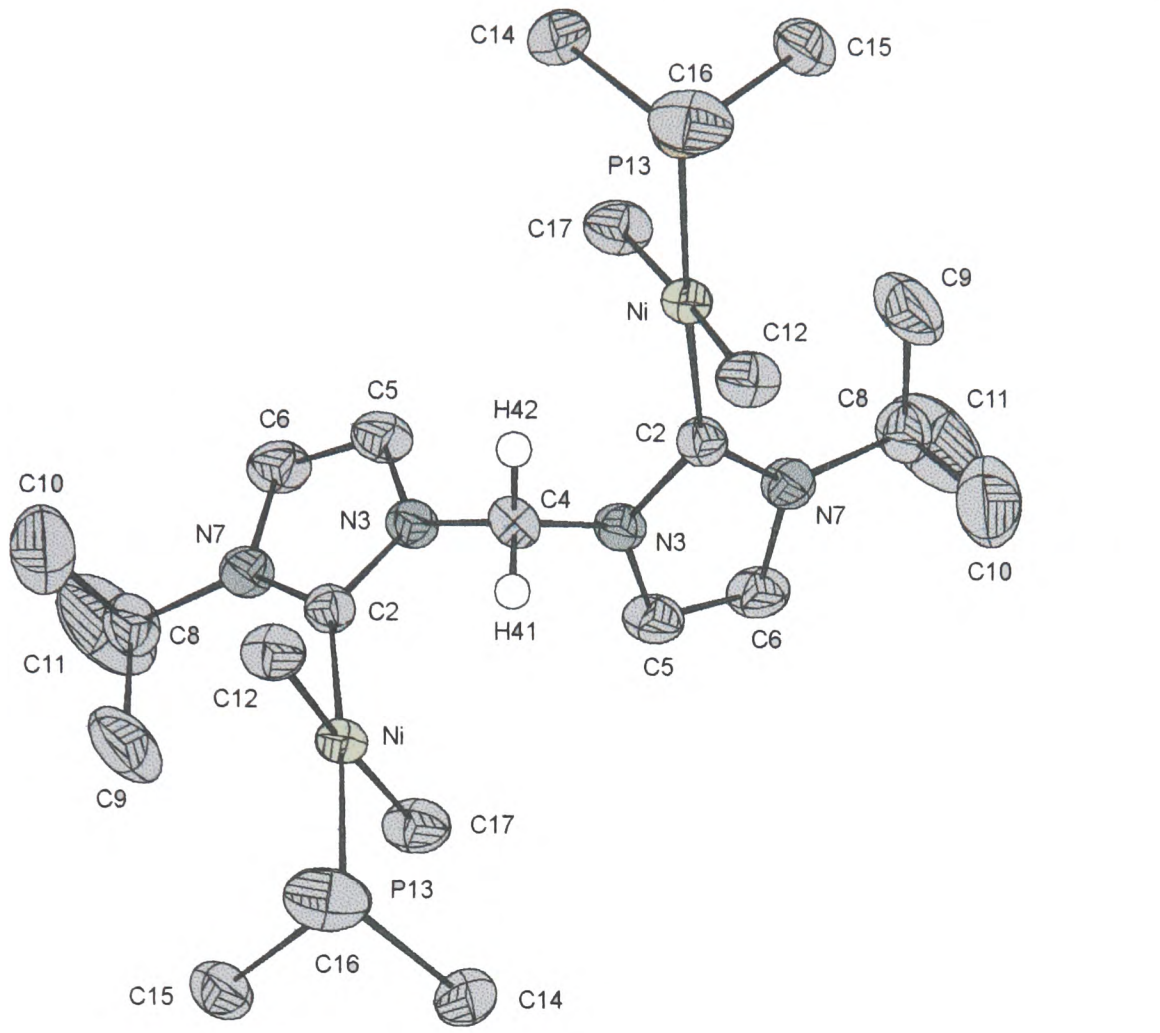

Figure 3.7 Two views of the X-ray structure of $[(\mu\text{-}^{tBu}CC^{meth})\{Ni(PMe_3)Me_2\}_2]$ (**12**). Hydrogen atoms except for H(41) and H(42) are omitted for clarity.

Bond	Length (Å)	Bond	Angle (°)
Ni-C(2)	1.879(3)	C(2)-Ni-C(12)	89.47(15)
Ni-C(12)	1.983(4)	C(2)-Ni-C(17)	89.40(15)
Ni-P(13)	2.1527(9)	C(2)-Ni-P(13)	175.1(1)
Ni-C(17)	2.001(4)	C(12)-Ni-C(17)	177.28(17)
C(2)-N(3)	1.367(4)	C(12)-Ni-P(13)	92.35(12)
C(2)-N(7)	1.365(4)	P(13)-Ni-C(17)	88.97(12)
N(3)-C(4)	1.449(4)	N(3)-C(2)-N(7)	103.3(3)
N(3)-C(5)	1.377(4)	C(2)-N(3)-C(5)	112.3(3)
C(5)-C(6)	1.355(5)	N(3)-C(4)-N(3')	111.87(22)
C(6)-N(7)	1.395(5)		
		ring twist*	80.4(3)

*The angle between the planes of the two heterocyclic rings.

Table 3.1 Selected bond lengths and angles for $[(\mu\text{-}^{tBu}CC^{meth})\{Ni(PMe_3)Me_2\}_2]$ (**12**).

3.2.3 Reaction Between $Ni(bpy)Me_2$ and $^{tBu}CC^{meth}$ (4)

In a second attempt to prepare the *cis*-dimethyl compound $Ni(^{tBu}CC^{meth})Me_2$, reaction in toluene at -78 °C between $Ni(bpy)Me_2$ and 1 equivalent $^{tBu}CC^{meth}$ (**4**) immediately gave a brown suspension, and gas evolution was observed on warming to room temperature. ^1H NMR spectroscopy of the diethyl ether extract showed a mixture of unidentifiable products (broad bands of peaks were observed in the *tert*-butyl and methylene bridge/imidazole ring proton regions). The reaction was repeated, and again slow gas evolution was observed on warming to room temperature, the resulting mixture being an intractable dark green/brown oil.

The reaction was repeated in d^8-toluene and monitored using ^1H NMR spectroscopy from -75 to +25 °C over 10 hours. Any quantitative analysis was hampered by the partial solubility of $Ni(bpy)Me_2$ at lower temperatures, leading to reaction occurring over a wide temperature range. Above -50 °C signals attributable to $Ni(^{tBu}CC^{meth})Me_2$ were observed which persisted to room temperature in various low concentrations relative to the by-

product bpy, unreacted $^{tBu}CC^{meth}$, and decomposition products (scheme 3.1). $Ni(bpy)Me_2$ was never observed in the NMR spectra, indicating rapid reaction with $^{tBu}CC^{meth}$ upon dissolution. The ^1H NMR pattern of the compound $Ni(^{tBu}CC^{meth})Me_2$ was recognised by its similarity to that of the palladium(II) analogue $Pd(^{tBu}CC^{meth})Me_2$ (**14**). Close examination of the spectra showed the possible presence of methane and/or ethane, which resonate in d^8-toluene at δ 0.23 and δ 0.82 respectively, although signals were of very low intensity and could be due to other decomposition products of $Ni(^{tBu}CC^{meth})Me_2$. On standing at room temperature for 24 hours $Ni(^{tBu}CC^{meth})Me_2$ could not be observed in the ^1H NMR spectrum. The ^1H NMR spectrum at +10 °C, which most clearly shows the signals for $Ni(^{tBu}CC^{meth})Me_2$, is shown in figure 3.8.

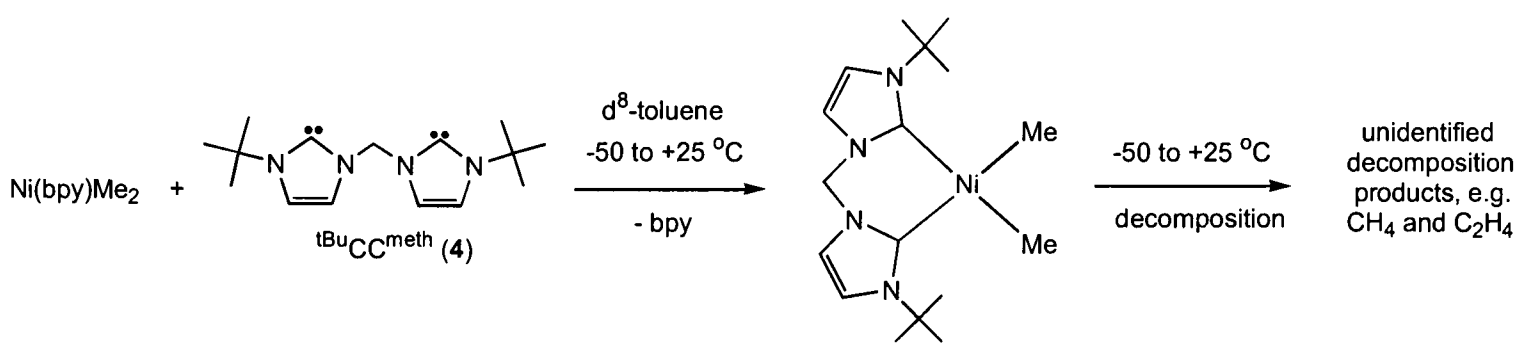

Scheme 3.1

The inability to isolate $Ni(^{tBu}CC^{meth})Me_2$, the observation of a gaseous decomposition product, most likely methane or ethane, and the formation and subsequent decomposition of $Ni(^{tBu}CC^{meth})Me_2$ over the temperature range -50 to +25 °C indicate that that the compound has a low thermal stability with respect to hydrocarbon elimination. This has also been observed in related chelating *bis*-phosphine chemistry, where Yamamoto et al. reported the thermal elimination of ethane from *bis*-phosphine dimethyl nickel(II) complexes. The rate of elimination was found to vary as a function of the number of carbon atoms bridging the phosphorus atoms.[10]

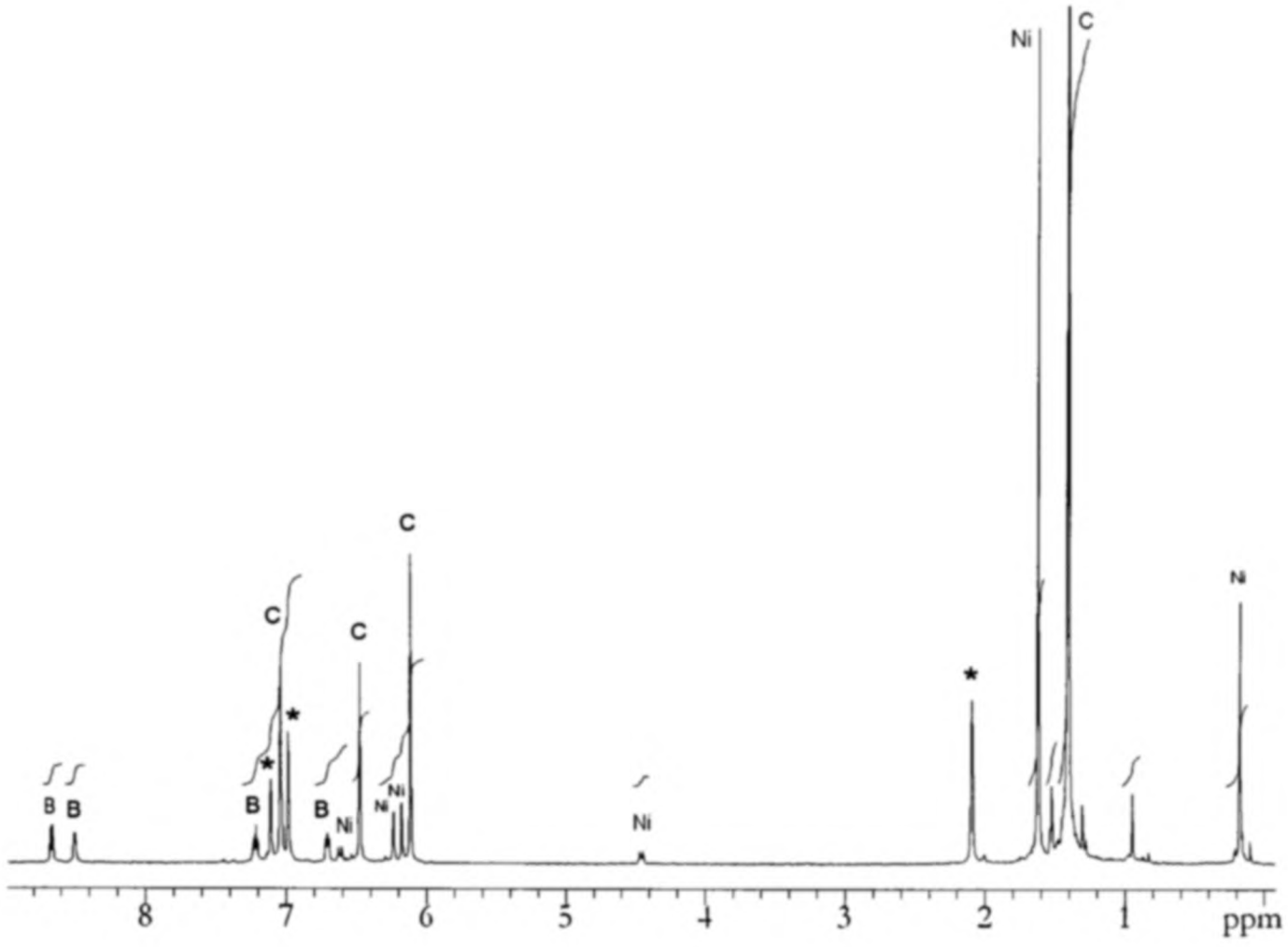

Figure 3.8 500 MHz ^{1}H NMR spectrum of the reaction in d^{8}-toluene between Ni(bpy)Me_2 and $^{tBu}CC^{meth}$ (**4**) at 10 °C. Ni = Ni($^{tBu}CC^{meth}$)Me_2, B = bpy, C = unreacted **4**, * = solvent.

3.2.4 Synthesis of Ni($^{tBu}CC^{eth}$)Me_2 (13)

Reaction in toluene between Ni(bpy)Me_2 and 1 equivalent $^{tBu}CC^{eth}$ (**5**) gives a golden solution to which pentane is added to precipitate the yellow solid Ni($^{tBu}CC^{eth}$)Me_2 (**13**) in high yield (Eq. 47).

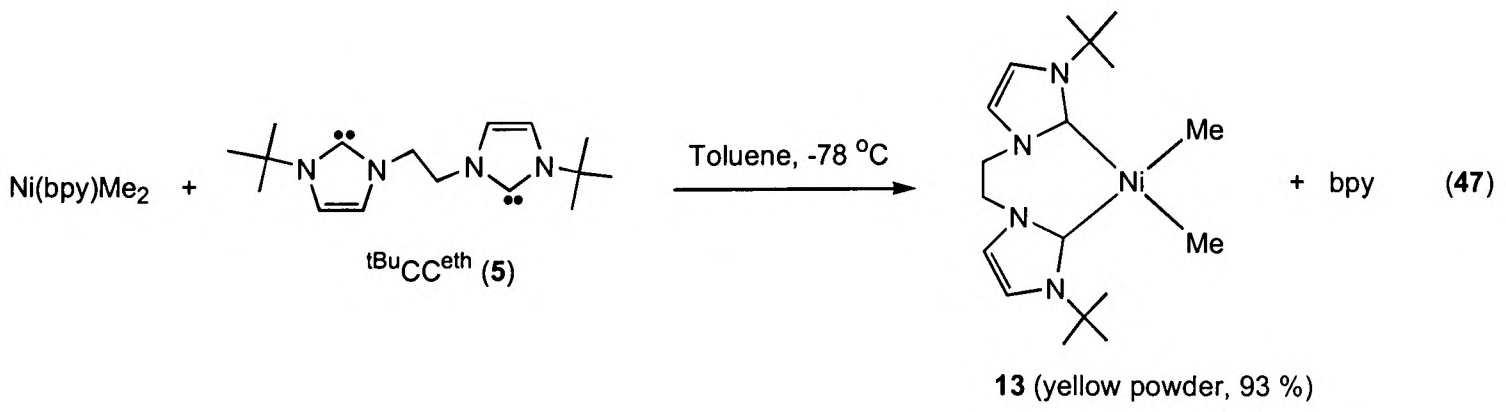

The compound **13** is air sensitive, and is stored at -20 °C to avoid thermal decomposition, which occurs at room temperature over several weeks (formation of insoluble orange-red decomposition products). **13** is soluble in toluene and common polar, aprotic organic solvents, but decomposes over several minutes in dichloromethane.

3.2.5 Characterisation of Ni(^{tBu}CC^{eth})Me$_2$ (13)

The compound **13** was characterised by elemental analysis, ^{1}H and ^{13}C{^{1}H} NMR spectroscopy, and X-ray crystal structure determination. Single crystals of sufficient quality for X-ray structure determination (performed by Dr Richard Douthwaite) were grown by cooling a diethyl ether solution of **13** to -20 °C. Selected bond lengths and angles are given in table 3.2. The asymmetric unit contains one molecule of **13**, shown in figure 3.9, and no solvent of crystallisation. The geometry at the nickel atom is essentially square planar with a dicarbene bite angle C(2)-Ni-C(14) = 88.9(2)° which is comparable to that of 88.4(4)° observed in the only other structurally characterised ethylene-bridged dicarbene nickel(II) complex [(^{tBu}CC^{eth})NiCl(PMe$_3$)][BPh$_4$] (**10**). The bite angle is also well within the range of those observed for nickel(II) complexes of chelating *bis*-phosphines which incorporate two-carbon-atom bridges such as dppe (85-90°).[11] A boat-like conformation similar to compound **10** is observed, and projection along the C(11)-C(12) vector shows a staggered conformation with a N(10)-C(11)-C(12)-N(13) torsion angle of 52.1(5)°, which is smaller than that observed for compound **10** (58.7(9)°). The twist angles of the heterocyclic rings relative to the coordination plane of **13** (76.7(4) and 62.1(4)°) are similar to those of **10** (73.5(9) and 62.3(8)°), and significantly larger than those of the methylene-bridged complexes **6** and **7**. The larger ring twist angles observed for the ethylene- relative to the methylene-bridged complexes serve to accommodate the longer bridge whilst reducing the requirement of a larger bite angle which would cause an unfavourable eclipsed conformation of the ethylene bridge hydrogen atoms. The Ni-C$_{Me}$ bond lengths (1.962(6) and 1.971(6) Å) are very similar to those found for the square planar *bis*-phosphine *cis*-dialkyl nickel complex (dppe)-2,3-dimethylene-nickela-cyclopentane (1.965 and 1.975 Å, no e.s.d.'s available),[12] and longer than those of Ni(bpy)Me$_2$ (1.923(4) Å)[9] which shows the greater *trans*-influence of ^{tBu}CC^{eth} relative to bpy because of the greater σ-donating capacity of the dicarbene ligand. The Ni-C$_{carbene}$ bond lengths (1.907(5) and 1.911(6) Å) are essentially identical to those of the nickel(II) monocarbene complex *trans*-

dichlororo*bis*(1,3-dicyclohexylimidazol-2-ylidene)nickel(II) (1.911(2) Å).[6] A similar degree of steric strain within the $^{tBu}CC^{eth}$ ligands of **13** and [($^{tBu}CC^{eth}$)NiCl(PMe_3)][BPh_4] (**10**) is implied. The sum of the angles of **13** at N(10) (359.8(15)°) and N(13) (359.9(15)°) are as expected for sp^2 hybridisation. However, as observed for compound **10**, the internal angles of the seven-membered ring C(2)-N(10)-C(11) (129.1(5)°) and C(12)-N(13)-C(14) (120.4(5)°) indicate that a degree of ring strain at N(10) may be present. The internal angles of the six-membered ring of the methylene-bridged carbene complex **7** show no such ring strain. In addition, the proximities of adjacent ^{t}Bu substituents within **13** and **10** are similar. Assuming free rotation about each N-C_{tBu} bond, distances between ^{t}Bu groups of 1.9 Å are estimated for **13** and **10**, compared to 2.3 Å observed for the $^{tBu}CC^{meth}$ compound **7**.

Bond	Length (Å)	Bond	Angle (°)
Ni-C(2)	1.907(5)	C(2)-Ni-C(14)	88.9(2)
Ni-C(14)	1.911(6)	C(2)-Ni-C(22)	92.4(3)
Ni-C(22)	1.972(6)	C(14)-Ni-C(22)	165.7(3)
Ni-C(23)	1.962(6)	C(2)-Ni-C(23)	176.3(3)
C(2)-N(3)	1.354(7)	C(14)-Ni-C(23)	90.8(3)
C(2)-N(10)	1.378(7)	N(3)-C(2)-N(10)	103.4(4)
C(8)-C(9)	1.322(9)	N(13)-C(14)-N(15)	102.9(5)
N(13)-C(14)	1.362(8)	Ni-C(2)-N(10)	121.3(4)
C(14)-N(15)	1.373(8)	C(2)-N(10)-C(11)	129.1(5)
C(20)-C(21)	1.34(1)	N(10)-C(11)-C(12)	116.3(5)
		C(11)-C(12)-N(13)	113.2(5)
		C(12)-N(13)-C(14)	120.4(5)
		N(13)-C(14)-Ni	112.0(4)
		C(2)-N(10)-C(9)	111.1(5)
		C(9)-N(10)-C(11)	119.6(5)
		C(12)-N(13)-C(21)	127.2(5)
		C(14)-N(13)-C(21)	112.3(5)
		ring $twist_{C(2)}$*	62.1(4)
		ring $twist_{C(14)}$	76.7(4)

* The angle between the coordination plane defined by nickel and carbene carbon atoms and the heterocyclic ring containing C(n)

Table 3.2 Selected bond lengths and angles for Ni($^{tBu}CC^{eth}$)Me_2 (**13**).

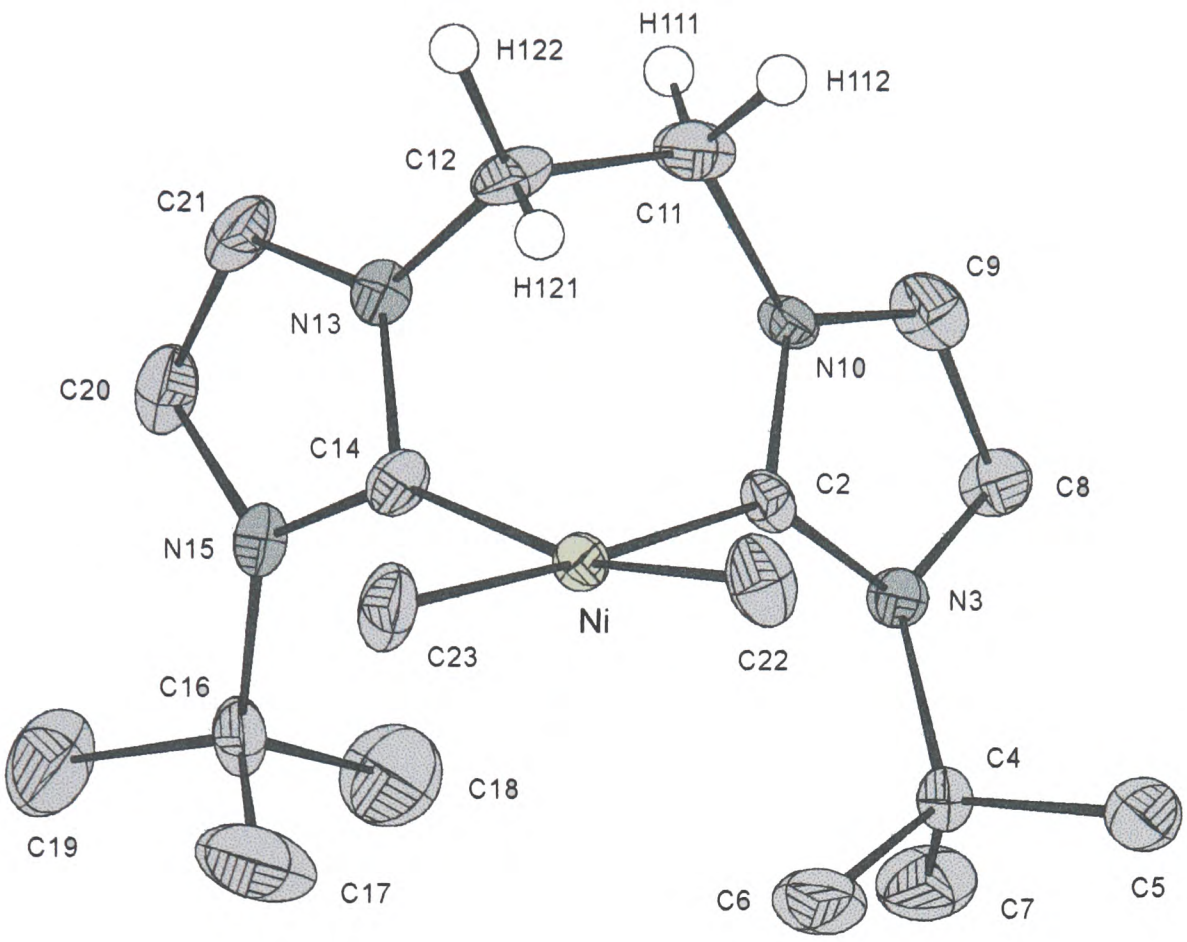

Figure 3.9 Two views of the X-ray structure of Ni(^{tBu}CC^{eth})Me$_2$ (**13**). Hydrogen atoms except for H(111), H(112), H(121) and H(122) are omitted for clarity.

The ^{1}H and $^{13}C\{^{1}H\}$ NMR spectra of **13** show signals consistent with C_{2v} symmetry (figure 3.10). Two resonances at δ 3.33 and 5.88 are observed for the four protons of the ethylene bridge, and a single resonance at δ 48.3 corresponds to the two ethylene bridge carbons. ^{1}H-^{13}C-$^{1}J_{CH}$ shift correlation NMR spectroscopy (figure 3.11), performed by Dr Daniel Haüßinger, showed correlations between each of the ethylene bridge proton resonances and the signal corresponding to the two ethylene bridge carbons. Both proton resonances correspond to two protons which are on different carbons of the ethylene bridge (an AA'BB' spin system). $^{1}J_{CH}$ correlations were also observed between the ^{1}H NMR methyl resonance (δ 0.13), *tert*-butyl resonance (δ 1.74) and two ring proton resonances (δ 6.08 and 6.35) and the respective $^{13}C\{^{1}H\}$ NMR methyl (δ -0.7), primary *tert*-butyl (δ 31.7) and two ring carbon resonances (δ 119.5, 117.1). The apparent horizontal mirror plane implied for **13** in the solution NMR spectra is attributed to a rocking vibration along the C(11)-C(12) vector, which causes the ethylene bridge protons labelled in the crystal structure as H(112) and H(121), as well as H(111) and H(122), to become equivalent pairs on the NMR timescale. ^{1}H NMR spectroscopy (d^{8}-toluene) of **13** at -80 °C did not result in appreciable broadening of the two signals ascribed to the ethylene bridge protons, which indicates a low barrier for this conformational change.

The equivalent carbene carbon atoms are observed at δ 197.6, which is a similar chemical shift to that of $[(\mu\text{-}^{tBu}CC^{meth})\{Ni(PMe_3)Me_2\}_2]$ (**12**) (δ 200.2), but is 28-42 ppm downfield with respect to the cationic nickel(II) carbene complexes **6-11**, and 8-28 ppm further downfield than the carbene carbon resonances of neutral monocarbene late transition metal (including nickel) halide complexes, which are in the range δ 170-190.[6,7]

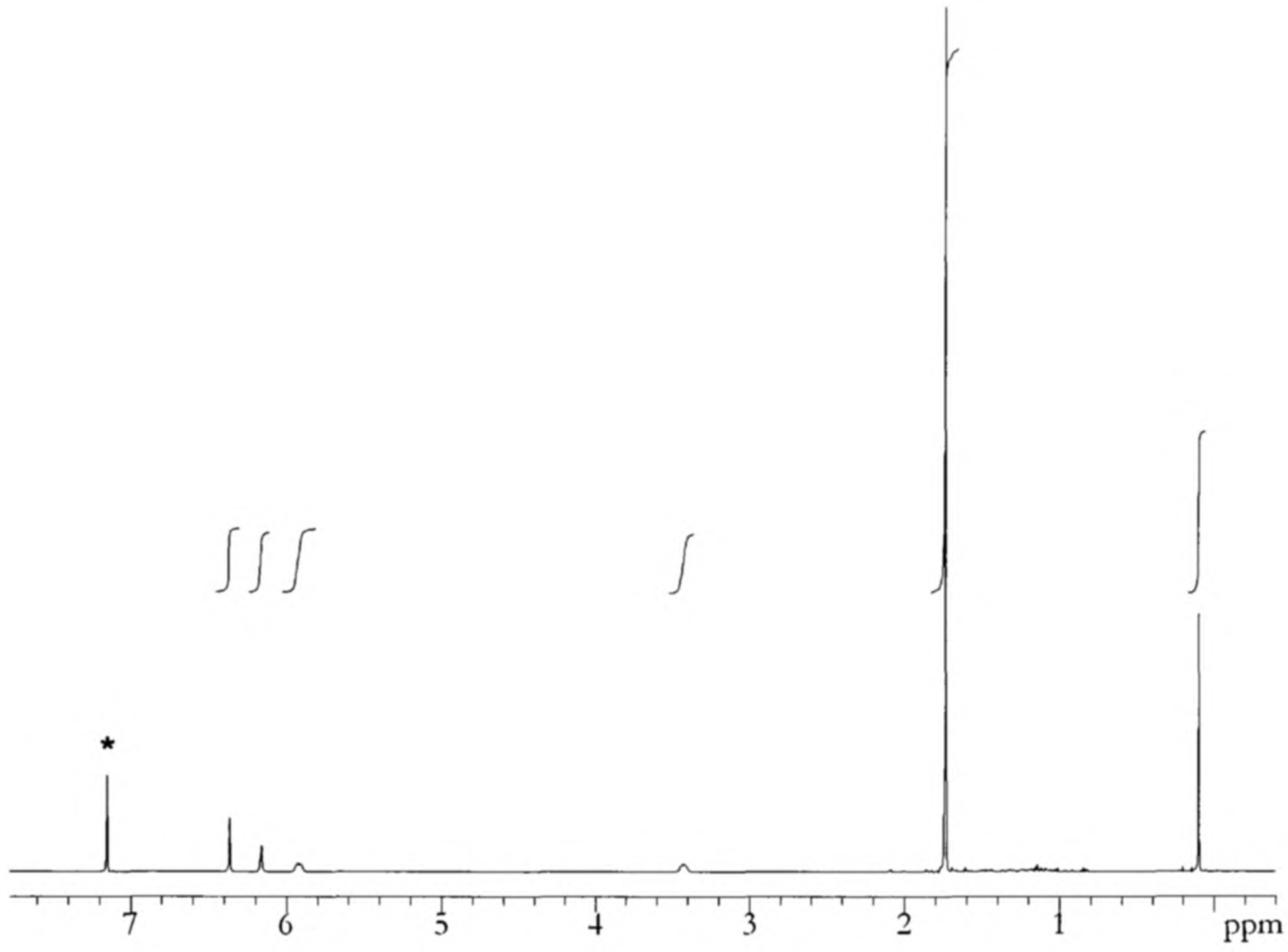

Figure 3.10 500 MHz ^{1}H and 125.7 MHz $^{13}C\{^{1}H\}$ NMR spectra of $Ni(^{tBu}CC^{eth})Me_2$ (**13**) in C_6D_6 (* = solvent).

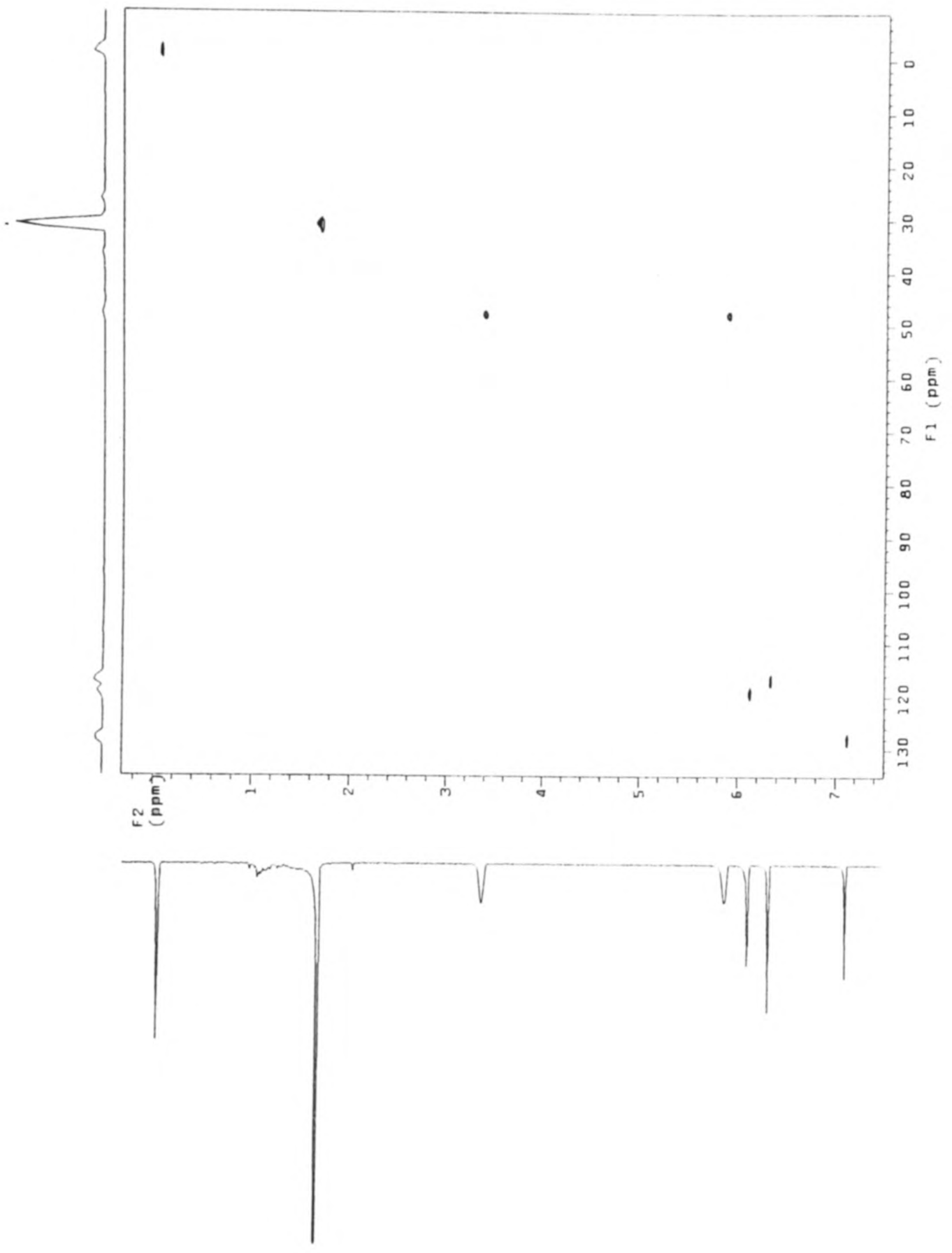

Figure 3.11 500 MHz ^{1}H-^{13}C-$^{1}J_{CH}$ shift correlation NMR spectrum of $Ni(^{tBu}CC^{eth})Me_2$ (**13**) in C_6D_6.

3.2.6 Thermal Decomposition of Ni(^{tBu}CC^{eth})Me$_2$ (13): Rate of Elimination of Methane

Following evidence described in section 3.2.3 that the compound Ni(^{tBu}CC^{meth})Me$_2$ has a low thermal stability with respect to hydrocarbon elimination, and in the light of observations by Yamamoto et al. that the rate of thermal elimination of ethane from *bis*-phosphine dimethyl nickel(II) complexes varies as a function of the number of carbon atoms bridging the phosphorus atoms,[10] it was decided to investigate the thermal decomposition of Ni(^{tBu}CC^{eth})Me$_2$ (**13**) for comparison with the methylene-bridged dicarbene analogue.

Diphenylmethane solutions of Ni(^{tBu}CC^{eth})Me$_2$, both with and without a 5-fold excess of 1,2-*bis*(diphenylphosphino)ethane (dppe), were heated to 70 °C for 2 hours before cooling to room temperature and releasing the volatiles directly into a mass spectrometer. In each case methane was detected as the only volatile decomposition product. Furthermore, the quantity of methane gas produced from the decomposition of a known amount of Ni(^{tBu}CC^{eth})Me$_2$ (in diphenylmethane) was accurately determined as 1 equivalent (experimental details are given in section 5.3.6). These observations are in contrast to those for chelating *bis*-phosphines, which are reported by Yamamoto et al. to eliminate ethane only.[10] The complexes Ni(dppe)Me$_2$ and Ni(dppp)Me$_2$ (dppp = 1,3-*bis*(diphenylphosphino)propane) could be isolated, whereas reactions to form the *bis*(diphenylphosphino)methane and 1,4-*bis*(diphenylphosphino)butane analogues gave products resulting from elimination of ethane. It was also observed that ethane elimination from Ni(dppe)Me$_2$ was catalysed by nickel decomposition products and that addition of excess dppe retarded this pathway giving cleaner first order kinetics. In order to investigate the observations of Yamamoto et al., who did not report details of gas analysis, a diphenylmethane solution of Ni(dppe)Me$_2$ was heated to 70 °C for 2 hours before cooling to room temperature and releasing the volatiles directly into a mass spectrometer. Ethane *and* methane were observed in essentially a 1:1 ratio. Addition of excess dppe in a separate experiment increased the ethane:methane ratio to 9:1. In a further report the solid state decomposition at 110 °C of Ni(dmpe)Me$_2$ gave ratios of methane:ethane:ethylene of 56:39:25.[13]

Rate constants, k, for the thermal elimination of methane from Ni(^{tBu}CC^{eth})Me$_2$ (**13**) were determined for the temperatures 50, 60, 70 and 80 °C, in d^8-toluene, by monitoring the decrease over time t in the integral value of the ^{1}H NMR methyl resonance, which is proportional to the concentration, x, of **13**. Microcal Origin version 5.0 was used to fit straight lines of gradient k to plots of $\ln(x_o/x)$ vs t (figure 3.13), where x_o is the concentration at t = 0. Estimated standard deviations in k (table 3.3) show good fits consistent with first order kinetics ($-dx/dt = kx$). The rate constant at a given temperature T was found to be independent of concentration, confirming first order kinetics.

The empirical activation energy, E, and pre-exponential factor, A, were calculated using the Arrhenius Equation, $k = A \exp(-E/RT)$. Plotting ln k vs 1/T gave E = 24.7(4) kcal mol^{-1} and A = 1.75 x 10^{12} s^{-1} (typical values of A for unimolecular reactions are in the range 10^{10}-10^{12} s^{-1}).[14] E and A were used to calculate the activation enthalpy and entropy,[14] which gave $\Delta H^{\ddagger}$ = 24.0(4) kcal mol^{-1} and $\Delta S^{\ddagger}$ = -4(1) cal K^{-1} mol^{-1}. Errors in E, H and S were estimated assuming temperature control of ± 0.5 K. A summary of the rate data is given in table 3.3.

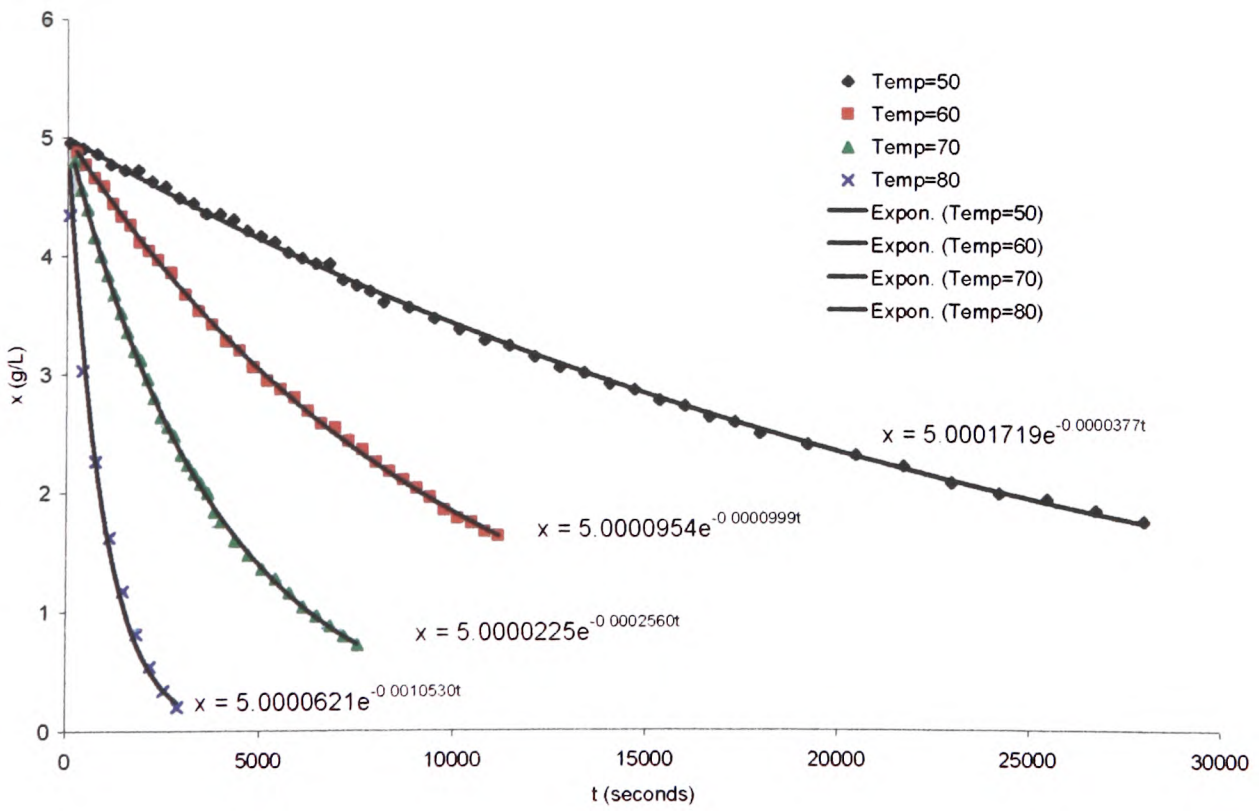

Figure 3.12 Graph showing the concentration, x, of Ni(^{tBu}CC^{eth})Me$_2$ (**13**) at time t, at 50, 60, 70 and 80 °C.

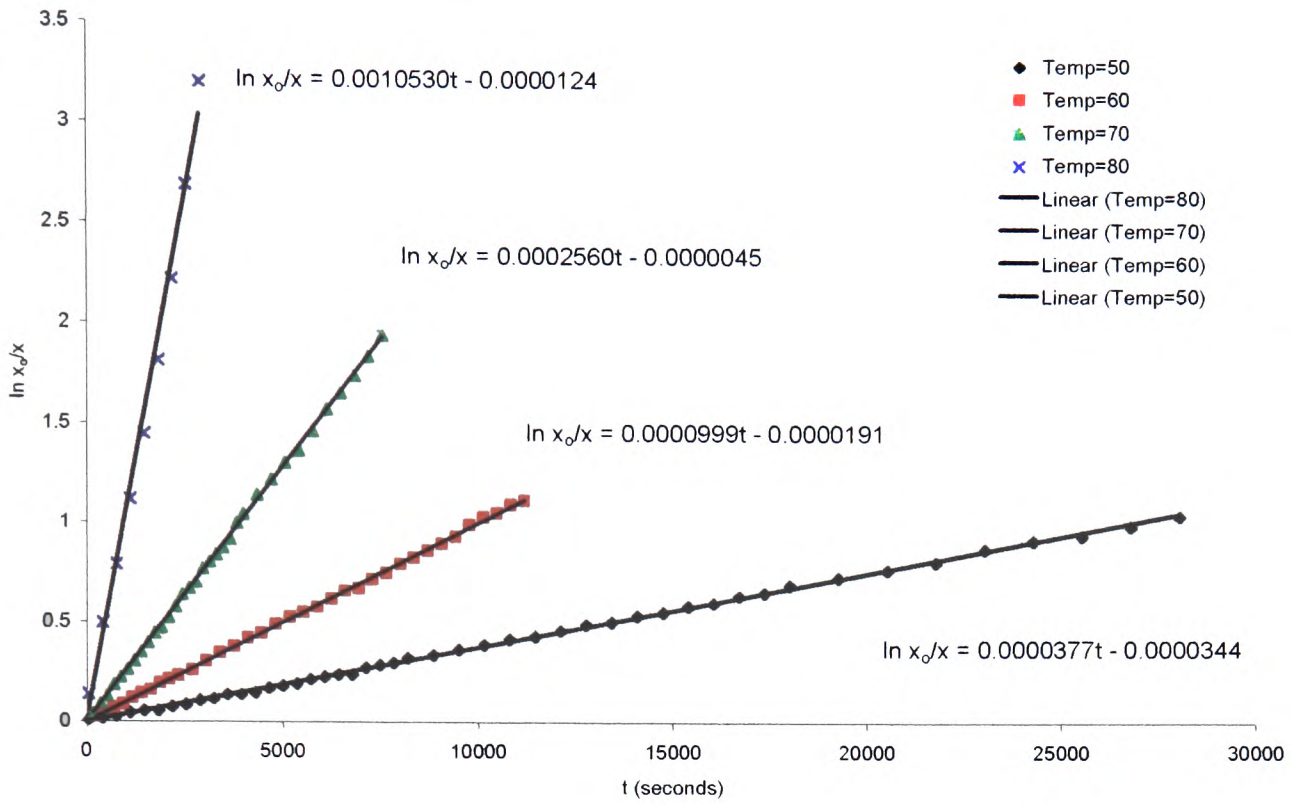

Figure 3.13 Graph showing ln x_o/x for Ni(^{tBu}CC^{eth})Me_2 (**13**) at time t, at 50, 60, 70 and 80 °C.

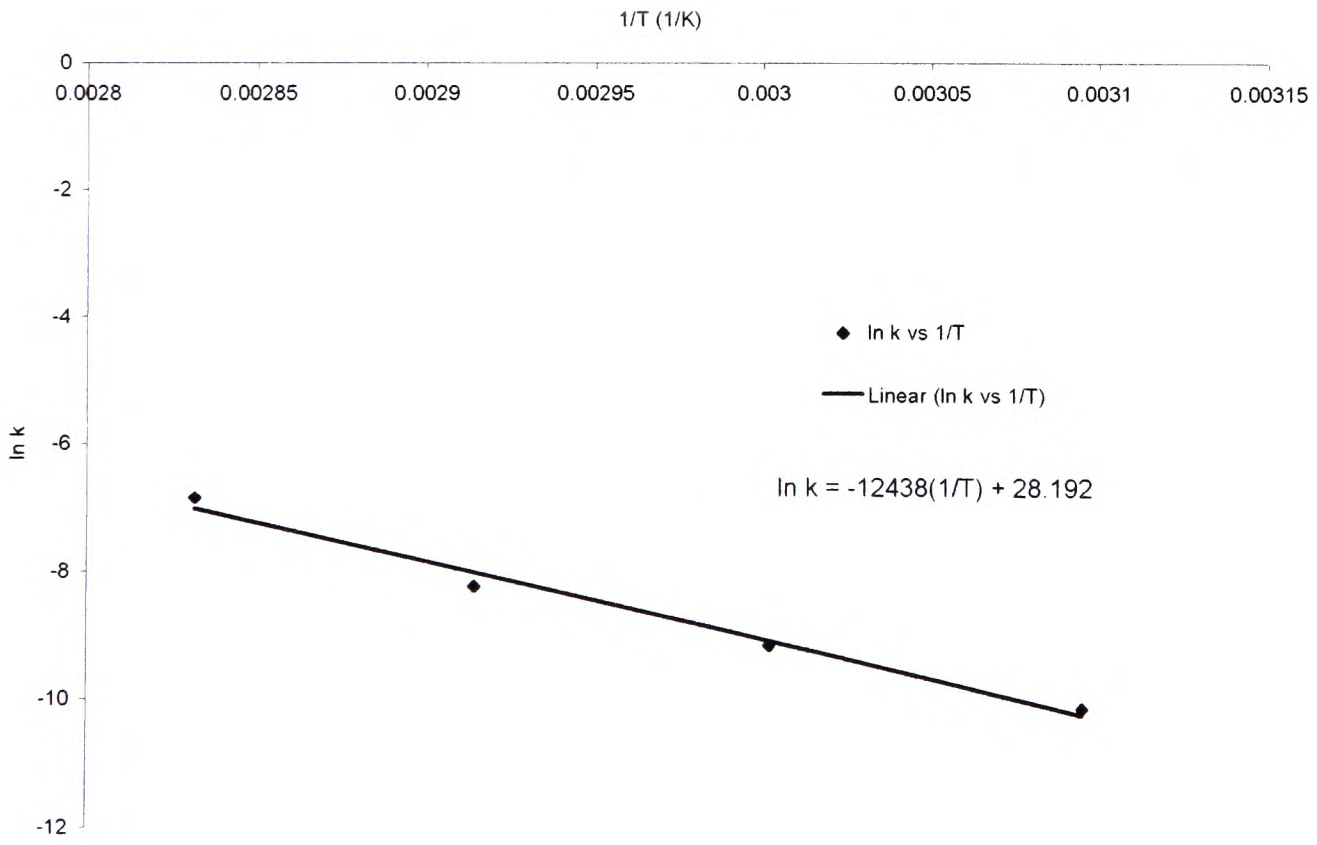

Figure 3.14 Plot of ln k vs 1/T for the thermal elimination of methane from Ni(^{tBu}CC^{eth})Me_2 (**13**).

T / °C	10^5 k / s^{-1} [a]	10^3 [**13**] / mol/L
50	3.77(2)	13.7
60	9.99(4)	13.7
70	25.6(9)	13.7
80	105(4)	13.7
70	26.0(3)	3.67
70	26.4(5)	19.27
70[b]	23.6(1)	13.7

[a] $\Delta H^{\ddagger}$ = 24.0(4) kcal mol^{-1}, $\Delta S^{\ddagger}$ = -4(1) cal K^{-1} mol^{-1}

[b] Added 5 fold excess of $^{tBu}CC^{eth}$ (**5**)

Table 3.3 Rate constants for the thermal elimination of methane from Ni($^{tBu}CC^{eth}$)Me_2 (**13**).

The low activation entropy, $\Delta S^{\ddagger}$, the independence of the rate constant k with respect to concentration, and the near-independence of k with respect to addition of excess dicarbene ligand (a slightly retarded rate is observed in this case) indicate a unimolecular pathway for the thermal elimination of methane from Ni($^{tBu}CC^{meth}$)Me_2 (**13**). The activation enthalpy, 24.0(4) kcal mol^{-1}, is lower than that observed for the thermal elimination of ethane from Ni(dppe)Me_2 ($\Delta H^{\ddagger}$ = 26.8 kcal mol^{-1}) and Ni(dppp)Me_2 ($\Delta H^{\ddagger}$ = 25.1 kcal mol^{-1}).[10]

Unimolecular elimination of methane from **13** could feasibly occur with concomitant formation of the transient nickel methylene species ($^{tBu}CC^{eth}$)Ni=CH_2, via the transition state shown in scheme 3.2.

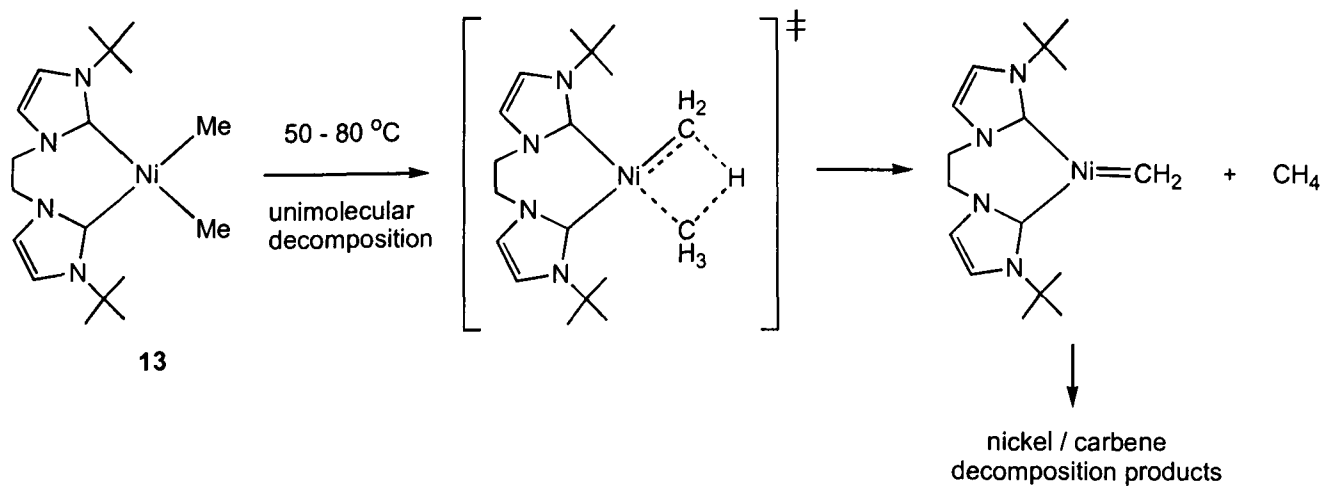

Scheme 3.2 Possible route for thermal elimination of methane from Ni($^{tBu}CC^{eth}$)Me_2 (**13**).

The observation of methane as the only gaseous thermal decomposition product of **13**, both in the absence and presence of excess dppe (which could act to retard decomposition pathways catalysed by nickel decomposition products) shows a preference for C-H rather than C-C bond formation. The absence of C-C coupled products such as ethane or ethylene, which have been observed in the thermal decomposition of chelating *bis*-phosphine nickel dimethyl compounds, can possibly be attributed to the greater σ-donating capacity of N-heterocyclic carbenes relative to tertiary phosphines. Ab initio calculations have shown that the covalent M-CH_3 bonds of *bis*-phosphine Pd and Pt *cis*-dimethyl complexes have one electron in an sp^3 hybrid orbital on the CH_3 and one electron in an spd hybrid orbital mainly on the metal.[15] It is stated in this work that the phosphine lone pairs form Lewis base / Lewis acid bonds to the metal by overlapping the empty valence s and p space of the metal. Furthermore, increasing the σ-donor strength of the phosphine ligands causes a greater overlap between the phosphine lone pairs and the metal s orbital, with the result that the metal spd hybrid orbitals lose s character and have to gain p character to stay orthogonal to the phosphine lone pairs. This increased p character raises the energy of the spd hybrids, bringing it closer to that of the methyl sp^3 orbitals, making the M-CH_3 bonds slightly stronger, which may cause the kinetic barrier for reductive elimination of ethane to be higher.[15] The greater σ-donating capacity of N-heterocyclic carbenes relative to tertiary phosphines could therefore account for an increase in the kinetic barrier of C-C relative to C-H bond formation in the case of nickel carbene complexes such as Ni(^{tBu}CC^{eth})Me_2 (**13**), explaining the thermal elimination of methane instead of ethane.

The difference in decomposition rate between Ni(^{tBu}CC^{meth})Me_2 and Ni(^{tBu}CC^{eth})Me_2 (**13**) is not readily rationalised. The bite angle observed for **13** is 88.9(2)°, and in the two related cations [(^{tBu}CC^{meth})NiCl(PMe_3)]$^+$ and [(^{tBu}CC^{eth})NiCl(PMe_3)]$^+$ the bite angle of ^{tBu}CC^{meth} (84.92(18)°) is smaller than ^{tBu}CC^{eth} (88.4(4)°). It was also observed in the cations that ^{tBu}CC^{meth} possibly exerts a greater steric influence at the nickel centre, a nonbonding interaction between the ^{t}Bu groups and the PMe_3 methyls causing a greater deviation from square planarity in the case of [(^{tBu}CC^{meth})NiCl(PMe_3)]$^+$. It therefore appears that the chemistry at the nickel centre, exemplified by thermal hydrocarbon elimination, is very sensitive to subtle variations in the nature of the dicarbene ligand, such as the bite angle and general ligand conformation determined by the backbone length $(CH_2)_n$.

3.2.7 Reaction Between Ni(^{tBu}CC^{eth})Me$_2$ (13) and B(C$_6$F$_5$)$_3$

In an attempt to form the cation [(^{tBu}CC^{eth})NiMe]$^+$ (a potential olefin polymerisation initiator similar to the Brookhart nickel(II) diimine systems shown in section 1.3.1) by methyl group abstraction using B(C$_6$F$_5$)$_3$ to form the counter anion [MeB(C$_6$F$_5$)$_3$]$^-$ (Eq. 48), reaction between Ni(^{tBu}CC^{eth})Me$_2$ (**13**) and 1 equivalent B(C$_6$F$_5$)$_3$ was performed. ^{11}B NMR spectroscopy of the NMR tube reaction in d^8-toluene showed a singlet at δ -9.3 characteristic of a 4-coordinate borate anion such as [MeB(C$_6$F$_5$)$_3$]$^-$, indicating that methyl abstraction had occurred. ^{19}F NMR spectroscopy was also consistent with the formation of [MeB(C$_6$F$_5$)$_3$]$^-$. However, the ^{1}H NMR spectrum showed a mixture of products (broad bands of peaks in the Ni-methyl, *tert*-butyl and imidazole ring proton regions), and a peak for [MeB(C$_6$F$_5$)$_3$]$^-$ at δ 1.1 was not discernable. The reaction was repeated on a 0.83 mmol scale, the resulting mixture an intractable dark red oil (^{1}H NMR spectroscopy of the diethyl ether extract showed a similar mixture of products).

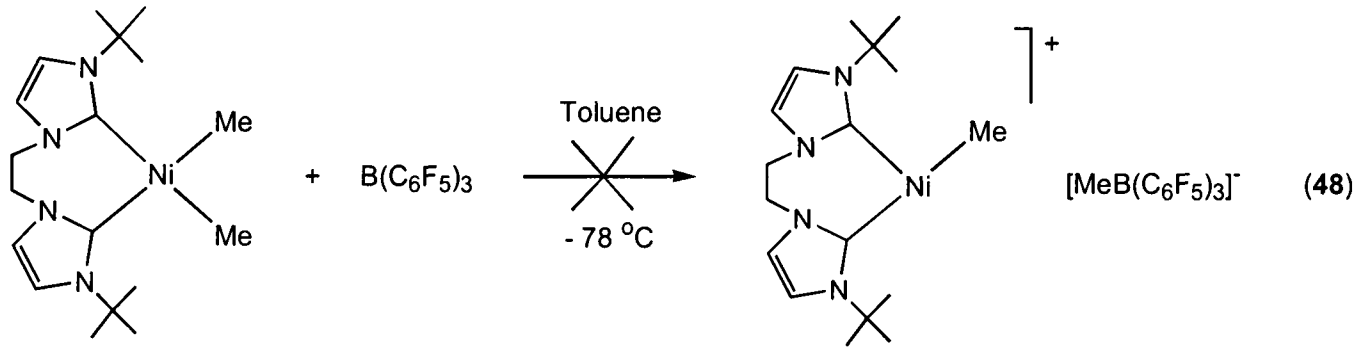

3.2.8 Reaction Between Ni(^{tBu}CC^{eth})Me$_2$ (13) and CO

Reaction between Ni(^{tBu}CC^{meth})Me$_2$ (**13**) and an excess of CO was carried out both on NMR-tube and 0.80 mmol scales. ^{1}H NMR spectroscopy of the NMR tube reaction mixture was consistent with the formation of acetone (δ 1.56 (s)). Acetone was not observed by ^{1}H NMR spectroscopy of the 0.80 mmol scale reaction mixture due to removal of volatiles under reduced pressure beforehand. ^{1}H NMR spectroscopy of the mixtures also showed that in both cases no starting material remained, and that the main non-volatile decomposition products were free ^{tBu}CC^{eth} and 1-*tert*-butylimidazole (the latter presumably a decomposition product of the former). The ^{1}H NMR spectra suggest coordination of CO and insertion into the Ni-Me bond to form the acyl complex [(^{tBu}CC^{meth})NiMe(COMe)],

followed by reductive elimination of acetone and decomposition of the resulting nickel carbene fragment to give free $^{tBu}CC^{eth}$ (scheme 3.3).

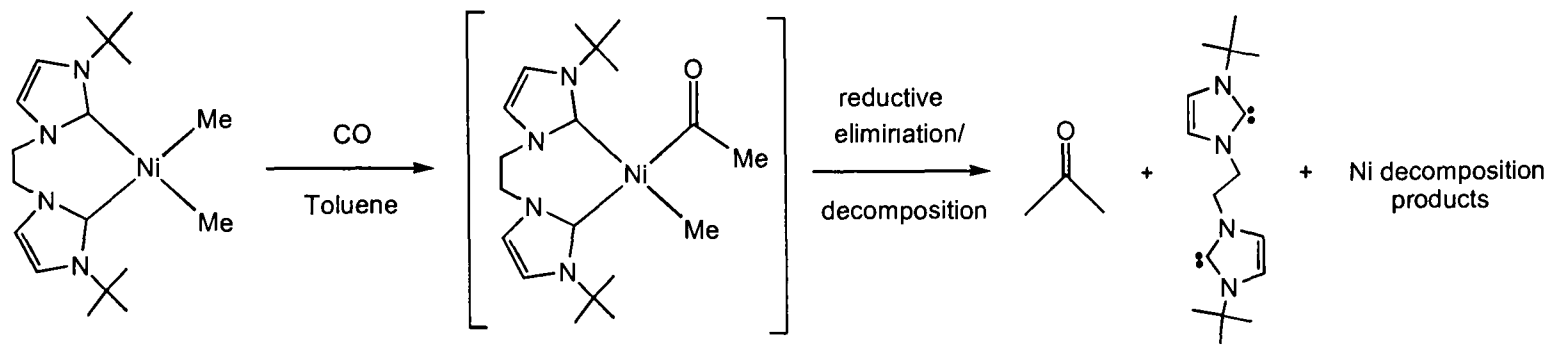

Scheme 3.3 Insertion of CO into an Ni-Me bond of Ni($^{tBu}CC^{eth}$)Me_2 (**13**), followed by reductive elimination of acetone.

3.3 Catalytic Studies of Ni(^{tBu}CC^{meth})Me$_2$

3.3.1 Ni(^{tBu}CC^{eth})Me$_2$ (13): Ethylene Polymerisation Studies

Following the synthesis of the originally-targetted compound Ni(^{tBu}CC^{meth})Me$_2$, the dicarbene ligand ^{tBu}CC^{eth} was investigated as an alternative ancillary ligand to the chelating diimines used in nickel(II) olefin polymerisation catalysis established by Brookhart (section 1.3.1).[16,17] Toluene solutions of **13** (10 μmol) and either methylaluminoxane or [Ph$_3$C][B(C$_6$F$_5$)$_4$] (co-catalysts) were stirred for 2 hours in the presence of 2 bar ethylene. No polymer formation was observed (Eq. 49) in runs 1-5 (table 3.4). Experimental details are given in section 5.3.11.

Run	MAO [Al] / [Ni]	[[Ph$_3$C][B(C$_6$F$_5$)$_4$]] / [^{i}Bu$_3$Al] / [Ni]	Temperature (°C)
1	500	-	22
2	1500	-	22
3	1500	-	58
4	-	1 / 30 / 1	22
5	-	1 / 0 / 1	22

NB. In run 4 the tri-*iso*-butylaluminium was added to the 50 mL toluene, prior to the addition of [Ph$_3$C][B(C$_6$F$_5$)$_4$] and Ni(^{tBu}CC^{eth})Me$_2$ (**13**), to act as a moisture scavanger.

Table 3.4 Summary of attempts at ethylene polymerisation using Ni(^{tBu}CC^{eth})Me$_2$ (**13**).

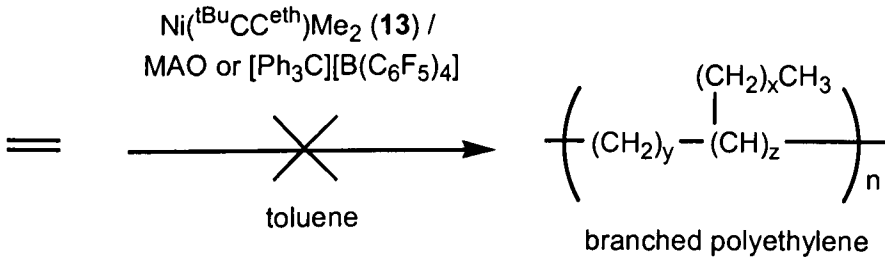

(49)

One possible reason for the inability of **13** to catalyse ethylene polymerisation is that the ^{tBu}CC^{eth} ligand is not bulky enough to retard axial approach of ethylene, which causes associative displacement and chain transfer, and prevents the formation of long polymer chains (section 1.3.1). The crystal structure of **13** shows that due to the boat-like conformation of the ^{tBu}CC^{eth} ligand, and the considerable deviation of the heterocyclic rings

from the nickel coordination plane, the bulky ^{t}Bu groups both point in the same direction away from the coordination plane. Therefore if the ^{t}Bu groups do serve to block axial approach of ethylene, it is only from one direction, and the ethylene bridge, which points in the opposite direction to the ^{t}Bu groups, is probably not bulky enough to prevent axial approach from the other direction. Another possible reason for the inactivity of **13** is that di-N-heterocyclic carbene nickel complexes are not as electrophilic as the active diimine nickel complexes, as a result of the greater σ donating capacity of the dicarbene relative to the diimine ligand and the greater electronegativity of nitrogen compared to carbon.

3.3.2 Ni(^{tBu}CC^{eth})Me$_2$ (13): Heck Coupling of 4-Bromoanisole with n-Butyl Acrylate

Although many frequently used C-C coupling reactions involve palladium catalysts (section 1.3.3), nickel(II) phosphine complexes have also been used as pre-catalysts for the cross coupling of organic halides with grignard reagents,[18] organolithium salts,[19] arylboronic acids (Suzuki coupling)[20] and olefins (Heck coupling). Heck coupling was observed by Kelkar et al. using $NiCl_2.H_2O/PPh_3$ in the presence of the base Na_2CO_3, achieving up to 100 % conversion in 19 hours (160 °C) using 1 mol % catalyst (turnover number (TON) = 100 (mol product / mol Ni)).[21] Furthermore the nickel(0) complexes $Ni[P(OR)_3]_4$ (R = Et, Ph) catalysed the coupling of aryl halides with alkenes such as styrene with quantitative conversion in 24 hours (150 °C) using 10 mol % Ni (TON = 10).[22] N-heterocyclic monocarbene nickel pre-catalysts for Suzuki coupling were also recently reported, with a higher activity observed for the arylnickel *bis*-monocarbene bromide complex than for the nickel *bis*-monocarbene diiodide complex (section 1.2.6.(f)).[5] The ability of Ni(^{tBu}CC^{eth})Me$_2$ (**13**) to catalyse the Heck coupling of 4-bromoanisole with n-butyl acrylate was therefore investigated.

4-bromoanisole and 1.4 equivalents n-butyl acrylate were refluxed in *N*,*N*-dimethylacetamide, in the presence of the bases sodium acetate and tetrabutylammonium acetate and 0.5 mol % Ni(^{tBu}CC^{eth})Me$_2$ (**13**). Experimental details are given in section 5.3.12. Yields, determined by GCMS, were found to be 0 % after 20 hours at 80 °C, 0 % after 20 hours at 100 °C and 3.5 % after 20 hours at 130 °C (TON = 7) (Eq. 50). The yield and turnover number are obviously very poor, with the best palladium Heck catalysts

achieving turnover numbers in the order 10^6 (section 1.3.3), and nickel catalysts achieving quantitative conversions within 24 hours. The low conversion is most likely attributable to the low thermal stability of Ni(^{tBu}CC^{eth})Me$_2$ (**13**), which eliminates methane to form decomposition products at elevated temperatures.

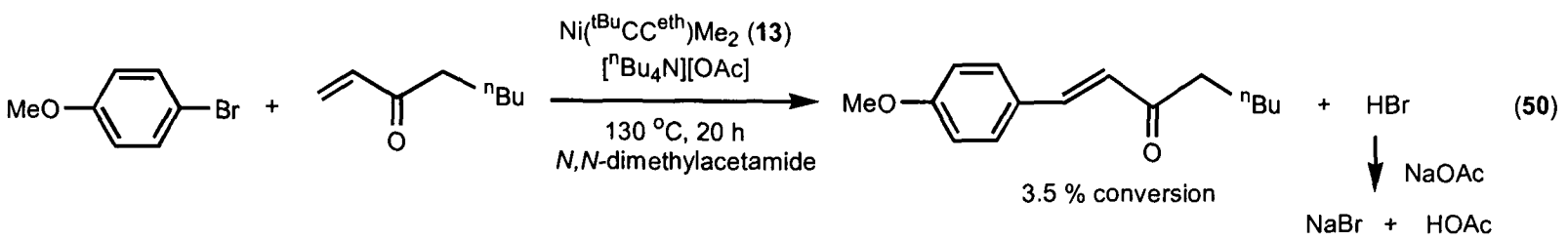

(**50**)

3.4 Palladium(II) Methyl Complexes of $^{tBu}CC^{meth}$ (4) and $^{tBu}CC^{eth}$ (5)

3.4.1 Synthesis of Pd($^{tBu}CC^{meth}$)Me_2 (14)

Reaction in THF between Pd(bpy)Me_2 and 1 equivalent $^{tBu}CC^{meth}$ (**4**) (Eq. 51) gave a dark orange suspension to which diethyl ether was added. The resulting orange supernatant was isolated and cooled to -80 °C, giving two crops of the beige microcrystalline solid Pd($^{tBu}CC^{meth}$)Me_2 (**14**) (combined yield = 63 %).

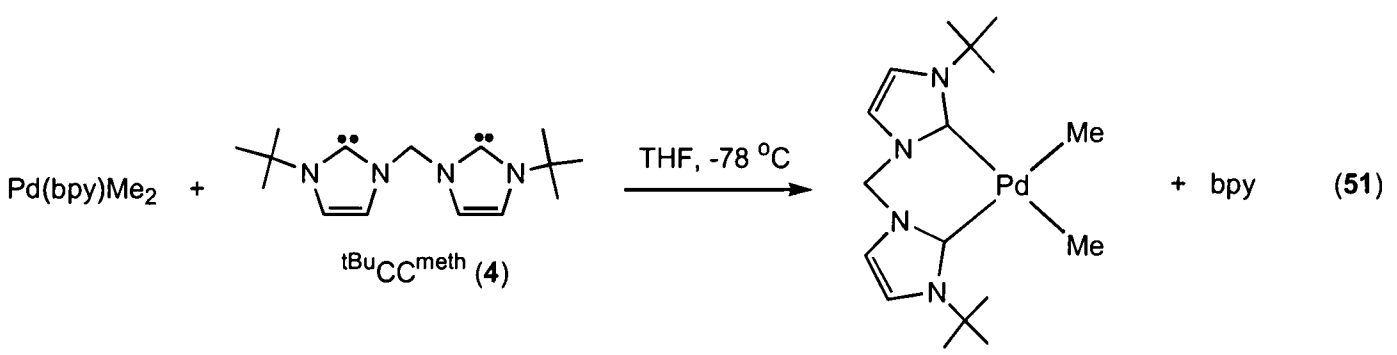

In contrast to the nickel analogue Ni($^{tBu}CC^{meth}$)Me_2, which cannot be isolated and decomposes upon formation above -50 °C, the compound **14** is air-stable for hours in the solid state, and is stored at room temperature under nitrogen without decomposition. This reflects the greater kinetic stability of palladium(II) *cis*-dialkyl compounds with respect to hydrocarbon elimination. The compound **14** is soluble in toluene and common polar, aprotic organic solvents, but is unstable in dichloromethane and decomposes within minutes in protic solvents such as alcohols and water.

3.4.2 Characterisation of Pd($^{tBu}CC^{meth}$)Me_2 (14)

The compound **14** was characterised by elemental analysis, and ^{1}H and $^{13}C\{^{1}H\}$ NMR spectroscopy. Attempts to grow single crystals suitable for structural characterisation by X-ray diffraction were unsuccessful. The ^{1}H and $^{13}C\{^{1}H\}$ NMR spectra (figure 3.16) are as expected for the molecular structure shown in equation 51, with the $^{tBu}CC^{meth}$ ligand chelating to the palladium centre, and the resulting six-membered palladacycle 'locked' in a boat conformation similar to that observed for the structurally-characterised $^{tBu}CC^{meth}$

complexes **6** and **7**. The ^{1}H NMR spectrum shows a similar pattern to that of Ni(^{tBu}CC^{meth})Me$_2$. A singlet for the Pd-Me groups is observed at δ 0.88 which is shifted 0.70 ppm downfield from that for the Ni-Me groups of Ni(^{tBu}CC^{meth})Me$_2$. Other ^{1}H NMR resonances of Ni(^{tBu}CC^{meth})Me$_2$ and Pd(^{tBu}CC^{meth})Me$_2$ are within 0.2 ppm. A single resonance for the *tert*-butyl groups is observed at δ 1.59, and two doublets ($^{2}J_{HH}$ = 13 Hz) at δ 6.25 and 6.41 are assigned to the magnetically inequivalent protons (labelled H_{exo} and H_{endo} in figure 3.15) of the methylene bridge, showing the structure to be rigid with respect to equilibration of these protons. This is probably due to steric congestion caused by the bulky ^{t}Bu groups that would be present in the planar intermediate of a 'butterfly-type' conformational movement of the ligand (figure 3.15). This is consistent with ^{1}H NMR spectroscopy of compounds synthesised by Herrmann et al., where a singlet is observed for the equivalent methylene bridge protons of Pd(^{Me}CC^{meth})X$_2$, and two doublets for the inequivalent methylene bridge protons of the *N*-^{t}Bu-substituted analogues Pd(^{tBu}CC^{meth})X$_2$ (X = Br, I).[3,23,24] The equivalent carbene carbon atoms of **14** are observed at δ 195.3, which is a similar chemical shift to that of Pd(^{tBu}CC^{eth})Me$_2$ (**15**) (δ193.2), but is ca. 37 ppm downfield with respect to the neutral palladium dihalide complexes Pd(tmiy)$_2$X$_2$ (X = Br, I) and is 9 and 15 ppm downfield with respect to the neutral palladium methyl halide complexes [Pd(Me)(1,3-dimethylimidazol-2-ylidene)$_2$Cl] and [Pd(Me)(tmiy)$_2$Cl] respectively (tmiy = 1,3,4,5-tetramethylimidazol-2-ylidene).[1,5] The carbene carbon resonances of the compounds Pd(^{R}CC^{meth})X$_2$ (R = Me, ^{t}Bu; X = Br, I) synthesised by Herrmann et al.[3,23,24] were not reported.

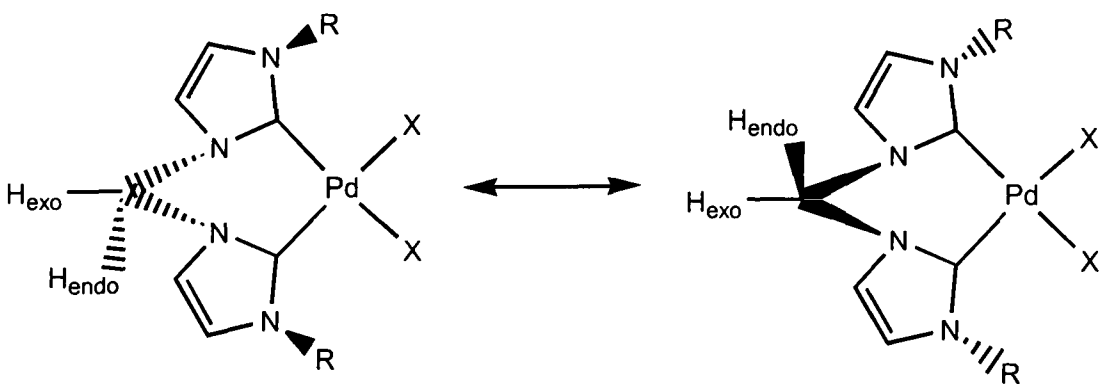

Figure 3.15 Interconversion of the magnetically inequivalent H_{exo} and H_{endo}, caused by a 'butterfly type' conformational movement of the ligand, occurs in the case of R = Me (X = Br, I) but not for R = ^{t}Bu (X = Br, I, Me).

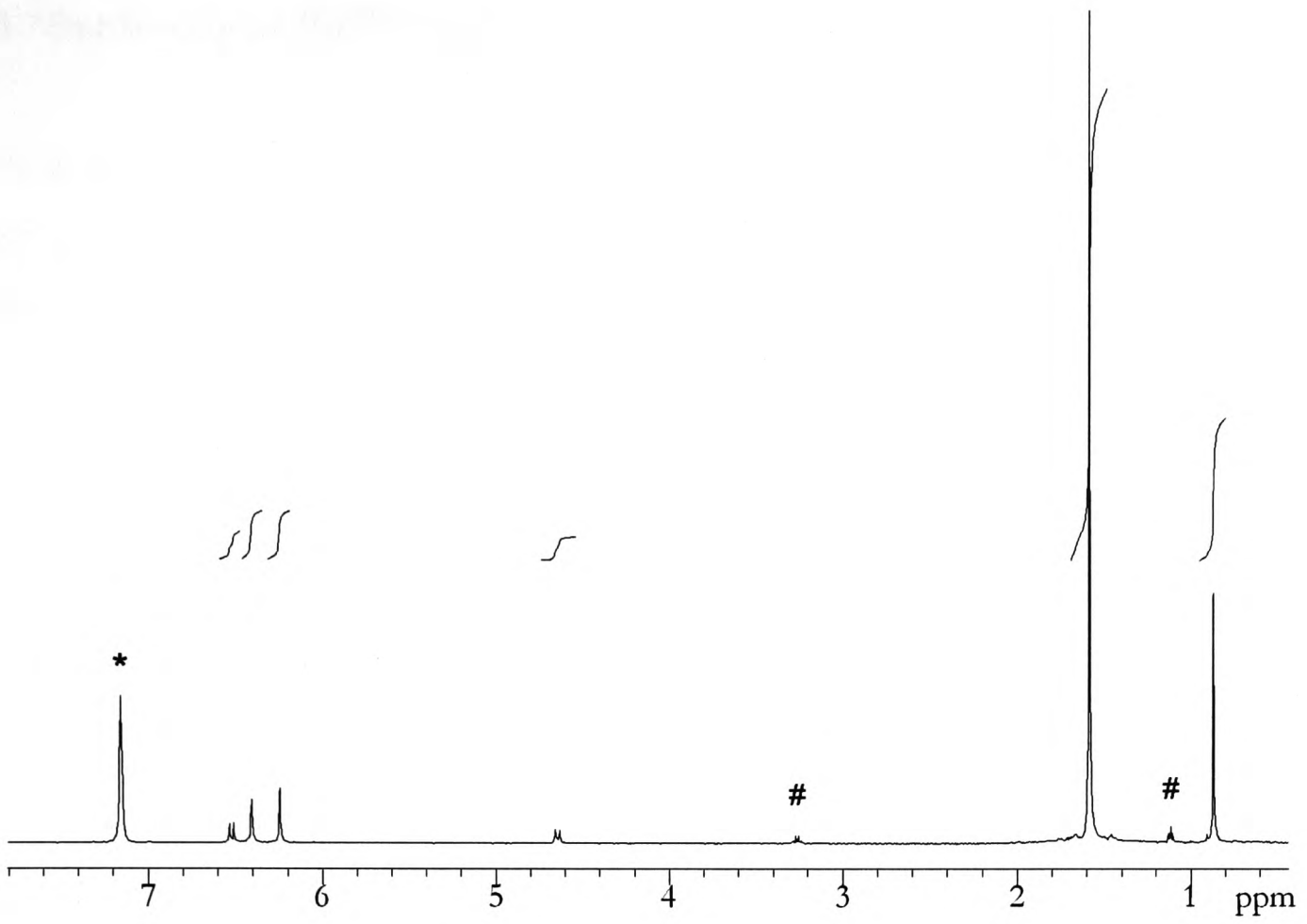

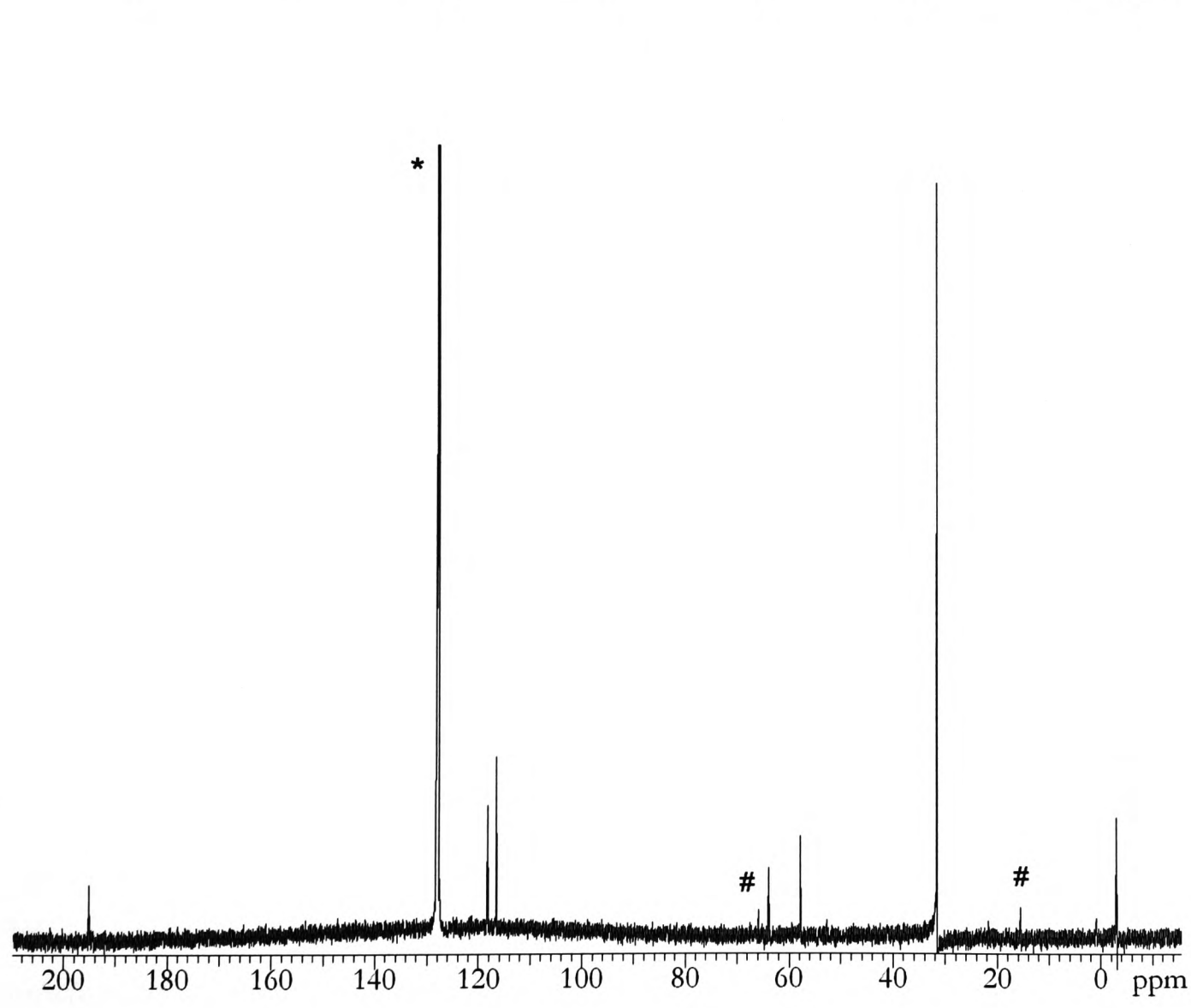

Figure 3.16 500 MHz ^{1}H and 125.7 MHz $^{13}C\{^{1}H\}$ NMR spectra of $Pd(^{tBu}CC^{meth})Me_2$ (**14**) in C_6D_6 (* = solvent, # = diethyl ether).

3.4.3 Synthesis of Pd(^{tBu}CC^{eth})Me$_2$ (15)

Reaction in THF between Pd(bpy)Me$_2$ and 1 equivalent ^{tBu}CC^{eth} (**5**) (Eq. 52) gave a dark orange suspension to which diethyl ether was added. The resulting orange supernatant was isolated and cooled to -80 °C which gave a white microcrystalline solid, Pd(^{tBu}CC^{eth})Me$_2$ (**15**), in 64 % yield.

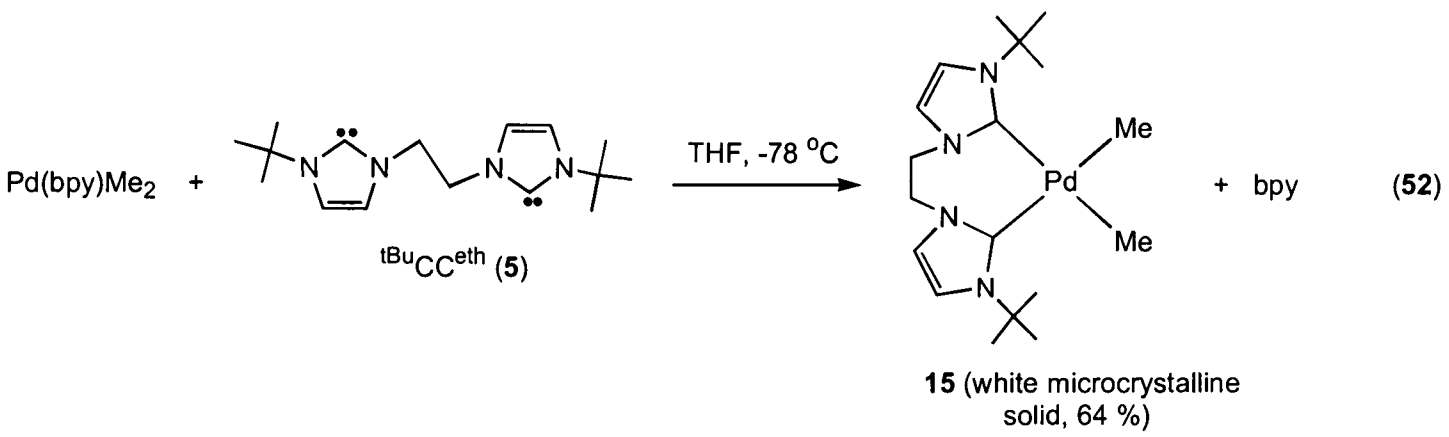

In contrast to the nickel analogue Ni(^{tBu}CC^{eth})Me$_2$ (**13**), which is air-sensitive, sensitive to the thermal elimination of methane and must be stored at -20 °C, the compound **15** is air-stable for hours in the solid state, and is stored at room temperature under nitrogen without decomposition. Again, this reflects the greater kinetic stability of palladium(II) *cis*-dialkyl compounds with respect to hydrocarbon elimination. **15** is soluble in toluene and common polar, aprotic organic solvents, but is unstable in dichloromethane and decomposes within minutes in protic solvents such as alcohols and water.

3.4.4 Characterisation of Pd(^{tBu}CC^{eth})Me$_2$ (15)

The compound **15** was characterised by elemental analysis, ^{1}H and ^{13}C{^{1}H} NMR spectroscopy, and X-ray crystal structure determination. Single crystals of sufficient quality for X-ray structure determination (performed by Dr Richard Douthwaite) were grown by cooling a diethyl ether solution of **15** to -20 °C. Selected bond lengths and angles are given in table 3.5. The asymmetric unit contains one molecule of **15**, shown in figure 3.17, and one molecule of diethyl ether as solvent of crystallisation. The geometry at the palladium atom is essentially square planar with a dicarbene bite angle C(3)-Pd-C(10) = 88.12(13)° which is comparable to those of 88.4(4)° and 88.9(2)° observed in the only other structurally characterised ethylene-bridged dicarbene complexes [(^{tBu}CC^{eth})NiCl(PMe$_3$)][BPh$_4$] (**10**) and Ni(^{tBu}CC^{eth})Me$_2$ (**13**) respectively. The bite angle of

15 is ca. 5° larger than observed for the methylene-bridged dicarbene palladium(II) diiodide complexes Pd(^{Me}CC^{meth})I_2 (83.2(3)°) and Pd(^{tBu}CC^{meth})I_2 (83.3(2)°).[3,23] A boat-like conformation similar to compounds **10** and **13** is observed, and projection along the C(7)-C(8) vector shows a staggered conformation with a N(4)-C(7)-C(8)-N(9) torsion angle of 50.7(4)°, which is slightly smaller that observed for the nickel(II) analogue **13** (52.1(5)°). The twist angles of the heterocyclic rings relative to the coordination plane of **15** (69.6(2) and 59.8(3)°) are also smaller than those of **13** (76.9(4) and 62.0(3)°). In order to maintain the similar bite angles observed for **13** and **15**, less ring twist is needed in the case of the palladium compound due to the longer (by ca. 0.17 Å) M-$C_{carbene}$ distances. The Pd-C_{Me} bond lengths (2.097(4) and 2.088(4) Å) are similar to that found for the square planar *bis*-monocarbene palladium complex [Pd(Me)(1,3-dimethylimidazol-2-ylidene)$_2$Cl] (2.117(8) Å),[1] and the Pd-$C_{carbene}$ bond lengths (2.070(3) and 2.089(3) Å) are slightly longer than those of the chelating dicarbene palladium(II) complex [Pd(^{tBu}CC^{meth})I_2] (2.004(3) Å).[23] A similar degree of ring strain within the metallocycles formed by the ^{tBu}CC^{eth} ligands of **15** and the nickel compounds **10** and **13** is implied. The sum of the angles of **15** at N(4) (360.0(9)°) and N(9) (360.0(11)°) are as expected for sp^2 hybridisation. However, as observed for compounds **10** and **13**, the internal angles of the seven-membered ring C(3)-N(4)-C(7) (120.6(3) °) and C(8)-N(9)-C(10) (130.3(4)°) indicate that a degree of ring strain at N(9) may be present. The internal angles of the six-membered ring of the methylene-bridged carbene complex **7** show no such ring strain. Due to the greater size of palladium compared to nickel, the proximity of adjacent ^{t}Bu substituents within **15** is less than for **13** and **10**. Assuming free rotation about each N-C_{tBu} bond, distances between ^{t}Bu groups of 2.2 Å (**15**) and 1.9 Å (**10** and **13**) are estimated. The estimated ^{t}Bu-^{t}Bu distance within **15** is more similar to that of the nickel ^{tBu}CC^{meth} compound **7** (2.3 Å).

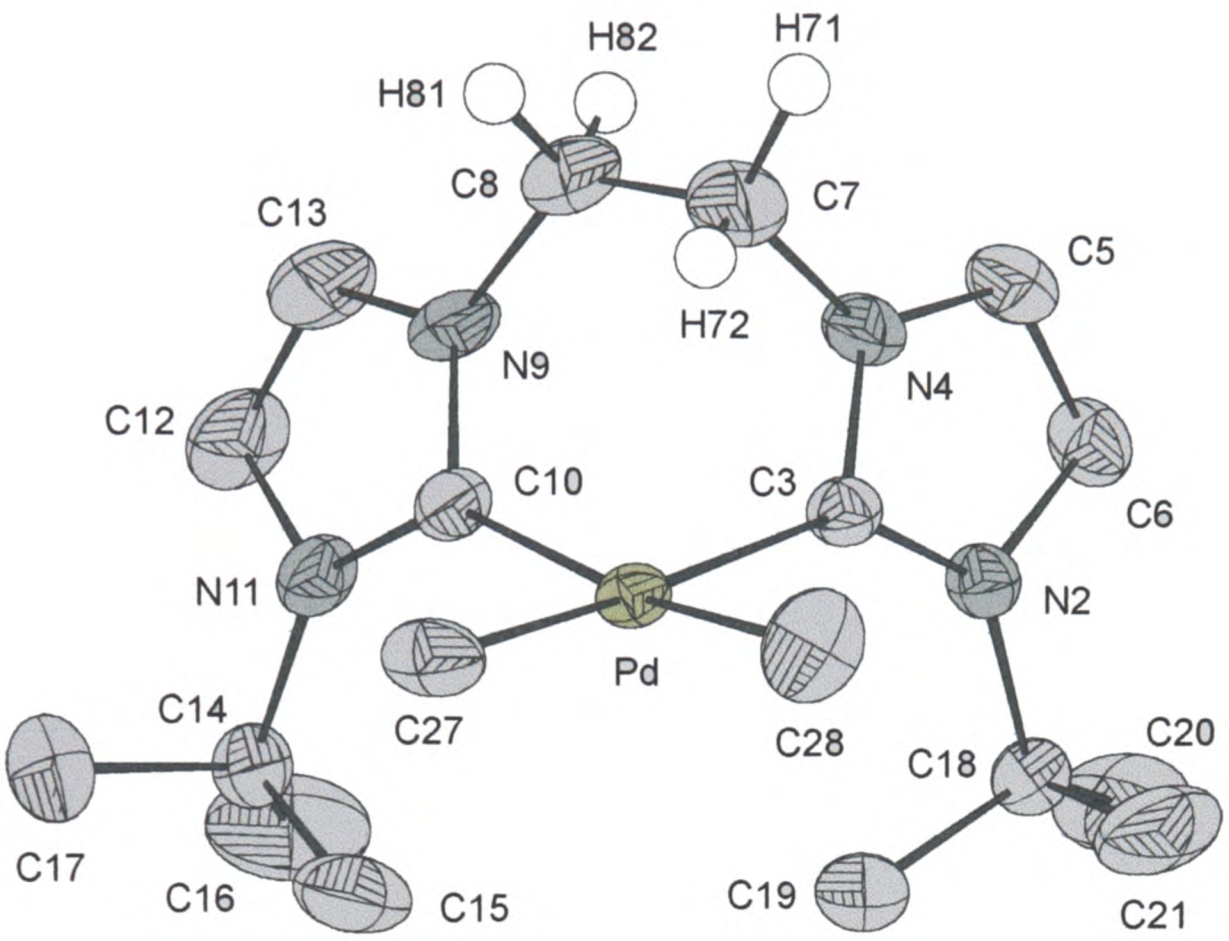

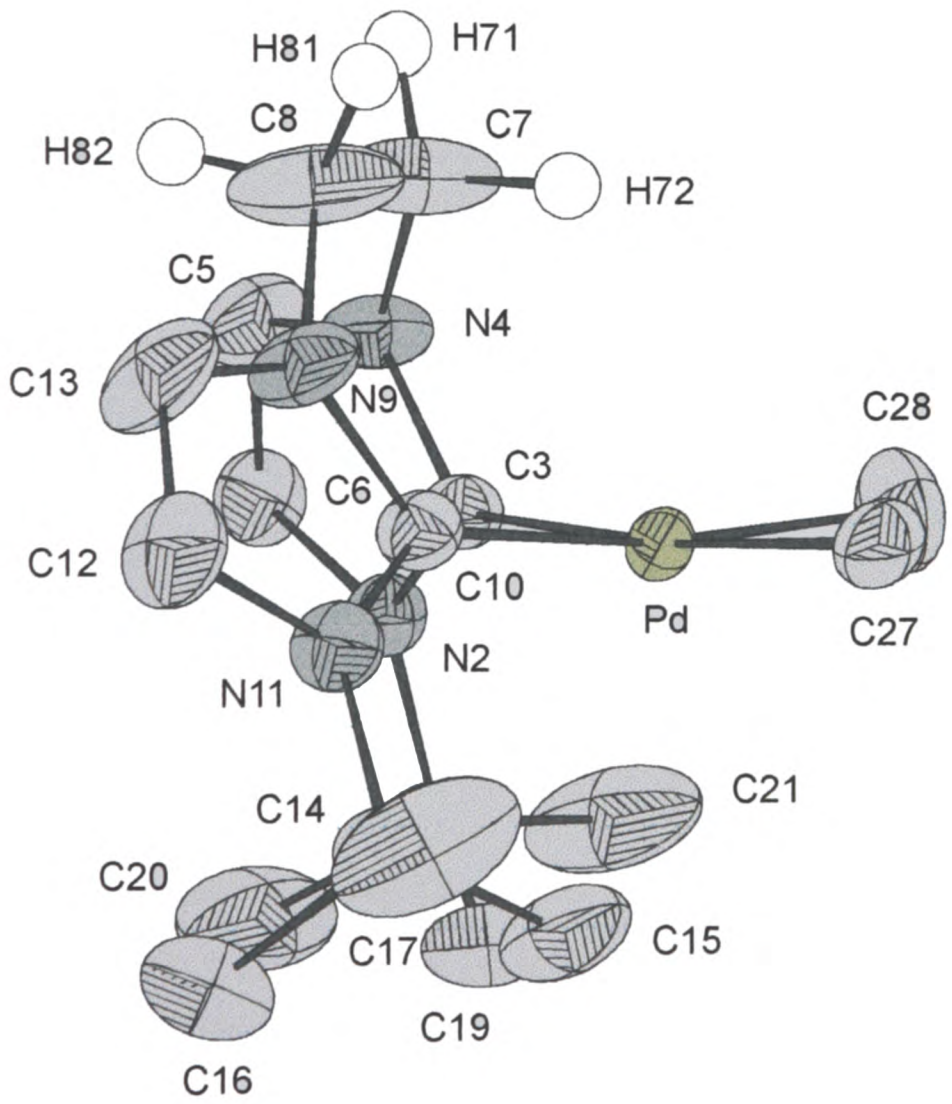

Figure 3.17 Two views of the X-ray structure of Pd(^{tBu}CC^{eth})Me$_2$ (**15**). Hydrogen atoms except for H(71), H(72), H(81) and H(82) are omitted for clarity.

Bond	Length (Å)	Bond	Angle (°)
Pd-C(3)	2.070(3)	C(3)-Pd-C(10)	88.12(13)
Pd-C(10)	2.089(3)	C(3)-Pd-C(27)	172.52(15)
Pd-C(27)	2.097(4)	C(10)-Pd-C(27)	95.78(16)
Pd-C(28)	2.088(4)	C(3)-Pd-C(28)	91.21(16)
C(3)-N(2)	1.356(4)	C(10)-Pd-C(28)	171.13(16)
C(3)-N(4)	1.350(4)	N(2)-C(3)-N(4)	103.7(3)
C(5)-C(6)	1.343(6)	N(9)-C(10)-N(11)	103.4(3)
C(10)-N(9)	1.361(4)	Pd-C(3)-N(4)	115.8(2)
C(10)-N(11)	1.364(4)	C(3)-N(4)-C(7)	120.6(3)
C(12)-C(13)	1.320(7)	N(4)-C(7)-C(8)	116.2(4)
		C(7)-C(8)-N(9)	123.0(4)
		C(8)-N(9)-C(10)	130.3(4)
		N(9)-C(10)-Pd	119.0(2)
		C(3)-N(4)-C(5)	112.2(3)
		C(5)-N(4)-C(7)	127.2(3)
		C(8)-N(9)-C(13)	118.0(4)
		C(10)-N(9)-C(13)	111.7(3)
		ring twist$_{C(3)}$*	69.6(2)
		ring twist$_{C(10)}$	59.8(3)

* The angle between the coordination plane defined by palladium and carbene carbon atoms and the heterocyclic ring containing C(n).

Table 3.5 Selected bond lengths and angles for Pd(^{tBu}CC^{eth})Me$_2$ (**15**).

As observed for the nickel analogue **13**, the ^{1}H and ^{13}C{^{1}H} NMR spectra (C_6D_6) of **15** show signals consistent with C_{2v} symmetry (figures 3.18 and 3.19). Two resonances at δ 3.26 and 5.48 are observed for the four protons of the ethylene bridge, and a single resonance at δ 48.9 corresponds to the two ethylene bridge carbons. Both proton resonances correspond to two protons which are on different carbons of the ethylene bridge (an AA'BB' spin system). A singlet for the Pd-Me groups is observed at δ 0.66 which is shifted 0.53 ppm downfield from that for the Ni-Me groups of Ni(^{tBu}CC^{eth})Me$_2$. A single

tert-butyl resonance is observed at δ 1.66 as well two ring proton resonances at δ 6.04 and 6.37. The apparent horizontal mirror plane implied for **15** in the solution NMR spectra is attributed to a rocking vibration along the C(7)-C(8) vector, which causes the ethylene bridge protons labelled in the crystal structure as H(72) and H(81), as well as H(71) and H(82), to become equivalent pairs on the NMR timescale.

The equivalent carbene carbon atoms of **15** are observed at δ 193.2, which is a similar chemical shift to that of Pd(^{tBu}CC^{meth})Me$_2$ (**14**) (δ195.3), but is ca. 35 ppm downfield with respect to the neutral palladium dihalide complexes Pd(tmiy)$_2$X$_2$ (X = Br, I) and is 7 and 13 ppm downfield with respect to the neutral palladium methyl halide complexes [Pd(Me)(1,3-dimethylimidazol-2-ylidene)$_2$Cl] and [Pd(Me)(tmiy)$_2$Cl] respectively (tmiy = 1,3,4,5-tetramethylimidazol-2-ylidene).[1,5] The carbene carbon resonances of the compounds Pd(^{R}CC^{meth})X$_2$ (R = Me, ^{t}Bu; X = Br, I) synthesised by Herrmann et al.[3,23,24] were not reported.

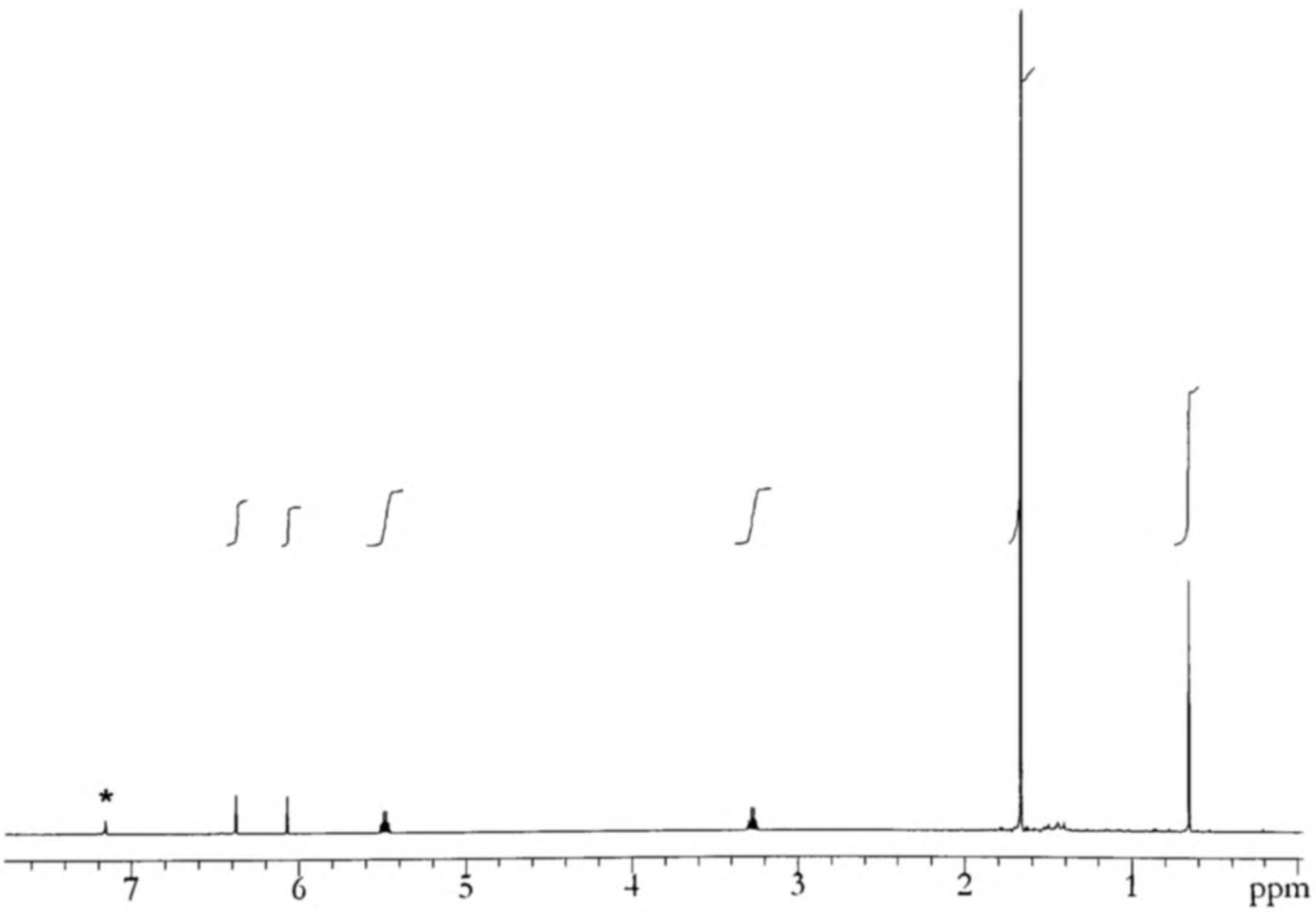

Figure 3.18 500 MHz ^{1}H NMR spectrum of Pd(^{tBu}CC^{eth})Me$_2$ (**15**) in C$_6$D$_6$ (* = solvent).

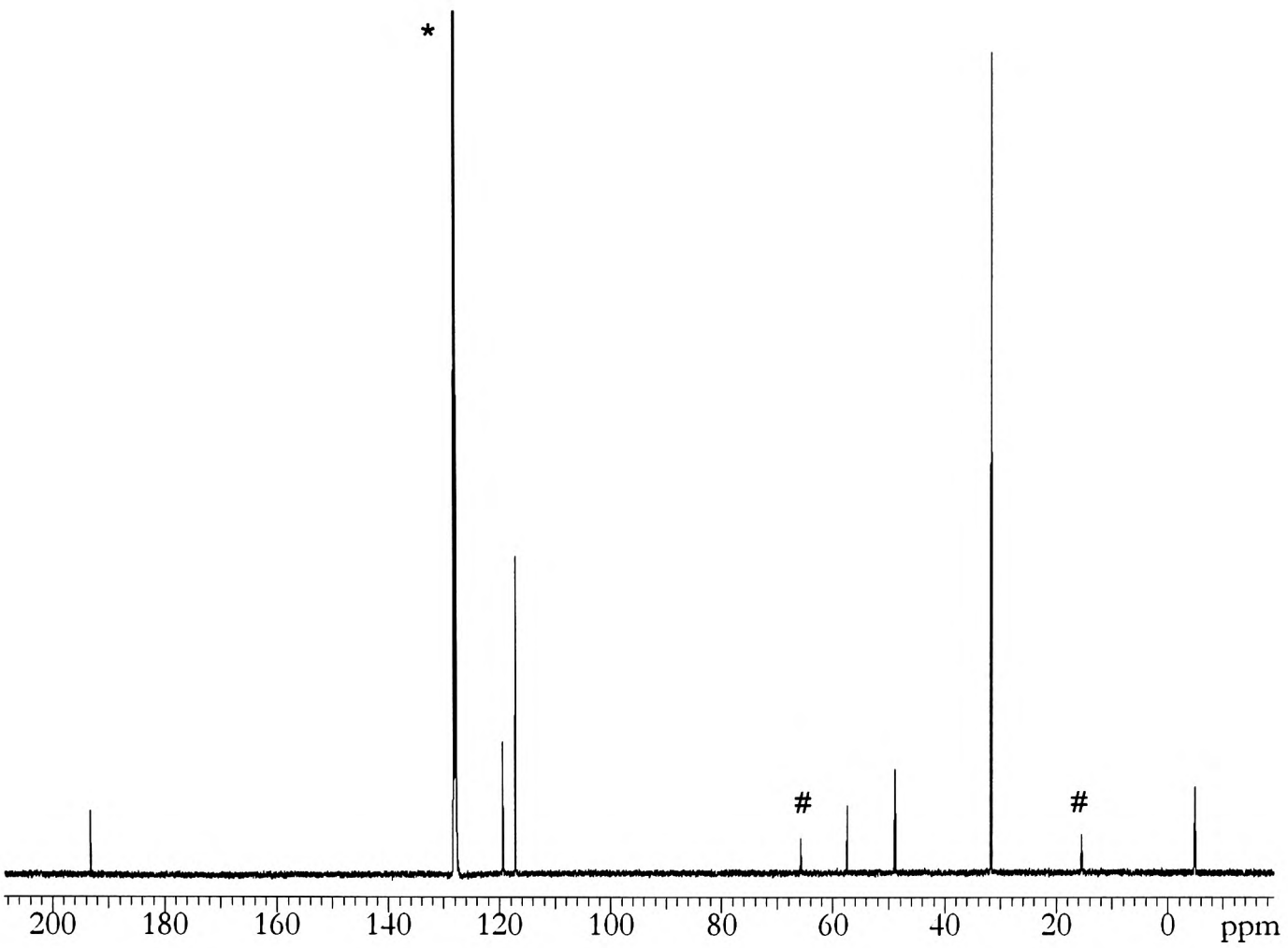

Figure 3.19 125.7 MHz $^{13}C\{^{1}H\}$ NMR spectrum of Pd($^{tBu}CC^{eth}$)Me_2 (**15**) in C_6D_6 (* = solvent, # = diethyl ether).

3.4.5 Syntheses of [($^{tBu}CC^{meth}$)PdMe(py)][OCD_3] (16) and [($^{tBu}CC^{eth}$)PdMe(py)][OCD_3] (17)

Mixtures of pyridine (py) and 1 equivalent of Pd($^{tBu}CC^{meth}$)Me_2 (**14**) or Pd($^{tBu}CC^{eth}$)Me_2 (**15**) were treated in air with an excess of CD_3OD, which gave colourless solutions of [($^{tBu}CC^{meth}$)PdMe(py)][OCD_3] (**16**) and [($^{tBu}CC^{eth}$)PdMe(py)][OCD_3] (**17**) respectively (Eq. 53), in quantitative yields, with concomitant evolution of a gas (presumably CH_3D).

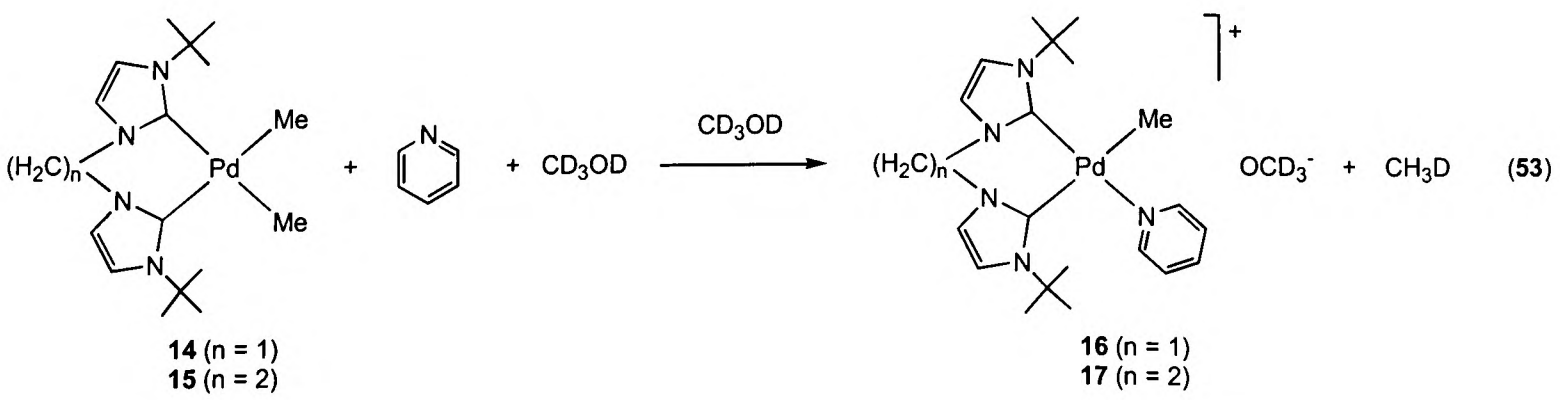

16 and **17** exist as air-stable colourless CD_3OD solutions. CH_3OH may also be used as the reaction solvent, although the resulting solutions cannot be characterised by NMR spectroscopy. Attempts to isolate **16** and **17** were unsuccessful. Removal of the volatiles gave pale yellow oils shown by ^1H NMR spectroscopy (CD_3OD) to be mixtures of unidentifiable decomposition products. Attempts to exchange the methoxide anion with PF_6 by addition of excess NH_4PF_6 gave similar intractable oils.

3.4.6 Characterisation of [(^{tBu}CC^{meth})PdMe(py)][OCD_3] (16) and [(^{tBu}CC^{eth})PdMe(py)][OCD_3] (17)

16 and **17** were characterised by electrospray mass spectrometry and ^1H and $^{13}C\{^1H\}$ NMR spectroscopy. The electrospray mass spectrum of **16** contained a single peak (m/z = 460 [M^+]) corresponding to the cation [(^{tBu}CC^{meth})PdMe(py)]$^+$. The electrospray mass spectrum of **17** contained peaks corresponding to the cation [(^{tBu}CC^{eth})PdMe(py)]$^+$ (m/z = 475 [M^+]) and the fragment [(^{tBu}CC^{eth})PdMe]$^+$ due to loss of pyridine (m/z = 396 [M^+-py]).

^1H NMR spectroscopy is consistent with the molecular structures of **16** and **17** shown in equation 53, in which the dicarbene ligands are chelating to the palladium atom with one N-heterocyclic carbene moiety *trans* to the pyridine ligand and the other *trans* to the methyl. The ^1H NMR spectra of **16** and **17** (figures 3.20 and 3.22) are similar to those of the cations [(^{tBu}CC^{meth})NiCl(PMe_3)]$^+$ and [(^{tBu}CC^{eth})NiCl(PMe_3)]$^+$ respectively: two magnetically inequivalent ^{t}Bu groups are observed (δ 1.31 and 1.80 (**16**), δ 1.44 and 1.81 (**17**)), and four inequivalent NC*H* heterocyclic ring protons (in the range δ 7.26-7.50). The methylene bridge protons of **16** are observed as two doublets (δ 6.20 and 6.92), and the ethylene bridge protons of **17** are observed as four multiplets (δ 4.54, 4.63, 5.44 and 6.22). The methyl groups resonate at δ 0.04 (**16**) and δ -0.10 (**17**). Finally, three multiplets are observed for the coordinated pyridine ligand (δ 7.53, 7.95 and 8.70 (**16**), δ 7.50, 7.94 and 8.59 (**17**)).

$^{13}C\{^1H\}$ NMR spectroscopy (figures 3.21 and 3.23) is also consistent with the molecular structures of **16** and **17** shown in equation 53. The inequivalent carbene carbon resonances are observed at δ 172.0 and 184.9 (**16**), and δ 169.0 and 181.3 (**17**). The values for **16** are shifted ca. 23 and 10 ppm upfield respectively, with respect to the neutral complex

$Pd(^{tBu}CC^{meth})Me_2$, and those for **17** are shifted ca. 24 and 12 ppm upfield with respect to the neutral complex $Pd(^{tBu}CC^{eth})Me_2$. These carbene carbon shifts of **16** and **17** are characteristic of cationic palladium(II) complexes of chelating di-N-heterocyclic carbenes.[25,26] Two inequivalent ^{t}Bu groups are observed (two quaternary and two methyl signals), as well as four inequivalent heterocyclic ring NCH carbons. Singlets are also observed for the methylene (**16**) and inequivalent ethylene (**17**) bridge carbons, the palladium methyl, and the pyridine *ortho, meta* and *para* carbons.

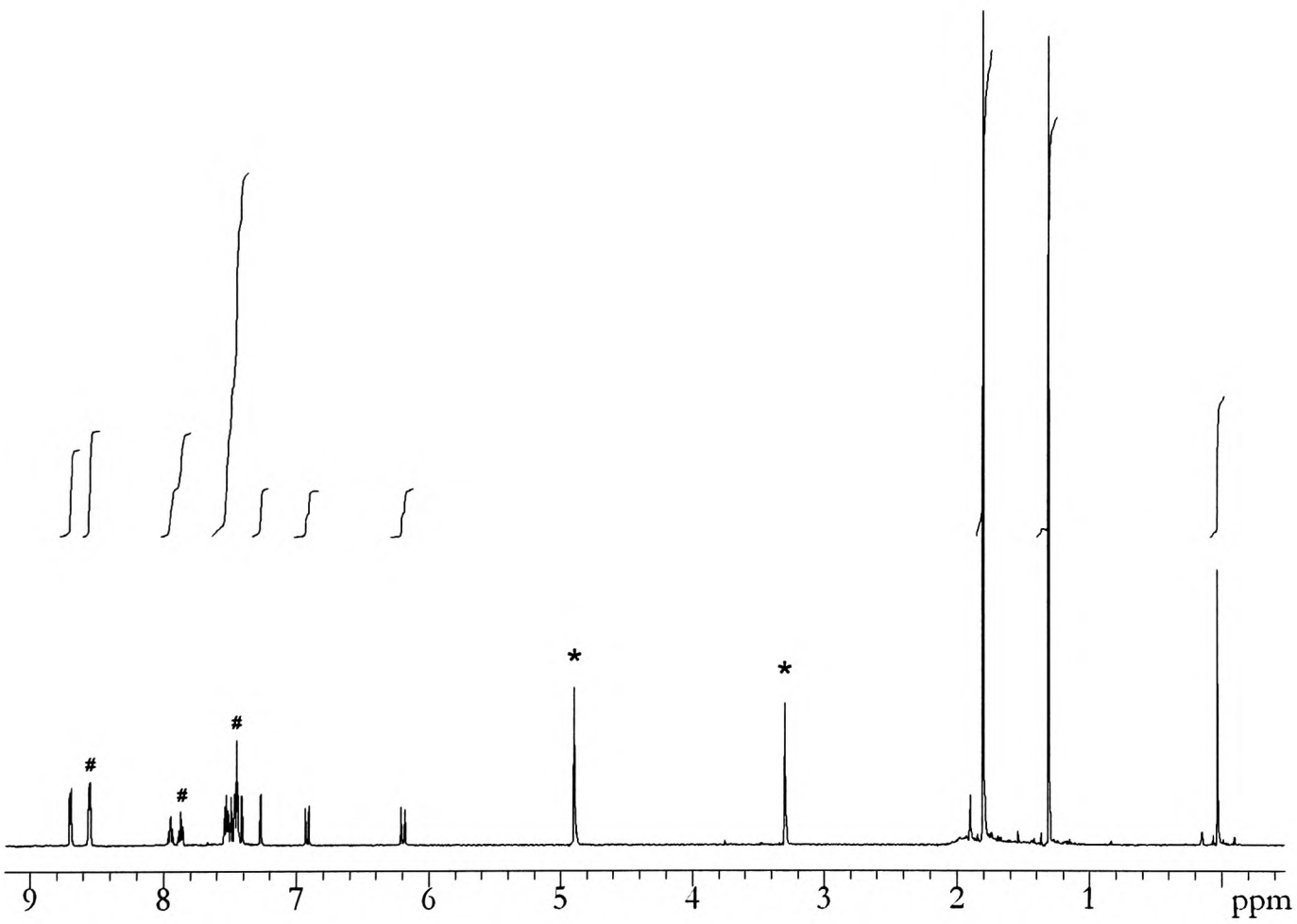

Figure 3.20 500 MHz ^{1}H NMR spectrum of $[(^{tBu}CC^{meth})PdMe(py)][OCD_3]$ (**16**) in CD_3OD (* = solvent, # = free pyridine).

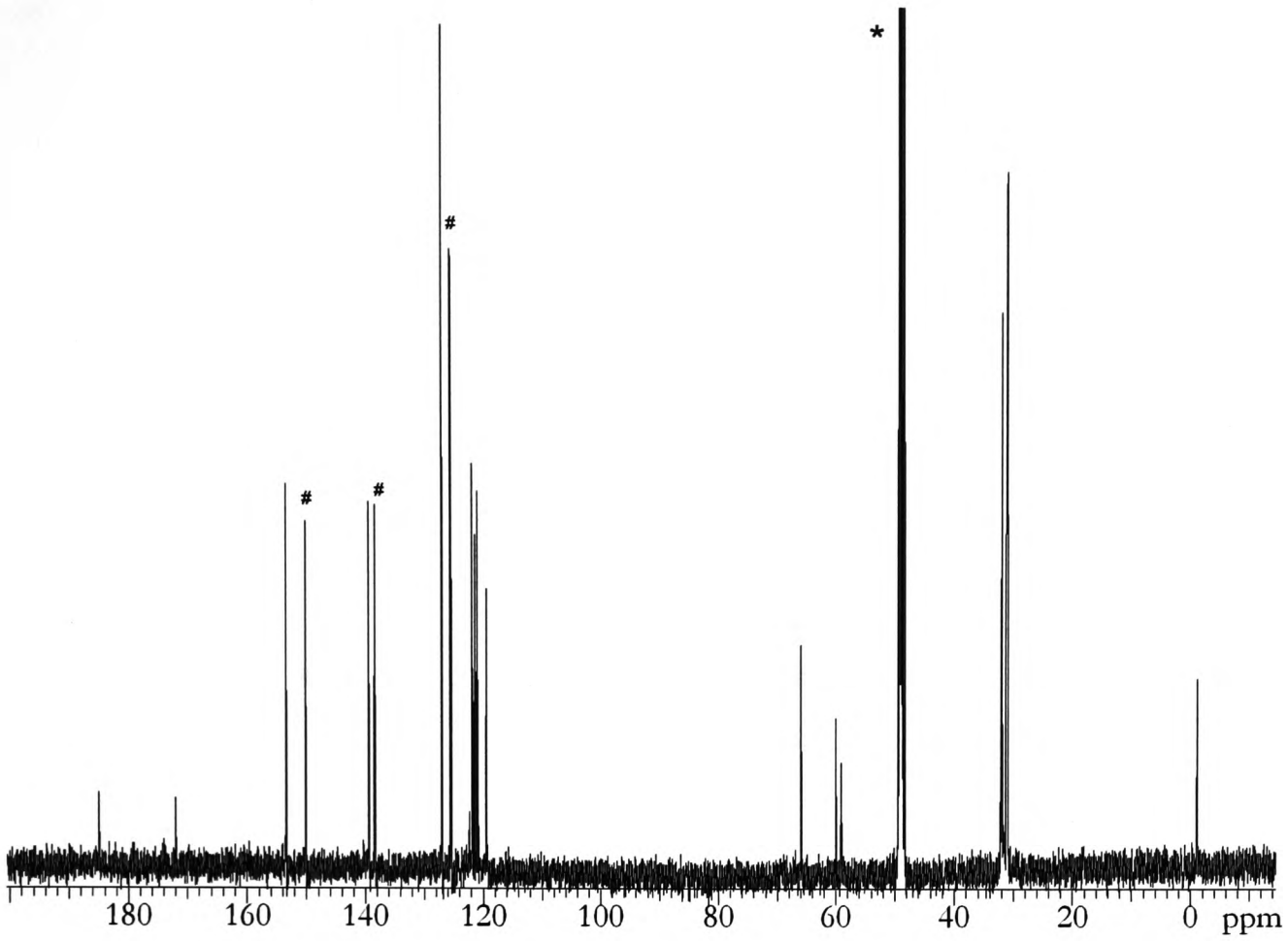

Figure 3.21 125.7 MHz $^{13}C\{^{1}H\}$ NMR spectrum of [($^{tBu}CC^{meth}$)PdMe(py)][OCD_3] (**16**) in CD_3OD (* = solvent, # = free pyridine).

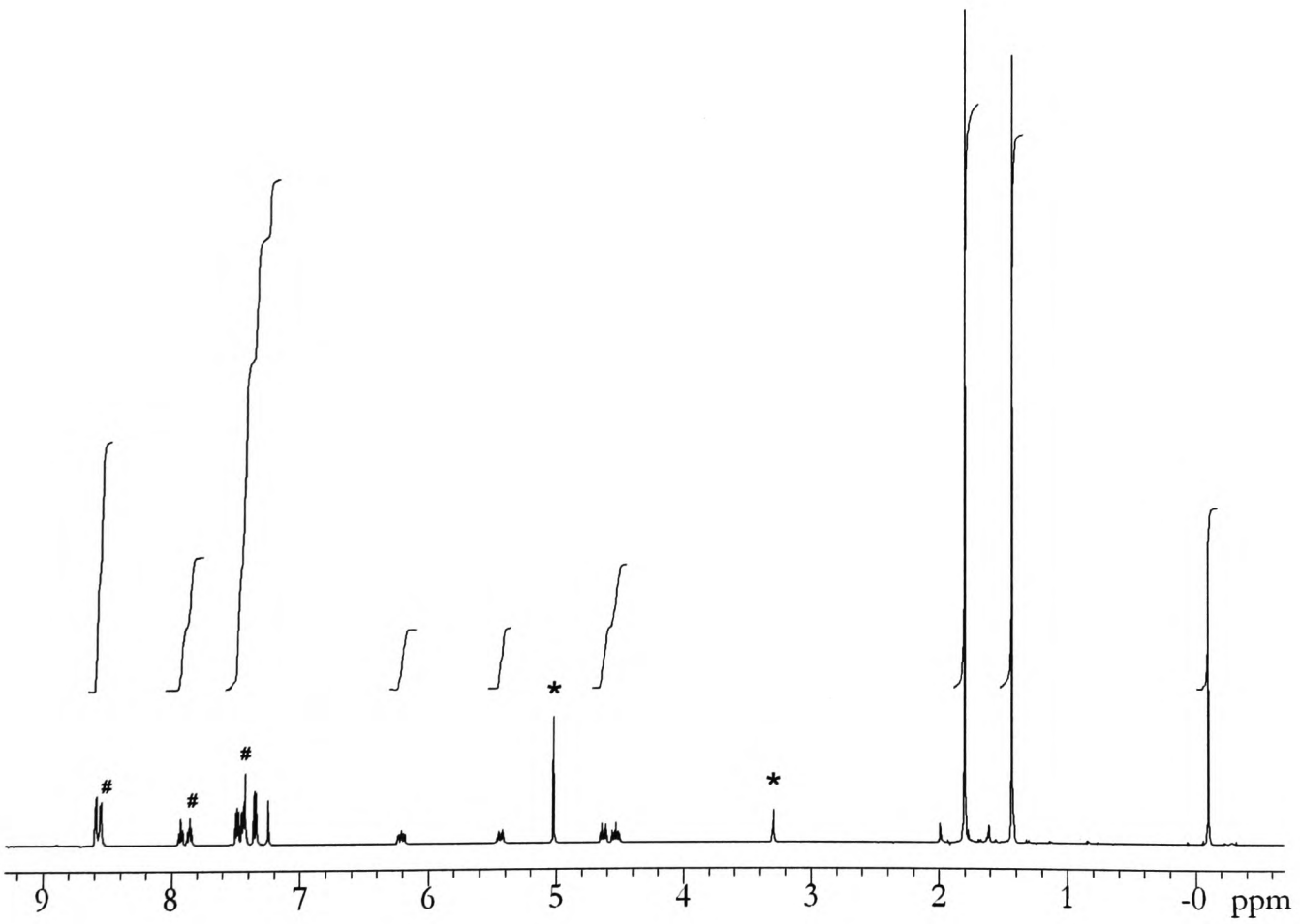

Figure 3.22 500 MHz ^{1}H NMR spectrum of [($^{tBu}CC^{eth}$)PdMe(py)][OCD_3] (**17**) in CD_3OD (* = solvent, # = free pyridine).

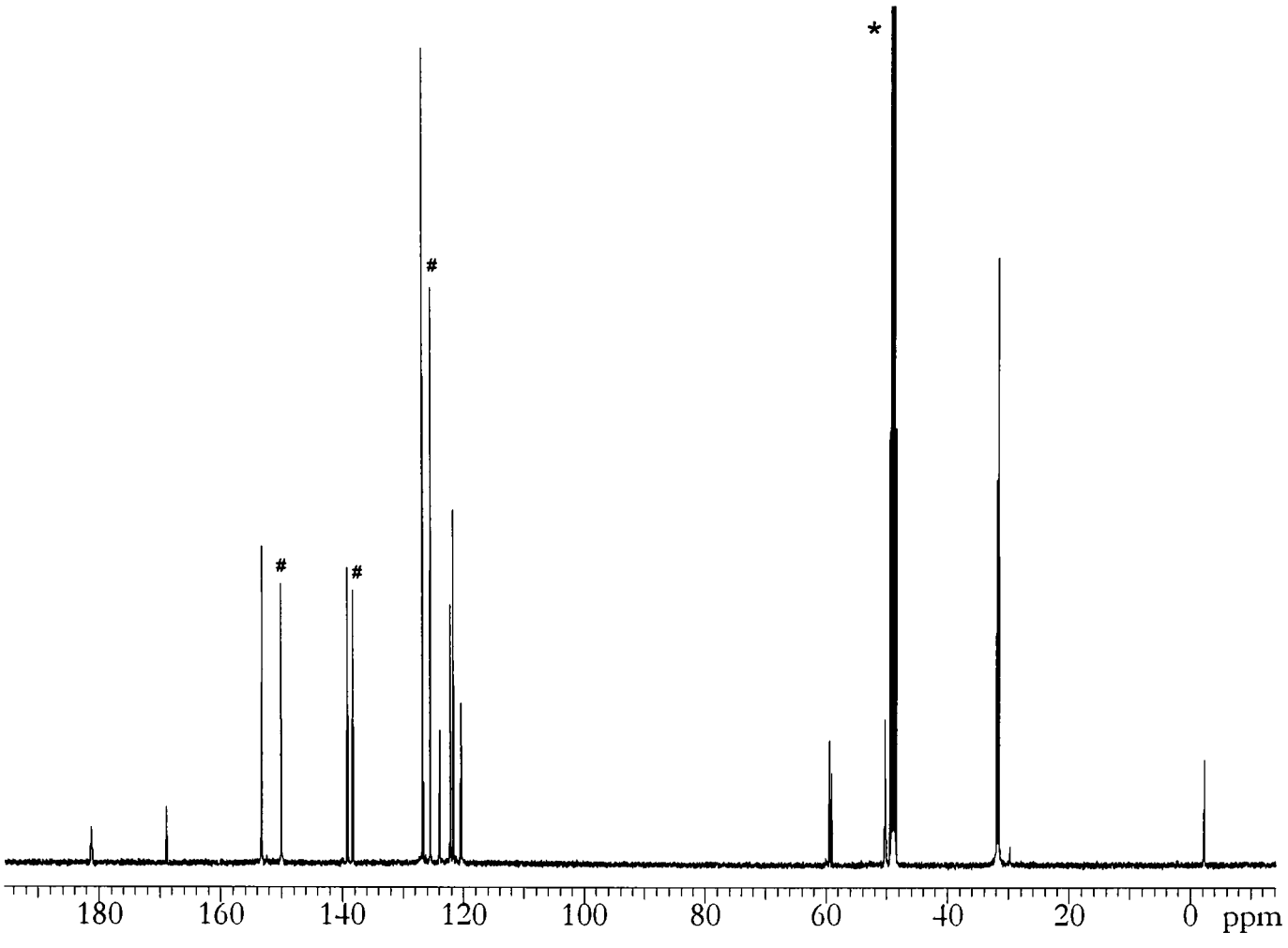

Figure 3.23 125.7 MHz $^{13}C\{^{1}H\}$ NMR spectrum of [($^{tBu}CC^{eth}$)PdMe(py)][OCD_3] (**17**) in CD_3OD (* = solvent, # = free pyridine).

3.4.7 Syntheses of [($^{tBu}C(D)C^{meth}$)PdMe(bpy)][OCD_3]$_2$ (18) and [($^{tBu}C(D)C^{eth}$)PdMe(bpy)][OCD_3]$_2$ (19)

Mixtures of 2,2'-bipyridyl (bpy) and 1 equivalent of Pd($^{tBu}CC^{meth}$)Me_2 (**14**) or Pd($^{tBu}CC^{eth}$)Me_2 (**15**) were treated in air with an excess of CD_3OD, which gave colourless solutions of [($^{tBu}C(D)C^{meth}$)PdMe(bpy)][OCD_3]$_2$ (**18**) and [($^{tBu}C(D)C^{eth}$)PdMe(bpy)][OCD_3]$_2$ (**19**) respectively (Eq. 54), in quantitative yields, with concomitant evolution of a gas (presumably CH_3D) ($^{tBu}C(D)C^{meth}$ = 1,1'-methylene-3,3'-di-*tert*-butyl(2-deuteroimidazolium)imidazol-2-ylidene, $^{tBu}C(D)C^{eth}$ = 1,1'-(1,2-ethylene)-3,3'-di-*tert*-butyl(2-deuteroimidazolium)imidazol-2-ylidene). **18** and **19** exist as air-stable colourless CD_3OD solutions. CH_3OH may also be used as the reaction solvent, although the resulting solutions cannot be characterised by NMR spectroscopy.

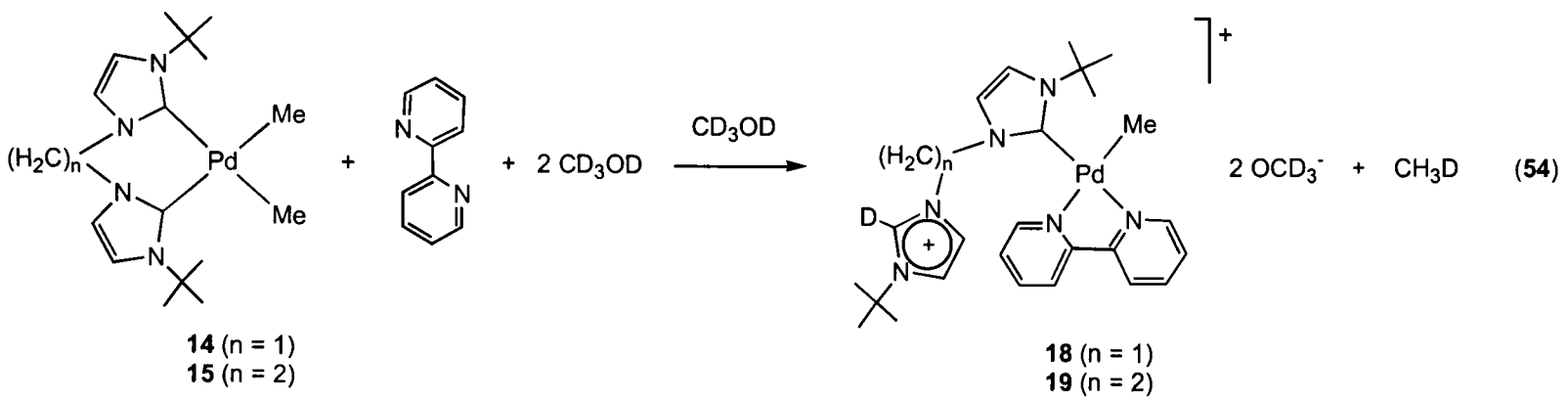

14 (n = 1)
15 (n = 2)

18 (n = 1)
19 (n = 2)

3.4.8 Characterisation of $[(^{tBu}C(D)C^{meth})PdMe(bpy)][OCD_3]_2$ (18)

The compound **18** was characterised by electrospray mass spectrometry and ^{1}H and $^{13}C\{^{1}H\}$ NMR spectroscopy. The electrospray mass spectrum contained peaks corresponding to the monocation $[(^{tBu}C(D)C^{meth})PdMe(bpy)]^{+}$ (m/z = 540 $[M^{+}]$), the dication $[(^{tBu}C(D)C^{meth})PdMe(bpy)]^{2+}$ (m/z = 270 $[M^{2+}]$), a monocationic fragment due to loss of ^{t}Bu (m/z = 484 $[M^{+}-{}^{t}Bu]$) and a dicationic fragment due to loss of ^{t}Bu (m/z = 242 $[M^{2+}-{}^{t}Bu]$).

^{1}H NMR spectroscopy (figure 3.24) is consistent with the molecular structure of **18** shown in equation 54 in which $^{tBu}C(D)C^{meth}$, a mono-N-heterocyclic carbene ligand whose N-substituents are ^{t}Bu and 1-methylene-2-deutero-3-*tert*-butylimidazolium, is coordinated to the palladium atom (via the N-heterocyclic carbene carbon) *cis* to the methyl. The methyl group resonates at δ 0.43 (s). Two magnetically inequivalent ^{t}Bu groups are observed (δ 1.41 and 1.82), and two inequivalent NC*H* heterocyclic ring protons (δ 7.86 and 7.97). The fact that only two resonances are observed for the four magnetically-inequivalent NC*H* ring protons (two on the N-heterocyclic carbene ring and two on the pendant imidazolium ring) is probably due to deuterium exchange with the the protons of the imidazolium ring, such that all three ring carbons are deuterated. Exchange of all three imidazolium ring protons with deuterium has previously been observed for 1-ethyl-3-methylimidazolium chloride in D_2O.[27] The methylene bridge protons are observed as a singlet (δ 6.74), showing freedom of rotation about the Pd-$C_{carbene}$ and N-(CH_2)-N bonds such that the methylene protons can be transformed by the mirror plane, σ_h, of intermediates of C_s symmetry on the NMR timescale. Finally, eight multiplets are observed for the chelating bipy ligand (in the range δ 7.55-8.77).

$^{13}C\{^{1}H\}$ NMR spectroscopy is also consistent with the molecular structure of **18** shown in equation 54. The carbene carbon resonance is observed at δ 173.3 which is characteristic of cationic N-heterocyclic carbene palladium(II) complexes.[25,26] The corresponding N(*C*D)N carbon of the pendant imidazolium ring is observed at δ 135.9, which is similar to the corresponding shifts of the diimidazolium dihalide salts **1** and **2** (δ 137.6), and similar to that of the complex [1,1'-methylene-3,3'-di-*tert*-butyl(imidazolium)imidazol-2-ylidene] palladium(II) triiodide synthesised by Herrmann et al. (section 1.2.5), which also incorporates a pendant imidazolium ring, (δ 136.7).[23] Two inequivalent ^{t}Bu groups are observed (two quaternary and two methyl signals) as well as a singlet for the methylene bridge carbon at δ 64.1, and the Pd-methyl signal is observed at δ -3.8. Only two carbon signals for the four magnetically-inequivalent N*C*H carbons are discernable. The peak height of the other two signals is reduced, presumably because of $^{1}J_{CD}$ and $^{2}J_{CD}$ coupling (as a result of exchange of the corresponding imidazolium NC*H* protons with deuterium), such that the carbon signals are impossible to distinguish from the baseline and the four other peaks in the region δ 120-125. Finally, ten signals are observed for the chelating bipy ligand (in the range δ 124.6-157.6).

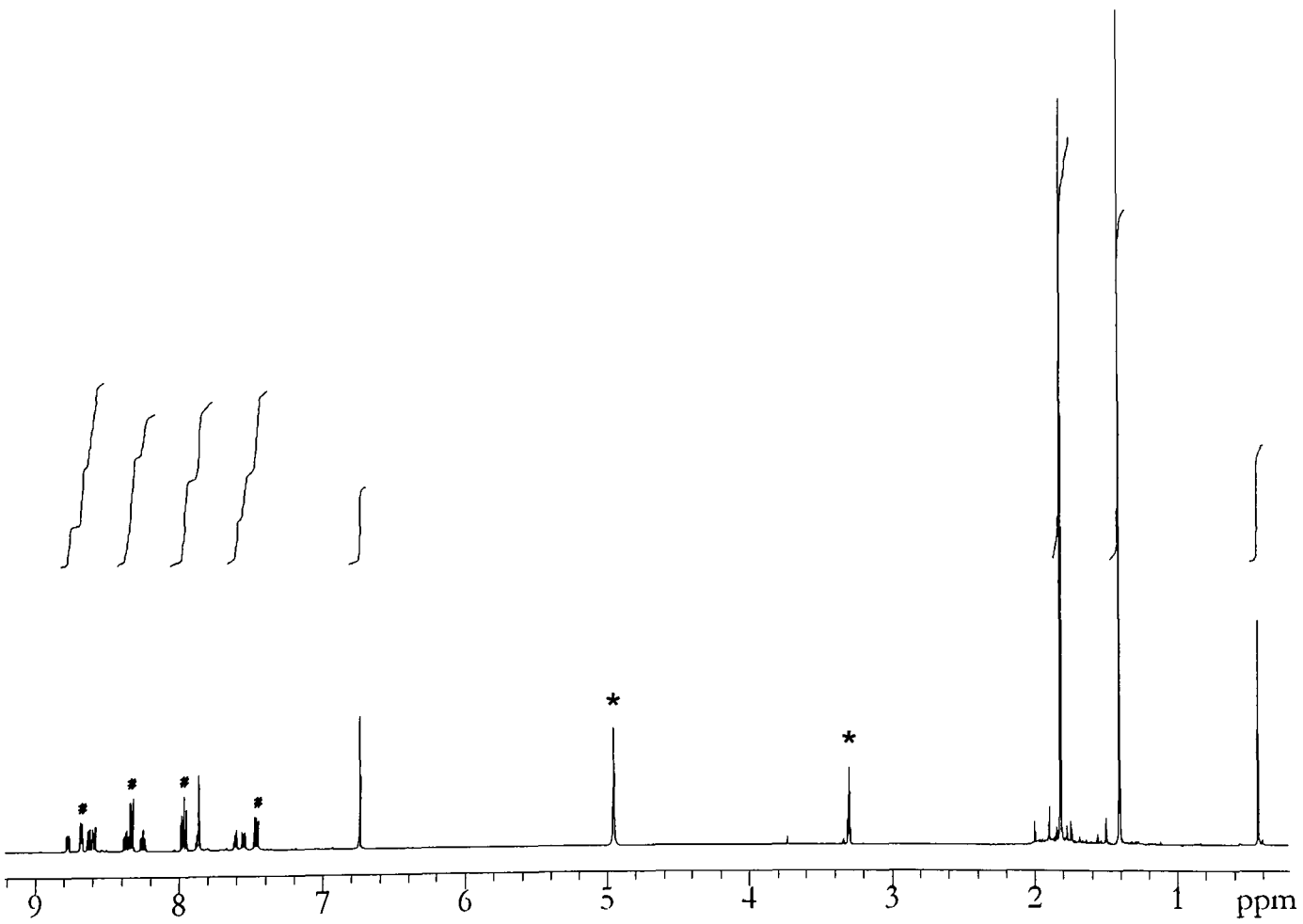

Figure 3.24 500 MHz ^{1}H NMR spectrum of [(^{tBu}C(D)C^{meth})PdMe(bpy)][OCD_3]$_2$ (**18**) (* = solvent, # = free bipy).

3.4.9 Characterisation of [(^{tBu}C(D)C^{eth})PdMe(bpy)][OCD$_3$]$_2$ (19)

The compound **19** was characterised by electrospray mass spectrometry and ^{1}H and ^{13}C{^{1}H} NMR spectroscopy. The electrospray mass spectrum contained peaks corresponding to the monocation [(^{tBu}C(D)C^{eth})PdMe(bpy)]$^+$ (m/z = 553 [M$^+$]), the dication [(^{tBu}C(D)C^{eth})PdMe(bpy)]$^{2+}$ (m/z = 277 [M^{2+}]), a monocationic fragment due to loss of ^{t}Bu (m/z = 498 [M$^+$-^{t}Bu]) and a dicationic fragment due to loss of ^{t}Bu (m/z = 249 [M^{2+}-^{t}Bu]).

^{1}H NMR spectroscopy (figure 3.25) is consistent with the molecular structure of **19** shown in equation 54 in which ^{tBu}C(D)C^{eth}, a mono-N-heterocyclic carbene ligand whose N-substituents are ^{t}Bu and 1-ethylene-2-deutero-3-*tert*-butylimidazolium, is coordinated to the palladium atom (via the N-heterocyclic carbene carbon) *cis* to the methyl. The methyl group resonates at δ 0.28 (s). Two magnetically inequivalent ^{t}Bu groups are observed (δ 1.63 and 1.82), and two inequivalent NC*H* heterocyclic ring protons (δ 7.55 and 7.79). The fact that only two resonances are observed for the four magnetically-inequivalent NC*H* ring protons (two on the N-heterocyclic carbene ring and two on the pendant imidazolium ring) is, again, probably due to deuterium exchange with the the protons of the imidazolium ring, such that all three ring carbons are deuterated. The ethylene bridge protons are observed as two rather than four multiplets at δ 4.77 (3H) and 5.39 (1H) indicating that two ethylene bridge protons are equivalent on the NMR timescale and the other two are not, which is presumably a result of freedom of rotation about the Pd-C$_{carbene}$ and N-(CH$_2$)-(CH$_2$)-N bonds. Finally, eight multiplets are observed for the chelating bipy ligand (in the range δ 7.62-8.71).

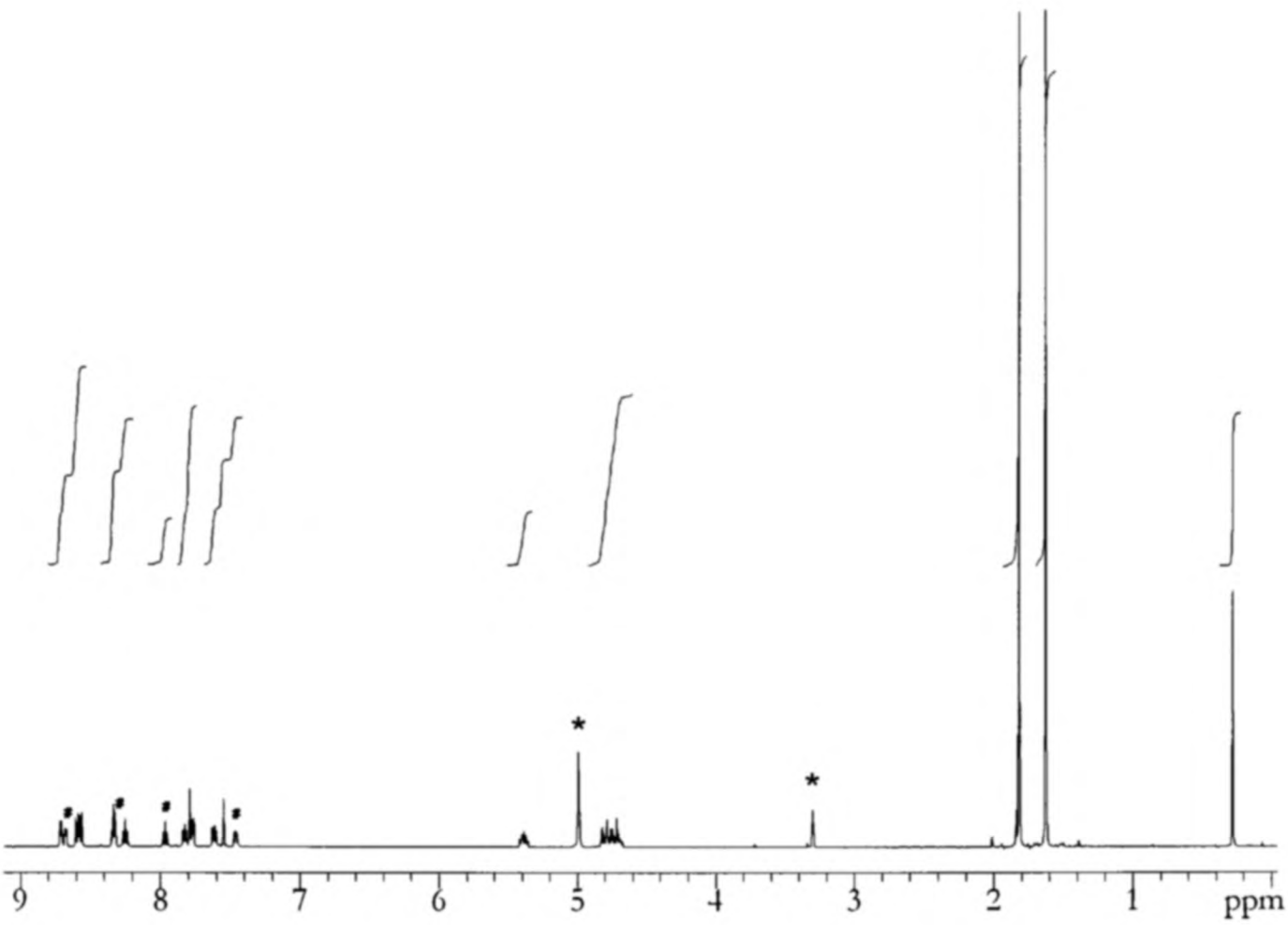

Figure 3.25 500 MHz ^{1}H NMR spectrum of [(^{tBu}C(D)C^{eth})PdMe(bpy)][OCD_3]$_2$ (**19**) (* = solvent, # = free bipy).

^{13}C{^{1}H} NMR spectroscopy is also consistent with the molecular structure of **19** shown in equation 54. The carbene carbon resonance is observed at δ 171.5 which is characteristic of cationic N-heterocyclic carbene palladium(II) complexes.[25,26] The corresponding N(*C*D)N carbon of the pendant imidazolium ring is observed at δ 135.8, which is similar to the corresponding shifts of the diimidazolium dihalide salt **3** (δ 136.6), and similar to that of the complex [1,1'-methylene-3,3'-di-*tert*-butyl(imidazolium)imidazol-2-ylidene] palladium(II) triiodide synthesised by Herrmann et al. (section 1.2.5), which also incorporates a pendant imidazolium ring, (δ 136.7).[23] Two inequivalent ^{t}Bu groups are observed (two quaternary and two methyl signals) as well as two singlets for the ethylene bridge carbons at δ 50.0 and 53.2, and the Pd-methyl signal is observed at δ -4.3. Only two carbon signals for the four magnetically-inequivalent N*C*H carbons are discernable. The peak height of the other two signals is reduced, presumably because of $^{1}J_{CD}$ and $^{2}J_{CD}$ coupling (as a result of exchange of the corresponding imidazolium NC*H* protons with deuterium), such that the carbon signals are impossible to distinguish from the baseline and

the four other peaks in the region δ 120-125. Finally, ten signals are observed for the chelating bipy ligand (in the range δ 124.4-157.7).

3.4.10 Reactions of Pd(^{tBu}CC^{eth})Me$_2$ (15) with B(C$_6$F$_5$)$_3$, HBF$_4$, and [Ph$_3$C][B(C$_6$F$_5$)$_4$]

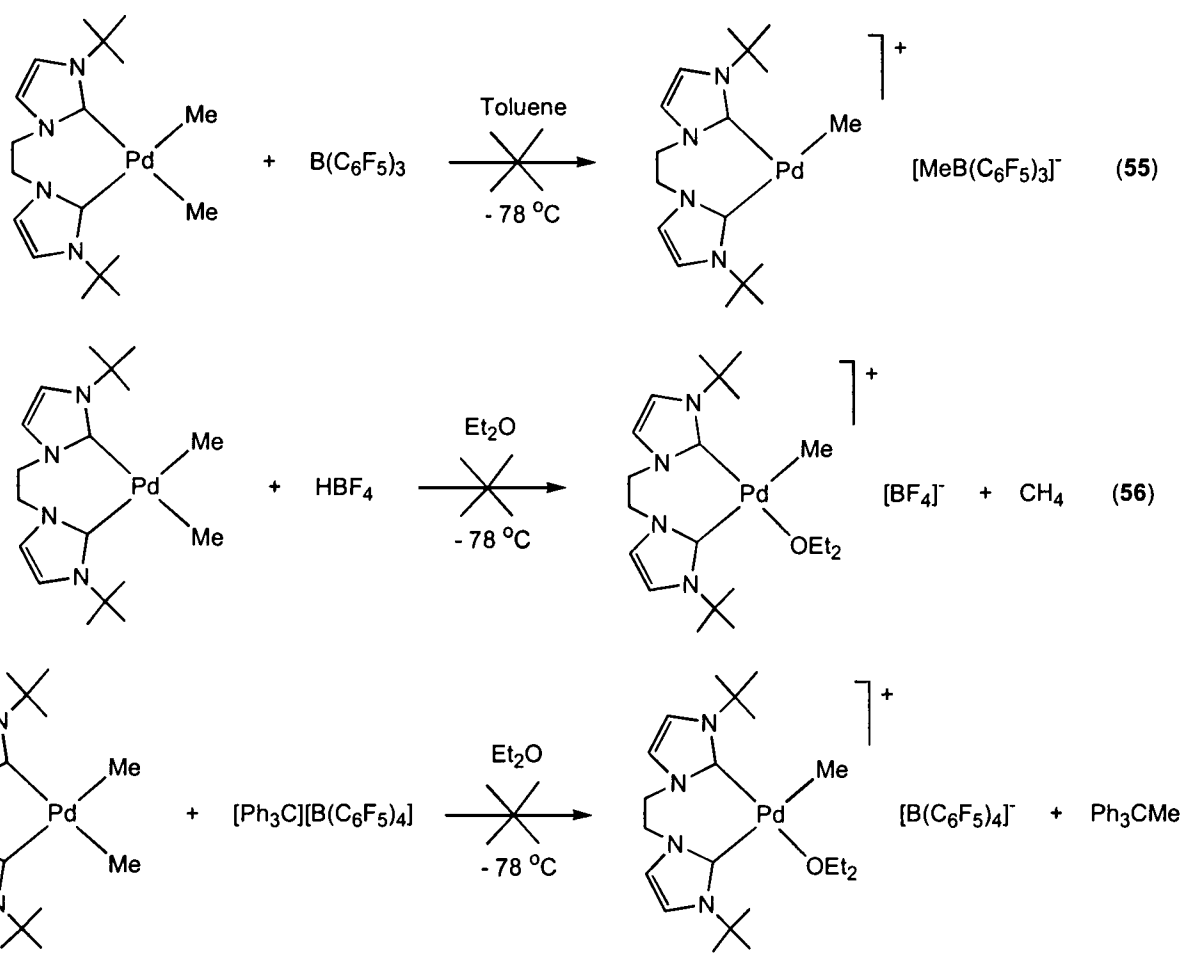

In an attempt to form the cation [(^{tBu}CC^{eth})PdMe]$^+$ (a potential olefin polymerisation initiator) by methyl group abstraction using B(C$_6$F$_5$)$_3$ to form the counter anion [MeB(C$_6$F$_5$)$_3$]$^-$, reaction between Pd(^{tBu}CC^{eth})Me$_2$ (**15**) and 1 equivalent B(C$_6$F$_5$)$_3$ was performed (Eq. 55). Similarly, in order to form the cationic weakly solvated complexes [(^{tBu}CC^{eth})PdMe(OEt$_2$)][BF$_4$] and [(^{tBu}CC^{eth})PdMe(OEt$_2$)][B(C$_6$F$_5$)$_4$], which are similar to diimine olefin polymerisation and diphosphine olefin/CO copolymerisation palladium catalysts (sections 1.3.1 and 1.3.2), reactions in diethyl ether between **15** and 1 equivalent HBF$_4$ (Eq. 56), and between **15** and 1 equivalent [Ph$_3$C][B(C$_6$F$_5$)$_4$] (Eq. 57), were attempted. In each case, after removal of the volatiles, intractable brown residues were obtained from the reaction mixture. ^{1}H NMR spectroscopy of the residues showed mixtures of unidentifiable products (broad bands of peaks in the Pd-methyl, *tert*-butyl and imidazole ring proton regions).

3.4.11 Reaction of Pd(^{tBu}CC^{eth})Me$_2$ (15) with [Ph$_3$C][B(C$_6$F$_5$)$_4$] in THF: Synthesis of [(^{tBu}CC^{eth})PdMe(THF)][B(C$_6$F$_5$)$_4$]

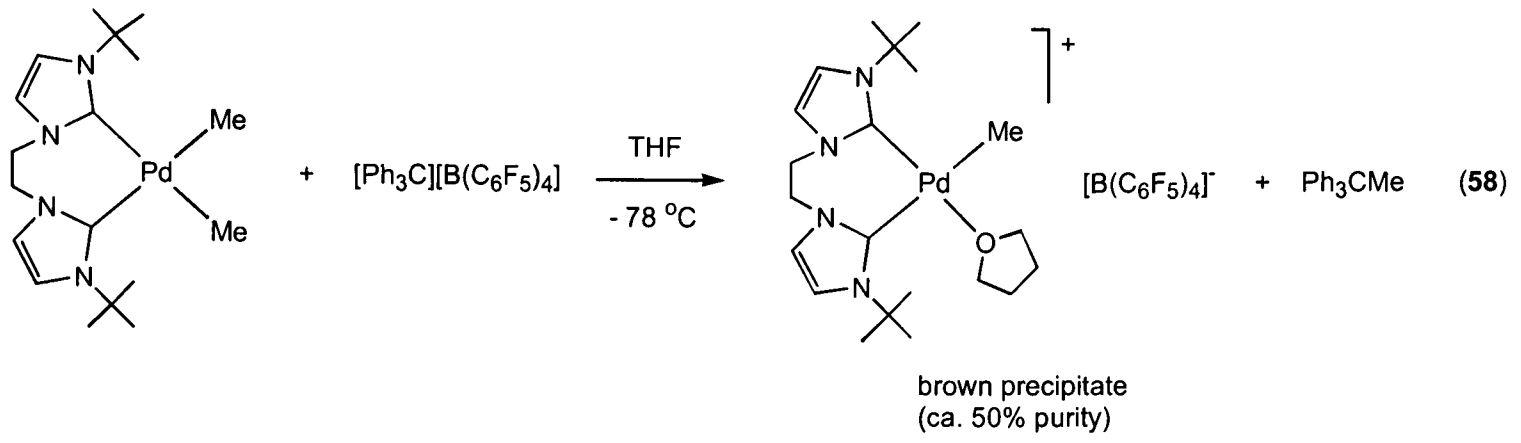

Reaction between Pd(^{tBu}CC^{meth})Me$_2$ (**15**) and 1 equivalent [Ph$_3$C][B(C$_6$F$_5$)$_4$] was carried out (Eq. 58) both on NMR-tube and 0.51 mmol scales, in d^8-THF and THF respectively. ^{1}H NMR spectroscopy of the NMR tube reaction mixture was consistent with the formation of the cationic weakly solvated complex [(^{tBu}CC^{eth})PdMe(THF)][B(C$_6$F$_5$)$_4$] and the by-product triphenylethane, but showed complete product decomposition after 48 hours at room temperature. A white precipitate is obtained upon adding an excess of 40-60 petroleum ether at -78 °C to the 0.51 mmol scale reaction mixture. The isolated precipitate turns brown on warming to room temperature, and is stored at -80 °C to avoid further decomposition. The product [(^{tBu}CC^{eth})PdMe(THF)][B(C$_6$F$_5$)$_4$] was observed by room temperature ^{1}H NMR spectroscopy of the precipitate (estimated purity = 50 %). The ^{1}H NMR pattern is similar to that of [(^{tBu}CC^{eth})PdMe(py)][OCD$_3$] (**17**). In d^8-THF the methyl group of [(^{tBu}CC^{eth})PdMe(THF)][B(C$_6$F$_5$)$_4$] resonates at δ 0.19 (s), and two resonances for the inequivalent ^{t}Bu groups are observed at δ 1.76 and 1.79. The four multiplets for the ethylene bridge protons are observed at δ 4.39, 4.62, 4.95 and 6.42, and the four inequivalent heterocyclic ring protons resonate in the range δ 7.29-7.42. Resonances for coordinated THF could not be distinguished from those of the residual protio NMR solvent.

3.4.12 Reaction of Pd(^{tBu}CC^{meth})Me$_2$ (14) with [Ph$_3$C][B(C$_6$F$_5$)$_4$] in THF: Synthesis of [(^{tBu}CC^{meth})PdMe(THF)][B(C$_6$F$_5$)$_4$]

Reaction in THF between Pd(^{tBu}CC^{meth})Me$_2$ (**14**) and 1 equivalent [Ph$_3$C][B(C$_6$F$_5$)$_4$] (Eq. 59) was performed following the synthesis of the cation [(^{tBu}CC^{eth})PdMe(THF)]$^+$ described above. As with the ethylene-bridged analogue, the white precipitate obtained upon adding

an excess of 40-60 petroleum ether to the reaction mixture at -78 °C turns brown on warming to room temperature, and is stored at -80 °C to avoid further decomposition. ^{1}H NMR spectroscopy of the precipitate in d^{8}-THF showed the desired product $[(^{tBu}CC^{meth})PdMe(THF)][B(C_6F_5)_4]$ (estimated purity = 50 %). The methyl group resonates at δ 0.12 (s), and two singlets for the inequivalent ^{t}Bu groups are observed at δ 1.67 and 1.78. Two doublets are observed for the methylene bridge protons at δ 6.07 and 6.77, and the four inequivalent heterocyclic ring protons resonate in the range δ 7.34-7.45. Signals for coordinated THF could not be distinguished from those for free THF / residual protio NMR solvent.

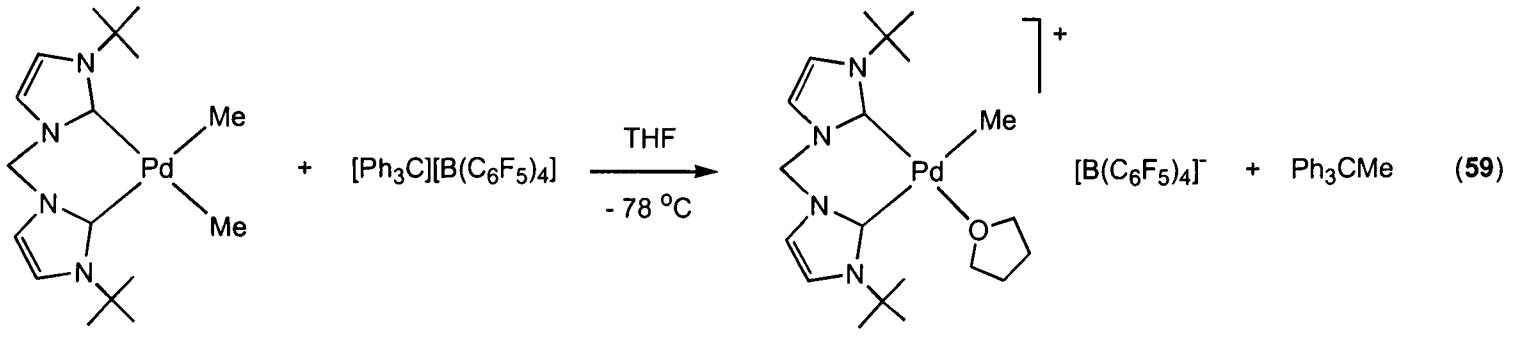

(59)

3.5 Catalytic Studies of Palladium(II) Dicarbene Compounds

Following the syntheses of the *cis*-dimethyl compounds Pd(^{tBu}CC^{meth})Me$_2$ (**14**) and Pd(^{tBu}CC^{eth})Me$_2$ (**15**), which were targetted as potential olefin polymerisation pre-catalysts analagous to the chelating diimine palladium(II) dimethyl pre-catalysts synthesised by Brookhart et al. (section 1.3.1),[16] and also as potentially highly-active pre-catalysts for the Heck coupling of aryl halides (section 1.3.3), the catalytic properties of **14** and **15** with respect to these reactions were investigated. Similarly, following the syntheses of the cations [(^{tBu}CC^{meth})PdMe(L)]$^+$ and [(^{tBu}CC^{eth})PdMe(L)]$^+$ (L = pyridine, THF) the catalytic properties of these compounds, as well as compounds **14** and **15**, were investigated with respect to ethylene / CO copolymerisation. This investigation was based on the similarity of the cations to *bis*-phosphine olefin / CO copolymerisation pre-catalysts of the type [(PR$_3$)$_2$Pd(R)(Solvent)]$^+$.[28,29] In addition, the chelating dicarbene ligands could have similar properties to chelating *bis*-phosphines, which significantly increase catalyst activity by enforcing *cis* coordination of the monomer and growing polymer chain, allowing insertion to occur more readily (section 1.3.2).[29,30]

3.5.1 Pd(^{tBu}CC^{meth})Me$_2$ (14) and Pd(^{tBu}CC^{eth})Me$_2$ (15): Ethylene Polymerisation Studies

Toluene solutions of **14** or **15** and either methylaluminoxane or [Ph$_3$C][B(C$_6$F$_5$)$_4$] (co-catalysts) were stirred for 2 hours in the presence of 2 bar ethylene. No polymer formation was observed (Eq. 60) in runs 1-5 (table 3.6) using either **14** or **15** (10 μmol). Experimental details are given in section 5.3.26.

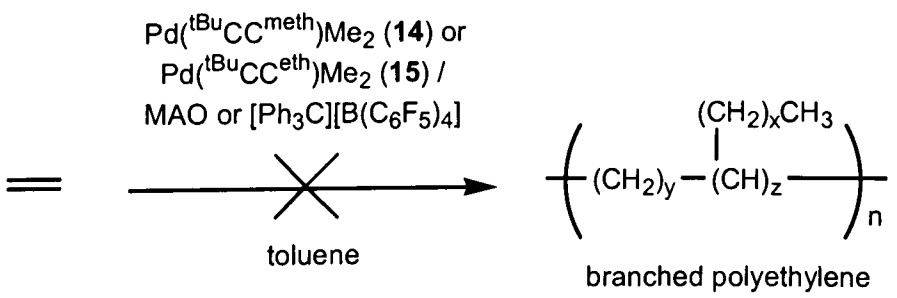

(**60**)

Run	MAO [Al] / [Ni]	$[[Ph_3C][B(C_6F_5)_4]]$ / $[^iBu_3Al]$ / [Ni]	Temperature (°C)
1	500	-	22
2	1500	-	22
3	1500	-	58
4	-	1 / 30 / 1	22
5	-	1 / 0 / 1	22

In run 4 the tri-*iso*-butylaluminium was added to the 50 mL toluene, prior to the addition of $[Ph_3C][B(C_6F_5)_4]$ and **14** or **15**, to act as a moisture scavanger.

Table 3.6 Summary of attempts at ethylene polymerisation using $Pd(^{tBu}CC^{meth})Me_2$ (**14**) and $Pd(^{tBu}CC^{eth})Me_2$ (**15**).

A possible reason for the inability of **14** and **15** to catalyse ethylene polymerisation is that the dicarbene ligands are not bulky enough to retard axial approach of ethylene, which causes associative displacement and chain transfer, and prevents the formation of long polymer chains (section 1.3.1). The crystal structures of the chelating $^{tBu}CC^{eth}$ complex **15,** the chelating $^{tBu}CC^{meth}$ nickel complexes **6** and **7**, and the chelating $^{tBu}CC^{meth}$ palladium complexes recently synthesised by Herrmann et al.[23] show that due to the boat conformations of the dicarbene ligands, and the considerable deviation of the heterocyclic rings from the coordination planes, the bulky ^{t}Bu groups both point in the same direction away from the coordination plane. Therefore if the ^{t}Bu groups of **14** and **15** do serve to block axial approach of ethylene, it is only from one direction. The methylene and ethylene bridges of $^{tBu}CC^{meth}$ and $^{tBu}CC^{eth}$ respectively, which point in the opposite direction to the ^{t}Bu groups, are probably not bulky enough to prevent axial approach from the other direction. Another possible reason for the inactivity of **14** and **15** is that palladium di-N-heterocyclic carbene complexes are not as electrophilic as the active palladium diimine complexes, as a result of the greater σ donating capacity of the dicarbene relative to the diimine ligand and the greater electronegativity of nitrogen compared to carbon.

3.5.2 Ethylene / CO Copolymerisation Studies

Run	Solvent / volume (ml)	Compound used as pre-catalyst	p-$C_6H_4O_2$
1	CD_3OD (10)	[($^{tBu}CC^{meth}$)PdMe(py)][OCD_3] (**16**) ($Pd(^{tBu}CC^{meth})Me_2$ (50 mg, 0.13 mmol) + py (10 mg, 0.13mmol))	-
2	CD_3OD (10)	[($^{tBu}CC^{eth}$)PdMe(py)][OCD_3] (**17**) ($Pd(^{tBu}CC^{eth})Me_2$ (55 mg, 0.13 mmol) + py (11 mg, 0.14 mmol))	-
3	THF (10)	[($^{tBu}CC^{meth}$)PdMe(THF)][$B(C_6F_5)_4$] (200 mg, 0.09 mmol at estimated 50% purity of compound)	13 mg, 0.12 mmol
4	THF (10)	[($^{tBu}CC^{eth}$)PdMe(THF)][$B(C_6F_5)_4$] (200 mg, 0.09 mmol at estimated 50% purity of compound)	-
5	CD_3OD (10)	($^{tBu}CC^{meth}$)$PdMe_2$ (**14**) (60 mg, 0.15 mmol)	-
6	CD_3OD (10)	($^{tBu}CC^{meth}$)$PdMe_2$ (**14**) (40 mg, 0.10 mmol)	13 mg, 0.12 mmol
7	CD_3OD (10)	($^{tBu}CC^{eth}$)$PdMe_2$ (**15**) (50 mg, 0.12 mmol)	-

Table 3.7 Summary of attempts at ethylene / CO copolymerisation using palladium(II) dicarbene compounds as the pre-catalysts.

$Pd(^{tBu}CC^{meth})Me_2$ (**14**), $Pd(^{tBu}CC^{eth})Me_2$ (**15**), [($^{tBu}CC^{meth}$)PdMe(py)][OCD_3] (**16**), [($^{tBu}CC^{eth}$)PdMe(py)][OCD_3] (**17**), [($^{tBu}CC^{meth}$)PdMe(THF)][$B(C_6F_5)_4$] and [($^{tBu}CC^{eth}$)PdMe(THF)][$B(C_6F_5)_4$] were tested for their ability to catalyse the copolymerisation of ethylene and CO. Solutions of the compounds were stirred for 2 hours at room temperature, and then for 16 hours at 50 °C in the presence of 40 bar 1:1 ethylene:CO. In two cases *p*-benzoquinone was also included, the presence of which was found by Herrmann et al. to increase copolymerisation turnover numbers in a previous study using palladium di-N-heterocyclic carbene pre-catalysts (section 1.2.6(g)).[24] The reaction temperature and the solvent of choice methanol were also in accordance with optimum conditions reported by Herrmann, although THF was chosen in the cases of [($^{tBu}CC^{meth}$)PdMe(THF)][$B(C_6F_5)_4$] and [($^{tBu}CC^{eth}$)PdMe(THF)][$B(C_6F_5)_4$], which rapidly decompose in protic solvents. No significant reduction in pressure of the autoclave was observed during any of runs 1-7 (table 3.7). In each case a black precipitate was formed whose infrared spectra did not contain a carbonyl stretch characteristic of poly(C_2H_4-*alt*-

CO) at 1692 cm^{-1}, and was shown by elemental analysis to be palladium black. ^1H NMR of the CD_3OD supernatants showed no trace of the pre-catalyst compounds.

A probable reason for the inactivity of **16** and **17** is that the pyridine ligand is too strong a σ donor and therefore not labile enough to be displaced by ethylene. Ligand displacement is regarded as a necessary step before ethylene insertion into the initial Pd-acyl bond, and hence copolymerisation, can occur (section 1.3.2).[28,29] THF is a weaker σ donor than pyridine, although may also not be labile enough for displacement by ethylene. This could account for the inactivity of the cations $[(^{tBu}CC^{meth})PdMe(THF)]^+$ and $[(^{tBu}CC^{eth})PdMe(THF)]^+$, as well as the fact that the solvent used in these cases was THF (an excess of coordinating solvent has previously be found to render copolymerisation catalysis inactive).[24] Another likely reason for the inactivity of $[(^{tBu}CC^{meth})PdMe(THF)]^+$ and $[(^{tBu}CC^{eth})PdMe(THF)]^+$ is their thermal sensitivity, which causes complete decomposition at room temperature within 48 hours, and may also have caused complete decomposition upon warming to 50 °C before copolymerisation could occur. To overcome the need for a ligand displacement step it was decided to test the activity of methanol solutions of **14** and **15**, in this case without the presence of pyridine. ^1H NMR spectroscopy of **14** and **15** in CD_3OD showed a mixture of unidentifiable decomposition products in both cases. For this reason it was decided to dissolve the compounds *inside* the autoclave, *after* pressurising with 40 bar 1:1 ethylene:CO, in the hope that a catalytically-active palladium dicarbene species could be stabilised before decomposition occurred. This was obviously not the case.

As well as the possible inability of pyridine and THF to undergo displacement by ethylene, and the possibility of catalyst decomposition due to thermal sensitivity, or solvolysis in the cases of **14** and **15**, a general reason for the inactivity could be the mild pressure employed (40 bar 1:1 ethylene:CO) in relation to that used by Herrmann and co-workers. Herrmann found that a methanol solution of the palladium dicarbene cation $[(^{Me}CC^{meth})Pd(MeCN)_2]^{2+}$ catalysed ethylene / CO copolymerisation at 50 °C, using 40-50 bar ethylene and 20-40 bar CO, including an 80 bar 1:1 ethylene:CO mixture which is double the pressure employed in this study.[24]

CO was bubbled through CD_3OD (1 mL) solutions of the cations $[(^{tBu}CC^{meth})PdMe(Py)][OCD_3]$ (**16**) (0.13 mmol) and $[(^{tBu}CC^{eth})PdMe(Py)][OCD_3]$ (**17**) (0.19 mmol) for 3 hours. In each case a deep red solution was formed. Standing at room temperature under argon for 24 hours caused the precipitation of palladium black, leaving colourless supernatants. ^1H NMR spectra of the red solutions and the colourless supernatants were essentially identical in each case, showing no trace of the starting materials, a mixture of unidentifiable dicarbene decomposition products (δ 1.0-2.2), free pyridine and a singlet at δ 1.7. The latter is possibly due to an acetyl decomposition product resulting from elimination of an initially-formed Pd-acyl group, although δ 1.7 did not correspond to the signals for possible elimination products d^1-acetaldehyde (MeCOD), d^3-methyl acetate ($MeCOOCD_3$) or acetone, which resonate in CD_3OD in the range δ 2.00-2.15.

The ^1H NMR spectra of the CD_3OD supernatants after reaction of **16** and **17** with CO were identical to those of the supernatants after copolymerisation experiments with these compounds. Therefore the presence of ethylene in the attempts at copolymerisation has no apparent effect, indicating that the pyridine ligand is too strong a σ donor and therefore not labile enough to be displaced by ethylene at a partial pressure of 20 bar (scheme 3.4).

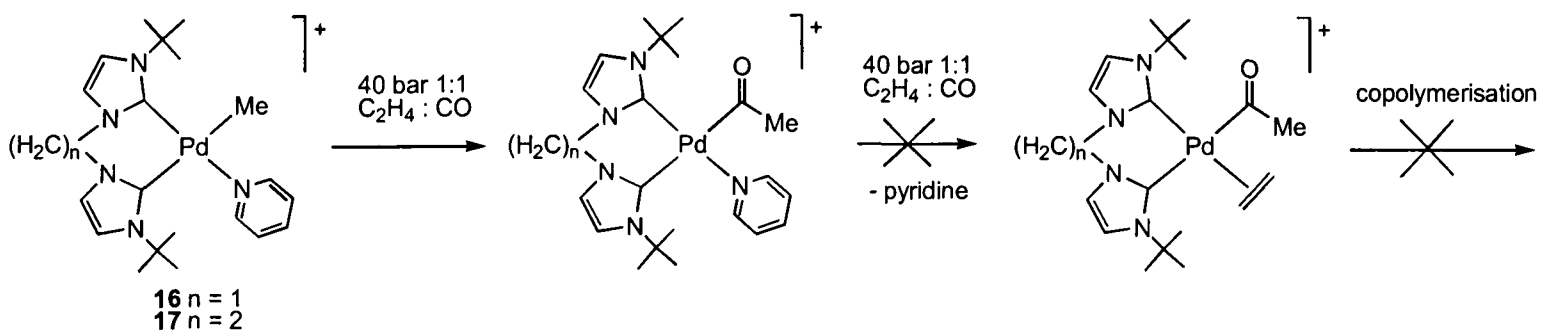

Scheme 3.4

3.5.3 Heck Coupling of 4-Bromoanisole with n-Butyl Acrylate

4-bromoanisole and 1.4 equivalents n-butyl acrylate were refluxed for 20 hours in *N*,*N*-dimethylacetamide, in the presence of the base sodium acetate and 0.5 mol % $Pd(^{tBu}CC^{meth})Me_2$ (**14**) or $Pd(^{tBu}CC^{eth})Me_2$ (**15**). In most cases $[^nBu_4N][OAc]$ was also added to the reaction mixture as a more soluble base. Experimental details are given in

section 5.3.12. Yields (determined by GCMS) and turnover numbers for various reaction conditions are given in table 3.8.

Run	Pre-catalyst used	Temperature (°C)	Yield (%)	TON*
1	None (control)	140	0	0
2†	**15**	140	2.3	4.6
3†	**15**	100	4.3	8.6
4†	**14**	140	0	0
5	**14**	80	12.6	25.2
6	**14**	100	21.2	42.4
7	**14**	120	68.3	136.6
8	**14**	140	75.3	150.6
9	**15**	80	19.5	39
10	**15**	100	18.6	37.2
11	**15**	120	47.8	95.6
12	**15**	140	60.1	120.2

*TON = turnover number (mol product / mol Pd). †No [$^{n}Bu_4N$][OAc] present in runs 2-4.

Table 3.8 Summary of Heck coupling experiments using pre-catalysts **14** and **15**.

The results in table 3.8 show that in the presence of the soluble base [$^{n}Bu_4N$][OAc] both **14** and **15** catalyse the Heck coupling of 4-bromoanisole with n-butyl acrylate (Eq. 61). **14** showed a significantly higher activity than **15** at all temperatures except 80 °C. Yields and turnover numbers were generally found to increase with increasing reaction temperature. The highest yields (75.3 % (**14**) and 60.1 % (**15**)) and TON's (150.6 (**14**) or 120.2 (**15**)) were found at 140 °C. In the absence of [$^{n}Bu_4N$][OAc] the pre-catalyst **14** was completely inactive, and yields obtained with **15** were reduced to below 5 %.

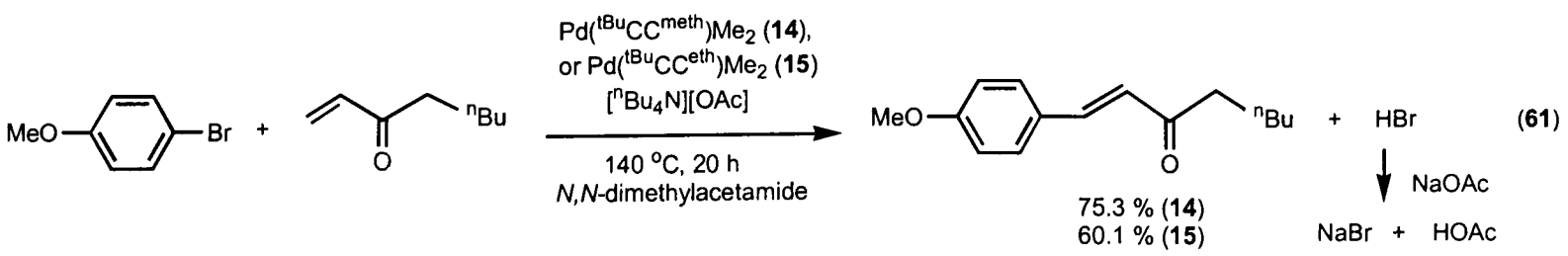

(61)

For the same reaction the chelating palladium(II) dicarbene complex $Pd(^{Me}CC^{meth})I_2$ achieves higher activities than **14** and **15** (95 % conversion after 12 hours, 0.5 mol % (TON = 190)), whereas the *bis*-monocarbene complex [Pd(1,3-dimethylimidazol-2-ylidene)I_2] has a lower activity (60 % conversion after 50 hours, 0.67 mol %, TON = 90). Both diiodide complexes show quantitative conversions, within 24 hours, of more activated, electron-poor aryl halides such as 4-bromoacetophenone, achieving TON's of up to 1000 (section 1.2.6(e)).[2-4] In the case of the diiodide complexes it was found that addition of a soluble base such as tetrabutylammonium acetate significantly reduced the induction time (e.g. from > 1 hour to minutes) required to form the catalytically-active Pd^0 species.[2] In contrast the highly-active *bis*-monocarbene complex [Pd(Me)(1,3-dimethylimidazol-2-ylidene)$_2$Cl] quantitatively converts aryl halides such as 4-bromoacetophenone (TON = 100500) with little or no induction period in the absence of a reducing agent. This was attributed to the presence of the methyl group on the palladium centre providing a facile pathway for formation of the active species (section 1.2.6(e)).[1] For this reason it was hoped that the methyl groups on the palladium centres of **14** and **15** would serve to markedly increase the activity of these compounds in relation to that of the chelating diiodide complex $Pd(^{Me}CC^{meth})I_2$. It was also hoped that the presence of a chelating dicarbene ligand rather than two monocarbene ligands would increase the activity of **14** and **15** in relation to [Pd(Me)(1,3-dimethylimidazol-2-ylidene)$_2$Cl], which is observed in the case of the di- and monocarbene diiodide complexes.

One possible reason for the lower activities of **14** and **15** compared to that of $Pd(^{Me}CC^{meth})I_2$ is a greater thermal stability, and hence longer lifetime at reaction temperatures, of the latter complex. The *cis* methyl groups of **14** and **15** most likely provide thermal decomposition pathways via hydrocarbon elimination which are not available to the diiodide compound. This would also explain the inactivity of **14** and the extremely low activity of **15** in the absence of the soluble base [$^nBuN_4$][OAc]: thermal decomposition of the pre-catalyst occurs during the resulting induction period, due to the high reaction temperature.

3.6 Summary and Conclusions

Reaction between $^{tBu}CC^{meth}$ (**4**) and $Ni(PMe_3)_2Me_2$ affords the novel dimer $[(\mu\text{-}^{tBu}CC^{meth})\{Ni(PMe_3)Me_2\}_2]$ (**12**), in which the $^{tBu}CC^{meth}$ ligand bridges two nickel atoms. Compound **12** is the first example of a group 10 metal complex incorporating a bridging dicarbene ligand, and also the first example of a structurally-characterised nickel *trans*-dimethyl complex. In contrast, reaction between **4** or $^{tBu}CC^{eth}$ (**5**) with $M(bpy)Me_2$ (M = Ni, Pd) affords the corresponding dicarbene nickel and palladium *cis*-dimethyl complexes, which were originally targeted for the investigation of dicarbene ligands as alternatives to chelating diphosphine and diimine ligands used in homogeneous catalysis (section 2.1). These are the first examples of simple *cis*-dihydrocarbyl complexes incorporating N-heterocyclic carbene ligands. $Ni(^{tBu}CC^{eth})Me_2$ (**13**) is isolated in near quantitative yield and was shown to undergo thermal elimination of methane at elevated temperatures. Kinetic studies on the thermal decomposition indicate that reductive elimination of methane from **13** proceeds by a unimolecular process with the activation parameters $\Delta H^{\ddagger}$ = 24.0(4) kcal mol^{-1} and $\Delta S^{\ddagger}$ = -4(1) cal K^{-1} mol^{-1}. In contrast, the methylene-bridged analogue $Ni(^{tBu}CC^{meth})Me_2$ could not be isolated and was observed, by ^1H NMR spectroscopy, to decompose upon formation above -50 °C. Concomitant gas evolution indicated thermal elimination of methane in which case $\Delta H^{\ddagger} < 24.0(4)$ kcal mol^{-1}. Chemistry at the nickel centre is therefore very sensitive to subtle variations in the nature of the chelating ligand, which was previously observed for nickel *cis*-dimethyl complexes of chelating *bis*-phosphines.[10] The X-ray structure of **13** showed a similar ligand conformation and bite angle (88.9(2)°) to those of the only other structurally characterised ethylene-bridged dicarbene nickel complex $[(^{tBu}CC^{eth})NiCl(PMe_3)][BPh_4]$ (**10**). Attempts to polymerise ethylene using **13** in the presence of co-catalysts MAO or $[Ph_3C][B(C_6F_5)_4]$ were unsuccessful, although a 3.5 % conversion in the Heck coupling of 4-bromoanisole with n-butyl acrylate was observed. $Pd(^{tBu}CC^{meth})Me_2$ (**14**) and $Pd(^{tBu}CC^{eth})Me_2$ (**15**) were isolated in 63 and 64 % yields respectively. Compound **15**, the first palladium compound incorporating an ethylene-bridged chelating dicarbene ligand, was structurally characterised, showing a similar ligand conformation and bite angle to those of the nickel analogue **13**. The bite angle, 88.12(13)°, is ca. 5° larger than observed for methylene-bridged dicarbene palladium(II) complexes.[3,23] **14** and **15** undergo clean reactions with 1 equivalent of pyridine in CD_3OD to form the compounds $[(^{tBu}CC^{meth})PdMe(py)][OCD_3]$

(**16**) and [(^{tBu}CC^{eth})PdMe(py)][OCD_3] (**17**) respectively. Similar reactions between **14** or **15** and 1 equivalent of bpy give the compounds [(^{tBu}C(D)C^{meth})PdMe(bpy)][OCD_3]$_2$ (**18**) and [(^{tBu}C(D)C^{eth})PdMe(py)][OCD_3]$_2$ (**19**), in which the carbene ligands are coordinated to palladium via only one heterocyclic ring, the other acting as a pendant imidazolium functionality. ^{1}H NMR spectroscopy showed that reaction in THF between [Ph_3C][$B(C_6F_5)_4$] and **14** or **15** affords the products [(^{tBu}CC^{meth})PdMe(THF)][$B(C_6F_5)_4$] and [(^{tBu}CC^{meth})PdMe(THF)][$B(C_6F_5)_4$], although attempts to isolate the solid compounds resulted in mixtures of ca. 50 % purity. Attempts to polymerise ethylene using **14** or **15** in the presence of co-catalysts MAO or [Ph_3C][$B(C_6F_5)_4$] were unsuccessful, as were attempts to copolymerise ethylene and CO using the following complexes as pre-catalysts: **14-17**, [(^{tBu}CC^{meth})PdMe(THF)][$B(C_6F_5)_4$] and [(^{tBu}CC^{meth})PdMe(THF)][$B(C_6F_5)_4$]. Both **14** and **15** catalysed the Heck coupling of the deactivated (electron-rich) aryl halide 4-bromoanisole, achieving 75.3 % and 60.1 % conversions, and turnover numbers of 150.6 and 120.2 respectively. Activities are higher than observed for *bis*-(1,3-dimethylimidazol-2-ylidene)palladium(II) diiodide and lower than observed for the chelating analogue Pd(^{Me}CC^{meth})I_2, for the same reaction.[2,3] The lower activity of **14** and **15** compared to Pd(^{Me}CC^{meth})I_2 is possibly attributable to a higher thermal stability of the diiodide compound relative to the dimethyl compounds. Examination of the X-ray structures of **13**, **15** and the ^{tBu}CC^{meth} nickel complexes shown in chapter 2 suggests that the inactivity of compounds **13-15** with respect to ethylene polymerisation could be due to lack of steric bulk provided by the ^{t}Bu groups and hydrocarbon bridges of the dicarbene ligands, allowing chain transfer processes to occur. Another possible reason is the decrease in electrophilicity of the Ni and Pd centres of **13-15** relative to those of the active diimine catalysts, owing to the greater σ-donating capacity of N-heterocyclic carbenes relative to N-donor ligands. A summary of the new chemistry described in chapter 3 is given in scheme 3.5.

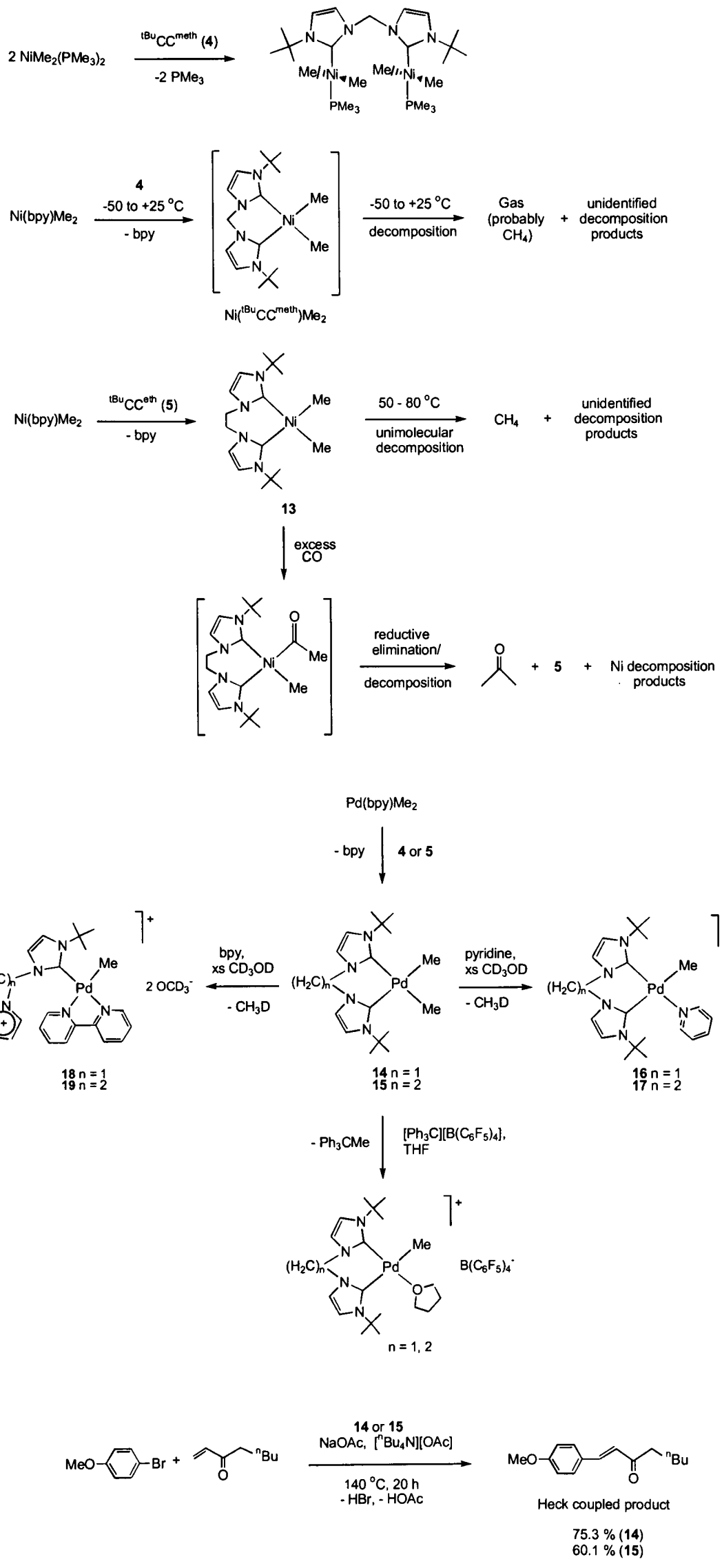

Scheme 3.5 Summary of the new chemistry described in chapter 3.

3.7 References

1) McGuinness, D. S.; Green, M. J.; Cavell, K. J.; Skelton, B. W.; White, A. H. *J. Organomet. Chem.* **1998**, *565*, 165.
2) Herrmann, W. A.; Elison, M.; Fischer, J.; Köcher, C.; Artus, G. R. J. *Angew. Chem. Int. Ed. Engl.* **1995**, *34*, 2371.
3) Herrmann, W. A.; Reisinger, C.-P.; Spiegler, M. *J. Organomet. Chem.* **1998**, *557*, 93.
4) Herrmann, W. A.; Böhm, V. P. W.; Reisinger, C.-P. *J. Organomet. Chem.* **1999**, *576*, 23.
5) McGuinness, D. S.; Cavell, K. J.; Skelton, B. W.; White, A. H. *Organometallics* **1999**, *18*, 1596.
6) Herrmann, W. A.; Gerstberger, G.; Spiegler, M. *Organometallics* **1997**, *16*, 2209.
7) Herrmann, W. A.; Elison, M.; Fischer, J.; Köcher, C. A., G.R.J. *Chem. Eur. J.* **1996**, *2*, 772.
8) Köcher, C.; Herrmann, W. A. *J. Organomet. Chem.* **1997**, *532*, 261.
9) Tucci, G. C.; Holm, R. H. *J. Am. Chem. Soc.* **1995**, *117*, 6489.
10) Kohara, T.; Yamamoto, T.; Yamamoto, A. *J. Organomet. Chem.* **1980**, *192*, 265.
11) Allen, F. H.; Davies, J. E.; Galloy, J. J.; Johnson, O.; Kennard, O.; Macrae, C. F.; Mitchell, E. M.; Mitchell, G. F.; Smith, J. M.; Watson, D. G. *J. Chem. Inf. Comput. Sci.* **1991**, *31*, 187.
12) Jolly, P. W.; Kruger, C.; Salz, R.; Sekutowski, J. C. *J. Organomet. Chem.* **1979**, *165*, C39.
13) Kaschube, W.; Pörschke, K. R.; Wilke, G. *J. Organomet. Chem.* **1988**, *355*, 525.
14) Gordon, A. J.; Ford, R. A. *The Chemist's Companion: A Handbook of Practical Data, Techniques, and References*; Wiley-Interscience: New York, 1972
15) Low, J. J.; Goddard III, W. A. *J. Am. Chem. Soc.* **1986**, *108*, 6115.
16) Johnson, L. K.; Killian, C. M.; Brookhart, M. *J. Am. Chem. Soc.* **1995**, *117*, 6414.
17) Killian, C. M.; Tempel, D. J.; Johnson, L. K.; Brookhart, M. *J. Am. Chem. Soc.* **1996**, *118*, 11664.
18) Tamao, K.; Sumitani, K.; Kumada, M. *J. Am. Chem. Soc.* **1972**, *94*, 4374.
19) Morrell, D. G.; Kochi, J. K. *J. Am. Chem. Soc.* **1975**, *97*, 7262.
20) Saito, S.; Saori, O.; Miyaura, N. *J. Org. Chem.* **1997**, *62*, 8024.
21) Kelkar, A. A.; Hanaoka, T.; Kubota, Y.; Sugi, Y. *Catalysis Lett.* **1994**, *29*, 69.
22) Iyer, S.; Ramesh, C.; Ramani, A. *Tetrahedron Lett.* **1997**, *38*, 8533.
23) Herrmann, W. A.; Schwarz, J.; Gardiner, M. G. *Organometallics* **1999**, *18*, 4082.
24) Gardiner, M. G.; Herrmann, W. A.; Reisinger, C.-P.; Schwarz, J.; Spiegler, M. *J. Organomet. Chem.* **1999**, *572*, 239.
25) Fehlhammer, W. P.; Bliss, T.; Kernbach, U.; Brüdgam, I. *J. Organomet. Chem.* **1995**, *490*, 149.
26) Herrmann, W. A.; Schwarz, J.; Gardiner, M. G.; Spiegler, M. *J. Organomet. Chem.* **1999**, *575*, 80.
27) Avent, A. G.; Chaloner, P. A.; Day, M. P.; Seddon, K. R.; Welton, T. *J. Chem. Soc. Dalton Trans.* **1994**, 3405.
28) Lai, T.-W.; Sen, A. *Organometallics* **1984**, *3*, 866.
29) Sen, A. *Acc. Chem. Res.* **1993**, *26*, 303.
30) Drent, E.; Budzelaar, P. H. M. *Chem. Rev.* **1996**, *96*, 663.

CHAPTER 4

Investigation of a New Rhodium C_{60} Catalyst: Evaluation of C_{60} as a Hydrogen Storage Medium

4.1 Introduction

The fullerene C_{60} is made up of a system of alternating single and double CC bonds in which π-electron delocalisation is small, causing it to react as an electron-deficient alkene. C_{60} does not undergo substitution reactions because of the high stability of the fullerene cage, but readily undergoes alkene addition reactions with electron-rich species including nucleophiles, bases and radicals. Furthermore, owing to its high electron affinity, C_{60} can behave as an oxidising agent forming anions C_{60}^{n-} (n = 1-6).[1]

C_{60} may therefore react with electron-rich transition metal precursors ML_x, either forming organometallic C_{60} π-adducts $ML_x(C_{60})$ or charge-transfer compounds $[ML_x]^{n+}[C_{60}]^{n-}$ (scheme 4.1). In addition, heterobonds X-Y can add across C_{60} double bonds to form compounds $C_{60}(X)_n(Y)_n$ (scheme 4.1).[1]

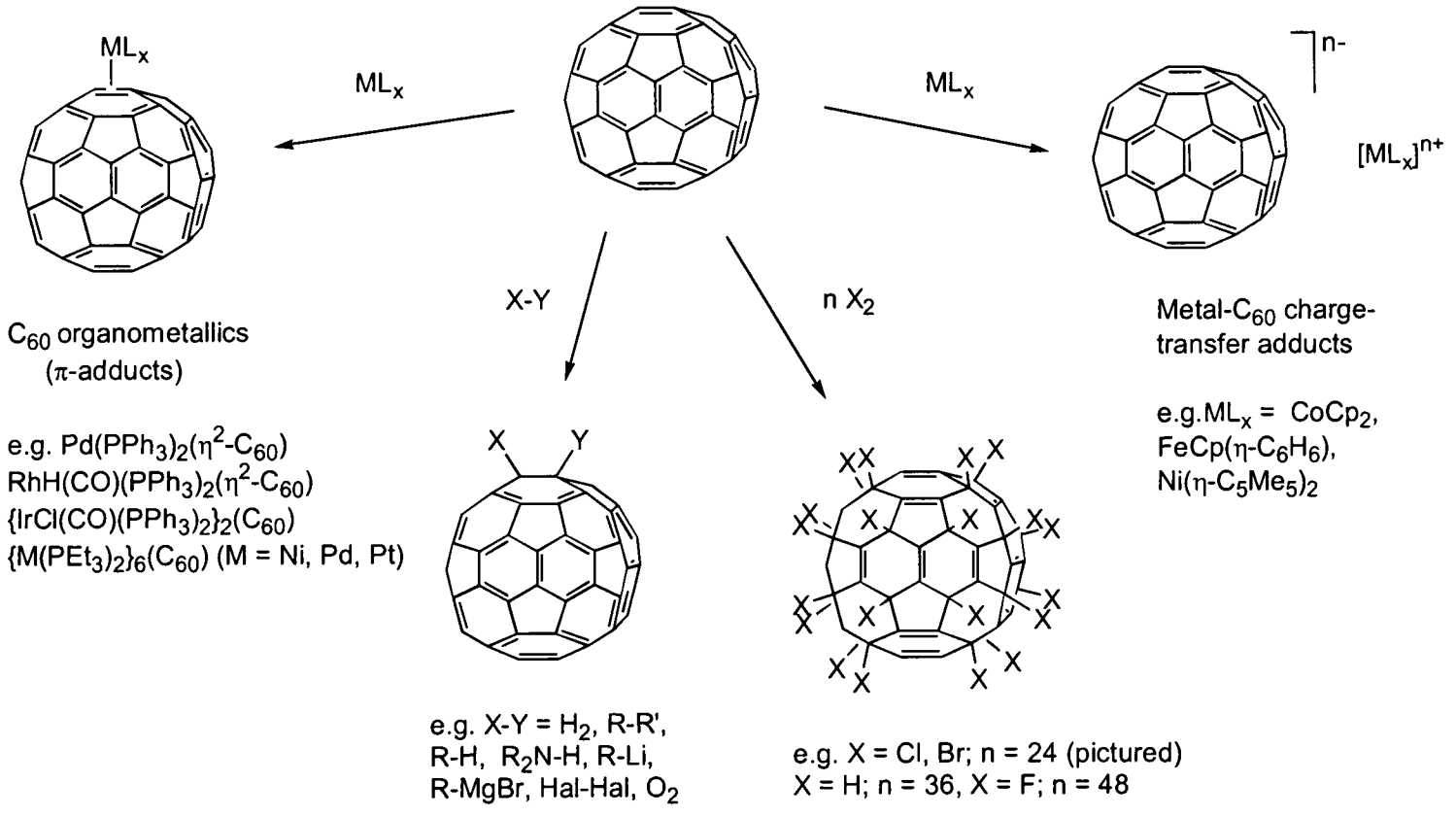

Scheme 4.1 Reactions of C_{60} with organometallic precursors, and with heterobonds X-Y.

The reactivity of C_{60} outlined above leads to the following ideas, which form the basis of the research described in chapter 4. Firstly, insoluble transition metal-C_{60} compounds such as the charge-transfer adducts are potential highly-active heterogeneous catalysts. In such

compounds the C_{60} can be regarded as a carbon support for a high concentration of discrete surface metal atoms. Secondly, it is conceivable that C_{60} could be catalytically hydrogenated to $C_{60}H_{60}$ representing a hydrogen uptake of 8.4 wt %. If hydrogen gas could subsequently be recovered from this product, C_{60} could form the basis of a hydrogen storage system useful to industry.

4.1.1 Hydrogen Storage

Hydrogen has attracted a great deal of attention as an energy source. Once it is generated (primarily from natural gas or petroleum refining), its use as a fuel creates neither air pollution nor greenhouse gas emissions. Despite this, hydrogen is not used as a common fuel because it is more expensive than other forms of energy (the cost per unit energy is 2-8 times that of natural gas). However, a standard first step in making hydrocarbon fuels is to react coal with steam to make synthesis gas (H_2 and CO). Given appropriate storage and transmission arrangements, a more efficient process would be to use the hydrogen generated by this process directly, as a fuel, rather than converting it to hydrocarbons which requires additional energy-consuming chemical steps. Therefore an economically viable system which allows the safe storage and transportation of hydrogen may allow hydrogen to become economically competitive with the major fuel sources.[2] Furthermore, high-capacity hydrogen storage systems are a long-sought goal of the automobile industry, which wants to use hydrogen-powered fuel cells to propel fuel-efficient and environmentally friendly vehicles.

Conventional storage of gaseous hydrogen at high pressures and ambient temperatures is not economically viable for transportation as a common fuel, and not practical for the automobile industry, because of the small amount of hydrogen stored per unit mass and per unit volume of container. Liquefaction is also expensive and impractical due to the low boiling point of hydrogen (20.4 K at 1 atm). Therefore leading contenders for commercially viable hydrogen storage systems are solids which reversibly adsorb large quantities of hydrogen at convenient temperatures and pressures.

Literally hundreds of intermetallic compounds RM_n adsorb hydrogen to form hydrides RM_nH_x, and have been investigated as hydrogen storage systems since the late 1970's.[2-4] R represents a hydride-forming element, and M a metal which is unreactive towards hydrogen

under ordinary conditions. The intermetallics $LaNi_5$ and FeTi, for example, react with hydrogen to form the hydrides $LaNi_5H_{6.7}$ and $FeTiH_{1.7}$ respectively, and the hydrogen can be added or removed very rapidly at various convenient temperatures and pressures (e.g. 20 °C, 1.5 atm ($LaNi_5$) or 40 °C, 3 atm (FeTi)).[2] $LaNi_5H_{6.7}$ and $FeTiH_{1.7}$ contain 1.6 and 1.7 wt % hydrogen respectively, and intermetallic compounds generally contain 0-2 % hydrogen by weight.[3,4] Although intermetallic compounds are safe hydrogen storage systems, and are widely used as electrodes in protonic batteries, intermetallic hydrogen storage for mass-transportation of hydrogen fuel would not be economically viable due to the low system-weight efficiency (the ratio of stored hydrogen weight to system weight). Similarly, low hydrogen/metal ratios would cause even modest intermetallic hydrogen reservoirs within cars to have enough mass that they would decrease performance and energy efficiency.

Hydrogen storage in carbon-based materials has the advantage of higher system-weight efficiencies due to the low atomic weight of carbon. Since the commencement of the research described in this chapter, reports of very high reversible adsorption of molecular hydrogen in single-walled nanotubes (SWNTs), alkali-doped graphite, and pure and alkali-doped graphite nanofibres (GNFs) has stimulated tremendous interest in the research community.[5-9] Furthermore the U.S. Department of Energy (DOE) Hydrogen Plan, which is concerned with the provision of an economical and safe hydrogen storage medium for a hydrogen-fuelled transportation system, has provided a commercially significant benchmark for the amount of reversible hydrogen absorption. This benchmark requires a system-weight efficiency of 6.5 wt % hydrogen and a volumetric density of 63 kg H_2 / m^3.[8] A summary of the recently-reported reversible gravimetric storage of hydrogen in various carbon materials is given in table 4.1, including the temperatures T and pressures P at which the hydrogen is adsorbed.

Material	Reference	Max wt % H_2	T (°C)	P (atm)
SWNTs (low purity)	7	5-10	17	0.39
SWNTs (high purity)	8	~4	27	0.39
GNFs (tubular)	6	11.26	25	112
GNFs (herringbone)	6	67.55	25	112
GNFs (platelet)	6	53.68	25	112
Graphite	6	4.52	25	112
GNFs	5	0.4	25-500	1
Li-GNFs	5	20.0	200-400	1
Li-Graphite	5	14.0	200-400	1
K-GNFs	5	14.0	40	1
K-Graphite	5	5.0	40	1
SWNTs (high purity)	9	8.25	-193	71
SWNTs (~50 % pure)	10	4.2	27	100

Table 4.1 Summary of reported gravimetric storage of H_2 in various carbon materials.

Adsorption of up to 67.55 wt % hydrogen was accomplished using graphite nanofibres (GNFs).[6] GNFs, which are stacks of one atom thick graphite (graphene) layers, have cross-sectional areas of 30-500 $Å^2$, lengths of 10-100 μm and are prepared by the catalysed desorption of carbon-containing gases (e.g. methane) over selected metal and alloy surfaces at 450-750 °C. Rodriguez et al. studied 'tubular' (90°), 'herringbone' (~45°) and 'platelet' (0°) GNFs, where the angle in parentheses indicates the direction of the nanofibre axis relative to the vector normal to the graphene sheets. At 112 atm and 25 °C the platelet and herringbone forms adsorbed remarkable amounts of H_2 (67.55 and 53.68 wt % respectively): 4-6 times more than the tubular form which itself adsorbs over twice as much as graphite under similar conditions (table 4.1). Herringbone GNFs were found to release about half of the stored hydrogen at room temperature and pressure. The authors proposed that an increased interplanar spacing for herringbone and platelet GNFs allowed for the adsorption of more layers of H_2 molecules between successive graphene layers. More recently Chen et al. found that lithium- and potassium-doped GNFs and lithium- and potassium-doped graphite reversibly adsorbed high quantities of H_2 at ambient pressures

(table 4.1).[5] Li-GNFs achieved 20 wt % gravimetric storage at temperatures between 200-400 °C, whereas K-GNFs adsorbed 14 wt % hydrogen at 40 °C. It was suggested that the greatly improved storage capacity of Li-GNFs relative to the virtually negligible storage (0.4 %) of undoped GNFs at ambient pressure was due to the catalytic dissociation of H_2, prior to adsorption, via metal hydride intermediates.

The hydrogen adsorption capacity of single-walled carbon nanotubes (SWNTs) was initially investigated by Dillon and co-workers using samples containing 1-2 wt % SWNTs.[7] Temperature-programmed desorption (TPD) experiments showed that hydrogen desorbed from both nanotube and activated carbon samples at the same temperature (-140 °C). However, in the case of the nanotube sample a second desorption occurred at 17 °C which was suggested might be due to the release of H_2 trapped inside the SWNTs. The hydrogen storage capacity of this higher temperature site was estimated to be in the range 5-10 wt % hydrogen. More recently Dillon et al. produced samples with a high concentration of short SWNTs, with open ends, in order to maximise the entry of hydrogen molecules into the SWNTs.[8] In this case a more accurate determination of the reversible hydrogen adsorption was possible, and was estimated to be ~4 wt % hydrogen at room temperature and 0.39 atm. It was also concluded, by opening and recapping the nanotubes, that most of the hydrogen is stored within the capillary rather than in the interstitial spaces between the SWNTs. A similar hydrogen storage capacity of 4.2 wt % hydrogen was reported for SWNTs at room temperature and 100 atm,[10] and Ye et al. observed a gravimetric hydrogen storage capacity of 8.25 wt %, at -193 °C and 71 atm, using high-purity 'cut' SWNTs.[9]

The results in table 4.1 show that carbon-based materials such as GNFs and SWNTs have potential as commercially-viable solid state hydrogen storage systems. In several cases the gravimetric adsorption of hydrogen observed for these materials is considerably greater than 6.5 wt % hydrogen, which is regarded as a commercially significant bechmark for system-weight efficiency.[8] The adsorption of up to 67.55 wt % hydrogen by GNFs at high pressure may enable larger quantities of hydrogen to be stored in relatively small tanks at lower pressures than is currently possible. In addition, storage of 14-20 wt % hydrogen by alkali-doped GNFs bodes well for the discovery of a commercially viable hydrogen storage system which reversibly adsorbs large quantities of hydrogen at more convenient pressures.

4.1.2 Hydrogenation of C_{60}

The first catalytic reduction of C_{60} was reported by Becker and co-workers in 1993 (Eq. 62).[11] A d^6-benzene solution of C_{60} was stirred in the presence of rhodium(0) on alumina, under a constant balloon pressure of hydrogen at room temperature. $C_{60}H_2$ was identified as the major product based on ^1H NMR spectroscopy, which showed the characteristic sharp singlet at δ 5.89 also observed by Henderson and Cahill who had previously isolated and characterised $C_{60}H_2$.[12]

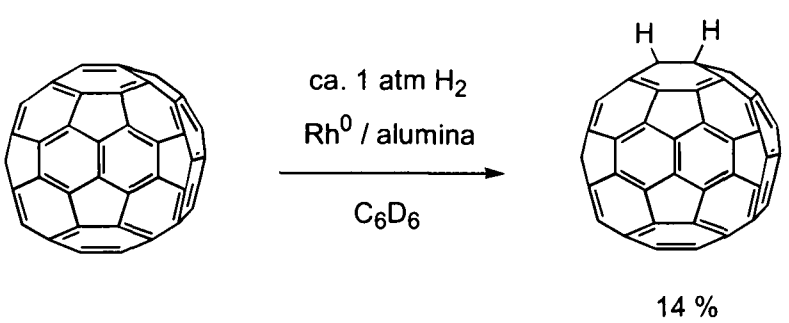

+ unidentified higher hydrogenation products, e.g. $C_{60}H_4$ and $C_{60}H_6$ **(62)**

In addition several reports existed which described the stoichiometric hydrogenation of C_{60}, to yield higher hydrofullerenes such as $C_{60}H_{18}$ and $C_{60}H_{36}$.

$C_{60}H_{36}$ was the first such hydrofullerene to be prepared and was obtained, under Birch reduction conditions, by Haufler and co-workers.[13] The product was identified by mass spectrometry and ^1H NMR spectroscopy showed a broad band between δ 2.5 and 4.2. A later mass spectroscopic study of the Birch reduction of C_{60} (Eq. 63) indicated the formation of hydrofullerenes ranging from $C_{60}H_{18}$ to $C_{60}H_{36}$ with the distribution centred on $C_{60}H_{32}$.[14] The variance between these and the earlier results was attributed to the different mass spectrometry techniques employed and to the thermal instability of the hydrofullerenes.

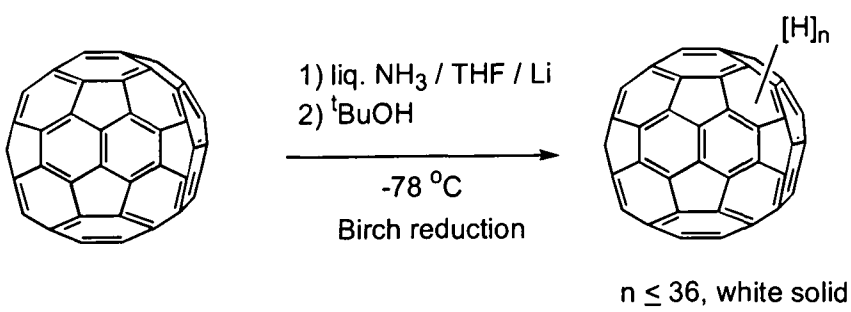

(63)

The observed stability of the hydrofullerene $C_{60}H_{36}$ was attributed to the high delocalisation energies of the four benzenoid rings at the tetrahedral positions of the *T* symmetry isomer

(figure 4.1). The *T* isomer was shown by several different quantum-chemical calculations to be the most stable of the possible structures of $C_{60}H_{36}$.[15,16]

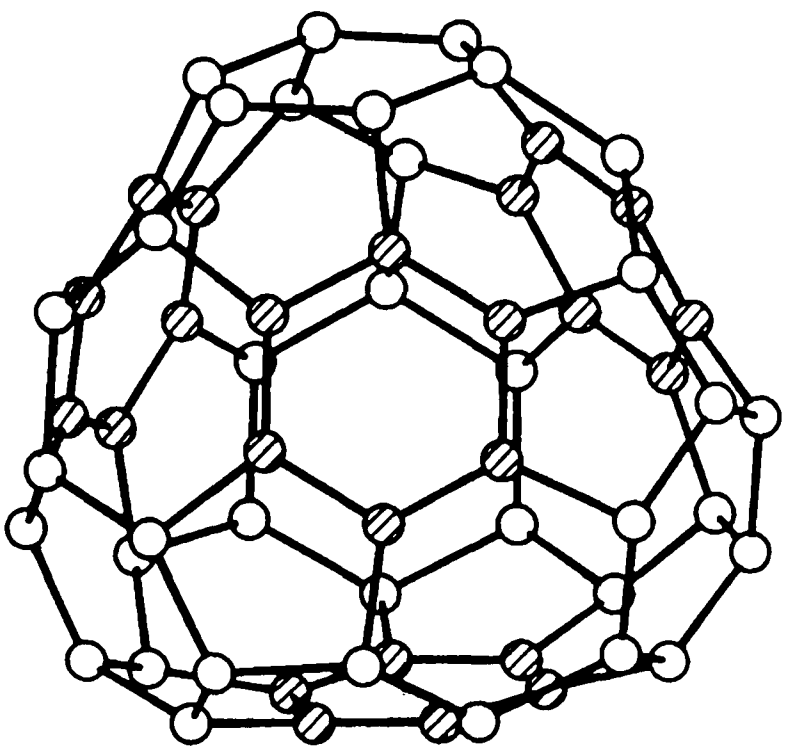

Figure 4.1 The *T* symmetry isomer of $C_{60}H_{36}$ in which all 12 double bonds are delocalised in four benzenoid rings (sp^2 carbon atoms are shaded).

Further reports claimed that hydrofullerenes $C_{60}H_{18}$ and $C_{60}H_{36}$ could be reproducibly synthesised by the transfer hydrogenation of C_{60} using 9,10'-dihydroanthracene.[17,18] A white solid product was isolated after reaction at 350 °C for 30 minutes and characterised by mass spectrometry as $C_{60}H_{36}$, whereas an increase in reaction time to 24 hours caused a decrease in the degree of hydrogenation, and the formation of a second product characterised as $C_{60}H_{18}$ (scheme 4.2).[18] Addition of the catalyst [7H]benzanthrene to the reaction mixture enabled lower reaction temperatures (250 °C) and possibly a higher degree of C_{60} hydrogenation: peaks in the mass spectrum of the reaction products were attributed to $C_{60}H_{36}$ and $C_{60}H_{44}$.[17] ^1H NMR spectroscopy of the hydrofullerene products showed a broad band between δ 2.5 and 4.2.

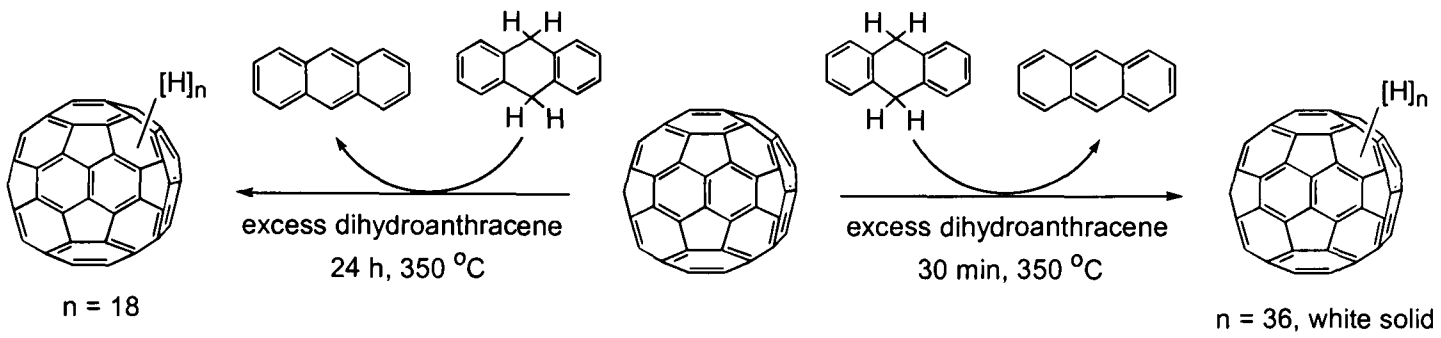

Scheme 4.2 Synthesis of $C_{60}H_{36}$ and $C_{60}H_{18}$ by transfer hydrogenation of C_{60} using 9,10-dihydroanthracene.

In 1993 Attalla and co-workers prepared a mixture of hydrofullerenes containing mainly $C_{60}H_{36}$ and $C_{70}H_{36}$, by hydrogen radical induced hydrogenation. A mixture of solid C_{60} and C_{70} (fullerite) was exposed to elevated hydrogen pressures (68 atm (cold)) at elevated temperatures (400 °C) in the presence of excess iodoethane (a promoter to generate hydrogen radical species, H). The products were characterised by FAB mass spectrometry. Similar experiments in the absence of iodoethane resulted in no hydrogenation. However, the following year $C_{60}H_n$ (n = 2-18) was prepared by direct hydrogenation of C_{60}, without the use of a catalyst or promoter.[19] Solid C_{60} was exposed to high pressure hydrogen gas (500-850 bar) at temperatures ranging from 300 to 350 °C, and products were identified by mass spectrometry.

In 1995 reduction of C_{60} using Zn / conc. HCl was reported, and the thermal stability of the product, $C_{60}H_{36}$, was investigated by mass spectrometry.[16] After 9 minutes at 650 °C a slight enhancement of the $C_{60}H_{18}$ peak relative to that of $C_{60}H_{36}$ was observed, and after 1 hour at this temperature peaks due to C_{60}, $C_{60}H_{18}$ and $C_{60}H_{36}$ were observed. Furthermore, it was stated that complete degradation to C_{60} eventually occurred, although the experimental evidence was not described.

The research outlined above (a) showed that catalytic hydrogenation of C_{60} is possible, (b) showed that C_{60} can be hydrogenated to higher hydrofullerenes $C_{60}H_n$, where generally n 36, and (c) suggested that the thermal decomposition of $C_{60}H_n$ to C_{60} + n/2 H_2 may possibly occur. Therefore, in order to evaluate C_{60} as a hydrogen storage medium (scheme 4.3) it seemed reasonable to (a) investigate the possibility of catalytic hydrogenation of C_{60} to

higher hydrofullerenes $C_{60}H_n$, and (b) investigate the thermal elimination of hydrogen gas from this product.

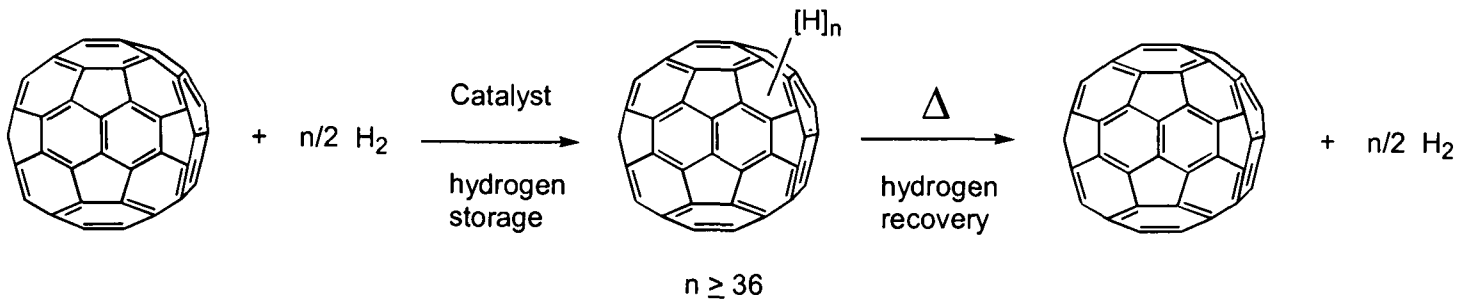

Scheme 4.3 C_{60} as a hydrogen storage medium.

After the commencement of the research described in this chapter the first catalytic hydrogenation of pure C_{60} to $C_{60}H_{36}$ was reported, using a carbon-supported palladium catalyst (Eq. 64). Best results were obtained using a hydrogen pressure of 70 atm at 180 °C, and the product was characterised by mass spectrometry.[20]

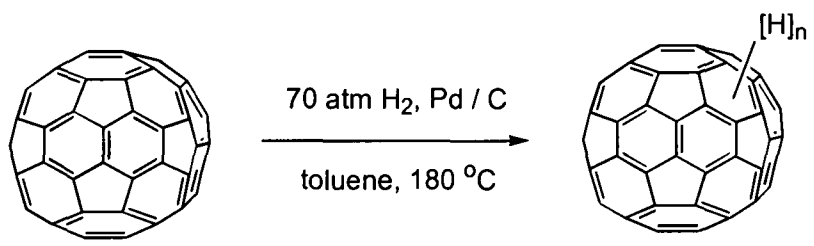

(64)

4.1.3 Transition Metal-C_{60} Heterogeneous Catalysts

Prior to the commencement of the research described in this chapter, two reports by Nagashima and co-workers demonstrated the use of C_{60} as a carbon support material for heterogeneous catalysis.[21,22] The insoluble compounds $C_{60}Pd_n$ (n = 1-7) and $C_{60}Pt_n$ (n ~ 1) were prepared (Eqs. 65 and 66) by reaction of C_{60} with $Pd_2(dba)_3.CHCl_3$ and $Pt(dba)_2$ respectively (dba = dibenzilideneacetone). The composition of C_{60} to Pd in the former compound was adjusted by changing the charged ratios of C_{60} to the palladium precursor (Eq. 65).

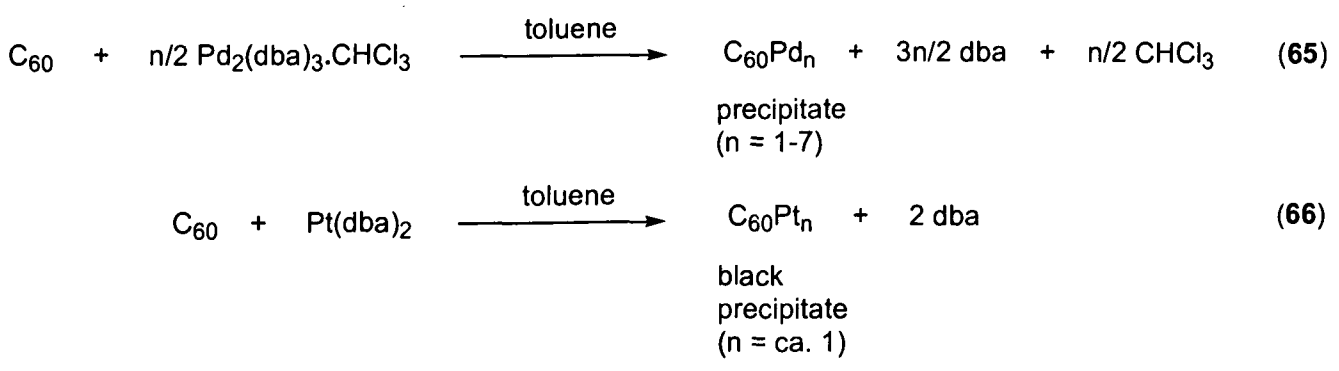

(65)

(66)

$C_{60}Pd_n$ was found to catalyse the hydrogenation of diphenylacetylene under a hydrogen atmosphere at room temperature where n > 3 (Eq. 67), and higher ratios of Pd to C_{60} resulted in an increase of the reaction rate. Compounds $C_{60}Pd_n$ where n < 3 were inactive. The catalytic hydrogenations of several different olefins (e.g. cyclooctene and PhCH=CHCOMe) over $C_{60}Pd_n$ (n = 4.61) also proceeded at room temperature under an atmosphere of hydrogen (Eq. 68). Furthermore, $C_{60}Pt_n$ (n ~ 1) catalysed the hydrogenation of diphenylacetylene under a hydrogen atmosphere at room temperature, to give a 3:7 mixture of *cis*-stilbene and diphenylethane (Eq. 69).[21,22]

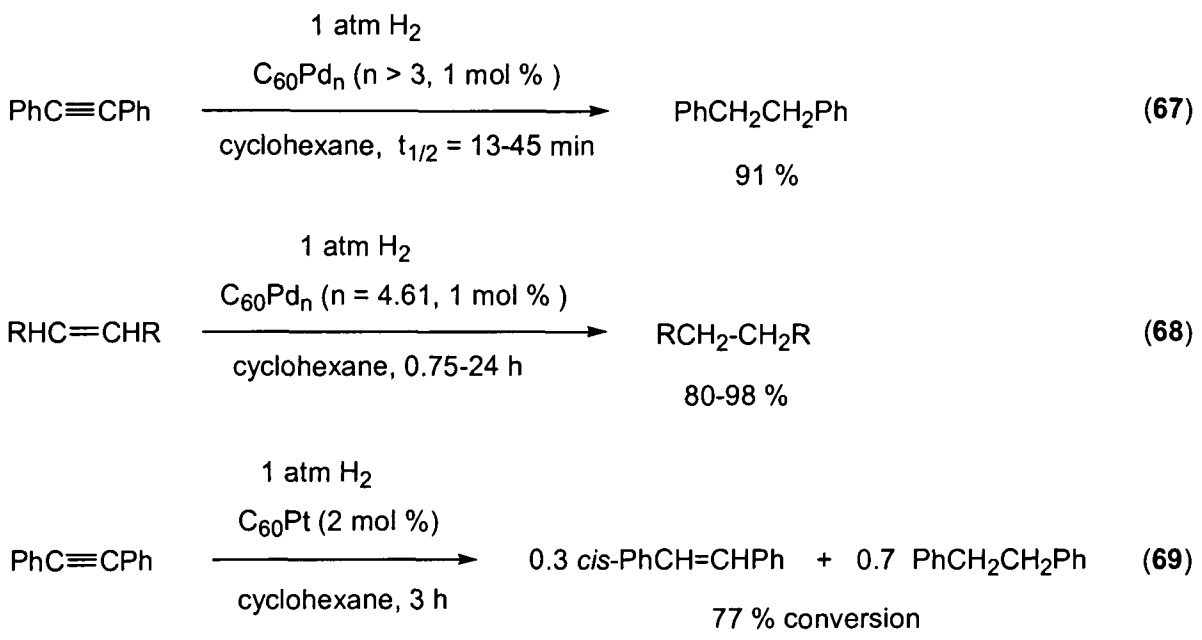

The results outlined above demonstrated the use of C_{60} as a carbon support for transition metal heterogeneous catalysis, in particular with respect to hydrogenation. Therefore, investigation of the rhodium C_{60} compound **20** (*vide infra*) seemed a reasonable starting point in the search for a highly-active heterogeneous catalyst which could possibly hydrogenate C_{60} itself. Several C_{60}-supported palladium,[23] platinum[24] and ruthenium[25-27] hydrogenation catalysts have been reported since the commencement of the research outlined in this chapter, although these were not studied with respect to C_{60} hydrogenation.

4.2 Synthesis and Characterisation of the Rhodium C_{60} Compound (20)

4.2.1 Synthesis

Reaction between C_{60} and 1.25 equivalents $[Rh(cyclooctene)_2Cl]_2$ gave a black precipitate and a colourless supernatant. The precipitate was isolated in 98 % yield for the compound $C_{60}[Rh(cyclooctene)Cl]_{2.5}$, which is consistent with the decomplexation of 1 cyclooctene per rhodium during reaction (Eq. 70).

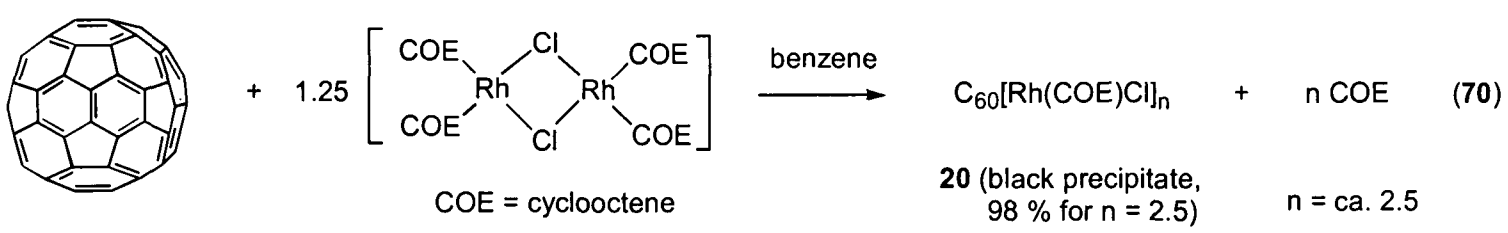

The supernatants obtained after reactions between C_{60} and 1 and 2 equivalents $[Rh(cyclooctene)_2Cl]_2$ were purple and yellow respectively, corresponding to unreacted C_{60} and $[Rh(cyclooctene)_2Cl]_2$ respectively. The presence of unreacted starting materials in each case indicates that the product does not have a stoichiometric Rh / C_{60} molar ratio of 2 or 4. Therefore, the colourless supernatant observed after reaction between C_{60} and 1.25 equivalents $[Rh(cyclooctene)_2Cl]_2$ is consistent with a non-stoichiometric Rh / C_{60} ratio of ca. 2.5 for the Rh C_{60} compound (**20**).

The compound **20**, a black powder, is insoluble in all common solvents, and was stored under nitrogen.

4.2.2 Characterisation

Characterisation of **20** was performed using elemental analysis, powder X-ray diffraction (XRD), infrared spectroscopy, and transmission electron microscopy (TEM) with energy dispersive X-ray (EDX) analysis.

The elemental analysis of **20** was erratic because microanalytical data obtained varied for different batches of the compound. It could not be determined whether this was due to

variation in the C_{60} / Rh stoichiometry from batch to batch because the carbon analyses varied, and were often too low, due incomplete combustion (a common problem with C_{60} compounds). The elemental analyses indicated that decomplexation of cyclooctene from rhodium had occurred during reaction, because the 'best fit' of the microanalytical data corresponded to loss of 1 cyclooctene per rhodium and formation of the compound $C_{60}[Rh(cyclooctene)Cl]_n$, where $n \sim 2.5$. The microanalytical data is given in section 5.4.1.

Powder XRD showed that **20** is amorphous.

Infrared spectroscopy showed C-H stretching absorptions at 2850 and 2922 cm^{-1} corresponding to coordinated cyclooctene. Furthermore, absorptions characteristic of C_{60} were observed at 523 cm^{-1} (s), 560 / 582 cm^{-1} (doublet) and 1169 cm^{-1} (broad): the splitting and broadening relative to the corresponding free C_{60} peaks at 526, 577 and 1184 cm^{-1} is due to symmetry reduction caused by C_{60}-metal adduct formation.[1]

TEM, performed by Dr Jeremy Sloan, showed that compound **20** consists of discrete spherical particles with a diameter in the range 200-500 nm (figure 4.2). EDX analysis of the particles confirmed the presence of rhodium and chlorine. The nature of the amorphous particles is not very well understood. However, it may be speculated that the C_{60} molecules are irregularly polymerised, with C_{60} units connected by rhodium atoms or by rhodium dimers as shown in figure 4.3. Although the C_{60}-Rh bonds are depicted as covalent η^2 metal-alkene π bonds, it is possible that a degree of charge-transfer from rhodium to C_{60} is occurring. The non-stoichiometric C_{60}:Rh ratio could easily be explained by a variation in the number of rhodium atoms bonded to each C_{60} molecule.

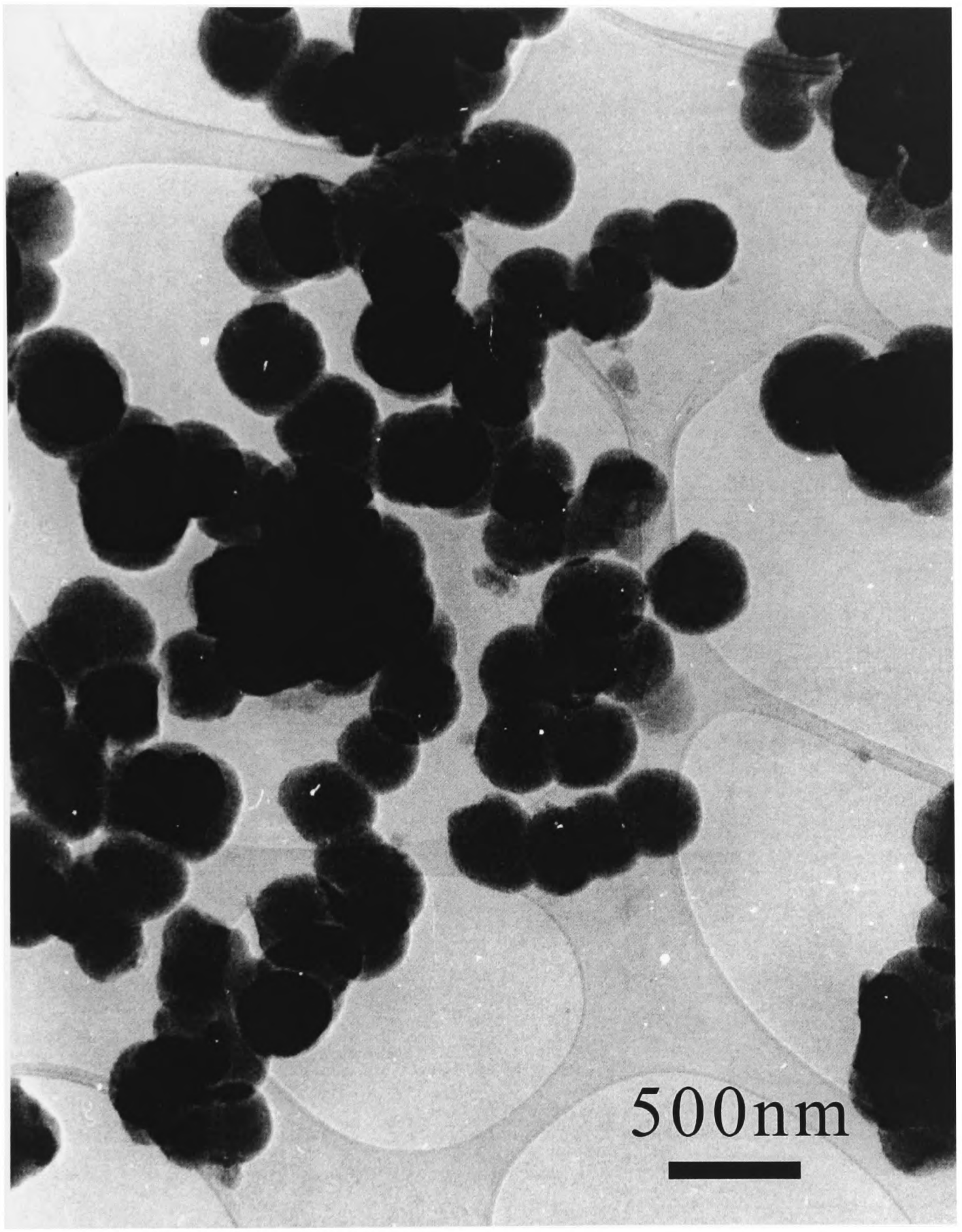

Figure 4.2 TEM image of the Rh C_{60} compound (**20**).

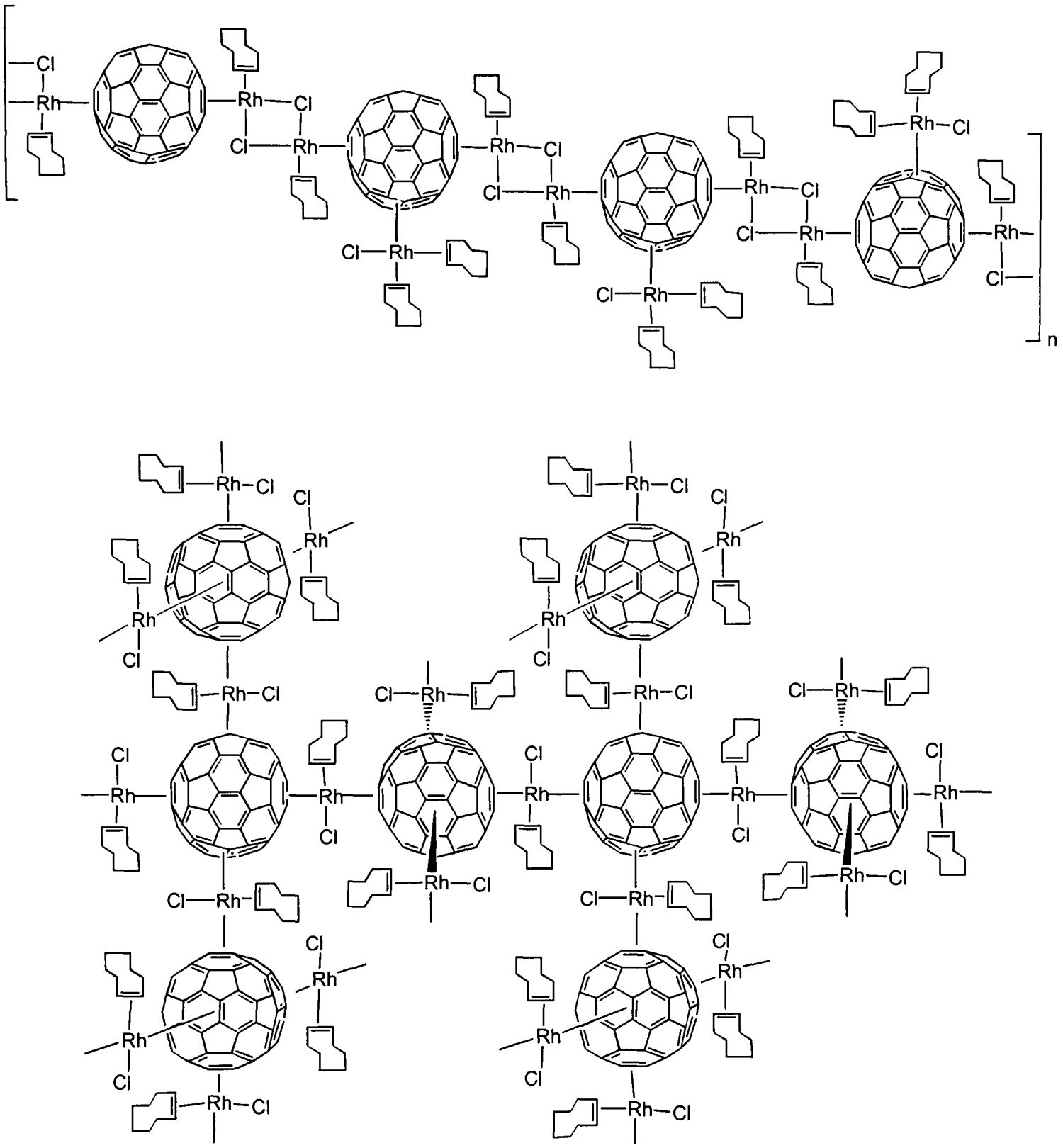

Figure 4.3 Two possible polymeric structures of the rhodium C_{60} compound.

4.2.3 Surface Area Measurement by the BET Method

Using the BET (Brunauer, Emmett and Teller) method, the rhodium C_{60} compound was found to have a high surface area of 156 m^2g^{-1}. The BET method is the standard technique for measuring the surface area of compounds, and involves the multilayer physical adsorption of an inert gas at constant temperature.[28,29] Nitrogen was used at liquid nitrogen temperature, 77 K.

The BET equation is:

$$\frac{P}{(n^s(P_o - P))} = \frac{(C-1)P}{(n^s_m C P_o)} + \frac{1}{(n^s_m C)}$$

n^s is the quantity of gas adsorbed at equilibrium pressure, P. P_o is the vapour pressure of the adsorbate (N_2) in the condensed state at the adsorption temperature (77 K), and n_m^s is the quantity of gas adsorbed at monolayer coverage. C is given by $C = \exp[(H_a-H_1)/RT]$, where H_a is the enthalpy of adsorption of the first layer and H_1 is the enthalpy of adsorption of the second and each subsequent layer.

Values of n^s at equilibrium pressures, P, are calculated by measuring the pressure decrease when known amounts of nitrogen gas are exposed to and therefore adsorbed by the sample.

A plot of $P/(n^s(P_o-P)$ against P/P_o gives a straight line graph in which the intercept is equal to $1/(n_m^s C)$ and the gradient is equal to $(C-1)/(n_m^s C)$. The value of n_m^s can then be obtained and the surface area per gram of catalyst calculated from:

$$\text{Surface Area} = \frac{a_m . n^s_m}{M}$$

M is the total mass of the sample used and a_m is the surface area of the adsorbate in the monolayer ($N_2 = 0.162\ nm^2 molecule^{-1}$).

The limit of the BET method when using liquid nitrogen is about 1-2 m^2g^{-1}.

In the case of compound **20** data points were entered into a Microsoft Excel spreadsheet written by Thomas Suhartanto, which solved the BET equation and calculated the surface area of the sample. Experimental details are given in section 5.4.2.

4.3 Catalytic Studies of the Rhodium C_{60} Compound (20)

In order to evaluate the catalytic activity of the rhodium C_{60} compound (**20**), the ability to catalyse the hydrogenation and hydroformylation of simple olefins was tested, as well as the ability to facilitate hydrogen storage via the catalytic hydrogenation of C_{60} to hydrofullerenes $C_{60}H_n$.

4.3.1 Ethylene Hydrogenation

$$H_2C{=}CH_2 \xrightarrow[25 - 300\ ^oC]{H_2,\ Rh\ C_{60}\ compound} C_2H_6 \quad (71)$$

100 %

A mixture of ethylene and hydrogen (ca. 14 % ethylene) was passed over compound **20** at ambient pressure and at temperatures in the range 25-300 °C. At various temperatures the product gas was allowed to pass directly into a gas chromatograph (GC runs 1-7), which showed 100 % conversion of ethylene to ethane in each case (Table 4.2, Eq. 71). Experimental details are given in section 5.4.3.

GC Run	Temperature (°C)	Ethane peak (r.t. = 1.64 mins) integral (%)	Ethylene peak (r.t. = 1.75 mins) integral (%)	Conversion (%)
1	30	100	0	100
2	50	100	0	100
3	100	100	0	100
4	140	100	0	100
5	200	100	0	100
6	300	100	0	100
7	25 (after 300)	100	0	100

Table 4.2 Summary of ethylene hydrogenation at various temperatures.

Elemental analysis of the rhodium C_{60} compound recovered after catalysis showed a reduction in chlorine and hydrogen contents to 1.5 % and 0.0 % respectively. Furthermore, the infrared spectrum contained no C-H stretching absorptions characteristic of

cyclooctene. The loss of cyclooctene could either be due to displacement by ethylene or hydrogen during catalysis, or to hydrogenation to cyclooctane and hence decomplexation, or to thermal dissociation at the elevated temperatures employed. The elevated temperatures would ensure subsequent evaporation of any free cyclooctene or cyclooctane. The observed decrease in chlorine content is possibly explained by the reductive elimination of HCl from an intermediate Rh(H)(Cl) moiety during catalysis.

TEM of the recovered Rh C_{60} catalyst, performed by Dr Jeremy Sloan, showed spherical particles of diameter in the range 200-500 nm as shown in figure 4.2. No change in the morphology of the Rh C_{60} compound was observed.

4.3.2 Cyclohexene Hydrogenation

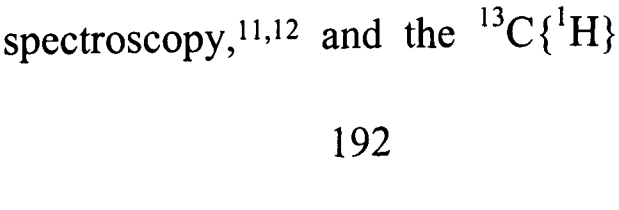

(72)

Quantitative conversion of cyclohexene to cyclohexane (Eq. 72) was observed by ^{1}H NMR spectroscopy after stirring a benzene solution of cyclohexene for 16 h at room temperature in the presence of 0.5 bar H_2 gas and **20** (ca. 0.5 mol % Rh). A control experiment showed that **20** does not catalyse the hydrogenation of benzene. Experimental details are given in section 5.4.4.

4.3.3 C_{60} Hydrogenation

The hydrogenation C_{60} to hydrofullerenes $C_{60}H_n$ was achieved upon stirring benzene solutions of C_{60} at 130 °C in the presence of **20** (29-100 mol % Rh). The value of n was observed to increase with increasing hydrogen pressure, P, and reaction time, t. Experimental details are given in sections 5.4.5, 5.4.6 and 5.4.7.

For P = 1.5 bar and t = 16 hours a brown-red solid was isolated from the reaction mixture after removal of the catalyst by filtration. The solid was shown to be a mixture of the product $C_{60}H_2$ (Eq. 73) and unreacted C_{60}. A singlet at δ 5.90 characteristic of $C_{60}H_2$ was observed by ^{1}H NMR spectroscopy,[11,12] and the $^{13}C\{^1H\}$ NMR spectrum showed the

presence of C_{60} (δ 143.3). The $C_{60}H_2$ product was not distinguishable from unreacted C_{60} by FAB mass spectrometry. A control experiment, identical except for the absence of the C_{60} substrate, was performed: ^1H NMR spectroscopy of the reaction mixture showed no peak at δ 5.90.

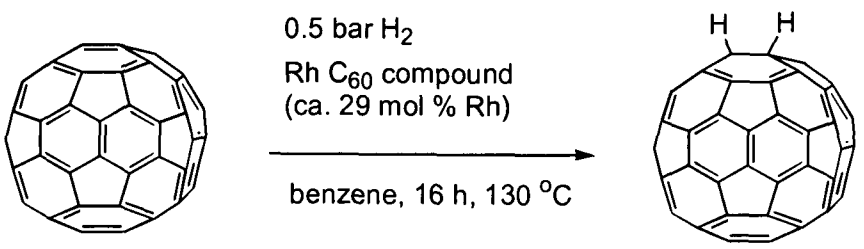

(73)

The degree of C_{60} hydrogenation was increased by increasing the reaction time, t, from 16 to 240 hours (Eq. 74). Again, after reaction the catalyst was removed by filtration and a brown-red solid was isolated from the resulting solution. FAB mass spectrometry indicated a mixture of hydrofullerenes $C_{60}H_n$ where n = 0-36 (figure 4.4). ^1H NMR spectroscopy (C_6D_6) showed a broad band in the range δ 2-5 characteristic of hydrofullerenes $C_{60}H_n$ where $n \leq 36$,[13,18] and $^{13}C\{^1H\}$ NMR spectroscopy showed the presence of unreacted C_{60} (δ 143.3).

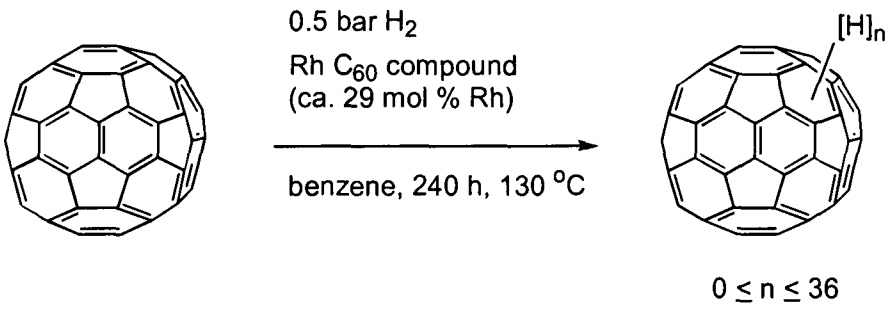

(74)

Using a hydrogen pressure of 40 bar and a reaction time of 240 hours, complete hydrogenation of C_{60} to $C_{60}H_{36}$ was observed (Eq. 75). The product, a brown-red solid, was isolated from the filtered reaction mixture in 78 % yield. FAB mass spectrometry is consistent with the formation of $C_{60}H_{36}$, and the spectrum (figure 4.5) is similar to those of hydrofullerenes obtained by the Birch reduction,[14] the reduction using Zn / HCl[16] and the transfer hydrogenation (using 9,10-dihydroanthracene)[18] of C_{60}. In addition, ^1H NMR spectroscopy showed a broad band in the range δ 2.6-4.5 and infrared spectroscopy showed strong C-H stretching absorptions at 2843 and 2911 cm^{-1} (figure 4.6) all of which is characteristic of $C_{60}H_{36}$.[13,16,18] No unreacted C_{60} was observed by $^{13}C\{^1H\}$ NMR

spectroscopy, which indicates that the increased hydrogen pressure of 40 bar caused the reaction to go to completion.

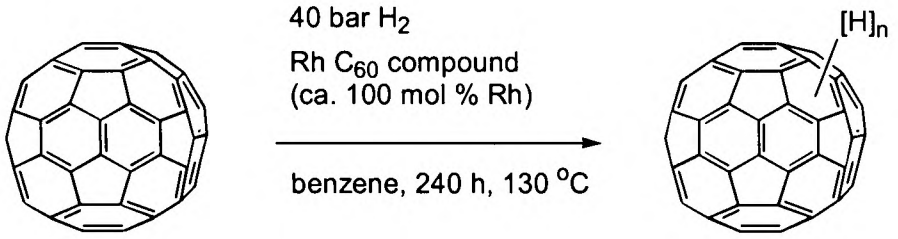

n = 36 (brown-red solid, 78 %)

(75)

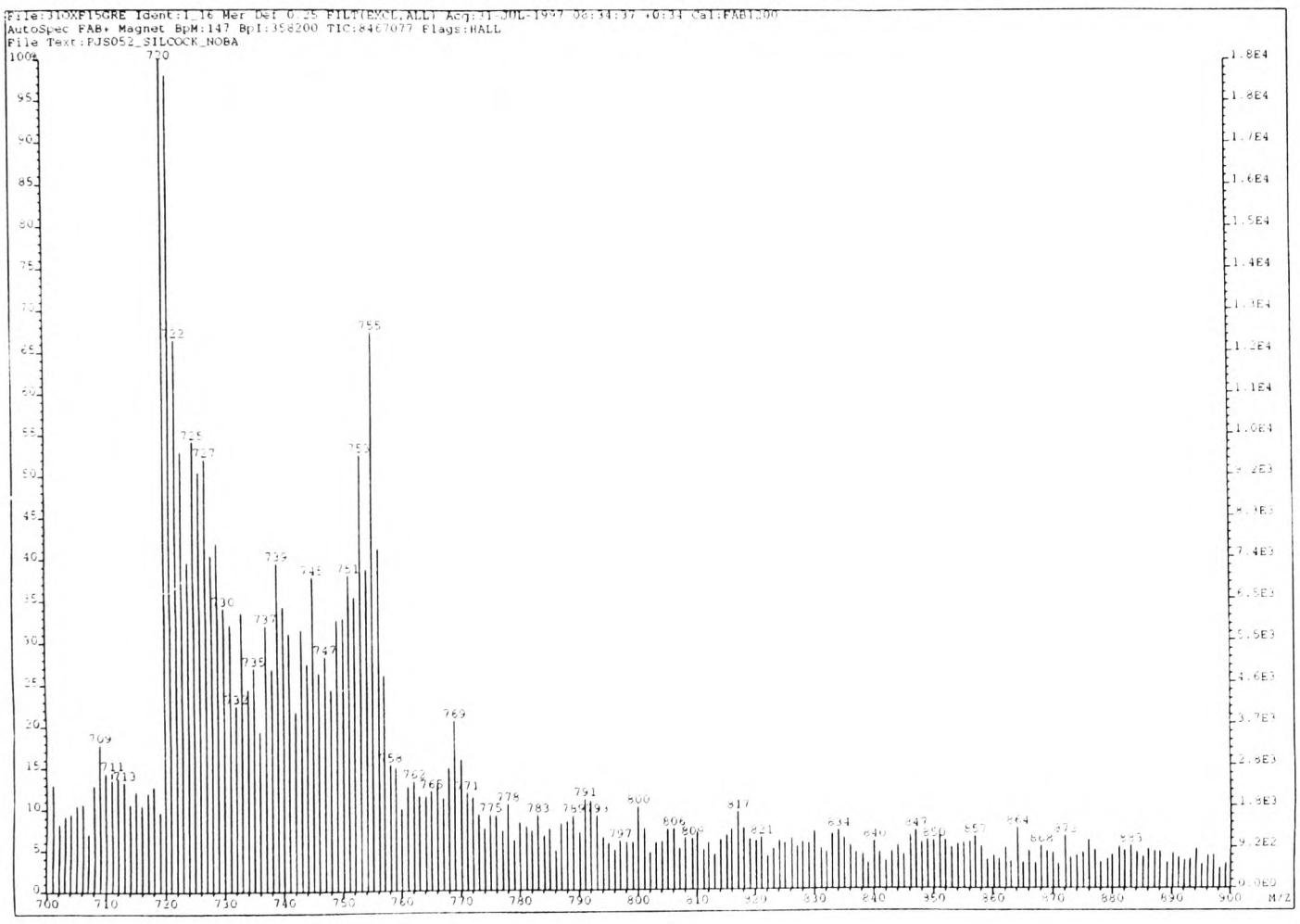

Figure 4.4 FAB mass spectrum of the C_{60} hydrogenation product where P = 0.5 bar and t = 240 hours.

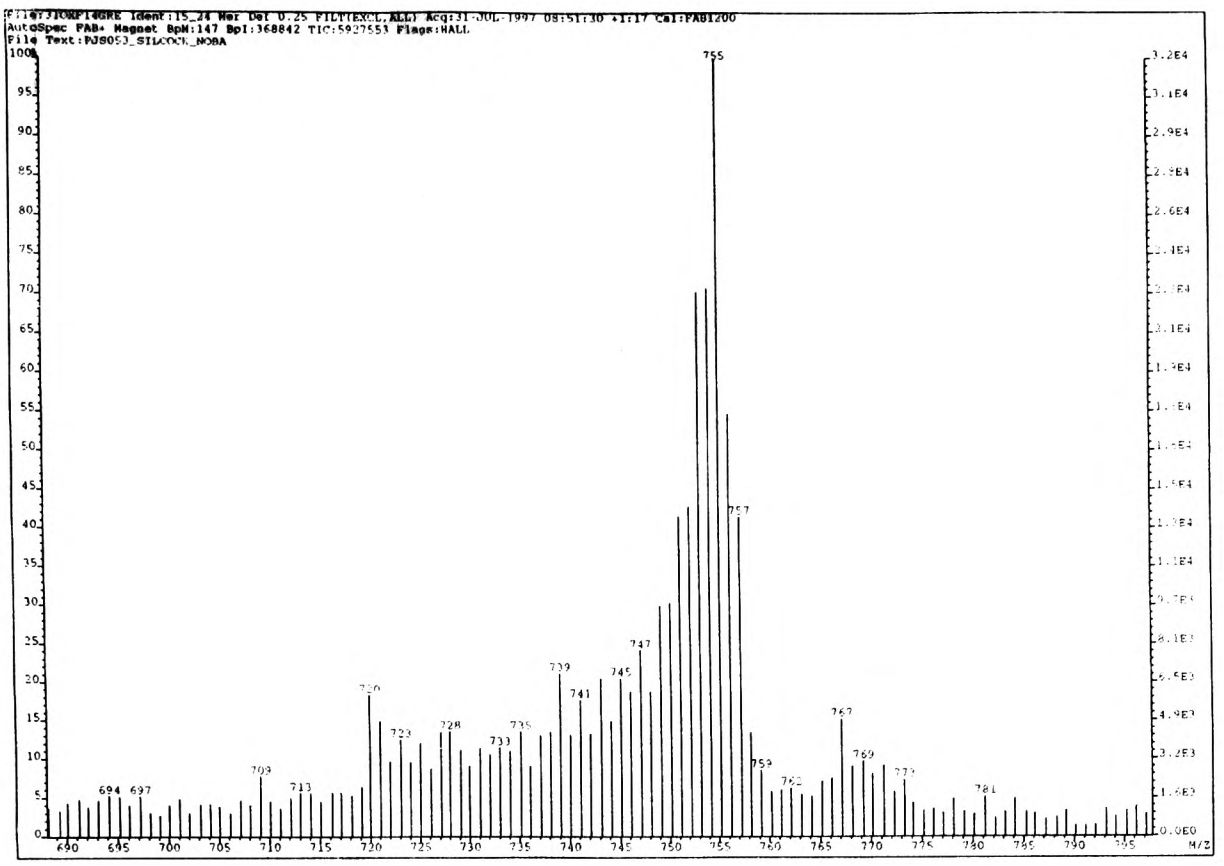

Figure 4.5 FAB mass spectrum of the C_{60} hydrogenation product $C_{60}H_{36}$ (P = 40 bar and t = 240 hours).

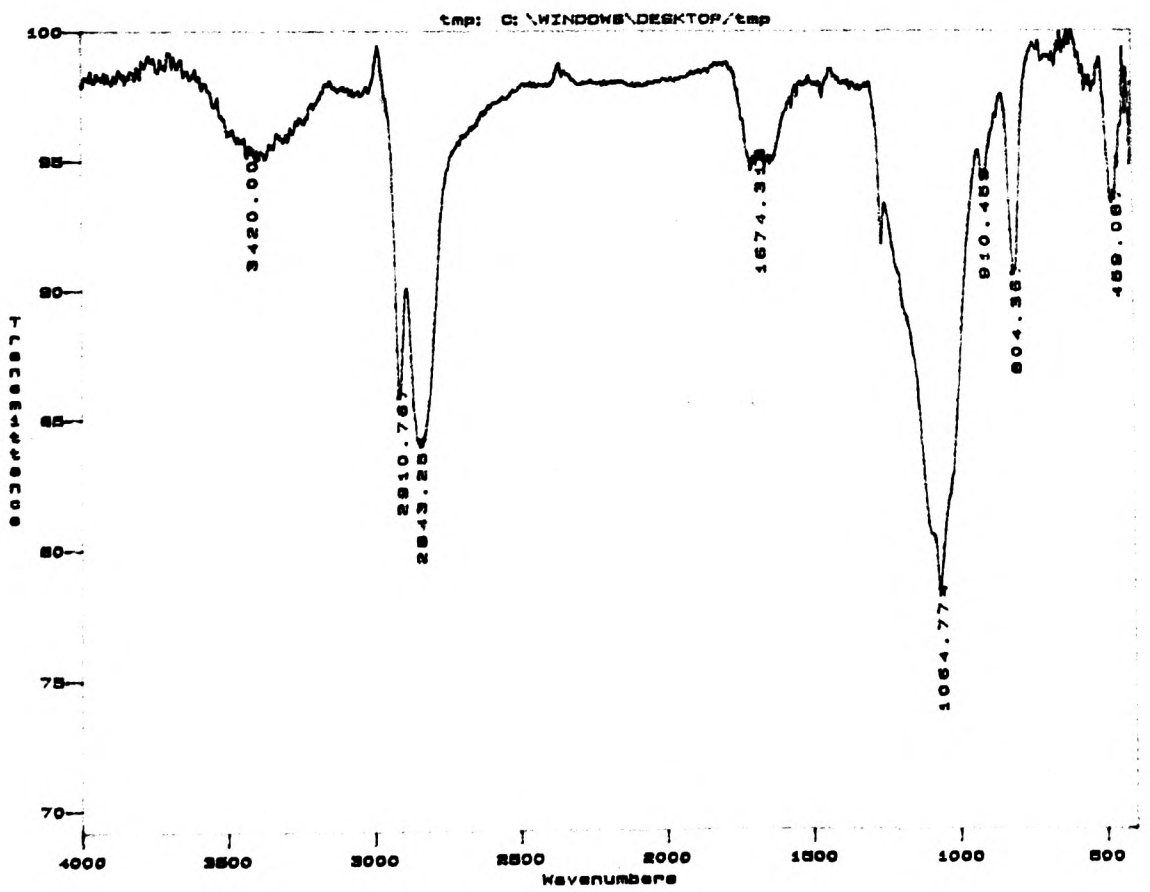

Figure 4.6 Infrared spectrum of the C_{60} hydrogenation product $C_{60}H_{36}$ (P = 40 bar and t = 240 hours).

After each C_{60} hydrogenation reaction the rhodium C_{60} catalyst was recovered from the reaction mixture by filtration, washed with benzene and residual volatiles removed under reduced pressure. For comparison with the micrographs of the Rh C_{60} compound **20** before catalysis, the resulting black powders were examined by Dr Jeremy Sloan using TEM (figures 4.7 and 4.8). In each case crystallites of metallic rhodium of less than 5 nm in diameter were observed within the particles of the Rh C_{60} compound after catalysis (figure 4.8). It is reasonable to suggest that prolonged exposure to hydrogen at 130 °C caused the reduction and subsequent agglomeration of rhodium within **20**. The observation of rhodium crystallites raises the question as to whether the observed catalytic ability of **20** is generally due to metallic rhodium rather than to discrete C_{60}-bonded Rh atoms.

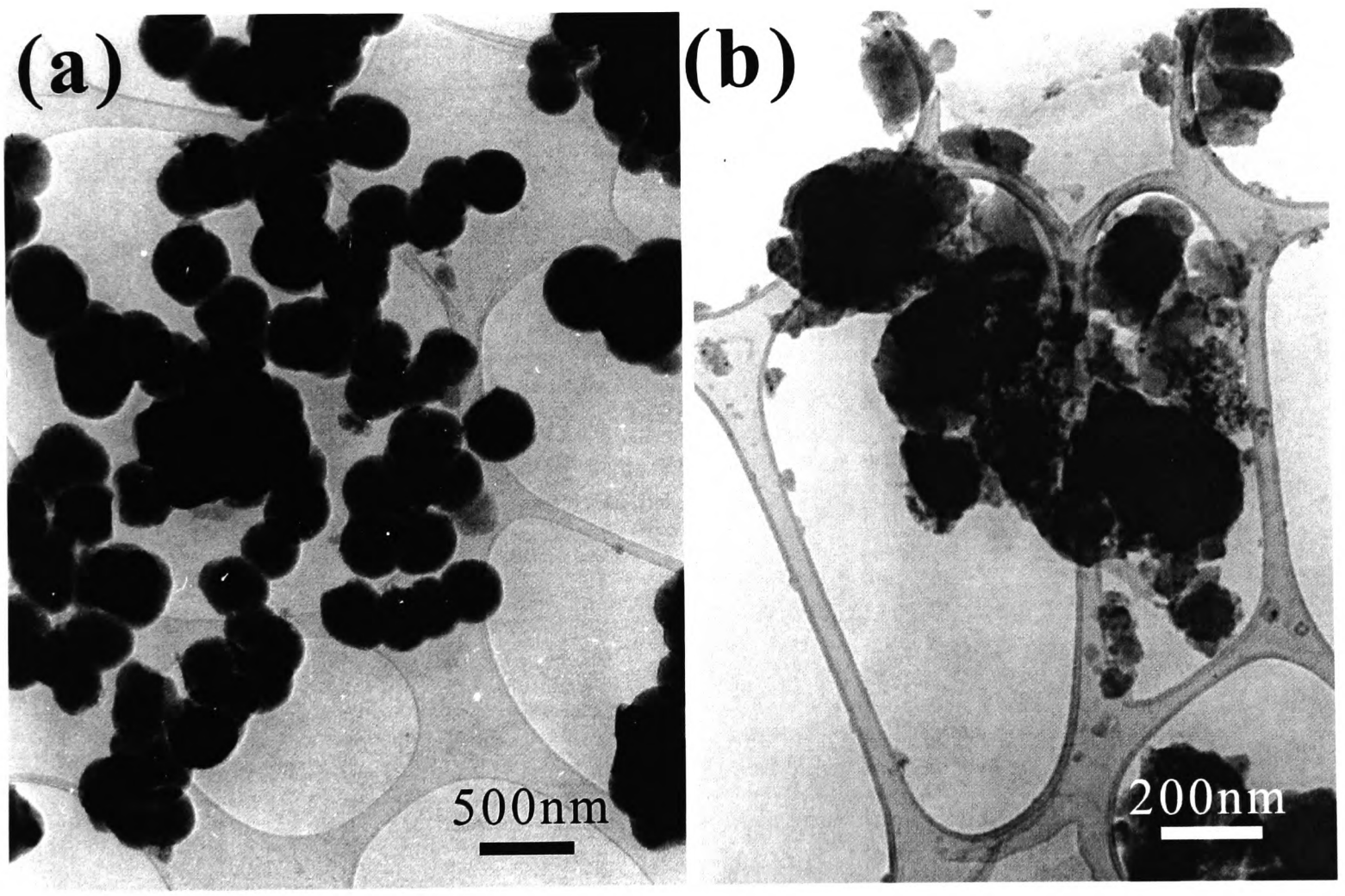

Figure 4.7 TEM images of the Rh C_{60} catalyst (a) before and (b) after C_{60} hydrogenation experiments.

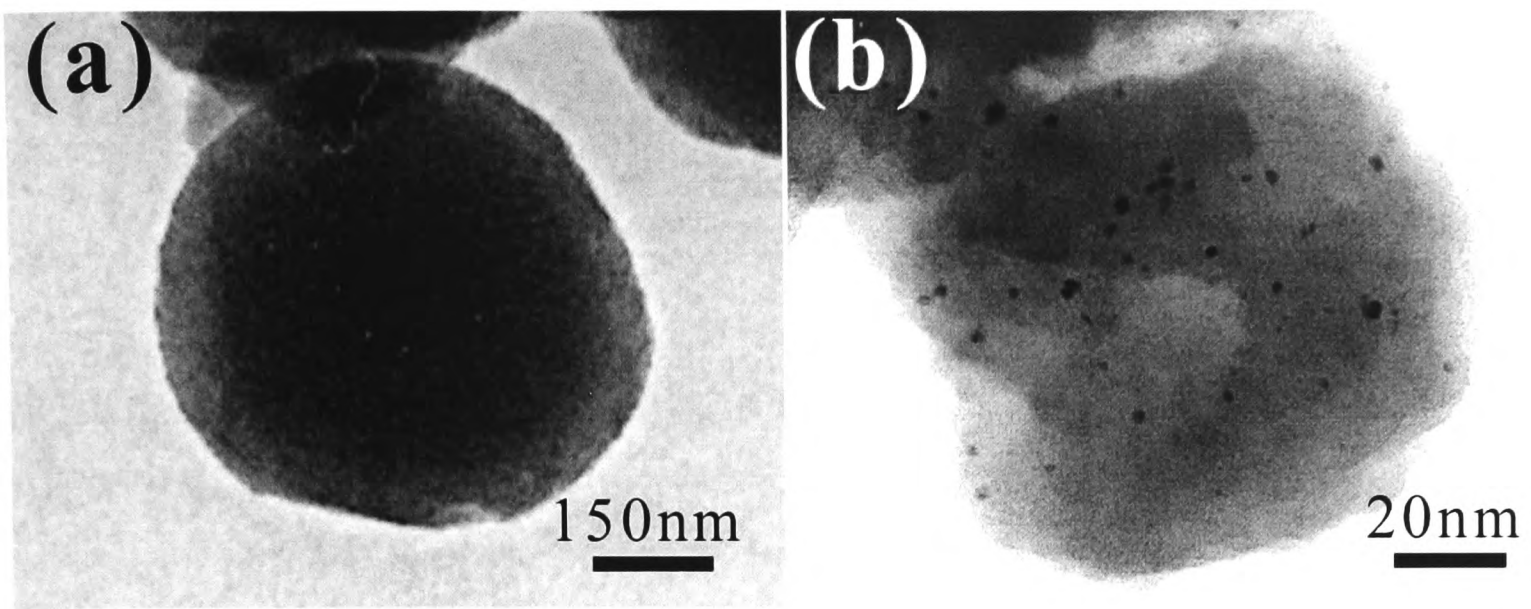

Figure 4.8 TEM images of single particles of the Rh C_{60} catalyst (a) before and (b) after C_{60} hydrogenation experiments. Crystallites of metallic rhodium are observed in (b).

4.3.4 Hydroformylation of 3,3-Dimethyl-1-butene and 1-Pentene

Compound **20** was found to be a pre-catalyst for the hydroformylation of the terminal olefins 3,3-dimethyl-1-butene (Eq. 76) and 1-pentene (Eq. 77). Although the reactions did not occur at room temperature, quantitative conversions were observed within 3 hours at 130 °C. In each case a pressure of 38 bar 1:1 H_2:CO was used, and ca. 0.2-0.3 mol % Rh. Experimental details are given in sections 5.4.8 and 5.4.9. Reactions were monitored by ^{1}H NMR spectroscopy which showed 100 % conversion of 3,3-dimethyl-1-butene to the linear-chain aldehyde 4,4-dimethyl pentan-1-al (Eq. 76). However, in the case of 1-pentene a 1:1 mixture of the linear- and branched-chain aldehydes was obtained (Eq. 77). Therefore, conversion of 3,3-dimethyl-1-butene to the linear-chain aldehyde only is not due to selectivity of the catalyst, but most likely to the steric bulk of the *tert*-butyl group which favours anti-Markovnikov addition to the olefin.

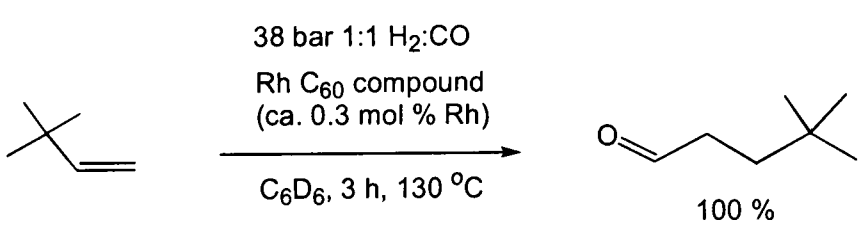

(76)

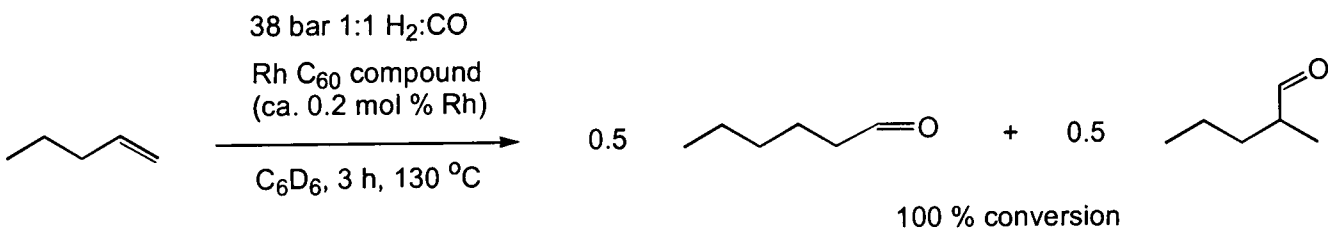

(77)

After hydroformylation the reaction mixtures were observed as red C_6D_6 solutions, with no solid Rh C_{60} compound remaining. In both cases intractable red solids were isolated from the reaction mixtures and residual volatiles removed. ^{1}H and ^{13}C{^{1}H} NMR spectroscopy showed mixtures of compounds with broad peaks in the methyl and methylene regions probably due to hydrocarbon residues originating from the alkene starting materials. The solid from the 1-pentene reaction was also examined by elemental analysis, FAB mass spectrometry and infrared spectroscopy (section 5.4.9) which indicated a mixture of C_{60} Rh chlorocarbonyl compounds. It is probable that the hydroformylation reactions described above are catalysed by rhodium species in solution rather than by the insoluble compound **20**. The fact that hydroformylation occurs at 130 °C but not at room temperature is possibly due to the requirement of elevated temperatures to convert **20** into the soluble catalytic species.

The observed ability of the insoluble Rh C_{60} compound (**20**) to catalyse the gas- and liquid-phase hydrogenation of simple olefins, as well as the hydrogenation of C_{60} to $C_{60}H_{36}$ confirms that C_{60} can be an appropriate support material for heterogeneous transition metal catalysis. It is uncertain as to whether the catalyst activity arises solely from the formation of metallic rhodium crystallites which were observed by TEM, or whether the compound **20** is itself an active heterogeneous catalyst.

The successful catalytic hydrogenation of C_{60} to $C_{60}H_{36}$ (an uptake of 5.0 wt % hydrogen) represents the first stage in the evaluation of C_{60} as a possible solid state hydrogen storage medium. The second stage, an investigation into the recovery of hydrogen gas from $C_{60}H_{36}$, is detailed in section 4.4.

4.4 Evaluation of C_{60} as a Hydrogen Storage Medium: Recovery of Hydrogen from $C_{60}H_{36}$

The catalytic hydrogenation of C_{60} to $C_{60}H_{36}$ represents a hydrogen uptake of 5 wt %, which is considerably greater than hydrogen uptake by conventional intermetallic hydrogen storage compounds (< 2 wt %).[2-4] Compared to other forms of carbon, such as graphite, undoped graphite nanofibres and single-walled nanotubes (SWNTs), C_{60} stores hydrogen at a relatively mild pressure (40 bar) although a catalyst and the elevated temperature of 130 °C is required, and the hydrogen uptake is not always as great (section 4.1). Although a hydrogen storage capacity of 5.0 wt % falls short of the 6.5 wt % benchmark regarded by the U.S. Department of Energy as a commercially significant value for system-weight efficiency,[8] 5.0 wt % is greater than the reported value for graphite and comparable to values observed for SWNTs (section 4.1), and the value could be improved to 8.4 wt % if hydrogenation to $C_{60}H_{60}$ is achieved in the future. Therefore C_{60} might still have potential as a useful hydrogen storage system, and the recovery of hydrogen by thermal elimination from $C_{60}H_{36}$ was investigated.

$C_{60}H_{36}$ was synthesised by the Birch reduction of C_{60} (Eq. 63) in order to obtain a large enough amount for an accurate determination of the quantity of hydrogen produced by thermal elimination. Experimental details for the Birch reduction, and characterising data for the product are given in section 5.4.10. ^{1}H NMR and infrared spectroscopy of the product was consistent with $C_{60}H_{36}$, and ^{13}C NMR spectroscopy showed that no unreacted C_{60} remained. Elemental analysis showed the presence of carbon and hydrogen, but was not accurate enough for determination of the exact carbon:hydrogen ratio due to the low carbon analysis as a result of incomplete combustion (a common problem with C_{60} compounds).

4.4.1 Thermal Decomposition of $C_{60}H_{36}$: Measurement of the Quantity of Hydrogen Evolved

A tube of known volume containing the Birch reduction product $C_{60}H_{36}$ (49 mg, 64.7 μmol) was attached to a high vacuum line which incorporated a volumetric system. The sample was degassed at room temperature and the absolute pressure reduced to 0.0 mmHg. The sample was isolated using a teflon stopcock and held for 1 hour at 110 °C before cooling to room temperature and releasing the gas produced into an accurately predetermined volume of glassware. The observed pressure increase was used to calculate the quantity of hydrogen evolved. This process was repeated for increasingly higher temperatures as shown in table 4.3. The amount of hydrogen gas evolved at each temperature as well as the overall total quantity was calculated (table 4.3). Experimental details are given in section 5.4.11.

Temperature (°C)	Time at temperature (mins)	Pressure increase (mmHg)	Amount H_2 evolved at temperature (μmol)	Amount H_2 evolved at temperature (% of theoretical maximum)	Pressure (mmHg)	Total amount H_2 evolved (μmol)	Total H_2 evolved (% of theoretical maximum)
110	60	3.3	13.7	1.2	3.3	13.7	1.2
180	60	3.4	14.0	1.2	6.7	27.7	2.4
250	60	1.0	4.2	0.3	7.7	31.9	2.7
340	60	3.1	12.8	1.1	10.8	44.7	3.8
440	60	42.4	175.5	15.1	53.2	220.2	18.9
550	90	56.3	233.0	20.0	109.5	453.2	38.9

Table 4.3 Quantity of hydrogen gas evolved by thermal decomposition of $C_{60}H_{36}$.

The results in table 4.3 show that significant quantities of gas are evolved when $C_{60}H_{36}$ is heated at and above 440 °C. Assuming all the gas is hydrogen, the total quantity evolved after heating at temperatures up to and including 550 °C corresponds to 38.9 % of the theoretical maximum amount from the 64.7 μmol $C_{60}H_{36}$ used. This corresponds to a loss of 14 H atoms per $C_{60}H_{36}$ to form 7 molecules H_2. Heating at temperatures up to and

including 340 °C only resulted in the evolution of less than 4 % of the theoretical maximum amount.

After the thermal decomposition experiments a black powder was recovered from the sample tube. The powder was insoluble in benzene, toluene and DMSO, all of which dissolve C_{60} itself and hydrofullerenes such as $C_{60}H_{36}$. Supernatants did not show the mauve colour characteristic of benzene or toluene solutions of C_{60}. The insoluble powder was suspended in C_6D_6 for ^1H and $^{13}C\{^1H\}$ NMR spectroscopy of any soluble parts. ^1H NMR spectroscopy showed no broad band in the range δ 2.6-4.5 characteristic of higher hydrofullerenes such as $C_{60}H_{36}$, and no singlet at δ 5.90 characteristic of $C_{60}H_2$. This evidence suggests that the lack of solubility is possibly due to products arising from decomposition of the C_{60} cage of the hydrofullerene. The $^{13}C\{^1H\}$ NMR spectrum, however, contained a peak at δ 144.3 of very low intensity corresponding to a trace amount of free C_{60}. This free C_{60} was also observed in the infrared spectrum which showed characteristic sharp absorbances at 525 and 576 cm^{-1} that were not present for the Birch reduction product (figure 4.9).

Infrared spectroscopy of the decomposed Birch reduction product shows evidence for reduced hydrogen content as a result of thermal decomposition. The C-H stretching absorptions at 2843 and 2910 cm^{-1} are ca. 25 % the intensity of those observed for the Birch reduction product, relative to peaks in fingerprint region (figure 4.9). Furthermore a reduction of the hydrogen content (from 5.8 to 1.9 %) is observed by elemental analysis although the microanalytical data is not accurate enough for quantitative comparisons.

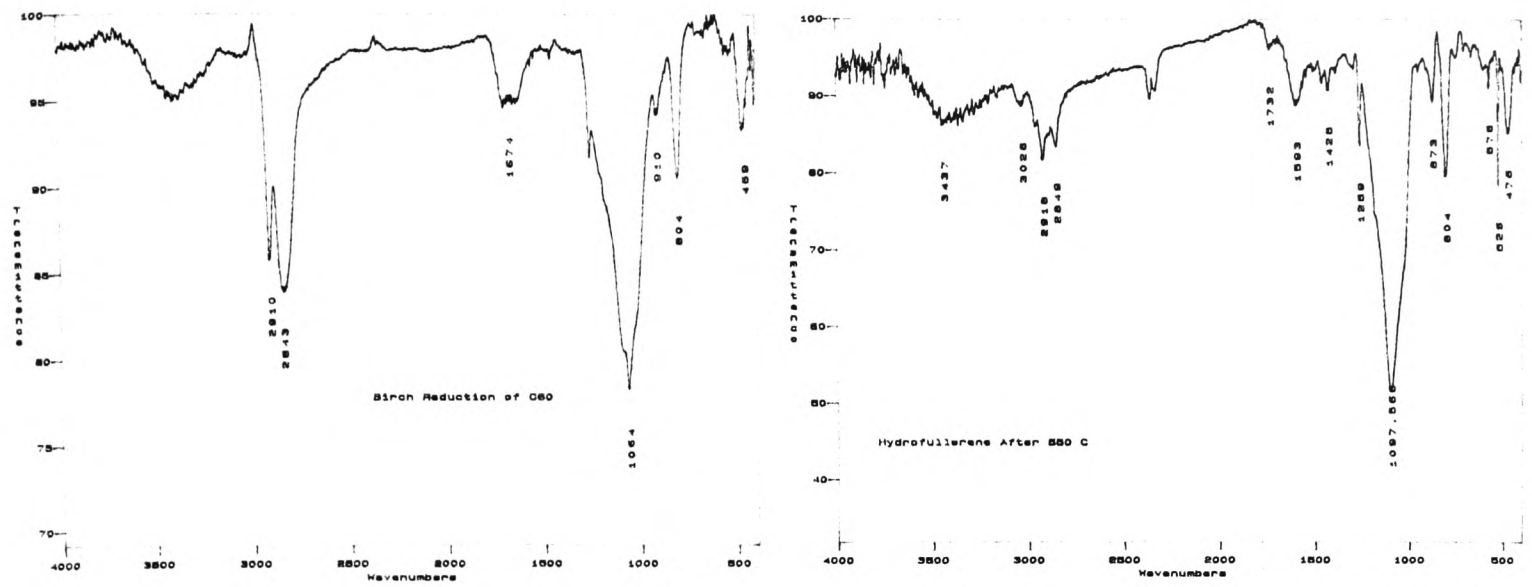

Figure 4.9 Infrared spectra of the Birch reduction product before (left) and after (right) thermal decomposition.

Although trace amounts of C_{60} by-product were observed by infrared and $^{13}C\{^1H\}$ NMR spectroscopy, the quantity of gas produced by thermal decomposition of $C_{60}H_{36}$ (38.9 % of the theoretical maximum of hydrogen) shows that complete decomposition to C_{60} and hydrogen gas did not occur, even after prolonged heating at 550 °C. Furthermore, the lack of solubility of the resulting residue, which contained no hydrofullerenes observable by ^1H NMR spectroscopy and only trace amounts of free C_{60}, indicates the presence of unknown decomposition products, possibly due to thermal decomposition of the C_{60} cage of the hydrofullerene. In this case temperatures above 550 °C would probably cause more such decomposition rather than recover any further hydrogen gas or C_{60}. Decomposition of the hydrofullerene cage would not only produce volatile hydrocarbons such as methane and ethane to contaminate the recovered hydrogen, but also render a hydrogen storage system non-reuseable (and therefore impractical). Besides these possible drawbacks, the incomplete recovery of hydrogen at temperatures up to 550 °C shows that C_{60} hydrogen storage is not reversible over a reasonable temperature range, which suggests that C_{60} could not form the basis of an economically viable hydrogen storage system.

4.5 Summary and Conclusions

The insoluble, amorphous rhodium C_{60} compound **20**, $C_{60}[Rh(cyclooctene)Cl]_n$ (n = ca. 2.5), was synthesised. Transmission electron microscopy showed a unique morphology consisting of discrete spherical particles with a diameter in the range 200-400 nm. A BET surface area measurement was performed which gave a value of 156 m^2g^{-1}. The compound **20** was found to catalyse the gas phase hydrogenation of ethylene and the liquid phase hydrogenation of cyclohexene at room temperature and ambient hydrogen pressures. Furthermore, **20** catalysed the hydrogenation of free C_{60}, at 130 °C, to give hydrofullerenes $C_{60}H_n$. The value of n was found to depend on the reaction time t and the hydrogen pressure P. For P = 40 bar and t = 240 hours, complete hydrogenation of C_{60} to $C_{60}H_{36}$ was observed which represents a hydrogen uptake of 5.0 wt %. For the C_{60} hydrogenation reactions, transmission electron microscopy of the recovered rhodium C_{60} compound **20** in each case showed the presence of crystallites of metallic rhodium, of less than 5 nm in diameter, within the particles of 200-400 nm diameter. It is therefore possible that the observed catalytic ability of compound **20** is generally due to *in situ* formation of metallic rhodium, rather than to the rhodium C_{60} compound itself. The compound **20** was also observed to be a pre-catalyst for the hydroformylation of terminal olefins, although no catalyst selectivity for linear- or branched-chain aldehydes was observed. For the evaluation of C_{60} as a solid state hydrogen storage medium, the thermal elimination of hydrogen gas from the hydrofullerene $C_{60}H_{36}$ was investigated. The total quantity of gas evolved on heating $C_{60}H_{36}$ at temperatures up to and including 550 °C corresponded to 38.9 % of the theoretical maximum amount of hydrogen. This corresponds to a loss of 14 H atoms per $C_{60}H_{36}$ to form 7 molecules H_2. Unlike hydrofullerenes, which could not be detected by ^1H NMR spectroscopy, the resulting solid residue was insoluble, and contained only trace amounts of free C_{60}, suggesting unknown decomposition products, possibly due to thermal decomposition of the C_{60} cage of the hydrofullerene. Such thermal decomposition would render a C_{60} hydrogen storage system non-reuseable and therefore impractical. Furthermore, the incomplete recovery of hydrogen at temperatures up to 550 °C shows that C_{60} hydrogen storage is not reversible over a reasonable temperature range, which suggests that C_{60} could not form the basis of an economically viable hydrogen storage system. A summary of the new chemistry described in chapter 4 is given in scheme 4.4.

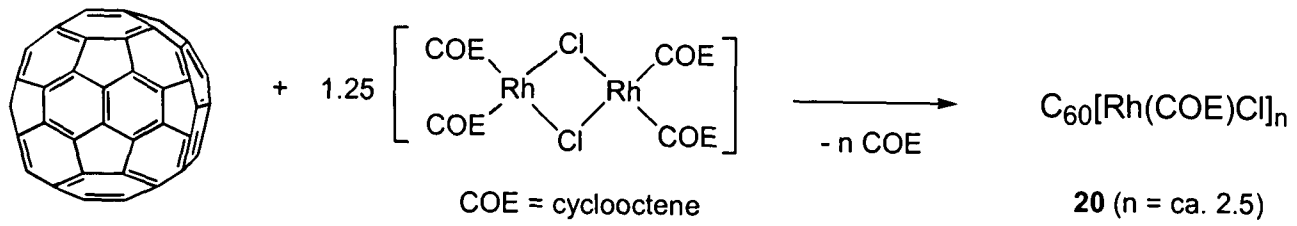

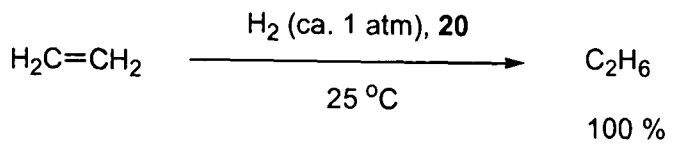

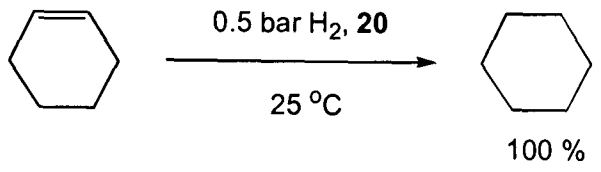

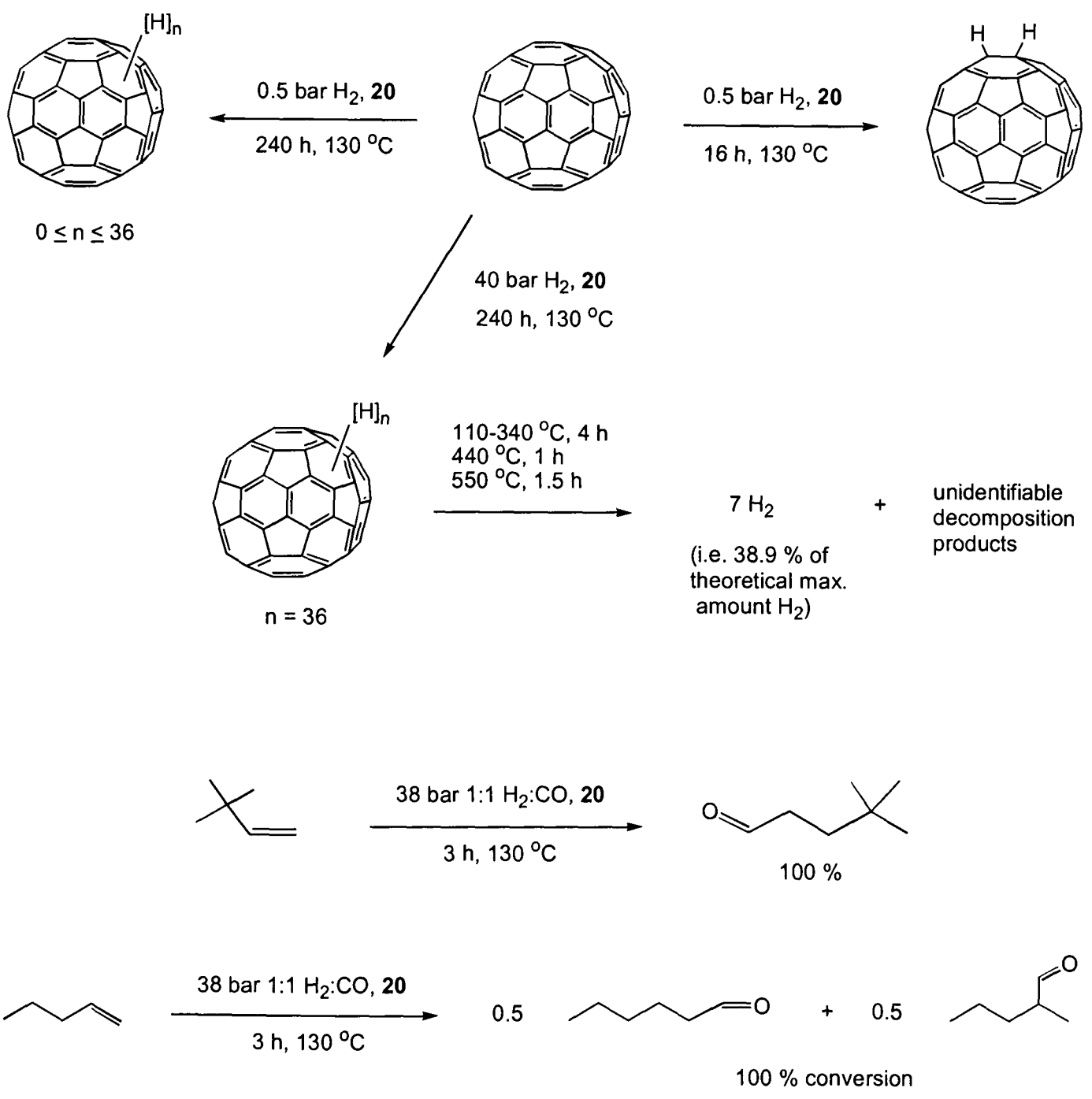

Scheme 4.4 Summary of the new chemistry described in chapter 4.

4.6 References

1) Stephens, A. H. H. *Studies in the Organometallic Chemistry of Buckminsterfullerene C60*; Stephens, A. H. H.; D.Phil. thesis; Christ Church: Oxford, 1996, pp 223.
2) Cohen, R. L.; Wernick, J. H. *Science* **1981**, *214*, 1081.
3) Bowman Jr., R. C. *Materials Science Forum* **1988**, *31*, 197.
4) Shilov, A. L.; Padurets, L. N.; Kost, M. E. *Russ. J. Phys. Chem.* **1985**, *59*, 1103.
5) Chen, P.; Wu, X.; Lin, J.; Tan, K. L. *Science* **1999**, *285*, 91.
6) Chambers, A.; Park, C.; Baker, R. T. K.; Rodriguez, N. M. *J. Phys. Chem. B.* **1998**, *102*, 4253.
7) Dillon, A. C.; Jones, K. M.; Bekkedahl, T. A.; Kiang, C. H.; Bethune, D. S.; Heben, M. J. *Nature (London)* **1997**, *386*, 377.
8) Dresselhaus, M. S.; Williams, K. A.; Eklund, P. C. *MRS Bulletin* **1999**, *November*, 45.
9) Ye, Y.; Ahn, C. C.; Witham, C.; Fultz, B.; Liu, J.; Rinzler, A. G.; Colbert, D.; Smith, K. A.; Smalley, R. E. *Appl. Phys. Lett.* **1999**, *74*, 2307.
10) Liu, C.; Fan, Y. Y.; Liu, M.; Cong, H. T.; Cheng, H. M.; Dresselhaus, M. S. *Science* **1999**, *286*, 1127.
11) Becker, L.; Evans, T. P.; Bada, J. L. *J. Org. Chem.* **1993**, *58*, 7630.
12) Henderson, C. C.; Cahill, P. A. *Science* **1993**, *259*, 1885.
13) Haufler, R. E.; Conceicao, J.; Chibante, L. P. F.; Chai, Y.; Byrne, N. E.; Flanagan, S.; Haley, M. M.; O'Brien, S. C.; Pan, C.; Xiao, Z.; Billups, W. E.; Ciufolini, M. A.; Hauge, R. H.; Margrave, J. L.; Wilson, L. J.; Curl, R. F.; Smalley, R. E. *J. Phys. Chem.* **1990**, *94*, 8634.
14) Banks, M. R.; Dale, M. J.; Gosney, I.; Hodgson, P. K. G.; Jennings, R. C. K.; Jones, A. C.; Lecoultre, J.; Langridge-Smith, P. R. R.; Maier, J. P.; Scrivens, J. H.; Smith, M. J. C.; Smyth, C. J.; Taylor, A. T.; Thorburn, P.; Webster, A. S. *J. Chem. Soc., Chem. Comm.* **1993**, 1149.
15) Okotrub, A. V.; Bulusheva, L. G.; Asanov, I. P.; Lobach, A. S.; Shulga, Y. M. *J. Phys. Chem. A* **1999**, *103*, 716.
16) Darwish, A. D.; Abdul-Sada, A. K.; Langley, G. J.; Kroto, H. W.; Taylor, R.; Walton, D. R. M. *J. Chem. Soc., Perkin Trans. 2* **1995**, 2359.
17) Gerst, M.; Beckhaus, H.-D.; Rüchardt, C.; Campbell, E. E. B.; Tellgmann, R. *Tett. Lett.* **1993**, *34*, 7729.
18) Rüchardt, C.; Gerst, M.; Ebenhoch, J.; Beckhaus, H.-D.; Campbell, E. E. B.; Tellgmann, R.; Schwarz, H.; Weiske, T.; Pitter, S. *Angew. Chem. Int. Ed. Engl.* **1993**, *32*, 584.
19) Jin, C.; Hettich, R.; Compton, R.; Joyce, D.; Blencoe, J.; Burch, T. *J. Phys. Chem.* **1994**, *98*, 4215.
20) Sui, Y.; Qian, J.; Zhang, J.; Zhou, X.; Gu, Z.; Wu, Y.; Fu, H.; Wang, J. *Fullerene science and Technology* **1996**, *4(5)*, 813.
21) Nagashima, H.; Kato, Y.; Yamaguchi, H.; Kimura, E.; Kawanishi, T.; Kato, M.; Saito, Y.; Haga, M.; Itoh, K. *Chem. Lett.* **1994**, 1207.
22) Nagashima, H.; Nakaoka, A.; Tajima, S.; Saito, Y.; Itoh, K. *Chem. Lett.* **1992**, 1361.
23) Yu, R.; Liu, Q.; Tan, K.-L.; Xu, G.-Q.; Ng, S. C.; Chan, H. S. O.; Hor, T. S. A. *J. Chem. Soc., Faraday Trans.* **1997**, *93*, 2207.
24) Coq, B.; Brotons, V.; Planeix, J. M.; de Ménorval, L. C.; Dutartre, R. *Journal of Catalysis* **1998**, *176*, 358.

25) Braun, T.; Wohlers, M.; Belz, T.; Schlögl, R. *Catalysis Letters* **1997**, *43*, 175.
26) Braun, T.; Wohlers, M.; Nowitzke, G.; Wortmann, G.; Uchida, Y.; Pfänder, N.; Schlögl, R. *Catalysis Letters* **1997**, *43*, 167.
27) Wohlers, M.; Herzog, B.; Belz, T.; Bauer, A.; Braun, T.; Rühle, T.; Schlögl, R. *Synthetic Metals* **1996**, *77*, 55.
28) Bond, G. C. *Heterogeneous Catalysis, Principles and Applications*; 2nd ed.; Clarendon Press: Oxford, 1987.
29) Brunauer, S.; Emmett, P. M.; Teller, E. *J. Am. Chem. Soc.* **1938**, *60*, 309.

CHAPTER 5

Experimental Details

5.1 General Experimental Details

5.1.1 Techniques

All manipulations of air- and/or moisture-sensitive materials were performed in an inert atmosphere using either a dual vacuum/argon line and standard Schlenk techniques, or in an inert atmosphere dry box containing nitrogen. The nitrogen was purified by passage over 4 Å molecular sieves, and BASF catalyst. Solvents and solutions were transferred through stainless steel cannulae using a positive pressure of argon. Filtrations were generally performed using modified stainless steel cannulae, which had been fitted with glass fibre filter discs. All glassware and cannulae were dried overnight at 150 °C before use.

5.1.2 Solvents and General Materials

Solvents were pre-dried by standing over 4 Å molecular sieves and then refluxed and distilled under a nitrogen atmosphere from phosphorus pentoxide or calcium hydride (dichloromethane, *ortho*-dichlorobenzene), potassium (benzene), sodium (DME, toluene) or sodium/potassium (1:3 w/w) alloy (40-60 petroleum ether, diethyl ether, pentane, THF).

Deuterated solvents (Aldrich) for NMR studies were refluxed and distilled from potassium metal (C_6D_6, d^8-toluene, d^8-THF), or from calcium hydride (CD_2Cl_2, CD_3CN, d^6-DMSO, d^5-pyridine) and stored in Young's ampoules under nitrogen. NMR solvents were transferred using a teat pipette in an inert atmosphere dry box, or by vacuum distillation using an all-glass apparatus.

5.1.3 Instrumental Methods

Solution NMR spectra were recorded using either a Brüker AM300 (^{1}H 300 MHz, ^{13}C 75.5 MHz, ^{31}P 121.6 MHz) or a Varian UNITY *plus* (^{1}H 500 MHz, ^{13}C 125.7 MHz, ^{31}P 202.4 MHz) spectrometer and are at room temperature unless otherwise stated. Spectra were referenced internally using the residual protio solvent (^{1}H) and solvent (^{13}C) resonances relative to tetramethylsilane (δ = 0 ppm), or externally using 85% H_3PO_4 in D_2O (^{31}P). All chemical shifts are in ppm and coupling constants are in Hz. The 2-D ^{1}H

NOESY, and ^{1}H-^{13}C-$^{n}J_{CH}$ shift correlation spectra were recorded by Dr Daniel Häußinger. All chemical shifts are in ppm and coupling constants are in Hz.

X-ray crystallography was performed by Dr Richard Douthwaite. Crystals were isolated under dinitrogen, covered with a polyfluoroether, and mounted on a glass fibre. Data were collected on an Eraf-Nonius DIP2000 image plate diffractometer with graphite-monochromated Mo Kα radiation (λ = 0.71069 Å). The images were processed with the DENZO and SCALEPACK programs.[1] All solution, refinement, and graphical calculations were performed using the CRYSTALS[2] and CAMERON[3] software packages. Crystal structures were solved by direct methods using the SIR 92 program[4] and were refined by full-matrix least squares on *F*. Non-hydrogen atoms were refined with anisotropic displacement parameters. Hydrogen atoms were generated and allowed to ride on their corresponding carbon atoms with fixed thermal parameters.

Electrospray **mass spectra** were recorded using a Micromass LC TOF electrospray ionisation mass spectrometer. EI mass spectra were recorded using a Micromass Autospec 500 OATOF high resolution mass spectrometer. GCMS chromatographs and spectra were recorded using a MassLab TRIO-1 electron impact GCMS. FAB mass spectrometry was performed by the EPSRC Mass Spectrometry Service at Swansea.

Elemental analyses were performed by the Microanalytical Department of the Inorganic Chemistry Laboratory, Oxford.

IR spectra were recorded on either a Mattson-Polaris or a Perkin Elmer 1710 fourier transform spectrometer.

Powder X-ray diffraction was performed using a Siemens D5000 diffractometer.

Transmission electron microscopy (TEM) was performed by Dr Jeremy Sloan using a JEOL 2010 electron microscope operated at 200 kV, or a JEOL 4000EX HRTEM operated at 400 kV. The 2010 microscope was fitted with a Link Pentafet energy dispersive X-ray (EDX) detector, linked to a Link eXL system, so that analysis of the characteristic X-rays produced by the samples could be undertaken. Samples were ground to a fine powder and

dispersed in AR grade chloroform. The dispersed sample was placed in an ultrasonic bath for 10-20 minutes before a drop of the suspension was placed on a copper grid and placed in the specimen holder. The specimen holder was placed in the side entry port of the microscope and the system was evacuated. After the microscope was tuned the sample was analysed.

5.1.4 Starting Material Preparations

The following materials were prepared following standard literature methods; $NiCl_2(PMe_3)_2$,[5] $NiCl_2(PPh_3)_2$,[6] $NiMe_2(PMe_3)_2$,[7] $AlMe_2OEt$,[8] $Pd(bpy)Cl_2$,[9] $Pd(bpy)Me_2$,[10] $Ni(dppe)Me_2$,[11] $[Rh(cyclooctene)_2Cl]_2$.[12]

Preparation of $NiBr_2(THF)_{1.5}$

A THF solution (100 mL) of $NiBr_2.H_2O$ (5.91 g, 25.0 mmol) was stirred at 50 °C for 2 h in the presence of 4 Å molecular sieves (previously activated at 120 °C under reduced pressure) which gave a dark supernatant and a pink precipitate. The precipitate was isolated by filtration, washed with THF (3 x 10 mL) and residual volatiles removed under reduced pressure. The resulting pink powder was characterised by elemental analysis as $NiBr_2(THF)_{1.5}$. Yield: 6.21 g, 76 %.

Elemental analysis found (calc. for $NiBr_2(THF)_{1.5}$) / % : C 21.81 (22.06), H 3.66 (3.70), Ni 17.75 (17.97), Br 48.33 (48.92).

Preparation of $Ni(bpy)Me_2$

$Ni(bpy)Me_2$ was synthesised in a similar manner to $Ni(bpy)Et_2$, prepared by Yamamoto et al.[13] To a diethyl ether suspension (75 mL) of nickel acetylacetonate (7.82 g, 29.7 mmol) and 2,2'-bipyridyl (11.62 g, 74.4 mmol) cooled to -78 °C was added a diethyl ether solution (5 mL) of dimethylaluminium monoethoxide (9.11 g, 89.2 mmol). The mixture was stirred at -78 °C for 2 h and stirred at room temperature for a further 12 h, which gave a pale green solid and a dark green supernatant. The volatiles were removed under reduced pressure and the residue extracted with diethyl ether (4 x 250 mL). The dark green extracts were combined, concentrated to a volume of 50 mL, and cooled to -80 °C for 12 h to give dark

green crystals which were isolated by filtration. A second crop of dark green crystals was isolated from the mother liquor after standing for 5 days at room temperature. Combined yield: 2.35 g, 32 %.

5.2 Experimental Details for Chapter 2

5.2.1 Preparation of 1-*tert*-Butylimidazole

An aqueous 40 % solution of glyoxal (147 ml, 1.28 mol), an aqueous 37 % solution of formaldehyde (97 ml, 1.28 mol) and propan-2-ol (10 ml) were placed in an addition funnel. A second addition funnel was filled with an aqueous 35 % solution of ammonia (70 ml, 1.28 mol) and *tert*-butylamine (136 ml, 1.28 mol). The contents of both funnels were added dropwise to propan-2-ol (20 ml) over 70 minutes, keeping the temperature below 70 °C, which gave a yellow suspension. Refluxing at 70-80 °C for 2 hours gave a red solution. The propan-2-ol and water were removed using a rotary evaporator (50 °C), and the product distilled under reduced pressure (4 mmHg). The fraction at 50-57 °C, a colourless to pale yellow liquid, was collected. Yield: 77.4 g, 49 %.

5.2.2 Preparation of 1,1'-Methylene*bis*(3-*tert*-butylimidazolium) Diiodide (1)

A mixture of 1-*tert*-butylimidazole (6.00 g, 48.3 mmol), diiodomethane (6.00 g, 22.4 mmol) and 1,4-dioxane (60 mL) was refluxed under reduced pressure for 24 h in an ampoule sealed with a teflon stopcock at 120 °C to give a white precipitate. The mixture was allowed to cool to room temperature. The precipitate was isolated by filtration, washed with ethanol (3 x 200 mL) and residual volatiles removed under reduced pressure. Yield: 8.73 g, 75 %.

5.2.3 Preparation of 1,1'-Methylene*bis*(3-*tert*-butylimidazolium) Dibromide (2)

A mixture of 1-*tert*-butylimidazole (21.00 g, 169.1 mmol), dibromomethane (14.00 g, 80.5 mmol) and 1,4-dioxane (100 mL) was refluxed under reduced pressure for 24 h in an ampoule sealed with a teflon stopcock at 150 °C to give a white precipitate. The mixture was allowed to cool to room temperature. The precipitate was isolated by filtration, washed with 1,4-dioxane (2 x 100 mL) and 40-60 petroleum ether (2 x 100 mL) and residual volatiles removed under reduced pressure. Yield: 31.90 g, 94 %.

5.2.4 Preparation of 1,1'-(1,2-Ethylene)*bis*(3-*tert*-butylimidazolium) Dibromide (3)

A mixture of 1-*tert*-butylimidazole (21.00 g, 169.1 mmol), 1,2-dibromoethane (15.13 g, 80.5 mmol) and 1,4-dioxane (100 mL) was refluxed under reduced pressure for 24 h in an ampoule sealed with a teflon stopcock at 150 °C to give a white precipitate. The mixture was allowed to cool to room temperature. The precipitate was isolated by filtration, washed with 1,4-dioxane (2 x 100 mL) and 40-60 petroleum ether (2 x 100 mL) and residual volatiles removed under reduced pressure. Yield: 33.70 g, 96 %.

5.2.5 Preparation of $^{tBu}CC^{meth}$ (4)

To a solid mixture of 1,1'-methylene*bis*(3-*tert*-butylimidazolium)dibromide (**2**) (12.90 g, 30.6 mmol) and potassium *bis*(trimethylsilyl)amide (13.40 g, 67.2 mmol) was added THF (350 mL) and the resulting white suspension stirred for 12 h at 25 °C to give a yellow suspension. The volatiles were removed under reduced pressure and the residue extracted with 40-60 petroleum ether (3 x 100 mL) to give an orange solution. The solution was cooled to -80 °C giving a white powder which was isolated by filtration. Yield: 5.00 g, 63 %.

5.2.6 Preparation of $^{tBu}CC^{eth}$ (5)

To a solid mixture of 1,1'-ethylene*bis*(3-*tert*-butylimidazolium)dibromide (**3**) (15.00 g, 34.4 mmol) and potassium *bis*(trimethylsilyl)amide (15.10 g, 75.7 mmol) was added THF (350 mL) and the resulting white suspension stirred for 12 h at 25 °C to give a yellow suspension. The volatiles were removed under reduced pressure and the residue extracted with THF (3 x 100 mL) to give an orange solution. The solution was cooled to -80 °C giving a white powder which was isolated by filtration. Yield: 5.700 g, 60 %.

5.2.7 Stability of $^{tBu}CC^{meth}$ (4) and $^{tBu}CC^{eth}$ (5) in C_6D_6 and CD_2Cl_2

Dry, degassed C_6D_6 (0.6 mL) solutions of $^{tBu}CC^{meth}$ (**4**) (0.020 g, 0.08 mmol) and $^{tBu}CC^{eth}$ (**5**) (0.020 g, 0.07 mmol) in flame-sealed NMR tubes were refluxed for 16 h at temperatures

within the range 90-140 °C before cooling to room temperature and recording the ^{1}H NMR spectra. The spectra of (**4**) and (**5**) were unchanged after refluxing at temperatures up to and including 100 °C. Decomposition products were observed after refluxing above this temperature: a 1:1 mixture of the free carbene and signals consistent with 1-*tert*-butylimidazole was observed after 16 h at 140 °C.

In contrast, ^{1}H NMR spectroscopy of $^{tBu}CC^{meth}$ (**4**) and $^{tBu}CC^{eth}$ (**5**) in dry, degassed CD_2Cl_2 showed that both compounds completely decomposed within minutes at 25 °C.

5.2.8 Preparation of $[Ni(^{tBu}CC^{meth})_2][Br]_2$ (6)

To an orange DME suspension (100 mL) of $NiBr_2$(DME) (1.000 g, 3.24 mmol) cooled to 0 °C was added 2 equiv of a similarly cooled DME solution (30 mL) of $^{tBu}CC^{meth}$ (**4**) (1.687 g, 6.48 mmol). The mixture was allowed to warm to room temperature over 2 h and stirred at room temperature for a further 2 h which gave a yellow supernatant and a pale yellow precipitate. The precipitate was isolated by filtration, washed with DME (2 x 30 mL) and then recrystallised from methanol (20 mL) at -30°C. Crude yield: 0.657 g, 27 %.

5.2.9 Preparation of $[(^{tBu}CC^{meth})NiCl(PMe_3)]Cl$ (7)

To a deep red toluene solution (20 mL) of $Ni(PMe_3)_2Cl_2$ (2.164 g, 7.68 mmol) was added a toluene solution (20 mL) of $^{tBu}CC^{meth}$ (**4**) (2.000 g, 7.68 mmol) which immediately gave a red supernatant and yellow precipitate. The precipitate was isolated by filtration, washed with toluene (2 x 15 mL) and diethyl ether (2 x 15 mL) and residual volatiles removed under reduced pressure. Yield: 3.400 g, 95 %.

5.2.10 Preparation of $[(^{tBu}CC^{meth})NiCl(PMe_3)][BPh_4]$ (8)

To a solid mixture of $Tl[BPh_4]$ (0.478 g, 0.91 mmol) and $[(^{tBu}CC^{meth})NiCl(PMe_3)]Cl$ (**7**) (0.425 g, 0.91 mmol) was added dichloromethane (30 mL) and the resulting yellow suspension stirred for 2 h at room temperature. Filtration of the suspension gave a yellow solution to which pentane (40 mL) was added to give a yellow precipitate. The precipitate

was isolated by filtration, washed with pentane (3 x 15 mL) and residual volatiles removed under reduced pressure. Yield: 0.350 g, 51 %.

5.2.11 Preparation of [(^{tBu}CC^{eth})NiCl(PMe$_3$)]Cl (9)

To a deep red solution (20 mL) of Ni(PMe$_3$)$_2$Cl$_2$ (1.170 g, 4.15 mmol) was added a toluene solution (20 mL) of ^{tBu}CC^{eth} (**5**) (1.140 g, 4.15 mmol) which immediately gave a yellow supernatant and yellow precipitate. The precipitate was isolated by filtration, washed with toluene (2 x 15 mL) and diethyl ether (2 x 15 mL) and residual volatiles were removed under reduced pressure. Yield: 1.700 g, 85 %.

5.2.12 Preparation of [(^{tBu}CC^{eth})NiCl(PMe$_3$)][BPh$_4$] (10)

To a solid mixture of Tl[BPh$_4$] (0.474 g, 0.91 mmol) and [(^{tBu}CC^{eth})NiCl(PMe$_3$)]Cl (**9**) (0.435 g, 0.91 mmol) was added dichloromethane (30 mL) and the resulting yellow suspension stirred for 2 h at room temperature. Filtration of the suspension gave a yellow solution to which pentane (40 mL) was added to give a yellow precipitate. The precipitate was isolated by filtration, washed with pentane (3 x 15 mL) and residual volatiles removed under reduced pressure. Yield: 0.542 g, 78 %.

5.2.13 Preparation of [Ni(^{tBu}CC^{meth})$_2$][Cl]$_2$ (11): Method 1

To a deep red *ortho*-dichlorobenzene solution (20 mL) of Ni(PMe$_3$)$_2$Cl$_2$ (0.216 g, 0.77 mmol) was added 2 equiv of an *ortho*-dichlorobenzene solution (20 mL) of ^{tBu}CC^{meth} (**4**) (0.400 g, 1.54 mmol) which gave a yellow supernatant and pale yellow precipitate. The mixture was stirred at room temperature for 2 h and then diethyl ether (40 mL) added to precipitate more yellow powder. The precipitate was isolated by filtration, washed with diethyl ether (3 x 15 mL) and residual volatiles removed under reduced pressure. Yield: 0.458 g, 92 %.

5.2.14 Preparation of $[Ni(^{tBu}CC^{meth})_2][Cl]_2$ (11): Method 2

To a yellow *ortho*-dichlorobenzene solution (20 mL) of (**7**) (0.466 g, 1.00 mmol) was added an *ortho*-dichlorobenzene solution (20 mL) of $^{tBu}CC^{meth}$ (**4**) (0.260 g, 1.00 mmol) which gave a yellow supernatant and pale yellow precipitate. Work up was performed as in method 1. Yield: 0.566 g, 87 %.

5.2.15 Preparation of $[Ni(^{tBu}CC^{meth})_2][Cl]_2$ (11): Method 3

To a yellow *ortho*-dichlorobenzene solution (20 mL) of (**9**) (0.720 g, 1.50 mmol) was added 2 equiv of an *ortho*-dichlorobenzene solution (20 mL) of $^{tBu}CC^{meth}$ (**4**) (0.820 g, 3.15 mmol) which gave a yellow supernatant and pale yellow precipitate. Work up was performed as in method 1. Yield: 0.880 g, 90 %.

Attempts to Synthesise $Ni(^{tBu}CC^{meth})X_2$ and $Ni(^{tBu}CC^{eth})Cl_2$ (X = Cl, Br)

5.2.16 Reaction of $^{tBu}CC^{meth}$ (4) with $NiBr_2(THF)_{1.5}$

To a purple THF solution (350 mL) of $NiBr_2(THF)_{1.5}$ (1.37 g, 4.19 mmol) was added a THF solution (50 mL) of $^{tBu}CC^{meth}$ (**4**) (1.12 g, 4.30 mmol) which gave an orange supernatant and beige precipitate. The precipitate was isolated by filtration, washed with THF (3 x 15 mL) and the residual volatiles removed under reduced pressure. The resulting beige powder was insoluble in non polar organic solvents, THF and dichloromethane, and soluble in DMSO, acetonitrile, and pyridine. Yield: 0.605 g (29 % based on an empirical formula $C_{15}H_{24}N_4NiBr_2$).

Elemental analysis found (calc. for $C_{15}H_{24}N_4NiBr_2$) / % : C 37.25 (37.62), H 5.36 (5.05), N 11.42 (11.70)

^1H NMR spectroscopy (d^6-DMSO and CD_3CN) showed a mixture of products (many peaks observed in the *tert*-butyl region (δ 1.0-2.5) and the methylene bridge / imidazole ring proton region (δ 6.5-8.5)).

FAB mass spectrum (possible fragment ions in parentheses):

m/z 753, 659 [NiBr(^{tBu}CC^{meth})$_2$], 578 [Ni(^{tBu}CC^{meth})$_2$ – H], 535 [Ni_2Br_2(^{tBu}CC^{meth}) – H], 399 [Ni(^{tBu}CC^{meth})Br], 318 [Ni(^{tBu}CC^{meth}) – H], 261 [^{tBu}CC^{meth}].
A molecular ion peak for (^{tBu}CC^{meth})$NiBr_2$ at m/z 479 was not observed
NB. ^{1}H NMR spectroscopy (d^6-DMSO) of the orange supernatant, after removal of the volatiles under reduced pressure, showed a mixture of products similar to the beige precipitate.

Reaction of the Beige Precipitate with Lewis Bases:

(i) PMe_3

To an *ortho*-dichlorobenzene suspension (20 mL) of the beige precipitate (0.135 g, 0.28 mmol based on an empirical formula $C_{15}H_{24}N_4NiBr_2$) was added an *ortho*-dichlorobenzene solution (20 mL) of PMe_3 (0.021 g, 0.28 mmol) to give an orange solution, which turned dark green before the addition was complete. Filtration of the mixture gave a dark green solution to which pentane (80 mL) was added to give a yellow precipitate. The precipitate was isolated by filtration, washed with pentane (3 x 15 mL) and residual volatiles removed under reduced pressure. The resulting yellow powder was soluble in dichloromethane, DMSO and acetonitrile. Yield: 0.043 g.

^{1}H NMR (d^6-DMSO): δ 1.26 (d, 9H, $^2J_{PH}$ = 10 Hz, P(CH_3)$_3$), 1.77 (s, 9H, C(CH_3)$_3$), 1.82 (s, 9H, C(CH_3)$_3$), 6.51 (d, 1H, $^2J_{HH}$ = 13 Hz, N(CH_2)N), 7.10 (d, 1H, $^2J_{HH}$ = 13 Hz, N(CH_2)N), 7.51 (vt, 1H, $^3J_{HH}$ = 2 Hz, $^5J_{PH}$ = 2 Hz, NC*H*), 7.63 (d, 1H, $^3J_{HH}$ = 2 Hz, NC*H*), 7.71 (d, 1H, $^3J_{HH}$ = 2 Hz, NC*H*), 7.81 (d, 1H, $^3J_{HH}$ = 2 Hz, NC*H*), corresponding to [(^{tBu}CC^{meth})NiBr(PMe_3)]Br by analogy with the chloride compound **7**. Impurity peaks were present in the *tert*-butyl region (δ 1.0-2.5), methylene bridge and imidazole ring proton region (δ 6.5-8.3) and a peak at δ 9.83 (imidazolium salt). Estimated purity based on ^{1}H NMR spectroscopy = 60 %.
Elemental analysis found (calc. for [(^{tBu}CC^{meth})NiBr(PMe_3)]Br) / % : C 39.26 (38.96), H 5.67 (5.99), N 10.04 (10.10).

(ii) d^5-Pyridine

^{1}H NMR (d^5-pyridine) of the beige precipitate was consistent with the formation of the compound [(^{tBu}CC^{meth})NiBr(C_5D_5N)]Br : δ 1.34 (s, 9H, C(C*H*$_3$)$_3$), 2.06 (s, 9H, C(C*H*$_3$)$_3$), 7.32 (d, 1H, $^3J_{HH}$ = 2 Hz, NC*H*), 7.42 (d, 1H, $^3J_{HH}$ = 2 Hz, NC*H*), 8.20 (d, 1H, $^2J_{HH}$ = 13 Hz, N(C*H*$_2$)N), 8.46 (d, 1H, $^3J_{HH}$ = 2 Hz, NC*H*), 8.81 (d, 1H, $^2J_{HH}$ = 13 Hz, N(C*H*$_2$)N), 8.89 (d, 1H, $^3J_{HH}$ = 2 Hz, NC*H*). Estimated purity = 90 %.

5.2.17 High Dilution Reaction of ^{tBu}CC^{meth} (4) with $NiBr_2(THF)_{1.5}$

To a THF solution (500 mL) of ^{tBu}CC^{meth} (**4**) (0.732 g, 2.81 mmol) was added a purple THF solution (500 mL) of $NiBr_2(THF)_{1.5}$ (0.872 g, 2.67 mmol) which gave a green supernatant and yellow precipitate. The precipitate was isolated by filtration, washed with THF (3 x 15 mL) and residual volatiles removed under reduced pressure. The resulting yellow powder was insoluble in non-polar organic solvents, THF and dichloromethane, but soluble in DMSO and SO_2. Yield: 0.611 g.

^{1}H NMR (d^6-DMSO): δ 1.31 (s, 18H, C(C*H*$_3$)$_3$), 6.84 (s, 2H, N(C*H*2)N), 7.59 (d, 2H, $^3J_{HH}$ = 2 Hz, NC*H*), 7.88 (d, 2H, $^3J_{HH}$ = 2 Hz, NC*H*). 0.5 equiv THF and < 0.1 equiv imidazolium salt and were also present. Estimated purity based on ^{1}H NMR spectroscopy = 90%.

^{13}C{^{1}H} NMR (d^6-DMSO): δ 30.4 (C(*C*H$_3$)$_3$), 58.7 (*C*(CH$_3$)$_3$), 63.6 (N(*C*H$_2$)N), 121.9 (N*C*H), 123.6 (N*C*H), 168.0 (N*C*N).

Elemental analysis found (calc. for C15H24N4NiBr$_2$(THF)$_{0.5}$) / % : C 41.87 (39.65), H 6.11 (5.48), N 11.72 (10.88), Ni 10.00 (11.40), Br 29.43 (31.03).

FAB mass spectrum (possible fragment ions in parentheses): m/z 753, 733, 669, 652, 578 [Ni(^{tBu}CC^{meth})$_2$ – H], 521, 399 [Ni(^{tBu}CC^{meth})Br], 318 [Ni(^{tBu}CC^{meth}) – H], 261 [^{tBu}CC^{meth}]. Molecular ion peaks for (^{tBu}CC^{meth})NiBr$_2$ (m/z 479) or for the bridging dimer [Br$_2$Ni(μ-^{tBu}CC^{meth})$_2$NiBr$_2$] implied by ^{1}H NMR δ 6.84 (**singlet**, 2H, N(C*H*$_2$)N) (m/z 958) were not observed.

Reaction of the Yellow Precipitate with Ethanol:

The yellow precipitate (0.230 g) was stirred in ethanol (45 mL) at 25 °C which gave a yellow solution after 10 mins. The volatiles were removed under reduced pressure, which gave a yellow solid. ^{1}H NMR was consistent with the formation of $[Ni(^{tBu}CC^{meth})_2][Br]_2$ (**6**):

^{1}H NMR (d^6-DMSO): δ 1.32 (s, 36H, C(CH_3)$_3$), 6.83 (d, 2H, $^{2}J_{HH}$ = 13 Hz, N(CH_2)N), 6.97 (d, 2H, $^{2}J_{HH}$ = 13 Hz, N(CH_2)N), 7.60 (d, 4H, $^{3}J_{HH}$ = 2 Hz, NC*H*), 7.91 (d, 4H, $^{3}J_{HH}$ = 2 Hz, NC*H*).

5.2.18 Reaction of $^{tBu}CC^{meth}$ (4) with $NiCl_2(PPh_3)_2$

To a dark red THF solution (20 mL) of $NiCl_2(PPh_3)_2$ (1.118 g, 1.71 mmol) was added a THF solution (20 mL) of $^{tBu}CC^{meth}$ (**4**) (0.445 g, 1.71 mmol) which gave a green supernatant and light green precipitate. The precipitate was isolated by filtration, washed with toluene (2 x 15 mL) and diethyl ether (2 x 15 mL) and residual volatiles removed under reduced pressure. The resulting green powder was insoluble in non-polar organic solvents, THF and dichloromethane, soluble in DMSO and partially soluble in CH_3CN. Yield: 0.392 g.

^{1}H NMR spectroscopy (d^6-DMSO and CD_3CN) showed a mixture of products (many peaks observed in the *tert*-butyl region (δ 1.0-2.5) and the methylene bridge / imidazole ring proton region (δ 6.5-8.5).
Elemental analysis found (calc. for $C15H24N4NiCl_2$) / % : C 39.44 (46.20), H 5.63 (6.20), N 10.65 (14.37), Ni 16.61 (15.05), Cl 20.46 (18.18).

Turquoise crystals were grown upon standing an acetonitrile solution of the green powder for 1 week, but were not of sufficient quality for X-ray crystal structure determination.
^{1}H NMR spectroscopy (d^6-DMSO) of the green supernatant, after removal of the volatiles under reduced pressure, showed a mixture of products similar to the light green precipitate.

Reaction of the Green Precipitate with PMe_3:

To a dichloromethane suspension (20 mL) of the green precipitate (0.227 g, 0.58 mmol based on an empirical formula $C_{15}H_{24}N_4NiCl_2$) was added PMe_3 (60 μL) (0.044 g, 0.58 mmol) to give an orange solution, which turned dark green after the addition was complete. Removal of the volatiles under reduced pressure gave a dark green solid which was washed with diethyl ether (3 x 15 mL) to give a yellow powder. Residual volatiles were removed under reduced pressure. Yield: 0.190 g.

^{1}H NMR (d^6-DMSO) corresponded to [(^{tBu}CC^{meth})NiCl(PMe_3)]Cl (**7**). The dominant impurity was diimidazolium salt (δ 1.58 (s, 9H, C(C*H*$_3$)$_3$), 6.77 (s, 2H, N(C*H*$_2$)N), 8.15 (d, 2H, $^3J_{HH}$ = 2 Hz, NC*H*), 8.42 (d, 2H, $^3J_{HH}$ = 2 Hz, NC*H*), 10.29 (s, 2H, N(C*H*)N)) although additional impurity peaks were present in the *tert*-butyl region (δ 1.0-2.5), methylene bridge and imidazole ring proton region (δ 6.5-8.3). Estimated purity based on ^{1}H NMR spectroscopy = 50 %.

Elemental analysis found (calc. for [(^{tBu}CC^{meth})NiCl(PMe_3)]Cl) / % : C 45.65 (46.39), H 6.47 (7.14), N 11.93 (12.02), Ni 9.94 (12.60), P 3.13 (6.65), Cl 15.86 (15.21).

5.2.19 Reaction of ^{tBu}CC^{eth} (5) with $NiCl_2(PPh_3)_2$

To a dark red THF solution (20 mL) of $NiCl_2(PPh_3)_2$ (1.120 g, 1.71 mmol) was added a THF solution (20 mL) of ^{tBu}CC^{eth} (**5**) (0.470 g, 1.71 mmol) which gave a brown supernatant and grey precipitate. The precipitate was isolated by filtration, washed with toluene (2 x 15 mL) and diethyl ether (2 x 15 mL) and residual volatiles removed under reduced pressure. The resulting grey powder was insoluble in non-polar organic solvents, THF and dichloromethane, soluble in DMSO and partially soluble in CH_3CN. Yield: 0.678 g.
^{1}H NMR spectroscopy (d^6-DMSO and CD_3CN) showed a mixture of products (many peaks observed in the *tert*-butyl region (δ 1.0-2.5) and the ethylene bridge / imidazole ring proton region (δ 6.0-8.5).

Elemental analysis found (calc. for C16H26N4NiCl$_2$) / % : C 41.94 (47.57), H 5.90 (6.49), N 10.90 (13.87), Ni 15.48 (14.53), Cl 20.30 (17.55).

Single turquoise crystals were grown from an acetonitrile solution of the grey powder after 1 week. X-ray crystal structure determination showed this compound to be 1,1'-(1,2-ethylene)*bis*(3-*tert*-butylimidazolium)tetrachloronickelate(II).

^{1}H NMR spectroscopy (d^6-DMSO) of the brown supernatant, after removal of the volatiles under reduced pressure, showed a mixture of products similar to the grey precipitate.

Attempts to Synthesise $[Ni(^{tBu}CC^{eth})_2][X]_2$ (X = Cl, Br)

5.2.20 Reaction of $^{tBu}CC^{eth}$ (5) with $NiCl_2(PMe_3)_2$

To a deep red *ortho*-dichlorobenzene solution (20 mL) of $Ni(PMe_3)_2Cl_2$ (0.257 g, 0.91 mmol) was added an *ortho*-dichlorobenzene solution (20 mL) of $^{tBu}CC^{meth}$ (**4**) (0.530 g, 1.93 mmol) which gave an orange solution after 10 mL of the $^{tBu}CC^{meth}$ (**4**) solution had been added. The solution remained orange after the addition was completed. The mixture was stirred for 16 h and no precipitate was formed. Diethyl ether (100 mL) was added which gave a pale yellow supernatant and a yellow precipitate. The precipitate was isolated by filtration, washed with diethyl ether (2 x 15 mL) and residual volatiles removed under reduced pressure. ^{1}H NMR spectroscopy (d^6-DMSO) showed that the product was pure $[(^{tBu}CC^{eth})NiCl(PMe_3)]Cl$ (**9**). Yield: 0.398 g, 91 %.

5.2.21 Reaction of $^{tBu}CC^{eth}$ (5) with $NiBr_2$(DME)

To an orange DME suspension (20 mL) of $NiBr_2$(DME) (0.680 g, 2.20 mmol) cooled to 0 °C was added 2 equiv of a DME solution (20 mL) of $^{tBu}CC^{eth}$ (**5**) (1.330 g, 4.85 mmol). The mixture was allowed to warm to room temperature over 2 h and stirred at room temperature for a further 2 h which gave a yellow supernatant and a yellow precipitate. The precipitate was isolated by filtration, washed with diethyl ether (2 x 15 mL) and residual volatiles removed under reduced pressure.

^{1}H NMR spectroscopy (CD_3OD) showed a mixture of products. Several peaks were observed in the *tert*-butyl region (δ 1.0-2.5) and imidazole ring proton region (δ 6.5-8.5). No ethylene bridge proton resonances were observed (the compound $[(^{tBu}CC^{eth})_2Ni][Br]_2$

would be expected to have at least two complex multiplets between δ 2.5 and δ 7.0 corresponding to ethylene bridge protons).

Attempts to Synthesise $[Ni(^{tBu}CC^{meth})(^{tBu}CC^{eth})][Cl]_2$

5.2.22 Attempted Reaction of $[(^{tBu}CC^{meth})NiCl(PMe_3)]Cl$ (7) with $^{tBu}CC^{eth}$ (5)

To an orange *ortho*-dichlorobenzene solution (20 mL) of $[(^{tBu}CC^{meth})NiCl(PMe_3)]Cl$ (**7**) (0.932 g, 2.00 mmol) was added an *ortho*-dichlorobenzene solution (20 mL) of $^{tBu}CC^{eth}$ (**5**) (0.549 g, 2.00 mmol) which gave an orange solution. The mixture was stirred at room temperature for 2 h and then diethyl ether (40 mL) added which gave a pale yellow supernatant and a yellow precipitate. The precipitate was isolated by filtration, washed with diethyl ether (3 x 15 mL) and residual volatiles removed under reduced pressure.

^1H NMR spectroscopy (d^6 - DMSO) showed that the yellow precipitate was the starting material $[(^{tBu}CC^{meth})NiCl(PMe_3)]Cl$ (**7**).

5.2.23 Reaction of $[(^{tBu}CC^{eth})NiCl(PMe_3)]Cl$ (9) with $^{tBu}CC^{meth}$ (4)

To an orange *ortho*-dichlorobenzene solution (20 mL) of $[(^{tBu}CC^{eth})NiCl(PMe_3)]Cl$ (**9**) (0.480 g, 1.00 mmol) was added an *ortho*-dichlorobenzene solution (20 mL) of $^{tBu}CC^{meth}$ (**4**) (0.260 g, 1.00 mmol) which gave an orange supernatant and a small amount of pale yellow precipitate. The mixture was stirred at room temperature for 2 h and then diethyl ether (40 mL) added to precipitate more yellow powder. The precipitate was isolated by filtration, washed with diethyl ether (3 x 15 mL) and residual volatiles removed under reduced pressure.

^1H NMR spectroscopy (d^6 - DMSO) showed that the yellow precipitate was a 1:1 mixture of $[(^{tBu}CC^{meth})_2Ni][Cl]_2$ (**11**) and the starting material $[(^{tBu}CC^{eth})NiCl(PMe_3)]Cl$ (**9**), and that the diethyl ether / *ortho*-dichlorobenzene supernatant contained the by-product $^{tBu}CC^{eth}$ (**5**).

Attempts to Reduce Ni(II) $^{tBu}CC^{meth}$ Compounds to Ni(0) Derivatives:

5.2.24 Reaction of $^{tBu}CC^{meth}$ (4) with $NiBr_2$(DME) and Na/Hg Amalgam

To a DME solution (20 mL) of $^{tBu}CC^{meth}$ (**4**) (1.687 g, 6.48 mmol) stirred in the presence of excess Na/Hg amalgam was added an orange DME suspension (20 mL) of $NiBr_2$(DME) (1.000 g, 3.24 mmol). The mixture was stirred for 16 h at 25 °C to give a red suspension, which was decanted from the Na/Hg residue. The volatiles were removed under reduced pressure to give a dark red solid which was extracted in turn with 40-60 petroleum ether (2 x 15 mL) and toluene (2 x 15 mL). The volatiles were removed under reduced pressure to give orange and red oils respectively.

^{1}H NMR spectroscopy (C_6D_6) of the petroleum ether extract showed a 2:1 mixture of free $^{tBu}CC^{meth}$ and free 1-*tert*-butylimidazole respectively.
^{1}H NMR spectroscopy (C_6D_6) of the toluene extract showed a broad band of peaks in the *tert*-butyl region (δ 1.0-2.5) and a broad band in the methylene bridge / imidazole ring proton region (δ 5.5-8.0), as well as a mixture of free $^{tBu}CC^{meth}$ and free 1-*tert*-butylimidazole.

5.2.25 Reaction of $[Ni(^{tBu}CC^{meth})_2][Cl]_2$ (11) with K

To a K mirror (0.100 g, 2.56 mmol) was added a yellow THF suspension (20 mL) of $[Ni(^{tBu}CC^{meth})_2][Cl]_2$ (**11**) (0.400 g, 0.62 mmol). The mixture was stirred for 16 h at 25 °C to give a red suspension. The volatiles were removed under reduced pressure to give a dark red solid which was extracted in turn with 40-60 petroleum ether (2 x 15 mL), toluene (2 x 15 mL), and THF (2 x 15 mL). The volatiles were removed under reduced pressure which gave an orange oil in each case.

^{1}H NMR spectroscopy (C_6D_6) of the petroleum ether extract showed a mixture of free $^{tBu}CC^{meth}$ and 1-*tert*-butylimidazole. ^{1}H NMR spectroscopy of the toluene extract showed the same, but with a broad band of peaks in the *tert*-butyl region (δ 1.0-2.5) and in the methylene bridge / imidazole ring proton region (δ 5.5-8.0). ^{1}H NMR spectroscopy (C_6D_6) of the THF extract showed the broad bands and no $^{tBu}CC^{meth}$ or 1-*tert*-butylimidazole.

5.2.26 Attempted Reduction of $[Ni(^{tBu}CC^{meth})_2][Cl]_2$ (11) with Zn

To a solid mixture of $[Ni(^{tBu}CC^{meth})_2][Cl]_2$ (**11**) (0.377 g, 0.51 mmol) and Zn powder (0.050 g, 0.76 mmol) was added THF (20 mL) which gave a pale yellow suspension. The mixture was stirred at 16 h at 25 °C. The volatiles were removed under reduced pressure and the yellow residue extracted in turn with 20 mL pentane, diethyl ether, toluene and THF. Removal of the volatiles under reduced pressure showed no significant extraction had occurred in each case. Extraction with methanol (10 mL) gave a yellow solution which, after removal of the volatiles under reduced pressure, was shown by ^{1}H NMR spectroscopy (CD_3OD) to be the starting material $[Ni(^{tBu}CC^{meth})_2][Cl]_2$ (**11**).

5.2.27 Attempted Reduction of $[(^{tBu}CC^{meth})NiCl(PMe_3)]Cl$ (7) with Zn

To a solid mixture of $[(^{tBu}CC^{meth})NiCl(PMe_3)]Cl$ (7) (0.260 g, 0.56 mmol) and Zn powder (0.055 g, 0.84 mmol) was added THF (20 mL) which gave a yellow suspension. The mixture was stirred for 16 h at 25 °C. The volatiles were removed under reduced pressure and the yellow residue extracted in turn with 20 mL pentane, diethyl ether, toluene and THF. Removal of the volatiles under reduced pressure showed no significant extraction had occurred in each case. Extraction with *ortho*-dichlorobenzene (20 mL) gave an orange solution to which pentane (40 mL) was added to precipitate a yellow powder, shown by ^{1}H NMR spectroscopy (d^6-DMSO) to be the starting material $[(^{tBu}CC^{meth})NiCl(PMe_3)]Cl$ (7).

5.2.28 Attempted Ethylene Polymerisation using $[(^{tBu}CC^{meth})NiCl(PMe_3)]Cl$ (7), and the Product of $^{tBu}CC^{meth}$ (4) + $NiBr_2(THF)_{1.5}$, as Co-Catalysts with MAO

A vacuum dried Fischer-Porter reactor was admitted with ethylene gas dried by passage through a column of 4 Å molecular sieves. Toluene (100 mL) was added, the absolute ethylene pressure increased to 2 bar and the solution stirred at 25 °C until saturated with ethylene. The stirring was then stopped so that a minimum of ethylene was released from solution on reducing the pressure to enable the methylaluminoxane (MAO) and the co-catalyst solutions to be added quickly, *via* cannulae, to the reactor. The ethylene pressure was then increased back to 2 bar, and the experiment started. The reaction mixture was stirred vigorously at 25 °C for 16 h and then at 60 °C for 16 h. The mixture was then

allowed to cool to room temperature before releasing the pressure and quenching with an excess of HCl in methanol. No polymer was observed in both cases, using 10 μmol Ni with a 100-fold molar excess of Al.

5.3 Experimental Details for Chapter 3

5.3.1 Preparation of [(μ-$^{tBu}CC^{meth}$){Ni(PMe_3)Me_2}$_2$] (12)

To a toluene solution (20 mL) of $NiMe_2(PMe_3)_2$ (0.381 g, 1.58 mmol) cooled to -78 °C was added a similarly cooled toluene solution (20 mL) of $^{tBu}CC^{meth}$ (**4**) (0.412 g, 1.58 mmol). The mixture was allowed to warm to 0 °C over 2 h and stirred at 0 °C for a further 4 h. The volatiles were removed under reduced pressure and the residue extracted with pentane (2 x 30 mL) to give a pale orange solution. The extract was concentrated to 10 mL and cooled to -20 °C which gave pale orange crystals of [(μ-$^{tBu}CC^{meth}$){Ni(PMe_3)Me_2}$_2$].C_5H_{12}. A second crop of crystals was isolated at -20 °C by concentration of the mother liquor. Combined yield: 0.150 g, 30 %.

5.3.2 Attempted Preparation of Ni($^{tBu}CC^{meth}$)Me_2

To a dark green toluene solution (20 mL) of Ni(bpy)Me_2 (0.376 g, 1.53 mmol) at -78 °C was added a similarly cooled toluene solution (20 mL) of $^{tBu}CC^{meth}$ (**4**) (0.399 g, 1.53 mmol) which immediately gave a brown-red supernatant and a brown precipitate. Slow evolution of gas was observed as the mixture was allowed to warm to room temperature over 2 h and stirred at room temperature for a further 12 h. The volatiles were removed under reduced pressure which gave a dark green/brown oil. Extraction with diethyl ether (40 mL) dissolved most of the residue to give a green solution, from which a product could not be crystallised after concentrating and cooling to -80 °C. ^{1}H NMR spectroscopy (C_6D_6) of the extract, after removal of the volatiles under reduced pressure, showed a mixture of unidentifiable products (broad bands of peaks were observed in both the *tert*-butyl region (δ 1.0-2.5) and methylene bridge/imidazole ring proton region (δ 5.5-8.0)).

5.3.3 NMR Tube Reaction Between Ni(bpy)Me_2 and $^{tBu}CC^{meth}$ (4)

d^8-Toluene (0.6 mL) was condensed on to a solid mixture of Ni(bpy)Me_2 (0.018 g, 0.073 mmol) and $^{tBu}CC^{meth}$ (**4**) (0.019 g, 0.073 mmol) at -173 °C and the Pyrex NMR tube flame-sealed under reduced pressure. The mixture was warmed to -78 °C and the reaction

monitored by ^{1}H NMR spectroscopy over 10 hours, allowing to equilibrate at each of the following temperatures in turn: -75, -65, -50, -40, -30, -20, -10, 0, +10, +25 °C and +25 °C after 24 h. The product Ni(^{tBu}CC^{meth})Me$_2$ (δ 0.18 (s, 6H, CH_3), 1.63 (s, 18H, C(CH_3)$_3$), 4.47 (d, 1H, $^{2}J_{HH}$ = 13 Hz, N(CH_2)N), 6.17 (d, 2H, $^{3}J_{HH}$ = 2 Hz, NC*H*), 6.25 (d, 2H, $^{3}J_{HH}$ = 2 Hz, NC*H*), 6.62 (d, 1H, $^{2}J_{HH}$ = 13 Hz, N(CH_2)N)) was identified between -50 and +25 °C in various low concentrations relative to free bpy (δ 6.73 (m), 7.24 (m), 8.50 (m), 8.65 (m)), the formation of which was also only observed above -50 °C, unreacted ^{tBu}CC^{meth} (**4**) and decomposition products. The starting material Ni(bpy)Me$_2$ was not observed. After 24 h at +25 °C the product Ni(^{tBu}CC^{meth})Me$_2$ could not be observed in the ^{1}H NMR spectrum.

5.3.4 Preparation of Ni(^{tBu}CC^{eth})Me$_2$ (13)

To a dark green toluene solution (20 mL) of Ni(bpy)Me$_2$ (0.435 g, 1.78 mmol) cooled to -78 °C was added a similarly cooled toluene solution (20 mL) of ^{tBu}CC^{eth} (**5**) (0.488 g, 1.78 mmol) which gave a dark green solution. The mixture was allowed to warm to room temperature over 2 h and stirred at room temperature for a further 14 h to give a golden solution. The solvent volume was reduced to 10 mL under reduced pressure and 40-60 petroleum ether (40 mL) added to give a yellow precipitate. The precipitate was isolated by filtration, washed with 40-60 petroleum ether (3 x 15 mL) and residual volatiles removed under reduced pressure. Yield: 0.600 g, 93 %.

5.3.5 Thermal Decomposition of Ni(^{tBu}CC^{eth})Me$_2$ (13): Rate Measurements

Yellow d^8 - toluene solutions (0.6 mL) of Ni(^{tBu}CC^{eth})Me$_2$ (**13**) (various known concentrations) in Pyrex NMR tubes flame-sealed under reduced pressure were allowed to equilibrate at elevated temperatures (50, 60, 70 or 80 °C). ^{1}H NMR spectra were automatically recorded at regular time intervals for up to 5 h to monitor the rate of decomposition using the integral value of the methyl peak (δ -0.08 in d^8-toluene).

5.3.6 Thermal Decomposition of Ni(^{tBu}CC^{eth})Me$_2$ (13) and Ni(dppe)Me$_2$: Detection of Gases Evolved

Yellow diphenylmethane solutions (0.25 mL) of either Ni(^{tBu}CC^{eth})Me$_2$ (**17**) (0.025 g, 0.07 mmol) or Ni(dppe)Me$_2$ (0.025g, 0.05 mmol) were heated to 70 °C for 2 h in Pyrex tubes sealed with a Teflon stopcock under reduced pressure. Solutions were allowed to cool to room temperature and tubes attached directly to a mass spectrometer. The stopcock was opened to release any volatile decomposition products into the mass spectrometer for detection.

5.3.7 Thermal Decomposition of Ni(^{tBu}CC^{eth})Me$_2$ (13): Measurement of the Quantity of Methane Gas Evolved

A yellow diphenylmethane solution (0.25 mL) of Ni(^{tBu}CC^{eth})Me$_2$ (**13**) (0.045 g, 0.124 mmol) was heated to 70 °C for 2 h in a Pyrex tube of known volume sealed with a teflon stopcock under reduced pressure. After cooling to room temperature the tube was attached to a high vacuum line which incorporated a volumetric system, and the absolute pressure was reduced to 0.0 mmHg. The stopcock was opened to release the evolved gas into a known total volume of glassware which included the sample tube (69.63 mL), which caused the pressure to increase to 29.6 mmHg. Atmospheric pressure was recorded as 760.3 mmHg, hence the total amount of methane evolved was calculated to be 0.120 mmol, 1 equivalent.

5.3.8 NMR Tube Reaction Between Ni(^{tBu}CC^{eth})Me$_2$ (13) and B(C$_6$F$_5$)$_3$

d^8 - Toluene (0.6 mL) was condensed on to a solid mixture of Ni(^{tBu}CC^{eth})Me$_2$ (**13**) (0.040 g, 0.11 mmol) and B(C$_6$F$_5$)$_3$ (0.056 g, 0.11 mmol) at -173 °C and the Pyrex NMR tube flame-sealed under reduced pressure. The mixture was warmed to room temperature which gave a yellow supernatant and a dark red oil.

^{1}H NMR spectroscopy showed a mixture of products (broad bands of peaks in the Ni-methyl and *tert*-butyl regions (δ 0.0-2.0, thus obscuring the peak for [MeB(C$_6$F$_5$)$_3$]$^-$ at δ 1.1) and in the imidazole ring proton region (δ 6.0-8.0)). ^{11}B NMR (coupled): δ -9.3 (s)

([$MeB(C_6F_5)_3$]$^-$), and 0.5 equiv free $B(C_6F_5)_3$ (δ 57 (s)). ^{19}F NMR: δ -162, -159, -127 ([$MeB(C_6F_5)_3$]$^-$), and 0.5 equiv free $B(C_6F_5)_3$ (δ -155, -137, -124).

5.3.9 Reaction Between Ni(^{tBu}CC^{eth})Me_2 (13) and $B(C_6F_5)_3$

To a yellow toluene solution (20 mL) of Ni(^{tBu}CC^{eth})Me_2 (**13**) (0.300 g, 0.83 mmol) cooled to -78 °C was added a similarly cooled toluene solution (20 mL) of $B(C_6F_5)_3$ (0.423 g, 0.83 mmol) which gave a yellow supernatant and a dark red oil. The mixture was allowed to warm to room temperature over 2 h and stirred for a further 2 h. The volatiles were removed under reduced pressure to give a dark red oil which was washed with 40-60 petroleum ether (2 x 15 mL). The oil was extracted with diethyl ether (2 x 15 mL) to give a dark orange solution. The volatiles were removed under reduced pressure to give an intractable dark red solid. Yield: 0.360 g.

^1H NMR spectroscopy (d^6-DMSO and CD_2Cl_2) showed a mixture of products (broad bands of peaks in the Ni-methyl and *tert*-butyl region (δ 0.0-2.0, thus obscuring the peak for $MeB(C_6F_5)_3$ at δ 1.1) and in the imidazole ring proton region (δ 6.0-8.0)).

5.3.10 NMR Tube Reaction Between Ni(^{tBu}CC^{eth})Me_2 (13) and CO

A yellow C_6D_6 solution (0.6 mL) of Ni(^{tBu}CC^{eth})Me_2 (**13**) (0.030 g, 0.08 mmol) was degassed and CO (< 1 atm) admitted into the NMR tube before flame sealing. The mixture was allowed to warm to room temperature and agitated for 30 mins.

^1H NMR spectroscopy (C_6D_6) showed no starting starting material and the formation of acetone (δ 1.56 (s)). The main decomposition products were free ^{tBu}CC^{eth} and 1-*tert*-butylimidazole (ca. 1:1).

5.3.11 Reaction Between Ni(^{tBu}CC^{eth})Me_2 (13) and CO

A yellow toluene solution (20 mL) of Ni(^{tBu}CC^{eth})Me_2 (**13**) (0.290 g, 0.80 mmol) was degassed and stirred under CO (0.5 bar) for 16 h which gave a red solution. The volatiles were removed under reduced pressure which gave a red solid. Yield: 0.240 g (90 % for loss

of methyl groups in the formation of acetone). ^{1}H NMR (C_6D_6) showed that no starting material was present. Decomposition products included a mixture of free $^{tBu}CC^{eth}$ and 1-*tert*-butylimidazole. The acetone peak at δ 1.56 was absent since all volatiles were removed under reduced pressure.

5.3.12 Attempted Ethylene Polymerisation using Ni($^{tBu}CC^{eth}$)Me_2 (13) as the Co-Catalyst With MAO and with $[Ph_3C][B(C_6F_5)_4]$

A vacuum dried Fischer-Porter reactor was admitted with ethylene gas dried by passage through a column of 4 Å molecular sieves. Toluene (50 mL) was added, the absolute ethylene pressure increased to 2 bar and the solution stirred at 25 °C until saturated with ethylene. The stirring was then stopped such that a minimum of ethylene was released from solution on reducing the pressure to enable toluene solutions of methylaluminoxane (MAO) or $[Ph_3C][B(C_6F_5)_4]$ and Ni($^{tBu}CC^{eth}$)Me_2 (**13**) (3.7 mg, 10 μmol) to be added quickly, *via* cannulae, to the reactor. The ethylene pressure was then increased back to 2 bar, and the experiment started. The reaction mixture was stirred vigorously at the appropriate reaction temperature for 2 h. The pressure was then released at room temperature and the reaction mixture quenched with an excess of HCl in methanol. No polymer formation was observed in runs 1-5 (see below).

Run	MAO [Al] / [Ni]	$[[Ph_3C][B(C_6F_5)_4]]$ / $[^iBu_3Al]$ / [Ni]	Temperature (°C)
1	500	-	22
2	1500	-	22
3	1500	-	58
4	-	1 / 30 / 1	22
5	-	1 / 0 / 1	22

In run 4 the tri-*iso*-butylaluminium was added to the 50 mL toluene, prior to the addition of $[Ph_3C][B(C_6F_5)_4]$ and **13**, to act as a moisture scavanger.

5.3.13 Attempted Heck Coupling of 4-Bromoanisole and n-Butyl Acrylate using Ni(^{tBu}CC^{eth})Me$_2$ (13) as the Catalyst

Sodium acetate (1.130 g, 13.8 mmol), tetrabutylammonium acetate (1.130 g, 3.75 mmol), 4-bromoanisole (2.338 g, 12.5 mmol), di-ethyleneglycol di-n-butylether (0.250 g, G.C. standard), n-butyl acrylate (2.243 g, 17.5 mmol) and a *N*,*N*-dimethylacetamide solution (5 mL) of Ni(^{tBu}CC^{eth})Me$_2$ (**13**) (0.023 g, 0.06 mmol, 0.5 mol %) were added to *N*,*N*-dimethylacetamide (10 mL) in a Rotaflo ampoule which gave a yellow solution. The mixture was degassed and refluxed at 80 °C, then at 100 °C and lastly at 130 °C for 20 h each time. Aliquots were removed after each temperature for analysis by GCMS (work-ups were achieved by pouring the mixture at room temperature into an excess of water, extracting with diethyl ether, and drying with magnesium sulphate). Yields were calculated by integration of the chromatograph peak for the product against the 4-bromoanisole peak, and also against the peak for the G.C. standard, di-ethyleneglycol di-n-butylether. Yield after 20 h at 80 °C: 0.0 %. Yield after 20 h at 100 °C: 0.0 %. Yield after 20 h at 130 °C: 3.5 % [Turnover number (TON) = 7 (mol product / mol Ni)].

5.3.14 Preparation of Pd(^{tBu}CC^{meth})Me$_2$ (14)

To an orange THF suspension (20 mL) of Pd(bpy)Me$_2$ (1.460 g, 4.99 mmol) cooled to -78°C was added a similarly cooled THF solution (20 mL) of ^{tBu}CC^{meth} (**4**) (1.300 g, 4.99 mmol) which gave an orange suspension. The reaction mixture was allowed to warm to room temperature over 2 h and stirred for a further 12 h which gave a dark orange suspension. The solvent volume was reduced to 10 mL under reduced pressure and diethyl ether (100 mL) added to give a beige precipitate and an orange supernatant. The supernatant was isolated by filtration and cooled to -80 °C for 20 h which gave a beige microcrystalline solid. The solid was isolated by filtration, washed with 40-60 petroleum ether (3 x 15 mL) and residual volatiles removed under reduced pressure. Yield: 0.581 g, 29 %.

A pure second crop was obtained by adding 40-60 petroleum ether (50 mL) to the mother liquor and cooling to -80 °C for 20 h which gave a beige microcrystalline solid (0.663 g). Work up was achieved as for the first crop. Combined yield: 1.244 g, 63 %.

5.3.15 Preparation of Pd(^{tBu}CC^{eth})Me$_2$ (15)

To an orange THF suspension (20 mL) of Pd(bpy)Me$_2$ (3.200 g, 10.93 mmol) cooled to -78°C was added a similarly cooled THF solution (20 mL) of ^{tBu}CC^{eth} (**5**) (3.000 g, 10.93 mmol) which gave an orange suspension. The reaction mixture was allowed to warm to room temperature over 2 h and stirred for a further 12 h which gave a dark orange suspension. The solvent volume was reduced to 20 mL under reduced pressure and diethyl ether (100 mL) added to give a white precipitate and an orange supernatant. The supernatant was isolated by filtration and cooled to -80 °C for 20 h which gave a white microcrystalline solid. The solid was isolated by filtration, washed with 40-60 petroleum ether (3 x 15 mL) and residual volatiles removed under reduced pressure. Yield: 2.870 g, 64 %.

5.3.16 Preparation of [(^{tBu}CC^{meth})PdMe(py)][OCD$_3$] (16)

To a mixture of Pd(^{tBu}CC^{meth})Me$_2$ (**14**) (0.060 g, 0.15 mmol) and pyridine (0.012 g, 0.15 mmol) was added CD$_3$OD (1 mL) which gave a colourless solution with concomitant evolution of a gas.

5.3.17 Preparation of [(^{tBu}CC^{eth})PdMe(py)][OCD$_3$] (17)

To a mixture of Pd(^{tBu}CC^{eth})Me$_2$ (**15**) (0.075 g, 0.18 mmol) and pyridine (0.014 g, 0.18 mmol) was added CD$_3$OD (1 mL) which gave a colourless solution with concomitant evolution of a gas.

5.3.18 Preparation of [(^{tBu}C(D)C^{meth})PdMe(bpy)][OCD$_3$]$_2$ (18)

To a solid mixture of Pd(^{tBu}CC^{meth})Me$_2$ (**14**) (0.034 g, 0.09 mmol) and 2,6-bipyridyl (0.014 g, 0.09 mmol) was added CD$_3$OD (1 mL) which gave a colourless solution with concomitant evolution of a gas.

5.3.19 Preparation of [(^{tBu}C(D)C^{eth})PdMe(bpy)][OCD_3]$_2$ (19)

To a solid mixture of Pd(^{tBu}CC^{eth})Me_2 (**15**) (0.060 g, 0.15 mmol) and 2,6-bipyridyl (0.023 g, 0.15 mmol) was added CD_3OD (1 mL) which gave a colourless solution with concomitant evolution of a gas.

5.3.20 Reaction Between Pd(^{tBu}CC^{eth})Me_2 (15) and $B(C_6F_5)_3$

To a pale yellow toluene solution (20 mL) of Pd(^{tBu}CC^{eth})Me_2 (**15**) (0.246 g, 0.60 mmol) cooled to -78 °C was added a similarly cooled toluene solution (20 mL) of $B(C_6F_5)_3$ (0.306 g, 0.60 mmol) which gave a yellow supernatant and a dark oil. The mixture was allowed to warm to room temperature over 2 h and stirred for a further 2 h. The volatiles were removed under reduced pressure to give an intractable brown solid. ^{1}H NMR spectroscopy (d^6-DMSO) showed an unidentifiable mixture of products (broad bands of peaks in the Pd-methyl, *tert*-butyl and imidazole ring proton regions).

5.3.21 Reaction Between Pd(^{tBu}CC^{eth})Me_2 (15) and HBF_4

To a pale yellow diethyl ether solution (20 mL) of Pd(^{tBu}CC^{eth})Me_2 (**15**) (0.190 g, 0.46 mmol) was added a diethyl ether solution (0.064 mL) of HBF_4 (0.041 g, 0.46 mmol) to give a colourless supernatant and beige precipitate. The mixture was stirred for 2 h at 25 °C. The volatiles were removed under reduced pressure to give an intractable brown solid. ^{1}H NMR spectroscopy (d^6-DMSO, CD_2Cl_2, CD_3CN) showed an unidentifiable mixture of products (broad bands of peaks in the Pd-methyl, *tert*-butyl and imidazole ring proton regions).

5.3.22 Reaction Between Pd(^{tBu}CC^{eth})Me_2 (15) and [Ph_3C][$B(C_6F_5)_4$] in Diethyl Ether

To a pale yellow diethyl ether solution (20 mL) of Pd(^{tBu}CC^{eth})Me_2 (**15**) (0.200 g, 0.49 mmol) cooled to -78 °C was added a similarly cooled diethyl ether solution (20 mL) of [Ph_3C][$B(C_6F_5)_4$] (0.449 g, 0.49 mmol) to give a colourless supernatant and brown oil. The mixture was allowed to warm to room temperature over 2 h and stirred for a further 2 h.

The volatiles were removed under reduced pressure to give a brown solid which was washed with 40-60 petroleum ether (3 x 15 mL) to give an intractable brown powder. Yield: 0.385 g. ^{1}H NMR spectroscopy (d^6-DMSO, d^5-pyridine) showed an unidentifiable mixture of products (broad bands of peaks in the Pd-methyl, *tert*-butyl and imidazole ring proton regions).

5.3.23 NMR Tube Reaction Between Pd(^{tBu}CC^{eth})Me$_2$ (15) and [Ph$_3$C][B(C$_6$F$_5$)$_4$]

d^8 - THF (0.6 mL) was condensed on to a solid mixture of Pd(^{tBu}CC^{eth})Me$_2$ (**15**) (0.019 g, 0.046 mmol) and [Ph$_3$C][B(C$_6$F$_5$)$_4$] (0.042 g, 0.046 mmol) at -173 °C and the Pyrex NMR tube flame-sealed under reduced pressure. The mixture was warmed to room temperature which gave a brown solution.

^{1}H NMR spectroscopy of the mixture immediately after warming to room temperature showed the product [(^{tBu}CC^{eth})PdMe(THF)][B(C$_6$F$_5$)$_4$]: δ 0.19 (s, 3H, *CH*$_3$), 1.76 (s, 9H, C(C*H*$_3$)$_3$), 1.79 (s, 9H, C(C*H*$_3$)$_3$), 4.39 (m, 1H, N(C$_2$*H*$_4$)N), 4.62 (m, 1H, N(C$_2$*H*$_4$)N), 4.95 (m, 1H, N(C$_2$*H*$_4$)N), 6.42 (m, 1H, N(C$_2$*H*$_4$)N), 7.29 (d, 2H, $^3J_{HH}$ = 2 Hz, NC*H*), 7.31 (d, 2H, $^3J_{HH}$ = 2 Hz, NC*H*), 7.39 (d, 2H, $^3J_{HH}$ = 2 Hz, NC*H*), 7.42 (d, 2H, $^3J_{HH}$ = 2 Hz, NC*H*). The by-product triphenylethane was also present. ^{1}H NMR spectroscopy showed product decomposition after the sealed NMR tube was left standing for 48 h at 25 °C.

5.3.24 Reaction Between Pd(^{tBu}CC^{eth})Me$_2$ (15) and [Ph$_3$C][B(C$_6$F$_5$)$_4$] in THF

To a pale yellow THF solution (20 mL) of Pd(^{tBu}CC^{eth})Me$_2$ (**15**) (0.211 g, 0.51 mmol) cooled to -78 °C was added a similarly cooled THF solution (20 mL) of [Ph$_3$C][B(C$_6$F$_5$)$_4$] (0.474 g, 0.51 mmol) to give a pale yellow solution. The mixture was stirred for 1 h at -78°C. The solvent volume was reduced to 10 mL under reduced pressure and 40-60 petroleum ether (100 mL) added at -78 °C which gave a colourless supernatant and white precipitate. The precipitate was isolated by filtration at -78 °C and residual volatiles removed under reduced pressure to give a white solid which turned brown on warming to room temperature. Yield: 0.300 g.

^{1}H NMR spectroscopy (d^5-pyridine) showed product (δ 0.18 (s, 3H, CH_3), 1.40 (s, 9H, C(CH_3)$_3$), 1.77 (s, 9H, C(CH_3)$_3$), 4.65 (m, 1H, N(C$_2H_4$)N), 4.73 (m, 1H, N(C$_2H_4$)N), 5.44 (m, 1H, N(C$_2H_4$)N), 6.34 (m, 1H, N(C$_2H_4$)N), 7.33 (d, 2H, $^3J_{HH}$ = 2 Hz, NC*H*), 7.40 (d, 2H, $^3J_{HH}$ = 2 Hz, NC*H*), 7.42 (d, 2H, $^3J_{HH}$ = 2 Hz, NC*H*), 7.46 (d, 2H, $^3J_{HH}$ = 2 Hz, NC*H*)) although resonances for coordinated THF could not be distinguished from those for free THF (δ 1.57 (m), 3.63 (m)). Estimated purity = 50 %.

5.3.25 Reaction Between Pd(^{tBu}CC^{meth})Me$_2$ (14) and [Ph$_3$C][B(C$_6$F$_5$)$_4$] in THF

To a pale yellow THF solution (20 mL) of Pd(^{tBu}CC^{meth})Me$_2$ (**14**) (0.162 g, 0.41 mmol) cooled to -78 °C was added a similarly cooled THF solution (20 mL) of [Ph$_3$C][B(C$_6$F$_5$)$_4$] (0.377 g, 0.41 mmol) to give a pale yellow solution. The mixture was stirred for 1 h at -78°C. The solvent volume was reduced to 10 mL under reduced pressure and 40-60 petroleum ether (100 mL) added at -78 °C which gave a colourless supernatant and white precipitate. The precipitate was isolated by filtration at -78 °C and residual volatiles removed under reduced pressure to give a white solid which turned brown on warming to room temperature. Yield: 0.280 g.

^{1}H NMR spectroscopy (d^8-THF) showed product (δ 0.12 (s, 3H, CH_3), 1.67 (s, 9H, C(CH_3)$_3$), 1.78 (s, 9H, C(CH_3)$_3$), 6.07 (d, 2H, $^2J_{HH}$ = 13 Hz, N(CH_2)N), 6.77 (d, 2H, $^2J_{HH}$ = 13 Hz, N(CH_2)N), 7.34 (d, 1H, $^3J_{HH}$ = 2 Hz, NC*H*), 7.38 (d, 1H, $^3J_{HH}$ = 2 Hz, NC*H*), 7.42 (d, 1H, $^3J_{HH}$ = 2 Hz, NC*H*), 7.45 (d, 1H, $^3J_{HH}$ = 2 Hz, NC*H*)) although resonances for coordinated THF could not be distinguished from those for free THF (δ 1.57 (m), 3.63 (m)). Estimated purity = 50 %.

5.3.26 Attempted Ethylene Polymerisation using Pd(^{tBu}CC^{meth})Me$_2$ (14) and Pd(^{tBu}CC^{eth})Me$_2$ (15) as Co-Catalysts with MAO and with [Ph$_3$C][B(C$_6$F$_5$)$_4$]

A vacuum dried Fischer-Porter reactor was admitted with ethylene gas dried by passage through a column of 4 Å molecular sieves. Toluene (50 mL) was added, the absolute ethylene pressure increased to 2 bar and the solution stirred at 25 °C until saturated with ethylene. The stirring was then stopped such that a minimum of ethylene was released from solution on reducing the pressure to enable toluene solutions of methylaluminoxane (MAO)

or $[Ph_3C][B(C_6F_5)_4]$ and either $Pd(^{tBu}CC^{meth})Me_2$ (**14**) (4.0 mg, 10 μmol) or $Pd(^{tBu}CC^{eth})Me_2$ (**15**) (4.1 mg, 10 μmol) to be added quickly, *via* cannulae, to the reactor. The ethylene pressure was then increased back to 2 bar, and the experiment started. The reaction mixture was stirred vigorously at the appropriate reaction temperature for 2 h. The pressure was then released at room temperature and the reaction mixture quenched with an excess of HCl in methanol. No polymer was observed in runs 1-5 (see below).

Run	MAO [Al] / [Ni]	$[[Ph_3C][B(C_6F_5)_4]]$ / $[^iBu_3Al]$ / [Ni]	Temperature (°C)
1	500	-	22
2	1500	-	22
3	1500	-	58
4	-	1 / 30 / 1	22
5	-	1 / 0 / 1	22

In run 4 the tri-*iso*-butylaluminium was added to the 50 mL toluene, prior to the addition of $[Ph_3C][B(C_6F_5)_4]$ and **14** or **15**, to act as a moisture scavanger.

5.3.27 Attempted Copolymerisation of Ethylene and CO using $Pd(^{tBu}CC^{meth})Me_2$ (14), $Pd(^{tBu}CC^{eth})Me_2$ (15), $[(^{tBu}CC^{meth})PdMe(py)][OCD_3]$ (16), $[(^{tBu}CC^{eth})PdMe(py)][OCD_3]$ (17), $[(^{tBu}CC^{meth})PdMe(THF)][B(C_6F_5)_4]$ and $[(^{tBu}CC^{eth})PdMe(THF)][B(C_6F_5)_4]$ as Pre-catalysts

The Pd pre-catalyst compound (0.09-0.20 mmol) together with 1,4-benzoquinone (0 or 0.12 mmol) was dissolved in 10 mL solvent and transferred under a flow of argon into a vacuum dried 200 mL Parr autoclave fitted with a teflon liner and equipped with a stirrer bar. The autoclave was charged with 40 bar 1:1 C_2H_4 : CO mixture, sealed, and stirred at room temperature for 2 h, and at 50 °C for a further 16 h. After reaction the autoclave was allowed to cool to room temperature before the remaining C_2H_4 / CO mixture was vented. No significant reduction in pressure of the autoclave was observed during any of runs 1-7 (see table below). In each case a black precipitate was formed whose infrared spectra contained no carbonyl stretch characteristic of poly(C_2H_4-*alt*-CO) at 1692 cm^{-1}, and was

shown by elemental analysis to be Pd metal. ^{1}H NMR of the CD_3OD supernatants showed no trace of the pre-catalyst compounds.

Run	Solvent / volume (ml)	Compound used as pre-catalyst	*p*-$C_6H_4O_2$
1	CD_3OD (10)	[(^{tBu}CC^{meth})PdMe(py)][OCD_3] (**16**) ($Pd(^{tBu}CC^{meth})Me_2$ (50 mg, 0.13 mmol) + py (10 mg, 0.13mmol))	-
2	CD_3OD (10)	[(^{tBu}CC^{eth})PdMe(py)][OCD_3] (**17**) ($Pd(^{tBu}CC^{eth})Me_2$ (55 mg, 0.13 mmol) + py (11 mg, 0.14 mmol))	-
3	THF (10)	[(^{tBu}CC^{meth})PdMe(THF)][$B(C_6F_5)_4$] (200 mg, 0.09 mmol at estimated 50% purity of compound)	13 mg, 0.12 mmol
4	THF (10)	[(^{tBu}CC^{eth})PdMe(THF)][$B(C_6F_5)_4$] (200 mg, 0.09 mmol at estimated 50% purity of compound)	-
5	CD_3OD (10)	(^{tBu}CC^{meth})$PdMe_2$ (**14**) (60 mg, 0.15 mmol)	-
6	CD_3OD (10)	(^{tBu}CC^{meth})$PdMe_2$ (**14**) (40 mg, 0.10 mmol)	13 mg, 0.12 mmol
7	CD_3OD (10)	(^{tBu}CC^{eth})$PdMe_2$ (**15**) (50 mg, 0.12 mmol)	-

5.3.28 Heck Coupling of 4-Bromoanisole and n-Butyl Acrylate using $Pd(^{tBu}CC^{meth})Me_2$ (14) and $Pd(^{tBu}CC^{eth})Me_2$ (15) as Pre-catalysts

Sodium acetate (2.250 g, 27.4 mmol), 4-bromoanisole (4.676 g, 25.0 mmol), di-ethyleneglycol di-n-butylether (0.500 g, G.C. standard), n-butyl acrylate (4.486 g, 35.0 mmol) and a *N*,*N*-dimethylacetamide solution (10 mL) of the pre-catalyst (0.5 mol %) were added to *N*,*N*-dimethylacetamide (20 mL) in a 100 mL 3-necked flask equipped with a thermometer and reflux condenser, against a counterflow of nitrogen. In most cases tetrabutylammonium acetate (2.26 g, 7.5 mmol) was also added to the reaction mixture, as a completely soluble base. The mixture was degassed and purged with nitrogen to ensure an inert reaction atmosphere, then refluxed at the appropriate reaction temperature for 20 h. Work-up was achieved by pouring the reaction mixture at room temperature into an excess of water, extracting with diethyl ether and drying with magnesium sulphate. The extraction was analysed by GCMS. The yield was calculated by integration of the chromatograph peak for the product against the 4-bromoanisole peak, and also against the peak for the

G.C. standard, di-ethyleneglycol di-n-butylether. See table below for yields and turnover numbers.

Run	Pre-catalyst used	Temperature (°C)	Yield (%)	TON*
1	None (control)	140	0	0
2†	**15**	140	2.3	4.6
3†	**15**	100	4.3	8.6
4†	**14**	140	0	0
5	**14**	80	12.6	25.2
6	**14**	100	21.2	42.4
7	**14**	120	68.3	136.6
8	**14**	140	75.3	150.6
9	**15**	80	19.5	39
10	**15**	100	18.6	37.2
11	**15**	120	47.8	95.6
12	**15**	140	60.1	120.2

*TON = turnover number (mol product / mol Pd). †No [$^{n}Bu_4N$][OAc] present in runs 2-4.

5.4 Experimental Details for Chapter 4

5.4.1 Reaction Between C_{60} and 1.25 Equivalents $[Rh(cyclooctene)_2Cl]_2$: Preparation of the Rhodium C_{60} Compound (20)

To a purple benzene solution (500 mL) of C_{60} (0.600 g, 0.83 mmol) was added a yellow benzene solution (40 mL) of $[Rh(Cyclooctene)_2Cl]_2$ (0.747 g, 1.04 mmol) which gave a colourless supernatant and black precipitate. The precipitate, insoluble in all common solvents, was isolated by filtration, washed with benzene (30 mL), pentane (3 x 30 mL) and the volatiles removed under reduced pressure. Yield: 1.090 g.

Elemental analyses found (calc. for $C_{60}[Rh(Cyclooctene)Cl]_{2.5}$) / % : C 67.16 ± 5.10 (71.60), H 2.25 ± 0.35 (2.63), Rh 18.85 ± 1.20 (19.17), Cl 9.17 ± 3.58 (6.60).
IR (KBr disc) / cm^{-1} : 2850 (ν(CH), s), 2922 (ν(CH), s), 523 (ν(C_{60}), s), 560 / 582 (ν(C_{60}), doublet, w), 1169 (ν(C_{60}), broad, w)
EDX analysis confirmed the presence of Rh and Cl within the particles of **20** observed by TEM.

5.4.2 BET Surface Area Measurement of the Rh C_{60} Compound (20)

The compound **20** (0.0344 g) was placed in a Pyrex tube of known volume and attached to a high vacuum line containing a previously-calibrated volumetric system made entirely of Pyrex glass. A sintered frit was incorporated between the sample tube and the volumetric system to prevent pumping away the compound **20** upon evacuation of the system. The sample was also separated from the volumetric system by a teflon stopcock. The system, including the sample tube, was evacuated and the sample degassed by heating to 150 °C for at least 1 hour under the reduced pressure. The sample was allowed to cool before the sample tube was immersed, to a standard level, in liquid nitrogen. Increasing amounts of nitrogen gas were introduced into the volumetric system, and each time the pressure was recorded before and after opening the teflon stopcock which allowed dosage to the sample. The sample was allowed to equilibrate for 2 minutes before readings of the equilibrium pressure, P, were taken. Data points were entered into a Microsoft Excel spreadsheet

written by Thomas Suhartanto, which solved the BET equation and calculated the surface area of the sample.

5.4.3 Catalytic Hydrogenation of Ethylene using the Rh C_{60} Compound (20)

The compound **20** (0.056 g) was packed between two glass wool plugs into the centre of a 50 cm long (5 mm diameter) Pyrex tube connected to a gas supply at one end and a gas chromatograph (GC) at the other. The Pyrex tube was surrounded by a stainless steel cylindrical jacket and ran through a tube furnace packed with glass wool. The sample tube was flushed with argon to ensure an inert atmosphere prior to hydrogenation runs. The argon flow was replaced at room temperature with a flow of ethylene (12.12 NmL / minute) and hydrogen (75.14 NmL / minute). The ethylene / hydrogen mixture was passed through the sample at all times, at temperatures from 30 to 300 °C, allowing 10 minutes for the sample to equilibrate to furnace temperature before GC runs were initiated. The GC retention times for ethane and ethylene gases were previously determined as 1.64 and 1.75 minutes respectively. 100 % conversion of ethylene to ethane was observed at all temperatures, including at 25 °C after allowing to cool from 300 °C.

Run	Temperature (°C)	Ethane peak (r.t. = 1.64 mins) integral (%)	Ethylene peak (r.t. = 1.75 mins) integral (%)	Conversion (%)
1	30	100	0	100
2	50	100	0	100
3	100	100	0	100
4	140	100	0	100
5	200	100	0	100
6	300	100	0	100
7	25 (after 300)	100	0	100

5.4.4 Catalytic Hydrogenation of Cyclohexene using the Rh C_{60} Compound (20)

To a black benzene suspension (50 mL) of **20** (0.082 g, ca. 0.5 mol % Rh) was added cyclohexene (3 mL, 29.58 mmol). An aliquot of the mixture was removed for ^{1}H NMR spectroscopy which showed the presence of benzene (δ 7.15 (s)) and cyclohexene (δ 1.67 (m), 2.05 (m), 5.74 (m)) only. The reaction mixture was degassed and then stirred under a constant pressure of hydrogen (0.5 bar) for 16 h at room temperature. ^{1}H NMR spectroscopy ($CDCl_3$) of the filtered reaction mixture showed the presence of cyclohexane (δ 1.53 (s)) and no cyclohexene, indicating quantitative conversion of cyclohexene to cyclohexane. A control experiment (identical except for the absence of cyclohexene) showed that **20** does not catalyse the hydrogenation of the benzene solvent.

5.4.5 Catalytic Hydrogenation of C_{60} using the Rh C_{60} Compound (20): H_2 Pressure = 1.5 bar, Reaction Time = 16 Hours

To a 600 mL ampoule containing a purple benzene solution (200 mL) of C_{60} (0.230 g, 0.32 mmol) was added **20** (0.050 g, ca. 29 mol % Rh) to give a black suspension. The ampoule was degassed and 1.5 bar hydrogen gas admitted before sealing with a teflon stopcock. The mixture was refluxed at 130 °C for 16 h. After allowing to cool to room temperature the pressure was released and the reaction mixture filtered which gave a red solution. The volatiles were removed under reduced pressure to give a brown-red solid. Yield: 0.209 g.

^{1}H NMR (C_6D_6): δ 5.90 (s)

^{13}C{^{1}H} NMR (C_6D_6): δ 143.3 (s)

FAB mass spectrometry: m/z 720 [C_{60}]; peaks due to $C_{60}H_2$ were not discernible

5.4.6 Catalytic Hydrogenation of C_{60} using the Rh C_{60} Compound (20): H_2 Pressure = 1.5 bar, Reaction Time = 240 Hours

To a 600 mL ampoule containing a purple benzene solution (200 mL) of C_{60} (0.230 g, 0.32 mmol) was added **20** (0.050 g, ca. 29 mol % Rh) to give a black suspension. The

ampoule was degassed and 1.5 bar hydrogen gas admitted before sealing with a teflon stopcock. The mixture was refluxed at 130 °C for 240 h. After allowing to cool to room temperature the pressure was released and the reaction mixture filtered which gave a red solution. The volatiles were removed under reduced pressure to give a brown-red solid. Yield: 0.204 g.

FAB mass spectrometry: m/z 720-755

^{1}H NMR (C_6D_6): δ 2-5 (br)

^{13}C{^{1}H} NMR (C_6D_6): δ 143.3 (s)

5.4.7 Catalytic Hydrogenation of C_{60} using the Rh C_{60} Compound (20): H_2 pressure = 40 bar, Reaction Time = 240 Hours

A purple benzene solution (50 mL) of C_{60} (0.066 g, 0.09 mmol) and **20** (0.050 g, ca. 100 mol % Rh) were transferred under nitrogen into a vacuum dried 200 mL Parr autoclave fitted with a teflon liner and equipped with a stirrer bar, to give a black suspension. The autoclave was charged with 40 bar H_2, sealed, and stirred at 130 °C for 240 h. The pressure of the autoclave rose to 55 bar after initial equilibration at 130 °C, before dropping to 43 bar after 10 days. After reaction the autoclave was allowed to cool to room temperature before the remaining H_2 was vented. The reaction mixture was filtered which gave a brown-red solution. The volatiles were removed under reduced pressure to give a brown-red solid. Yield: 0.054 g, 78 %.

FAB mass spectrometry: m/z 755 [$C_{60}H_{36}$ - H]

IR (KBr disc) / cm^{-1} : 2843 (ν(CH), s), 2911 (ν(CH), s)

^{1}H NMR (C_6D_6): δ 2.6-4.5 (br)

^{13}C{^{1}H} NMR (C_6D_6): No singlet at δ 143.3

5.4.8 Hydroformylation of 3,3-Dimethyl 1-Butene using the Rh C_{60} Compound (20)

3,3-dimethyl 1-butene (3.000 g, 35.65 mmol) in C_6D_6 (10 mL) and **20** (0.055 g, ca. 0.3 mol % Rh) were transferred under nitrogen into a vacuum dried 200 mL Parr autoclave

fitted with a teflon liner and equipped with a stirrer bar, to give a black suspension. The autoclave was charged with 38 bar 1:1 H_2 : CO mixture, sealed, and stirred at room temperature for 24 h after which no significant drop in the autoclave pressure was observed. The H_2 / CO mixture was vented and an aliquot of the black suspension removed for ^{1}H NMR spectroscopy which showed that only the starting material 3,3-dimethyl 1-butene was present in solution (δ 0.96 (s, 9H, C(C*H*$_3$)$_3$), 4.88 (m, 2H, C*H*$_2$CH), 5.82 (m, 1H, CH$_2$C*H*)). The autoclave was re-charged with 38 bar 1:1 H_2 : CO mixture and sealed. The temperature was increased to 130 °C causing an initial pressure increase to 44 bar, and the reaction mixture stirred for a further 3 h after which the pressure had decreased to 35 bar. The autoclave was allowed to cool to room temperature (causing the pressure to decrease to 29 bar) before the remaining H_2 / CO mixture was vented. The reaction mixture had become a red solution, with no black Rh C_{60} compound remaining.

^{1}H NMR spectroscopy of the reaction mixture showed the terminal aldehyde product (4,4-dimethyl pentan-1-al) only: δ 0.68 (s, 9H, C(C*H*$_3$)$_3$), 1.24 (m, 2H, C*H*$_2$), 1.87 (m, 2H, C*H*$_2$), 9.39 (s, 1H, C*H*O). No alkene starting material remained.

The volatiles were removed from the reaction mixture under reduced pressure which gave a red solid. ^{1}H and ^{13}C{^{1}H} NMR spectroscopy (C_6D_6) showed a mixture of compounds (broad bands observed in the *tert*-butyl regions (δ 0.6-1.2 (^{1}H) and δ 22-32 (^{13}C{^{1}H})) and methylene regions (δ 1.4-2.4 (^{1}H) and δ 35-42 (^{13}C{^{1}H})).

5.4.9 Hydroformylation of 1-Pentene using the Rh C_{60} Compound (20)

1-pentene (2.800 g, 40.00 mmol) in C_6D_6 (10 mL) and **20** (0.034 g, ca. 0.2 mol % Rh) were transferred under nitrogen into a vacuum dried 200 mL Parr autoclave fitted with a teflon liner and equipped with a stirrer bar, to give a black suspension. The autoclave was charged with 38 bar 1:1 H_2 : CO mixture, sealed, and stirred at 130 °C for 3 h after which time the pressure had decreased from an initial 44 bar at 130 °C to 35 bar. The autoclave was allowed to cool to room temperature (causing the pressure to decrease to 29 bar) before the remaining H_2 / CO mixture was vented. The reaction mixture had become a red solution, with no black Rh C_{60} compound remaining.

^{1}H NMR spectroscopy of the reaction mixture showed a ca. 1:1 mixture of the terminal and branched aldehyde products hexan-1-al and 2-methyl pentan-1-al: δ 9.31 (m, 1H, C*H*O) and δ 9.38 (m, 1H, C*H*O). Methyl, methylene and methine proton resonances for the aldehydes were observed between δ 0.7 and δ 2.0. No alkene starting material remained.

Pentane (50 mL) was added to the reaction mixture which gave a pale red supernatant and a red-brown precipitate. The precipitate was isolated by filtration and residual volatiles removed under reduced pressure.

Elemental analysis / % : C 70.30, H 4.70, Rh 14.13, Cl 6.78

^{1}H and ^{13}C{^{1}H} NMR spectroscopy (C_6D_6): broad peaks observed in alkyl regions (δ 0.6-2.5 (^{1}H) and δ 15-35 (^{13}C{^{1}H}))

FAB mass spectrum: m/z 262, 350, 547, 720 [C_{60}], 811, 823 [C_{60}Rh], broad distribution in the range m/z 720-950 (C_{60} compounds)

IR (KBr disc) / cm^{-1} : 527 (ν(C_{60}), br), 2030 (ν(CO) Rh chlorocarbonyl region, s), 2858 (ν(CH), s), 2869 (ν(CH), s), 2929 (ν(CH), s)

5.4.10 Birch Reduction of C_{60}: Preparation of $C_{60}H_{36}$

To a 500 mL 3-necked flask equipped with an ammonia condenser (with exit to Hg bubbler) and a solids addition tube containing Li metal (0.386 g, 55.62mmol) was added C_{60} (0.400 g, 0.56 mmol) and THF (50 mL) against a counterflow of argon. The reaction vessel and the ammonia condenser were cooled to -78 °C before liquid ammonia (250 mL) was introduced directly into the 3-necked flask. After the ammonia had equilibrated to the -78 °C reaction temperature the Li metal was introduced into the mixture from the solids addition tube to give an intense blue solution. The mixture was stirred at -78 °C for 1 h before *tert*-butyl alcohol (50 mL) was added. The mixture was stirred and allowed to warm to room temperature over 6 h, by which time all the liquid ammonia had evaporated into the fume cupboard via the Hg bubbler. The reaction mixture was transferred onto a Schlenk frit and filtered which gave a brown solid. The solid was washed with THF (2 x 100 mL), ethanol (2 x 100 mL), acetone (2 x 100 mL) and pentane (2 x 100 mL), and residual volatiles removed under reduced pressure, which gave a beige powder. Yield: 0.122 g, 29 %.

IR (KBr disc) / cm^{-1} : 2843 (ν(CH), s), 2911 (ν(CH), s)

^{1}H NMR (C_6D_6): δ 2.6-4.5 (br)

$^{13}C\{^{1}H\}$ NMR (C_6D_6): No singlet at δ 143.3

Elemental analysis (calc. for $C_{60}H_{36}$) / % : C 86.00 (95.21), H 5.81 (4.79), Li 0.03 (0.00)

5.4.11 Thermal Decomposition of the Birch Reduction Product $C_{60}H_{36}$: Measurement of the Quantity of Hydrogen Evolved

The Birch reduction product $C_{60}H_{36}$ (0.049 g, 64.7 μmol) in a Pyrex tube of known volume sealed with a teflon stopcock was attached to a high vacuum line which incorporated a volumetric system. The stopcock was opened, and the absolute pressure reduced to 0.0 mmHg at room temperature. The stopcock was closed, and the Pyrex tube surrounded by a tube furnace. The temperature of the sample, measured by a thermocouple, was increased to the appropriate temperature (see table) and held for 1.0 or 1.5 h (see table) before allowing the sample to cool back to room temperature. The stopcock was subsequently opened to release any gas produced by thermal decomposition into a known total volume of glassware which included the sample tube. The pressure increase was noted, the stopcock closed and the sample heated to the next, higher temperature. After allowing to cool the stopcock was opened again to record any further pressure increase. This process was repeated: measurements were taken at 6 temperatures in total. The amount of hydrogen gas evolved at each temperature as well as the overall total quantity was calculated. Atmospheric pressure was recorded as 758.2 mmHg. The total volume of glassware used was calculated prior the experiment as 70.60 mL.

Temperature (°C)	Time at temperature (mins)	Pressure increase (mmHg)	Amount H_2 evolved at temperature (μmol)	Amount H_2 evolved at temperature (% of theoretical maximum)	Pressure (mmHg)	Total amount H_2 evolved (μmol)	Total H_2 evolved (% of theoretical maximum)
110	60	3.3	13.7	1.2	3.3	13.7	1.2
180	60	3.4	14.0	1.2	6.7	27.7	2.4
250	60	1.0	4.2	0.3	7.7	31.9	2.7
340	60	3.1	12.8	1.1	10.8	44.7	3.8
440	60	42.4	175.5	15.1	53.2	220.2	18.9
550	90	56.3	233.0	20.0	109.5	453.2	38.9

After heating to 550 °C a black insoluble powder (0.036 g) was recovered from the sample tube.

IR (KBr disc) / cm^{-1} : 526 (ν(C_{60}), w), 576 (ν(C_{60}), w), 2843 (ν(CH), w) 2911 (ν(CH), w)

^1H NMR (C_6D_6): No broad band in the range δ 2.6-4.5

$^{13}C\{^1H\}$ NMR (C_6D_6): δ 144.3 (very low intensity - trace amount of free C_{60})

Elemental analysis / % : C 87.82, H 1.90

5.5 References

1) Otwinowski, Z.; Minor, W. *Methods Enzymol.* **1997**, *276*, 307.
2) Watkin, D. J.; Prout, C. K.; Carruthers, J. R.; Betteridge, P. W. *CRYSTALS, Issue 10*; Chemical Crystallography Laboratory: Oxford, U.K., 1996
3) Watkin, D. J.; Prout, C. K.; Pearce, L. J. *CAMERON*; Chemical Crystallography Laboratory: Oxford, U.K., 1996
4) Altomare, A.; Cascarano, G.; Guagliardi, A.; Burla, M. C.; Polidori, G.; Camalli, M. *J. Appl. Crystallogr.* **1994**, *27*, 435.
5) Dahl, O. *Acta Chem. Scand.* **1969**, *23*, 2342.
6) Venanzi, L. M. *J. Chem. Soc.* **1958**, 719.
7) Klein, H.-F.; Karsch, H. H. *Chem. Ber.* **1972**, *105*, 2628.
8) Pasynkiewics, S.; Pikul, S.; Poplawska, J. *J. Organomet. Chem.* **1985**, *293*, 125.
9) Wimmer, F. L.; Wimmer, S.; Castan, P. *Inorganic Syntheses* **1992**, *29*, 185.
10) Calvin, G.; Coates, G. E. *J. Chem. Soc.* **1960**, 2008.
11) Kohara, T.; Yamamoto, T.; Yamamoto, A. *J. Organomet. Chem.* **1980**, *192*, 265.
12) van der Ent, A.; Onderdelinden, A. L. *Inorganic Syntheses* **1973**, *14*, 92.
13) Saito, T.; Uchida, Y.; Misono, A.; Yamamoto, A.; Morifuji, K.; Ikeda, S. *J. Am. Chem. Soc.* **1966**, *88*, 5198.

CHAPTER 6

Characterising Data

6.1 Data Characterising 1,1'-Methylene*bis*(3-*tert*-butylimidazolium) Diiodide (1)

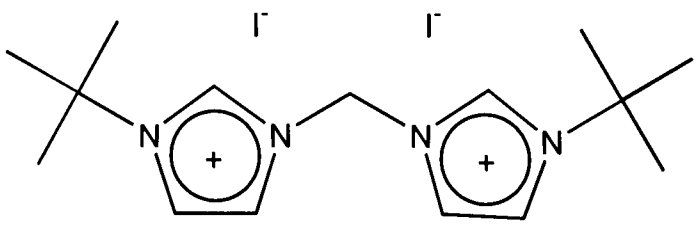

Description: Air-stable cream coloured powder.

Elemental analysis: $C_{15}H_{26}N_4I_2$. $0.4(C_4H_8O_2)$

Found (Calc.) / %: C 36.09 (36.16), H 4.96 (5.34), N 10.09 (10.16)

^{1}H NMR data (300 MHz, CD_3OD, 25 °C)**:**

1.71 [s, 18H, $C(CH_3)_3$] 6.73 [s, 2H, $N(CH_2)N$]

8.03 [d, 2H, $^3J_{HH}$ = 2Hz, NC*H*] 8.07 [d, 2H, $^3J_{HH}$ = 2Hz, NC*H*]

9.84 [s, 2H, N(C*H*)N]

3.66 [s, $C_4H_8O_2$] (1,4-dioxane solvent)

On standing a CD_3OD solution of (**1**) for 24 h the peak at δ 9.84 ppm disappears, accompanied by an increase in intensity of the CD_3OH residual protio solvent peak (δ 4.8 ppm) indicating that complete H / D exchange has occurred.

^{13}C{^{1}H} NMR data (125.7 MHz, CD_3OD, 25 °C)**:**

29.6 [s, $C(CH_3)_3$] 59.7 [s, $N(CH_2)N$]

62.4 [s, $C(CH_3)_3$] 122.4 [s, NCH]

123.9 [s, NCH] 137.6 [s, N(CH)N]

68.1 [s, $C_4H_8O_2$] (1,4-dioxane solvent)

6.2 Data Characterising 1,1'-Methylene*bis*(3-*tert*-butylimidazolium) Dibromide (2)

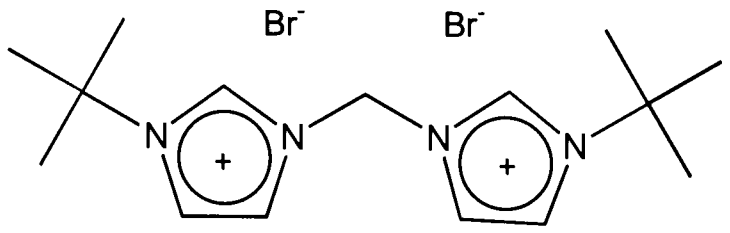

Description: Air-stable cream coloured powder.

Elemental analysis: $C_{15}H_{26}N_4Br_2$. $0.4(C_4H_8O_2)$

Found (Calc.) / %: C 43.31 (43.59), H 6.48 (6.43), N 11.97 (12.25)

^{1}H NMR data (500 MHz, CD_3OD, 25 °C):

1.71 [s, 18H, $C(CH_3)_3$]
8.06 [vt, 2H, $^3J_{HH}$ = 2Hz, $^4J_{HH}$ = 2 Hz, NC*H*]
8.19 [vt, 2H, $^3J_{HH}$ = 2Hz, $^4J_{HH}$ = 2 Hz, NC*H*]
9.84 [t, 2H, $^4J_{HH}$ = 2 Hz, N(C*H*)N]
6.83 [s, 2H, $N(CH_2)N$]

3.66 [s, $C_4H_8O_2$] (1,4-dioxane solvent)

On standing a CD_3OD solution of (**2**) for 24 h the peak at δ 9.84 ppm disappears, accompanied by an increase in intensity of the CD_3OH residual protio solvent peak (δ 4.8 ppm) indicating that complete H / D exchange has occurred.

^{13}C{^{1}H} NMR data (125.7 MHz, CD_3OD, 25 °C):

29.6 [s, $C(CH_3)_3$]
62.4 [s, $C(CH_3)_3$]
123.9 [s, NCH]
59.7 [s, $N(CH_2)N$]
122.4 [s, NCH]
137.6 [s, N(CH)N]

68.1 [s, $C_4H_8O_2$] (1,4-dioxane solvent)

6.3 Data Characterising 1,1'-(1,2-Ethylene)*bis*(3-*tert*-butylimidazolium) Dibromide (3)

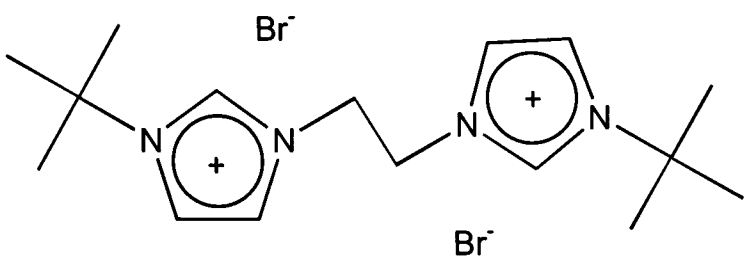

Description: Air-stable cream coloured powder.

Elemental analysis: $C_{16}H_{28}N_4Br_2$

Found (Calc.) / %: C 43.61 (44.05), H 6.45 (6.47), N 12.65 (12.84), Br 37.02 (36.63)

^{1}H NMR data (500 MHz, CD_3OD, 25 °C)**:**

1.68 [s, 18H, C(C*H*$_3$)$_3$]

4.91 [s, 4H, N(C$_2$*H*$_4$)N]

7.72 [vt, 2H, $^3J_{HH}$ = 2Hz, $^4J_{HH}$ = 2 Hz, NC*H*]

7.97 [vt, 2H, $^3J_{HH}$ = 2Hz, $^4J_{HH}$ = 2 Hz, NC*H*]

9.49 [t, 2H, $^4J_{HH}$ = 2 Hz, NC*H*]

^{13}C{^{1}H} NMR data (125.7 MHz, CD_3OD, 25 °C)**:**

29.8 [s, C(*C*H$_3$)$_3$]

61.9 [s, *C*(CH$_3$)$_3$]

124.1 [s, N*C*H]

49.9 [s, N(*C*$_2$H$_4$)N]

122.0 [s, N*C*H]

136.6 [s, N(*C*H)N]

6.4 Data Characterising $^{tBu}CC^{meth}$ (4)

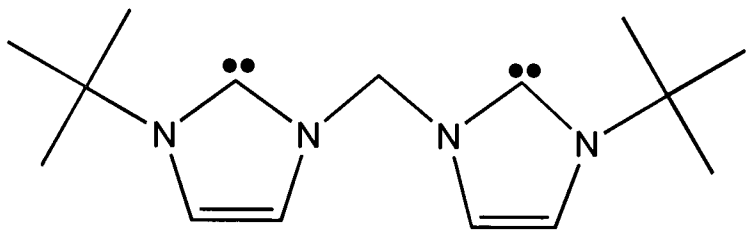

Description: Air-sensitive white powder.
Must be stored below -20 °C.

Mass spectrum (EI): m/z 204 [M^+ - ^{t}Bu], 147 [M^+ - 2(^{t}Bu)], 124 [*tert*-butylimidazole], 69 [imidazole], 57 [^{t}Bu]

^{1}H NMR data (500 MHz, C_6D_6, 25 °C):

1.41 [s, 18H, C(C*H*$_3$)$_3$] 6.22 [s, 2H, N(C*H*$_2$)N] 6.50 [d, 2H, $^3J_{HH}$ = 2 Hz]
7.11 [d, 2H, $^3J_{HH}$ = 2 Hz]

^{13}C{^{1}H} NMR data (125.7 MHz, C_6D_6, 25 °C):

31.2 [s, C(*C*H$_3$)$_3$] 55.7 [s, *C*(CH$_3$)$_3$] 66.3 [s, N(*C*H$_2$)N] 116.7 [s, N*C*H]
117.7 [s, N*C*H] 214.5 [s, N*C*N]

^{1}H-^{13}C-$^1J_{CH}$ shift correlated NMR data (125.7 MHz, C_6D_6, 25 °C):

Cross-peaks (^{1}H, ^{13}C):

1.41, 31.2 [C(*CH*$_3$)$_3$] 6.22, 66.3 [N(*CH*$_2$)N]
6.50, 116.7 [N*CH*] 7.11, 117.7 [N*CH*]

6.5 Data Characterising $^{tBu}CC^{eth}$ (5)

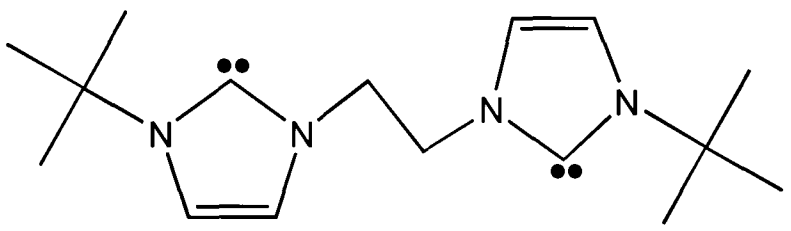

Description: Air-sensitive white powder.

Must be stored below -20°C.

Mass spectrum (EI): m/z 274 [M^+], 217 [M^+ - ^{t}Bu], 161 [M^+ - 2(^{t}Bu)],
150 [M^+ - *tert*-butylimidazole], 124 [*tert*-butylimidazole],
69 [imidazole], 57 [^{t}Bu]

^{1}H NMR data (500 MHz, C_6D_6, 25 °C):

1.47 [s, 18H, C(CH_3)$_3$]

4.41 [s, 4H, N(C$_2H_4$)N]

6.35 [d, 2H, $^3J_{HH}$ = 2 Hz]

6.55 [d, 2H, $^3J_{HH}$ = 2 Hz]

^{13}C{^{1}H} NMR data (125.7 MHz, C_6D_6, 25 °C):

31.3 [s, C(CH$_3$)$_3$]

52.8 [s, N(C_2H$_4$)N]

55.7 [s, C(CH$_3$)$_3$]

115.2 [s, NCH]

119.1 [s, NCH]

214.0 [s, NCN]

6.6 Data Characterising $[Ni(^{tBu}CC^{meth})_2][Br]_2$ (6)

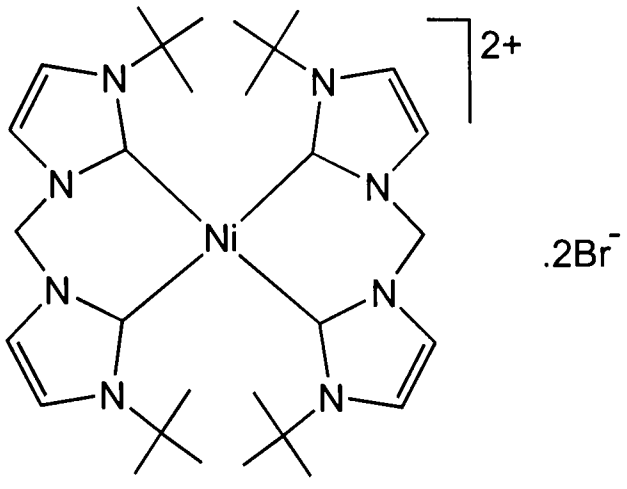

Description: Air-stable pale yellow powder.

Mass spectrum (Electrospray)**:**

m/z (%) 289 (80) [M^{2+}], 336 (10) [impurity], 342 (10) [impurity]

^{1}H NMR data (500 MHz, CD_3OD, 25 °C)**:**

1.45 [s, 18H, $C(CH_3)_3$]
6.65 [d, 1H, $^{2}J_{HH}$ = 14 Hz, $N(CH_2)N$]
7.11 [d, 1H, $^{2}J_{HH}$ = 14 Hz, $N(CH_2)N$]
7.51 [d, 2H, $^{3}J_{HH}$ = 2 Hz, NC*H*]
7.76 [d, 2H, $^{3}J_{HH}$ = 2 Hz, NC*H*]

^{13}C{^{1}H} NMR data (125.7 MHz, CD_3OD, 25 °C)**:**

31.9 [s, $C(CH_3)_3$]
60.9 [s, $C(CH_3)_3$]
65.8 [s, $N(CH_2)N$]
123.4 [s, NCH]
125.0 [s, NCH]
170.3 [NCN]

6.7 Data Characterising [(^{tBu}CC^{meth})NiCl(PMe$_3$)]Cl (7)

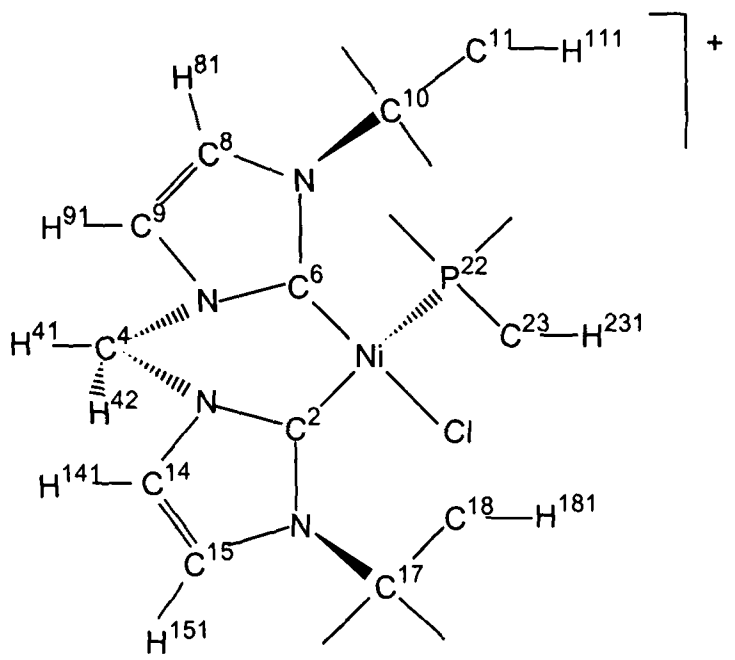

Atom labels from crystal structure

Description: Moderately air-stable yellow powder.

^{1}H and ^{13}C{^{1}H} NMR assignments (CD_2Cl_2, 25 °C):

Carbon atom label	^{13}C{^{1}H} NMR (125.7 MHz) data	Corresponding hydrogen atom label	Corresponding ^{1}H NMR (500 MHz) data
C^{23}	13.9 (d, $^1J_{PC}$ = 29 Hz)	H^{231}	1.23 (d, 9H, $^2J_{PH}$ = 10 Hz)
C^{11}	31.2 (d, $^5J_{PC}$ = 2 Hz)	H^{111}	1.87 (s, 9H)
C^{18}	31.4 (s)	H^{181}	1.79 (s, 9H)
C^{10}	59.1 (s)	-	-
C^{17}	59.1 (s)	-	-
C^4	63.6 (s)	H^{42}	6.91 (d, 1H, $^2J_{HH}$ = 13 Hz)
		H^{41}	8.26 (d, 1H, $^2J_{HH}$ = 13 Hz)
C^{15}	119.4 (d, $^{4 \text{ or } 5}J_{PC}$ = 5 Hz)	H^{151}	6.95 (vt, 1H, $^3J_{HH}$ = 2 Hz, $^5J_{PH}$ = 2 Hz)
C^8	120.5 (s)	H^{81}	7.02 (d, 1H, $^3J_{HH}$ = 2 Hz)
C^{14}	122.9 (s)	H^{141}	7.97 (d, 1H, $^3J_{HH}$ = 2 Hz)
C^9	125.9 (s)	H^{91}	8.43 (d, 1H, $^3J_{HH}$ = 2 Hz)
C^6	162.6 (d, $^2J_{PC}$ = 40 Hz)	-	-
C^2	165.7 (d, $^2J_{PC}$ = 117 Hz)	-	-

^{1}H and $^{13}C\{^{1}H\}$ NMR (CD_2Cl_2) assignments were made with the aid of ^{1}H-^{13}C-$^{1}J_{CH}$ shift correlation NMR spectroscopy, ^{1}H-^{13}C-$^{n}J_{CH}$ (n > 1) shift correlation NMR spectroscopy and ^{1}H NOESY NMR spectroscopy.

^{1}H NMR data (500 MHz, d^6-DMSO, 25 °C):

1.21 [d, 9H, $^{2}J_{PH}$ = 10 Hz, P(CH_3)$_3$]
1.75 [s, 9H, C(CH_3)$_3$]
1.84 [s, 9H, C(CH_3)$_3$]
6.76 [d, 1H, $^{2}J_{HH}$ = 13 Hz, N(CH_2)N]
7.10 [d, 1H, $^{2}J_{HH}$ = 13 Hz, N(CH_2)N]
7.51 [vt, 1H, $^{3}J_{HH}$ = 2 Hz, $^{5}J_{PH}$ = 2Hz, NC*H*]
7.66 [d, 1H, $^{3}J_{HH}$ = 2 Hz, NC*H*]
7.76 [d, 1H, $^{3}J_{HH}$ = 2 Hz, NC*H*]
7.88 [d, 1H, $^{3}J_{HH}$ = 2 Hz, NC*H*]

$^{1}H\{^{31}P\}$ NMR data (500 MHz, d^6-DMSO, 25 °C):

Identical to ^{1}H NMR data (500 MHz, d^6-DMSO, 25 °C) except for:

1.21 [s, 9H, P(CH_3)$_3$]
7.51 [d, 1H, $^{3}J_{HH}$ = 2 Hz, NC*H*]

$^{13}C\{^{1}H\}$ NMR data (125.7 MHz, d^6-DMSO, 25 °C):

12.8 [d, $^{1}J_{PC}$ = 30 Hz, P(*C*H$_3$)$_3$]
30.3 [s, C(*C*H$_3$)$_3$]
30.7 [s, C(*C*H$_3$)$_3$]
58.5 [s, *C*(CH$_3$)$_3$]
58.7 [s, *C*(CH$_3$)$_3$]
63.8 [s, N(*C*H$_2$)N]
120.3 [d, $^{4\text{ or }5}J_{PC}$ = 5 Hz, N*C*H]
121.8 [s, N*C*H]
122.0 [s, N*C*H]
124.3 [s, N*C*H]
161.6 [d, $^{2}J_{PC}$ = 39 Hz, N*C*N]
165.8 [d, $^{2}J_{PC}$ = 114 Hz, N*C*N]

$^{31}P\{^{1}H\}$ NMR data (202.4 MHz, d^6-DMSO, 25 °C):

-12.3 [s, *P*(CH$_3$)$_3$]

Mass spectrum (Electrospray): m/z (%) 429 (100) [M^+]

6.8 Data Characterising [(^{tBu}CC^{meth})NiCl(PMe$_3$)][BPh$_4$] (8)

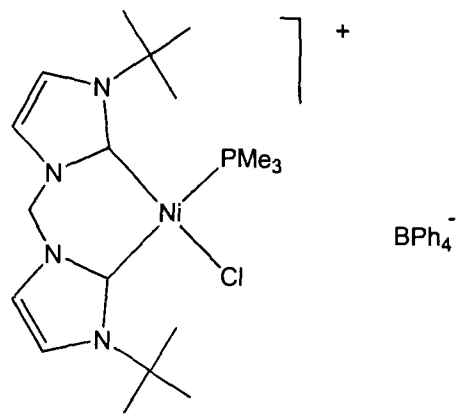

Description: Moderately air-stable yellow powder.

Mass spectrum (Electrospray): m/z (%) 429 (100) [M^+]

^{1}H NMR data (500 MHz, d^6-DMSO, 25 °C):

1.21 [d, 9H, $^2J_{PH}$ = 10 Hz, P(CH_3)$_3$]
1.76 [s, 9H, C(CH_3)$_3$]
1.84 [s, 9H, C(CH_3)$_3$]
6.43 [d, 1H, $^2J_{HH}$ = 13 Hz, N(CH_2)N]
6.79 [m, 4H, *para*-BPh$_4$]
6.93 [m, 8H, BPh$_4$]
7.11 [d, 1H, $^2J_{HH}$ = 13 Hz, N(CH_2)N]
7.18 [m, 8H, BPh$_4$]
7.48 [vt, 1H, $^3J_{HH}$ = 2 Hz, $^5J_{PH}$ = 2 Hz, NC*H*]
7.58 [d, 1H, $^3J_{HH}$ = 2 Hz, NC*H*]
7.68 [d, 1H, $^3J_{HH}$ = 2 Hz, NC*H*]
7.74 [d, 1H, $^3J_{HH}$ = 2 Hz, NC*H*]

^{13}C{^{1}H} NMR data (125.7 MHz, d^6-DMSO, 25 °C):

12.9 [d, $^1J_{PC}$ = 29 Hz, P(CH_3)$_3$]
30.3 [s, C(*C*H$_3$)$_3$]
30.7 [s, C(*C*H$_3$)$_3$]
58.7 [s, *C*(CH$_3$)$_3$]
58.9 [s, *C*(CH$_3$)$_3$]
64.0 [s, N(*C*H$_2$)N]
120.4 [s, N*C*H]
121.7 [s, BPh$_4$]
121.9 [s, N*C*H]
122.1 [s, N*C*H]
124.4 [s, N*C*H]
125.5 [m, BPh$_4$]
135.7 [m, BPh$_4$]
161.9 [d, $^2J_{PC}$ = 39 Hz, N*C*N]
163.5 [q, $^1J_{BC}$ = 49 Hz, *ipso*-BPh$_4$]
165.8 [d, $^2J_{PC}$ = 114 Hz, N*C*N]

^{31}P{^{1}H} NMR data (202.4 MHz, d^6-DMSO, 25 °C): -12.3 [s, *P*(CH$_3$)$_3$]

6.9 Data Characterising [(^{tBu}CC^{eth})NiCl(PMe$_3$)]Cl (9)

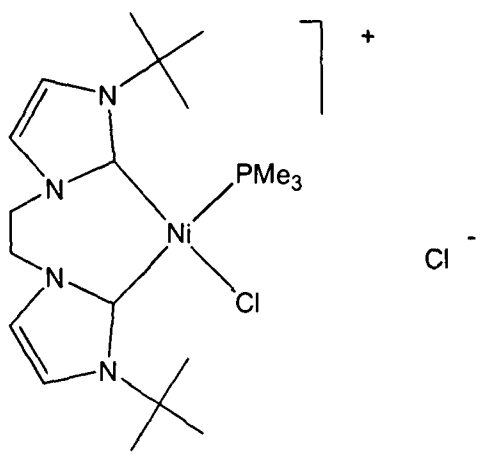

Description: Moderately air-stable yellow powder.

Mass spectrum (Electrospray): m/z (%) 443 (100) [M^+]

^{1}H NMR data (500 MHz, d^6-DMSO, 25 °C):

1.14 [d, 9H, $^2J_{PH}$ = 10 Hz, P(CH_3)$_3$]
1.82 [s, 9H, C(CH_3)$_3$]
1.95 [s, 9H, C(CH_3)$_3$]
4.74 [m, 1H, N(C$_2H_4$)N]
4.88 [m, 1H, N(C$_2H_4$)N]
5.75 [m, 1H, N(C$_2H_4$)N]
6.49 [m, 1H, N(C$_2H_4$)N]
7.57 [d, 1H, $^3J_{HH}$ = 2 Hz, NC*H*]
7.58 [d, 1H, $^3J_{HH}$ = 2 Hz, NC*H*]
7.63 [d, 1H, $^3J_{HH}$ = 2 Hz, NC*H*]
7.69 [d, 1H, $^3J_{HH}$ = 2 Hz, NC*H*]

^{13}C{^{1}H} NMR data (125.7 MHz, d^6-DMSO, 25 °C):

12.5 [d, $^1J_{PC}$ = 29 Hz, P(CH_3)$_3$]
30.4 [s, C(*C*H$_3$)$_3$]
30.9 [s, C(*C*H$_3$)$_3$]
47.2 [s, N(*C*$_2$H$_4$)N]
48.1 [s, N(*C*$_2$H$_4$)N]
58.24 [s, *C*(CH$_3$)$_3$]
58.28 [s, *C*(CH$_3$)$_3$]
121.2 [s, NCH]
122.7 [s, NCH]
123.5 [d, $^{4\text{ or }5}J_{PC}$ = 3 Hz, NCH]
124.9 [s, NCH]
155.0 [d, $^2J_{PC}$ = 40 Hz, NCN]
162.6 [d, $^2J_{PC}$ = 112 Hz, NCN]

^{31}P{^{1}H} NMR data (202.4 MHz, d^6-DMSO, 25 °C): -11.9 [s, *P*(CH$_3$)$_3$]

6.10 Data Characterising [(^{tBu}CC^{eth})NiCl(PMe$_3$)][BPh$_4$] (10)

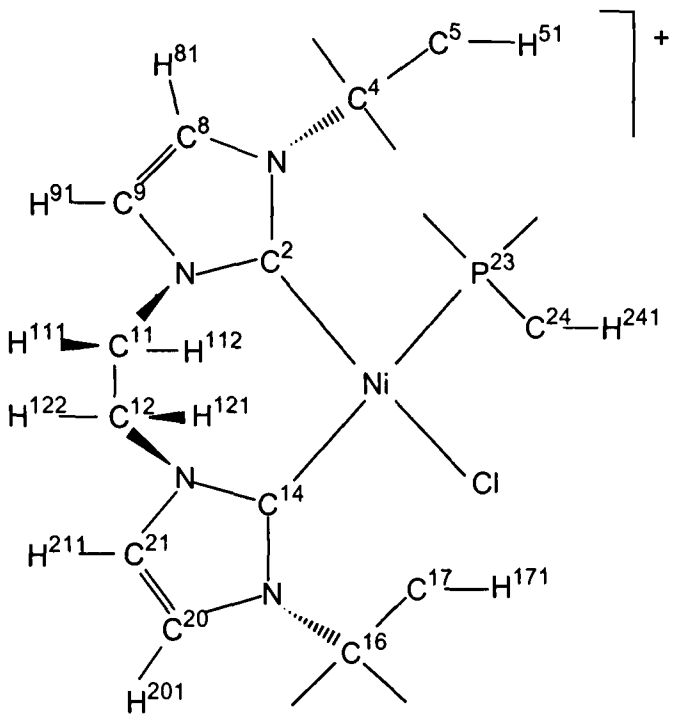

BPh_4^-

Atom labels from crystal structure

Description: Moderately air-stable yellow powder.

^{1}H and ^{13}C{^{1}H} NMR assignments (d^6 - DMSO, 25 °C)**:**

Carbon atom label	^{13}C{^{1}H} NMR (125.7 MHz) data	Corresponding hydrogen atom label	Corresponding ^{1}H NMR (500 MHz) data
C^{24}	13.4 (d, $^1J_{PC}$ = 29 Hz)	H^{241}	1.11 (d, 9H, $^2J_{PH}$ = 10 Hz)
C^5	31.2 (s)	H^{51}	1.91 (s, 9H)
C^{17}	31.7 (s)	H^{171}	1.80 (s, 9H)
C^{12}	48.1 (s)	H^{122}	4.77 (m, 1H)
		H^{121}	6.42 (m, 1H)
C^{11}	48.9 (s)	H^{111}	4.67 (m, 1H)
		H^{112}	5.74 (m, 1H)
C^{16}	59.08 (s)	-	-
C^4	59.10 (s)	-	-
C^{20}	122.0 (d, $^{4 \text{ or } 5}J_{PC}$ = 4 Hz)	H^{201}	7.51 (dd, 1H, $^3J_{HH}$ = 2 Hz, $^5J_{PH}$ = 1.5 Hz)
para-BPh_4	122.3 (s)	*para*-BPh_4	6.77 (m, 4H)
C^8	123.5 (s)	H^{81}	7.60 (d, 1H, $^3J_{HH}$ = 2Hz)
C^{21}	124.3 (d, $^{4 \text{ or } 5}J_{PC}$ = 4 Hz)	H^{211}	7.47 (d, 1H, $^3J_{HH}$ = 2Hz)
C^9	125.7 (s)	H^{91}	7.52 (d, 1H, $^3J_{HH}$ = 2Hz)
BPh_4	126.1 (q, $^{2 \text{ or } 3}J_{BC}$ = 10 Hz)	BPh_4	6.90 (m, 8H)
BPh_4	136.4 (m)	BPh_4	7.16 (m, 8H)
C^2	156.0 (d, $^2J_{PC}$ = 41 Hz)	-	-
C^{14}	163.4 (d, $^2J_{PC}$ = 111 Hz)	-	-
ipso-BPh_4	164.2 (q, $^1J_{BC}$ = 49 Hz)	-	-

^{1}H and $^{13}C\{^{1}H\}$ NMR (d^6-DMSO) assignments were made with the aid of ^{1}H-^{13}C-$^{1}J_{CH}$ shift correlation NMR spectroscopy, ^{1}H-^{13}C-$^{n}J_{CH}$ (n > 1) shift correlation NMR spectroscopy and ^{1}H NOESY NMR spectroscopy.

Mass spectrum (Electrospray):

m/z (%) 443 (100) [M^+]

$^{1}H\{^{31}P\}$ NMR data (500 MHz, d^6-DMSO, 25 °C):

Identical to ^{1}H NMR data (500 MHz, d^6-DMSO, 25 °C) except for:

1.11 [s, 9H, $P(CH_3)_3$]
7.51 [d, 1H, $^{3}J_{HH}$ = 2 Hz, NC*H*]

$^{31}P\{^{1}H\}$ NMR data (202.4 MHz, d^6-DMSO, 25 °C):

-13.5 [s, $P(CH_3)_3$]

6.11 Data Characterising $[Ni(^{tBu}CC^{meth})_2][Cl]_2$ (11)

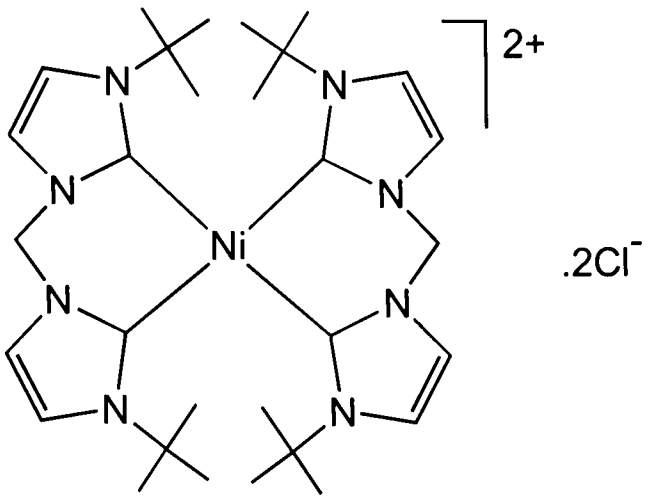

Description: Air-stable pale yellow powder.

Mass spectrum (Electrospray): m/z (%) 289 (100) $[M^{2+}]$

^{1}H NMR data (500 MHz, CD_3OD, 25 °C):

1.45 [s, 18H, $C(CH_3)_3$]

6.65 [d, 1H, $^2J_{HH}$ = 14 Hz, $N(CH_2)N$]

7.11 [d, 1H, $^2J_{HH}$ = 14 Hz, $N(CH_2)N$]

7.51 [d, 2H, $^3J_{HH}$ = 2 Hz, NC*H*]

7.76 [d, 2H, $^3J_{HH}$ = 2 Hz, NC*H*]

$^{13}C\{^1H\}$ NMR data (125.7 MHz, CD_3OD, 25 °C):

31.9 [s, $C(CH_3)_3$]

60.9 [s, $C(CH_3)_3$]

65.8 [s, $N(CH_2)N$]

123.4 [s, NCH]

125.0 [s, NCH]

170.3 [NCN]

6.12 Data Characterising [(μ-$^{tBu}CC^{meth}$){Ni(PMe_3)Me_2}$_2$] (12)

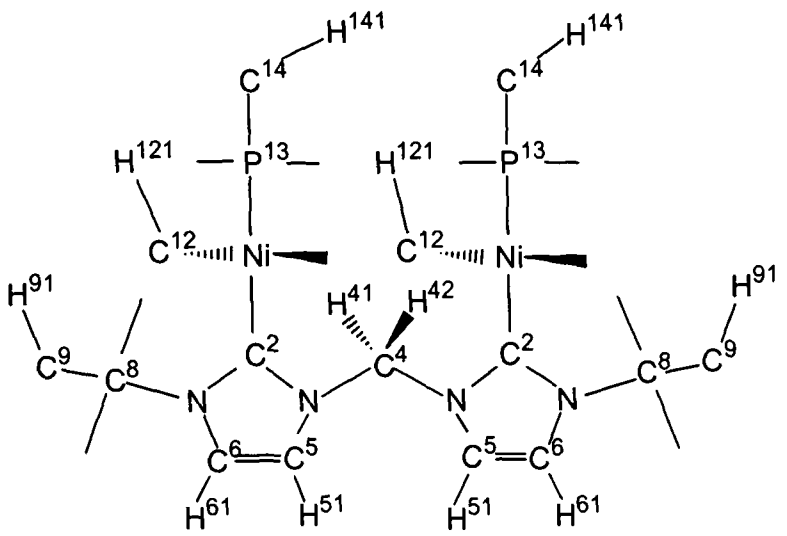

Atom labels from crystal structure

Description: Air-sensitive pale orange crystals.

Elemental analysis: $C_{25}H_{54}N_4Ni_2P_2$. 0.5 C_5H_{12}

Found (Calc.) / %: C 52.65 (52.75), H 9.36 (9.66), N 9.45 (9.66)

^{1}H and ^{13}C{^{1}H} NMR assignments (d^8-toluene, 25 °C):

Carbon atom label	^{13}C{^{1}H} NMR (125.7 MHz) data	Corresponding hydrogen atom label	Corresponding ^{1}H NMR (500 MHz) data
C^{12}	-9.2 (broad)	H^{121}	-0.64 (d, 12H, $^3J_{PH}$ = 11 Hz)
C^{14}	13.5 (d, $^1J_{PC}$ = 23 Hz)	H^{141}	1.05 (d, 18H, $^2J_{PH}$ = 8 Hz)
C^9	31.5 (s)	H^{91}	1.70 (s, 18H)
C^8	57.0 (s)	-	-
C^4	66.1 (s)	H^{41} and H^{42}	7.90 (s, 2H)
C^6	119.11 (d, $^4J_{PC}$ = 4 Hz)	H^{61}	6.42 (d, $^3J_{HH}$ = 2Hz)
C^5	119.14 (d, $^4J_{PC}$ = 4 Hz)	H^{51}	7.42 (d, $^3J_{HH}$ = 2Hz)
C^2	200.2 (d, $^2J_{PC}$ = 106 Hz)	-	-

^{31}P{^{1}H} NMR data (202.4 MHz, d^8-toluene, 25 °C):

-3.83 [s, $P(CH_3)_3$]

$^{1}H\{^{31}P\}$ NMR data (500 MHz, d^8-toluene, 25 °C)**:**

Identical to ^{1}H NMR data (500 MHz, $CD_3C_6D_5$, 25 °C) except for:

-0.64 [s, 12H, $Ni(CH_3)_2$]
1.05 [s, 18H, $C(CH_3)_3$]

^{1}H and $^{13}C\{^{1}H\}$ NMR (d^8-toluene) assignments were made with the aid of ^{1}H-^{13}C-$^{1}J_{CH}$ shift correlation NMR spectroscopy, ^{1}H-^{13}C-$^{n}J_{CH}$ ($n > 1$) shift correlation NMR spectroscopy and ^{1}H NOESY NMR spectroscopy.

6.13 Data Characterising Ni(^{tBu}CC^{eth})Me$_2$ (13)

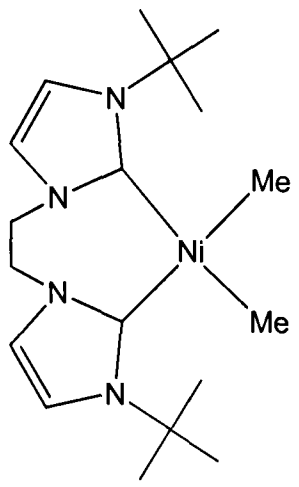

Description: Air-sensitive yellow powder. Must be stored below -20 °C.

Elemental analysis: $C_{18}H_{32}N_4Ni$

Found (Calc.) / %: C 59.43 (59.53), H 8.62 (8.88), N 15.58 (15.43)

^{1}H NMR data (500 MHz, C_6D_6, 25 °C)**:**

0.13 [s, 6H, Ni(CH_3)$_2$] 1.74 [s, 18H, C(CH_3)$_3$]

3.33 [m, 2H, N(C$_2H_4$)N] 5.88 [m, 2H, N(C$_2H_4$)N]

6.08 [d, 2H, $^3J_{HH}$ = 2 Hz, NC*H*] 6.35 [d, 2H, $^3J_{HH}$ = 2 Hz, NC*H*]

^{13}C{^{1}H} NMR data (125.7 MHz, C_6D_6, 25 °C)**:**

-0.7 [s, Ni(*C*H$_3$)$_2$] 31.7 [s, C(*C*H$_3$)$_3$] 48.3 [s, N(*C*$_2$H$_4$)N]

56.9 [s, *C*(CH$_3$)$_3$] 117.1 [s, N*C*H] 119.5 [s, N*C*H]

197.6 [s, N*C*N]

^{1}H-^{13}C-$^1J_{CH}$ shift correlated NMR data (125.7 MHz, C_6D_6, 25 °C)**:**

Cross-peaks (^{1}H, ^{13}C):

0.13, -0.7 [Ni(*CH*$_3$)$_2$] 1.74, 31.7 [C(*CH*$_3$)$_3$] 3.33, 48.3 [N(*C*$_2$*H*$_4$)N]

5.88, 48.3 [N(*C*$_2$*H*$_4$)N] 6.08, 119.5 [N*C*H] 6.35, 117.1 [N*C*H]

6.14 Data Characterising Pd(^{tBu}CC^{meth})Me$_2$ (14)

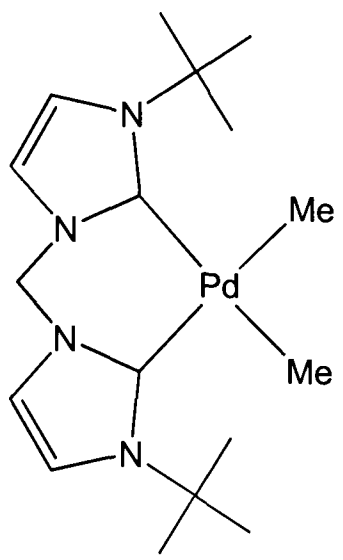

Description: Moderately air-stable beige microcrystalline solid.

Elemental analysis: $C_{17}H_{30}N_4Pd$

Found (Calc.) / %: C 51.44 (51.45), H 7.64 (7.62), N 14.02 (14.12)

^{1}H NMR data (500 MHz, C_6D_6, 25 °C)**:**

0.88 [s, 6H, Pd(CH_3)$_2$]
1.59 [s, 18H, C(CH_3)$_3$]
4.65 [d, 1H, $^2J_{HH}$ = 13 Hz, N(CH_2)N]
6.25 [d, 2H, $^3J_{HH}$ = 2 Hz, NCH]
6.41 [d, 2H, $^3J_{HH}$ = 2 Hz, NCH]
6.54 [d, 1H, $^2J_{HH}$ = 13 Hz, N(CH_2)N]

^{13}C{^{1}H} NMR data (125.7 MHz, C_6D_6, 25 °C)**:**

-3.0 [s, Pd(CH$_3$)$_2$]
31.5 [s, C(CH$_3$)$_3$]
57.8 [s, C(CH$_3$)$_3$]
64.0 [s, N(CH$_2$)N]
116.6 [s, NCH]
118.3 [s, NCH]
195.3 [s, NCN]

6.15 Data Characterising Pd(^{tBu}CC^{eth})Me$_2$ (15)

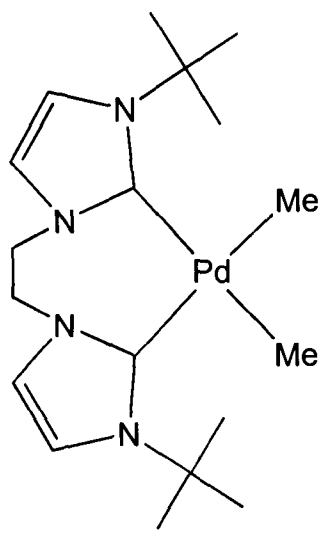

Description: Moderately air-stable white microcrystalline solid.

Elemental analysis: $C_{18}H_{32}N_4Pd$

Found (Calc.) / %: C 52.19 (52.62), H 8.22 (7.85), N 13.26 (13.64)

^{1}H NMR data (500 MHz, C_6D_6, 25 °C):

0.66 [s, 6H, Pd(CH_3)$_2$]
1.66 [s, 18H, C(CH_3)$_3$]
3.26 [m, 2H, N(C$_2H_4$)N]
5.48 [m, 2H, N(C$_2H_4$)N]
6.04 [d, 2H, $^3J_{HH}$ = 2 Hz, NCH]
6.37 [d, 2H, $^3J_{HH}$ = 2 Hz, NCH]

^{13}C{^{1}H} NMR data (125.7 MHz, C_6D_6, 25 °C):

-4.8 [s, Pd(CH$_3$)$_2$]
31.8 [s, C(CH$_3$)$_3$]
48.9 [s, N(C_2H$_4$)N]
57.5 [s, C(CH$_3$)$_3$]
117.2 [s, NCH]
119.5 [s, NCH]
193.2 [s, NCN]

6.16 Data Characterising [(^{tBu}CC^{meth})PdMe(py)][OCD_3] (16)

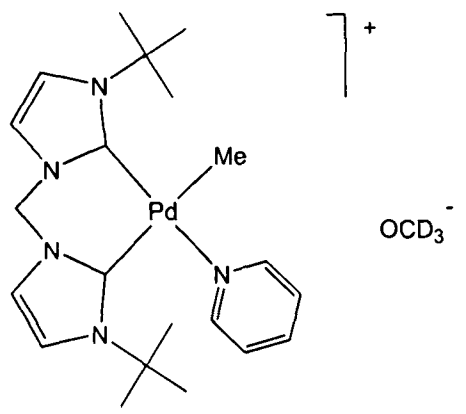

Description: Air-stable colourless CD_3OD solution.

Mass spectrum (Electrospray): m/z (%) 460 (100) [M^+]

^{1}H NMR data (500 MHz, CD_3OD, 25 °C):

0.04 [s, 3H, Pd(CH_3)]
1.31 [s, 9H, C(CH_3)$_3$]
1.80 [s, 9H, C(CH_3)$_3$]
6.20 [d, 1H, $^2J_{HH}$ = 14 Hz, N(CH_2)N]
6.92 [d, 1H, $^2J_{HH}$ = 14 Hz, N(CH_2)N]
7.28 [d, 1H, $^3J_{HH}$ = 2 Hz, NC*H*]
7.42 [d, 1H, $^3J_{HH}$ = 2 Hz, NC*H*]
7.46 [d, 1H, $^3J_{HH}$ = 2 Hz, NC*H*]
7.50 [d, 1H, $^3J_{HH}$ = 2 Hz, NC*H*]
7.53 [m, 2H, Pd(NC_5H_5)]
7.95 [m, 1H, Pd(NC_5H_5)]
8.70 [m, 2H, Pd(NC_5H_5)]

Free py: 7.45 [m, 2H] 7.87 [m, 1H] 8.56 [m, 2H]

^{13}C{^{1}H} NMR data (125.7 MHz, CD_3OD, 25 °C):

-1.1 [s, Pd(CH_3)]
31.1 [s, C(CH_3)$_3$]
32.0 [s, C(CH_3)$_3$]
59.1 [s, C(CH_3)$_3$]
60.0 [s, C(CH_3)$_3$]
66.0 [s, N(CH_2)N]
119.5 [s, NCH]
121.0 [s, NCH]
121.5 [s, NCH]
121.9 [s, NCH]
127.0 [s, Pd(NC_5H_5)]
139.4 [s, Pd(NC_5H_5)]
153.4 [s, Pd(NC_5H_5)]
172.0 [s, NCN]
184.9 [s, NCN]

Free py: 125.6 [s] 138.4 [s] 150.1 [s]

6.17 Data Characterising [(^{tBu}CC^{eth})PdMe(py)][OCD_3] (17)

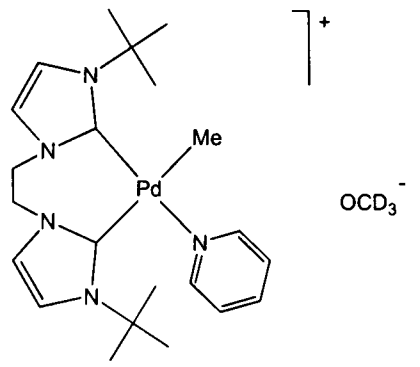

Description: Air-stable colourless CD_3OD solution.

Mass spectrum (Electrospray): m/z (%) 475 (90) [M^+], 396 (10) [M^+ - Py]

^{1}H NMR data (500 MHz, CD_3OD, 25 °C):

-0.10 [s, 3H, Pd(CH_3)]
1.44 [s, 9H, C(CH_3)$_3$]
1.81 [s, 9H, C(CH_3)$_3$]
4.54 [m, 1H, N(C_2H_4)N]
4.63 [m, 1H, N(C_2H_4)N]
5.44 [m, 1H, N(C_2H_4)N]
6.22 [m, 1H, N(C_2H_4)N]
7.26 [d, 1H, $^3J_{HH}$ = 2 Hz, NC*H*]
7.35 [d, 1H, $^3J_{HH}$ = 2 Hz, NC*H*]
7.37 [d, 1H, $^3J_{HH}$ = 2 Hz, NC*H*]
7.43 [d, 1H, $^3J_{HH}$ = 2 Hz, NC*H*]
7.50 [m, 2H, Pd(NC_5H_5)]
7.94 [m, 1H, Pd(NC_5H_5)]
8.59 [m, 2H, Pd(NC_5H_5)]

Free py: 7.45 [m, 2H] 7.87 [m, 1H] 8.56 [m, 2H]

^{13}C{^{1}H} NMR data (125.7 MHz, CD_3OD, 25 °C):

-2.2 [s, Pd(CH_3)]
31.7 [s, C(CH_3)$_3$]
32.0 [s, C(CH_3)$_3$]
50.25 [s, N(C_2H_4)N]
50.30 [s, N(C_2H_4)N]
59.1 [s, *C*(CH_3)$_3$]
59.5 [s, *C*(CH_3)$_3$]
120.5 [s, N*C*H]
121.7 [s, N*C*H]
122.3 [s, N*C*H]
124.0 [s, N*C*H]
126.8 [s, Pd(NC_5H_5)]
139.2 [s, Pd(NC_5H_5)]
153.3 [s, Pd(NC_5H_5)]
169.0 [s, N*C*N]
181.3 [s, N*C*N]

Free py: 125.6 [s] 138.4 [s] 150.1 [s]

6.18 Data Characterising [(^{tBu}C(D)C^{meth})PdMe(bpy)][OCD_3]$_2$ (18)

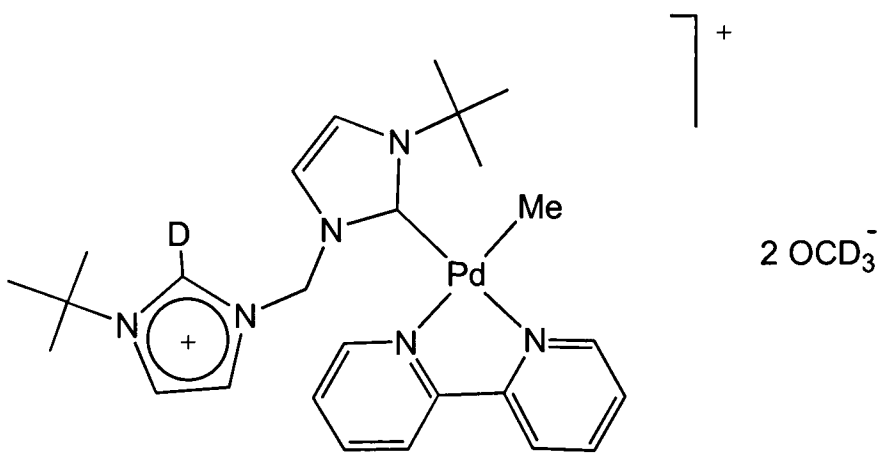

Description: Air-stable colourless CD_3OD solution.

Mass spectrum (Electrospray)**:**

m/z (%) 540 (25) [M^+], 484 (25) [M^+ - ^{t}Bu], 270 (25) [M^{2+}], 242 (25) [(M - ^{t}Bu)$^{2+}$]

^{1}H NMR data (500 MHz, CD_3OD, 25 °C)**:**

0.43 [s, 3H, Pd(CH_3)]
1.41 [s, 9H, C(CH_3)$_3$]
1.82 [s, 9H, C(CH_3)$_3$]
6.74 [s, 2H, N(CH_2)N]
7.55 [m, 1H, Pd($N_2C_{10}H_8$)]
7.61 [m, 1H, Pd($N_2C_{10}H_8$)]
7.86 [d, 1H, $^3J_{HH}$ = 2 Hz, NCH]
7.87 [m, 1H, Pd($N_2C_{10}H_8$)]
7.97 [d, 1H, $^3J_{HH}$ = 2 Hz, NCH]
8.25 [m, 1H, Pd($N_2C_{10}H_8$)]
8.37 [m, 1H, Pd($N_2C_{10}H_8$)]
8.59 [m, 1H, Pd($N_2C_{10}H_8$)]
8.63 [m, 1H, Pd($N_2C_{10}H_8$)]
8.77 [m, 1H, Pd($N_2C_{10}H_8$)]

Free bpy: 7.46 [m], 7.97 [m], 8.33 [m], 8.68 [m]

$^{13}C\{^1H\}$ NMR data (125.7 MHz, CD_3OD, 25 °C):

-3.8 [s, Pd(*C*H_3)]
31.7 [s, C(*C*H_3)$_3$]
62.1 [s, *C*(CH$_3$)$_3$]
122.4 [s, N*C*H]
124.6 [s, Pd(N$_2$*C*$_{10}$H$_8$)]
128.5 [s, Pd(N$_2$*C*$_{10}$H$_8$)]
135.9 [s, N(*C*D)N]
142.0 [s, Pd(N$_2$*C*$_{10}$H$_8$)]
151.3 [s, Pd(N$_2$*C*$_{10}$H$_8$)]
157.6 [s, Pd(N$_2$*C*$_{10}$H$_8$)]

29.5 [s, C(*C*H$_3$)$_3$]
61.2 [s, *C*(CH$_3$)$_3$]
64.1 [s, N(*C*H$_2$)N]
123.4 [s, N*C*H]
124.8 [s, Pd(N$_2$*C*$_{10}$H$_8$)]
128.8 [s, Pd(N$_2$*C*$_{10}$H$_8$)]
141.7 [s, Pd(N$_2$*C*$_{10}$H$_8$)]
149.4 [s, Pd(N$_2$*C*$_{10}$H$_8$)]
155.6 [s, Pd(N$_2$*C*$_{10}$H$_8$)]
173.3 [s, N*C*N]

Free bpy:

122.6 [s] 125.3 [s] 138.7 [s] 150.3 [s] 157.2 [s]

The ^{1}H NMR spectrum of (**18**) contains only two resonances for the four magnetically inequivalent NC*H* ring protons. This is probably due to deuterium exchange with the two NC*H* protons of the pendant imidazolium ring. Exchange of all three imidazolium ring protons with deuterium has previously been observed for 1-ethyl-3-methylimidazolium chloride in D_2O.[1] Only two carbon signals for the four magnetically inequivalent NCH carbons are discernable. The other two signals are impossible to distinguish from the baseline and the four other peaks in the region δ 120-125, probably due to peak height reduction because of the $^1J_{CD}$ and $^2J_{CD}$ coupling.

6.19 Data Characterising [(^{tBu}C(D)C^{eth})PdMe(bpy)][OCD$_3$]$_2$ (19)

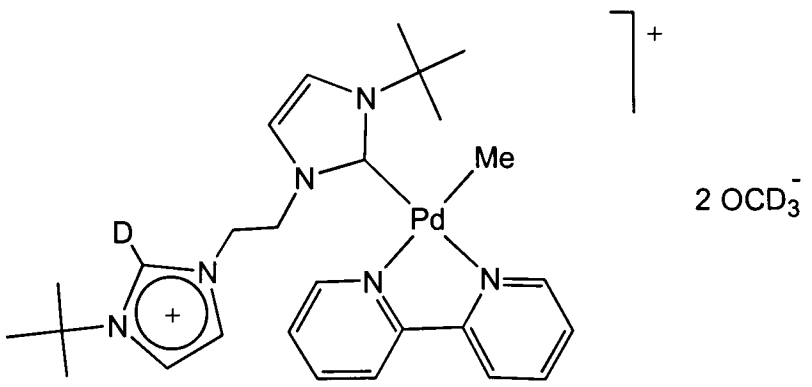

Description: Air-stable colourless CD_3OD solution.

Mass spectrum (Electrospray)**:**

m/z (%) 553 (25) [M^+], 498 (10) [M^+ - ^{t}Bu], 277 (40) [M^{2+}], 249 (25) [(M - ^{t}Bu)$^{2+}$]

^{1}H NMR data (500 MHz, CD_3OD, 25 °C)**:**

0.28 [s, 3H, Pd(C*H*$_3$)]
1.63 [s, 9H, C(C*H*$_3$)$_3$]
1.82 [s, 9H, C(C*H*$_3$)$_3$]
4.77 [m, 3H, N(C$_2$*H*$_4$)N]
5.39 [m, 1H, N(C$_2$*H*$_4$)N]
7.55 [d, 1H, $^3J_{HH}$ = 2 Hz, NC*H*]
7.62 [m, 1H, Pd(N$_2$C$_{10}$*H*$_8$)]
7.77 [m, 1H, Pd(N$_2$C$_{10}$*H*$_8$)]
7.79 [d, 1H, $^3J_{HH}$ = 2 Hz, NC*H*]
7.83 [m, 1H, Pd(N$_2$C$_{10}$*H*$_8$)]
8.25 [m, 1H, Pd(N$_2$C$_{10}$*H*$_8$)]
8.34 [m, 1H, Pd(N$_2$C$_{10}$*H*$_8$)]
8.57 [m, 1H, Pd(N$_2$C$_{10}$*H*$_8$)]
8.60 [m, 1H, Pd(N$_2$C$_{10}$*H*$_8$)]
8.71 [m, 1H, Pd(N$_2$C$_{10}$*H*$_8$)]

Free bpy:

7.46 [m], 7.97 [m], 8.33 [m], 8.68 [m]

$^{13}C\{^1H\}$ NMR data (125.7 MHz, CD_3OD, 25 °C):

-4.3 [s, Pd(CH_3)]
31.8 [s, C(CH_3)$_3$]
53.2 [s, N(C_2H_4)N]
61.7 [s, C(CH$_3$)$_3$]
123.5 [s, NCH]
124.7 [s, Pd(N$_2C_{10}$H$_8$)]
128.8 [s, Pd(N$_2C_{10}$H$_8$)]
141.5 [s, Pd(N$_2C_{10}$H$_8$)]
149.2 [s, Pd(N$_2C_{10}$H$_8$)]
155.7 [s, Pd(N$_2C_{10}$H$_8$)]
171.5 [s, NCN]
29.7 [s, C(CH_3)$_3$]
50.0 [s, N(C_2H_4)N]
60.5 [s, C(CH$_3$)$_3$]
121.7 [s, NCH]
124.4 [s, Pd(N$_2C_{10}$H$_8$)]
128.3 [s, Pd(N$_2C_{10}$H$_8$)]
135.8 [s, N(CD)N]
141.8 [s, Pd(N$_2C_{10}$H$_8$)]
151.3 [s, Pd(N$_2C_{10}$H$_8$)]
157.7 [s, Pd(N$_2C_{10}$H$_8$)]

Free bpy:

122.6 [s]	125.3 [s]	138.7 [s]	150.3 [s]	157.1 [s]

The ^{1}H NMR spectrum of (**19**) contains only two resonances for the four magnetically inequivalent NCH ring protons. This is probably due to deuterium exchange with the two NCH protons of the pendant imidazolium ring. Exchange of all three imidazolium ring protons with deuterium has previously been observed for 1-ethyl-3-methylimidazolium chloride in D_2O.[1] Only two carbon signals for the four magnetically inequivalent NCH carbons are discernable. The other two signals are impossible to distinguish from the baseline and the four other peaks in the region δ 120-125, probably due to peak height reduction because of the $^1J_{CD}$ and $^2J_{CD}$ coupling.

6.20 References

1) Avent, A. G.; Chaloner, P. A.; Day, M. P.; Seddon, K. R.; Welton, T. *J. Chem. Soc. Dalton Trans.* **1994**, 3405.

APPENDICES

X-Ray Crystal Structure Data

A. X-Ray Structure Analysis of 1,1'-Methylene*bis*(3-*tert*-butylimidazolium) Dibromide (2)

A.1 Summary of Crystallographic Data

Empirical formula	$C_{15}H_{26}Br_2N_4.2H_2O$	
Formula weight	458.24	
Temperature	180 K	
Wavelength (Mo-Kα)	0.71073 Å	
Crystal system	Monoclinic	
Space group	$P2_1/c$	
Unit cell dimensions	a = 7.216(1) Å	α= 90°
	b = 18.161(2) Å	β= 101.69(2)°
	c = 15.510(2) Å	γ = 90°
Volume	1990.5 $Å^3$	
Z	4	
Density (calculated)	1.52 Mg/m^3	
Absorption coefficient	4.05 mm^{-1}	
F(000)	917.27	
Crystal size	0.2 x 0.3 x 0.3 mm^3	
θ range for data collection	1.72 to 26.45°	
Index ranges	$-8\leq h\leq 8$, $0\leq k\leq 22$, $0\leq l\leq 19$	
Reflections collected	8662	
Independent reflections	4079 [R(int) = 0.086]	
Absorption correction	None	
Refinement method	Full-matrix least-squares on F	
Weighting scheme	Chebychev parameters 5.40, 0.275 and 4.30	
Data / parameters [$I>3\sigma(I)$]	2440/209	
Goodness-of-fit on F	1.0844	
Largest final shift	0.001476	
Final R indices	$R = 0.0425$, $wR_w = 0.0510$	
Residual density	0.77 and –1.26 $e.Å^{-3}$	

A.2 Interatomic Distances (Å) and Angles (°) for 1,1'-Methylene*bis*(3-*tert*-butylimidazolium) Dibromide (2)

N(3)	- C(4)	1.315(5)	
N(3)	- C(7)	1.383(5)	
N(3)	- C(18)	1.493(5)	
C(4)	- N(5)	1.336(5)	
N(5)	- C(6)	1.386(5)	
N(5)	- C(8)	1.449(5)	
C(6)	- C(7)	1.342(6)	
C(8)	- N(9)	1.455(5)	
N(9)	- C(10)	1.329(5)	
N(9)	- C(13)	1.380(5)	
C(10)	- N(11)	1.322(5)	
N(11)	- C(12)	1.381(5)	
N(11)	- C(14)	1.511(5)	
C(12)	- C(13)	1.334(6)	
C(14)	- C(15)	1.507(6)	
C(14)	- C(16)	1.511(7)	
C(14)	- C(17)	1.500(7)	
C(18)	- C(19)	1.502(6)	
C(18)	- C(20)	1.508(6)	
C(18)	- C(21)	1.521(6)	

C(4)	- N(3)	- C(7)	108.2(3)
C(4)	- N(3)	- C(18)	126.5(3)
C(7)	- N(3)	- C(18)	125.3(3)
N(3)	- C(4)	- N(5)	109.0(3)
C(4)	- N(5)	- C(6)	108.6(3)
C(4)	- N(5)	- C(8)	125.8(3)
C(6)	- N(5)	- C(8)	125.5(3)
N(5)	- C(6)	- C(7)	106.2(3)
N(3)	- C(7)	- C(6)	108.1(3)
N(5)	- C(8)	- N(9)	111.0(3)
C(8)	- N(9)	- C(10)	124.0(3)
C(8)	- N(9)	- C(13)	127.2(3)
C(10)	- N(9)	- C(13)	108.8(3)
N(9)	- C(10)	- N(11)	108.4(3)
C(10)	- N(11)	- C(12)	108.4(3)
C(10)	- N(11)	- C(14)	125.2(3)
C(12)	- N(11)	- C(14)	126.4(3)
N(11)	- C(12)	- C(13)	107.7(3)
N(9)	- C(13)	- C(12)	106.7(3)
N(11)	- C(14)	- C(15)	107.6(4)
N(11)	- C(14)	- C(16)	108.4(4)
C(15)	- C(14)	- C(16)	109.6(4)
N(11)	- C(14)	- C(17)	107.1(4)
C(15)	- C(14)	- C(17)	112.1(5)
C(16)	- C(14)	- C(17)	111.8(5)
N(3)	- C(18)	- C(19)	108.8(3)
N(3)	- C(18)	- C(20)	107.7(3)
C(19)	- C(18)	- C(20)	111.0(4)
N(3)	- C(18)	- C(21)	107.2(3)
C(19)	- C(18)	- C(21)	109.3(4)
C(20)	- C(18)	- C(21)	112.6(5)
C(6)	- N(5)	- C(8)	125.5(3)
N(5)	- C(6)	- C(7)	106.2(3)
N(3)	- C(7)	- C(6)	108.1(3)
N(5)	- C(8)	- N(9)	111.0(3)
C(8)	- N(9)	- C(10)	124.0(3)
C(8)	- N(9)	- C(13)	127.2(3)
C(10)	- N(9)	- C(13)	108.8(3)
N(9)	- C(10)	- N(11)	108.4(3)
C(10)	- N(11)	- C(12)	108.4(3)
C(10)	- N(11)	- C(14)	125.2(3)
C(12)	- N(11)	- C(14)	126.4(3)
N(11)	- C(12)	- C(13)	107.7(3)
N(9)	- C(13)	- C(12)	106.7(3)
N(11)	- C(14)	- C(15)	107.6(4)
N(11)	- C(14)	- C(16)	108.4(4)
C(15)	- C(14)	- C(16)	109.6(4)
N(11)	- C(14)	- C(17)	107.1(4)
C(15)	- C(14)	- C(17)	112.1(5)
C(16)	- C(14)	- C(17)	111.8(5)
N(3)	- C(18)	- C(19)	108.8(3)
N(3)	- C(18)	- C(20)	107.7(3)
C(19)	- C(18)	- C(20)	111.0(4)
N(3)	- C(18)	- C(21)	107.2(3)
C(19)	- C(18)	- C(21)	109.3(4)
C(20)	- C(18)	- C(21)	112.6(5)

A.3 Fractional Atomic Coordinates and Isotropic Thermal Parameters for All Non-Hydrogen Atoms of 1,1'-Methylene*bis*(3-*tert*-butylimidazolium) Dibromide (2)

Atom	x/a	y/b	z/c	U(iso)	Occ
Br(1)	0.16011(6)	0.13759(3)	0.94763(3)	0.0503	
Br(2)	-0.05463(8)	0.11992(4)	0.64512(4)	0.0739	
N(3)	0.4168(4)	-0.01850(17)	0.8308(2)	0.0325	
C(4)	0.3682(5)	0.0443(2)	0.7902(2)	0.0342	
N(5)	0.5245(4)	0.08305(17)	0.78797(19)	0.0329	
C(6)	0.6799(5)	0.0435(2)	0.8312(3)	0.0401	
C(7)	0.6116(5)	-0.0195(2)	0.8577(3)	0.0399	
C(8)	0.5302(6)	0.1562(2)	0.7512(3)	0.0396	
N(9)	0.5465(4)	0.21210(16)	0.81951(19)	0.0320	
C(10)	0.4049(5)	0.2553(2)	0.8311(2)	0.0350	
N(11)	0.4694(4)	0.30140(17)	0.8962(2)	0.0355	
C(12)	0.6583(6)	0.2861(2)	0.9281(3)	0.0437	
C(13)	0.7067(5)	0.2308(2)	0.8805(3)	0.0412	
C(14)	0.3559(7)	0.3623(2)	0.9273(3)	0.0455	
C(15)	0.4005(7)	0.3617(3)	1.0265(3)	0.0566	
C(16)	0.1480(8)	0.3462(3)	0.8945(4)	0.0720	
C(17)	0.4138(11)	0.4330(3)	0.8905(5)	0.0899	
C(18)	0.2858(5)	-0.0776(2)	0.8486(3)	0.0369	
C(19)	0.0859(6)	-0.0547(3)	0.8107(4)	0.0652	
C(20)	0.3363(9)	-0.1474(3)	0.8060(5)	0.0766	
C(21)	0.3115(8)	-0.0846(3)	0.9481(3)	0.0655	
O(22)	0.1633(6)	0.2800(2)	0.6435(2)	0.0820	
O(23)	0.1355(15)	-0.0196(7)	0.549(1)	0.2533	

A.4 Anisotropic Thermal Parameters For 1,1'-Methylene*bis*(3-*tert*-butylimidazolium) Dibromide (2)

Atom	u(11)	u(22)	u(33)	u(23)	u(13)	u(12)
Br(1)	0.0417(3)	0.0495(3)	0.0565(3)	0.0033(2)	0.00237(18)	0.00934(18)
Br(2)	0.0490(3)	0.1073(5)	0.0680(4)	0.0405(3)	0.0182(2)	0.0206(3)
N(3)	0.0302(16)	0.0349(17)	0.0315(15)	-0.0043(12)	0.0042(11)	0.0050(12)
C(4)	0.0332(19)	0.037(2)	0.0314(18)	-0.0033(15)	0.0029(14)	0.0029(14)
N(5)	0.0346(16)	0.0318(15)	0.0320(16)	-0.0026(13)	0.0063(12)	0.0034(12)
C(6)	0.0289(19)	0.040(2)	0.051(2)	0.0004(17)	0.0076(15)	0.0042(15)
C(7)	0.032(2)	0.038(2)	0.048(2)	-0.0016(17)	0.0055(15)	0.0064(15)
C(8)	0.046(2)	0.041(2)	0.033(2)	0.0016(15)	0.0125(16)	0.0046(16)
N(9)	0.0333(16)	0.0309(15)	0.0315(15)	0.0044(12)	0.0059(12)	0.0018(11)
C(10)	0.0338(19)	0.039(2)	0.0311(17)	0.0050(15)	0.0040(14)	0.0043(14)
N(11)	0.0408(18)	0.0335(16)	0.0310(15)	0.0033(13)	0.0043(12)	0.0043(13)
C(12)	0.044(2)	0.036(2)	0.047(2)	-0.0011(17)	-0.0013(17)	-0.0040(16)
C(13)	0.033(2)	0.038(2)	0.049(2)	0.0047(17)	0.0001(16)	0.0040(15)
C(14)	0.061(3)	0.039(2)	0.039(2)	-0.0013(18)	0.0149(18)	0.0070(18)
C(15)	0.064(3)	0.072(3)	0.035(2)	-0.007(2)	0.0120(19)	0.003(2)
C(16)	0.062(3)	0.078(4)	0.068(3)	-0.015(3)	-0.004(3)	0.035(3)
C(17)	0.156(7)	0.036(3)	0.102(5)	0.010(3)	0.083(5)	0.016(3)
C(18)	0.036(2)	0.035(2)	0.040(2)	-0.0025(16)	0.0085(15)	0.0004(15)
C(19)	0.036(2)	0.054(3)	0.099(4)	0.009(3)	-0.001(2)	-0.0071(19)
C(20)	0.082(4)	0.043(3)	0.120(5)	-0.026(3)	0.058(4)	-0.009(2)
C(21)	0.063(3)	0.086(4)	0.048(3)	0.013(3)	0.012(2)	-0.021(3)
O(22)	0.099(3)	0.087(3)	0.0493(19)	-0.010(2)	-0.0096(19)	0.019(2)
O(23)	0.18(1)	0.240(12)	0.346(17)	0.072(11)	0.06(1)	-0.025(8)

A.5 Fractional Atomic Coordinates and Isotropic Thermal Parameters for Hydrogen Atoms of 1,1'-Methylene*bis*(3-*tert*-butylimidazolium) Dibromide (2)

Atom	x/a	y/b	z/c	U(iso)	Occ
H(171)	0.3478	0.4762	0.9115	0.0788	
H(201)	0.2497	-0.1886	0.8158	0.0708	
H(202)	0.4698	-0.1617	0.8307	0.0708	
H(203)	0.3210	-0.1399	0.7402	0.0708	
H(213)	0.2821	-0.0364	0.9743	0.0635	
H(41)	0.2429	0.0637	0.7640	0.0500	
H(61)	0.8175	0.0628	0.8423	0.0500	
H(81)	0.6550	0.1560	0.7229	0.0500	
H(101)	0.2704	0.2518	0.7937	0.0500	
H(82)	0.3971	0.1642	0.7090	0.0500	
H(71)	0.6854	-0.0628	0.8873	0.0500	
H(151)	0.3179	0.3943	1.0515	0.0500	
H(152)	0.5338	0.3692	1.0529	0.0500	
H(192)	0.0583	-0.0042	0.8433	0.0500	
H(172)	0.5371	0.4422	0.9063	0.0500	
H(131)	0.8183	0.2002	0.8821	0.0500	
H(191)	-0.0025	-0.0893	0.8233	0.0500	
H(212)	0.4513	-0.0980	0.9833	0.0500	
H(153)	0.3763	0.3112	1.0452	0.0500	
H(193)	0.0821	-0.0500	0.7360	0.0500	
H(173)	0.3992	0.4342	0.8235	0.0500	
H(121)	0.7621	0.3218	0.9692	0.0500	
H(211)	0.2067	-0.1173	0.9671	0.0500	
H(161)	0.1152	0.2986	0.9206	0.0500	
H(162)	0.0709	0.3868	0.9130	0.0500	
H(163)	0.1203	0.3422	0.8290	0.0500	

B. X-ray Structure Analysis of $[Ni(^{tBu}CC^{meth})_2][Br]_2$ (6)

B.1 Summary of Crystallographic Data

Empirical formula	$C_{30}H_{48}Br_2N_8Ni.4MeOH$	
Formula weight	867.44	
Temperature	180 K	
Wavelength (Mo-Kα)	0.71073 Å	
Crystal system	Monoclinic	
Space group	$P2_1/c$	
Unit cell dimensions	a = 11.414(2) Å	α= 90°
	b = 14.919(1) Å	β= 115.00(1)°
	c = 13.376(2) Å	γ = 90°
Volume	2064.3(6) $Å^3$	
Z	4	
Density (calculated)	1.37 Mg/m^3	
Absorption coefficient	2.43 mm^{-1}	
F(000)	875.22	
Crystal size	0.2 x 0.2 x 0.3 mm^3	
θ range for data collection	1.98 to 26.50°.	
Index ranges	$0\leq h\leq 14$, $0\leq k\leq 18$, $-16\leq l\leq 14$	
Reflections collected	5406	
Independent reflections	4103 [R(int) = 0.029]	
Absorption correction	None	
Refinement method	Full-matrix least-squares on F	
Weighting scheme	Chebychev parameters 3.83, 1.44 and 2.85	
Data / parameters [$I>3\sigma(I)$]	2857/223	
Goodness-of-fit on F	1.1913	
Largest final shift	0.007510	
Final R indices	$R = 0.0574$, $wR_w = 0.0704$	
Residual density	0.75 and -0.59 $e.Å^{-3}$	

B.2 Interatomic Distances (Å) and Angles (°) for $[Ni(^{tBu}CC^{meth})_2][Br]_2$ (6)

NI(2) - C(3)	1.936(4)
NI(2) - C(3)	1.936(4)
NI(2) - C(7)	1.928(4)
NI(2) - C(7)	1.928(4)
C(3) - N(4)	1.366(5)
C(3) - N(17)	1.354(6)
N(4) - C(5)	1.433(6)
N(4) - C(15)	1.386(6)
C(5) - N(6)	1.454(5)
N(6) - C(7)	1.346(5)
N(6) - C(10)	1.378(5)
C(7) - N(8)	1.354(5)
N(8) - C(9)	1.377(6)
N(8) - C(11)	1.501(5)
C(9) - C(10)	1.336(7)
C(11) - C(12)	1.511(7)
C(11) - C(13)	1.495(7)
C(11) - C(14)	1.527(6)
C(15) - C(16)	1.326(7)
C(16) - N(17)	1.386(6)
N(17) - C(18)	1.500(6)
C(18) - C(19)	1.512(7)
C(18) - C(20)	1.521(6)
C(18) - C(21)	1.509(7)
C(22) - O(23)	1.411(2)
O(24) - C(25)	1.413(2)

C(3) - NI(2) - C(3)	179.99
C(3) - NI(2) - C(7)	83.57(17)
C(3) - NI(2) - C(7)	96.43(17)
C(3) - NI(2) - C(7)	96.43(17)
C(3) - NI(2) - C(7)	83.57(17)
C(7) - NI(2) - C(7)	179.99
NI(2) - C(3) - N(4)	114.3(3)
NI(2) - C(3) - N(17)	141.5(3)
N(4) - C(3) - N(17)	104.1(4)
C(3) - N(4) - C(5)	123.1(4)
C(3) - N(4) - C(15)	111.5(4)
C(5) - N(4) - C(15)	124.0(4)
N(4) - C(5) - N(6)	107.8(3)
C(5) - N(6) - C(7)	122.4(3)
C(5) - N(6) - C(10)	125.0(3)
C(7) - N(6) - C(10)	112.4(4)
NI(2) - C(7) - N(6)	115.7(3)
NI(2) - C(7) - N(8)	139.9(3)
N(6) - C(7) - N(8)	104.0(3)
C(7) - N(8) - C(9)	110.2(3)
C(7) - N(8) - C(11)	127.8(3)
C(9) - N(8) - C(11)	121.7(3)
N(8) - C(9) - C(10)	108.2(4)
N(6) - C(10) - C(9)	105.2(4)
N(8) - C(11) - C(12)	110.0(4)
N(8) - C(11) - C(13)	109.0(4)
C(12) - C(11) - C(13)	111.9(5)
N(8) - C(11) - C(14)	107.5(4)
C(12) - C(11) - C(14)	106.8(4)
C(13) - C(11) - C(14)	111.5(4)
N(4) - C(15) - C(16)	105.7(4)
C(15) - C(16) - N(17)	108.7(4)
C(3) - N(17) - C(16)	110.0(4)
C(3) - N(17) - C(18)	129.7(4)
C(16) - N(17) - C(18)	119.4(4)
N(17) - C(18) - C(19)	111.6(4)
N(17) - C(18) - C(20)	106.8(4)
C(19) - C(18) - C(20)	110.0(4)
N(17) - C(18) - C(21)	108.8(4)
C(19) - C(18) - C(21)	109.9(4)
C(20) - C(18) - C(21)	109.6(5)

B.3 Fractional Atomic Coordinates and Isotropic Thermal Parameters for All Non-Hydrogen Atoms of $[Ni(^{tBu}CC^{meth})_2][Br]_2$ (6)

Atom	x/a	y/b	z/c	U(iso)	Occ
Br(1)	0.30934(5)	0.52540(4)	0.14250(5)	0.0496	
Ni(2)	1.0000	0.5000	0.5000	0.0238	
C(3)	1.0406(4)	0.5075(2)	0.6557(4)	0.0265	
N(4)	0.9354(3)	0.5032(2)	0.6793(3)	0.0303	
C(5)	0.8107(4)	0.4737(3)	0.6014(4)	0.0321	
N(6)	0.8289(3)	0.3937(2)	0.5475(3)	0.0301	
C(7)	0.9203(4)	0.3882(3)	0.5089(4)	0.0283	
N(8)	0.9158(3)	0.3015(2)	0.4778(3)	0.0311	
C(9)	0.8198(5)	0.2566(3)	0.4939(4)	0.0405	
C(10)	0.7648(4)	0.3138(3)	0.5381(4)	0.0379	
C(11)	1.0078(5)	0.2534(3)	0.4427(4)	0.0373	
C(12)	1.1348(5)	0.3032(3)	0.4836(6)	0.0525	
C(13)	0.9469(6)	0.2441(4)	0.3199(5)	0.0518	
C(14)	1.0364(6)	0.1621(3)	0.4995(5)	0.0485	
C(15)	0.9705(5)	0.5120(3)	0.7915(4)	0.0343	
C(16)	1.0979(5)	0.5220(3)	0.8374(4)	0.0355	
N(17)	1.1417(4)	0.5182(2)	0.7554(3)	0.0315	
C(18)	1.2840(4)	0.5102(3)	0.7870(4)	0.0326	
C(19)	1.3138(5)	0.5138(4)	0.6871(5)	0.0522	
C(20)	1.3267(6)	0.4206(4)	0.8454(5)	0.0544	
C(21)	1.3531(5)	0.5853(4)	0.8653(5)	0.0553	
C(22)	0.593(1)	0.1782(7)	0.1761(8)	0.0965	
O(23)	0.4835(12)	0.2243(9)	0.1727(16)	0.4170	
O(24)	0.6992(13)	0.852(1)	0.2061(14)	0.2667	
C(25)	0.5810(11)	0.8574(11)	0.1109(15)	0.2267	

B.4 Anisotropic Thermal Parameters for $[Ni(^{tBu}CC^{meth})_2][Br]_2$ (6)

Atom	u(11)	u(22)	u(33)	u(23)	u(13)	u(12)
Br(1)	0.0339(3)	0.0662(4)	0.0453(4)	0.0107(2)	0.0133(3)	0.0027(2)
Ni(2)	0.0239(4)	0.0223(3)	0.0244(4)	-0.0004(3)	0.0093(3)	-0.0001(3)
C(3)	0.026(2)	0.0233(18)	0.028(2)	0.0007(15)	0.0090(18)	-0.0003(14)
N(4)	0.0292(18)	0.0315(17)	0.032(2)	-0.0008(14)	0.0151(16)	-0.0008(14)
C(5)	0.032(2)	0.033(2)	0.034(3)	-0.0048(16)	0.017(2)	-0.0017(16)
N(6)	0.0308(18)	0.0276(16)	0.031(2)	-0.0012(13)	0.0120(16)	-0.0041(13)
C(7)	0.029(2)	0.0252(19)	0.029(2)	-0.0006(15)	0.0107(18)	-0.0016(15)
N(8)	0.0331(18)	0.0227(16)	0.034(2)	-0.0029(13)	0.0113(17)	-0.0019(13)
C(9)	0.044(3)	0.030(2)	0.046(3)	-0.0050(18)	0.017(2)	-0.0087(18)
C(10)	0.035(2)	0.035(2)	0.045(3)	-0.0012(18)	0.017(2)	-0.0105(17)
C(11)	0.043(2)	0.026(2)	0.040(3)	-0.0049(17)	0.015(2)	0.0016(17)
C(12)	0.039(3)	0.035(2)	0.085(5)	-0.005(2)	0.028(3)	0.0012(19)
C(13)	0.059(3)	0.057(3)	0.038(3)	0.003(2)	0.019(3)	0.018(2)
C(14)	0.059(3)	0.029(2)	0.058(4)	0.005(2)	0.025(3)	0.005(2)
C(15)	0.041(3)	0.034(2)	0.029(3)	-0.0007(16)	0.017(2)	0.0020(17)
C(16)	0.041(2)	0.036(2)	0.028(3)	-0.0030(16)	0.014(2)	-0.0015(17)
N(17)	0.035(2)	0.0290(18)	0.033(2)	-0.0004(14)	0.0168(19)	-0.0008(13)
C(18)	0.026(2)	0.036(2)	0.026(3)	0.0021(16)	0.0021(19)	0.0021(16)
C(19)	0.029(2)	0.082(4)	0.045(4)	0.006(3)	0.015(2)	0.005(2)
C(20)	0.048(3)	0.049(3)	0.061(4)	0.019(3)	0.018(3)	0.013(2)
C(21)	0.038(3)	0.061(3)	0.063(4)	-0.019(3)	0.018(3)	-0.014(2)
C(22)	0.096(6)	0.120(7)	0.092(7)	0.037(5)	0.058(6)	0.002(6)
O(23)	0.259(17)	0.59(4)	0.30(2)	0.23(2)	0.012(15)	-0.25(2)
O(24)	0.170(12)	0.228(14)	0.39(2)	-0.126(16)	0.101(14)	-0.01(1)
C(25)	0.069(7)	0.250(19)	0.32(2)	-0.203(19)	0.04(1)	-0.051(9)

B.5 Fractional Atomic Coordinates and Isotropic Thermal Parameters for Hydrogen Atoms of $[Ni(^{tBu}CC^{meth})_2][Br]_2$ (6)

Atom	x/a	y/b	z/c	U(iso)	Occ
H(51)	0.7708	0.5222	0.5462	0.0318	
H(52)	0.7557	0.4605	0.6409	0.0318	
H(91)	0.7924	0.1925	0.4734	0.0391	
H(101)	0.6933	0.3012	0.5617	0.0382	
H(121)	1.1976	0.2707	0.4619	0.0481	
H(122)	1.1750	0.3070	0.5676	0.0481	
H(123)	1.1223	0.3654	0.4538	0.0481	
H(131)	1.0061	0.2110	0.2936	0.0542	
H(132)	0.9265	0.3042	0.2825	0.0542	
H(133)	0.8631	0.2087	0.2938	0.0542	
H(141)	1.0973	0.1270	0.4801	0.0487	
H(142)	1.0762	0.1704	0.5834	0.0487	
H(143)	0.9538	0.1269	0.4793	0.0487	
H(151)	0.9105	0.5109	0.8291	0.0323	
H(161)	1.1538	0.5296	0.9181	0.0342	
H(191)	1.4083	0.5071	0.7102	0.0486	
H(192)	1.2818	0.5705	0.6461	0.0486	
H(193)	1.2679	0.4616	0.6362	0.0486	
H(201)	1.4199	0.4105	0.8672	0.0525	
H(202)	1.3077	0.4183	0.9121	0.0525	
H(203)	1.2758	0.3703	0.7936	0.0525	
H(211)	1.4485	0.5827	0.8871	0.0562	
H(212)	1.3373	0.5823	0.9337	0.0562	
H(213)	1.3204	0.6458	0.8290	0.0562	

C. X-Ray Structure Analysis of [(^{tBu}CC^{meth})NiCl(PMe$_3$)]Cl (7)

C.1 Summary of Crystallographic Data

Empirical formula	$C_{18}H_{33}Cl_2N_4PNi.1.2CH_2Cl_2$	
Formula weight	558.01	
Temperature	180 K	
Wavelength (Mo-Kα)	0.71073 Å	
Crystal system	Monoclinic	
Space group	C2/c	
Unit cell dimensions	a = 27.711(3) Å	α= 90°
	b = 11.812(1) Å	β= 125.79(2)°
	c = 21.145(2) Å	γ = 90°
Volume	5614.3(5) Å^3	
Z	8	
Density (calculated)	1.32 Mg/m^3	
Absorption coefficient	1.16 mm^{-1}	
F(000)	2338.49	
Crystal size	0.2 x 0.2 x 0.3 mm^3	
θ range for data collection	1.72 to 26.33°	
Index ranges	-34≤h≤28, 0≤k≤14, 0≤l≤26	
Reflections collected	9300	
Independent reflections	5527 [R(int) = 0.037]	
Absorption correction	None	
Refinement method	Full-matrix least-squares on F	
Weighting scheme	Chebychev parameters 0.718, 0.580 and 0.467	
Data / parameters [I>3σ(I)]	2964/271	
Goodness-of-fit on F	1.0587	
Largest final shift	0.000983	
Final R indices	R = 0.0515, wR$_w$ = 0.0540	
Residual density	1.17 and –1.11 e.Å^{-3}	

C.2 Interatomic Distances (Å) and Angles (°) for [(^{tBu}CC^{meth})NiCl(PMe$_3$)]Cl (7)

NI(1) - C(2)	1.939(4)
NI(1) - C(6)	1.874(4)
NI(1) - P(22)	2.2074(14)
NI(1) - CL(26)	2.1956(11)
C(2) - N(3)	1.357(5)
C(2) - N(16)	1.343(5)
N(3) - C(4)	1.447(5)
N(3) - C(14)	1.382(5)
C(4) - N(5)	1.453(5)
N(5) - C(6)	1.351(5)
N(5) - C(9)	1.384(5)
C(6) - N(7)	1.338(5)
N(7) - C(8)	1.399(5)
N(7) - C(10)	1.491(6)
C(8) - C(9)	1.328(7)
C(10) - C(11)	1.521(6)
C(10) - C(12)	1.539(6)
C(10) - C(13)	1.518(7)
C(14) - C(15)	1.340(7)
C(15) - N(16)	1.381(6)
N(16) - C(17)	1.511(6)
C(17) - C(18)	1.516(7)
C(17) - C(19)	1.524(7)
C(17) - C(20)	1.525(7)
P(22) - C(23)	1.782(7)
P(22) - C(24)	1.818(6)
P(22) - C(25)	1.810(5)
CL(27)- C(28)	1.721(7)
C(28) - CL(29)	1.749(7)
C(30) - CL(31)	1.721(5)
C(30) - CL(31)	1.721(5)
C(30) - CL(32)	1.725(5)

C(2) - NI(1) - C(6)	85.04(15)
C(2) - NI(1) - P(22)	155.72(13)
C(6) - NI(1) - P(22)	91.98(12)
C(2) - NI(1) - CL(26)	93.99(11)
C(6) - NI(1) - CL(26)	177.69(14)
P(22) - NI(1) - CL(26)	88.05(5)
NI(1) - C(2) - N(3)	112.0(3)
NI(1) - C(2) - N(16)	142.3(3)
N(3) - C(2) - N(16)	104.3(3)
C(2) - N(3) - C(4)	123.1(3)
C(2) - N(3) - C(14)	111.1(3)
C(4) - N(3) - C(14)	125.7(3)
N(3) - C(4) - N(5)	108.4(3)
C(4) - N(5) - C(6)	120.5(3)
C(4) - N(5) - C(9)	127.5(3)
C(6) - N(5) - C(9)	110.0(3)
NI(1) - C(6) - N(5)	116.3(3)
NI(1) - C(6) - N(7)	137.0(3)
N(5) - C(6) - N(7)	106.7(3)
C(6) - N(7) - C(8)	108.6(3)
C(6) - N(7) - C(10)	128.9(3)
C(8) - N(7) - C(10)	121.9(3)
N(7) - C(8) - C(9)	108.1(4)
N(5) - C(9) - C(8)	106.5(3)
N(7) - C(10) - C(11)	110.8(3)
N(7) - C(10) - C(12)	109.1(4)
C(11) - C(10) - C(12)	110.0(4)
N(7) - C(10) - C(13)	107.8(4)
C(11) - C(10) - C(13)	108.8(4)
C(12) - C(10) - C(13)	110.3(4)
N(3) - C(14) - C(15)	106.3(4)
C(14) - C(15) - N(16)	107.0(4)
C(2) - N(16) - C(15)	111.1(4)
C(2) - N(16) - C(17)	128.2(3)
C(15) - N(16) - C(17)	120.5(3)
N(16) - C(17) - C(18)	107.9(4)
N(16) - C(17) - C(19)	108.3(4)
C(18) - C(17) - C(19)	110.3(4)
N(16) - C(17) - C(20)	109.1(3)
C(18) - C(17) - C(20)	110.4(4)
C(19) - C(17) - C(20)	110.7(4)
NI(1) - P(22) - C(23)	106.6(2)
NI(1) - P(22) - C(24)	118.0(2)
C(23) - P(22) - C(24)	104.6(3)
NI(1) - P(22) - C(25)	121.39(18)
C(23) - P(22) - C(25)	101.4(3)
C(24) - P(22) - C(25)	102.5(3)
CL(27)- C(28) - CL(29)	112.3(4)
CL(31)- C(30) - CL(31)	109.4(20)
CL(31)- C(30) - CL(32)	125.3(10)
CL(31)- C(30) - CL(32)	125.3(10)

C.3 Fractional Atomic Coordinates and Isotropic Thermal Parameters for [(^{tBu}CC^{meth})NiCl(PMe$_3$)]Cl (7)

Atom	x/a	y/b	z/c	U(iso)	Occ
Ni(1)	0.79142(2)	0.02064(5)	0.50424(3)	0.0330	
C(2)	0.85954(16)	0.0788(3)	0.6023(2)	0.0342	
N(3)	0.88708(13)	0.1638(3)	0.59173(19)	0.0345	
C(4)	0.87757(17)	0.1856(4)	0.5179(2)	0.0376	
N(5)	0.87844(14)	0.0782(3)	0.48511(19)	0.0340	
C(6)	0.84630(16)	-0.0105(4)	0.4819(2)	0.0354	
N(7)	0.86523(14)	-0.1017(3)	0.46476(19)	0.0354	
C(8)	0.91063(18)	-0.0687(4)	0.4582(2)	0.0428	
C(9)	0.91985(18)	0.0415(4)	0.4730(2)	0.0433	
C(10)	0.8496(2)	-0.2231(4)	0.4628(3)	0.0440	
C(11)	0.8000(2)	-0.2347(4)	0.4733(3)	0.0529	
C(12)	0.8301(2)	-0.2751(4)	0.3844(3)	0.0541	
C(13)	0.9046(2)	-0.2830(5)	0.5297(3)	0.0592	
C(14)	0.92726(18)	0.2196(4)	0.6610(3)	0.0448	
C(15)	0.92540(19)	0.1672(4)	0.7157(3)	0.0484	
N(16)	0.88494(14)	0.0798(3)	0.67931(19)	0.0381	
C(17)	0.8770(2)	-0.0043(4)	0.7264(2)	0.0459	
C(18)	0.9379(2)	-0.0299(5)	0.8004(3)	0.0648	
C(19)	0.8372(2)	0.0493(5)	0.7460(3)	0.0638	
C(20)	0.8487(3)	-0.1119(5)	0.6786(3)	0.0601	
Cl(21)	1.02423(5)	0.2796(1)	0.59683(7)	0.0491	
P(22)	0.71687(4)	0.02763(11)	0.37926(6)	0.0437	
C(23)	0.7007(3)	0.1737(6)	0.3545(3)	0.0728	
C(24)	0.6463(2)	-0.0345(6)	0.3487(4)	0.0770	
C(25)	0.7252(3)	-0.0219(7)	0.3051(3)	0.0806	
Cl(26)	0.72782(5)	0.06441(11)	0.53042(7)	0.0502	
Cl(27)	0.8680(1)	0.4215(2)	0.41273(15)	0.1169	
C(28)	0.9320(3)	0.4252(6)	0.4173(4)	0.0763	
Cl(29)	0.9298(1)	0.3303(2)	0.35214(12)	0.1284	
C(30)	1.0000	0.4446(18)	0.2500	0.09(1)	0.113(8)
Cl(31)	1.0004(12)	0.529(2)	0.3167(13)	0.079(8)	0.057(4)
Cl(32)	1.0000	0.2986(18)	0.2500	0.096(9)	0.113(8)

C.4 Anisotropic Thermal Parameters for [(^{tBu}CC^{meth})NiCl(PMe$_3$)]Cl (7)

Atom	u(11)	u(22)	u(33)	u(23)	u(13)	u(12)
Ni(1)	0.0302(2)	0.0412(3)	0.0333(3)	-0.0071(2)	0.0217(2)	-0.0028(2)
C(2)	0.0329(18)	0.041(2)	0.034(2)	-0.0072(17)	0.0222(17)	-0.0056(16)
N(3)	0.0351(16)	0.038(2)	0.0343(18)	-0.0048(14)	0.0222(15)	-0.0033(14)
C(4)	0.038(2)	0.036(3)	0.041(2)	-0.0022(18)	0.0239(19)	-0.0047(17)
N(5)	0.0363(16)	0.037(2)	0.0358(18)	-0.0046(14)	0.0250(15)	-0.0048(14)
C(6)	0.0344(18)	0.044(3)	0.0291(19)	-0.0019(17)	0.0196(16)	0.0019(17)
N(7)	0.0376(17)	0.040(2)	0.042(2)	-0.0045(14)	0.0309(16)	-0.0021(14)
C(8)	0.040(2)	0.057(3)	0.043(2)	-0.004(2)	0.030(2)	-0.000(2)
C(9)	0.044(2)	0.059(4)	0.041(2)	-0.002(2)	0.0333(19)	-0.002(2)
C(10)	0.052(2)	0.040(3)	0.049(3)	-0.0006(19)	0.035(2)	-0.0007(19)
C(11)	0.065(3)	0.044(3)	0.073(3)	-0.011(2)	0.053(3)	-0.009(2)
C(12)	0.060(3)	0.057(3)	0.052(3)	-0.014(2)	0.037(3)	-0.002(2)
C(13)	0.064(3)	0.057(4)	0.059(3)	0.006(2)	0.037(3)	0.010(2)
C(14)	0.039(2)	0.047(3)	0.047(3)	-0.012(2)	0.024(2)	-0.0116(18)
C(15)	0.041(2)	0.059(3)	0.044(3)	-0.018(2)	0.024(2)	-0.012(2)
N(16)	0.0356(17)	0.048(2)	0.037(2)	-0.0065(15)	0.0247(16)	-0.0040(15)
C(17)	0.052(2)	0.055(3)	0.033(2)	-0.0022(18)	0.0264(19)	-0.0028(19)
C(18)	0.070(3)	0.075(4)	0.048(3)	0.007(3)	0.033(2)	0.003(3)
C(19)	0.073(3)	0.082(4)	0.062(3)	0.003(3)	0.054(3)	0.002(3)
C(20)	0.081(4)	0.056(3)	0.053(3)	0.003(2)	0.044(3)	-0.011(2)
Cl(21)	0.0499(6)	0.0579(8)	0.0513(7)	0.0121(5)	0.0362(6)	0.0091(5)
P(22)	0.0338(5)	0.0549(8)	0.0392(6)	-0.0073(5)	0.0196(5)	0.0014(5)
C(23)	0.071(3)	0.069(4)	0.061(4)	0.004(3)	0.029(3)	0.017(3)
C(24)	0.057(3)	0.098(5)	0.061(3)	-0.013(3)	0.026(3)	-0.021(3)
C(25)	0.067(3)	0.125(6)	0.045(3)	0.000(3)	0.031(3)	0.034(3)
Cl(26)	0.0401(5)	0.0688(8)	0.0538(6)	-0.0147(5)	0.0343(5)	-0.0036(5)
Cl(27)	0.1321(17)	0.1105(17)	0.1457(19)	0.0688(14)	0.1024(16)	0.0504(13)
C(28)	0.084(4)	0.069(4)	0.061(4)	-0.003(3)	0.035(3)	-0.007(3)
Cl(29)	0.1200(16)	0.149(2)	0.0792(13)	-0.0137(12)	0.0374(12)	0.0543(14)

C.5 Fractional Atomic Coordinates and Isotropic Thermal Parameters for Hydrogen Atoms of [(^{tBu}CC^{meth})NiCl(PMe$_3$)]Cl (7)

Atom	x/a	y/b	z/c	U(iso)	Occ
H(41)	0.9093	0.2370	0.5251	0.0437	
H(42)	0.8376	0.2238	0.4803	0.0437	
H(81)	0.9336	-0.1195	0.4458	0.0559	
H(91)	0.9517	0.0892	0.4754	0.0485	
H(111)	0.7893	-0.3167	0.4725	0.0775	
H(112)	0.8125	-0.2017	0.5253	0.0775	
H(113)	0.7631	-0.1936	0.4310	0.0775	
H(121)	0.8193	-0.3574	0.3827	0.0718	
H(122)	0.8623	-0.2698	0.3773	0.0718	
H(123)	0.7937	-0.2345	0.3407	0.0718	
H(131)	0.8956	-0.3664	0.5301	0.0753	
H(132)	0.9383	-0.2776	0.5249	0.0753	
H(133)	0.9174	-0.2497	0.5811	0.0753	
H(141)	0.9534	0.2838	0.6686	0.0504	
H(151)	0.9496	0.1889	0.7723	0.0542	
H(181)	0.9331	-0.0859	0.8332	0.0765	
H(182)	0.9648	-0.0613	0.7893	0.0765	
H(183)	0.9552	0.0419	0.8323	0.0765	
H(191)	0.8310	-0.0047	0.7780	0.0870	
H(192)	0.8566	0.1202	0.7786	0.0870	
H(193)	0.7975	0.0704	0.6981	0.0870	
H(201)	0.8448	-0.1701	0.7106	0.0652	
H(202)	0.8770	-0.1470	0.6672	0.0652	
H(203)	0.8103	-0.0977	0.6295	0.0652	
H(231)	0.6675	0.1843	0.2985	0.0500	
H(232)	0.7373	0.2146	0.3651	0.0500	
H(233)	0.6900	0.2121	0.3875	0.0500	
H(241)	0.6165	-0.0264	0.2893	0.0500	
H(242)	0.6516	-0.1190	0.3598	0.0500	
H(243)	0.6301	0.0011	0.3741	0.0500	
H(251)	0.6872	-0.0115	0.2517	0.0500	
H(252)	0.7575	0.0231	0.3074	0.0500	
H(253)	0.7367	-0.1036	0.3130	0.0500	
H(281)	0.9679	0.4043	0.4734	0.0500	
H(282)	0.9401	0.5043	0.4078	0.0500	

D. X-ray Structure Analysis of [(^{tBu}CC^{eth})NiCl(PMe$_3$)][BPh$_4$] (10)

D.1 Summary of Crystallographic Data

Empirical formula	$C_{43}H_{55}BPClN_4Ni.1.5CH_2Cl_2$	
Formula weight	891.27	
Temperature	180 K	
Wavelength (Mo-Kα)	0.71073 Å	
Crystal system	Triclinic	
Space group	P(-1)	
Unit cell dimensions	a = 12.085(3) Å	α= 77.73(1)°
	b = 13.467(2) Å	β= 85.86(1)°
	c = 14.190(2) Å	γ = 86.48(2)°
Volume	2248.3 Å^3	
Z	2	
Density (calculated)	1.29 Mg/m^3	
Absorption coefficient	0.71 mm^{-1}	
F(000)	920.74	
Crystal size	0.2 x 0.3 x 0.3 mm^3	
θ range for data collection	1.79 to 26.45°.	
Index ranges	-14≤h≤15, -16≤k≤16, 0≤l≤17	
Reflections collected	9382	
Independent reflections	5852 [R(int) = 0.048]	
Absorption correction	None	
Refinement method	Full-matrix least-squares on F	
Weighting scheme	w = 1/(0.0010(F) + 3σ^2(F) + 3)	
Data / parameters [I>3σ(I)]	4603/505	
Goodness-of-fit on F	1.1229	
Largest final shift	0.000808	
Final R indices	R = 0.0950, wR$_w$ = 0.1097	
Residual density	0.89 and -0.55 e.Å^{-3}	

D.2 Interatomic Distances (Å) and Angles (°) for [(^{tBu}CC^{eth})NiCl(PMe$_3$)][BPh$_4$] (10)

NI(1) - CL(22)	2.200(2)
NI(1) - P(23)	2.203(3)
NI(1) - C(2)	1.857(7)
NI(1) - C(14)	1.915(8)
CL(27)- C(28)	1.717(17)
CL(29)- C(28)	1.659(17)
P(23) - C(24)	1.800(9)
P(23) - C(25)	1.81(1)
P(23) - C(26)	1.81(1)
N(3) - C(2)	1.327(9)
N(3) - C(4)	1.501(11)
N(3) - C(8)	1.400(11)
N(10) - C(2)	1.349(9)
N(10) - C(9)	1.377(11)
N(10) - C(11)	1.448(11)
N(13) - C(12)	1.469(11)
N(13) - C(14)	1.36(1)
N(13) - C(21)	1.381(12)
N(15) - C(14)	1.356(9)
N(15) - C(16)	1.500(11)
N(15) - C(20)	1.391(13)
C(4) - C(5)	1.503(15)
C(4) - C(6)	1.515(13)
C(4) - C(7)	1.509(17)
C(8) - C(9)	1.322(14)
C(11) - C(12)	1.504(13)
C(16) - C(17)	1.508(15)
C(16) - C(18)	1.509(13)
C(16) - C(19)	1.534(16)
C(20) - C(21)	1.321(14)
C(30) - C(31)	1.370(12)
C(30) - C(35)	1.411(13)
C(30) - B(36)	1.665(11)
C(31) - C(32)	1.403(11)
C(32) - C(33)	1.357(15)
C(33) - C(34)	1.354(15)
C(34) - C(35)	1.394(11)
C(37) - C(38)	1.401(12)
C(37) - C(42)	1.385(13)
C(37) - B(36)	1.659(13)
C(38) - C(39)	1.412(14)
C(39) - C(40)	1.333(16)
C(40) - C(41)	1.388(15)
C(41) - C(42)	1.391(13)
C(43) - C(44)	1.392(12)
C(43) - C(48)	1.394(12)
C(43) - B(36)	1.601(14)
C(44) - C(45)	1.379(15)
C(45) - C(46)	1.388(16)
C(46) - C(47)	1.371(16)
C(47) - C(48)	1.379(14)
C(49) - C(50)	1.409(11)
C(49) - C(54)	1.36(1)
C(49) - B(36)	1.640(12)
C(50) - C(51)	1.372(13)
C(51) - C(52)	1.365(13)
C(52) - C(53)	1.369(12)
C(53) - C(54)	1.369(11)
CL(101- C(101)	1.710(18)
CL(101- C(101)	1.716(19)

CL(22)- NI(1) - P(23)	88.2(1)
CL(22)- NI(1) - C(2)	171.3(2)
P(23) - NI(1) - C(2)	89.5(3)
CL(22)- NI(1) - C(14)	92.0(2)
P(23) - NI(1) - C(14)	167.4(2)
C(2) - NI(1) - C(14)	88.4(4)
NI(1) - P(23) - C(24)	110.3(3)
NI(1) - P(23) - C(25)	119.0(4)
C(24) - P(23) - C(25)	101.5(5)
NI(1) - P(23) - C(26)	116.2(4)
C(24) - P(23) - C(26)	103.9(5)
C(25) - P(23) - C(26)	104.1(6)
C(2) - N(3) - C(4)	128.4(6)
C(2) - N(3) - C(8)	108.9(7)
C(4) - N(3) - C(8)	122.1(7)
C(2) - N(10) - C(9)	110.4(7)
C(2) - N(10) - C(11)	121.9(6)
C(9) - N(10) - C(11)	127.7(7)
C(12) - N(13) - C(14)	130.6(7)
C(12) - N(13) - C(21)	117.7(7)
C(14) - N(13) - C(21)	111.7(7)
C(14) - N(15) - C(16)	129.7(8)
C(14) - N(15) - C(20)	110.3(7)
C(16) - N(15) - C(20)	119.9(7)
NI(1) - C(2) - N(3)	139.0(6)
NI(1) - C(2) - N(10)	114.6(5)
N(3) - C(2) - N(10)	106.3(6)
N(3) - C(4) - C(5)	110.6(8)
N(3) - C(4) - C(6)	109.8(8)
C(5) - C(4) - C(6)	108.7(10)
N(3) - C(4) - C(7)	107.3(9)
C(5) - C(4) - C(7)	110.3(9)
C(6) - C(4) - C(7)	110.1(10)
N(3) - C(8) - C(9)	108.0(8)
N(10) - C(9) - C(8)	106.3(8)
N(10) - C(11) - C(12)	111.3(7)
N(13) - C(12) - C(11)	116.0(7)
NI(1) - C(14) - N(13)	122.8(5)
NI(1) - C(14) - N(15)	132.8(6)
N(13) - C(14) - N(15)	103.8(7)
N(15) - C(16) - C(17)	112.0(6)
N(15) - C(16) - C(18)	107.6(8)
C(17) - C(16) - C(18)	110.2(10)
N(15) - C(16) - C(19)	107.1(9)
C(17) - C(16) - C(19)	109.1(9)
C(18) - C(16) - C(19)	110.8(9)
N(15) - C(20) - C(21)	107.8(8)
N(13) - C(21) - C(20)	106.4(8)
CL(27)- C(28) - CL(29)	114.7(9)
C(31) - C(30) - C(35)	115.3(7)
C(31) - C(30) - B(36)	123.5(7)
C(35) - C(30) - B(36)	121.1(8)
C(30) - C(31) - C(32)	121.7(8)
C(31) - C(32) - C(33)	121.2(9)
C(32) - C(33) - C(34)	119.4(8)
C(33) - C(34) - C(35)	119.8(9)
C(30) - C(35) - C(34)	122.6(9)
C(38) - C(37) - C(42)	114.4(8)
C(38) - C(37) - B(36)	121.8(8)
C(42) - C(37) - B(36)	123.7(7)
C(37) - C(38) - C(39)	121.0(10)
C(38) - C(39) - C(40)	121.9(9)
C(39) - C(40) - C(41)	119.5(9)
C(40) - C(41) - C(42)	118.1(10)
C(37) - C(42) - C(41)	125.0(9)
C(44) - C(43) - C(48)	113.9(9)
C(44) - C(43) - B(36)	122.7(8)
C(48) - C(43) - B(36)	123.3(8)
C(43) - C(44) - C(45)	124.2(9)
C(44) - C(45) - C(46)	119.0(10)
C(45) - C(46) - C(47)	119.4(11)
C(46) - C(47) - C(48)	119.7(10)
C(43) - C(48) - C(47)	123.8(9)
C(50) - C(49) - C(54)	115.5(7)
C(50) - C(49) - B(36)	120.9(7)
C(54) - C(49) - B(36)	123.4(7)
C(49) - C(50) - C(51)	122.1(8)

C(50) - C(51) - C(52)	119.8(8)	C(37) - B(36) - C(43)	112.7(7)
C(51) - C(52) - C(53)	119.5(8)	C(30) - B(36) - C(49)	108.0(6)
C(52) - C(53) - C(54)	120.0(8)	C(37) - B(36) - C(49)	106.3(7)
C(49) - C(54) - C(53)	123.1(7)	C(43) - B(36) - C(49)	111.1(7)
C(30) - B(36) - C(37)	110.1(6)	C(101)- CL(101- C(101)	63.3(17)
C(30) - B(36) - C(43)	108.6(7)	CL(101- C(101)- CL(101)	116.7(17)

D.3 Fractional Atomic Coordinates and Isotropic Thermal Parameters for All Non-Hydrogen Atoms of [(^{tBu}CC^{eth})NiCl(PMe$_3$)][BPh$_4$] (10)

Atom	x/a	y/b	z/c	U(iso)	Occ
Ni(1)	0.27674(7)	0.87976(7)	0.65987(7)	0.0245	
Cl(22)	0.2285(2)	1.04124(17)	0.60772(18)	0.0483	
Cl(27)	0.2877(4)	0.3314(4)	0.5733(4)	0.1250	
Cl(29)	0.0576(4)	0.3778(4)	0.5489(4)	0.1368	
P(23)	0.23973(18)	0.90220(18)	0.80845(16)	0.0358	
N(3)	0.3037(6)	0.6570(5)	0.7429(5)	0.0351	
N(10)	0.4479(5)	0.7461(5)	0.7178(5)	0.0344	
N(13)	0.4526(5)	0.8632(6)	0.5145(5)	0.0374	
N(15)	0.2978(6)	0.8759(6)	0.4483(5)	0.0420	
C(2)	0.3371(6)	0.7506(5)	0.7092(6)	0.0308	
C(4)	0.1912(8)	0.6169(7)	0.7394(7)	0.0492	
C(5)	0.1013(8)	0.6959(8)	0.7526(7)	0.0503	
C(6)	0.1751(11)	0.523(1)	0.8192(11)	0.0910	
C(7)	0.1866(11)	0.590(1)	0.6420(11)	0.0778	
C(8)	0.3960(8)	0.5927(8)	0.7718(7)	0.0496	
C(9)	0.4844(8)	0.6483(8)	0.7576(7)	0.0508	
C(11)	0.5139(6)	0.8344(7)	0.6847(7)	0.0411	
C(12)	0.5453(7)	0.8497(8)	0.5783(7)	0.0474	
C(14)	0.3412(6)	0.8676(6)	0.5353(5)	0.0309	
C(16)	0.1787(9)	0.8838(8)	0.4231(6)	0.0511	
C(17)	0.1002(8)	0.8631(8)	0.5118(7)	0.0551	
C(18)	0.156(1)	0.990(1)	0.3651(9)	0.0779	
C(19)	0.1654(12)	0.8041(11)	0.3624(9)	0.0845	
C(20)	0.382(1)	0.8801(8)	0.3757(7)	0.0539	
C(21)	0.4780(8)	0.8715(9)	0.4168(7)	0.0536	
C(24)	0.3213(8)	1.0013(8)	0.8309(7)	0.0467	
C(25)	0.272(1)	0.7991(9)	0.9086(7)	0.0569	
C(26)	0.0985(8)	0.9428(9)	0.8377(9)	0.0610	
C(28)	0.1530(14)	0.3035(13)	0.6117(14)	0.1168	
C(30)	0.1365(6)	0.2721(6)	0.9692(6)	0.0318	
C(31)	0.0542(7)	0.3404(6)	0.9895(6)	0.0341	
C(32)	-0.0431(7)	0.3588(7)	0.9390(7)	0.0487	
C(33)	-0.0609(8)	0.3073(8)	0.8694(8)	0.0524	
C(34)	0.0168(8)	0.2374(8)	0.8480(7)	0.0507	
C(35)	0.1144(7)	0.2197(7)	0.8970(6)	0.0426	
C(37)	0.3603(6)	0.2926(6)	0.9526(6)	0.0344	
C(38)	0.4476(8)	0.3384(8)	0.9843(7)	0.0536	
C(39)	0.5423(8)	0.3677(9)	0.9228(8)	0.0565	
C(40)	0.5517(8)	0.3557(8)	0.8316(9)	0.0564	
C(41)	0.4665(9)	0.3129(8)	0.7956(8)	0.0558	
C(42)	0.3743(8)	0.2829(8)	0.8572(7)	0.0478	
C(43)	0.2400(7)	0.2965(6)	1.1209(6)	0.0355	
C(44)	0.2452(7)	0.4003(7)	1.1167(7)	0.0457	
C(45)	0.2282(8)	0.4449(8)	1.1959(8)	0.0528	
C(46)	0.2046(8)	0.384(1)	1.2862(9)	0.0607	
C(47)	0.1994(7)	0.2808(9)	1.2947(7)	0.0523	
C(48)	0.2153(7)	0.2396(7)	1.2134(7)	0.0411	
C(49)	0.2760(6)	0.1245(6)	1.0556(5)	0.0296	
C(50)	0.1867(7)	0.0590(7)	1.0745(6)	0.0421	
C(51)	0.2027(8)	-0.0444(7)	1.1035(7)	0.0435	
C(52)	0.3078(8)	-0.0865(6)	1.1155(6)	0.0418	
C(53)	0.3959(7)	-0.0247(7)	1.0998(6)	0.0399	
C(54)	0.3786(6)	0.0783(6)	1.0701(6)	0.0329	
B(36)	0.2537(8)	0.2483(7)	1.0266(7)	0.0354	
Cl(101)	0.4478(8)	0.6016(6)	0.4930(8)	0.1099	0.5000
C(101)	0.470(3)	0.4956(18)	0.445(2)	0.2855	0.5000

D.4 Anisotropic Thermal Parameters for [(^{tBu}CC^{eth})NiCl(PMe$_3$)][BPh$_4$] (10)

Atom	u(11)	u(22)	u(33)	u(23)	u(13)	u(12)
Ni(1)	0.0226(5)	0.0244(5)	0.0257(5)	-0.0026(4)	-0.0049(4)	-0.0014(4)
Cl(22)	0.0530(13)	0.0311(11)	0.0576(14)	-0.002(1)	-0.0062(11)	0.0030(9)
Cl(27)	0.118(3)	0.108(3)	0.161(5)	-0.057(3)	-0.012(3)	0.006(3)
Cl(29)	0.118(4)	0.126(4)	0.165(5)	-0.014(4)	-0.029(3)	-0.032(3)
P(23)	0.0331(11)	0.0429(12)	0.0350(11)	-0.015(1)	-0.0029(9)	-0.0025(9)
N(3)	0.041(4)	0.032(4)	0.030(3)	0.001(3)	-0.008(3)	0.002(3)
N(10)	0.027(3)	0.040(4)	0.035(4)	-0.008(3)	-0.007(3)	0.008(3)
N(13)	0.031(3)	0.049(4)	0.032(4)	-0.013(4)	0.011(3)	-0.003(3)
N(15)	0.047(4)	0.043(4)	0.035(4)	-0.003(4)	-0.006(3)	-0.009(3)
C(2)	0.039(4)	0.013(3)	0.041(5)	-0.005(3)	-0.012(4)	0.002(3)
C(4)	0.053(5)	0.037(5)	0.055(6)	-0.001(5)	-0.007(5)	-0.014(4)
C(5)	0.047(5)	0.048(6)	0.051(6)	0.006(5)	-0.007(4)	-0.022(4)
C(6)	0.079(8)	0.052(7)	0.120(12)	0.034(8)	-0.005(8)	-0.017(6)
C(7)	0.077(8)	0.068(8)	0.10(1)	-0.048(8)	-0.012(8)	-0.013(6)
C(8)	0.054(6)	0.053(6)	0.039(5)	-0.005(5)	-0.005(4)	0.010(5)
C(9)	0.058(6)	0.052(6)	0.044(5)	-0.015(5)	-0.019(5)	0.022(5)
C(11)	0.027(4)	0.052(5)	0.047(5)	-0.013(4)	-0.007(4)	-0.005(4)
C(12)	0.040(5)	0.052(6)	0.051(5)	-0.013(5)	-0.002(4)	-0.004(4)
C(14)	0.036(4)	0.036(4)	0.021(3)	-0.000(3)	-0.013(3)	-0.011(3)
C(16)	0.067(6)	0.052(6)	0.033(5)	0.004(4)	-0.027(5)	-0.014(5)
C(17)	0.050(5)	0.062(7)	0.052(6)	-0.002(5)	-0.021(5)	-0.002(5)
C(18)	0.082(8)	0.075(9)	0.061(7)	0.029(7)	-0.019(6)	-0.007(7)
C(19)	0.11(1)	0.09(1)	0.059(7)	-0.012(7)	-0.029(7)	-0.041(8)
C(20)	0.077(7)	0.057(6)	0.028(4)	-0.013(5)	0.006(5)	-0.010(5)
C(21)	0.048(5)	0.068(7)	0.045(5)	-0.020(6)	0.017(4)	-0.008(5)
C(24)	0.046(5)	0.054(6)	0.047(5)	-0.025(5)	0.004(4)	-0.012(4)
C(25)	0.081(7)	0.058(6)	0.034(5)	-0.011(5)	-0.005(5)	-0.006(5)
C(26)	0.035(5)	0.079(8)	0.079(8)	-0.042(7)	0.004(5)	-0.002(5)
C(28)	0.108(12)	0.085(11)	0.135(15)	0.022(11)	0.017(11)	-0.013(9)
C(30)	0.027(4)	0.034(4)	0.036(4)	-0.008(4)	-0.003(3)	-0.004(3)
C(31)	0.037(4)	0.036(4)	0.028(4)	-0.001(4)	0.000(3)	-0.008(4)
C(32)	0.037(5)	0.048(6)	0.058(6)	-0.005(5)	-0.006(4)	0.004(4)
C(33)	0.041(5)	0.053(6)	0.066(7)	-0.009(5)	-0.026(5)	-0.004(4)
C(34)	0.050(5)	0.054(6)	0.049(6)	-0.007(5)	-0.016(5)	-0.012(5)
C(35)	0.044(5)	0.044(5)	0.039(5)	-0.006(4)	-0.005(4)	0.001(4)
C(37)	0.033(4)	0.028(4)	0.042(5)	-0.004(4)	-0.004(4)	-0.002(3)
C(38)	0.056(6)	0.047(6)	0.054(6)	0.005(5)	-0.014(5)	-0.013(5)
C(39)	0.036(5)	0.070(7)	0.057(6)	0.008(6)	-0.006(4)	-0.019(5)
C(40)	0.045(5)	0.042(5)	0.071(7)	0.010(5)	0.009(5)	-0.003(4)
C(41)	0.059(6)	0.052(6)	0.054(6)	-0.010(5)	0.020(5)	-0.008(5)
C(42)	0.043(5)	0.051(6)	0.053(6)	-0.017(5)	0.002(4)	-0.013(4)
C(43)	0.036(4)	0.035(4)	0.037(4)	-0.005(4)	-0.016(4)	0.004(3)
C(44)	0.043(5)	0.050(5)	0.046(5)	-0.010(5)	-0.022(4)	0.005(4)
C(45)	0.048(5)	0.049(6)	0.068(7)	-0.023(5)	-0.022(5)	0.008(4)
C(46)	0.041(5)	0.081(8)	0.074(8)	-0.048(7)	-0.019(5)	0.016(5)
C(47)	0.037(5)	0.080(8)	0.039(5)	-0.009(5)	-0.008(4)	0.006(5)
C(48)	0.039(5)	0.044(5)	0.042(5)	-0.016(4)	-0.002(4)	0.010(4)
C(49)	0.032(4)	0.032(4)	0.024(4)	-0.005(3)	-0.000(3)	-0.006(3)
C(50)	0.038(5)	0.046(5)	0.040(5)	-0.007(4)	0.003(4)	-0.002(4)
C(51)	0.050(5)	0.040(5)	0.039(5)	-0.006(4)	0.006(4)	-0.013(4)
C(52)	0.062(6)	0.028(4)	0.032(4)	0.000(4)	-0.002(4)	-0.004(4)
C(53)	0.046(5)	0.042(5)	0.033(4)	-0.007(4)	-0.014(4)	0.005(4)
C(54)	0.026(4)	0.037(4)	0.037(4)	-0.010(4)	-0.001(3)	-0.003(3)
B(36)	0.033(5)	0.031(5)	0.041(5)	-0.001(4)	-0.009(4)	-0.003(4)
Cl(101)	0.126(7)	0.074(5)	0.113(7)	-0.002(5)	0.059(5)	-0.012(4)
C(101)	0.32(8)	0.48(12)	0.10(3)	-0.10(5)	0.12(4)	-0.29(8)

D.5 Fractional Atomic Coordinates and Isotropic Thermal Parameters for Hydrogen Atoms of [(^{tBu}CC^{eth})NiCl(PMe$_3$)][BPh$_4$] (10)

Atom	x/a	y/b	z/c	U(iso)
H(51)	0.0277	0.6672	0.7494	0.0584
H(52)	0.1066	0.7126	0.8173	0.0584
H(53)	0.1107	0.7579	0.7009	0.0584
H(61)	0.1009	0.4964	0.8140	0.0963
H(62)	0.1792	0.5419	0.8823	0.0963
H(63)	0.2345	0.4695	0.8109	0.0963
H(71)	0.1132	0.5631	0.6377	0.0931
H(72)	0.1971	0.6535	0.5903	0.0931
H(73)	0.2473	0.5386	0.6329	0.0931
H(81)	0.3937	0.5168	0.7988	0.0574
H(91)	0.5628	0.6236	0.7715	0.0624
H(111)	0.5832	0.8237	0.7213	0.0467
H(112)	0.4699	0.8949	0.6991	0.0467
H(121)	0.5890	0.9116	0.5599	0.0623
H(122)	0.5910	0.7888	0.5670	0.0623
H(171)	0.0221	0.8683	0.4920	0.0674
H(172)	0.1099	0.9138	0.5522	0.0674
H(173)	0.1170	0.7928	0.5501	0.0674
H(181)	0.0761	0.9975	0.3473	0.0895
H(182)	0.1675	1.0407	0.4059	0.0895
H(183)	0.2056	1.0035	0.3057	0.0895
H(191)	0.0891	0.8057	0.3429	0.1013
H(192)	0.2185	0.8182	0.3023	0.1013
H(193)	0.1874	0.7343	0.4005	0.1013
H(201)	0.3715	0.8871	0.3051	0.0628
H(211)	0.5537	0.8694	0.3843	0.0651
H(311)	0.0638	0.3776	1.0419	0.0377
H(321)	-0.0995	0.4121	0.9553	0.0539
H(331)	-0.1313	0.3188	0.8345	0.0612
H(341)	0.0062	0.1999	0.7953	0.0649
H(351)	0.1711	0.1670	0.8810	0.0528
H(381)	0.4435	0.3499	1.0516	0.0667
H(391)	0.6035	0.3982	0.9482	0.0608
H(401)	0.6205	0.3757	0.7876	0.0608
H(411)	0.4700	0.3038	0.7273	0.0671
H(421)	0.3148	0.2507	0.8308	0.0586
H(441)	0.2605	0.4443	1.0519	0.0553
H(451)	0.2341	0.5193	1.1882	0.0664
H(461)	0.1904	0.4149	1.3443	0.0762
H(471)	0.1856	0.2365	1.3598	0.0584
H(481)	0.2095	0.1654	1.2207	0.0482
H(501)	0.1095	0.0881	1.0664	0.0469
H(511)	0.1366	-0.0875	1.1171	0.0531
H(521)	0.3201	-0.1621	1.1353	0.0448
H(531)	0.4730	-0.0554	1.1086	0.0485
H(541)	0.4443	0.1214	1.0601	0.0418
H(241)	0.3029	1.0117	0.8987	0.0500
H(242)	0.3025	1.0674	0.7847	0.0500
H(243)	0.4017	0.9836	0.8225	0.0500
H(251)	0.2510	0.8202	0.9715	0.0500
H(252)	0.3539	0.7804	0.9058	0.0500
H(253)	0.2303	0.7379	0.9059	0.0500
H(261)	0.0894	0.9513	0.9062	0.0500
H(262)	0.0779	1.0100	0.7939	0.0500
H(263)	0.0455	0.8913	0.8285	0.0500
H(281)	0.1417	0.3181	0.6862	0.0500
H(282)	0.1393	0.2312	0.6219	0.0500

E. X-Ray Structure Analysis of 1,1'-(1,2-Ethylene)*bis*(3-*tert*-butylimidazolium) Tetrachloronickelate(II)

E.1 Summary of Crystallographic Data

Empirical formula	$C_{16}H_{28}N_4NiCl_4$	
Formula weight	476.93	
Temperature	180 K	
Wavelength (Mo-Kα)	0.71073 Å	
Crystal system	Monoclinic	
Space group	$P2_1/a$	
Unit cell dimensions	a = 11.425(1) Å	α= 90°
	b = 12.802(1) Å	β= 97.01(2)°
	c = 14.835(1) Å	γ = 90°
Volume	2153.6 Å^3	
Z	4	
Density (calculated)	1.47 Mg/m^3	
Absorption coefficient	1.41 mm^{-1}	
F(000)	995.29	
Crystal size	0.2 x 0.2 x 0.3 mm^3	
θ range for data collection	1.69 to 26.43°	
Index ranges	-14≤h≤14, 0≤k≤15, 0≤l≤28	
Reflections collected	11673	
Independent reflections	4637 [R(int) = 0.066]	
Absorption correction	None	
Refinement method	Full-matrix least-squares on F	
Weighting scheme	Chebychev parameters 2.23, -0.0847 and 1.89	
Data / parameters [I>3σ(I)]	2338/227	
Goodness-of-fit on F	1.0700	
Largest final shift	0.000310	
Final R indices	R = 0.0477, wR_w = 0.0477	
Residual density	0.59 and -0.52 e.Å^{-3}	

E.2 Interatomic Distances (Å) and Angles (°) for 1,1'-(1,2-Ethylene)*bis*(3-*tert*-butylimidazolium) Tetrachloronickelate(II)

NI(1) - CL(2)	2.2708(13)
NI(1) - CL(3)	2.2443(13)
NI(1) - CL(4)	2.2515(14)
NI(1) - CL(5)	2.2483(14)
N(6) - C(15)	1.373(6)
N(6) - C(16)	1.331(6)
N(6) - C(20)	1.459(6)
N(7) - C(11)	1.367(6)
N(7) - C(12)	1.332(6)
N(7) - C(22)	1.449(6)
N(8) - C(10)	1.382(6)
N(8) - C(16)	1.315(6)
N(8) - C(17)	1.491(6)
N(9) - C(12)	1.314(6)
N(9) - C(13)	1.378(6)
N(9) - C(14)	1.491(6)
C(10) - C(15)	1.335(7)
C(11) - C(13)	1.337(7)
C(14) - C(19)	1.509(7)
C(14) - C(21)	1.502(7)
C(14) - C(24)	1.504(7)
C(17) - C(18)	1.519(7)
C(17) - C(23)	1.509(7)
C(17) - C(25)	1.509(7)
C(20) - C(22)	1.514(7)

CL(2) - NI(1) - CL(3)	121.61(6)
CL(2) - NI(1) - CL(4)	102.45(6)
CL(3) - NI(1) - CL(4)	108.35(5)
CL(2) - NI(1) - CL(5)	112.30(6)
CL(3) - NI(1) - CL(5)	100.75(5)
CL(4) - NI(1) - CL(5)	111.51(6)
C(15) - N(6) - C(16)	108.2(4)
C(15) - N(6) - C(20)	127.6(4)
C(16) - N(6) - C(20)	124.3(4)
C(11) - N(7) - C(12)	108.4(4)
C(11) - N(7) - C(22)	127.8(4)
C(12) - N(7) - C(22)	123.7(4)
C(10) - N(8) - C(16)	108.4(4)
C(10) - N(8) - C(17)	125.9(4)
C(16) - N(8) - C(17)	125.6(4)
C(12) - N(9) - C(13)	107.8(4)
C(12) - N(9) - C(14)	125.5(4)
C(13) - N(9) - C(14)	126.5(4)
N(8) - C(10) - C(15)	107.1(4)
N(7) - C(11) - C(13)	106.8(4)
N(7) - C(12) - N(9)	109.1(4)
N(9) - C(13) - C(11)	107.9(4)
N(9) - C(14) - C(19)	107.7(4)
N(9) - C(14) - C(21)	106.8(4)
C(19) - C(14) - C(21)	111.6(4)
N(9) - C(14) - C(24)	108.7(4)
C(19) - C(14) - C(24)	110.9(5)
C(21) - C(14) - C(24)	110.9(5)
N(6) - C(15) - C(10)	107.4(4)
N(6) - C(16) - N(8)	108.9(4)
N(8) - C(17) - C(18)	108.0(4)
N(8) - C(17) - C(23)	108.9(4)
C(18) - C(17) - C(23)	111.4(4)
N(8) - C(17) - C(25)	106.5(4)
C(18) - C(17) - C(25)	110.4(5)
C(23) - C(17) - C(25)	111.5(5)
N(6) - C(20) - C(22)	109.6(4)
N(7) - C(22) - C(20)	109.7(4)

E.3 Fractional Atomic Coordinates and Isotropic Thermal Parameters for All Non-Hydrogen Atoms of 1,1'-(1,2-Ethylene)*bis*(3-*tert*-butylimidazolium) Tetrachloronickelate(II)

Atom	x/a	y/b	z/c	U(iso)	Occ
Ni(1)	0.30333(5)	0.44545(5)	0.75158(4)	0.0250	
Cl(2)	0.5005(1)	0.4145(1)	0.76669(9)	0.0344	
Cl(3)	0.23079(12)	0.6082(1)	0.75464(8)	0.0378	
Cl(4)	0.24190(12)	0.3750(1)	0.61493(8)	0.0368	
Cl(5)	0.21528(12)	0.36964(11)	0.86230(9)	0.0396	
N(6)	0.4258(3)	0.1200(3)	0.6230(3)	0.0247	
N(7)	0.3518(3)	0.1331(3)	0.8567(3)	0.0260	
N(8)	0.4504(3)	0.2117(3)	0.5051(2)	0.0245	
N(9)	0.4242(3)	0.1862(3)	0.9898(2)	0.0248	
C(10)	0.3895(4)	0.1225(4)	0.4751(3)	0.0285	
C(11)	0.3038(4)	0.0717(4)	0.9181(3)	0.0302	
C(12)	0.4232(4)	0.2024(4)	0.9023(3)	0.0278	
C(13)	0.3497(5)	0.1037(4)	1.0007(3)	0.0313	
C(14)	0.4862(4)	0.2524(4)	1.0635(3)	0.0293	
C(15)	0.3747(4)	0.0659(4)	0.5484(3)	0.0294	
C(16)	0.4708(4)	0.2081(4)	0.5942(3)	0.0280	
C(17)	0.4935(4)	0.2941(4)	0.4464(3)	0.0307	
C(18)	0.3867(5)	0.3478(4)	0.3954(4)	0.0393	
C(19)	0.3937(5)	0.3121(4)	1.1067(4)	0.0388	
C(20)	0.4329(5)	0.0890(4)	0.7181(3)	0.0325	
C(21)	0.5542(5)	0.1796(5)	1.1299(4)	0.0459	
C(22)	0.3269(4)	0.1310(4)	0.7586(3)	0.0303	
C(23)	0.5691(5)	0.3702(4)	0.5055(4)	0.0432	
C(24)	0.5678(6)	0.3258(5)	1.0224(4)	0.0488	
C(25)	0.5635(5)	0.2388(5)	0.3808(4)	0.0501	

E.4 Anisotropic Thermal Parameters 1,1'-(1,2-Ethylene)*bis*(3-*tert*-butylimidazolium) Tetrachloronickelate(II)

Atom	u(11)	u(22)	u(33)	u(23)	u(13)	u(12)
Ni(1)	0.0244(3)	0.0252(3)	0.0254(3)	-0.0005(3)	0.0039(2)	0.0022(3)
Cl(2)	0.0232(6)	0.0388(7)	0.0410(7)	0.0012(5)	0.0031(5)	-0.0011(5)
Cl(3)	0.0550(8)	0.0278(6)	0.0299(6)	-0.0008(5)	0.0025(6)	0.0096(5)
Cl(4)	0.0392(7)	0.0372(7)	0.0319(6)	-0.0079(5)	-0.0041(5)	0.0014(5)
Cl(5)	0.0371(7)	0.0417(8)	0.0418(7)	0.0137(6)	0.0129(5)	0.0041(6)
N(6)	0.0225(19)	0.024(2)	0.027(2)	0.0006(16)	0.0039(15)	0.0049(15)
N(7)	0.030(2)	0.025(2)	0.0225(19)	0.0003(16)	0.0043(16)	-0.0007(16)
N(8)	0.0240(19)	0.025(2)	0.024(2)	0.0013(15)	0.0022(15)	-0.0012(16)
N(9)	0.031(2)	0.024(2)	0.0197(19)	0.0003(16)	0.0054(15)	-0.0002(16)
C(10)	0.029(2)	0.024(2)	0.032(3)	-0.002(2)	0.0023(19)	-0.0027(19)
C(11)	0.033(3)	0.023(3)	0.036(3)	-0.002(2)	0.012(2)	-0.0063(19)
C(12)	0.028(2)	0.023(2)	0.033(3)	-0.000(2)	0.0037(19)	-0.0021(19)
C(13)	0.037(3)	0.027(3)	0.032(3)	0.007(2)	0.013(2)	-0.003(2)
C(14)	0.031(3)	0.032(3)	0.024(2)	0.002(2)	0.0041(19)	-0.003(2)
C(15)	0.028(2)	0.028(3)	0.031(3)	-0.001(2)	0.0003(19)	-0.0042(19)
C(16)	0.024(2)	0.031(3)	0.028(2)	-0.007(2)	0.0015(18)	0.001(2)
C(17)	0.030(3)	0.024(2)	0.039(3)	0.001(2)	0.010(2)	-0.003(2)
C(18)	0.039(3)	0.037(3)	0.042(3)	0.008(2)	0.001(2)	0.005(2)
C(19)	0.045(3)	0.038(3)	0.035(3)	-0.009(2)	0.008(2)	0.003(2)
C(20)	0.037(3)	0.042(3)	0.020(2)	-0.000(2)	0.012(2)	0.010(2)
C(21)	0.042(3)	0.057(4)	0.037(3)	0.001(3)	-0.003(2)	0.013(3)
C(22)	0.025(3)	0.038(3)	0.027(2)	-0.000(2)	-0.0005(19)	-0.002(2)
C(23)	0.037(3)	0.029(3)	0.062(4)	0.003(3)	-0.001(3)	-0.011(2)
C(24)	0.048(4)	0.058(4)	0.041(3)	-0.014(3)	0.007(3)	-0.026(3)
C(25)	0.051(4)	0.047(4)	0.060(4)	0.009(3)	0.035(3)	0.005(3)

E.5 Fractional Atomic Coordinates and Isotropic Thermal Parameters for Hydrogen Atoms of 1,1'-(1,2-Ethylene)*bis*(3-*tert*-butylimidazolium) Tetrachloronickelate(II)

Atom	x/a	y/b	z/c	U(iso)	Occ
H(101)	0.3615	0.1016	0.4097	0.0316	
H(111)	0.2461	0.0132	0.9030	0.0342	
H(121)	0.4714	0.2564	0.8730	0.0302	
H(131)	0.3325	0.0739	1.0614	0.0341	
H(151)	0.3346	-0.0041	0.5507	0.0316	
H(161)	0.5142	0.2608	0.6335	0.0267	
H(181)	0.4130	0.4043	0.3548	0.0497	
H(182)	0.3366	0.3802	0.4386	0.0497	
H(183)	0.3379	0.2959	0.3561	0.0497	
H(191)	0.4316	0.3589	1.1563	0.0431	
H(192)	0.3384	0.2632	1.1322	0.0431	
H(193)	0.3473	0.3573	1.0591	0.0431	
H(201)	0.5073	0.1205	0.7522	0.0328	
H(202)	0.4377	0.0118	0.7236	0.0328	
H(211)	0.5980	0.2206	1.1814	0.0484	
H(212)	0.4965	0.1317	1.1569	0.0484	
H(213)	0.6104	0.1364	1.1003	0.0484	
H(221)	0.3072	0.2019	0.7350	0.0286	
H(222)	0.2584	0.0825	0.7408	0.0286	
H(231)	0.6006	0.4258	0.4662	0.0416	
H(232)	0.6407	0.3319	0.5379	0.0416	
H(233)	0.5254	0.4031	0.5509	0.0416	
H(241)	0.6094	0.3715	1.0712	0.0664	
H(242)	0.6245	0.2878	0.9903	0.0664	
H(243)	0.5173	0.3729	0.9779	0.0664	
H(251)	0.5940	0.2941	0.3398	0.0650	
H(252)	0.6315	0.2025	0.4143	0.0650	
H(253)	0.5118	0.1901	0.3427	0.0650	

F. X-Ray Structure Analysis of [(μ-^{tBu}CC^{meth}){Ni(PMe$_3$)Me$_2$}$_2$] (12)

F.1 Summary of Crystallographic Data

Empirical formula	$C_{25}H_{54}N_4Ni_2P_2.C_5H_{12}$	
Formula weight	662.22	
Temperature	180 K	
Wavelength (Mo-Kα)	0.71073 Å	
Crystal system	Monoclinic	
Space group	C2/c	
Unit cell dimensions	a = 14.644(1) Å	α= 90°
	b = 18.135(1) Å	β= 105.94(2)°
	c = 14.682(1) Å	γ = 90°
Volume	3749.1 Å^3	
Z	8	
Density (calculated)	1.16 Mg/m^3	
Absorption coefficient	1.11 mm^{-1}	
F(000)	1403.04	
Crystal size	0.2 x 0.2 x 0.3 mm^3	
θ range for data collection	1.69 to 26.34°	
Index ranges	-18≤h≤17, 0≤k≤22, 0≤l≤18	
Reflections collected	5936	
Independent reflections	3642 [R(int) = 0.027]	
Absorption correction	None	
Refinement method	Full-matrix least-squares on F	
Weighting scheme	Chebychev parameters 3.10, 0.218 and 2.32	
Data / parameters [I>3σ(I)]	2291/164	
Goodness-of-fit on F	1.0254	
Largest final shift	0.001064	
Final R indices	R = 0.0419, wR$_w$ = 0.0490	
Residual density	1.72 and -0.65 e.Å^{-3}	

F.2 Interatomic Distances (Å) and Angles (°) for [(μ-^{tBu}CC^{meth}){Ni(PMe$_3$)Me$_2$}$_2$] (12)

NI(1)	-	C(2)	1.879(3)	C(2)	- NI(1) -	C(12)	89.47(15)
NI(1)	-	C(12)	1.983(4)	C(2)	- NI(1) -	P(13)	175.1(1)
NI(1)	-	P(13)	2.1527(9)	C(12)	- NI(1) -	P(13)	92.35(12)
NI(1)	-	C(17)	2.001(4)	C(2)	- NI(1) -	C(17)	89.40(15)
C(2)	-	N(3)	1.367(4)	C(12)	- NI(1) -	C(17)	177.28(17)
C(2)	-	N(7)	1.365(4)	P(13)	- NI(1) -	C(17)	88.97(12)
N(3)	-	C(4)	1.449(4)	NI(1)	- C(2) -	N(3)	124.7(2)
N(3)	-	C(5)	1.377(4)	NI(1)	- C(2) -	N(7)	132.0(2)
C(5)	-	C(6)	1.335(5)	N(3)	- C(2) -	N(7)	103.3(3)
C(6)	-	N(7)	1.395(5)	C(2)	- N(3) -	C(4)	122.9(3)
N(7)	-	C(8)	1.483(4)	C(2)	- N(3) -	C(5)	112.3(3)
C(8)	-	C(9)	1.477(7)	C(4)	- N(3) -	C(5)	124.7(2)
C(8)	-	C(10)	1.518(8)	N(3)	- C(4) -	N(3)	111.9(4)
C(8)	-	C(11)	1.493(8)	N(3)	- C(5) -	C(6)	106.2(3)
P(13)	-	C(14)	1.818(4)	C(5)	- C(6) -	N(7)	107.6(3)
P(13)	-	C(15)	1.820(4)	C(2)	- N(7) -	C(6)	110.5(3)
P(13)	-	C(16)	1.827(5)	C(2)	- N(7) -	C(8)	127.1(3)
C(100)	-	C(102)	1.47(2)	C(6)	- N(7) -	C(8)	122.1(3)
C(102)	-	C(103)	1.44(3)	N(7)	- C(8) -	C(9)	112.2(3)
				N(7)	- C(8) -	C(10)	106.6(4)
				C(9)	- C(8) -	C(10)	109.2(5)
				N(7)	- C(8) -	C(11)	109.5(4)
				C(9)	- C(8) -	C(11)	109.7(5)
				C(10)	- C(8) -	C(11)	109.6(6)
				NI(1)	- P(13) -	C(14)	119.62(15)
				NI(1)	- P(13) -	C(15)	109.99(14)
				C(14)	- P(13) -	C(15)	102.5(2)
				NI(1)	- P(13) -	C(16)	121.46(16)
				C(14)	- P(13) -	C(16)	99.4(2)
				C(15)	- P(13) -	C(16)	100.9(2)
				C(100)	- C(102) -	C(103)	105.2(22)
				C(102)	- C(103) -	C(102)	103.1(36)

F.3 Fractional Atomic Coordinates and Isotropic Thermal Parameters for All Non-Hydrogen Atoms of $[(\mu\text{-}^{tBu}CC^{meth})\{Ni(PMe_3)Me_2\}_2]$ (12)

Atom	x/a	y/b	z/c	U(iso)	Occ
Ni(1)	0.15549(3)	0.11046(2)	0.63062(3)	0.0332	
C(2)	0.1576(2)	0.16642(19)	0.7388(2)	0.0345	
N(3)	0.08492(18)	0.16966(16)	0.78062(19)	0.0362	
C(4)	0.0000	0.1249(2)	0.7500	0.0360	
C(5)	0.1051(3)	0.2160(2)	0.8579(3)	0.0456	
C(6)	0.1915(3)	0.2433(2)	0.8656(3)	0.0473	
N(7)	0.22400(19)	0.21285(16)	0.7930(2)	0.0396	
C(8)	0.3217(3)	0.2258(2)	0.7857(3)	0.0523	
C(9)	0.3341(4)	0.2002(4)	0.6943(5)	0.1013	
C(10)	0.3879(4)	0.1826(5)	0.8656(5)	0.1166	
C(11)	0.3444(5)	0.3061(4)	0.7979(7)	0.1205	
C(12)	0.2029(3)	0.0240(2)	0.7128(3)	0.0493	
P(13)	0.16301(6)	0.05218(5)	0.50514(6)	0.0404	
C(14)	0.0695(3)	0.0645(3)	0.3955(3)	0.0653	
C(15)	0.2688(3)	0.0801(3)	0.4717(3)	0.0587	
C(16)	0.1743(4)	-0.0482(3)	0.5041(4)	0.0687	
C(17)	0.1020(3)	0.1974(2)	0.5496(3)	0.0510	
C(100)	0.489(1)	0.0837(9)	0.0897(12)	0.2017	
C(102)	0.4906(13)	0.0358(12)	0.1711(16)	0.2587	
C(103)	0.5000	0.085(2)	0.2500	0.3323	

F.4 Anisotropic Thermal Parameters for [(μ-^{tBu}CC^{meth}){Ni(PMe$_3$)Me$_2$}$_2$] (12)

Atom	u(11)	u(22)	u(33)	u(23)	u(13)	u(12)
Ni(1)	0.0372(2)	0.0338(2)	0.0304(2)	-0.00158(17)	0.01247(15)	-0.00102(18)
C(2)	0.0354(15)	0.0340(16)	0.0349(16)	0.0029(13)	0.0108(12)	-0.0005(13)
N(3)	0.0377(13)	0.0383(15)	0.0345(14)	-0.0030(11)	0.0132(11)	-0.0005(11)
C(4)	0.036(2)	0.033(2)	0.042(3)	0.0000	0.0170(18)	0.0000
C(5)	0.053(2)	0.048(2)	0.0393(19)	-0.0089(15)	0.0196(15)	0.0021(16)
C(6)	0.057(2)	0.048(2)	0.0379(19)	-0.0119(15)	0.0146(15)	-0.0027(17)
N(7)	0.0415(14)	0.0403(16)	0.0375(16)	-0.0087(12)	0.0120(11)	-0.0076(12)
C(8)	0.0445(19)	0.057(2)	0.057(2)	-0.0099(19)	0.0169(16)	-0.0157(17)
C(9)	0.065(3)	0.155(6)	0.100(4)	-0.063(4)	0.050(3)	-0.056(3)
C(10)	0.058(3)	0.178(8)	0.110(5)	0.038(5)	0.016(3)	0.007(4)
C(11)	0.122(5)	0.089(5)	0.181(8)	-0.051(5)	0.092(5)	-0.059(4)
C(12)	0.059(2)	0.044(2)	0.046(2)	0.0036(16)	0.0179(17)	0.0070(17)
P(13)	0.0444(5)	0.0440(5)	0.0355(5)	-0.0063(4)	0.0155(3)	-0.0012(4)
C(14)	0.055(2)	0.096(4)	0.042(2)	-0.018(2)	0.0091(17)	0.002(2)
C(15)	0.052(2)	0.075(3)	0.056(2)	-0.015(2)	0.0257(18)	-0.007(2)
C(16)	0.101(3)	0.047(2)	0.067(3)	-0.010(2)	0.037(3)	-0.006(2)
C(17)	0.066(2)	0.045(2)	0.046(2)	0.0082(16)	0.0218(17)	0.0122(17)
C(100)	0.211(9)	0.157(11)	0.254(17)	-0.00000(1)	0.092(11)	-0.00000(1)
C(102)	0.268(9)	0.214(11)	0.311(17)	-0.00000(1)	0.108(11)	-0.00000(1)
C(103)	0.342(9)	0.288(11)	0.385(17)	-0.00000(1)	0.128(11)	0.00000(1)

F.5 Fractional Atomic Coordinates and Isotropic Thermal Parameters for Hydrogen Atoms of [(μ-$^{tBu}CC^{meth}$){Ni(PMe_3)Me_2}$_2$] (12)

Atom	x/a	y/b	z/c	U(iso)	Occ
H(41)	-0.0054	0.0925	0.8039	0.0424	
H(42)	0.0054	0.0925	0.6961	0.0424	
H(51)	0.0613	0.2268	0.8991	0.0543	
H(61)	0.2268	0.2792	0.9139	0.0545	
H(91)	0.4022	0.2092	0.6914	0.1012	
H(92)	0.3225	0.1453	0.6865	0.1012	
H(93)	0.2904	0.2261	0.6397	0.1012	
H(101)	0.4568	0.1903	0.8681	0.1299	
H(102)	0.3816	0.2026	0.9308	0.1299	
H(103)	0.3733	0.1297	0.8637	0.1299	
H(111)	0.4114	0.3164	0.7929	0.1189	
H(112)	0.3407	0.3245	0.8611	0.1189	
H(113)	0.2994	0.3361	0.7468	0.1189	
H(141)	0.0825	0.0350	0.3433	0.0500	
H(142)	0.0064	0.0507	0.4041	0.0500	
H(143)	0.0662	0.1189	0.3760	0.0500	
H(151)	0.2732	0.0530	0.4136	0.0500	
H(152)	0.3277	0.0687	0.5247	0.0500	
H(153)	0.2675	0.1345	0.4589	0.0500	
H(161)	0.1775	-0.0644	0.4392	0.0500	
H(162)	0.2352	-0.0634	0.5515	0.0500	
H(163)	0.1197	-0.0717	0.5194	0.0500	
H(121)	0.2114	-0.0188	0.6734	0.0500	
H(122)	0.2666	0.0366	0.7584	0.0500	
H(123)	0.1576	0.0113	0.7500	0.0500	
H(171)	0.0920	0.1849	0.4808	0.0500	
H(172)	0.1472	0.2403	0.5658	0.0500	
H(173)	0.0397	0.2123	0.5598	0.0500	

G. X-Ray Structure Analysis of Ni(^{tBu}CC^{eth})Me$_2$ (13)

G.1 Summary of Crystallographic Data

Empirical formula	$C_{18}H_{32}N_4Ni$	
Formula weight	363.17	
Temperature	180 K	
Wavelength (Mo-Kα)	0.71073 Å	
Crystal system	Orthorhombic	
Space group	$P2_12_12_1$	
Unit cell dimensions	a = 9.901(1) Å	α= 90°
	b = 12.701(2) Å	β= 90°
	c = 15.309(2) Å	γ = 90°
Volume	1925.1 Å^3	
Z	4	
Density (calculated)	1.25 Mg/m^3	
Absorption coefficient	1.02 mm^{-1}	
F(000)	785.16	
Crystal size	0.2 x 0.2 x 0.2 mm^3	
θ range for data collection	1.71 to 26.79°	
Index ranges	0≤h≤12, 0≤k≤15, 0≤l≤19	
Reflections collected	8876	
Independent reflections	2276 [R(int) = 0.064]	
Absorption correction	None	
Refinement method	Full-matrix least-squares on F	
Weighting scheme	w = 1/(0.0010(F) + 3σ^2(F) + 3)	
Data / parameters [I>3σ(I)]	2200/209	
Goodness-of-fit on F	1.0313	
Largest final shift	0.000445	
Final R indices	R = 0.0550, wR$_w$ = 0.0664	
Residual density	0.63 and -0.77 e.Å^{-3}	

G.2 Interatomic Distances (Å) and Angles (°) for Ni(^{tBu}CC^{eth})Me$_2$ (13)

NI(1) - C(2)	1.907(5)
NI(1) - C(14)	1.911(6)
NI(1) - C(22)	1.972(6)
NI(1) - C(23)	1.962(6)
C(2) - N(3)	1.354(7)
C(2) - N(10)	1.378(7)
N(3) - C(4)	1.499(7)
N(3) - C(8)	1.394(7)
C(4) - C(5)	1.516(9)
C(4) - C(6)	1.517(9)
C(4) - C(7)	1.522(9)
C(8) - C(9)	1.322(9)
C(9) - N(10)	1.392(8)
N(10) - C(11)	1.455(8)
C(11) - C(12)	1.51(1)
C(12) - N(13)	1.455(8)
N(13) - C(14)	1.362(8)
N(13) - C(21)	1.387(8)
C(14) - N(15)	1.373(8)
N(15) - C(16)	1.496(8)
N(15) - C(20)	1.385(8)
C(16) - C(17)	1.514(11)
C(16) - C(18)	1.488(11)
C(16) - C(19)	1.502(11)
C(20) - C(21)	1.34(1)

C(2) - NI(1) - C(14)	88.9(2)
C(2) - NI(1) - C(22)	92.4(3)
C(14) - NI(1) - C(22)	165.7(3)
C(2) - NI(1) - C(23)	176.3(3)
C(14) - NI(1) - C(23)	90.8(3)
C(22) - NI(1) - C(23)	87.0(3)
NI(1) - C(2) - N(3)	135.2(4)
NI(1) - C(2) - N(10)	121.3(4)
N(3) - C(2) - N(10)	103.4(4)
C(2) - N(3) - C(4)	128.8(5)
C(2) - N(3) - C(8)	111.2(5)
C(4) - N(3) - C(8)	120.0(5)
N(3) - C(4) - C(5)	107.8(5)
N(3) - C(4) - C(6)	112.0(5)
C(5) - C(4) - C(6)	109.3(6)
N(3) - C(4) - C(7)	108.3(5)
C(5) - C(4) - C(7)	110.1(6)
C(6) - C(4) - C(7)	109.3(6)
N(3) - C(8) - C(9)	107.6(6)
C(8) - C(9) - N(10)	106.7(5)
C(2) - N(10) - C(9)	111.1(5)
C(2) - N(10) - C(11)	129.1(5)
C(9) - N(10) - C(11)	119.6(5)
N(10) - C(11) - C(12)	116.3(5)
C(11) - C(12) - N(13)	113.2(5)
C(12) - N(13) - C(14)	120.4(5)
C(12) - N(13) - C(21)	127.2(5)
C(14) - N(13) - C(21)	112.3(5)
NI(1) - C(14) - N(13)	112.0(4)
NI(1) - C(14) - N(15)	144.9(5)
N(13) - C(14) - N(15)	102.9(5)
C(14) - N(15) - C(16)	123.9(5)
C(14) - N(15) - C(20)	111.2(5)
C(16) - N(15) - C(20)	124.0(5)
N(15) - C(16) - C(17)	108.4(6)
N(15) - C(16) - C(18)	107.7(6)
C(17) - C(16) - C(18)	111.0(7)
N(15) - C(16) - C(19)	110.0(6)
C(17) - C(16) - C(19)	108.3(8)
C(18) - C(16) - C(19)	111.5(7)
N(15) - C(20) - C(21)	107.5(6)
N(13) - C(21) - C(20)	106.1(6)

G.3 Fractional Atomic Coordinates and Isotropic Thermal Parameters for All Non-Hydrogen Atoms of Ni(^{tBu}CC^{eth})Me$_2$ (13)

Atom	x/a	y/b	z/c	U(iso)	Occ
Ni(1)	0.33680(7)	0.36989(5)	0.64523(5)	0.0183	
C(2)	0.4811(5)	0.2704(4)	0.6444(4)	0.0195	
N(3)	0.5998(5)	0.2603(4)	0.6875(3)	0.0211	
C(4)	0.6641(7)	0.3343(5)	0.7515(4)	0.0266	
C(5)	0.7965(7)	0.3716(6)	0.7125(5)	0.0433	
C(6)	0.5750(8)	0.4287(6)	0.7704(6)	0.0488	
C(7)	0.6900(9)	0.2744(7)	0.8359(4)	0.0446	
C(8)	0.6656(7)	0.1673(4)	0.6643(4)	0.0262	
C(9)	0.5889(7)	0.1182(5)	0.6065(4)	0.0292	
N(10)	0.4749(5)	0.1805(4)	0.5941(3)	0.0186	
C(11)	0.3747(7)	0.1501(5)	0.5294(4)	0.0316	
C(12)	0.2381(7)	0.2031(5)	0.5364(4)	0.0292	
N(13)	0.1792(5)	0.1955(4)	0.6233(3)	0.0247	
C(14)	0.2198(6)	0.2620(5)	0.6880(4)	0.0226	
N(15)	0.1493(5)	0.2262(4)	0.7593(3)	0.0241	
C(16)	0.1745(6)	0.2627(5)	0.8508(5)	0.0313	
C(17)	0.1840(11)	0.3817(7)	0.8503(6)	0.0628	
C(18)	0.3034(9)	0.2147(9)	0.8807(6)	0.0644	
C(19)	0.059(1)	0.2316(11)	0.9085(6)	0.0773	
C(20)	0.0709(6)	0.1397(6)	0.7381(5)	0.0330	
C(21)	0.0886(6)	0.1203(5)	0.6530(5)	0.0305	
C(22)	0.4388(7)	0.4707(5)	0.5728(5)	0.0331	
C(23)	0.1850(6)	0.4689(5)	0.6385(5)	0.0338	

G.4 Anisotropic Thermal Parameters for Ni(^{tBu}CC^{eth})Me$_2$ (13)

Atom	u(11)	u(22)	u(33)	u(23)	u(13)	u(12)
Ni(1)	0.0171(3)	0.0160(3)	0.0218(3)	-0.0012(3)	-0.0006(3)	0.0021(3)
C(2)	0.020(3)	0.020(2)	0.019(2)	0.001(3)	0.006(3)	0.000(2)
N(3)	0.019(2)	0.023(2)	0.021(2)	-0.002(2)	-0.002(2)	0.003(2)
C(4)	0.018(3)	0.035(3)	0.027(3)	-0.007(2)	0.002(3)	-0.000(3)
C(5)	0.040(4)	0.043(4)	0.047(4)	-0.016(4)	0.014(3)	-0.017(4)
C(6)	0.042(4)	0.049(4)	0.056(5)	-0.031(4)	-0.010(4)	0.013(4)
C(7)	0.054(5)	0.053(4)	0.026(4)	-0.002(3)	-0.009(3)	-0.005(4)
C(8)	0.026(3)	0.023(2)	0.029(3)	-0.001(2)	-0.005(3)	0.003(3)
C(9)	0.038(3)	0.014(3)	0.035(3)	0.001(3)	0.008(3)	0.002(3)
N(10)	0.020(2)	0.020(2)	0.016(2)	-0.0039(19)	0.0001(19)	0.0050(19)
C(11)	0.036(4)	0.032(3)	0.027(3)	-0.010(3)	-0.002(3)	-0.000(3)
C(12)	0.031(4)	0.033(3)	0.024(3)	-0.004(3)	-0.011(3)	-0.008(3)
N(13)	0.020(2)	0.027(2)	0.027(3)	-0.0035(19)	-0.000(2)	-0.001(2)
C(14)	0.018(3)	0.026(3)	0.024(3)	0.002(2)	-0.006(2)	0.001(2)
N(15)	0.015(3)	0.028(2)	0.029(3)	0.001(2)	0.001(2)	0.000(2)
C(16)	0.016(3)	0.046(3)	0.032(3)	-0.003(3)	0.004(3)	0.002(3)
C(17)	0.089(7)	0.055(5)	0.044(4)	-0.021(4)	0.012(5)	-0.008(5)
C(18)	0.046(5)	0.088(7)	0.060(6)	-0.011(5)	-0.018(4)	0.016(5)
C(19)	0.048(6)	0.154(11)	0.030(4)	-0.004(6)	0.005(4)	-0.038(7)
C(20)	0.021(3)	0.030(3)	0.047(4)	0.003(3)	0.003(3)	-0.003(3)
C(21)	0.023(3)	0.025(3)	0.044(4)	-0.001(3)	-0.004(3)	-0.009(2)
C(22)	0.034(4)	0.028(3)	0.037(4)	0.009(3)	0.012(3)	0.002(3)
C(23)	0.017(3)	0.033(3)	0.051(4)	-0.001(3)	0.002(3)	0.002(2)

G.5 Fractional Atomic Coordinates and Isotropic Thermal Parameters for Hydrogen Atoms of Ni(^{tBu}CC^{eth})Me$_2$ (13)

Atom	x/a	y/b	z/c	U(iso)	Occ
H(51)	0.8434	0.4211	0.7539	0.0464	
H(52)	0.8589	0.3086	0.7033	0.0464	
H(53)	0.7830	0.4070	0.6554	0.0464	
H(61)	0.6161	0.4759	0.8148	0.0434	
H(62)	0.4830	0.4033	0.7966	0.0434	
H(63)	0.5523	0.4691	0.7166	0.0434	
H(71)	0.7307	0.3227	0.8819	0.0436	
H(72)	0.7531	0.2139	0.8268	0.0436	
H(73)	0.6026	0.2454	0.8619	0.0436	
H(81)	0.7520	0.1409	0.6884	0.0302	
H(91)	0.6127	0.0498	0.5757	0.0292	
H(111)	0.3590	0.0718	0.5340	0.0320	
H(112)	0.4130	0.1652	0.4696	0.0320	
H(121)	0.2505	0.2799	0.5206	0.0313	
H(122)	0.1753	0.1708	0.4921	0.0313	
H(171)	0.2025	0.4114	0.9082	0.0617	
H(172)	0.1043	0.4149	0.8226	0.0617	
H(173)	0.2673	0.4015	0.8105	0.0617	
H(181)	0.3255	0.2397	0.9417	0.0648	
H(182)	0.3019	0.1391	0.8771	0.0648	
H(183)	0.3789	0.2441	0.8408	0.0648	
H(191)	0.0793	0.2542	0.9719	0.0694	
H(192)	0.0567	0.1495	0.9116	0.0694	
H(193)	-0.0265	0.2575	0.8901	0.0694	
H(201)	0.0113	0.0973	0.7786	0.0360	
H(211)	0.0451	0.0608	0.6165	0.0344	
H(123)	0.2178	0.5386	0.6144	0.0500	
H(124)	0.1431	0.4792	0.6957	0.0500	
H(125)	0.1151	0.4406	0.5956	0.0500	
H(122)	0.3824	0.5358	0.5623	0.0500	
H(123)	0.5239	0.4921	0.6035	0.0500	
H(124)	0.4618	0.4385	0.5152	0.0500	

H. X-ray Structure Analysis of Pd(^{tBu}CC^{eth})Me$_2$ (15)

H.1 Summary of Crystallographic Data

Empirical formula	$C_{18}H_{32}N_4Pd.C_4H_{10}O$	
Formula weight	485.02	
Temperature	180 K	
Wavelength (Mo-Kα)	0.71073 Å	
Crystal system	Monoclinic	
Space group	$P2_1/n$	
Unit cell dimensions	a = 10.141(1) Å	α= 90°
	b = 10.001(1) Å	β= 94.24(2)°
	c = 24.746(2) Å	γ = 90°
Volume	2502.9 Å^3	
Z	4	
Density (calculated)	1.29 Mg/m^3	
Absorption coefficient	0.75 mm^{-1}	
F(000)	1019.41	
Crystal size	0.2 x 0.2 x 0.3 mm^3	
θ range for data collection	1.68 to 26.42°	
Index ranges	-12≤h≤12, 0≤k≤12, 0≤l≤30	
Reflections collected	12317	
Independent reflections	5329 [R(int) = 0.036]	
Absorption correction	None	
Refinement method	Full-matrix least-squares on F	
Weighting scheme	Chebychev parameters 1.41, 0.137 and 0.986	
Data / parameters [I>3σ(I)]	3583/253	
Goodness-of-fit on F	1.0803	
Largest final shift	0.008433	
Final R indices	R = 0.0331, wR$_w$ = 0.0391	
Residual density	1.14 and –1.59 e.Å^{-3}	

H.2 Interatomic Distances (Å) and Angles (°) for Pd(^{tBu}CC^{eth})Me$_2$ (15)

PD(1) - C(3)	2.070(3)
PD(1) - C(10)	2.089(3)
PD(1) - C(27)	2.097(4)
PD(1) - C(28)	2.088(4)
N(2) - C(3)	1.356(4)
N(2) - C(6)	1.395(4)
N(2) - C(18)	1.493(4)
C(3) - N(4)	1.350(4)
N(4) - C(5)	1.376(5)
N(4) - C(7)	1.459(5)
C(5) - C(6)	1.343(6)
C(7) - C(8)	1.394(8)
C(8) - N(9)	1.475(6)
N(9) - C(10)	1.361(4)
N(9) - C(13)	1.364(5)
C(10) - N(11)	1.364(4)
N(11) - C(12)	1.396(5)
N(11) - C(14)	1.485(5)
C(12) - C(13)	1.320(7)
C(14) - C(15)	1.494(6)
C(14) - C(16)	1.550(7)
C(14) - C(17)	1.500(7)
C(18) - C(19)	1.512(6)
C(18) - C(20)	1.542(7)
C(18) - C(21)	1.495(7)
O(22) - C(23)	1.414(6)
O(22) - C(25)	1.396(6)
C(23) - C(24)	1.461(9)
C(25) - C(26)	1.461(11)

C(3) - PD(1) - C(10)	88.12(13)
C(3) - PD(1) - C(27)	172.52(15)
C(10) - PD(1) - C(27)	95.78(16)
C(3) - PD(1) - C(28)	91.21(16)
C(10) - PD(1) - C(28)	171.13(16)
C(27) - PD(1) - C(28)	83.94(19)
C(3) - N(2) - C(6)	111.2(3)
C(3) - N(2) - C(18)	126.4(3)
C(6) - N(2) - C(18)	122.3(3)
PD(1) - C(3) - N(2)	140.4(2)
PD(1) - C(3) - N(4)	115.8(2)
N(2) - C(3) - N(4)	103.7(3)
C(3) - N(4) - C(5)	112.2(3)
C(3) - N(4) - C(7)	120.6(3)
C(5) - N(4) - C(7)	127.2(3)
N(4) - C(5) - C(6)	106.7(3)
N(2) - C(6) - C(5)	106.3(3)
N(4) - C(7) - C(8)	116.2(4)
C(7) - C(8) - N(9)	123.0(4)
C(8) - N(9) - C(10)	130.3(4)
C(8) - N(9) - C(13)	118.0(4)
C(10) - N(9) - C(13)	111.7(3)
PD(1) - C(10) - N(9)	119.0(2)
PD(1) - C(10) - N(11)	137.6(2)
N(9) - C(10) - N(11)	103.4(3)
C(10) - N(11) - C(12)	110.3(3)
C(10) - N(11) - C(14)	129.9(3)
C(12) - N(11) - C(14)	119.7(3)
N(11) - C(12) - C(13)	106.9(4)
N(9) - C(13) - C(12)	107.5(4)
N(11) - C(14) - C(15)	112.8(3)
N(11) - C(14) - C(16)	106.9(4)
C(15) - C(14) - C(16)	108.0(4)
N(11) - C(14) - C(17)	108.5(4)
C(15) - C(14) - C(17)	111.4(5)
C(16) - C(14) - C(17)	109.1(5)
N(2) - C(18) - C(19)	110.1(3)
N(2) - C(18) - C(20)	108.1(3)
C(19) - C(18) - C(20)	108.5(4)
N(2) - C(18) - C(21)	109.5(3)
C(19) - C(18) - C(21)	110.1(4)
C(20) - C(18) - C(21)	110.4(5)
C(23) - O(22) - C(25)	113.1(5)
O(22) - C(23) - C(24)	109.6(4)
O(22) - C(25) - C(26)	110.0(5)

H.3 Fractional Atomic Coordinates and Isotropic Thermal Parameters for All Non-Hydrogen Atoms of Pd(^{tBu}CC^{eth})Me$_2$ (15)

Atom	x/a	y/b	z/c	U(iso)	Occ
Pd(1)	0.64757(2)	0.07526(2)	0.883693(9)	0.0274	
N(2)	0.6766(3)	0.3941(3)	0.86643(11)	0.0324	
C(3)	0.6614(3)	0.2800(3)	0.89497(12)	0.0311	
N(4)	0.6598(3)	0.3228(3)	0.94667(12)	0.0431	
C(5)	0.6756(4)	0.4591(4)	0.95094(16)	0.0480	
C(6)	0.6875(4)	0.5052(3)	0.90058(16)	0.0421	
C(7)	0.6436(6)	0.2282(6)	0.99056(17)	0.0726	
C(8)	0.5147(6)	0.1869(6)	0.99752(17)	0.0793	
N(9)	0.4246(3)	0.1353(4)	0.95279(12)	0.0474	
C(10)	0.4511(3)	0.0874(3)	0.90326(13)	0.0338	
N(11)	0.3291(3)	0.0565(3)	0.87966(12)	0.0395	
C(12)	0.2316(4)	0.0846(5)	0.91502(19)	0.0594	
C(13)	0.2926(5)	0.1309(6)	0.96015(19)	0.0652	
C(14)	0.2906(4)	0.0046(4)	0.82450(16)	0.0466	
C(15)	0.4065(5)	-0.0186(6)	0.79182(19)	0.0694	
C(16)	0.2016(7)	0.1123(8)	0.7952(2)	0.0973	
C(17)	0.2117(8)	-0.1209(7)	0.8299(3)	0.1024	
C(18)	0.6913(4)	0.4041(4)	0.80696(14)	0.0426	
C(19)	0.6128(5)	0.2948(5)	0.77718(16)	0.0548	
C(20)	0.6355(8)	0.5405(6)	0.7872(2)	0.0937	
C(21)	0.8342(5)	0.3930(9)	0.7966(2)	0.1007	
O(22)	0.1614(3)	0.5860(4)	0.92216(13)	0.0617	
C(23)	0.1835(6)	0.4951(6)	0.8801(2)	0.0815	
C(24)	0.3247(7)	0.4657(7)	0.8802(3)	0.0914	
C(25)	0.0284(5)	0.6196(9)	0.9246(3)	0.1017	
C(26)	0.0133(8)	0.7130(11)	0.9691(4)	0.1421	
C(27)	0.6539(5)	-0.1341(4)	0.88013(16)	0.0470	
C(28)	0.8511(4)	0.0609(5)	0.8770(2)	0.0582	

H.4 Anisotropic Thermal Parameters for Pd(^{tBu}CC^{eth})Me$_2$ (15)

Atom	u(11)	u(22)	u(33)	u(23)	u(13)	u(12)
Pd(1)	0.03112(13)	0.02647(12)	0.02510(13)	-0.00062(11)	0.00585(8)	0.00472(12)
N(2)	0.0376(15)	0.0270(14)	0.0326(14)	-0.0012(11)	0.0025(11)	0.0006(11)
C(3)	0.0349(16)	0.0312(15)	0.0273(17)	0.0013(13)	0.0014(13)	0.0002(14)
N(4)	0.060(2)	0.0409(17)	0.0274(15)	-0.0007(12)	-0.0047(14)	-0.0105(14)
C(5)	0.062(2)	0.042(2)	0.040(2)	-0.0132(16)	0.0037(18)	-0.0046(18)
C(6)	0.049(2)	0.0302(19)	0.046(2)	-0.0038(15)	-0.0006(16)	0.0001(16)
C(7)	0.106(4)	0.077(3)	0.032(2)	0.011(2)	-0.015(2)	-0.033(3)
C(8)	0.101(4)	0.108(5)	0.029(2)	0.010(2)	0.004(2)	-0.047(4)
N(9)	0.0459(17)	0.068(2)	0.0299(15)	-0.0020(15)	0.0155(13)	-0.0081(16)
C(10)	0.0336(16)	0.0387(18)	0.0297(15)	0.0020(14)	0.0058(12)	-0.0009(14)
N(11)	0.0300(14)	0.0520(19)	0.0376(15)	0.0025(13)	0.0089(12)	-0.0032(13)
C(12)	0.0367(19)	0.084(3)	0.060(3)	-0.002(2)	0.0205(18)	0.001(2)
C(13)	0.056(3)	0.091(3)	0.052(3)	-0.015(2)	0.032(2)	-0.007(2)
C(14)	0.0356(19)	0.064(3)	0.040(2)	-0.0015(18)	0.0011(15)	-0.0144(18)
C(15)	0.047(2)	0.119(4)	0.042(2)	-0.027(3)	0.0028(19)	-0.010(3)
C(16)	0.101(5)	0.128(6)	0.059(3)	0.003(3)	-0.019(3)	0.037(4)
C(17)	0.133(6)	0.099(4)	0.078(4)	-0.028(3)	0.033(4)	-0.073(4)
C(18)	0.052(2)	0.043(2)	0.0327(18)	0.0039(15)	0.0028(15)	-0.0106(17)
C(19)	0.067(3)	0.064(3)	0.0326(19)	0.0011(18)	-0.0013(18)	-0.015(2)
C(20)	0.172(7)	0.059(3)	0.049(3)	0.018(2)	0.001(4)	0.001(4)
C(21)	0.054(3)	0.203(8)	0.048(3)	-0.012(4)	0.020(2)	-0.040(4)
O(22)	0.0426(15)	0.085(2)	0.0559(17)	-0.0082(16)	-0.0046(12)	0.0035(16)
C(23)	0.086(4)	0.088(4)	0.069(4)	-0.027(3)	-0.005(3)	-0.014(3)
C(24)	0.090(4)	0.100(5)	0.086(4)	-0.030(4)	0.015(3)	0.017(4)
C(25)	0.044(3)	0.157(7)	0.103(5)	-0.003(5)	0.001(3)	0.007(3)
C(26)	0.081(4)	0.220(11)	0.127(7)	-0.030(7)	0.019(4)	0.073(6)
C(27)	0.074(3)	0.0302(17)	0.0368(19)	-0.0029(16)	0.0055(17)	0.0115(19)
C(28)	0.0357(19)	0.066(3)	0.074(3)	0.006(2)	0.0119(19)	0.012(2)

H.5 Fractional Atomic Coordinates and Isotropic Thermal Parameters for Hydrogen Atoms of Pd(^{tBu}CC^{eth})Me$_2$ (15)

Atom	x/a	y/b	z/c	U(iso)	Occ
H(51)	0.6791	0.5155	0.9850	0.0532	
H(61)	0.7025	0.6002	0.8889	0.0389	
H(121)	0.1325	0.0747	0.9075	0.0698	
H(131)	0.2505	0.1569	0.9943	0.0750	
H(151)	0.3774	-0.0530	0.7549	0.0718	
H(152)	0.4701	-0.0848	0.8101	0.0718	
H(153)	0.4571	0.0681	0.7873	0.0718	
H(161)	0.1734	0.0857	0.7576	0.1099	
H(162)	0.1214	0.1306	0.8158	0.1099	
H(163)	0.2523	0.2012	0.7937	0.1099	
H(171)	0.1853	-0.1620	0.7943	0.1217	
H(172)	0.2673	-0.1912	0.8524	0.1217	
H(173)	0.1309	-0.1039	0.8502	0.1217	
H(191)	0.6219	0.3014	0.7373	0.0614	
H(192)	0.6460	0.2051	0.7904	0.0614	
H(193)	0.5169	0.3031	0.7842	0.0614	
H(201)	0.6404	0.5506	0.7472	0.0978	
H(202)	0.6834	0.6150	0.8065	0.0978	
H(203)	0.5379	0.5464	0.7951	0.0978	
H(211)	0.8499	0.3953	0.7578	0.0967	
H(212)	0.8885	0.4629	0.8169	0.0967	
H(213)	0.8702	0.3011	0.8116	0.0967	
H(231)	0.1321	0.4071	0.8861	0.0947	
H(232)	0.1471	0.5308	0.8439	0.0947	
H(241)	0.3441	0.4004	0.8507	0.1098	
H(242)	0.3596	0.4274	0.9159	0.1098	
H(243)	0.3746	0.5511	0.8737	0.1098	
H(251)	-0.0279	0.5382	0.9310	0.1057	
H(252)	-0.0087	0.6632	0.8898	0.1057	
H(261)	-0.0795	0.7420	0.9729	0.1589	
H(262)	0.0494	0.6728	1.0050	0.1589	
H(263)	0.0686	0.7978	0.9639	0.1589	
H(127)	0.5845	-0.1667	0.8519	0.0500	
H(128)	0.6356	-0.1725	0.9160	0.0500	
H(129)	0.7426	-0.1638	0.8699	0.0500	
H(128)	0.8707	0.0627	0.8380	0.0500	
H(129)	0.8972	0.1391	0.8961	0.0500	
H(130)	0.8858	-0.0237	0.8941	0.0500	
H(71)	0.6845	0.2664	1.0252	0.0500	
H(72)	0.6961	0.1434	0.9824	0.0500	
H(81)	0.5183	0.1180	1.0269	0.0500	
H(82)	0.4692	0.2699	1.0117	0.0500	